In compliance with the
Canadian Privacy Legislation
some supporting forms
may have been removed from
this dissertation.

While these forms may be included
in the document page count,
their removal does not represent
any loss of content from the dissertation.

University of Alberta

Solid-Liquid Separation of Laterite Slurries

by

Shahid Azam ©

A thesis submitted to the Faculty of Graduate Studies and Research
in partial fulfillment of the requirements for the degree of
Doctor of Philosophy

in

Geoenvironmental Engineering

Department of Civil and Environmental Engineering

Edmonton, Alberta

Fall 2003

National Library
of Canada

Acquisitions and
Bibliographic Services

395 Wellington Street
Ottawa ON K1A 0N4
Canada

Bibliothèque nationale
du Canada

Acquisisitons et
services bibliographiques

395, rue Wellington
Ottawa ON K1A 0N4
Canada

Your file Votre référence
ISBN: 0-612-87932-1
Our file Notre référence
ISBN: 0-612-87932-1

The author has granted a non-exclusive licence allowing the National Library of Canada to reproduce, loan, distribute or sell copies of this thesis in microform, paper or electronic formats.

The author retains ownership of the copyright in this thesis. Neither the thesis nor substantial extracts from it may be printed or otherwise reproduced without the author's permission.

L'auteur a accordé une licence non exclusive permettant à la Bibliothèque nationale du Canada de reproduire, prêter, distribuer ou vendre des copies de cette thèse sous la forme de microfiche/film, de reproduction sur papier ou sur format électronique.

L'auteur conserve la propriété du droit d'auteur qui protège cette thèse. Ni la thèse ni des extraits substantiels de celle-ci ne doivent être imprimés ou aturement reproduits sans son autorisation.

Canada

University of Alberta

Library Release Form

Name of Author: Shahid Azam

Title of Thesis: Solid-Liquid Separation of Laterite Slurries

Degree: Doctor of Philosophy

Year This Degree Granted: 2003

Permission is hereby granted to the University of Alberta Library to reproduce single copies of this thesis and to lend or sell such copies for private, scholarly or scientific research purposes only.

The author reserves all other publication and other rights in association with the copyright in the thesis, and except as herein before provided, neither the thesis nor any substantial portion thereof may be printed or otherwise reproduced in any material form whatever without the author's prior written permission.

26 August 2003

University of Alberta

Faculty of Graduate Studies and Research

The undersigned certify that they have read, and recommend to the Faculty of Graduate Studies and Research for acceptance, a thesis entitled Solid-Liquid Separation of Laterite Slurries submitted by Shahid Azam in partial fulfillment of the requirements for the degree of Doctor of Philosophy in Geoenvironmental Engineering.

Dr. Rick J. Chalaturnyk, Supervisor

Dr. J. Don Scott, Co-Supervisor

Dr. David C. Sego

Dr. Tong Yu

Dr. Marvin J. Dudas

Dr. Loretta Li

June 17, 2003

Abstract

The pressure acid leaching process is the most widely used method for extracting economic metals from laterites. The solid-liquid separation of the laterite ore slurries prepared prior to leaching influences the efficiency of this method. Likewise, the solid-liquid separation of the pressure acid leach (PAL) laterite slurries in the counter current decantation (CCD) circuit affects the amount of the removed liquid. Given the increasing demand for Ni and Co, there was an exigent need to conduct a comprehensive and fundamental study of this class of materials. The objective of this work was to understand and improve the solid-liquid separation of laterite slurries using laboratory investigations: geotechnical index properties, mineralogy, pore water chemistry, morphology, sedimentation, consolidation and hydraulic conductivity. It was found that the geotechnical characteristics of laterites depend on ore geology and the metal extraction process. Sesquioxide-rich laterite ores and hematite-rich laterite PALs have 90% and 70% of the material finer than 0.075 mm, at pH = 7.0 and pH $\leq$ 1.0, respectively. Both of these materials are nonsegregating at 15% solids. An anionic polymer with 75% charge, 17.5 x 10^6 g/mol MW and 12 ppm dosage was found to optimize both hydraulic conductivity and compressibility of laterite ore slurries. For laterite PAL slurries, a cationic polymer with 10% charge, 17.5 x 10^6 g/mol MW and 4 ppm dosage was the most viable. Sedimentation, not consolidation, governs the solid-liquid separation process of laterite slurries because of effective flocculation during initial stages. Hydraulic conductivity and compressibility during consolidation depend on efficient removal of both pore water and water entrapped in flocs. A polymer factor was developed that combines the various parameters of synthetic polymers and was found to correlate with the solid-liquid separation behavior of polymer modified laterite slurries.

Acknowledgements

All praise is to God for guiding mankind in the eternal search of the worlds for truth. I feel honored in glorifying Him in the sincerest way through this small accomplishment. I wish and pray that this humble contribution plays a pivotal role in the current historic transformation of geotechnical engineering into geoenvironmental engineering.

I am extremely fortunate to have a loving wife, Shehla, who made my home a heaven on earth. She took charge of my personal and professional growth ever since we tied the knot. My two little angels, Ayesha and Maria, have made my life really enjoyable and eventful for the last four years. I am indebted to my parents, brothers and sisters for their love and affection throughout my academic career. The emotional and moral support of my family and friends is highly regarded.

I feel privileged to have worked under the kind supervision of Dr. Rick J. Chalaturnyk and Dr. J. Don Scott. Their erudite guidance, ceaseless encouragement, and constructive criticism are genuinely appreciated. Let me put on record my gratitude for my committee members whose invaluable comments and suggestions made this research undertaking possible. The meticulous manuscript reading and the useful critique by my external examiner, Dr. Loretta Li, are greatly valued.

Special thanks to Dr. Marvin J. Dudas and Dr. Stephen Talman for their critical assessments of my work throughout this research. The help and support of Mr. Gerry Cyre, Mr. Stephen Gamble and Mr. Gilbert Wong during the laboratory investigations are sincerely acknowledged.

I am grateful to Natural Sciences and Engineering Research Council of Canada for granting financial assistance. Thanks to the Metallurgical Technologies Division of Dynatec Corporation, Canada, and to Ciba Specialty Chemicals Canada Inc. for providing material support.

Table of Contents

1 Introduction

1.1 GENERAL 1
1.2 PROBLEM STATEMENT 2
1.3 RESEARCH OBJECTIVES AND FRAMEWORK 3
1.4 DISSERTATION OUTLINE 4
1.5 SUMMARY 5

2 Literature Review

2.1 GENERAL 6
2.2 GEOLOGY OF LATERITE ORES 7
  2.2.1 General 7
  2.2.2 Occurrence and Origin 7
  2.2.3 Laterite Profiles 10
2.3 CHARACTERISTICS OF LATERITE ORE SLURRIES 12
  2.3.1 General 12
  2.3.2 Geotechnical Index Properties 13
  2.3.3 Mineralogy 16
  2.3.4 Pore Water Chemistry 19
  2.3.5 Morphology 20
  2.3.6 Solid-Liquid Separation 21
2.4 PRESSURE ACID LEACHING 22
  2.4.1 General 22
  2.4.2 The Mining Operation 23
    2.4.2.1 General 23
    2.4.2.2 Feed Preparation 23
    2.4.2.3 Acid Leaching 25
    2.4.2.4 Counter Current Decantation 28
  2.4.3 Geoenvironmental Issues 30
    2.4.3.1 General 30
    2.4.3.2 Solid-Liquid Separation 30
    2.4.3.3 Waste Management 30

2.5 CHARACTERISTICS OF LATERITE PAL SLURRIES 31
- 2.5.1 General 31
- 2.5.2 Geotechnical Index Properties 31
- 2.5.3 Mineralogy 32
- 2.5.4 Pore Water Chemistry 33
- 2.5.5 Morphology 33
- 2.5.6 Solid-Liquid Separation 34

2.6 COLLOID-POLYMER-ELECTROLYTE INTERACTION 35
- 2.6.1 General 35
- 2.6.2 Characteristics of Colloidal Slurries 35
  - *2.6.2.1 General* 35
  - *2.6.2.2 Double Layer Theory* 36
  - *2.6.2.3 Morphology* 41
  - *2.6.2.4 Solid-Liquid Separation* 46
- 2.6.3 Characteristics of Polymer Solutions 52
  - *2.6.3.1 General* 52
  - *2.6.3.2 Polymer Composition* 53
  - *2.6.3.3 Surface Tension* 55
  - *2.6.3.4 Radius of Gyration* 57
  - 2.6.3.5 *Chain Configuration* 58
- 2.6.4 Polymer Adsorption on Colloidal Surfaces 59
  - *2.6.4.1 General* 59
  - *2.6.4.2 Adsorption Isotherms* 61
  - *2.6.4.3 Adsorbed Conformations* 62
  - *2.6.4.4 Factors Affecting Adsorption* 64
  - *2.6.4.5 Polymer Induced Flocculation* 65

2.7 POLYMER MODIFICATION OF LATERITE SLURRIES 66
- 2.7.1 General 66
- 2.7.2 Solid-Liquid Separation 67
- 2.7.3 Polymer Selection 68
  - *2.7.3.1 General* 68
  - *2.7.3.2 Ionic Polymers* 69
  - *2.7.3.3 Nonionic Polymers* 70
  - *2.7.3.4 Polymer Characteristics* 71
- 2.7.4 Research Hypothesis 71

2.8 SUMMARY 74

3 Research Methodology

3.1 GENERAL 75

3.2 MATERIALS 76

- 3.2.1 General 76
- 3.2.2 Laterite Slurries 76
- 3.2.3 Synthetic Polymers 78
- 3.2.4 Sample Preparation 80
- 3.2.5 Safety Hazards 81

3.3 RESEARCH PROGRAM 82

- 3.3.1 General 82
- 3.3.2 Laboratory Investigation 82
- 3.3.3 Statistical Analysis 83
- 3.3.4 Numerical Simulation 83
- 3.3.5 Laterite Slurry Characteristics Diagram 84

3.4 LABORATORY INVESTIGATION 84

- 3.4.1 General 84
- 3.4.2 Geotechnical Index Properties 86
  - *3.4.2.1 General* 86
  - *3.4.2.2 Water Content* 87
  - *3.4.2.3 Specific Gravity* 88
  - *3.4.2.4 Grain Size Distribution* 89
  - *3.4.2.5 Segregation* 90
  - *3.4.2.6 Consistency Limits* 92
- 3.4.3 Mineralogy 93
  - *3.4.3.1 General* 93
  - *3.4.3.2 X-Ray Diffraction Analysis* 93
  - *3.4.3.3 Ion Exchange* 94
- 3.4.4 Pore Water Chemistry 96
  - *3.4.4.1 General* 96
  - *3.4.4.2 pH and Electrical Conductivity* 96
  - *3.4.4.3 Electrolyte Concentration* 97
- 3.4.5 Morphology 98
  - *3.4.5.1 General* 98
  - *3.4.5.2 Sample Preparation* 99
  - 3.4.5.3 *Scanning Electron Microscopy* 99

3.4.6 Solid-Liquid Separation 101

3.4.6.1 General 101

3.4.6.2 Sedimentation Test 101

3.4.6.3 Consolidation Test 104

3.5 STATISTICAL ANALYSIS 111

3.5.1 General 111

3.5.2 Theoretical Background 112

3.5.2.1 General 112

3.5.2.2 Variables 112

3.5.2.3 Relationships 113

3.5.2.4 Statistical Significance 114

3.5.2.5 Sample Size 114

3.5.2.6 Distribution Function 115

3.5.3 Application 116

3.5.3.1 General 116

3.5.3.2 Design of Experiments 116

3.5.3.3 Analysis of Variance 118

3.5.3.4 Sedimentation 119

3.5.3.5 Consolidation 120

3.5.3.6 Model Validation 120

3.6 NUMERICAL SIMULATION 121

3.6.1 General 121

3.6.2 Thickeners 121

3.6.3 Application 124

3.6.3.1 General 124

3.6.3.2 Sedimentation 124

3.6.3.3 Consolidation 124

3.7 LATERITE SLURRY CHARACTERISTICS DIAGRAM 125

3.7.1 General 125

3.7.2 Construction 127

3.7.3 Application 129

3.7.3.1 General 129

3.7.3.2 Soil Structure 129

3.7.3.3 Soil Behavior 130

3.8 SUMMARY 130

4 Characteristics of Laterite Ore Slurries

4.1 GENERAL 133
4.2 GEOTECHNICAL INDEX PROPERTIES 134
  4.2.1 General 134
  4.2.2 Water Content 134
  4.2.3 Specific Gravity 136
  4.2.4 Grain Size Distribution 137
  4.2.5 Segregation 139
  4.2.6 Consistency Limits 143
4.3 MINERALOGY 145
  4.3.1 General 145
  4.3.2 X-Ray Diffraction 145
  4.3.3 Anion Exchange 151
  4.3.4 Cation Exchange 153
4.4 PORE WATER CHEMISTRY 155
  4.4.1 General 155
  4.4.2 pH and Electrical Conductivity 155
  4.4.3 Electrolyte Concentration 157
4.5 MORPHOLOGY 159
  4.5.1 General 159
  4.5.2 Scanning Electron Microscopy 159
  4.5.3 Elemental Analysis 166
4.6 SOLID-LIQUID SEPARATION 168
  4.6.1 General 168
  4.6.2 Diameter-Height Ratio 168
  4.6.3 Sedimentation 170
  4.6.4 Consolidation 177
    4.6.4.1 General 177
    4.6.4.2 Test Results 177
    4.6.4.3 Morphology 185
4.7 NUMERICAL SIMULATION 190
  4.7.1 General 190
  4.7.2 Laboratory Data 191
  4.7.3 Storage Thickener 191
4.8 LATERITE SLURRY CHARACTERISTICS DIAGRAM 196
4.9 SUMMARY AND CONCLUSIONS 198

5 Characteristics of Laterite PAL Slurries

5.1 GENERAL 200
5.2 GEOTECHNICAL INDEX PROPERTIES 201
    5.2.1 General 201
    5.2.2 Water Content 201
    5.2.3 Specific Gravity 203
    5.2.4 Grain Size Distribution 204
    5.2.5 Segregation 206
    5.2.6 Consistency Limits 210
5.3 MINERALOGY 212
    5.3.1 General 212
    5.3.2 X-Ray Diffraction 212
    5.3.3 Anion Exchange 217
    5.3.4 Cation Exchange 219
5.4 PORE WATER CHEMISTRY 221
    4.9.1 General 221
    4.9.2 pH and Electrical Conductivity 221
    4.9.3 Electrolyte Concentration 223
5.5 MORPHOLOGY 225
    5.5.1 General 225
    5.5.2 Scanning Electron Microscopy 225
    5.5.3 Elemental Analysis 233
5.6 SOLID-LIQUID SEPARATION 235
    5.6.1 General 235
    5.6.2 Diameter-Height Ratio 235
    5.6.3 Sedimentation 238
    5.6.4 Consolidation 244
        4.9.3.1 General 244
        4.9.3.2 Test Results 245
        4.9.3.3 Morphology 255
5.7 NUMERICAL SIMULATION 258
    5.7.1 General 258
    5.7.2 Laboratory Data 259
    5.7.3 CCD Thickener 262
5.8 LATERITE SLURRY CHARACTERISTICS DIAGRAM 264
5.9 SUMMARY AND CONCLUSIONS 266

6 Polymer Modification of Laterite Ore Slurries
6.1 GENERAL 268
6.2 GEOTECHNICAL INDEX PROPERTIES 269
  6.2.1 General 269
  6.2.2 Segregation 269
  6.2.3 Consistency Limits 272
6.3 SEDIMENTATION 274
  6.3.1 General 274
  6.3.2 Ionic Polymers 274
    6.3.2.1 General 274
    6.3.2.2 Initial Hydraulic Conductivity 276
    6.3.2.3 Morphology 287
    6.3.2.4 Statistical Analysis 294
  6.3.3 Nonionic Polymers 296
    6.3.3.1 General 296
    6.3.3.2 Initial Hydraulic Conductivity 296
    6.3.3.3 Morphology 301
    6.3.3.4 Statistical Analysis 301
6.4 CONSOLIDATION 304
  6.4.1 General 304
  6.4.2 Ionic Polymers 304
    6.4.2.1 General 304
    6.4.2.2 Hydraulic Conductivity-Void Ratio 306
    6.4.2.3 Void Ratio-Effective Stress 315
    6.4.2.4 Statistical Analysis 322
  6.4.3 Nonionic Polymers 326
    6.4.3.1 General 326
    6.4.3.2 Hydraulic Conductivity-Void Ratio 327
    6.4.3.3 Void Ratio-Effective Stress 327
    6.4.3.4 Statistical Analysis 330
6.5 NUMERICAL SIMULATION 333
  6.5.1 General 333
  6.5.2 Analyzed Data 333
  6.5.3 Storage Thickener 333
6.6 LATERITE SLURRY CHARACTERISTICS DIAGRAM 339
6.7 SUMMARY AND CONCLUSIONS 341

7 Polymer Modification of Laterite PAL Slurries

7.1 GENERAL 343
7.2 GEOTECHNICAL INDEX PROPERTIES 344
7.2.1 General 344
7.2.2 Segregation 344
7.2.3 Consistency Limits 347
7.3 SEDIMENTATION 349
7.3.1 General 349
7.3.2 Ionic Polymers 349
7.3.2.1 General 349
7.3.2.2 Initial Hydraulic Conductivity 352
7.3.2.3 Morphology 359
7.3.2.4 Statistical Analysis 366
7.3.3 Nonionic Polymers 368
7.3.3.1 General 368
7.3.3.2 Initial Hydraulic Conductivity 368
7.3.3.3 Morphology 373
7.3.3.4 Statistical Analysis 373
7.4 CONSOLIDATION 376
7.4.1 General 376
7.4.2 Ionic Polymers 376
7.4.2.1 General 376
7.4.2.2 Hydraulic Conductivity-Void Ratio 378
7.4.2.3 Void Ratio-Effective Stress 386
7.4.2.4 Statistical Analysis 393
7.4.3 Nonionic Polymers 397
7.4.3.1 General 397
7.4.3.2 Hydraulic Conductivity-Void Ratio 398
7.4.3.3 Void Ratio-Effective Stress 398
7.4.3.4 Statistical Analysis 401
7.5 NUMERICAL SIMULATION 404
7.5.1 General 404
7.5.2 Analyzed Data 404
7.5.3 CCD Thickener 404
7.6 LATERITE SLURRY CHARACTERISTICS DIAGRAM 410
7.7 SUMMARY AND CONCLUSIONS 412

8 Conclusions, Application, Recommendations

8.1 GENERAL 414
8.2 RESEARCH METHODOLOGY 415
8.3 OBSERVATIONS AND CONCLUSIONS 417
  8.3.1 General For All Laterite Slurries 417
    8.3.1.1 Observations 417
    8.3.1.2 Conclusions 417
  8.3.2 Laterite Ore Slurries 418
    8.3.2.1 Observations 418
    8.3.2.2 Conclusions 418
  8.3.3 Laterite PAL Slurries 419
    8.3.3.1 Observations 419
    8.3.3.2 Conclusions 420
  8.3.4 Conclusions For Polymer Modified Laterite Ore Slurries 421
  8.3.5 Conclusions For Polymer Modified laterite PAL Slurries 422
8.4 SIGNIFICANCE AND APPLICATION 423
8.5 RECOMMENDATIONS 425

References 426

A Test Data of Chapter Six

A.1 GENERAL 441

B Test Data of Chapter Seven

B.1 GENERAL 491

List of Tables

Table 3.1: Process conditions for laterite PAL samples 77
Table 3.2: Designations and characteristics of various polymers used 79
Table 3.3: Summary of the laboratory investigation program 85
Table 3.4: Designation of polymer parameters for use in experimental design 117
Table 4.1: Geotechnical index properties of laterite ore slurries 135
Table 4.2: Percent amount of various minerals in laterite ores 149
Table 4.3: Anion exchange of laterite ores 152
Table 4.4: Cation exchange of laterite ores 154
Table 4.5: Pore water chemistry of laterite ore slurries 156
Table 4.6: Summary of sedimentation test results for laterite ore slurries 174
Table 4.7: Changes during solid-liquid separation of laterite ore slurry 181
Table 5.1: Geotechnical index properties of laterite PAL slurries 202
Table 5.2: Percent amount of various minerals in laterite PALs 216
Table 5.3: Anion exchange of laterite PALs 218
Table 5.4: Cation exchange of laterite PALs 220
Table 5.5: Pore water chemistry of laterite PAL slurries 222
Table 5.6: Summary of sedimentation test results for laterite PAL slurries 242
Table 5.7: Changes during solid-liquid separation of laterite PAL slurry 249
Table 6.1: k_i of laterite ore slurry modified with various ionic polymers 278
Table 6.2: k_i of laterite ore slurry modified with various nonionic polymers 298
Table 6.3: log k-e parameters for laterite ore slurry modified with ionic polymers 309
Table 6.4: e-log σ' parameters for laterite ore slurry modified with ionic polymers 318
Table 6.5: Summary of analyzed data for laterite ore slurry 334
Table 7.1: k_i of laterite PAL slurry modified with various ionic polymers 353
Table 7.2: k_i of laterite PAL slurry modified with various nonionic polymers 370
Table 7.3: log k-e parameters for laterite PAL slurry modified with ionic polymers 380
Table 7.4: e-log σ' parameters for laterite PAL slurry modified with ionic polymers 388

Table 7.5: Summary of analyzed data for laterite pal slurry 405

Table A.1: Consistency limits of laterite ore modified with various ionic polymers 442

Table A.2: Consistency limits of laterite ore modified with various nonionic polymers 443

Table A.3: Solids content at start and end of sedimentation tests for laterite ore slurry modified with various ionic polymers 444

Table A.4: Solids content at start and end of sedimentation tests for laterite ore slurry modified with various nonionic polymers 445

Table A.5: Solids content at start and end of consolidation tests for laterite ore slurry modified with various ionic polymers 446

Table A.6: Solids content at start and end of consolidation tests for laterite ore slurry modified with various nonionic polymers 447

Table A.7: pH and EC after sedimentation and consolidation tests for laterite ore slurry modified with various ionic polymers 448

Table A.8: pH and EC after sedimentation and consolidation tests for laterite ore slurry modified with various nonionic polymers 449

Table B.1: Consistency limits of laterite PAL modified with various ionic polymers 492

Table B.2: Consistency limits of laterite PAL modified with various nonionic polymers 493

Table B.3: Solids content at start and end of sedimentation tests for laterite PAL slurry modified with various ionic polymers 494

Table B.4: Solids content at start and end of sedimentation tests for laterite PAL slurry modified with various nonionic polymers 495

Table B.5: Solids content at start and end of consolidation tests for laterite PAL slurry modified with various ionic polymers 496

Table B.6: Solids content at start and end of consolidation tests for laterite PAL slurry modified with various nonionic polymers 497

Table B.7: pH and EC after sedimentation and consolidation tests for laterite PAL slurry modified with various ionic polymers 498

Table B.8: pH and EC after sedimentation and consolidation tests for laterite PAL slurry modified with various nonionic polymers 499

List of Figures

Figure 2.1: Global distribution of laterite ores 8
Figure 2.2: Typical laterite profiles for humid and dry climates 11
Figure 2.3: Effect of geology and environment on plasticity of laterite ores 15
Figure 2.4: Composition of various types of laterite ores 18
Figure 2.5: Schematic of the feed preparation process 24
Figure 2.6: Schematic of the acid leaching process 26
Figure 2.7: Schematic of the counter current decantation process 29
Figure 2.8: Schematic of the double layer and its effect on flocculation 37
Figure 2.9: Schematic of various types of soil fabrics for colloidal particles 42
Figure 2.10: Schematic of important fabric features 44
Figure 2.11: Solid-Liquid Separation of soil slurries 47
Figure 2.12: Typical behavior of soil slurries (after Suthaker 1995) 51
Figure 2.13: Schematic of polymer adsorption on colloidal surfaces 63
Figure 2.14: Hypothetical model for polymer modification of laterite slurries 72
Figure 3.1: Setup for sedimentation test 103
Figure 3.2: Setup for consolidation test 105
Figure 3.3: Schematic of two cell types for consolidation testing 106
Figure 3.4: Calibration of devices used for the consolidation test 109
Figure 3.5: Schematic of a typical thickener used in the metal extraction process 123
Figure 3.6: Laterite slurry characteristics diagram 126
Figure 4.1: Grain size distribution of laterite ore slurries 138
Figure 4.2: Segregation test results for laterite ore slurries 140
Figure 4.3: Segregation limit for various laterite ore slurries 142
Figure 4.4: Plasticity chart for laterite ores 144
Figure 4.5: X-ray diffraction patterns of bulk samples of laterite ores 146
Figure 4.6: Stiff diagrams for laterite ore slurries 158
Figure 4.7: Scanning electron micrographs of limonite ore slurry (Cuba) 160
Figure 4.8: Scanning electron micrographs of limonite-saprolite ore slurry (Philippines) 161
Figure 4.9: Scanning electron micrographs of limonite-saprolite ore slurry (Australia) 162

Figure 4.10: Scanning electron micrographs of saprolite ore slurry (Indonesia) 163
Figure 4.11: Elemental analysis of SEM specimens of laterite ore slurries 167
Figure 4.12: Sedimentation test results for various Do/Ho 169
Figure 4.13: Effect of Do/Ho on sedimentation of limonite-saprolite ore slurry from Philippines 171
Figure 4.14: Sedimentation test results for laterite ore slurries 172
Figure 4.15: Water release rate for various laterite ore slurries 173
Figure 4.16: Consolidation of limonite-saprolite ore slurry 178
Figure 4.17: Void Ratio of limonite-saprolite ore slurry 179
Figure 4.18: Solids Content of limonite-saprolite ore slurry 180
Figure 4.19: Excess Pore pressure of limonite-saprolite ore slurry 183
Figure 4.20: Hydraulic conductivity of limonite-saprolite ore slurry 184
Figure 4.21: Hydraulic conductivity-void ratio relation for limonite-saprolite ore slurry 186
Figure 4.22: Void ratio-effective stress relation for limonite-saprolite ore slurry 187
Figure 4.23: Scanning electron micrographs of limonite-saprolite ore slurry (Philippines) on vertically cut specimen 188
Figure 4.24: Scanning electron micrographs of limonite-saprolite ore slurry (Philippines) on laterally cut specimen 189
Figure 4.25: Simulation of sedimentation test results 192
Figure 4.26: Hydraulic conductivity-void ratio relation for laterite ore slurries 193
Figure 4.27: Predicted behavior in the storage thickener 194
Figure 4.28: LSCD for laterite ore slurries 197
Figure 5.1: Grain size distribution of laterite PAL slurries 205
Figure 5.2: Segregation test results for laterite PAL slurries 207
Figure 5.3: Segregation limit for various laterite PAL slurries 209
Figure 5.4: Plasticity chart for laterite PALs 211
Figure 5.5: X-ray diffraction patterns of bulk samples of laterite PALs 213
Figure 5.6: Stiff diagrams for laterite PAL slurries 224
Figure 5.7: Scanning electron micrographs of limonite PAL slurry (Cuba) 226
Figure 5.8: Scanning electron micrographs of limonite-saprolite PAL slurry (Philippines) 227
Figure 5.9: Scanning electron micrographs of limonite-saprolite PAL slurry (Australia) 228
Figure 5.10: Scanning electron micrographs of saprolite PAL slurry 229

(Indonesia)
Figure 5.11: Elemental analysis of SEM specimens of laterite PAL slurries 234
Figure 5.12: Sedimentation test results for various Do/Ho 236
Figure 5.13: Effect of Do/Ho on sedimentation of limonite-saprolite PAL slurry from Philippines 237
Figure 5.14: Sedimentation test results for laterite PAL slurries 240
Figure 5.15: Water release rate for various laterite PAL slurries 241
Figure 5.16: Consolidation of limonite-saprolite PAL slurry 246
Figure 5.17: Void Ratio of limonite-saprolite PAL slurry 247
Figure 5.18: Solids Content of limonite-saprolite PAL slurry 248
Figure 5.19: Excess Pore pressure of limonite-saprolite PAL slurry 250
Figure 5.20: Hydraulic conductivity of limonite-saprolite PAL slurry 251
Figure 5.21: Hydraulic conductivity-void ratio relation for limonite-saprolite PAL slurry 253
Figure 5.22: Void ratio-effective stress relation for limonite-saprolite PAL slurry 254
Figure 5.23: Scanning electron micrographs of limonite-saprolite PAL slurry (Philippines) on vertically cut specimen 256
Figure 5.24: Scanning electron micrographs of limonite-saprolite PAL slurry (Philippines) on laterally cut specimen 257
Figure 5.25: Simulation of sedimentation test results 260
Figure 5.26: Hydraulic conductivity-void ratio relation for laterite PAL slurries 261
Figure 5.27: Predicted behavior in the CCD thickener 263
Figure 5.28: LSCD for laterite PAL slurries 265
Figure 6.1: Segregation test results for laterite ore slurry modified with 4 ppm of different polymers 270
Figure 6.2: Segregation limit for laterite ore slurry modified with 4 ppm of various polymers 271
Figure 6.3: Plasticity chart for laterite ore slurry modified with various polymers 273
Figure 6.4: Sedimentation test results for laterite ore slurry modified with various anionic polymers 275
Figure 6.5: Sedimentation test results for laterite ore slurry modified with various cationic polymers 277
Figure 6.6: Effect of various polymer parameters on k_i of laterite ore slurry 279
Figure 6.7: Variation of k_i with polymer factor 285

Figure 6.8: SEM of laterite ore slurry modified with 10% charge (low)-17.5 x 10^6 g/mol MW (high)-04 ppm (low) anionic polymer 288

Figure 6.9: SEM of laterite ore slurry modified with 75% charge (high)-17.5 x 10^6 g/mol MW (high)-04 ppm (low) anionic polymer 289

Figure 6.10: SEM of laterite ore slurry modified with 10% charge (low)-17.5 x 10^6 g/mol MW (high)-04 ppm (low) cationic polymer 290

Figure 6.11: SEM of laterite ore slurry modified with 75% charge (high)-17.5 x 10^6 g/mol MW (high)-04 ppm (low) cationic polymer 291

Figure 6.12: Relationship between measured and predicted k_i of laterite ore slurry modified with ionic polymers 295

Figure 6.13: Sedimentation test results using nonionic polymers 297

Figure 6.14: Effect of nonionic polymer parameters on k_i of laterite ore slurry 299

Figure 6.15: SEM of laterite ore slurry modified with 12.5 x 10^6 g/mol MW (medium)-08 ppm dosage (medium) nonionic polymer 302

Figure 6.16: Relationship between measured and estimated k_i of laterite ore slurry modified with polymers 303

Figure 6.17: k-e relationships for laterite ore slurry modified with various anionic polymers 307

Figure 6.18: k-e relationships for laterite ore slurry modified with various cationic polymers 308

Figure 6.19: k-e relationship for laterite ore slurry modified with various ionic polymers 310

Figure 6.20: Effect of gradient on hydraulic conductivity of laterite ore slurry modified with ionic polymers 311

Figure 6.21: e-σ' relationships for laterite ore slurry modified with various anionic polymers 316

Figure 6.22: e-σ' relationships for laterite ore slurry modified with various cationic polymers 317

Figure 6.23: e-σ' relationship for laterite ore slurry modified with various ionic polymers 319

Figure 6.24: Relationship between measured and estimated k of laterite ore slurry modified with ionic polymers 323

Figure 6.25: Relationship between measured and estimated e of laterite ore slurry modified with ionic polymers 324

Figure 6.26: Significance of polymer characteristics on solid-liquid separation of laterite ore slurry 325

Figure 6.27: k-e relationships for laterite ore slurry 328

Figure 6.28: e-σ' relationship for laterite ore slurry 329

Figure 6.29: Relationship between measured and estimated k of polymer modified laterite ore slurry 331

Figure 6.30: Relationship between measured and estimated e of polymer modified laterite ore slurry 332

Figure 6.31: Predicted behavior in the storage thickener 335

Figure 6.32: Performance of the selected polymer in the storage thickener 336

Figure 6.33: LSCD for polymer modified laterite ore slurry 340

Figure 7.1: Segregation test results for laterite PAL slurry modified with 4 ppm of different polymers 345

Figure 7.2: Segregation limit for laterite PAL slurry modified with 4 ppm of various polymers 346

Figure 7.3: Plasticity chart for laterite PAL slurry modified with various polymers 348

Figure 7.4: Sedimentation test results for laterite PAL slurry modified with various anionic polymers 350

Figure 7.5: Sedimentation test results for laterite PAL slurry modified with various cationic polymers 351

Figure 7.6: Effect of various polymer parameters on k_i of laterite PAL slurry 354

Figure 7.7: Variation of k_i with polymer factor 356

Figure 7.8: SEM of laterite PAL slurry modified with 10% charge (low)-17.5 x 10^6 g/mol (high) MW-04 ppm (low) anionic polymer 360

Figure 7.9: SEM of laterite PAL slurry modified with 75% charge (high)-17.5 x 10^6 g/mol (high) MW-04 ppm (low) anionic polymer 361

Figure 7.10: SEM of laterite PAL slurry modified with 10% charge (low)-17.5 x 10^6 g/mol (high) MW-04 ppm (low) cationic polymer 362

Figure 7.11: SEM of laterite PAL slurry modified with 75% charge (low)-17.5 x 10^6 g/mol (high) MW-04 ppm (low) cationic polymer 363

Figure 7.12: Relationship between measured and estimated k_i of laterite PAL slurry modified with ionic polymer 367

Figure 7.13: Sedimentation test results using nonionic polymers 369

Figure 7.14: Effect of nonionic polymer parameters on k_i of laterite PAL slurry 371

Figure 7.15: SEM of laterite PAL slurry modified with 12.5 x 10^6 g/mol (medium) MW-08 ppm (medium) nonionic polymer 374

Figure 7.16: Relationship between measured and estimated k_i of laterite PAL slurry modified with polymers 375

Figure 7.17: k-e relationships for laterite PAL slurry modified with ionic polymers 379

Figure 7.18: k-e relationships for laterite PAL slurry 381
Figure 7.19: Effect of hydraulic gradient on hydraulic conductivity of laterite PAL slurry 382
Figure 7.20: e-σ' relationships for laterite PAL slurry modified with ionic polymers 387
Figure 7.21: e-σ' relationships for laterite PAL slurry 389
Figure 7.22: Relationship between measured and estimated k of laterite PAL slurry modified with ionic polymers 394
Figure 7.23: Relationship between measured and estimated e of laterite PAL slurry modified with ionic polymers 395
Figure 7.24: Significance of polymer parameters on solid-liquid separation of laterite PAL slurry 396
Figure 7.25: k-e relationships for laterite PAL slurry 399
Figure 7.26: e-σ' relationships for laterite PAL slurry 400
Figure 7.27: Relationship between measured and estimated k for polymer modified laterite PAL slurry 402
Figure 7.28: Relationship between measured and estimated e for polymer modified laterite PAL slurry 403
Figure 7.29: Predicted behavior in the CCD thickener 406
Figure 7.30: Performance of the selected polymer in the CCD thickener 407
Figure 7.31: LSCD for polymer modified laterite PAL slurries 411
Figure A.1: Determination of k_i for laterite ore slurry modified with 10% charge (low) anionic polymers 450
Figure A.2: Determination of k_i for laterite ore slurry modified with 75% charge (high) anionic polymers 451
Figure A.3: Determination of k_i for laterite ore slurry modified with 10% charge (low) cationic polymers 452
Figure A.4: Determination of k_i for laterite ore slurry modified with 75% charge (high) cationic polymers 453
Figure A.5: Determination of k_i using low MW nonionic polymer 454
Figure A.6: Determination of k_i using medium MW nonionic polymer 455
Figure A.7: Determination of k_i using high MW nonionic polymer 456
Figure A.8: Consolidation Test#1 457
Figure A.9: Hydraulic conductivity during Test#1 458
Figure A.10: Consolidation Test#2 459
Figure A.11: Hydraulic conductivity during Test#2 460
Figure A.12: Consolidation Test#3 461
Figure A.13: Hydraulic conductivity during Test#3 462

Figure A.14: Consolidation Test#4 463
Figure A.15: Hydraulic conductivity during Test#4 464
Figure A.16: Consolidation Test#5 465
Figure A.17: Hydraulic conductivity during Test#5 466
Figure A.18: Consolidation Test#6 467
Figure A.19: Hydraulic conductivity during Test#6 468
Figure A.20: Consolidation Test#7 469
Figure A.21: Hydraulic conductivity during Test#7 470
Figure A.22: Consolidation Test#8 471
Figure A.23: Hydraulic conductivity during Test#8 472
Figure A.24: Consolidation Test#9 473
Figure A.25: Hydraulic conductivity during Test#9 474
Figure A.26: Consolidation Test#10 475
Figure A.27: Hydraulic conductivity during Test#10 476
Figure A.28: Consolidation Test#11 477
Figure A.29: Hydraulic conductivity during Test#11 478
Figure A.30: Consolidation Test#12 479
Figure A.31: Hydraulic conductivity during Test#12 480
Figure A.32: Consolidation Test#13 481
Figure A.33: Hydraulic conductivity during Test#13 482
Figure A.34: Consolidation Test#14 483
Figure A.35: Hydraulic conductivity during Test#14 484
Figure A.36: Consolidation Test#15 485
Figure A.37: Hydraulic conductivity during Test#15 486
Figure A.38: Consolidation Test#16 487
Figure A.39: Hydraulic conductivity during Test#16 488
Figure A.40: Consolidation Test#17 489
Figure A.41: Hydraulic conductivity during Test#17 490
Figure B.1: Determination of k_i for laterite PAL slurry modified with 10% charge (low) anionic polymers 500
Figure B.2: Determination of k_i for laterite PAL slurry modified with 75% charge (high) anionic polymers 501
Figure B.3: Determination of k_i for laterite PAL slurry modified with 10% charge (low) cationic polymers 502
Figure B.4: Determination of k_i for laterite PAL slurry modified with 75% charge (high) cationic polymers 503
Figure B.5: Determination of k_i using low MW nonionic polymer 504

Figure B.6: Determination of k_i using medium MW nonionic polymer 505
Figure B.7: Determination of k_i using high MW nonionic polymer 506
Figure B.8: Consolidation Test#1 507
Figure B.9: Hydraulic conductivity during Test#1 508
Figure B.10: Consolidation Test#2 509
Figure B.11: Hydraulic conductivity during Test#2 510
Figure B.12: Consolidation Test#3 511
Figure B.13: Hydraulic conductivity during Test#3 512
Figure B.14: Consolidation Test#4 513
Figure B.15: Hydraulic conductivity during Test#4 514
Figure B.16: Consolidation Test#5 515
Figure B.17: Hydraulic conductivity during Test#5 516

List of Symbols

A	Electrolyte concentration (mg/L)
A	Coefficient in hydraulic conductivity-void ratio relationship
AEC	Anion exchange capacity (cmol(-)/Kg)
B	Power in hydraulic conductivity-void ratio relationship
C	Clay content required to fill voids of the coarse matrix (%)
C	Coefficient in void ratio-effective stress relationship
CEC	Cation exchange capacity (cmol(+)/Kg)
C_p	Polymer charge (%)
D	Dielectric constant of the liquid medium
D	Power in void ratio-effective stress relationship
$\mathrm{D_o}$	Diameter of the slurry sample (cm)
D_p	Polymer dosage (mg/L)
E	Surface free energy of a polymer in solution (J)
EC	Electrical conductivity (μS/cm)
ESP	Exchangeable sodium percentage
G_s	Specific gravity of soil
G_{sc}	Specific gravity of the clay size fraction
G_{ss}	Specific gravity of the coarse size fraction
G_{sol}	Surface free energy of the solvent in polymer solution (J)
G_{seg}	Surface free energy of one polymer segment (J)
H	Height of the slurry sample at a given time (cm)
H	Square well depth or attractive energy of a polymer in solution (J)
$\mathrm{H_o}$	Initial height of the slurry sample (cm)
I	Ionic strength of soil water (moles/L)
I_s	Segregation index (%)
I_p	Plasticity index (%)
L	Height of soil sample (cm)
L	Length of one segment of polymer chain (m)
L_1	Measure of the interaction energy between adsorbed segments
L_2	Equilibrium constant
M	Mass of one polymer segment (kg)
MW_p	Polymer molecular weight (g/mol)
N	Number of segments in a polymer chain

N	Number of observed results
N_A	Avogadro's number = 6.023×10^{23}
PAL	Pressure acid leach
pH	Logarithm of the reciprocal of H^+ ion concentration in soil water
PZC	Point of zero charge
Q	Flow volume through soil sample (cm^3/sec)
R_F	Flory Radius (m)
R_G	Radius of gyration (m)
S^2	Sample variance
T	Temperature (^{o}K)
TAEC	Total anion exchange capacity (cmol(-)/Kg)
TCEC	Total cation exchange capacity (cmol(+)/Kg)
TDS	Total dissolved solids (mg/L)
T_p	Polymer type
T_θ	Theta temperature (^{o}K)
V_f	Fluidization velocity of water in a slurry (cm/sec)
V_s	Settling velocity of a slurry (cm/sec)
Y	Response of statistical model corresponding to the observed value
a	Surface area of soil sample (cm^2)
c	Mass concentration of polymer per unit volume of solution (kg/m^3)
d	Linear distance between the two ends of the coiled polymer (m)
d	Inter-atomic spacing (Å)
e	Void ratio
e	Electronic charge, 1.602×10^{-19} (C)
e_s	Maximum void ratio of the coarse fraction taken as 0.9
f	Flexibility of rotation of hydrocarbon molecule about the C—C bond
h	Head difference across soil sample (cm)
k	Hydraulic conductivity (cm/sec)
k	Boltzmann constant, 1.38×10^{-23} ($J\ ^{o}K^{-1}$)
m	Molecular mass of the polymer (kg)
n	Order of diffraction peaks
n_{io}	Electrolyte concentration at the reference state
p	Probability of cell occupation by a polymer
q	Fraction of total colloidal surface covered by the polymer (%)
r	Number of lattice cells joined together in a single polymer molecule
s	Solids content (%)

t	Time (sec)
u	Pore Pressure (kPa)
w	Water content (%)
w_l	Liquid limit (%)
w_p	Plastic limit (%)
w_s	Shrinkage limit (%)
x	Distance from the colloidal surface (m)
$\underline{x}$	Sample mean
x_i	Observed result
x_1	Coefficient in statistical model
x_2	Coefficient in statistical model
x_3	Coefficient in statistical model
x_4	Coefficient in statistical model
z	Coordination number
α	Intra-molecular expansion factor
β	Fraction of the sphere occupied by polymer molecule
χ_s	Flory-Huggins parameter for exchange free energy
δ	Average number of adsorbed polymer segments
ε	Static permittivity of the liquid medium ($C^2J^{-1}m^{-1}$)
ε_o	Permittivity of vacuum, 8.8542×10^{-12} ($C^2J^{-1}m^{-1}$)
ϕ	Volume fraction of the polymer (%)
γ^*	Non dimensional constant
γ_s	Unit weight of the soil solids (g/cm^3)
γ_w	Unit weight of water (g/cm^3)
η	Dynamic viscosity of the liquid (Ns/m^2)
η_o	Dynamic viscosity of the polymer (Ns/m^2)
λ	Wavelength of Cu X-ray source (Å)
ν_i	Valence of ion of type *i*
ρ	Density of polymer solution (kg/m^3)
Ω	Cell volume (m^3)
σ	Total stress (kPa)
σ'	Effective Stress (kPa)
υ	Volume of one segment in a polymer chain (m^3)
ξ	Zeta potential
Ψ	Electrical potential

Chapter 1

Introduction

1.1 GENERAL

Wet mineral processing operations generate soil slurries, which contain large amounts of liquid. In such operations, the liquid phase of the slurry is separated from the solid phase under self-weight. The solid-liquid separation behavior of slurry materials is governed by various interrelated compositional and environmental factors, both of which are determined by ore geology and the extraction technology. Management of mine slurries requires a thorough knowledge of sedimentation, consolidation, and hydraulic conductivity principles.

Laterite ores are one of the major sources of economic metals. According to Golightly (1979a), these ores contain about 80% of known nickel (Ni) reserves on land with sizeable amounts of cobalt (Co). Metals are generally extracted using the pressure acid leaching (PAL) method. This process uses selective dissolution of Ni and Co in an acidic media at elevated temperature and pressure (Chalkey & Toirac 1997). The method requires the conversion of the raw ores to slurries prior to pressure acid leaching. The leaching operation, in turn, generates slurries, which possess an entirely different set of physical and chemical features. Due to the diversity in composition and the environment, an understanding of the solid-liquid separation behavior of laterite slurries needs a methodical investigation.

This chapter introduces the subject area and determines the scope of the study. First, the problem is formulated by stating the most important issues related to the management of laterite slurries. Next, the research objectives and the framework to accomplish those objectives are presented. This is followed by outlining the organization of this dissertation. Finally, a summary of this chapter is provided.

1.2 PROBLEM STATEMENT

The pressure acid leaching process is the most widely used method for extracting economic metals from laterite ores due to its high recovery, low environmental risk, and economic viability (Motteram et al. 1996). The solid-liquid separation of the laterite ore slurries prepared prior to leaching influences the efficiency of this method. Likewise, the solid-liquid separation of the laterite PAL slurries in the counter current decantation (CCD) circuit affects the yield. Given the increasing demand of Ni and Co, there was an exigent need to conduct a comprehensive study of this class of materials. Further, a fundamental undertaking was necessary to capture the influence of laterite geology and the pressure acid leaching process. A knowledge of the solid-liquid separation behavior of laterite slurries is beneficial both for the mining industry and the geotechnical engineering community. Results of this study could be used to improve process efficiency and productivity under actual conditions as well as to assess slurry disposal methods and to manage tailings ponds. The application of basic soil mechanics concepts to a hydrometallurgical process broadens the scope of geotechnical engineering.

1.3 RESEARCH OBJECTIVES AND FRAMEWORK

The main objective of this work is to understand and improve the solid-liquid separation of laterite slurries. The specific objectives are listed below:

- To determine geotechnical index properties for preliminary slurry assessment
- To investigate the influence of mineralogy and pore water chemistry on solid-liquid separation behavior
- To study the of effect of microstructure on solid-liquid separation behavior
- To study solid-liquid separation behavior by determining sedimentation, consolidation and hydraulic conductivity

The research framework required to accomplish the main objective resulted in a stepwise approach. The first step was to develop a clear understanding of laterite slurry behavior under ambient process conditions by capturing the influence of ore geology and pressure acid leaching. Therefore, a comprehensive characterization was conducted for both laterite ore and PAL slurries.

Improvement of the solid-liquid separation behavior of laterite slurries was based on the principle of *no alteration in actual process conditions*. This necessitated the use of synthetic polymers because of their ability to interact with the solid phase in a given medium while still remaining chemically inert.

Laboratory investigation called for developing special protocols owing to various peculiarities of laterite slurries. First, laterite soils illustrate variations in engineering characteristics when exposed to air or heating (Townsend 1985).

Second, when these soils are converted to slurries, characteristics of the latter are entirely different from normal soils. Third, the extraction process causes mineralogical changes during leaching. Therefore, all routine testing procedures had to be modified to capture the characteristics of this distinct class of materials.

Finally, this study had to be beneficial for both the mining industry and the geotechnical engineering community. This required the extrapolation of laboratory data to predict field performance. For improved efficiency and productivity, laboratory results had to be statistically validated and numerically simulated. Likewise, the results had to be presented in a way that is useful for assessing alternative slurry disposal methods.

1.4 DISSERTATION OUTLINE

This chapter is followed by a thorough survey of the published literature that provides a theoretical basis for this research work. Chapter Two mainly focuses on various aspects related to laterite geology, pressure acid leaching, characteristics of laterite slurries, and polymer modification of these materials.

Chapter Three presents the methodology for conducting this research. This chapter describes the materials and the laboratory testing methods, gives an account of the statistical and numerical techniques for data analysis, and proposes a Laterite Slurry Characteristics Diagram (LSCD) for summarizing data.

Chapter Four and Five present the results of laboratory testing conducted to characterize various laterite ore and PAL slurries, respectively. Likewise, Chapter

Six and Seven discuss the results of laboratory investigation and modeling for polymer modified laterite slurries using a selected ore and the corresponding PAL, respectively. These four chapters fulfill the main research objective, that is, to understand and improve the solid-liquid separation of laterite slurries.

Lastly, Chapter Eight summarizes the main conclusions derived from the findings of this research and provides recommendations for future work.

1.5 SUMMARY

The pressure acid leaching process is the most widely used method for extracting economic metals from laterite ores. The efficiency and the yield of this method depend on the solid-liquid separation of the laterite ore and PAL slurries, respectively. Given the increasing demand of Ni and Co, there was an exigent need to understand and improve the solid-liquid separation of laterite slurries. This objective was achieved using the following framework:

- Understanding laterite slurry behavior under ambient process conditions
- Devising a polymer amelioration method for improved solid-liquid separation
- Developing a detailed laboratory characterization protocol
- Predicting field performance from laboratory data

This dissertation is divided into eight chapters. The first three chapters provide an introduction, literature review and research methodology for this work. The next four chapters present, analyze and discuss the results obtained during this research. The last chapter summarizes the main conclusions.

Chapter 2

Literature Review

2.1 GENERAL

This chapter presents a comprehensive literature review of various interrelated aspects pertaining to the solid-liquid separation of laterite slurries. First, the geological features of laterite ores and the geotechnical characteristics of the corresponding slurries are given. Next, the acid leach metal extraction process is described with all necessary details; the major geoenvironmental issues associated with this mining operation are identified. This is followed by an account of the characteristics of laterite PAL slurries. These four sections provide an overview of the material characteristics under ambient process conditions.

Synthetic polymers were chosen to improve the solid-liquid separation behavior of laterite slurries for the metal extraction process. A detailed literature survey related to the interactions of colloidal particles with synthetic polymers in an electrolyte medium is given. This review helps in understating the expected behavior of polymer modified laterite slurries and in selecting appropriate polymers for this class of materials. Based on such a theoretical background, a research hypothesis is propounded for effective polymer modification of laterite slurries. The chapter concludes by providing a summary of the main points learnt during this literature survey.

2.2 GEOLOGY OF LATERITE ORES

2.2.1 General

The term laterite is derived from a Latin word *later* meaning brick. This term was first given to some weather resistant and rapid hardening Indian soils used for brick construction (Buchanan 1807). According to Alexander & Caddy (1962), laterites are rich in secondary oxides of iron and aluminum and may contain quartz and clay minerals but are devoid of bases and primary silicates.

Economic metal bearing laterite ores are produced by weathering of parent rocks. Variation in mineral composition in the weathered profile leads to significant differences in engineering behavior of these ores (Lohnes et al. 1971). Further, test conditions can cause an inadequate assessment of material properties and hence results of one area cannot be used in another area with certainty (Terzaghi 1958). Therefore, a clear understanding of the geological origin and the weathered profile of a laterite ore is key to economic metal recovery.

2.2.2 Occurrence and Origin

Laterite ores mainly occur in tropical areas of the Pacific Ocean such as Indonesia, Philippines, New Caledonia, and Australia. Sizeable amounts of laterite ores are found in Cuba, Brazil, Colombia, Guatemala, and some central African countries (Golightly 1981). Most of these laterites are very old and their development associated with Pliocene, Pleistocene, and Middle or Late Tertiary surfaces (Ruhe 1954). Condensed from Nixon & Skipp (1957) and Saunders & Fookes (1970), Figure 2.1 gives a world map showing laterite ore distribution.

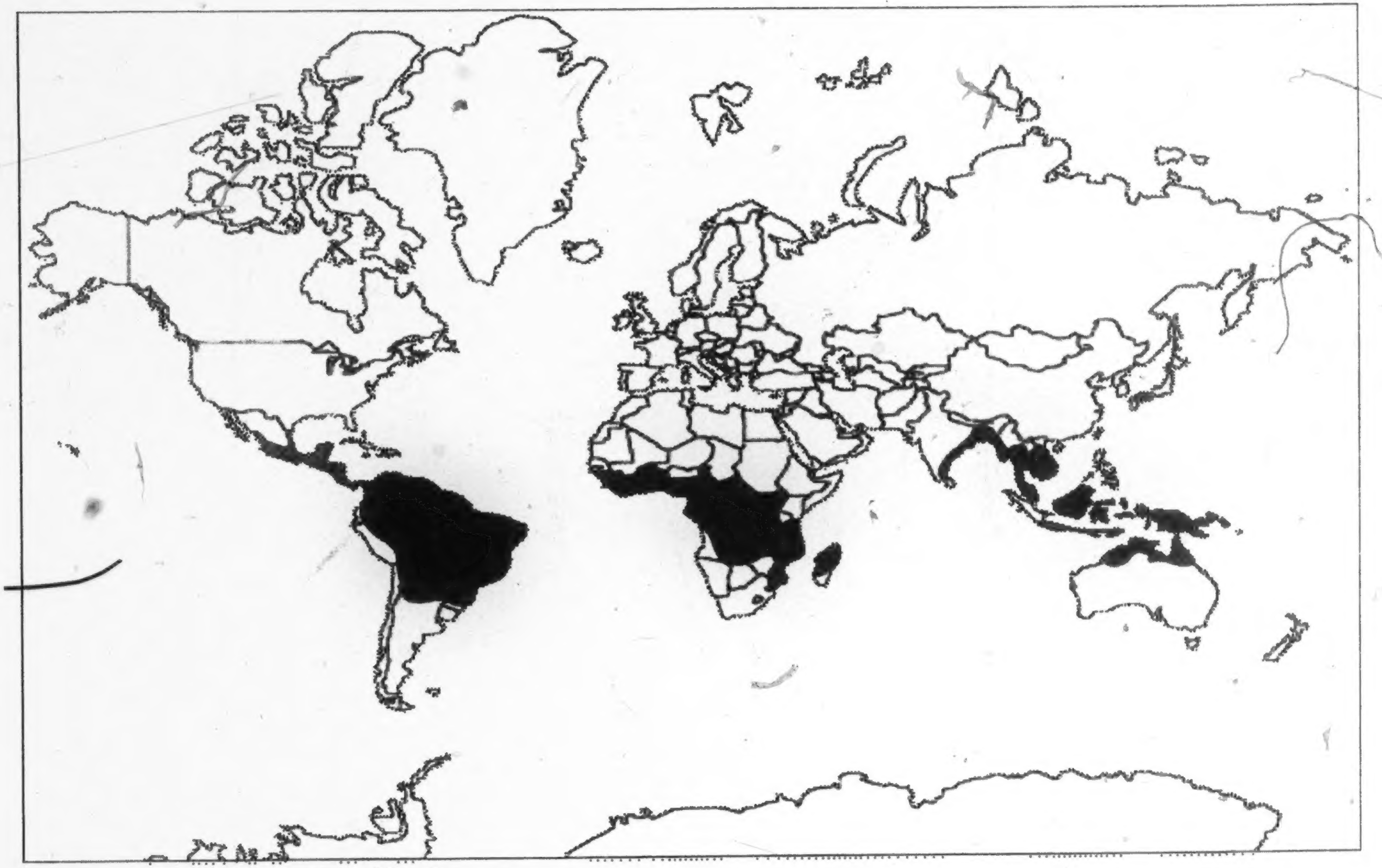

Figure 2.1: Global distribution of laterite ores

The parent material of laterite ores is an olivine-rich igneous rock called peridotite that contains up to 0.3% nickel (Gidigasu 1974). The peridotite bedrock is either composed of fresh olivine, $(Mg, Fe)_2SiO_4$, or its hydrated derivative known as serpentine. These bedrocks undergo extensive physical and chemical weathering that involves rapid breakdown of feldspar and ferro-magnesium minerals, and are converted to laterite ores (Grant 1974). The oxidation reaction that involves alteration of Mg and SiO_2 (*serpentinization*) is associated with up to 70% swelling and a permeability increase (Krause et al. 1997). Exchange of Ni in soil water for Mg in serpentine clay occurs as follows (Golightly1979a):

$$Mg_3Si_2O_5\,(OH)_4 + 3\,Ni^{2+} \rightarrow Ni_3Si_2O_5\,(OH)_4 + 3\,Mg^{2+} \qquad (2.1)$$

Weathering of ultramafic (ferro-magnesium-rich) bedrocks to laterites occurs in three stages. The first stage is the *decomposition* of primary minerals and the release of constituent elements such as Si, Al, Fe, Ca, Mg, Ni, K and Na, in simple ionic form (Loughnan 1969). This is followed by *laterization* that involves leaching of silica and accumulation of sesquioxides (Pickering 1962). Suitable conditions for laterization include intense and prolonged weathering at less than neutral pH (Mohr & Van Baren 1954). The last phase is *desiccation*, which refers to the dehydration of sesquioxide-rich material and secondary minerals (Sherman et al. 1953). The dehydration of hydrated iron oxides involves a loss of water and crystallization of amorphous iron colloids into dense crystalline iron minerals (Hamilton 1964). The time required for the conversion of primary minerals to laterite ores is of the order of 3×10^6 years (Burger 1995).

Climate, topography, mineralogy of parent rock and geomorphic history control the development of laterite ores (Golightly 1979b). Due to high temperature, extended periods of abundant rainfall, and acidic environment, tropical regions present the natural setting for laterization (Gidigasu 1972). Under such conditions, the weathering process is accelerated due to unidirectional downward water flow. Laterites of Cuba and Philippines have formed swiftly by the conversion of olivine to silica and goethite (Troly et al. 1979) by the process:

$$Fe_2SiO_4 + 2\,H^+ + O_2 \rightarrow SiO_2 + 2\,FeO(OH) \tag{2.2}$$

In other areas such as Australia, weathering had been slow owing to relatively dryer conditions, which, in turn, led to the formation of smectite clays along with goethite (Burger 1979) according to the following reaction:

$$4\,Fe_2SiO_4 + 8\,H^+ + 4\,O_2 \rightarrow Fe_2Si_4O_{10}\,(OH)_2 + 6\,FeO(OH) \tag{2.3}$$

2.2.3 Laterite Profiles

Laterite profiles generally exhibit various zones due to dissolution of original minerals, movement of elements in solution and precipitation of elements at other locations (Golightly 1979a). Figure 2.2, which is modified after Krause et al. (1997), gives typical profiles for both dry and humid equatorial climates. This figure shows that for both climates, laterite profiles have an average thickness of 20 to 50 m (Baghala & Papangelakis 1998a). Further, most laterite ores are overlain by a hard crust of hematite with low nickel content at the surface. Below this iron capping, a region of hematite-rich goethite is encountered. According to Krause et al. (1997), this zone contains a negligible amount of nickel.

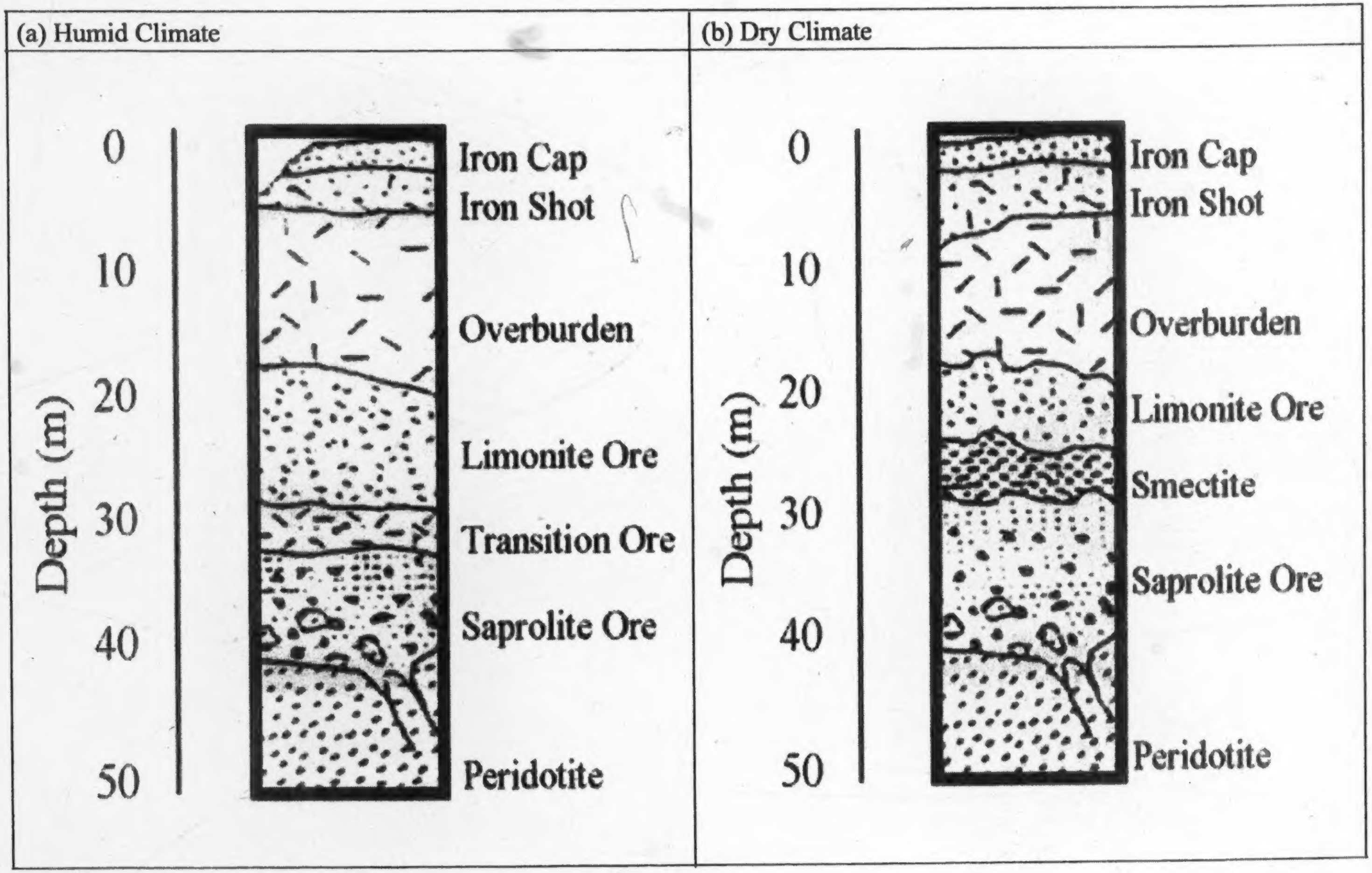
(a) Humid Climate
Depth (m)
0
10
20
30
40
50
Iron Cap
Iron Shot
Overburden
Limonite Ore
Transition Ore
Saprolite Ore
Peridotite
(b) Dry Climate
Depth (m)
0
10
20
30
40
50
Iron Cap
Iron Shot
Overburden
Limonite Ore
Smectite
Saprolite Ore
Peridotite

Figure 2.2: Typical laterite profiles for humid and dry climates

Below the overburden is found a limonite zone that is predominantly composed of mixed iron oxides (geothite and hematite); aluminum is present as gibbsite (Chalkley & Toirac 1997). This extremely fine-grained ore commonly contains from 1.0 to 1.6% nickel. Further, the water content of this zone varies from 10% for arid deposits to 50% for tropical deposits.

The transition zone that consists of clay minerals, traces of crystalline quartz, and variable amounts of iron oxides, underlie the limonite zone (Mitchell 1993). The clay minerals are formed as a result of extreme disintegration, strong hydration and minimal leaching (Tourtelot 1973). Such conditions are brought about by scanty and sporadic rainfall prevalent in dry climates (McMahone 1989).

Above the bedrock occurs a saprolite zone that retains most of the parent rock minerals. This zone is derived from the *in situ* decomposition of parent material and contains large boulders (Golightly 1981). Saprolite is characterized by high Mg and SiO_2 content and large compositional variation with depth. The Ni content in a mined saprolite varies between 1.6 and 3.0% (Krause et al. 1997).

2.3 CHARACTERISTICS OF LATERITE ORE SLURRIES

2.3.1 General

Slurries are composed of solid particles dispersed in a liquid (van Olphen 1977). The colloidal particles have large surface areas, charged interfaces, and the ability to flocculate (Mitchell 1993). This section highlights the influence of composition and geology on the characteristics of laterite ore slurries.

2.3.2 Geotechnical Index Properties

Laterite ore slurries have reddish shades due to the various degrees of iron, titanium, and manganese hydration. According to Maignien (1966), these shades become progressively darker with age.

It is generally accepted that laterite soils have significantly higher values of specific gravity than most sedimentary soils (Gidigasu & Bhatia 1971). This is mainly attributed to the presence of iron oxides for which specific gravity ranges from 4.26 for goethite to 5.26 for hematite (Gidigasu 1976).

Grain size distribution of laterite soils is a function of the nature of the parent material, genesis, degree of weathering, geologic origin, location in the topographic site and depth in the profile (Gidigasu 1976). These soils cover a large succession of materials from fresh to concretionary rock. The presence, quantity, distribution and degree of weathering of materials finer than 1 mm govern the behavior of such soils (Gidigasu 1974).

The weathering process results in coating of the colloidal particles by sesquioxides of iron and aluminum (Mitchell & Sitar 1982). Due to such coating coarser aggregations of silt and sand sized range are developed thereby suppressing the surface characteristics of the colloids (Townsend 1985). The micro-aggregates are formed due to one or both of the following reasons: (i) cementation that is caused by precipitation and irreversible dehydration of iron and aluminum gels (Morin & Todor 1975) and (ii) flocculation, which is promoted by the presence of iron in solution (D'Hoore & Fripiat 1954). Such aggregates of cemented particles are susceptible to mechanical weathering (Mitchell 1993). Small sized grains and narrow grain size distribution (homogenous particles) in laterite ore slurries are associated with reduced aggregation and minimum settling (Schramm 1996; Yariv & Cross 1979).

Figure 2.3 highlights the influence of (a) parent rock type, (b) clay size fraction, (c) weathering condition and (d) rainfall distribution on the plasticity of laterite soils. Although given separately, this figure suggests that the influence of all factors should be considered conjointly because of their mutual interrelation; the A-line differentiates between active clays (above) and silty clays (below).

Figure 2.3 (a) shows that laterite soils derived from igneous parent rocks plot below the A-line and a liquid limit higher than 50%. On the contrary, laterites derived from sedimentary parent rocks plot above the A-line and have a liquid limit that depends upon the nature of the clay minerals (Cruz 1969).

Figure 2.3 (b) shows that plasticity characteristics of laterite ores do not correlate well with clay size fraction (material finer than 0.002 mm). This is due to variations in clay mineral type (de Graft-Johnson et al. 1972) and partial or complete sesquioxide coating of clay particles (Townsend 1985).

Figure 2.3 (c) differentiates ferruginous ores from ferralitic ores (Remillon 1967). The former are formed under dry climates in well-drained savannah vegetation whereas the latter are developed in humid tropical marshy rainforests. This figure shows that ores from both weathering conditions plot above A-line but ferruginous ores have lower liquid limits owing to their high sesquioxide content.

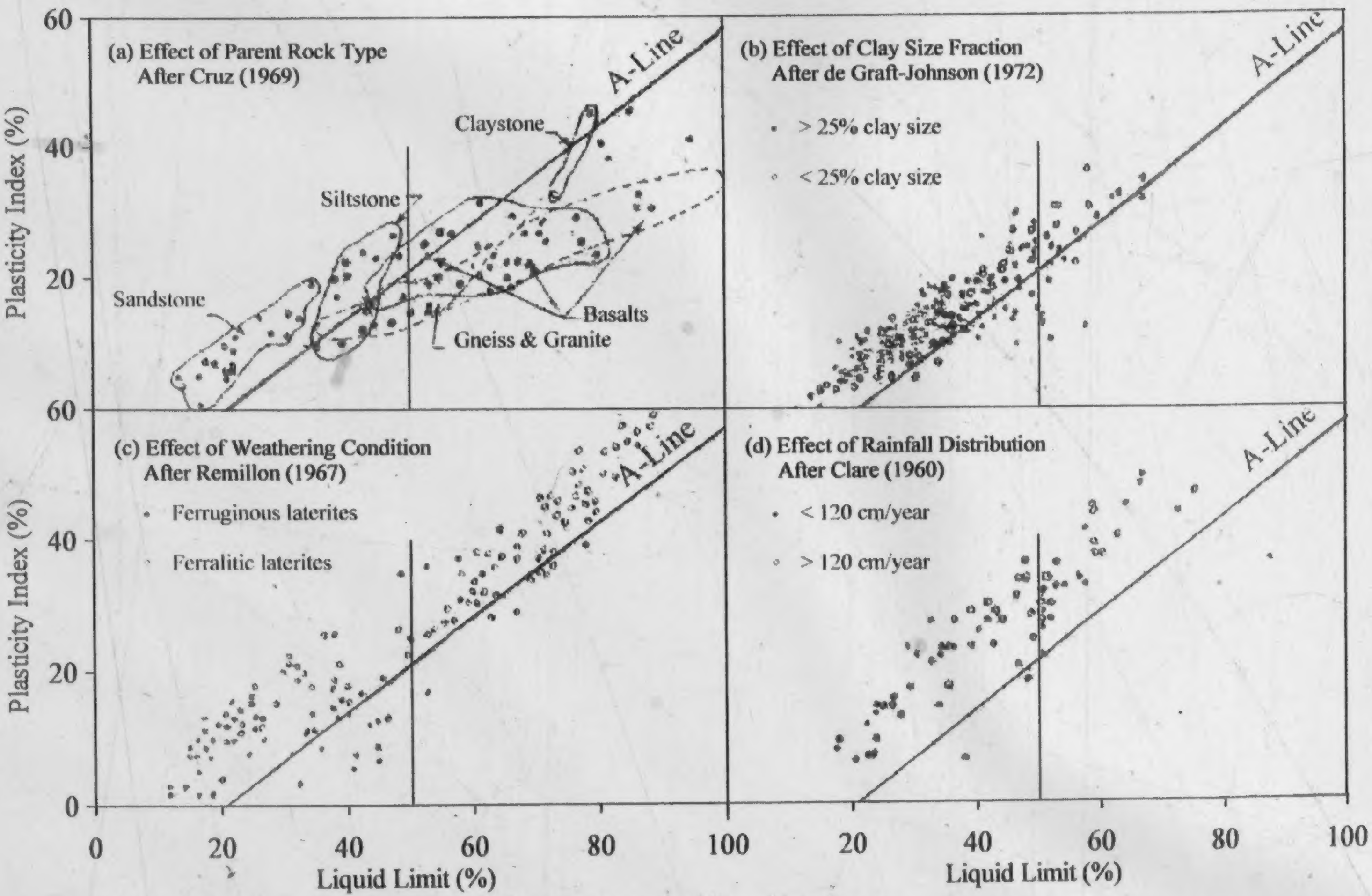

Figure 2.3: Effect of geology and environment on plasticity of laterite ores

Figure 2.3 (d) shows that laterites formed under most rainfall conditions plot above the A-line. Similarly, laterites developed in areas receiving an average annual precipitation of less than 120 cm have liquid limit below 50% and the reverse is true for regions getting more than 120 cm of rainfall per year.

2.3.3 Mineralogy

Mineralogical composition governs the size, shape, and surface characteristics of soil particles. It determines the interaction of the solid phase with the fluid phase and hence affects the solid-liquid separation behavior. Thus, knowledge of mineralogy is fundamental to the understanding of laterite ore slurries.

Mineralogy of laterite ores varies between the boundaries given in equations 2.2 and 2.3 owing to variation in geology and environment. The various zones of laterite profiles are associated with specific mineralogy that leads to a distinct behavior (Gidigasu 1976). The presence or absence of a mineral in a laterite ore depends upon its solubility with respect to other minerals of similar chemical composition (Golightly 1979a). As described earlier, weathering of peridotite follows the three stages of decomposition, laterization and desiccation. During this weathering process, minerals of lower solubility such as silica, smectite and goethite replace unstable minerals like olivine and serpentine. Although clay minerals such as kaolinite, chrysotile, hydrous mica, chlorite and smectite are found in laterite ores (Loughnan 1969; Morrin & Parry 1969), smaller sesquioxide minerals govern the engineering response of these materials due to their mobility and solubility (Maignien 1966).

Figure 2.4, which is modified after Golightly (1979a), gives composition of various types of laterite ores. This figure shows that most varieties of laterite ores fall in the triangular area enclosed by two limiting curves. Boundary AB depicts the progressive weathering of olivine and serpentine to limonite whereas curve CD follows a serpentine-smectite-limonite evolution: silica-rich varieties fall above this curve. Figure 2.4, which also gives contours of iron content, shows increasing Fe percentage during the various stages of laterite ore development.

The significance of mineralogical composition arises from the surface charges of various mineral species. Clay particles possess a negatively charged surface that attracts cations. Many of these cations are exchangeable as they can be replaced by other cations (Mitchell 1993). Conversely, sesquioxides have a positively charged surface and variations in surface charge depend on the pH of the pore fluid.

The capacity of anion and cation exchange in laterite ores owes its origin to the parent material and the degree of weathering. Anion exchange, which arises from the protonation of hydroxyl groups on the edges of clay minerals and on the surfaces of sesquioxides, is inversely proportional to the pH of the pore fluid. Cation exchange in laterite ores depends on the type and amount of clay mineral and coating of these minerals by fine sesquioxide gels (Gidigasu 1971). Such coatings tend to reduce the electro-chemical activity on clay mineral surfaces (Townsend et al. 1971). Therefore, characteristics of laterite ore slurries depend on the extent of sesquioxide coating and on the pore fluid chemistry.

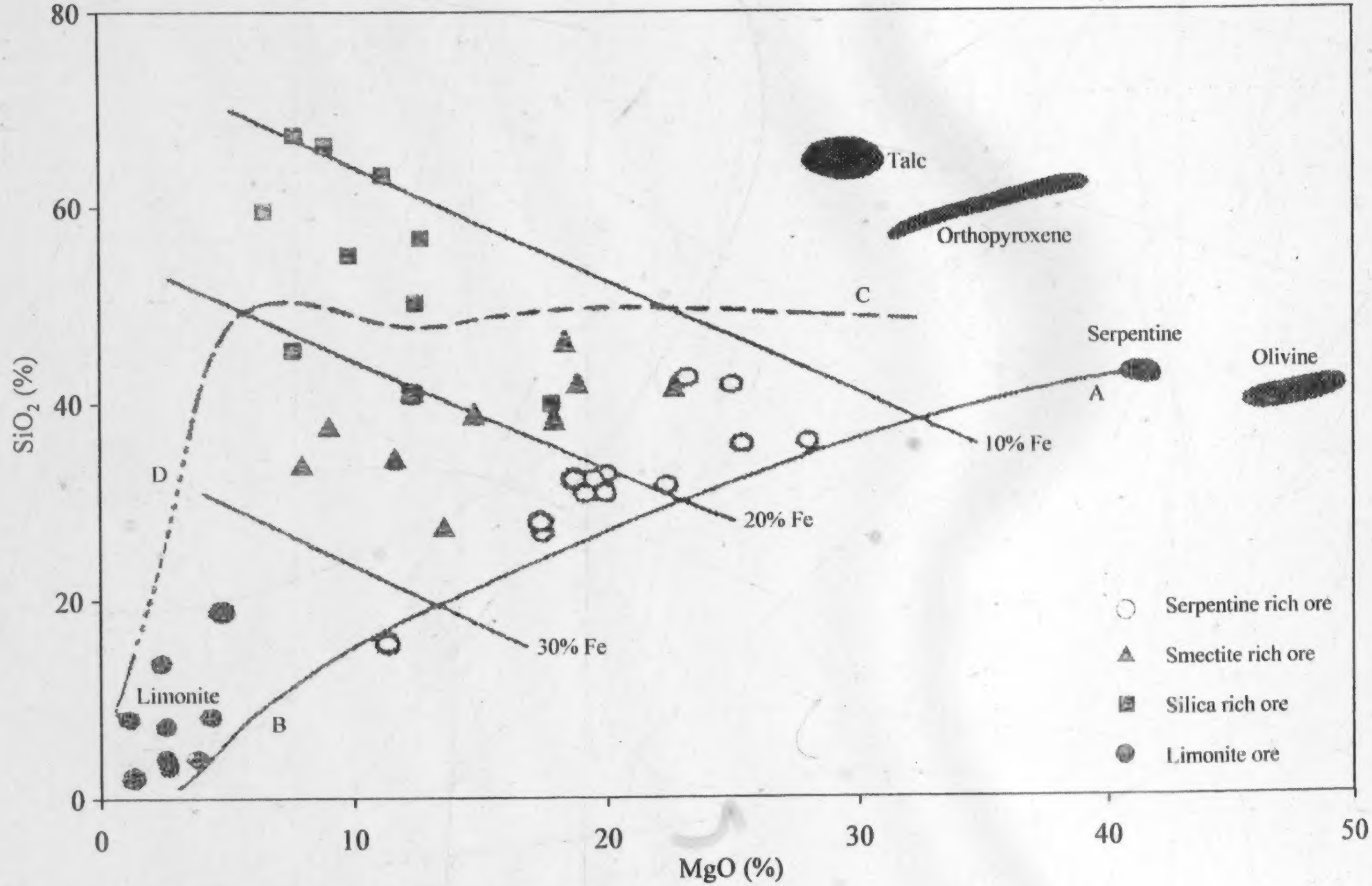

Figure 2.4: Composition of various types of laterite ores

2.3.4 Pore Water Chemistry

Pore water chemistry is one of the key factors influencing the engineering behavior of soils. The physico-chemical interactions at the interface of pore water and colloidal slurry results in the development of a double layer of electrolytes around the colloids (Mitchell 1993). Changing the chemical composition of the pore water can alter the properties of this double layer thereby affecting the solid-liquid separation behavior of the slurry (Sposito 1984). A detailed account of the double layer theory is presented later in this chapter. This section describes the origin of two of the most important water characteristics for laterite ores: pH and electrolyte concentration (Winterkorn 1948; Winterkorn & Moorman 1941).

Depending on climate and vegetation, a neutral to slightly acidic pH characterizes a weathering laterite environment (Gidgasu 1976). The higher the rainfall and hence the degree of leaching the lower the pH. Data presented by Gidigasu (1971) suggests that the pH decreases with depth as the root zone of plants gradually diminishes.

The type and amount of an electrolyte in the pore water depends on mineral solubility and water movement, which is governed by weathering conditions (Golightly 1979a). Figure 2.4 suggests that due to the high solubility of serpentine, its pore water should be rich in Mg^{2+} and Si^{4+}. Concentration of these ions is progressively decreased with increased weathering and reaches a minimum for limonite ores. Depending on the weathering environment, Na^{+}, K^{+}, Ca^{2+} and SO_4^{2-} may get dissolved in pore water of smectite and silica rich ores.

2.3.5 Morphology

Morphology of soil slurries has profound effect on sedimentation, consolidation and hydraulic conductivity. Arrangement of individual particles, particle groups and pore spaces in a soil slurry predominantly depends on soil mineralogy and pore water chemistry (Mitchell 1993). Determination of laterite slurry morphology is obligatory to evaluate the development of solid-liquid separation behavior of such materials. A detailed discussion about various types and scales of soil fabrics and their significance in the solid-liquid separation behavior is given later in this chapter. This section briefly describes the *in situ* morphology of laterite soil as developed under local geological, climatic and environmental conditions.

Laterite soils have been described as vesicular, concretionary, cellular, vermicular, slag-like, pisolithic and concrete-like masses (Gidigasu 1976). Such variable descriptions of this class of materials indicate their range from unconsolidated and scarcely coherent soils to hard rock-like masses with a wide variety of intermediate forms (Haldemann et al. 1979). Further, this morphological variability is due to the nature and extent of clod formation in different types of laterite ores. According to Greenland et al. (1968), aggregates as large as silt and even sand size are formed as sesquioxides of iron and aluminum coat clay minerals to various degrees. The oppositely charged sesquioxide and clay mineral surfaces and an acidic environment favor such coating (Mitchell 1993).

2.3.6 Solid-Liquid Separation

The most important geoenvironmental issue in wet mineral processing operations is the generation of soil slurries containing large amounts of liquid. Effective separation of solids and liquids in these slurries reduces the running cost of such operations. Solid-liquid separation is characterized by sedimentation and consolidation and the variation of hydraulic conductivity under these two stages. A detailed discussion about these geotechnical aspects of engineering behavior is given later in this chapter. This section describes the solid-liquid separation behavior of laterite ore slurries.

Laterite ore slurries are streams of low solids content prepared prior to the acid leaching process. For increased process efficiency, an understating of the solid-liquid separation behavior of these materials is obligatory. Based on the preceding literature review of geotechnical index properties, mineralogy, pore water chemistry and morphology of laterite ores, an understating of the anticipated solid-liquid separation behavior can be developed. Generally, the high specific gravity, the large grain size derived from sesquioxide coating of soil particles and the near neutral environments should result in good solid-liquid separation. Incidentally, no record was found in the published literature that presents experimental data on solid-liquid separation of laterite ore slurries. The presence of various mineral species and the effect of the slurry preparation method may cause changes in the above mentioned expected behavior. This research was investigates such variations in the behavior of laterite ore slurries.

2.4 PRESSSURE ACID LEACHING

2.4.1 General

The two main processing technologies for treating nickel laterite ores are smelting and acid leaching. Smelting is used for the saprolite ore (Reid 1996) whereas for the limonite ore, the acid leach process is generally preferred (Duyvesteyn et al. 1979). This preference for the latter extraction method is due to the incentive to obtain relatively pure nickel as well as cobalt from large untapped limonite reserves because of a marked decline in the number of available sources of saprolite ores (Matheson 1996). However, the process is not confined to limonite ore only and has undergone extensive modification to meet the requirements of the mining industry since its inception in Cuba in the 1960s. Queneau et al. (1984) extended the application of this process to the entire ore body: limonite ore, transition ore and saprolite ore. The excessive acid requirement was overcome by separating the ore into a fine low-Mg fraction for direct leaching and a coarse high-Mg fraction that was pretreated before leaching. To further reduce the operational cost, limonite-saprolite mixtures are now leached in one step (Chalkley & Toirac 1997). Currently, due to its high recovery, low environmental risk and economic viability, acid leaching is considered as the method of choice for metal extraction from almost any type of laterite ore (Baghala & Papangelakis 1998a). This section provides a detailed account of important stages in the sulfuric acid leaching metal extraction process as well as the geoenvironmental issues associated with this mining operation.

2.4.2 The Mining Operation

2.4.2.1 General

The sulfuric acid leaching process, commonly used in most industrial units, typically involves several stages of operation. These include feed preparation, acid leaching, counter current decantation, neutralization, sulfide precipitation, and waste disposal. However, the hydrometallurgical processes for obtaining metals from the pregnant liquor and the trivial geotechnical aspects of tailings management are beyond the scope of this work. To provide a background for this research, this section describes the first three stages of the mining operation.

2.4.2.2 Feed Preparation

Figure 2.5, taken from Carlson & Simmons (1960) shows the slurry preparation flow sheet to obtain suitable plant feed from the mined ore using water and wet screening. The raw ore is recovered with scrappers and draglines and transported to the slurry plant by trucks. The ore is fed into the plant by apron feeder and inclined conveyor belt. A shaking grizzly with 12.5 cm (5 in) bar spacing scalps off the stray rock and the undersize goes directly to the log washers. The slurry overflowing the log washers is finished by two stages of screening, with primary screens having 1.0 cm (3/8 in) openings to protect the 20-mesh secondary screens (0.85 mm opening). The oversize from the shaking grizzly is scrubbed free of ore in a cylindrical scrubber and fed into the primary screen. Conversely, the oversize rock from the cylindrical scrubber is combined with the oversize from the primary and the secondary screens and eventually disposed off.

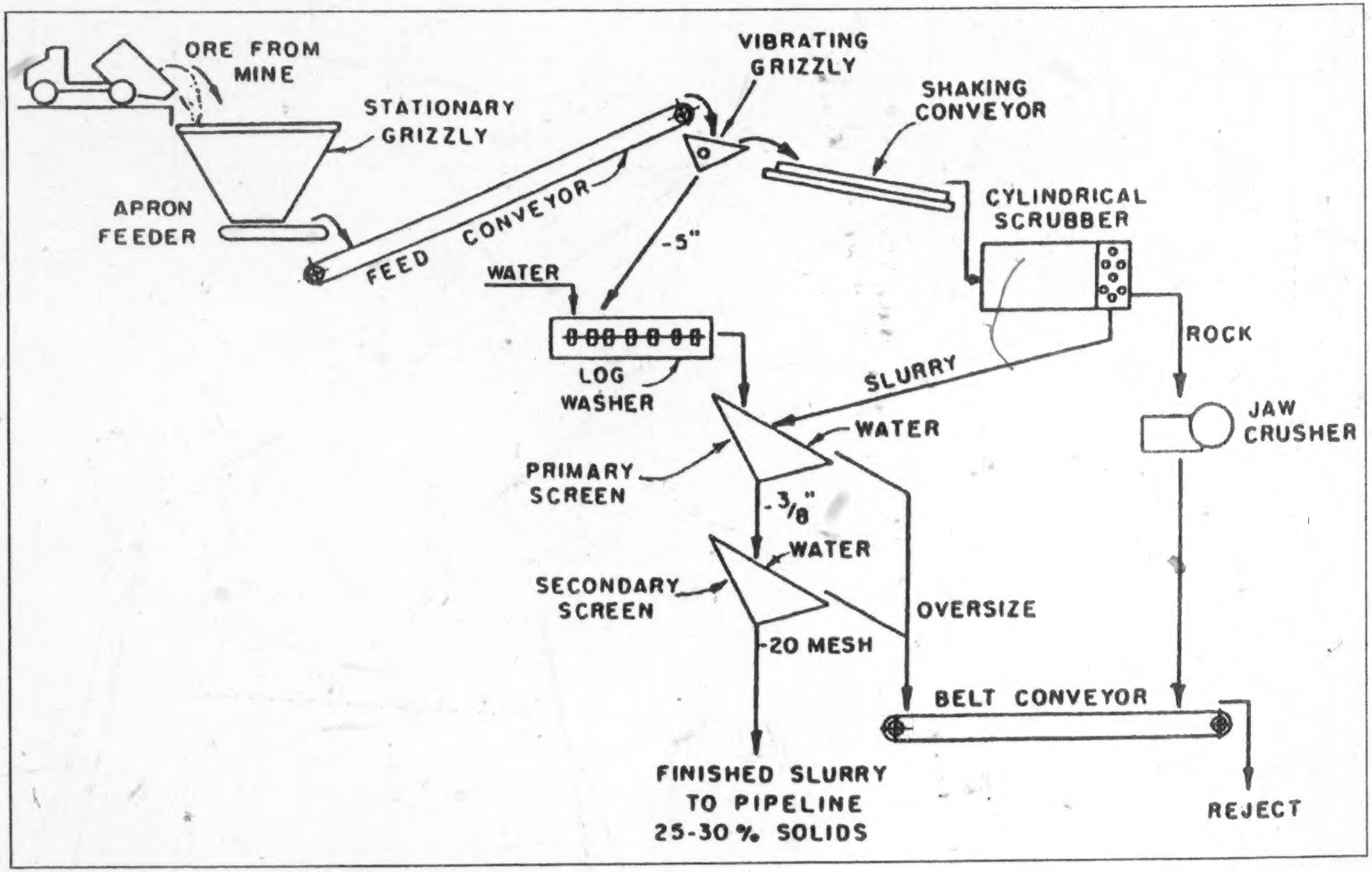
ORE FROM MINE
STATIONARY GRIZZLY
APRON FEEDER
FEED CONVEYOR
VIBRATING GRIZZLY
SHAKING CONVEYOR
CYLINDRICAL SCRUBBER
-5"
WATER
LOG WASHER
ROCK
SLURRY
JAW CRUSHER
WATER
PRIMARY SCREEN
-3/8"
WATER
SECONDARY SCREEN
OVERSIZE
-20 MESH
BELT CONVEYOR
FINISHED SLURRY TO PIPELINE 25-30% SOLIDS
REJECT

Figure 2.5: Schematic of the feed preparation process

Gravity pipes move raw ore slurry with a solids content of about 25%, to a storage thickener. The purpose of the storage thickener is to increase the solids content at which the slurry is pumpable. A high solids content material ensures minimum acid and steam consumption during leaching and maximum leach throughput. Depending on the type of raw ore, underflow solids content from the storage thickener vary significantly but values in the range of 35 to 40% are common (Carlson & Simons 1960). Overflow water is re-circulated to the slurry preparation plant during the thickening process that is usually carried out for a maximum of one day. The solid-liquid separation behavior of the ore slurry in the storage thickener can be improved by using synthetic polymers.

2.4.2.3 Acid Leaching

Figure 2.6, which is also taken from Carlson & Simmons (1960), gives a schematic flow sheet of the acid leaching operation. The ore slurry from the storage thickener is pumped to a slurry preheater where it is heated up to a temperature of 75 °C (170 °F) by direct absorption of 200 kPa (30 psi) steam. The heated slurry is stored in a mechanically agitated storage tank that has a design capacity commensurate with the operation. The slurry is picked up by a rubber lined centrifugal booster pump and fed to the high-pressure slurry pump. This latter pump feeds the slurry to the slurry heater tower of the reactor train. Once again, the slurry is heated by direct injection of steam at 4000 to 6000 kPa (600 to 900 psi); the reaction temperature typically ranges between 250 and 280 °C (475 and 550 °F).

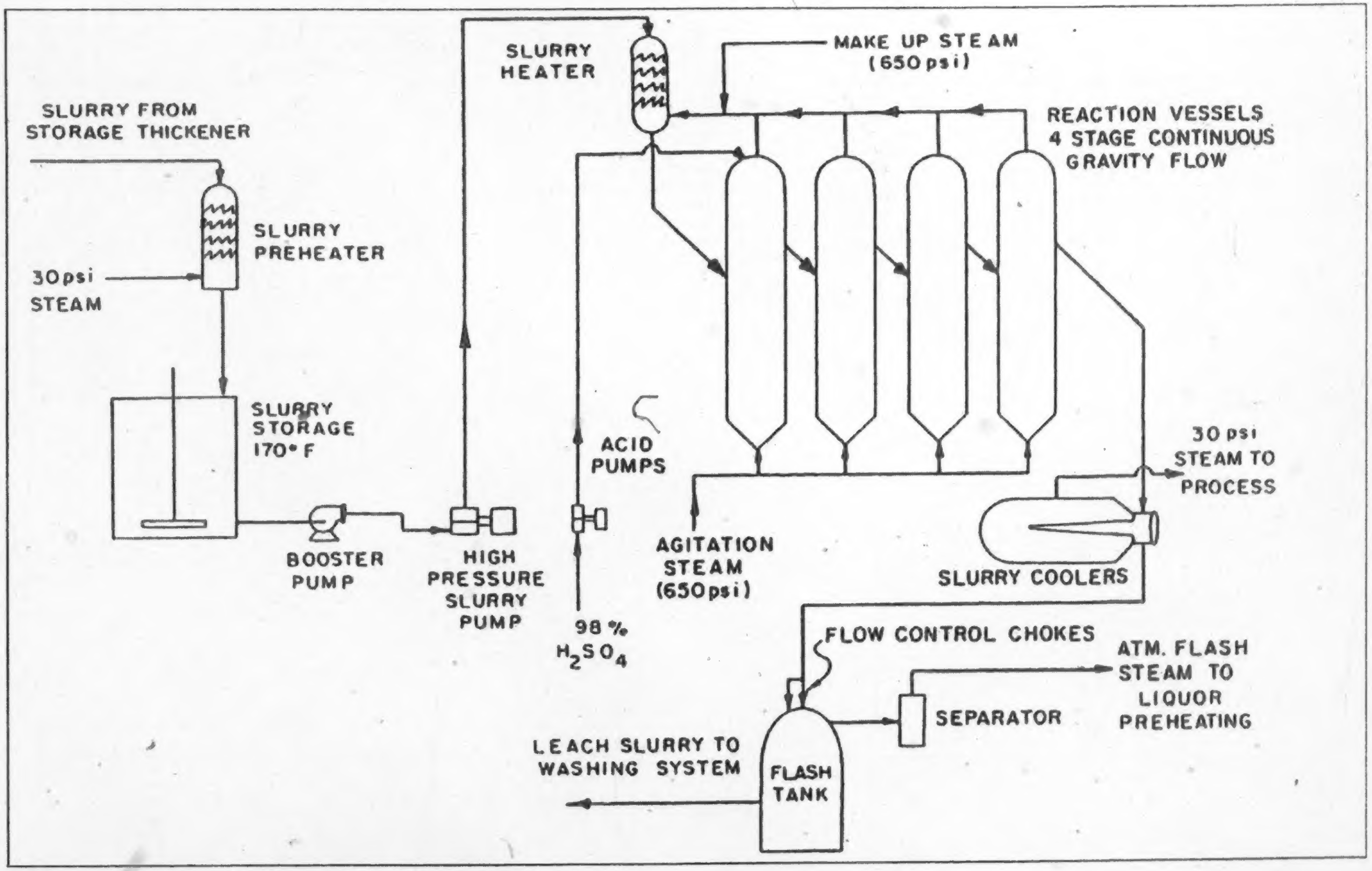
SLURRY FROM STORAGE THICKENER
SLURRY PREHEATER
30psi STEAM
SLURRY STORAGE 170° F
BOOSTER PUMP
HIGH PRESSURE SLURRY PUMP
SLURRY HEATER
MAKE UP STEAM (650psi)
REACTION VESSELS 4 STAGE CONTINUOUS GRAVITY FLOW
ACID PUMPS
98 % H_2SO_4
AGITATION STEAM (650psi)
30 psi STEAM TO PROCESS
SLURRY COOLERS
FLOW CONTROL CHOKES
ATM. FLASH STEAM TO LIQUOR PREHEATING
SEPARATOR
LEACH SLURRY TO WASHING SYSTEM
FLASH TANK

Figure 2.6: Schematic of the acid leaching process

The ore feed is allowed to flow by gravity from the slurry heater into the four-stage reaction vessels. Sulfuric acid at 98% concentration is fed into the first reaction vessel using a plunger pump. To induce circulation, the high-pressure steam (4000 to 6000 kPa) provides agitation in the reaction vessels. Due to negligible condensation of the agitation steam, it is reused after necessary makeup in the slurry heater. The leached slurry overflowing the fourth stage of the reaction vessels is allowed to pass through an exchanger where it is cooled and the recovered steam heat is reused. The slurry is then passed through special flow-control chokes into a flash tank. Again the steam generated in the flash tank under atmospheric pressure is reused for heating elsewhere in the mining operation. From the flash tank the leached slurry is allowed to enter the next stage, which is called as the counter current decantation (CCD).

Acid leaching involves selective dissolution of nickel and cobalt from the ore using sulfuric acid. Divalent metal (M) oxides (NiO and CoO) are soluble under autoclave conditions and react with acid according to the following reaction (Chou et al. 1977):

$$MO_{(s)} + 2\,H^{+} \rightarrow M^{2+} + H_2O \qquad (2.4)$$

The sulfuric acid leaching process depends on several interrelated parameters such as temperature, pressure, leaching kinetics, acid consumption, and ore type (Tuovinen & Jason 1984). Understanding of the interaction of these parameters is important from a hydrometallurgical viewpoint but is beyond the scope of this research work.

2.4.2.4 Counter Current Decantation

Following acid leaching, the slurry is allowed to flow by gravity to a multi-stage counter current decantation wash circuit. Given schematically in Figure 2.7, the purpose of this process is metal separation from the leach residue. This is achieved by washing the leach residue with water and collecting soluble nickel and cobalt at the front end as the overflow.

Overflow solution from the CCD wash circuit is pumped to the reduction and neutralization section. First, the solution is treated with hydrogen sulfide gas to reduce Fe^{3+} to Fe^{2+} and Cr^{4+} to Cr^{3+} and to precipitate copper as copper sulfide. Then, it is neutralized with calcium carbonate by continuous agitation as the pH is monitored at regular intervals of time. Nickel and cobalt precipitate from the neutral solution by hydrogen sulfide gas in the sulfide precipitation plant: Mg, Mn, Fe and Al remain in solution. The reaction takes place in mechanically agitated horizontal autoclaves.

Underflow slurries from the first thickener are diluted by adding process water and overflow solution from the third thickener prior to feeding to the next thickener and so on. This ensures minimal variation in pH that ranges from 1.0 to 2.0. The waste slurries collected at the back end of the CCD circuit are treated to meet the regulatory criteria and are finally disposed of to a tailings pond.

To increase yield, synthetic polymers are added at all stages of the CCD circuit with decreasing dosage from the first to the last thickener. These flocculants improve the solid-liquid separation behavior of the leached slurry.

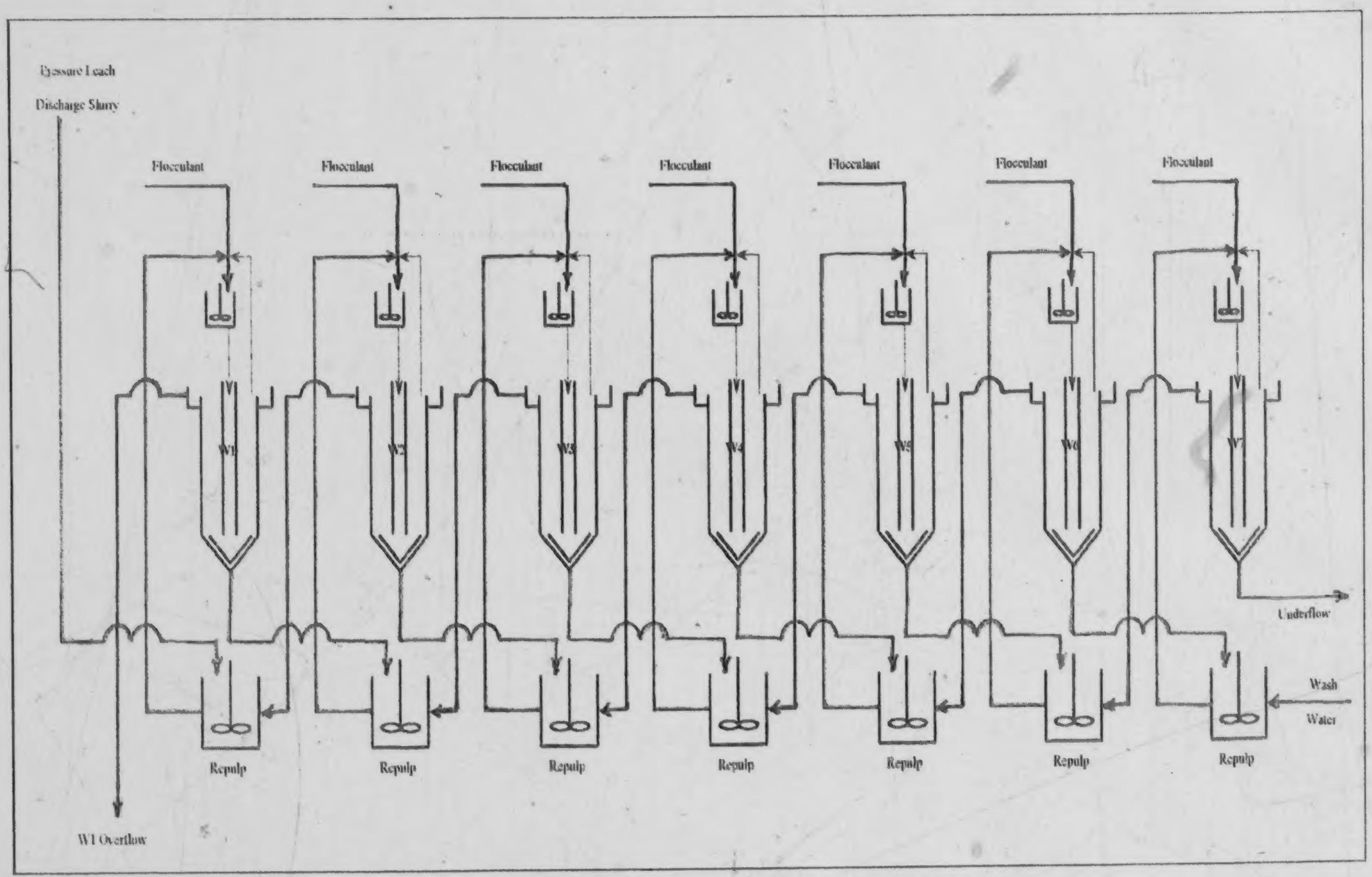
Pressure Leach
Discharge Slurry
Flocculant
Flocculant
Flocculant
Flocculant
Flocculant
Flocculant
Flocculant
W1
W2
W3
W4
W5
W6
W7
Underflow
Wash
Water
Repulp
Repulp
Repulp
Repulp
Repulp
Repulp
Repulp
W1 Overflow

Figure 2.7: Schematic of the counter current decantation process

2.4.3 Geoenvironmental Issues

2.4.3.1 General

Geoenvironmental issues associated with the sulfuric acid pressure leaching process are multi-disciplinary. Studies aiming at devising methods that optimize both yield and risk are usually carried out in conjunction. Although, this research focuses on the former, salient issues related to the solid-liquid separation and waste management of laterite slurries are noted here.

2.4.3.2 Solid-Liquid Separation

The solid-liquid separation of laterite ore slurries prepared prior to leaching and of laterite PAL slurries in the CCD circuit affect process efficiency and yield, respectively. Polymer modification methods for ore and PAL slurries can be devised to increase both efficiency and production of the extraction process. Therefore, these mine slurries can be effectively managed using geotechnical engineering concepts of sedimentation, consolidation and hydraulic conductivity.

2.4.3.3 Waste Management

An appreciation of the economics and technology is necessary as these govern the waste handling method of the placed material (Morgenstern & Scott 1995). Since, stability is ensured for unsaturated states (Küpper et al. 1992), liquefaction may result in saturated conditions (Bishop 1977). Process water composition renders contaminant migration an important issue. Emission of sulfur oxides and acid mist from the plant should meet the regulatory criteria (Chalkley & Toirac 1997).

2.5 CHARACTERITICS OF LATERITE PAL SLURRIES

2.5.1 General

Laterite slurries generated by the pressure acid leaching process possess an entirely different set of characteristics compared to the ore slurries. The leaching process causes changes in both the solid and the liquid phases of the slurries, thereby influencing the solid-liquid separation behavior of these materials. This section gives a description of the important aspects related to the characteristics of laterite PAL slurries.

2.5.2 Geotechnical Index Properties

Laterite PAL slurries have a dark brown color, which is generally irrespective of the ore type and the leaching conditions. The values of specific gravity for laterite PAL slurries are higher than laterite ore slurries owing to mineral transformations during the leaching operation (Tindall & Muir 1998). Such changes causes precipitation of various types of minerals on soil particles thereby resulting in a coarse grained material. Due to the predominant effect of grain size distribution on the solid-liquid separation behavior of laterite slurries, it is important to investigate variations in the grain size growth in each type of laterite ore. Further, no experimental data on the consistency or the plasticity characteristics of laterite PAL slurries was found in the published literature. This research generated a complete data set on the geotechnical index properties of various types of laterite PAL slurries for a preliminary evaluation of this class of materials.

2.5.3 Mineralogy

Conversion of goethite into hematite is the main reaction occurring during the acid leaching process. This mineral transformation, which conserves the amount of sulfuric acid, occurs in two steps; dissolution of goethite and precipitation of hematite, according to the following reactions (Tindall & Muir 1998):

$$2\ FeO(OH)_{(s)} + 3\ H_2SO_4 \rightarrow 2\ Fe^{3+} + 3\ SO_4^{2-} + 4\ H_2O \qquad (2.5)$$

$$2\ Fe^{3+} + 3\ SO_4^{2-} + 4\ H_2O \rightarrow Fe_2O_{3\ (s)} + 3\ H_2SO_4 + H_2O \qquad (2.6)$$

Similar distinct dissolution and precipitation paths lead to the following overall reaction for the conversion of boehmite to hydronium-substituted alunite (Chou et al. 1977):

$$3\ AlO(OH)_{(s)} + 2\ H_2SO_4 + H_2O \rightarrow (H_3O)Al_3(SO_4)_2(OH)_{6\ (s)} \qquad (2.7)$$

In saprolite ores, Ni-rich magnesium silicates (serpentine) dissolve rapidly and form amorphous silica and magnesium sulfate according to the following reaction:

$$2\ Mg_3Si_2O_5(OH)_{4\ (s)} + 6\ H_2SO_4 \rightarrow 6\ MgSO_4 + 4\ SiO_{2\ (s)} + 10\ H_2O \qquad (2.8)$$

The above reaction also shows that blending saprolite ore with limonite ore utilizes the high Mg content of the former, thereby consuming part of the free acid in solution (Baghala & Papangelakis 1998a).

Anion exchange is the critical parameter governing the behavior of laterite PAL slurries under acidic condition (Dixon & Weed 1989). Similarly, the presence of small amount of clay minerals as well as amorphous materials can significantly affect the behavior of these slurries.

2.5.4 Pore Water Chemistry

Pore fluid chemistry as described by the pressure acid leaching process leads to variation in physico-chemical interactions that governs the mechanical behavior of laterite PAL slurries. The pH values for the PAL slurries are usually well below the point of zero charge (PZC) as the predominant hematite mineral in these slurries has a PZC range of 7.5 to 8.5. According to Rubisov & Papangelakis (1999), such conditions are favorable for coating of soil particles by hematite. However, the presence of other ion types in solution also affects the engineering behavior of these slurries. This research studies the mineral interaction in a given environment and the resulting behavior of the slurries.

2.5.5 Morphology

Morphology depicts the interaction between mineralogy and pore water chemistry. For laterite PAL slurries, precipitation of hematite and alunite on soil particles causes fundamental changes in soil characteristics. Such precipitation is accompanied by an increase in grain size that in turn affects morphology and the mechanical response of the PAL slurries. Hematite and alunite coat soil particles to form platelets with dimensions of 50 Å diameter and 10 Å thickness, below the point of zero charge (PZC) of these minerals (Rubisov & Papangelakis 1999). According to the same authors, the PZC of these minerals is near neutral, which is above the pH of the PAL slurries in most industrial applications (Tindall & Muir 1998). Microscopic observations reveal goethite morphology as *needle-like*, whereas hematite is seen as a *nearly spherical particle* (Krause et al. 1997).

2.5.6 Solid-Liquid Separation

Laterite PAL slurries are streams of medium solids content generated by the pressure acid leaching process. The leaching operation causes changes in the solid and liquid phases of the laterite PAL slurries. Such changes are manifested in the solid-liquid separation behavior of these materials. Transformation of iron minerals cause grain size growth and an increase in the specific gravity of the solid phase. Likewise, change from near neutral to acidic conditions results in a different set of physico-chemical interactions between the minerals and the pore water. Based on the preceding discussion of the changes caused by the leaching process and the new set of interactions resulting therefrom, an understanding of the expected solid-liquid separation behavior can be developed.

Laterite PAL slurries settle much faster than their respective ore slurries under self-weight due to larger and heavier grain size (Briceno & Osseo-Asare 1995a: Krause et al. 1998). Likewise, the mineral content in the ore affects the settling behavior of the leached materials. According to Briceno & Osseo-Asare (1995b), oxide-silicate material (PAL from limonite-saprolite ore) has lower settling rate than iron-rich material (PAL from limonite ore) owing to the presence of a gelatinous/siliceous product in the PAL slurry of the former ore. Briceno & Osseo-Asare (1995c) also suggests that the behavior of PAL slurries can be effectively improved by using synthetic polymers. This research undertakes a comprehensive experimental program to improve the solid-liquid separation behavior of laterite PAL slurries.

2.6 COLLOID-POLYMER-ELECTROLYTE INTERACTION

2.6.1 General

The solid-liquid separation behavior of laterite slurries can be effectively ameliorated using synthetic polymers, which are known to flocculate the slurries thereby increasing grain size and density. Different polymers achieve this objective to various degrees due to the combined effect of several interrelated parameters. These factors are derived from the physical, chemical and electrical characteristics of the system constituents; namely, colloidal slurry particles, chains of synthetic polymers and the electrolytes in the liquid medium. A clear understanding of these parameters is key to efficient solid-liquid separation of laterite slurries. The discussion given here on colloid-polymer-electrolyte interaction is divided into three sections. First, characteristics of colloidal slurries are given. Second, characteristics of synthetic polymers in solution form are described. Third, the interaction of these two solid phases in a liquid medium is discussed using the title polymer adsorption on colloidal surfaces.

2.6.2 Characteristics of Colloidal Slurries

2.6.2.1 General

This section first describes the interaction between colloidal surfaces and the electrolyte solution in the form of double layer theory. Then the effect of such interactions on soil morphology is presented. Finally, the evolution of the solid-liquid separation behavior with variations in time and loading conditions as well as soil morphology is given.

2.6.2.2 Double Layer Theory

Hydrophobic colloids possess electrically charged surfaces. The sign and magnitude of this charge is a function of the character of the colloid, pH and the general ionic characteristics of water (Sawyer et al. 1994). To preserve electrical neutrality in a colloid-water system, a double layer of ions is developed in the vicinity of the colloid. Figure 2.8a, which shows a double layer of ions adjacent to a negatively charged colloid, illustrates a Stern layer of positively charged ions adsorbed to the colloidal surface and a diffuse layer of mixed ions (Chapman 1913). The concentration of ions is greatest at the colloidal surface and decreases with distance. Due to the opposite movement of colloidal particles and counterions, there exists a shear surface at the colloid-liquid interface. An estimate of the surface potential is a lower value known as the zeta potential (ζ), which develops between the Stern layer and the diffuse layer (Hunter 1981). In its general form, the double layer equation can be written as follows (Mitchell 1993):

$$\frac{d^2\psi}{d\,x^2} = -\frac{e}{\varepsilon}\sum v_i n_{io}\exp\left(\frac{-v_i e\,\psi}{k\,T}\right) \tag{2.9}$$

where, Ψ = Electrical potential (work needed to bring a positive unit charge from the reference state to the specified point in the electric field),

x = Distance from the surface (m),

e = Electronic charge (1.602×10^{-19} C),

ε = Static permittivity of medium ($C^2\ J^{-1}\ m^{-1}$) = ε_o (permittivity of vacuum, $8.8542 \times 10^{-12}\ C^2\ J^{-1}\ m^{-1}$) x D (dielectric constant),

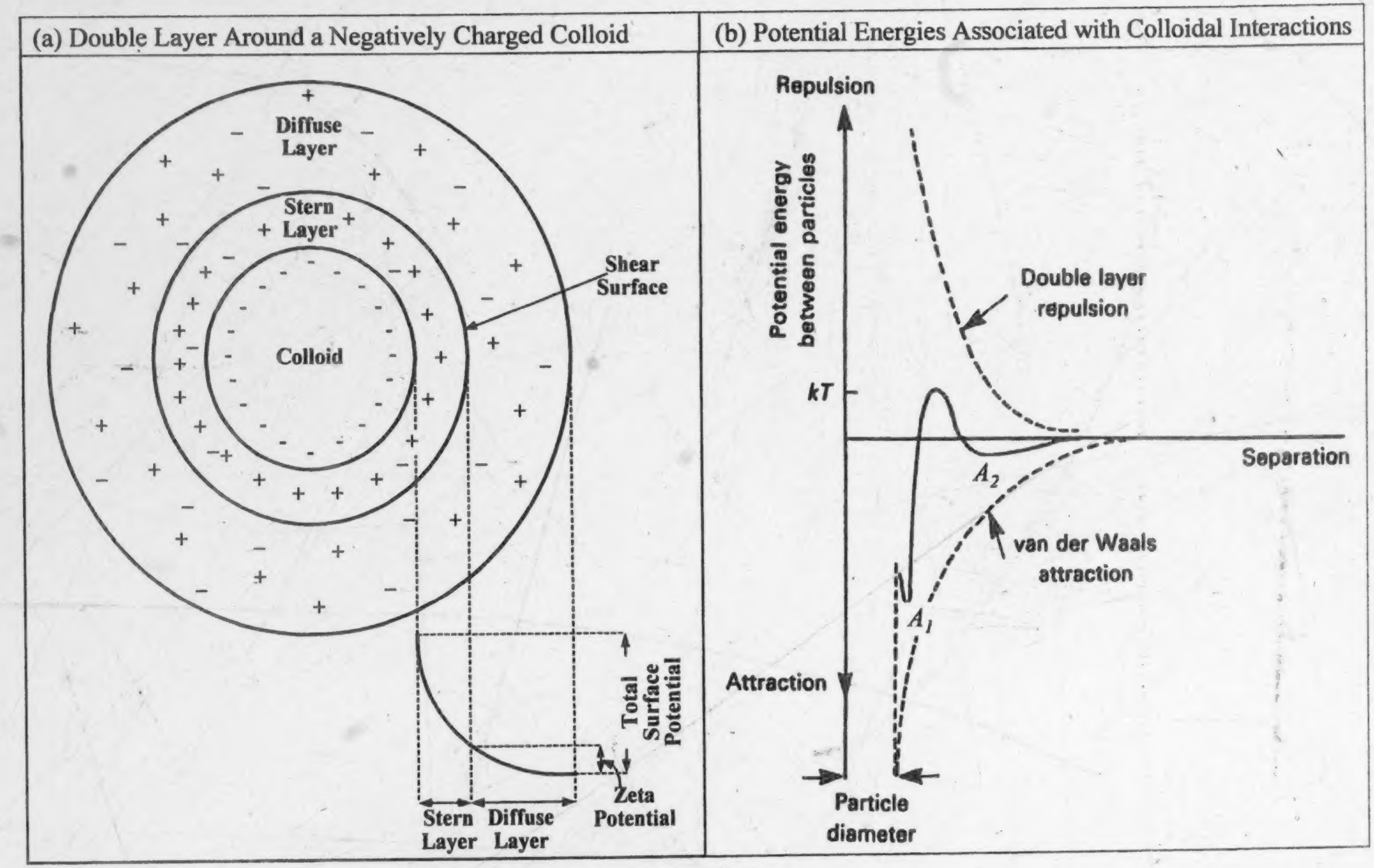
(a) Double Layer Around a Negatively Charged Colloid
Diffuse Layer
Stern Layer
Colloid
Shear Surface
Total Surface Potential
Zeta Potential
Stern Layer
Diffuse Layer
(b) Potential Energies Associated with Colloidal Interactions
Repulsion
Potential energy between particles
kT
Attraction
Double layer repulsion
Separation
A2
van der Waals attraction
A1
Particle diameter

Figure 2.8: Schematic of the double layer and its effect on flocculation

v_I = Valence of cation of type i,

n_{io} = Electrolyte concentration at the reference state,

k = Boltzmann constant (1.38×10^{-23} J $^{o}K^{-1}$), and

T = Temperature (^{o}K)

Ion distribution adjacent to a charged surface can be quantitatively estimated by solving equation (2.9). For a single cation and anion species of equal valence ($i = 2$, $v^+ = v^- = v$, $n_o^+ = n_o^- = n_o$), equation (2.9) simplifies to the Poisson-Boltzmann equation as given below:

$$\frac{d^2\psi}{d x^2} = \frac{2 n_o v e}{\varepsilon} \sinh\left(\frac{v e \psi}{k T}\right) \qquad (2.10)$$

Babcock (1963), Bolt (1956) and van Olphen (1977) proposed solutions to equation (2.10). These solutions can be applied to a good approximation for the case $i = 2$ but $v^+ \neq v^-$. Even for the more complex case of multiple counterions, solutions are given by Collis-George & Bozeman (1970) and van Olphen (1977).

When two colloidal particles approach one another the double layer positive repulsion opposes the negative attraction arising from van der Waals interactions. Figure 2.8b gives typical trends of potential energies associated with these forces and the resultant of these potentials. The resultant shows a primary deep minimum at A_1 corresponding to contact between the particles and a secondary shallow minimum at A_2. At A_1 the particles are joined together firmly to result in irreversible flocculation and the formation of unbreakable clusters. Conversely, at A_2 the particles are loosely held together at relatively larger separation distances. According to Tabor (1991), particles are not able to escape from one another in this latter type of flocculation because of the their lower thermal energy (*kT*) at A_2.

Flocculation of colloids is governed by the thickness of the double layer (*1/K*) and the surface potential. In general, the thinner the electrical double layer and hence a smaller surface potential, the stronger the tendency for particle associations (Mitchell 1993). Ion and potential distribution in a double layer depends on many interrelated system variables. A good perception of these parameters is given by the following equation:

$$\frac{1}{K} = \left(\frac{\varepsilon_o D\, k\, T}{2\, n_o e^2 v^2} \right)^{1/2} \qquad (2.11)$$

High concentration of electrolyte results in suppression of the double layer. For negatively charged colloids, the increased amount of cations reduces concentration gradient between the colloid and the solution thereby reducing the surface potential (Verwey & Overbeek 1948). This results in a shrunk double layer due to a decreased tendency of cations to diffuse away from the colloid. Further, double layer compression is more pronounced for multivalent cations due to their preferential adsorption. Collis-George & Bozeman (1970) showed that in a system containing monovalent and divalent cations, the latter concentrate near the colloid surface. Generally, trivalent cations (Al^{3+} and Fe^{3+}) cause the thinnest double layer followed by divalent cations (Ca^{2+} and Mg^{2+}) and monovalent cations (Na^+ and K^+) are known for thicker double layers (Mitchell 1993).

The tendency of the OH^- ion (exposed at clay surfaces) to dissociate is strongly affected by the pH of the pore fluid. Depending on the PZC of the system, the tendency for H^+ release in acidic media is lower and results in lower negative charge on clay particles. This results in positive edge to negative surface interaction, which leads to flocculation (Mitchell 1993). In addition, alumna (exposed at clay edges) ionizes positively at low pH (Sposito 1989).

The effect of the product of dielectric constant and temperature on double layer thickness is marginal but may be important in certain applications. Since, D values of most pollutants (hydrocarbons and organic materials) are lower than that of distilled water, they reduce double layer thickness (Sposito 1984). This reduction is further highlighted at elevated temperatures due to the associated decrease in dielectric constant. However, Mitchell (1993) has reported that an increase in temperature may also cause an increase in double layer thickness. Therefore, the combined effect of D*T* is contradictorily reported in the literature.

The foregoing discussion was related to classical double layer theory, which was developed for a colloidal clay with negatively charged surface. This theory can be used for laterite slurries as their colloidal particles also possess a surface electric charge in the presence of water, which is polar in nature. This charge owes its origin to ionization (pH dependent surface hydrolysis), and diffusion of electrolytes (Schramm 1996). Due to charge variation at the interface of water and solid particles, a diffuse double layer is created that influences the behavior of these slurries (Sposito 1984).

2.6.2.3 Morphology

Engineering behavior of soils is usually understood by considering the soil mass as a continuum. However, soils are actually composed of discrete particles, particle groups and pore spaces. Therefore, a better understanding of soil behavior can be achieved by studying it in conjunction with soil morphology. This is more important for soil slurries owing to variations in soil morphology with variations in water content. This section gives a description about the various types and scales of soil fabrics and their significance in the solid-liquid separation behavior of laterite slurries.

Figure 2.9 gives a schematic of various types of soil fabrics for colloidal particles. Based on both theory and observations, this figure shows that electrically charged colloids can act independently as well as mutually. In the former case, these particles can either be dispersed or associated edge-to-face thereby making a *cardhouse* (Goldschmidt 1926). When acting mutually, colloidal particles form aggregates or *books* by aligning face-to-face (Sloane & Kell 1966). The books can be dispersed or can be associated edge-to-face fashion, which is called a *bookhouse* (Mitchell 1993). Both the cardhouse and the bookhouse are called *flocculated* soil fabrics. Variations in various types of fabrics resulting either from independently acting colloids or from mutually acting colloids depend on water content. For soil slurries, water content decreases during sedimentation and consolidation. This research develops a qualitative correlation between soil fabric and the solid-liquid separation behavior of laterite slurries.

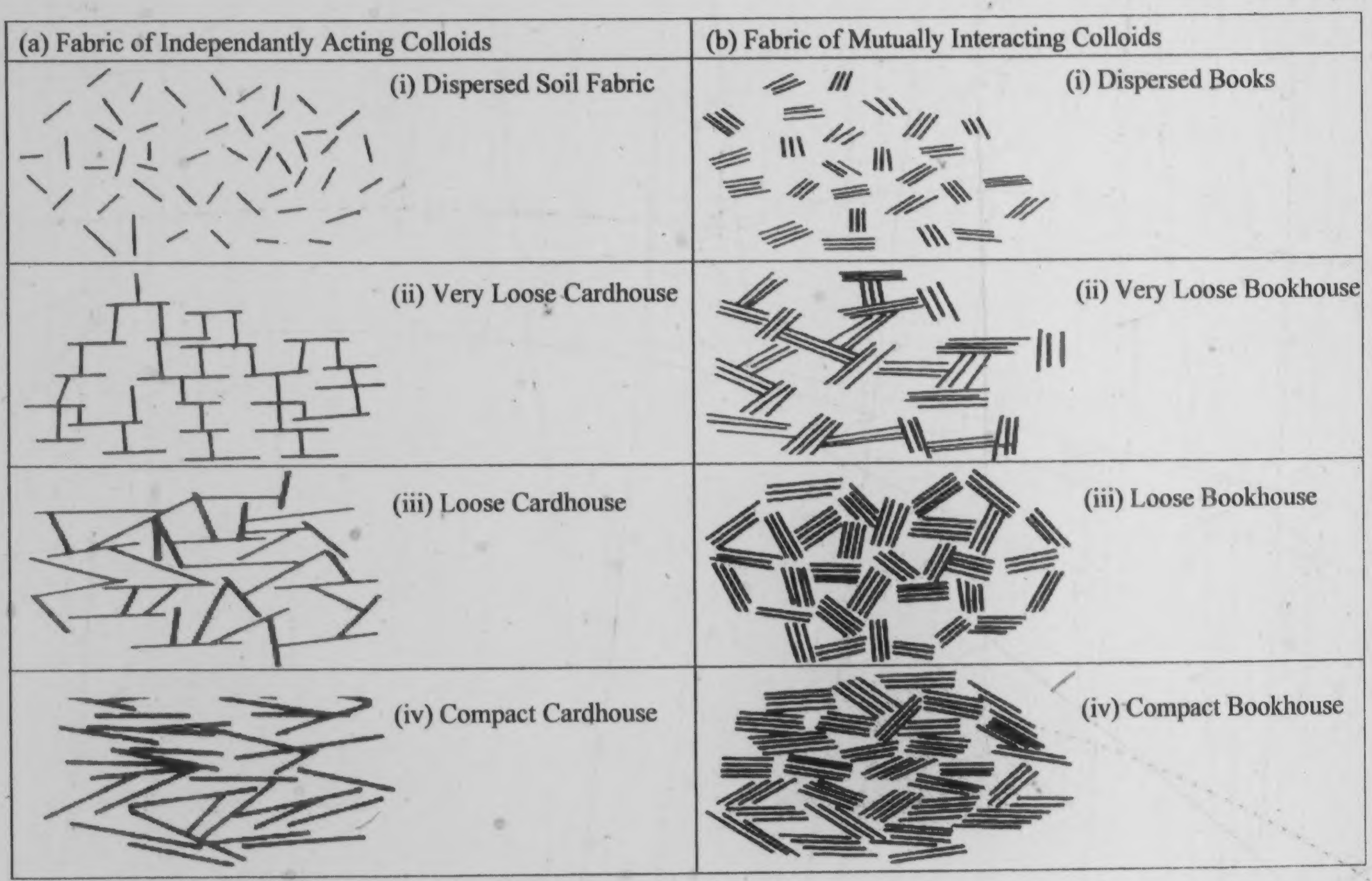
(a) Fabric of Independantly Acting Colloids
(b) Fabric of Mutually Interacting Colloids
(i) Dispersed Soil Fabric
(i) Dispersed Books
(ii) Very Loose Cardhouse
(ii) Very Loose Bookhouse
(iii) Loose Cardhouse
(iii) Loose Bookhouse
(iv) Compact Cardhouse
(iv) Compact Bookhouse

Figure 2.9: Schematic of various types of soil fabrics for colloidal particles

Soils are composed of clay and coarse size grains. The clay particles have a grain size less than 0.002 mm and include clay minerals as well as amorphous and siliceous materials whereas silt and sand are the coarse grained materials. Figure 2.10 describes important fabric features of soils comprising of these two types of clay forming materials. A connector of clay between two coarse grains results from a loose cardhouse of the former material (Figure 2.10a). Similarly, an array of books is similar to the interviewing bunches of clay between coarse grains as shown in Figure 2.10b. Likewise, Figure 2.10c and 2.10d differentiates between irregular and regular aggregations, respectively. Irregular aggregations correspond to a cardhouse microstructure of clay particles whereas regular aggregations, which have defined physical boundaries, are made up of units of a bookhouse fabric.

The mechanism of particle association depends on the type of particle (size, shape and charge) and on the type of pore fluid (pH, type of ions and ionic strength). Laterite slurries are predominantly composed of fine, positively charged particles. These needle-like goethite and spherical hematite coat clay platelets to variable extent. The pore fluid has a neutral to highly acidic pH, low to very high ionic strength, and the presence of multivalent ions in the latter. Further, synthetic polymers also influences soil microstructure. All of these permutations allow for the possible development of a wide variety of soil fabrics. For enhanced understanding of the solid-liquid separation behavior of laterite slurries, the mechanisms of some of these soil fabrics are described where appropriate.

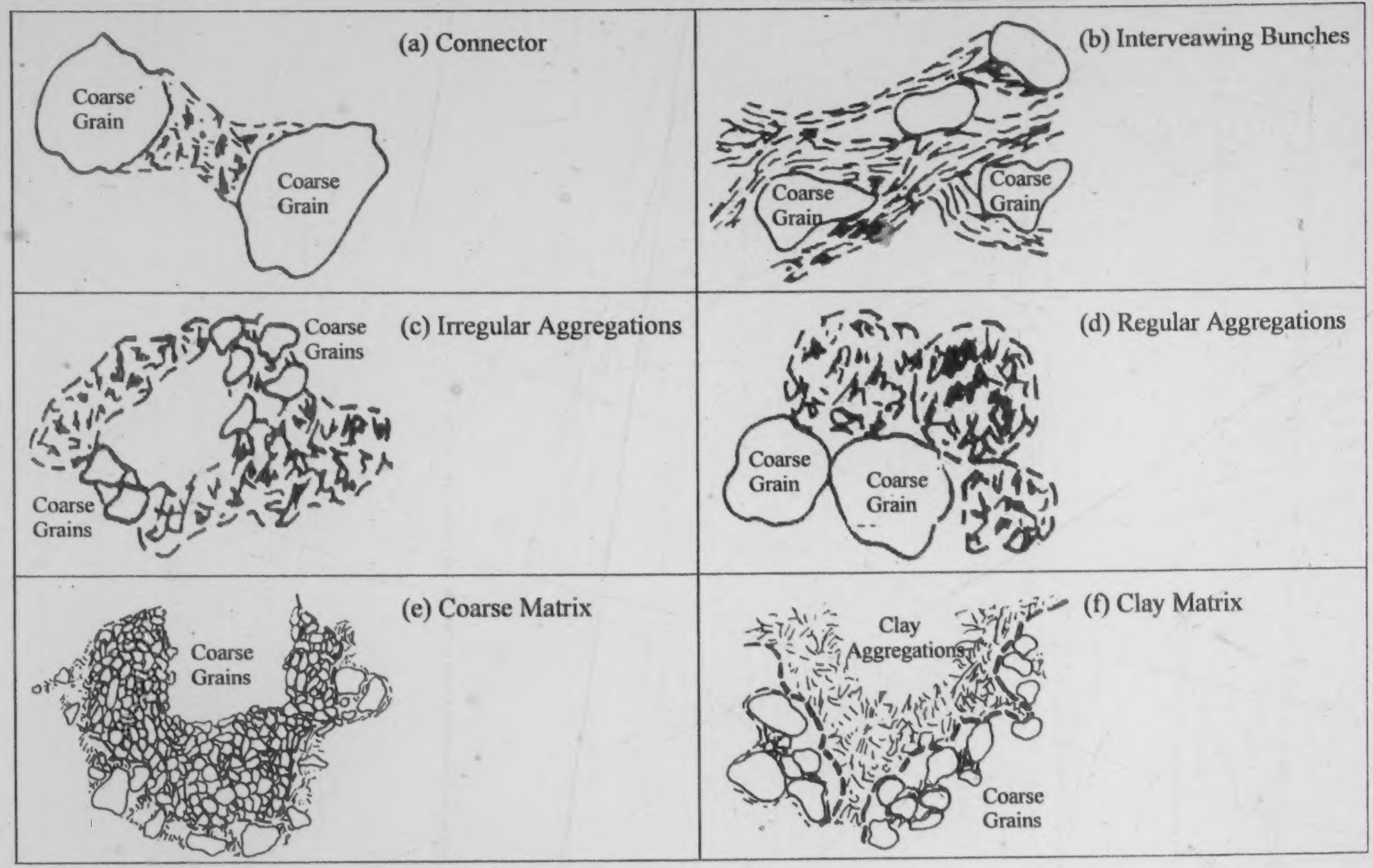
(a) Connector
Coarse Grain
Coarse Grain
(b) Interveawing Bunches
Coarse Grain
Coarse Grain
Coarse Grains
(c) Irregular Aggregations
Coarse Grains
(d) Regular Aggregations
Coarse Grain
Coarse Grain
Coarse Grains
(e) Coarse Matrix
Clay Aggregations
(f) Clay Matrix
Coarse Grains

Figure 2.10: Schematic of important fabric features

Figure 2.10 also distinguishes between two types of soil matrix, of which both result from a combination of the above features and depend on soil composition. A coarse matrix (Figure 2.10e) is defined as one in which the coarse grains touch one another. The void ratio of the coarse particles can reach a maximum of 0.9 for a simple cubic arrangement of equal spheres. Under such conditions, clay is present in the pore space between the coarse grains. On the contrary, the coarse grains do not touch one another in a clay matrix as shown in Figure 2.10f. In a coarse matrix, soil behavior is dominated by the size, shape, angularity and distribution of the coarse grains. On the other hand, the engineering behavior in a clay matrix depends on the interactions between colloids and water containing electrolytes. The current research focuses on this latter soil matrix due to the large amount of water and electrolytes in laterite ore and PAL slurries.

The structure or fabric of a soil can be considered relative to three levels of scale: microfabric, minifabric, and macrofabric (Olsen 1962; Yong & Sheeran 1973). A microfabric consists of particles assemblage and the interassemblage pore spaces. Typical microfabric units are up to a few tens of micrometers. Minifabric contains the assemblage of a few microfabric units and the interassemblage pore spaces between these units. The size of a minifabric is generally in the range of a few hundred micrometers. Finally, the macrofabric is representative of the entire soil mass and contains cracks, fissure and laminations that correspond to the transassemblage pore spaces between the aggregations of minifabric units.

Different fabric scales influence different aspects of engineering behavior of soils. Time dependant phenomena such as creep are influenced by the microfabric. Physico-chemical interactions are better understood by studying soil minifabric. Soil behavior involving such interactions includes sedimentation and hydraulic conductivity. Mechanical behavior such as shear strength and consolidation of *in situ* soils is governed by macrofabric.

Solid-liquid separation of laterite slurries mainly depends on minifabric but a general study of the entire fabric scale is warranted for a better understanding of this class of materials. Generally, a flocculated soil fabric is associated with rapid sedimentation because the particles move down as a massive block under gravity. On the other hand, individual particles move down independently in a dispersed soil and hence both the rate and the amount of sedimentation are smaller (Mitchell 1993).

2.6.2.4 Solid-Liquid Separation

Solid-liquid separation is characterized by sedimentation and consolidation and the variation of hydraulic conductivity under these two stages. Over most of the last century, the geotechnical engineering community formulated the fundamentals of these concepts. The community successfully used these basic concepts in engineering practice and in the process accumulated a voluminous literature. This section gives important aspects of these three fundamental geotechnical engineering concepts. Figure 2.11 summarizes the solid-liquid separation of soil slurries.

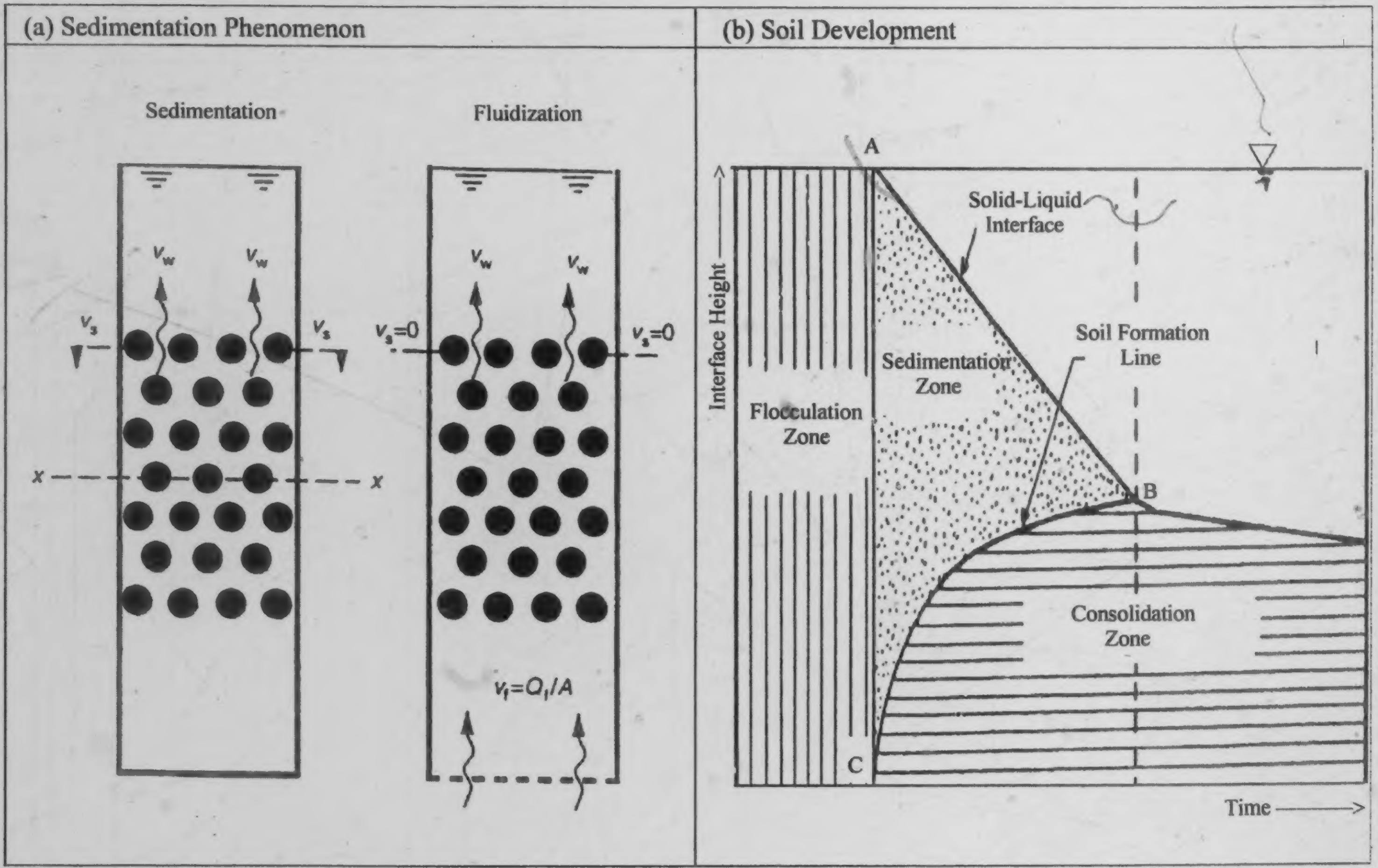
(a) Sedimentation Phenomenon
Sedimentation
Fluidization
v_w
v_s
$v_s=0$
x
$v_f=Q_f/A$
(b) Soil Development
A
B
C
Solid-Liquid Interface
Soil Formation Line
Sedimentation Zone
Flocculation Zone
Consolidation Zone
Interface Height
Time

Figure 2.11: Solid-Liquid Separation of soil slurries

Kynch (1952) and Richardson & Zaki (1954) established the theoretical background of sedimentation. Whereas the latter authors showed that the drag force depends on the relative velocity of the solid and the liquid phases, it was Kynch (1952) who realized that slurry settling is a transient process. These theories were approximate because of the assumption of *nondeformable slurry.* Notable works that provided experimental data on sedimentation include Been (1980), Imai (1980), Imai (1981) and McRoberts & Nixon (1976). Based on these theoretical and experimental developments, Pane & Schiffman (1985) postulated their model for the sedimentation behavior of soil slurries. They concluded that slurry behavior depends on the initial void ratio, the hydraulic conductivity and the effective stress. Later, they developed a method for the direct determination of hydraulic conductivity during sedimentation (Pane & Schiffman 1997).

Figure 2.11a that explains the sedimentation phenomenon, shows that the solid grains fall under gravity through water,. During this process, the water is forced upwards whereas the solid grains tend to rearrange and achieve greater packing. At a certain *fluidization velocity of water* (V_w)*,* the solid grains are held suspended by upward water flow and they do not change their position with time. The fluidization velocity of water is equal and opposite to the *settling velocity* (V_s) of the solid grains; both depend on the soil porosity that can be readily translated to void ratio (e). Further, since the solid grains are entirely supported by water, the total stress (σ) is equal to the pore pressure (u). Therefore, the effective stress (σ'), which is the difference of total stress and pore pressure, equates to zero.

For a sedimentation soil slurry, the hydraulic conductivity (k), measured in cm/sec similar to Vs, can be determined using the following equations:

$$k = \frac{Vs\,(1 + e)}{\gamma^*} \tag{2.12}$$

$$\gamma^* = \frac{\gamma_s - \gamma_w}{\gamma_w} \tag{2.13}$$

where, γ^* = Non dimensional constant

γ_s = Unit weight of the soil solids (g/cm^3)

γ_w = Unit weight of water (g/cm^3)

Figure 2.11b describes the development of soil formation during the solid-liquid separation process in the form of interface height versus time. This figure shows that based on physico-chemical interactions, slurry may exhibit an initial lag due to flocculation prior to undergoing sedimentation (Imai 1981). Sedimentation starts at point A and proceeds to result in straight-line portion of the solid-liquid separation curve. Simultaneously, a generally invisible *soil formation line* starts at point C. Eventually, the two lines coincide at point B and the settling velocity abruptly decreases, indicating the completion of sedimentation stage. Thereafter, the solid-liquid separation curve exhibits a slow and gradual decrease in slope as the soil undergoes consolidation under self-weight. The time required for complete self-weight consolidation is generally two orders of magnitude larger than that required for sedimentation (Pane & Schiffman 1997).

Consolidation refers to that stage of the solid-liquid separation process in which the solid grains transmit effective stresses (Terzaghi 1943). Depending on soil type, two types of consolidation can be distinguished. Primary consolidation arises when the stress-strain properties of the soil skeleton are independent of time. Conversely, secondary consolidation is the result of an intrinsic time-dependent response of the soil skeleton owing to viscous resistance (Buisman 1936; Mitchell 1993). Both of these consolidation types take place simultaneously but one or the other may dominate for different types of slurry materials.

During sedimentation, the hydraulic conductivity (k) can be computed according to equation 2.12. Similarly, the effective stresses can be calculated from knowledge of the buoyant unit weight of soil ($\gamma' = \gamma_s - \gamma_w$), and the height of the sedimenting sample (H) according to the following equation:

$$\sigma' = \frac{\gamma' H}{2} \tag{2.14}$$

The solid-liquid separation behavior of soil slurries is explained by e-σ' and k-e relationships. Figure 2.12, which is modified after Suthaker (1995), gives these two relationships for the oil sands fine tailings. Figure 2.12a shows that at low effective stresses, the former relationship strongly depends on the initial solids content of the slurry. Although the latter relationship is independent of the initial slurry solids content, Figure 2.12b shows a poor correlation at high void ratios. This research focuses on understanding and improving the solid-liquid separation behavior of laterite slurries at high void ratio and low effective stress.

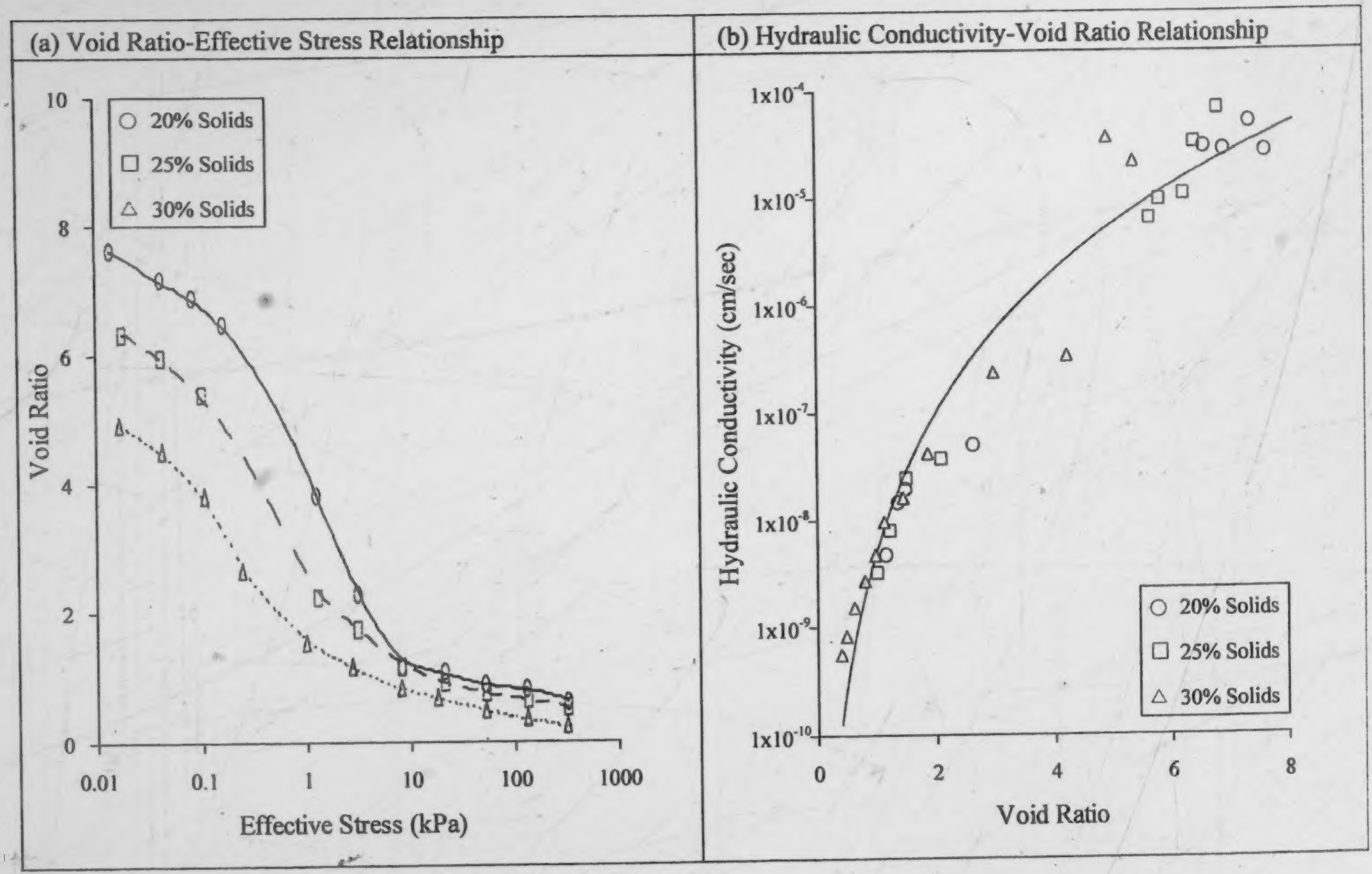

Figure 2.12: Typical behavior of soil slurries (after Suthaker 1995)

2.6.3 Characteristics of Polymer Solutions

2.6.3.1 General

The word polymer is a combination of two Greek words, namely; *poly* means many and *mer* means part. According to the International Union of Pure and Applied Chemistry (IUPAC), a polymer is a substance composed of molecules characterized by the multiple repetition of one or more species of atoms or groups of atoms (constitutional repeating units) linked to each other in amounts sufficient to provide a set of properties that do not vary markedly with the addition of one or a few of the constitutional repeating units.

Water-soluble synthetic polymers are generally used for most industrial applications involving solid-liquid separation of slurries. At the onset of such applications, a polymer-water solution is usually prepared. Characteristics of these polymer solutions depend on the distance from the interface as well as on the bonding between the units, which make up the polymer molecule (Jones & Richards 1999). The distance from the interface governs the interactions between segments of adjacent polymer chains. Such enthalpy related interactions determine surface tension of polymers. On the contrary, covalent bonding dictates the configurational entropy that influences the equilibrium state of the polymer. In turn, these configurations govern the subsequent colloid-polymer interactions. This section describes the salient features of water-soluble polymers in solution. Discussion focuses on polymer composition, surface tension, radius of gyration and chain configurations.

2.6.3.2 Polymer Composition

The basic building block of polymers is called a *monomer* that has a molecular weight of 50 to 100 g/mole. By the process of polymerization, large numbers of monomers are assembled and converted to a polymer that has a molecular weight in the range of 10^3 to 10^7 g/mole. Water-soluble polymers can be divided into two main categories: nonionic or *homopolymers* and ionic or *polyelectrolytes* (Farinato et al. 1999). Both of these polymer categories dissolve in water owing to the presence of functional groups. Whereas different types of ionic and nonionic polymers are commercially available, the polymers that are widely used in many industrial operations are polyacrylamides (PAA). This is because of the fact that a variety of polymers having a wide range of molecular weight can be prepared from acrylamides. This section describes the chemical composition of three types of polyacrylamides: nonionic, anionic and cationic.

Nonionic polymers of acrylamide are made from a large number (*n*) of repeated monomers, as given in the following expression:

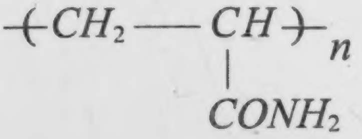

$$-\!\!\left(CH_2 - \underset{\displaystyle CONH_2}{\underset{|}{CH}}\right)\!\!-_n \tag{2.15}$$

By control of reaction conditions during the polymer manufacturing process, the molecular weight of a polymer can be changed by varying the number of monomers present in one molecule of that polymer. In water solutions, hydration of acrylamide nonionic polymers mainly takes place due to the presence of the functional group —$CONH_2$.

Adding suitable ionic moieties convert nonionic acrylamides to ionic polymers. Generally, anionic polymers contain sodium acrylate whereas cationic polymers possess dimethylaminoethyacrylate methyl chloride (DMAEA MC). These two moieties are respectively shown in the following expressions:

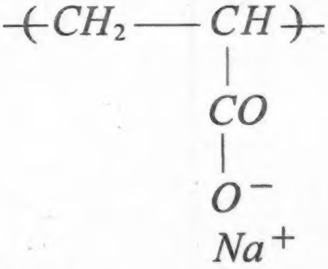

$$\begin{array}{rc} -\!(CH_2 - & CH)\!- \\ & | \\ & CO \\ & | \\ & O^- \\ & Na^+ \end{array} \qquad (2.16)$$

Sodium acrylate

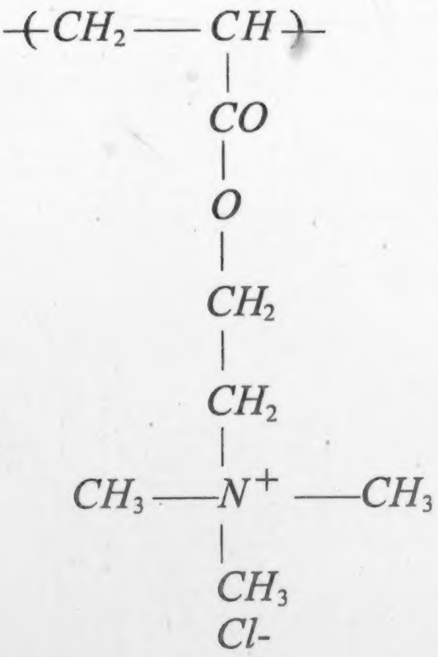

$$\begin{array}{rcl} -\!(CH_2 - & CH)\!- & \\ & | & \\ & CO & \\ & | & \\ & O & \\ & | & \\ & CH_2 & \\ & | & \\ & CH_2 & \\ & | & \\ CH_3 - & N^+ & - CH_3 \\ & | & \\ & CH_3 & \\ & Cl\text{-} & \end{array} \qquad (2.17)$$

Dimethylaminoethyacrylate methyl chloride (DMAEA MC)

Acrylamide based polyelectrolytes comprise the most useful materials for industrial applications involving solid-liquid separation. The macroions possess formal anionic and cationic charges on the polymer whereas the associated counterions ensure overall charge neutrality. The ionic nature of the polymer chains affects their dimension in solution, with intramolecular charge repulsions tending to increase the solvated coil size (Farinato et al. 1999). The charge bearing moieties in anionic polymers are oxygen based whereas those in cationic polymers are nitrogen based. These moieties help the macroions to remain fully ionized over large pH ranges including acidic and basic solutions.

2.6.3.3 Surface Tension

Polymer solutions are characterized by surface tension that can be related to intermolecular forces using statistical mechanics. This is due to the fact that the mechanics of interfaces can be determined from knowledge of the polymer density and composition as well as their spatial variability (Jones & Richards 1999). Hence, the density of a polymer solution varies from a bulk value at the polymer surface to a minimum value at some distance away from that surface. The distance denoting such a density profile is related to the length that characterizes the range of intermolecular forces. These intermolecular forces depend upon surface free energy and lead to cohesion in polymer-water solutions. Theoretically, the surface free energy is written as a function of the square of the gradient of the density profile according to the *square gradient theory.* This theory is described here.

Two polymer molecules interact by strong short-range repulsive forces when they are brought close together and by week long-range attractive forces when they are pulled apart. The potential, which has a shape similar to the resultant given in Figure 2.8b, changes to a discrete function for a lattice fluid model. In such a model, an individual polymer molecule can only occupy one unshared cell in space. If the nearest neighboring cells are occupied, there is an associated attractive energy (*H*) and an infinite potential barrier that prevents two polymer molecules occupying the same cell. The entropy of each cell in such a model is related to the probability of cell occupation that is, in turn, proportional to the density of the polymer solution. Similarly, for a given coordination number (*z*), the internal energy of the nearest cells may be obtained by converting the bell-shaped curve to a square. Therefore, the surface free energy of the system is composed of the configurational entropy of the polymer and the concentration gradients. The surface free energy of a synthetic polymer solution is given as follows:

$$E = \frac{kTp\ln(\mathrm{p})}{r} + (1-p)\ln(1-p) + \frac{zHp(1-p)}{2} \qquad (2.18)$$

where, E = Surface free energy (J),

p = Probability of cell occupation = ρ (Density of polymer solution, kg/m^3) x Ω (Cell volume, m^3) / *m* (Polymer molecular mass, kg)

r = Number of lattice cells joined together in one polymer molecule,

H = Square well depth (J)

2.6.3.4 Radius of Gyration

Theoretically, a polymer chain can achieve any configuration out of a large number of available possibilities. However, for simplicity actual dimensions of the polymer can be averaged and its configuration may be approximated to a spherical shape (Jones & Richards 1999). This approximation allows the determination of radius of gyration, which is the average distance of the whole polymer molecule from the center of the mass.

$$R_G^2 = \frac{1}{6} d^2 = \frac{1}{9} NL^2 \tag{2.19}$$

where, R_G = Radius of gyration (m),

d = Linear distance between the two ends of the coiled polymer (m)

N = Number of segments in a polymer chain, and

L = Length of the segment (m)

This definition can be used to calculate the empty space inside the globule formed by a polymer chain. The portion of the total volume of the globule occupied by a single molecule of a given synthetic polymer can be determined as follows:

$$\beta = \frac{6\upsilon}{N^{0.5} L^3} \tag{2.20}$$

where, β = Fraction of the sphere occupied by polymer molecule, and

υ = Volume of each segment of the polymer chain (m^3)

In general, for most polymers bulk of the sphere is empty space. For example, Tabor (1991) reported $\beta = 0.13$ for polyethylene.

Equations (2.19) and (2.20) apply to an *ideal solvent*, one that does not facilitate interactions between polymer segments. Therefore, the polymer adopts a randomly fluctuating three-dimensional structure or *random coil* configuration (Atkins 1988); the length of unperturbed coil is defined by radius of gyration.

2.6.3.5 Chain Configurations

In actual solutions, polymer segments can attract or repel each other. For *non-ideal solvents,* the intra-molecular interactions result in a variety of chain configurations. Polymer dimensions can be larger or smaller than R_G by an intra-molecular expansion factor, α. This new polymer size is called the Flory Radius, R_F and is defined as follows:

$$R_F = \alpha R_G \tag{2.21}$$

A *good solvent* does not allow its displacement and keeps the segments apart; chain swelling. Such a solvent can even straighten the polymer chain to a certain extent thereby resulting in increased flocculation. Due to repulsion between segments in such a solvent, complete polymer solubility is ensured and $\alpha \geq 1$. Conversely, in a *poor solvent*, it is energetically favorable for the segments to come closer together, a phenomenon known as chain contraction. Further, because of strong attraction due to van der Waals forces, the coil collapse into a compact structure and $\alpha < 1$. A poor solvent can be transformed to a good solvent either by adding a salt or by bringing its temperature to a critical point known as the theta temperature (T_θ). A solvent at this temperature is known as a *θ-solvent.*

The viscosity of a good solvent affects that of the whole solution and is a measure of the movement of polymer coil through the liquid medium. The following equation gives the unit change in viscosity:

$$\frac{\eta-\eta_o}{\eta_o} = 2.5\,\varphi = \frac{0.42\,N_A L^3}{m^{0.67}} M^{0.5}\,c \qquad (2.22)$$

where, η = Dynamic viscosity of the liquid (Ns/m^2),

η_o = Dynamic viscosity of the polymer (Ns/m^2),

ϕ = Volume fraction of the polymer,

N_A = Avogadro's number = 6.023×10^{23},

M = Mass of one segment (kg),

M = Molecular mass of the polymer (kg), and

C = Polymer mass concentration per unit volume of solution (kg/m^3)

This equation highlights that the solvent does not flow through the polymer sphere despite the large volume of the former compared to that of the polymer. In fact, the polymer globule carrying the liquid moves through the solution. This hydrodynamic phenomenon is known as the Zimm theory.

2.6.4 Polymer Adsorption on colloidal Surfaces

2.6.4.1 General

Synthetic polymers form complexes when they uncoil and adsorb onto colloidal surfaces (Theng 1974). Optimum flocculation occurs when the polymer chains achieve their maximum extension, which depends on the pH and the ionic strength of the system (Slater et al. 1969). Colloid-polymer interactions in a given electrolyte medium are best explained by Flory-Huggins parameter for exchange free energy (χ_s). This parameter denotes the free energy change in bringing polymer segment from solvent to colloid surface. Since segment attachment is accompanied by displacement of the solvent molecules, χ_s is expressed in terms of the entropies of the segment and the solvent according to the following equation:

$$\chi_S = \frac{G_{sol} - G_{seg}}{kT} \tag{2.23}$$

where, G_{sol} = Surface free energy of the solvent (J),

G_{seg} = Surface free energy of the segment (J),

In equation (2.23), the term ($\chi_s kT$) gives the difference in free energy between those due to segment/surface and solvent/surface contact, respectively. This equation further suggests that adsorption of polymer chains onto a colloidal surface can occur only when χ_s is positive.

Polymer adsorption on colloidal surfaces is generally exothermic and increases with the molecular weight of the polymer, reflecting the increased contribution of van der Waals forces to the overall adsorption energy (Theng 1979). Using diffusion theory and assuming the colloid surface as a reflecting wall, Frisch (1955) defined the average number of adsorbed segments (δ) in a chain consisting of N segments and having a flexibility, f (ease of rotation of the hydrocarbon molecule about the C--C bond) as being equal to $(N/f)^{0.5}$.

P

This section describes important concepts related to polymer adsorption on colloidal surfaces. These include adsorption isotherms, adsorbed conformations, factors affecting adsorption and finally flocculation caused by synthetic polymers.

2.6.4.2 Adsorption Isotherms

For the case of a single segment and considering that solvent adsorption is absent, Frisch & Simha (1957) developed the following equation for polymer adsorption onto colloid particles that gives results comparable to the Langmuir isotherm:

$$\frac{q}{1-q}\exp^{(2L_1q)}=(L2\,c)^{1\delta} \tag{2.24}$$

where, q = Fraction of total colloidal surface covered by the polymer,

L_1 = Measure of the interaction energy between adsorbed segments,

L_2 = Equilibrium constant

Adsorption isotherms generally show an initial monotonous increase in q with increasing c and a gradual approach to a constant q-value thereafter. Such a shape is mainly due to the high affinity of long-chain polymers for colloids. This affinity decreases for low molecular weight polymers, for which the isotherms become more rounded (Muthukumar 1999). Further, the shape of the isotherm also depends on solvent quality. In good solvents, adsorption increases with molecular weight and this effect is more pronounced for low molecular weight polymers. In θ-solvents such an increase in adsorption is independent of the polymer molecular weight. Moreover, for the same molecular weight, adsorption is higher in θ-solvents than in good solvents, particularly for higher molecular weight polymers (Scheutjens et al.1993).

2.6.4.3 Adsorbed Conformations

Synthetic polymers alter the electrical double layer around the particle as illustrated in Figure 2.13a (Theng 1974; Vincent 1974). This figure shows that any modification of the inner Stern layer is due to the presence of trains, whereas that of the outer diffuse layer is ascribable to the loop and tail segments of the adsorbed polymer molecule (Lyklema 1976). These changes in the double layer push the water molecules farther away from the particle resulting in solid-liquid separation in the system.

Long chain polymers, which are soluble in a given solvent, attach to colloids at many points either due to high surface charges or due to entropy changes. Under both conditions, the free ends of the polymer chains waggle around in the solvent. The thermal energy of these chains helps in facilitating the polymer molecules to adopt any of the numerous available conformations (Muthukumar 1999). These configurations are governed by the flexibility of the hydrocarbon chain.

Figure 2.13b gives possible conformations of a single polymer when it is brought closer to a colloid. This figure shows that as the bound fraction of the polymer decreases, double layer thickness increases and eventually the chain reaches a *mushroom* conformation, where it is grafted onto the colloidal surface by one segment. In this case, the layer thickness is approximately equal to ($2R_G$).

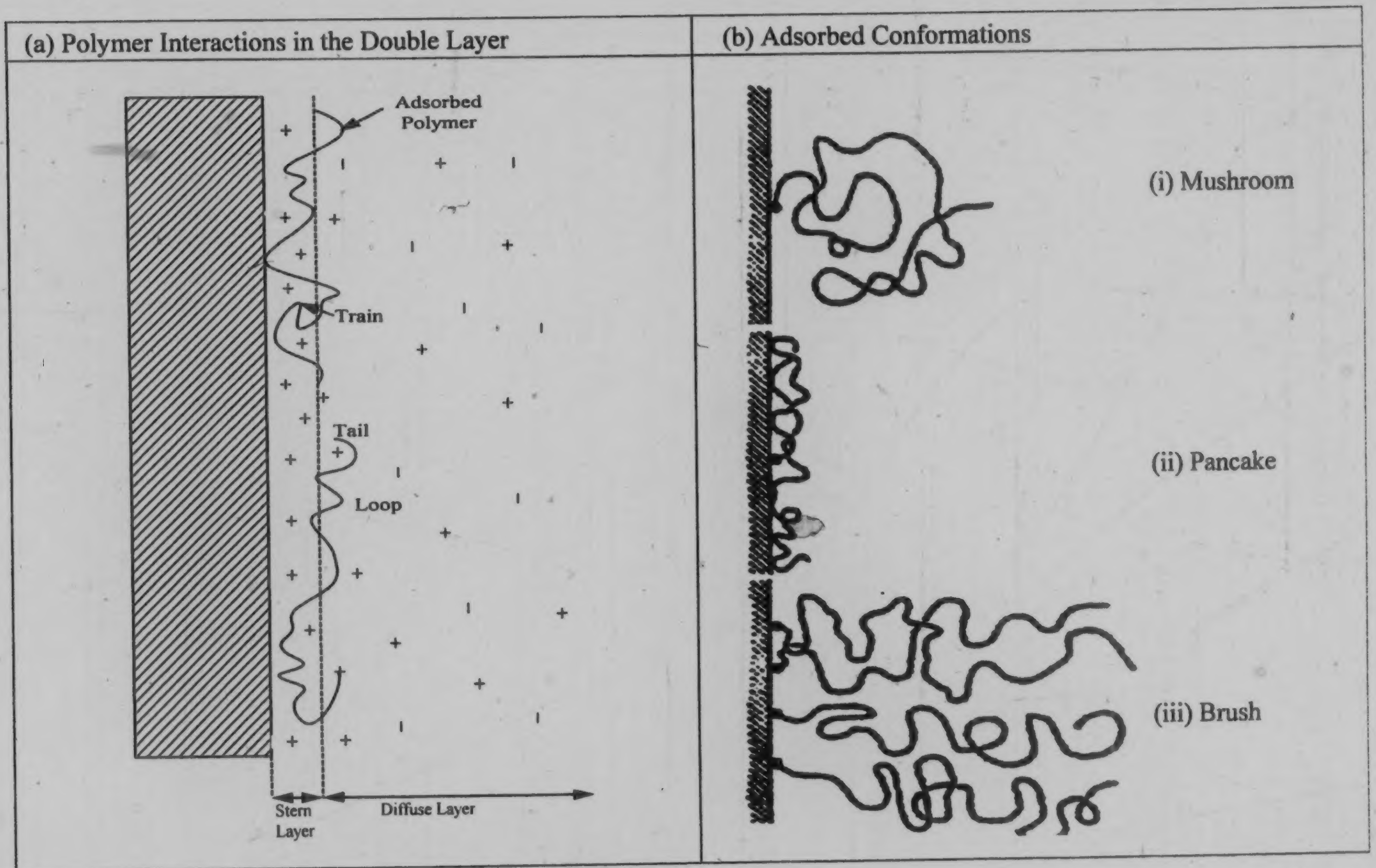
(a) Polymer Interactions in the Double Layer

(b) Adsorbed Conformations

Adsorbed Polymer
Train
Tail
Loop
Stern Layer
Diffuse Layer
(i) Mushroom
(ii) Pancake
(iii) Brush

Figure 2.13: Schematic of polymer adsorption on colloidal surfaces

Conversely, as the bound fraction increases, the adsorbed polymer adopts a flatter conformation. Referred to as a *pancake,* this confirmation results due to the fact that the polymer is attached at many points. Under such conditions, layer thickness reaches a minimum of segment length for an infinite polymer chain length. This is the desired conformation for maximum flocculation.

In the case of numerous polymers, as the amount of adsorbed polymer increases, lateral displacement of the adsorbed segments takes place to accommodate more polymers. When polymer population reaches to the point of chain overlap, chains undergo stretching perpendicular to the colloidal surface and adopt the *brush* conformation. In the limiting case, adsorbed layer thickness is equal to polymer chain length. This case results from an over dosage of the polymer and causes dispersion.

2.6.4.4 Factors Affecting Adsorption

For polymers devoid of any charge, adsorption is governed by the Flory-Huggins parameter χ_s that represents the exchange free energy between the solvent molecule and the polymer segment. This is the free energy change required to bring the polymer segment from the solvent to the colloidal surface. On the other hand, for charged polymers the predominant factors influencing polymer adsorption onto colloidal surfaces are derived from electrostatic interactions. These interactions depend on the surface charge of the solid particles, the polymer charge, the polymer molecular mass, and the salt concentration in the pore fluid.

2.6.4.5 Polymer Induced Flocculation

Synthetic polymers consisting of macromolecules, progressively unfolds and adsorbs onto more than one colloid in a three-phase system (Linke & Booth 1960). This results in the formation of flocs, which are composed of large number of loosely joined solid particles. This phenomenon is called *bridging* and it occurs through hydrogen bonding between the colloidal particle and the undissociated ion of the polymer. The size of flocs is related to the extent and strength of interparticle bridging, which depends on the polymer chain length and the segment-surface interaction (Theng 1979). In general, high molecular weight polymers cause greater flocculation in a given environment (Schamp & Huylebroeck 1973). The use of lower molecular weight polymers for similar results depends on the thickness of the double layer, which reduces with increasing ionic strength (Mitchell 1993).

Electrostatic attraction enhances flocculation of oppositely charged polymers and solid particles. For negatively charged particles, cationic polymers are used to neutralize charge and induce flocculation; *charge patching*. Upon charge neutralization, positive and negative charged patches remain on the surface, causing electrostatic attraction. Flocculation of anionic polymers can be improved by adding activating ions to neutralize the negative charges of the solid phase prior to polymer addition.

Flocculation is initiated by the rapid agglomeration of sub-micron size particles through diffusion collisions followed by slower growth of larger flocs through hydrodynamic collision (Kitchener 1972). Successful flocculation needs enough time for the desired agglomerate size and density to form (Mortland 1970). This necessitates an adequate stirring system to maximize collision opportunities, prevent particle deposition, and minimize floc destruction by shearing forces (Jankovics 1965).

Generally, the required polymer dosage for effective flocculation is much less than that needed for surface saturation ($q = 0.5$). An optimum dosage is the one below which flocculation increases due to polymer adsorption and above which flocculation decreases owing to colloidal protection (Briceno & Osseo-Asare 1995c). This latter phenomenon occurs when polymer is adsorbed onto the particles to such an extent that vacant adsorption sites are no longer available for bridging (La Mer & Smellie 1962). According to Linke & Booth (1960), the existence of an optimum polymer dosage is common polymer feature and it suggests that the bridging mechanism is operative (Mortensen 1962).

2.7 POLYMER MODIFICATION OF LATERITE SLURRIES

2.7.1 General

The main objective of this research is to ameliorate the solid-liquid separation behavior of laterite slurries. This section describes the expected solid-liquid separation behavior of polymer modified laterite slurries. After providing a criterion of polymer selection for these slurries, a hypothesis is proposed to serve as a basis for this research undertaking.

2.7.2 Solid-Liquid Separation

The solid-liquid separation process of slurries involves the two stages of sedimentation and consolidation (Allen 1981; Pane 1985; Suthaker 1995). The predominance of any particular stage depends upon the initial solids content and the degree of flocculation. Based on the literature review given in this chapter, this section describes the expected solid-liquid separation behavior of polymer modified laterite slurries.

In dilute slurries, dispersed colloidal particles settle individually and their removal depends upon specific gravity and grain size (Svarovsky 1981; van Olphen 1977). This is called particulate settling and is characterized by a graded and hazy supernatant liquid, which gradually clarifies with time (Briceno & Osseo-Asare 1995b). Laterite slurries, which either contain sesquioxide coated colloidal particles (ore slurries) or exhibit grain size growth (PAL slurries), are expected to be flocculated in most cases. Further, synthetic polymers would impart additional flocculation. Therefore, particulate settling is not anticipated for these materials.

The progressive increase in size due to flocculation ultimately reach a point where the grains are entrapped, forming a three dimensional network within which all flocs settle at the same velocity as a group. This is known as sedimentation and is characterized by clear liquor behind the settling granular assemblage (Allen 1981). Under such conditions, the settling velocity is influenced by the weight of the solids of the upper layer transmitted to the lower layer (Kynch 1952; Richardson & Zaki 1954). It is anticipated that sedimentation would dominate the solid-liquid separation behavior of polymer modified laterite slurries. This is because during sedimentation colloid-polymer-electrolyte interactions are likely to be maximized.

Consolidation refers to that stage of the solid-liquid separation process in which the solid grains transmit effective stresses (Terzaghi 1943). Consolidation tests would help in understanding the mechanical behavior of polymer modified laterite slurries. As such, these tests are expected to provide data, which explains the progressive decrease and eventual minimization of the colloid-polymer-electrolyte interactions with loading.

This research is expected to provide data for a geotechnical understanding of the solid-liquid separation behavior of polymer modified laterite slurries. Such an understanding would include the determination of void ratio-effective stress relationship and hydraulic conductivity-void ratio relationship during sedimentation and consolidation.

2.7.3 Polymer Selection

2.7.3.1 General

Appropriate synthetic polymer for laterite slurries should bring about maximum solid-liquid separation without deteriorating other slurry characteristics important for these materials (Farinato et al. 1999). This section describes two types of polymers (ionic and nonionic) and various polymer characteristics influencing colloid-polymer-electrolyte interactions.

2.7.3.2 Ionic Polymers

Ion exchange (Bidwell et al. 1970), hydrogen bonding (Kohl & Taylor 1961), or a combination of both (Ahlrichs 1962) together with van der Waals interactions (Joyace & Worrall 1970) and ligand exchange (Ruehrwein & Ward 1952) has been postulated as bonding mechanisms for colloid-polyelectrolyte systems. The participation of the crystal edges in polyelectrolyte uptake is supported by the fact that the amount adsorbed correlates with the ion exchange capacity of the colloids (Warkentin & Miller 1958).

Adsorption of anionic polymer is markedly reduced when the pH of the medium is raised from acidic to neutral (Neal et al. 1985). This is because of the increased extension of the polyanion chain induced by intramolecular charge repulsion (hydrolysis) that offsets any bond formation (Theng 1979). In addition, the presence of sesquioxides (PZC ≅ 6.8 to 8.5) in the highly acidic suspension facilitates anion adsorption as the phenomenon occurs only at pH values below the PZC (Prafitt 1978). Polyanions can act as effective flocculating agents of clay slurries despite the fact that both the polymer and the clay mineral carry a net negative surface charge (Sakaguchi & Nagase 1966).

Cationic polymers tend to get sorbed onto colloidal surfaces because of opposite charges. The larger the number of cationic sites on the polymer molecule the more the latter uncoils into solution promoting interparticle bridging and hence flocculation (Ueda & Harada 1968a). Such flocculation is very successful in active clay mineral suspensions under high pH (Ueda & Harada 1968b).

This efficiency of anionic polymers is due to their extended chain conformation in solution (Michaels 1954). In neutral and acidic conditions and in the presence of positively charged soil particles, polyanions should be the first choice. Similarly, the use of cationic polymers for laterite slurries in neutral and acidic environments needs to be investigated (Petzold & Lukwitz 1998).

2.7.3.3 Nonionic Polymers

Nonionic polymers possess numerous polar groups along their chains, which interact with colloidal particles and the medium. Unlike polyelectrolytes whose chains are stretched out due to charge repulsion, nonionic polymers tend to adopt a random coil shape in dispersions (Theng 1979). The flocculating efficiency of such polymers can be increased using high molecular weight thereby increasing the coil dimension to the size of the mean interparticle separation (Kuzkin et al.1964). Under favorable environmental conditions, nonionic polymers are strongly and irreversibly adsorbed onto colloidal surfaces (Schamp & Huylebroeck 1973).

Briceno & Osseo-Asare (1995c) have shown that using nonionic polyacrylamide-based polymers can effectively ameliorate the dewatering behavior of laterite PAL slurries. This success was attributed to the ion-dipole and surface-segment hydrogen bonding of positively charged metal oxides and colloidal edges with the polymer, facilitated by the low pH of the medium (Kavanagh et al. 1975). Therefore, these polymers are suitable candidates for flocculating laterite slurries.

2.7.3.4 Polymer Characteristics

Three fundamental polymer characteristics influence colloid-polymer-electrolyte interactions. These include polymer charge, polymer molecular weight and polymer dosage. Briceno & Osseo-Asare (1995c) reported an improvement in the mechanical properties of laterite PAL slurries with an increase in polymer dosage. The same authors believe that the higher the molecular weight of a polymer, the better its performance in flocculating the slurries. This can be the result of the greater adsorption of the polymer onto the colloidal particles because of an increase in its molecular size. No data is available in the published literature that describes the effect of polymer charge on the behavior of laterite slurries. This research undertakes a parametric study to investigate the relative influence of these polymer characteristics on the solid-liquid separation of laterite slurries.

2.7.4 Research Hypothesis

This section presents a hypothetical model for polymer modification of laterite slurries. This model provides a basis for a comprehensive laboratory investigation program and for selecting appropriate polymers for two types of laterite slurries: ore slurries in neutral environment and PAL slurries under acidic conditions. For both these types of laterite slurries, the hypothesis remains essentially the same. Figure 2.14 shows the hypothetical model for polymer modification of laterite slurries. This figure shows that the hypothesis comprises of three stages: model development, model validation and model prediction. These three stages are described in detail here.

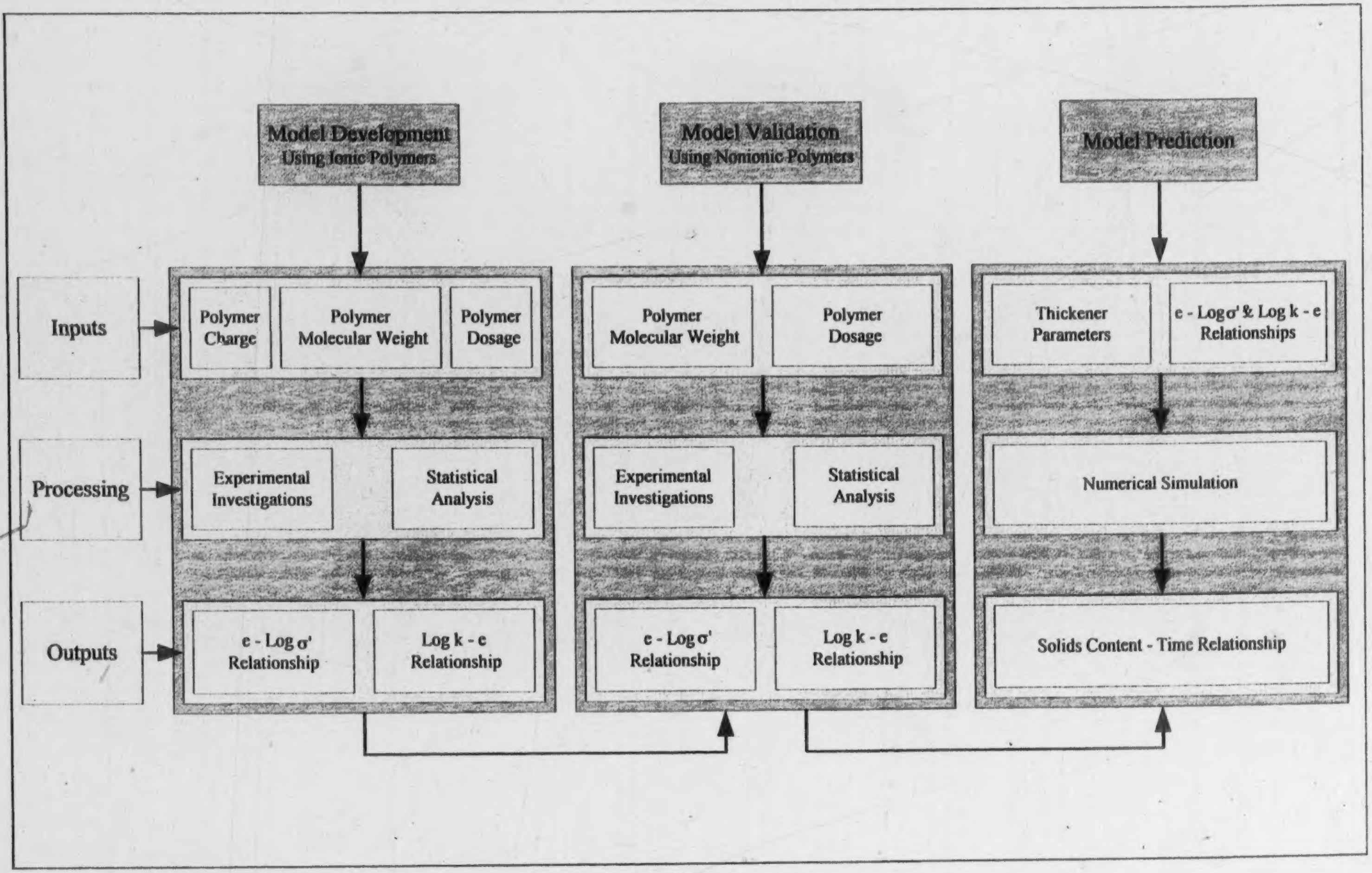
Model Development
Using Ionic Polymers
Model Validation
Using Nonionic Polymers
Model Prediction
Inputs
Processing
Outputs
Polymer Charge
Polymer Molecular Weight
Polymer Dosage
Experimental Investigations
Statistical Analysis
e - Log σ' Relationship
Log k - e Relationship
Polymer Molecular Weight
Polymer Dosage
Experimental Investigations
Statistical Analysis
e - Log σ' Relationship
Log k - e Relationship
Thickener Parameters
e - Log σ' & Log k - e Relationships
Numerical Simulation
Solids Content - Time Relationship

Figure 2.14: Hypothetical model for polymer modification of laterite slurries

The model would be developed using anionic and cationic polymers. The inputs include polymer characteristics such as charge, molecular weight and dosage. Using low and high values of these input parameters, a total of sixteen sedimentation-consolidation tests need to be conducted. Laboratory data would be analyzed and presented in the form of void ratio-effective stress and hydraulic conductivity-void ratio relationships. Statistical analysis would be used to determine the best fits for these two relationships. Results from both techniques would be studied in conjunction to understand the influence of input parameters on the solid-liquid separation behavior of polymer modified laterite slurries.

Model validation would be carried out using nonionic polymers and therefore the inputs would be reduced to polymer molecular weight and dosage. This time, low, medium and high values would be taken for these inputs and a total of nine sedimentation-consolidation tests would be conducted. Again, laboratory data and statistical analysis would be used to determine void ratio-effective stress and hydraulic conductivity-void ratio relationships. The best fits for these relationships are expected to approximate those from the above.

Using the physical parameters of thickeners and the best fit obtained previously, a numerical simulation would be conducted to predict the solid-liquid separation behavior of polymer modified laterite slurries. Such prediction would extrapolate laboratory data under field conditions. The output of this stage would be a solids content-time relationship that could be compared to the ones obtained for ore and PAL slurries to estimate the improvement due to polymer addition.

2.8 SUMMARY

This chapter presented a detailed and comprehensive literature review to provide a theoretical basis for this research work. Various interrelated aspects pertaining to the solid-liquid separation behavior of laterite slurries for the sulfuric acid pressure leaching process were discussed. This section provides a summary of some of the important points learnt from this literature review.

- Climate, topography, mineralogy of parent rock and geomorphic history controls the development of laterite ores. Characteristics of laterite ore slurries are governed by sesquioxide coating of soil particles.
- Sulfuric acid pressure leaching is the method of choice to for metal extraction from laterite slurries. This process occurs at a temperature and pressure of up to 280 °C and 6000 kPa, respectively.
- The leaching operation causes mineral transformations, which are associated with grain size growth that in turn affects the characteristics of laterite PAL slurries.
- Solid-liquid separation of laterite ore and PAL slurries can be improved using synthetic polymers. Understanding of the colloid-polymer-electrolyte interactions is key to successful amelioration.
- Based on the above material characteristics and literature review, a hypothetical model is proposed for selecting appropriate polymers for improving solid-liquid separation behavior of laterite slurries.

Chapter 3

Research Methodology

3.1 GENERAL

This chapter gives an account of the research methodology followed during the course of the study. First, the materials are described including details about the various types of samples and the associated safety hazards. Second, the various stages of the research program are laid out giving a theoretical background of each stage. Third, a detailed description of the various types of tests conducted during this research is given. These include tests for the determination of geotechnical index properties, x-ray diffraction analysis, pH, electrical conductivity, and electrolyte concentration, scanning electron microscopy, sedimentation and large-strain consolidation. Background information on various testing techniques as well as the modifications adapted in this study to suite the particular requirements of this class of materials is provided. Next, the analysis technique adopted to provide a statistical basis to this research. This technique is described with reference to its application to sedimentation and consolidation. This is followed by a description of the numerical simulation techniques used for both sedimentation and consolidation. Then, the role of laterite slurry characteristics diagram is highlighted for a geotechnical understanding of laterite slurries. Finally, a summary of this chapter is given.

3.2 MATERIALS

3.2.1 General

This section first describes various laterite slurries as well as synthetic polymers obtained for use in the research work. Then, it describes the preparation of various types of sample from the received materials. Lastly, it gives an account of the safety hazards associated with this class of materials.

3.2.2 Laterite Slurries

The Metallurgical Technologies Division of Dynatec Corporation, Canada, provided laterite slurry samples. These included underflow ore slurry samples from the storage thickener and underflow PAL slurry samples from the counter current decantation (CCD) wash circuit. These samples, which are designated as Type A and Type B, respectively, were transported to the Department of Civil and Environmental Engineering, University of Alberta for laboratory investigations. All samples were received in 20 L plastic containers.

Four laterite ore slurry samples were selected for geotechnical characterization from various parts of the globe: Cuba, Philippines, Australia and Indonesia. The Cuban sample represented a limonite ore whereas the Indonesian sample denoted a saprolite ore; the Philippines and the Australian samples corresponded to two distinct varieties of limonite and saprolite ores blends. Similarly, for the same ore slurry samples, the corresponding PAL slurry samples were also obtained using consistent process conditions. Table 3.1 gives the process conditions during the autoclave operation for laterite PAL samples.

Table 3.1: Process conditions for laterite PAL samples

Parameter	Sample Type and Origin			
	Limonite PAL	Limonite-Saprolite PAL		Saprolite PAL
	Cuba	Philippines	Australia	Indonesia
Temperature (^oC)	245	260	255	250
Pressure (kPa)	4100	4100	4100	4000
Reaction Time (min)	60	60	60	50

3.2.3 Synthetic Polymers

Ciba Specialty Chemicals Canada Inc. provided various acrylamide-based polymers (anionic, cationic and nonionic) in powder from. The chemical composition of these synthetic polymers is similar to those described in Chapter Two. Table 3.2 describes the charge (C_p) and molecular weight (MW_p) characteristics of various types of polymers used during this research work.

The powdered polymers were dissolved in distilled water prior to their application to the slurry. For each test, a fresh concentrated *stock solution* was prepared. To preclude the effect of flocculant aging, this solution was instantly diluted to a *test solution* that was immediately used. The stock solution was prepared by weighing 0.5 grams of dry powdered polymer in a clean dry 250 mL beaker. Then, 1 mL of methanol (for anionic and nonionic polymers) or acetone (for cationic polymers) was added as the powder was swirled for an even distribution. Next, 99 mL of distilled water was added and a magnetic stirrer rod was immersed in the beaker. The beaker containing all of the above ingredients was put on a stirring machine for 1 hour at a moderate speed of 12 rpm.

To dilute the stock solution to 0.05% test solution for dosing, added 10 mL of the stock solution to 90 mL of distilled water. Thus, 1 mL of the test solution contained 0.5 mg of dry polymer. When divided by the total volume of the slurry (L), this gave the amount of 1 mL of test solution in the slurry in mg/L. To get the volume of dosage in mL, the desired amount in mg/L was divided by the previously obtained amount.

Table 3.2: Designations and characteristics of various polymers used

Type	C_p (%)	MW_p x 10^6 (g/mol)[†]	Trade Name[‡]
Anionic	10 (Low)	7.5 (Low)	Magnafloc 24
	10 (Low)	17.5 (High)	Magnafloc 338
	75 (High)	7.5 (Low)	Magnafloc 1017
	75 (High)	17.5 (High)	Magnafloc 919
Cationic	10 (Low)	7.5 (Low)	Percol 140
	10 (Low)	17.5 (High)	Zetag 7692
	75 (High)	7.5 (Low)	Zetag 7504
	75 (High)	17.5 (High)	Zetag 7689
Nonionic	———	7.5 (Low)	Percol 374
	———	12.5 (Medium)	Magnafloc 351
	———	17.5 (High)	Magnafloc 333

[†] Approximate values with a variation of ± 1 x 10^6 (g/mol)

[‡] Trade names belong to Ciba Specialty Chemicals Canada Inc.

3.2.4 Sample Preparation

Four different types of samples were tested in the laboratory. As stated earlier, Type A samples denoted the four laterite ores whereas Type B samples designated the corresponding PAL samples. Two more sample types were prepared using various synthetic polymers. These included Type C, which were the polymer modified ore slurries and Type D that designated polymer modified PAL samples.

Type C and Type D samples were prepared by adding the required dosage to the slurry samples. A low and a high dosage were selected for ionic polymers whereas a medium dosage was also used for nonionic polymers. These low, medium and high dosages corresponded to 4, 8 and 12 mg/L, respectively, of the total volume of the slurry or to 53, 106 and 159 g/ton, respectively, when based on dry mass of polymer and solids in the slurry. These dosages were based on a thorough literature review (e.g. Briceno & Osseo-Asare 1995c) as well as on consultations with the Metallurgical Technologies Division of Dynatec Corporation, Canada and Ciba Specialty Chemicals Canada Inc.

Polymer modified samples were prepared by mixing the required dosage from the test solution with the known volume of the slurry. Based on consultation and experimentation, 15% initial solids content was selected and consistently used in this research. Obtained from knowledge of the polymer amount in mg/L, the desired polymer volume was introduced to the slurry sample using a graduated plastic syringe. To minimize floc breakage, ingredients were mixed using a steel plunger that was rotated at a moderate rate of 12 rpm for 5 minutes.

3.2.5 Safety Hazards

Type A and Type C samples were mainly neutral (pH ≈ 7) whereas Type B and Type D samples were highly acidic with a pH ≈ 1 and containing small amount of residual sulfuric acid. According to the Workplace Hazardous Materials Information Systems (WHMIS), these latter two sample types are considered hazardous. To work safely with these materials, a WHMIS training course was attended under the auspices of the Office of Environmental Health and Safety, University of Alberta.

Protective measures generally consisted of means of preventing direct contact with samples. Typically, this included chemical resistant laboratory coats and hand gloves, safety glasses, face shields, and appropriate respiratory protection. Further, the laboratory space was well ventilated by exhaust fans to minimize exposure to vapor from sulfuric acid at ambient temperatures. In case of emergency, eyewash and shower, a first aid box and telephone contact with the doctor were made available.

Minor spills and leaks were usually diluted and neutralized with soda ash, or lime whereas large spills were generally contained. Due to limited amount of available material, the hierarchy of laboratory testing was managed in such a way that allowed the use of the same samples for more than one test. The waste materials were stored in an isolated and confined area thereby minimizing the possibility of contaminating the surrounding environment. Finally, these materials were disposed off to a landfill in accordance with the regulatory criteria.

3.3 RESEARCH PROGRAM

3.3.1 General

Understanding of the solid-liquid separation of laterite slurries is the key geoenvironmental issue associated with the sulfuric acid leaching metal extraction process. Polymer modification methods for both the ore and PAL slurries can be devised to increase the yield and the efficiency of this method. For this purpose, a comprehensive research program was enacted to characterize and ameliorate the engineering behavior of laterite slurries. This program comprised of four stages: laboratory investigations, statistical analyses, numerical simulations, and the use of laterite slurry characteristics diagram (LSCD). This section describes the role of each of these stages in the research program.

3.3.2 Laboratory Investigation

Laboratory investigations were the largest portion of this research program. It comprised of a characterization phase and an amelioration phase. In the first phase, five distinct categories of characteristics were investigated for Type A and Type B slurries using various laboratory testing techniques. These categories included geotechnical index properties, mineralogy, pore water chemistry, morphology and solid-liquid separation. The main focus in the second phase was on the determination of the solid-liquid separation behavior of Type C and Type D samples. Some of the geotechnical index properties and morphological observations were also made during this phase to understand improvement in the engineering of laterite slurries with the use of synthetic polymers.

3.3.3 Statistical Analysis

Results of laboratory investigations in phase two were statistically analyzed to illustrate the significance of the various polymer parameters such as charge, molecular weight and dosage. Described in detail later in this chapter, these analyses were aimed at the derivation of a statistical model to elucidate the solid-liquid separation behavior of polymer modified laterite slurries. For this purpose, the sedimentation and consolidation tests were designed in such a way to capture the effect of all of the independent variables. The model was developed by selecting a low and a high value for each of the ionic polymer parameter (*factors*) and thereby conducting sixteen tests. For validating the model, nine more tests were conducted using nonionic polymers with each factor considered at three *levels*; low, medium and high.

3.3.4 Numerical Simulation

To predict field performance from the laboratory and the statistical data, numerical simulations were conducted independently for both sedimentation and consolidation. For Type A and Type B samples, numerical simulations were based on laboratory data. On the other hand, numerical simulations for Type C and type D samples were based on statistical analyses that were, in turn, derived from laboratory investigations. For both of these cases, physical parameters of the thickeners were used to determine the solids content-time relationship for various types of laterite samples. Results from both cases were compared to estimate the improvement due to polymer modification.

3.3.5 Laterite Slurry Characteristics Diagram

To understand the geotechnical behavior of laterite slurries, their constituent phases were combined into a single ternary diagram called the laterite slurry characteristics diagram (LSCD). Such a diagram eliminates the need for multiple two-dimensional plots and has been effectively used to predict viable tailings disposal methods of Alberta oil-sand (Morgenstern & Scott 1995). In this research, the LSCD was used to correlate the structure (morphology) and the behavior (solid-liquid separation) of laterite slurries. Data obtained from laboratory testing, statistical analysis and numerical simulation techniques were plotted on this ternary diagram. The LSCD was used as a tool to understand sedimentation and consolidation and the evolution of hydraulic conductivity during those processes. Salient features of the LSCD are described later in this chapter.

3.4 LABORATORY INVESTIGATION

3.4.1 General

This section gives an account of the various laboratory tests performed during this research. Details of the different testing procedures and deviation from standards to suite laterite slurries are described where appropriate. Likewise, sample preparation methods for certain tests are also given. To provide a general overview, the entire laboratory investigation program is given in Table 3.2, which is followed by describing each testing category.

Table 3.3. Summary of the laboratory investigation program

Characteristic	Test	Number of Tests for Sample Type*			
		A	B	C	D
Geotechnical Index Properties	Water Content (%)	12	12	32 + 18	32 + 18
		2	2	32 + 2	8 + 2
	Specific Gravity	4	4		
	Grain Size Distribution	4	4		
	Segregation	4	4	4	4
	Consistency Limits	4	4	16 + 9	16 + 9
Mineralogy	XRD	4	4		
	AEC and CEC	4	4		
Pore Water Chemistry	pH and EC	4	4	16 + 9	16 + 9
		1	1	16 + 1	4 + 1
	Electrolyte Concentration	4	4		
Morphology	SEM and EDXA	4	4	4 + 1	4 + 1
		2	2		
Solid-Liquid Separation	Sedimentation	4	4	16 + 9	16 + 9
	Consolidation	1	1	16 + 1	4 + 1

Note: For the same test appearing in two rows, the upper and the lower values mean sedimentation and consolidation tests, respectively. Likewise, for Type C and D samples, the first and the second values pertain to ionic and nonionic polymers, respectively.

Table 3.3 shows that five distinct categories of engineering characteristics were determined during this research work. These included geotechnical index properties, mineralogy, pore water chemistry, morphology and solid-liquid separation. These characteristics were determined for four sample types using various testing procedures.

Laboratory investigations were conducted in two phases. First, Type A and B samples were characterized to understand the engineering behavior of laterite ore and PAL slurries under ambient process conditions. Improvement of the solid-liquid separation behavior of laterite slurries was based on the results of Type A and Type B samples. As such, engineering characteristics of polymer modified laterite slurries were determined for a selected ore of Type C and the corresponding PAL of Type D.

Table 3.3 also gives the number of tests performed for each sample type. The table indicates that a complete geotechnical characterization was done for Type A and B samples to develop fundamental understanding of these materials. On the other hand, the bulk of the testing for Type C and D samples was focused on the improvement of the solid-liquid separation behavior.

3.4.2 Geotechnical Index Properties

3.4.2.1 General

Laterite soils are prone to changes in properties caused by drying and exposure to air. Oven drying leads to partial or complete dehydration of the clay minerals that can result in permanent changes in soil properties (Frost 1976). Even air-drying at ambient temperature can cause changes that cannot be reversed by re-wetting (Fourie 1997). This necessitated modification of all routine laboratory testing methods. This section presents a review of the modified testing procedures for determining geotechnical index properties of laterite soils.

3.4.2.2 Water Content

Gravimeteric water content (w) is defined as the ratio of the mass of water in a given volume of soil to that of the soil particles in the same volume. Expressed as a percentage, water content is generally determined according to the ASTM Standard Test Method for Laboratory Determination of Water (Moisture) Content of Soil and Rock by Mass (D 2216-98). In this method, the sample is oven-dried at a temperature of 110 ± 5 °C, which can cause removal of structural water from residual soils (Holtz & Kovacs 1981). Therefore, Fourie (1997) suggested that water content of such soils should be determined at a temperature of 50 °C. Although, this reduced oven temperature could result in an underestimation of water content, such discrepancies are negligible owing to the large amount of water present in the slurries. Further, the use of a consistent procedure for all tests involving heating ensured compatibility of results.

Water content was translated to solids content (s), which is the mass of soil solids divided by the total mass of the soil. Based on basic relationships, such conversion was made according to the following equation:

$$s = \frac{1}{1+w} \tag{2.1}$$

Table 3.3 indicates that water content was determined for both the ore and the PAL slurries. This established the amount of water used for slurry preparation and during CCD washing, respectively. To ensure an initial solids content of 15%, water content was always measured for all slurry samples prepared for both sedimentation and consolidation tests. Similarly, water content at the completion of each test was also determined to ascertain the estimated values.

3.4.2.3 Specific Gravity

Specific gravity (*Gs*) is the ratio of the mass of a unit volume of a material at a standard temperature (4 °C) to the mass in air of the same volume of gas-free distilled water at the stated temperature. This parameter is usually determined according to the ASTM Standard Test Method for Specific Gravity of Soil Solids by Water Pycnometer (D 854-00). To preclude the effect of pre-test drying of the slurry, Fourie (1997) proposed that the dry mass of the specimen should be calculated at a temperature of 50 °C after the completion of the test; air removal was achieved by vacuum and did not involve heating. These two alterations were adapted to the standard ASTM procedure during this study. As given in Table 3.3, specific gravity was determined in the laboratory for four ore samples and four PAL samples. This gave a first indication of the composition of various samples.

Specific gravity of soil was used to calculate void ratio (e), which is the ratio of the volume of voids to the volume of solids. Assuming complete saturation and using unity for the specific gravity of water, void ratio can be estimated from knowledge of solids content according to the equation:

$$\bar{e} = Gs\left(\frac{1-s}{s}\right) \tag{2.2}$$

Equations (2.1) and (2.2) were two of the most useful equations in this study as they described basic geotechnical engineering terms associated with solid-liquid separation of laterite slurries. Table 3.3 shows that the specific gravity was determined for the four types of laterite ore slurries and their corresponding PAL slurries.

3.4.2.4 Grain Size Distribution

Grain size distribution analyses are generally performed according to the ASTM Standard Test Method for Particle-Size Analysis of Soils (D422-63(1998)). This procedure was modified to account for laterite soils due to high ionic concentration of the pore water and the fact that initial dry mass of the slurry is not known as pre-test drying was to be avoided. Therefore, the soil sample was divided into two sub-samples; one for determining dry mass of the soil and the other for grain size analyses (Dusseault & Scott 1983). First, an hydrometer analysis was performed on dry soil after dispersion of the soil mass was assured (Lamb 1951). To preclude the effect of hindered settling during the hydrometer test (Vitton & Sadler 1997), about 25 g of dry soil was used in the test. Based on experimentation, this amount was found to be appropriate for laterite soils. In the hydrometer, the soil was suspended by agitation with dilute alkaline sodium hexametaphosphate, which acts as a dispersing agent (Townsend et al. 1971;

Wintermeyer & Kinter 1954). This was followed by a sieve analysis on the same material washed with distilled water.

Results of the combined hydrometer and sieve analyses yield two important parameters. The fines content is defined as the percentage of mass finer than 0.075 mm in the total mass of soil solids. Similarly, the clay content is the amount of mass finer than 0.002 mm in the total mass of the soil solids and is expressed as a percentage. Whereas the former grain size determines mechanical properties of a soil slurry, the latter grain size controls the physico-chemical phenomena at the solid-liquid interface.

Table 3.3 shows that the combined hydrometer and sieve analyses were conducted for four ore slurries and four PAL slurries. These tests revealed the gradation of various laterite samples obtained as a result of the slurry preparation procedure or the acid leaching operation.

3.4.2.5 Segregation

One of the undesirable properties of many types of slurry is segregation of coarse and fine grains. Segregation tests were conducted by taking different initial solids content of the same slurry in separate 150 mL graduated cylinders and allowing the slurries to settle under self-weight. After twenty four hours, the sediment was divided into equally spaced layers (denoted by i) and the solids content of each layer (s_i) was determined separately. This measured solids content was plotted versus the normalized height, obtained by dividing the mid height of a layer (H_i) by the total sediment height (H_f) after twenty four hours. The resulting solids content profile with depth was bisected by an average value of the measured solids content (s_{avg}). Using this average solids content, percentage of segregation (S) was calculated for each layer according to the following equation:

$$S\,(\%) = \frac{100}{2H_f}\,(s_i - s_{avg})(H_{i+1} - H_{i-1}) \qquad (2.3)$$

The sum of segregation percentage for all layers was divided by the average solids content to obtain the segregation index (I_s) for each value of initial solids content. These data of segregation index were plotted versus the corresponding initial solids content and a value pertaining to 5% segregation was chosen as I_s.

Segregation index is defined as the initial solids content that corresponds to minimum variation in the solids content profile with depth. Alternatively, large deviations from the average solids content render the material segregating whereas proximity of measured solids content to s_{avg} means a nonsegregating material. Based on experimentation, the minimum possible segregation for laterite slurries was found to be in the range of 2 to 5%. Allowing for experimental errors, 5% segregation was used as the boundary between segregating and nonsegregating materials.

Table 3.3 indicates that the segregation index was determined for four ore slurries and four PAL slurries as well as for the polymer modified ore and PAL slurries. Determination of segregation index for the latter sample types included four tests with selected ionic polymers.

3.4.2.6 Consistency Limits

The presence of water can especially affect the engineering behavior of fine-grained fraction of soils. Consistency limits provide a standardized scale for comparison of engineering behavior. Expressed as percentage, the liquid limit (w_l) and plastic limit (w_p) are water contents at critical stages in soil behavior. These limits were determined according to the ASTM Standard Test Methods for Liquid Limit, Plastic Limit, and Plasticity Index of Soils (D 4318-00). Related to and derived from consistency limits are the consistency indices, which are useful parameters in identification and classification of fine-grained soils. Plasticity index (I_p), which indicates the range of water contents over which a soil is plastic, is numerically equal to the difference of the two limits.

Consistency limits for laterite soils are affected by pre-drying (Rouse et al. 1986) and mixing time (Wesley & Matuschika 1988). The effect of drying prior to testing may be attributed to increased cementation due to sesquioxide oxidation (Townsend 1985). The consistency limits were determined by gradual drying of the high water content slurries at the proposed oven temperature of 50 °C. This greatly reduced the effect of water addition, pre-drying and mixing on soil consistency. To further, minimize the breakdown of clay clusters in the soil, mixing time was restricted to five minutes as suggested by Fourie (1997). To facilitate easy comparison between various samples, the influence of increased electrolyte concentration in pore water at low water contents was not taken into consideration.

Consistency limits were determined for the four ore and the four PAL slurries as well as for twenty five Type C and twenty five Type D samples. The polymer modified slurries included sixteen samples with ionic polymers and nine samples containing nonionic polymers.

3.4.3 Mineralogy

3.4.3.1 General

Mineralogy was determined for four laterite ore samples and four laterite PAL samples. This section describes the testing and analysis procedures to determine mineralogy. These include x-ray diffraction analysis for mineral identification and semiquantitative measurement, and tests to determine the exchangeable anion and cations associated with a given mineral composition.

3.4.3.2 X-ray diffraction Analysis

Mineralogical composition was investigated by X-ray diffraction (XRD) analysis using a Phillips diffractometer, Model Pw 1710. The diffractometer uses a Cu broad focus tube at 40 kV and 25 mA, equipped with a curved crystal monochromator. The scanning speed and interval of data collection was 1° 2θ/min. To observe all diffraction peaks associated with each constituent mineral, the angle scanned was 4 to 80°. Such a large scanned angle allowed the exact qualitative determination of various mineral types. To conduct XRD analysis, slurry samples were first oven-dried at 50 °C and subsequently ground manually in a porcelain mortar pestle to powdered form. To obtain a tangible mineralogy, grain size distributions identical to ambient process conditions were obtained; the maximum grain size was 0.85 mm. Randomly oriented samples were prepared by lightly pressing the powdered samples into rectangular metal holders, 20 mm x 10 mm size. The top surface of the specimen was pressed against a rough glass surface to maximize randomness in surface packing (Grim 1968).

X-ray diffraction is based on the fact that no two minerals have the same spacing of inter-atomic planes in three dimensions (Kinter & Diamond 1956). The angles ($2\theta^{\circ}$) at which diffraction occurred and the atomic spacing (d) calculated there from were used for mineralogical identification. Using 1.5418 Å as wavelength (λ) of Cu X-ray source and $n = 1,2,3$ for first, second and third order diffraction peaks, atomic spacing was calculated according to Bragg's equation:

$$d = \frac{n\lambda}{2\sin\theta} \tag{2.4}$$

To ascertain various mineral types in a sample, the diffraction patterns were matched with the standard patterns prepared by the Joint Committee of Powder Diffraction Data Service (JCPDS). Comparing the areas under the peaks allowed semiquantitative estimates of the various minerals present in each sample (Kilmer & Alexander 1949).

3.4.3.3 Ion Exchange

For the measurement of individual ions, a mixture of 10 g of soil and 40 mL of either deionized water (for anions) or 1 *M* NH_4OAc (for cations) was prepared in a tube that was agitated for 5 minutes in a reciprocal shaker. After a rest period of

24 hours, the tube was again agitated for 15 minutes and its contents were filtered through a Whatman No. 42 filter paper.

Anions such as Cl^-, NO_3^-, and SO_4^{2-} were determined by the ion chromatography method using a high performance liquid chromator, Model Dionex AS 50. For this purpose, the filtrate was drawn into a 3 mL syringe and the sample was pumped into the chromator. After 10 min, the machine generated discrete bands by passing the sample through a column filled with a specially designed anion exchange resin. After identifying the anionic components of the sample, the same separated bands were used to quantify individual anions; concentrations were corrected using appropriate dilution factors. The individual anions and their summation, which is called as the anion exchange capacity (AEC) were expressed as cmol(-)/kg of dry soil (Mitchell 1993).

Ammonium acetate method measured cations such as Na^+, K^+, Ca^{2+} Mg^{2+}, Fe^{2+}, and Al^{3+} (Bascomb 1964; Gillman 1979). For this purpose, the filtrate was washed with 1 *M* NH_4OAc and 250 mL leachate was collected in a volumetric flask for analysis. Concentrations of individual cations were corrected using appropriate dilution factors and the concentration of blanks prepared for each run.

Total cation exchange capacity (CEC) was independently determined by leaching ammonium saturated soil with 1 *M* KCl and analyzing the 250 mL extract. From a knowledge of equivalent weight of different ions (mg/meq), ion concentration (mg/L) was converted to CEC in cmol(+)/Kg using the following equation (Mitchell, 1993):

$$CEC = \left(\frac{\text{Ion Conc.}}{\text{Eq. Wt}}\right)\left(\frac{250\text{ mL}}{100\text{ g of soil}}\right) \tag{2.5}$$

The cation exchange capacity was translated to exchangeable sodium percentage (ESP) according to the following equation:

$$ESP = \left(\frac{Na^{+}}{CEC}\right) \text{x}\,100 \tag{2.6}$$

Exchangeable sodium percentage is one of the most important factors in understanding the evolution of soil morphology. According to Mitchell (1993), soils with $ESP<2$ possess a flocculated fabric whereas those with $ESP \geq 2$ are susceptible to dispersion.

3.4.4 Pore Water Chemistry

3.4.4.1 General

Pore water chemistry was carried out on four laterite ore samples and four laterite PAL samples. This section describes the testing procedures used for the determination of pH, electrical conductivity and electrolyte concentrations.

3.4.4.2 pH and Electrical Conductivity

The pH of soil water is expressed as logarithm to the base of 10 of the reciprocal of hydrogen ion concentration. Similarly soil electrical conductivity (EC), which is the inverse of resistivity, is measured in micro siemens per centimeter. Accument 50 that allows precision and accuracy was used for measurement of both pH and conductivity. The pH was determined according to the ASTM

Standard Test Method for pH of Soils (D4972-01). Similarly, electrical conductivity was measured as per ASTM Standard Test Methods for Electrical Conductivity and Resistivity of Water D1125-95(1999). For pH measurement, the instrument was periodically calibrated with solutions at pH = 3, 5 and 7.

Table 3.3 indicates that the pH and the EC were determined after all of the sedimentation and the consolidation tests. Based on observations, it was found that the addition of polymers had negligible effect on both pH and EC of the slurry samples. This is attributed to the small dosages (maximum 12 mg/L) of polymers used in this research.

3.4.4.3 Electrolyte Concentration

Concentrations of Na^+, K^+, Ca^{2+}, Mg^{2+}, Mn^{2+}, Al^{3+}, Fe^{3+}, Ni^{3+}, Co^{3+}, and Si^{4+} ions were determined by the Inductively Coupled Plasma method using a Thermal Jarrell Ash IRIS Advantage. The Automated Ferricyanide Method using Colorimetric Centripetal Analyzer (COBAS FARA II), determined the concentration of Cl^- ion in solution. The concentration of other anions such as NO_3^-, HCO_3^- and SO_4^{2-} in the pore water was determined according to ASTM Standard Test Method for Anions in Water by Chemically Suppressed Ion Chromatography (D4327-97) using Dionex DX-500. The sum of the concentrations of measured anions and cations was recorded as the total dissolved solids (TDS) in mg/L. Similarly, from a knowledge of individual electrolyte concentrations (A) and valence (v), ionic strength (I) was calculated in moles/L according to the following equation:

$$I = \frac{1}{2} \sum A v^2 \tag{2.7}$$

The pore fluid chemistry was determined for the four ore slurries and the corresponding PAL slurries. Based on theory, no change in the chemical composition of the pore water was envisaged. Therefore, the concentration of various ions pore water in the slurry samples of polymer modified materials was not measured.

The theoretical basis was provided by calculating the maximum amount of dissociated charge from the polymer for complete adsorption using 12 mg/L dosage. Table 3.2 indicates that the maximum charge for anionic polymers was 50% and that for cationic polymers was 80%. The estimated maximum amount of released Na^+ for the former polymers was 6.0 mg/L. Similarly, the amount of liberated Cl^- for the latter polymers could be as high as 9.6 mg/L. In contrast, the TDS of the ore slurry was 550 mg/L (Chapter Four) and that of the PAL slurry was 88407 mg/L (Chapter Five). This meant that the maximum dissociated charge from the polymers was at least 57 times (and up to 14735 times) that of the TDS of the pore fluid. Therefore, the detailed pore fluid chemistry for polymer modified samples was not investigated.

3.4.5 Morphology

3.4.5.1 General

Scanning electron microscopy (SEM) was used for morphological assessment of laterite slurries. Manufactured by Japan Electron Optics Limited (JEOL), the microscope (JSM-6301FXV) performed assessment of fabric as well as elemental analyses using Energy Dispersive X-ray Analyzer (EDXA). To ensure an intact fabric with minimal disturbance to the solid phase, slurry samples were prepared using cryogenic techniques (Erol et al. 1976). Despite the reported phenomenon of freezing artifact (Mikula 1988), the microstructure explains several distinct features of slurries (Scott et al. 1985) and was used to characterize slurries in an empirical way (Mikula et al. 1989). This section describes the sample preparation method and the cryogenic technique for conducting scanning electron microscopy.

3.4.5.2 Sample Preparation

Slurry samples were drawn by vertically inserting a 3 mm circular plastic straw and gently plugging it with the thumb to create suction. To ensure an intact fabric, the straw containing the sample was immediately immersed in liquid nitrogen at a temperature of -208 °C. After complete freezing, the straw was clipped and peeled off. A batch of three samples was glued to the cryogenic sample holder using TISSUE-TEK OCT 4583 compound. Each batch was immersed in liquid nitrogen and individual samples were fractured with a side cutter to avoid condensation on the fracture surface. Specimens were stored in the cryogenic system (Emitek K1200) of the microscope at a temperature of -195 °C.

3.4.5.3 Scanning Electron Microscopy

The samples were placed in the SEM sample chamber after the latter was flushed with argon to remove water vapor and vacuum cleaned using a rotary pump.

Samples were allowed to sublimate at a temperature of -40 °C and examined at low voltage (2.5 kV) till all the ice was removed. Thereafter, all samples were transferred to the cryogenic preparation chamber at a temperature of -155 °C, where they were sputtered with a fine film gold. Finally, the samples were put back in the SEM chamber for visual and photographic examination. Scanning and recording speeds were 450 frame/sec and 40 sec/frame, respectively. The incident electron beam was at an average vertical distance of 30 mm and the voltage was kept at 2.5 to 5 kV. For EDXA spectra, voltage was kept at 10 to 15 kV. Generally, the micrographs were taken at representative locations with enlargements of 15, 200, 500, 2000 times. However, for highlighting some peculiar features, higher enlargements such as 5000 and 10000 were also used occasionally.

Table 3.3 indicates that scanning electron microscopy was performed for six laterite ore samples and six laterite PAL samples. For both of these sample types, four specimens were taken from each of the ore and the corresponding PAL slurries after the sedimentation tests. The remaining two specimens were taken at the end of consolidation; one in each of the vertical and horizontal directions. Based on the results, specimens in the polymer modified laterite samples were selected only from slurries after sedimentation tests. For Type C samples, four specimens were selected from slurries modified with ionic polymers and one with nonionic polymers. Scanning electron microscopy was also conducted on the corresponding specimens of Type D.

3.4.6 Solid-Liquid Separation

3.4.6.1 General

Determination of the solid-liquid separation behavior of laterite slurries comprised of conducting sedimentation tests and consolidation tests. Table 3.3 indicates that the sedimentation tests were performed for four ore samples and four PAL samples as well as twenty-five Type C samples and twenty-five Type D samples. Among the polymer modified slurries, sixteen tests were conducted using ionic polymers and nine with nonionic polymers. On the other hand, consolidation tests were conducted for a selected ore and its corresponding PAL. Consolidation tests were conducted on all of the ionic polymers added laterite ore slurries as well as one selected sample from the nonionic polymer added laterite ore slurries. In contrast, four ionic polymer modified and one nonionic polymer modified laterite PAL slurries were selected for consolidation testing.

3.4.6.2 Sedimentation Test

Sedimentation tests were conducted using 8.5 cm diameter graduated cylinders. Based on experimentation, the initial height of the sample was kept as 8.5 cm to give a height to diameter ratio of 1.0 at the start of the test. To mimic process conditions and to facilitate easy comparison, the initial solids content was kept at 15% for all the sedimentation tests. This initial solids content pertained to negligible segregation for most laterite slurries and, based on consultations with the chemical and the mining industry, was the maximum value at which polymers interact with laterite colloids.

Figure 3.1 illustrates the setup for conducting the sedimentation test. As shown in this figure, the slurry sample was poured in the graduated cylinder up to a height of 8.5 cm and was allowed to settle under self-weight. The solid-liquid interface movement was captured at equal intervals of time using a camcorder. The camcorder was connected to a computer that stored the captured frames in a digital format. After the completion of the sedimentation test, the digital frame files were carefully viewed and the data were recorded as interface height versus time. This procedure minimized the observation error because of the facility to digitally enlarge and refine the captured solid-liquid interface. For additional accuracy, some of the tests were replicated using an identical fresh sample tested in a different size mold (initial part of the consolidation test).

The slope of the initial straight-line portion of the sedimentation curve was used to determine the initial hydraulic conductivity according to the theoretical formulations of Pane & Schiffman (1997), presented in Chapter Two. The sedimentation data was further translated to void ratio-time and solids content-time curves using equation 2.2. First, the initial void ratio (e_o) was calculated from knowledge of the initial solids content (s_o). Then, the void ratio (e_1) pertaining to the next time reading was obtained by multiplying the initial void ratio with the interface height at that time. In turn, the next solids content (s_1) that corresponded to e_1 was estimated by rearranging equation 2.2. In this fashion, the variation of void ratio and solids content with the elapsed time during the sedimentation test was calculated.

Figure 3.1: Setup for sedimentation test

3.4.6.3 Consolidation Test

The standard odometer test could not be used for laterite slurries due to the large anticipated strain, the inability of determining hydraulic conductivity during the test and the test duration (Suthaker & Scott 1994). Several advanced testing techniques developed to overcome these problems were surveyed. These included the constant rate of deformation (CRD) test (Lee, 1981), the constant hydraulic gradient (CHG) test (Lowe et al. 1969), the constant rate of loading (CRL) test (Aboshi et al. 1979), and the constant loading (CL) test (Janbu et al. 1981). It was found that although these tests are faster than the conventional odometer test, their applicability is restricted by the assumptions of the infinitesimal consolidation theory on which they are based (Znidarcic et al. 1984). Further, the seepage test (Imai, 1979) was suspected to yield erroneous results due to possible sample rebound at test completion.

The slurry consolidation test (Pollock 1988; Suthaker 1995) was selected due to its ability of measuring large strains and the fact that it minimizes the above mentioned experimental and theoretical errors. Further, this test allowed the direct determination of hydraulic conductivity after the completion of each loading stage. To avoid the inversion of the finite-strain consolidation theory due to the associated assumptions, long test duration for consolidation of laterite slurries was accepted in this research.

Figure 3.2 shows the consolidation test setup whereas Figure 3.3 gives the schematic diagrams of two types of cells used during this research.

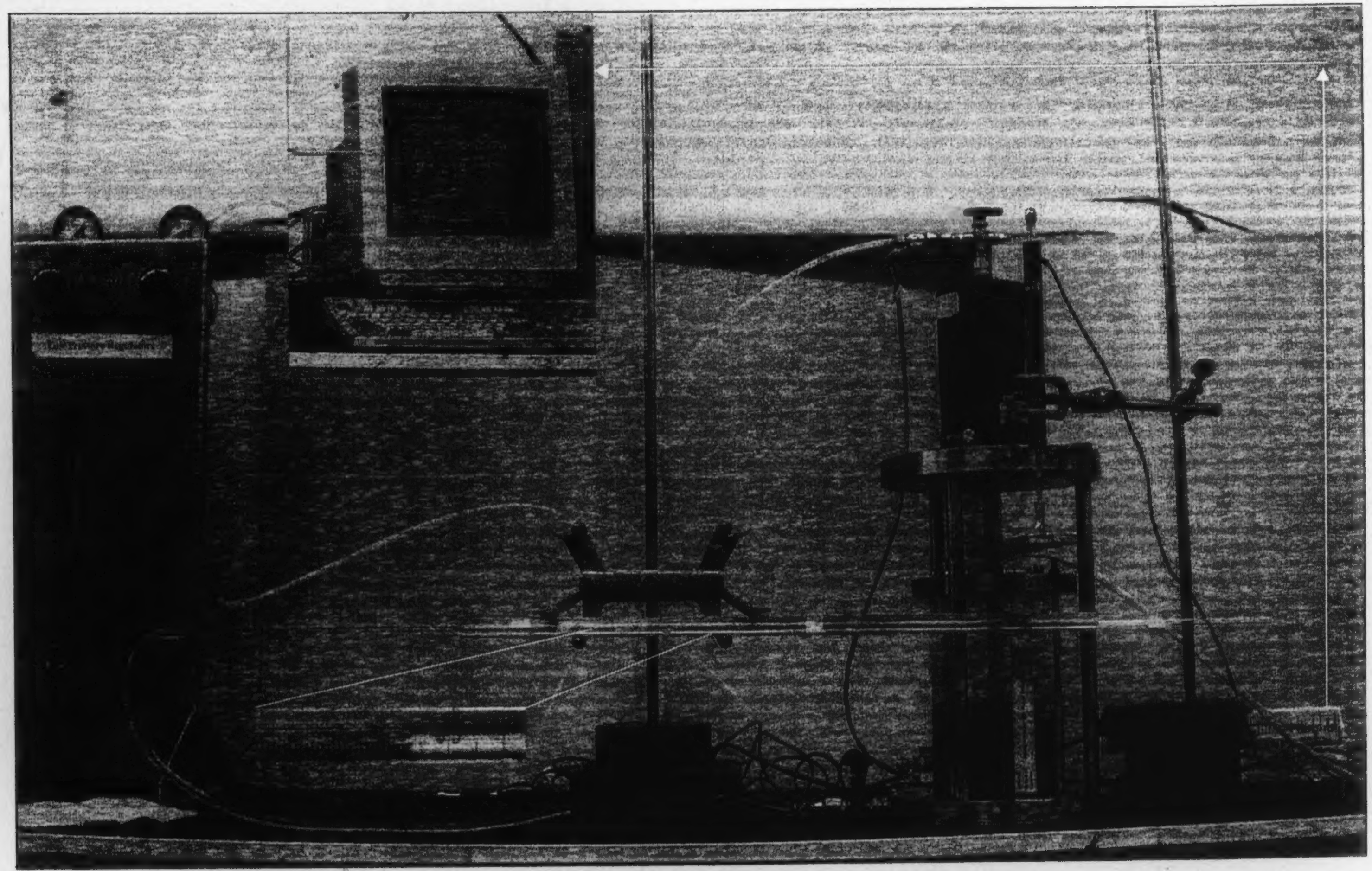

Figure 3.2: Setup for consolidation test

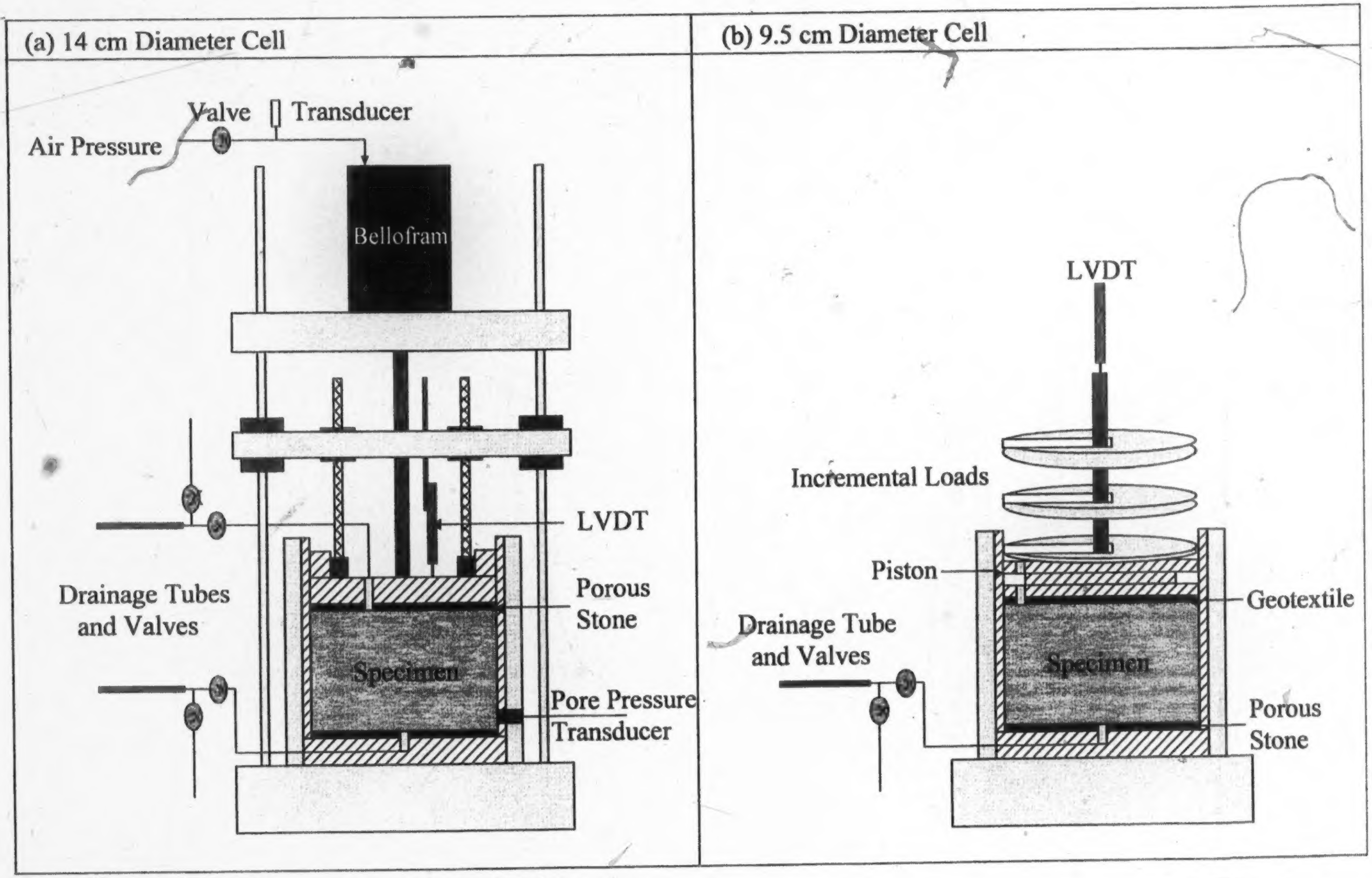
(a) 14 cm Diameter Cell
Valve
Transducer
Air Pressure
Bellofram
LVDT
Drainage Tubes and Valves
Porous Stone
Specimen
Pore Pressure Transducer
(b) 9.5 cm Diameter Cell
LVDT
Incremental Loads
Piston
Geotextile
Drainage Tube and Valves
Specimen
Porous Stone

Figure 3.3: Schematic of two cell types for consolidation testing

A 14 cm diameter cell allowed the application of high loads using air pressure and the determination of pore pressure during the test. This cell was used for the ore and the PAL slurries to understand the solid-liquid separation behavior for these materials. On the other hand, the 9.5 cm diameter cell was used for polymer modified slurries because of the improved engineering behavior and the associated preclusion of high loads and pore pressure measurements during the test. Due to the reduced test duration for this latter cell, a larger number of samples could be tested.

The 14 cm internal diameter cell had a wall thickness of 0.75 cm. To measure pore pressure, a 0.16 cm diameter hole was drilled in the wall close to the base. The top and bottom plates had a network of circumferential and radial grooves to facilitate dewatering. To each of these plates, a porous stone was fastened and was used as a filter; both plates were connected to external ports. Further, each plate had a pair of 'O' rings, which prevented sample escape, ensured minimal friction and improved stability. The cell body was connected to the bottom plate using four equidistant 1.25 cm rods supported by a frame.

The 9.5 cm internal diameter cell had a wall thickness of 0.50 cm. In this apparatus, the bottom plate was identical to the 14 cm diameter cell and similarly connected to an outside port. The piston was cut from a PVC rod and had eight equidistant 0.50 cm diameter holes along the periphery for drainage; a geotextile was used as a filter. The piston had two plates and a 1.0 mm extended geotextile to prevent sample escape and ensure minimal friction and tilting.

In the larger cell, compressed air pressure regulated by a pressure gage was applied to the sample using a bellofram diaphragm system. On the other hand, a known mass of load was applied to the sample in the smaller cell. For both types of cells, Linear Variable Displacement Transducers (LVDT) connected to the data acquisition system measured vertical displacement of the top cap due to load application.

For use in the consolidation test, the test equipment was first calibrated. As stated earlier, these included a diaphragm air cylinder (Type SS from Bellofram Corporation) for transferring air pressure from the air source to the loading ram; a 200 kPa pore pressure transducer (MPX2200 from Motorola Inc.); and a 15 cm linear potentiometer (HLP300 from Penny & Giles Controls Ltd.). The diaphragm and the transducer were calibrated by connecting these in series with a proving ring and applying a regulated air pressure. Likewise, the linear potentiometer was calibrated using a linear potentiometer calibrator. Figure 3.4 gives the calibration of the diaphragm and the two measuring devices.

The consolidation test was conducted on specimens at an initial solids content of 15%. First, the slurry was allowed to undergo self-weight and the solid-liquid interface movement was monitored similar to the sedimentation test. Next, the top cap was placed on the cell and lowered to the slurry-water interface. Using the conventional step loading procedure, loads were applied when no more change in void ratio was observed under the previous load. Load increments for the larger cell included self-weight, 0.5, 1, 2, 4, 8, 16, 32, and 64 kPa and those of

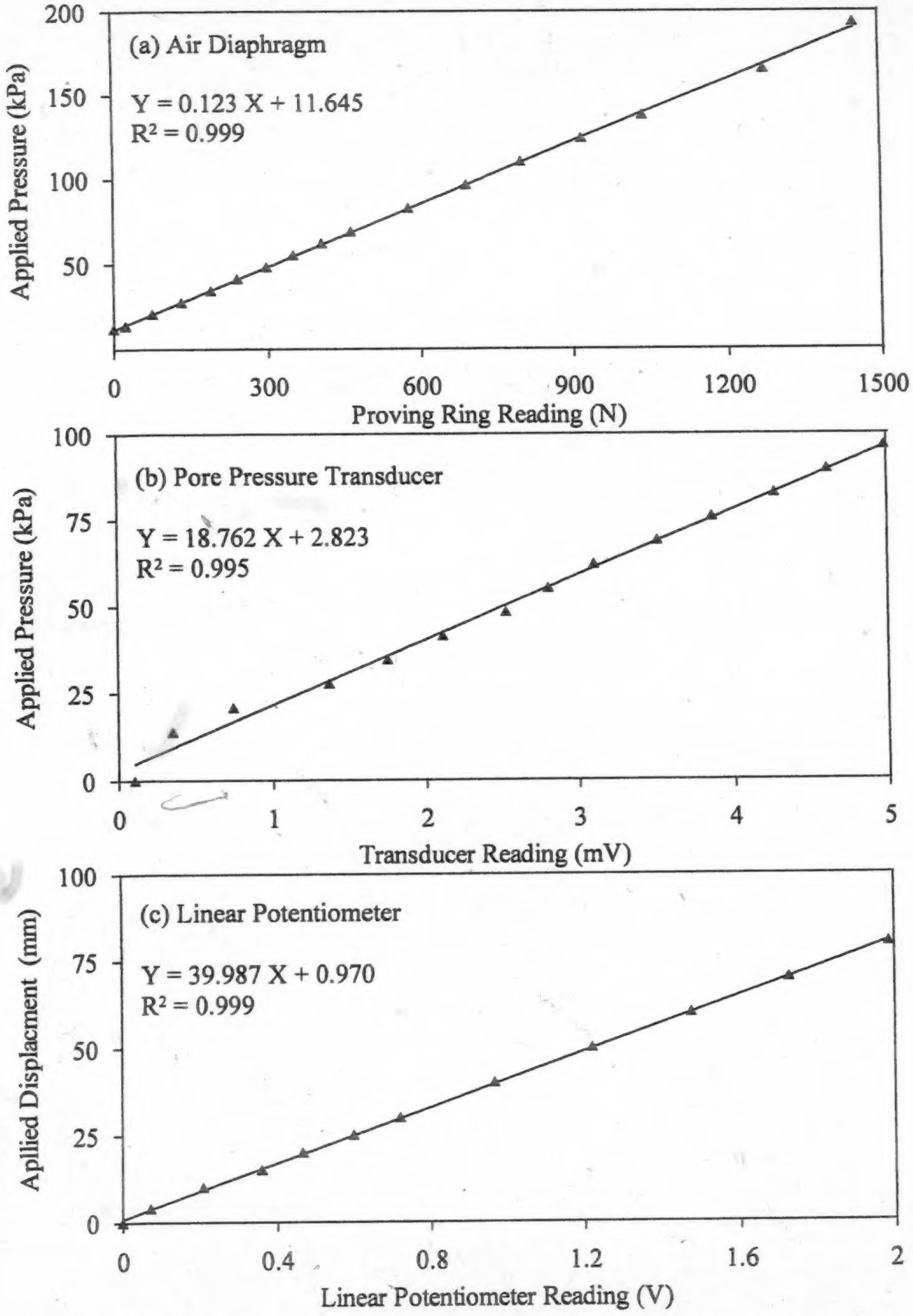

Figure 3.4: Calibration of devices used for the consolidation test

the smaller cell were self-weight, 0.5, 1, 2, 4, and 8 kPa. To simulate thickener conditions in the extraction process, a single upward drainage path was permitted during the test. For the large cell, water was collected from the upper drainage tube whereas for the small cell, a syringe was used for removing extra water. At all times during the test, water level was kept 1.0 cm above sample top.

Hydraulic conductivity was determined at the end of each load increment using the constant head method. This test was conducted similar to the ASTM Standard Test Method for Permeability of Granular Soils (D2434-68(2000)). For this purpose, water was passed through the sample from bottom to top. Flow of water was measured for one hour for the large cell and one half hour for the small cell. Based on experimentation, these durations were found to be enough for obtaining a steady state flow. Hydraulic conductivity (k, cm/sec) was calculated from knowledge of flow volume (Q, cm^3/sec) collected in time (t, sec), sample height (L, cm), surface area (a, cm^2) and head difference (h, cm) according to the following version of Darcy's law:

$$k = \frac{Q\,L}{a\,h} \tag{2.8}$$

Both the void ratio and the solids content were determined and plotted as functions of time as described previously. From knowledge of excess pore pressure data, the effective stress corresponding to each stress increment was calculated. The void ratio at the end of each load increment was plotted versus the resulting effective stress. On the same plot, a best-fit curve was developed for the experimental data to be called as the void ratio-effective stress relationship for the entire test. Hydraulic conductivity measured at the end of each load increment was plotted versus the void ratio and the data was fitted to the most appropriate curve to obtain the hydraulic conductivity-void ratio relationship.

Consolidation test were conducted to determine the above governing relationships, which were subsequently used to model thickener performance. Despite the low effective stresses in these thickeners, a number of load increments were used to obtain a representative correlation. To minimize floc deformation, a maximum of about 8 to 9 kPa loading was used for polymer modified materials. Experimentation showed that under the low applied stresses, it is difficult to liberate the entrapped water from the flocs.

3.5 STATISTICAL ANALYSIS

3.5.1 General

Statistical analyses were conducted for polymer modified laterite slurries including Type C and Type D samples. This section first provides a theoretical background of various statistical terms. This is followed by highlighting the significance and the application of statistical analysis for understanding the improved behavior of polymer modified slurries. Finally, this section shows how statistical analyses were used in this research to study the effect of various polymer parameters on the sedimentation and the consolidation behavior of laterite slurries.

3.5.2 Theoretical Background

3.5.2.1 General

This introductory section describes those basic concepts and the underlying assumptions of statistics, which are relevant to this research work. Therefore, this section develops the theoretical foundations necessary for a fundamental understanding of the quantitative nature of applied research based on experimentation. As such, the focus of this section is mostly on the functional aspects of the theoretical concepts.

3.5.2.2 Variables

The term *variable* refers to those things, items and entities, which are measured, controlled, or manipulated in research. In experimental research, some variables are manipulated (*independent variables*) and the effects of this manipulation on *dependent variables* are usually measured. Based on the type and scale of measurement, variables can be classified into four broad classes: nominal, ordinal, interval and ratio. *Nominal variables* such as gender and race can be assessed only in terms of categories but cannot be distinctly ranked or quantified. On the contrary, *ordinal variables* like economic status allow ranking but not quantification. *Interval variables* allow both ranking and quantification and include measurement of both time and space: examples include many types of scalars and vectors. Finally, *ratio variables* are similar to interval variables but they feature an identifiable absolute zero such as the Kelvin temperature.

3.5.2.3 Relationships

Data analysis in experimental research determines the relationship between independent and dependent variables provided that the values of those variables are distributed consistently in a sample of observations. Two basic features including the *magnitude* and the *reliability* characterize a relationship. Magnitude refers to the size or amount of variation in a relationship. On the other hand, reliability pertains to the truthfulness or the representativeness of the observed data for generalization. In other words, reliability is the probability of a relationship to recur for replicated samples drawn from the same *population* of items.

Relationships determine the extent of proportionality between two variables. The correlation line between two variables is called the *least squares line* because it is obtained by minimizing the sum of the squared distances of all the data points from the line. The magnitude of a relationship is determined by the *coefficient of determination* (R^2). The significance of a correlation with a particular magnitude depends on the sample size and the *outliers*. Outliers are atypical observations, which affect the slope of the correlation line and thereby R^2. To improve a correlation, certain outliers can be excluded from the analysis. However, such preclusion depends on the physical phenomena: some outliers are extreme observations. Therefore, scientific conclusions are always drawn by examining both the R^2 and the variation in data.

3.5.2.4 Statistical Significance

The statistical significance of a result is denoted by the p-value, which is based on the assumption that the observed relationship between variables in a sample occurs by chance (Brownlee, 1960). Generally, a higher p-value is associated with a lower probability of the observed relationship being indicative of the relationship between the respective variables in the population. Therefore, the p-value indicates the probability of error involved in accepting observed results. In most experimental studies, results that yield $p \leq 0.005$ are called highly significant, $p \leq 0.01$ are considered significant whereas $p \leq 0.05$ is known as borderline significant.

3.5.2.5 Sample Size

Magnitude and reliability of relationships between variables are inter-dependent provided sample size is kept constant. Typically, the larger the magnitude of the relationship between variables in a sample of a particular size, the more reliable the relationship. Further, the probability of obtaining by chance a strong and a significant relationship between variables is relatively high for small sample size. Therefore, the necessary minimum sample size increases as the magnitude of the effect to be observed decreases. If no relationship exists between two variables, then the required sample size would approach the population size that is assumed to be infinitely large. In most experimental studies, sample size is determined by the number and the maximum possible values of the dependent variables to be observed.

3.5.2.6 Distribution Function

The link between the magnitude and the significance of a scientific relationship between different variables gives the p-value and the probability of error involved in rejecting the relationship. For simplicity, the probability function is generally derived from an assumed normal distribution. According to Pearson (1894), this bell shaped curve is defined by a sample mean ($\underline{x}$) and a sample variance (S^2). These two fundamental statistical concepts are mathematically described by the following two equations:

$$\underline{x} = \frac{\sum x_i}{N} \tag{2.9}$$

$$S^2 = \frac{\sum (x_i - \underline{x})^2}{(N-1)} \tag{2.10}$$

where, x_i = observed result

N = number of observed results

Generally, design of experiments based on normal distribution necessitates a large enough sample size. This is because all types of shape for the sampling distribution approach a normal with an increase in sample size (Fisher, 1928). Therefore, all influencing parameters required for a good design of experiment can be determined from background knowledge of population variance and regardless of the type of distribution. Likewise, a sample size can be computed in case population variance is unknown and such determination is also independent of the type of distribution curve.

3.5.3 Application

3.5.3.1 General

Designing a proper experimental program, conducting meticulous testing and performing thorough analysis of the observed data lead to drawing reliable conclusions. This section describes the statistical methodology used in this research. First, the design of experiments is presented with a focus on the 2^k factorial designs. This is followed by presenting the procedure for the analysis of variance (ANOVA) and the use of the statistical software, MINITAB, is described in detail. Next, the application of the above statistical techniques to both sedimentation and consolidation of polymer modified laterite slurries is given with special focus on the development and validation of the statistical models.

3.5.3.2 Design of Experiments

One of the aims of this research was to understand the statistical significance of various polymer parameters on the solid-liquid separation of laterite slurries. For this purpose, a 2^k factorial design of experiments was adopted to develop a statistical model. This method minimized the number of experiments by considering each factor at two levels: high and low. Table 3.4 gives the designation of various polymer characteristics used in this experimental design. This table denotes all the lows by –1 and all the highs by +1. Similarly, anionic polymers are symbolized by –1 and cationic polymers by +1. Such a notation is generally used for simplicity in the analysis of properly designed experiments (Montgomery 1991).

Table 3.4: Designation of polymer parameters for use in experimental design

Type	Charge	MW	Dosage
Anionic = -1	Low = -1	Low = -1	Low = -1
			High = +1
		High = +1	Low = -1
			High = +1
	High = +1	Low = -1	Low = -1
			High = +1
		High = +1	Low = -1
			High = +1
Cationic = +1	Low = -1	Low = -1	Low = -1
			High = +1
		High = +1	Low = -1
			High = +1
	High = +1	Low = -1	Low = -1
			High = +1
		High = +1	Low = -1
			High = +1

Since, the validity of results only depends on the size of the sample, each specimen, arising from a combination of the four factors in Table 3.4, was picked randomly. Further, a separate polymer stock solution was prepared for each specimen. This precluded the experimental bias that could possibly be induced by the use of the same polymer stock solution for more than one test. In some cases, replicate specimens were prepared to provide additional reliability to the statistical model.

Four separate types of models were prepared for: (i) sedimentation of polymer modified laterite ore slurries; (ii) consolidation of polymer modified laterite ore slurries; (iii) sedimentation of polymer modified laterite PAL slurries; and (iv) consolidation of polymer modified laterite PAL slurries.

3.5.3.3 Analysis of Variance

The theory of analysis of variance (ANOVA) is beyond the scope of this work. However, it is important to understand that the analysis is conducted to obtain statistical significance by partitioning the total variance into components and comparing these components under hypothetical situations. It is also noteworthy to realize that a good experimental design is obligatory to carry out proper analysis of variance. As can be observed from Table 3.4, laboratory tests were conducted by varying only one factor at a time thereby minimizing the number of tests. The main reason of using this powerful tool was to statistically analyze the complex phenomena of colloid-polymer-electrolyte interaction for understanding the solid-liquid separation behavior of laterite slurries.

Analysis of variance was conducted using the statistical software called MINITAB (Release 13.30). A factorial design depicted in Table 3.4 was created in the form of the given notations of –1 (for anionic polymers, low charge, low molecular weight and low dosage) and +1 (for cationic polymers, high charge, high molecular weight and high dosage). The observed data obtained from laboratory tests was used as an input. The output of ANOVA resulted in a model equation comprising of the four factors, representing each of the polymer parameters, and the significance (p-value) of each of these factors. The equation was usually of the following form:

$$Y = (x_1\, T_P) \pm (x_2\, C_P) \pm (x_3\, MW_P) \pm (x_4\, D_P) \tag{2.11}$$

where, Y = model response corresponding to the observed value

x_1, x_2, x_3, x_4 = model coefficients

T_p, C_p, MW_p, D_p = polymer type, charge, molecular weight, dosage, respectively

3.5.3.4 Sedimentation

Two independent statistical models were developed to study the sedimentation behavior of polymer modified laterite slurries. These included separate models for each of the polymer modified laterite ore slurries and the polymer modified laterite PAL slurries. Both models were based on sixteen tests as shown in Table 3.4. Replicate data was obtained for the former model from the initial stage of the consolidation tests. On the contrary, because of the minimal variation in observations, no replicate data was obtained for the latter model. The input and the output variable was the initial hydraulic conductivity (k_i).

3.5.3.5 Consolidation

Two types of independent statistical models were developed to study the consolidation behavior of polymer modified laterite slurries. Again, these models included one each for the polymer modified laterite ore and PAL slurries. As shown in Table 3.4, the former model was developed on the basis of sixteen tests without replication. The latter model was built on four observed results and twelve dummy data points based on the observed data.

To study the consolidation behavior of polymer modified laterite slurries, *log k-e* and *e-log* σ' relationships were modeled. These power relationships were translated to k values at known void ratios and to e values at known effective stresses. Therefore, the were first converted to a single points, which were subsequently used in statistical analysis.

3.5.3.6 Model Validation

To validate the aforementioned statistical models, additional laboratory testing was carried out. This included two sets of nine sedimentation tests for each of the laterite ore and PAL slurries. For these tests, the slurries were modified with low, medium and high molecular weight ionic polymers using low, medium and high dosages. Similarly, one consolidation test was conducted for each of the laterite ore and PAL slurries modified with a medium molecular weight ionic polymer and a medium dosage. Details of these tests were previously given in Table 3.3. The observed data were compared with the corresponding estimated data from statistical models.

3.6 NUMERICAL SIMULATION

3.6.1 General

Numerical simulations were conducted to extrapolate laboratory and statistical data for predicting field performance of the storage and the CCD thickeners used in the acid leaching process. Separate computer programs were used to model the sedimentation and large-strain consolidation behavior of laterite slurries for the two types of thickeners. This section first describes the salient features of the two thickeners and then gives an account of modeling the sedimentation and consolidation behavior of laterite slurries for the metal extraction process.

3.6.2 Thickeners

Thickening is the most cost effective method for solid-liquid separation of laterite slurries. Other alternatives such as filtration or centrifugation are either costly or difficult to apply to laterite slurries in the pressure acid leaching process. This section briefly describes the main functions of the two types of thickeners under study and their operation during the extraction process.

The storage thickener performs two functions. First, it thickens the slurry feed to the autoclave thereby minimizing the liquor volume. This increases autoclave capacity as well as efficiency by reducing the energy and acid requirement. Second, this thickener acts as a buffer storage tank between the feed preparation and the acid leaching stages. The main function of the CCD thickener is to rapidly separate the solids from the pregnant liquor. Further, a higher amount of the separated materials is required for increased yield.

Figure 3.5 illustrates the operation of a typical thickener used in the metal extraction process for laterite slurries. This figure shows that these cylindrical vessels have an inverted conical base. A dilute slurry is generally fed at the top and allowed to undergo solid-liquid separation under self-weight. The process is similar to that described earlier in this chapter and illustrated in Figure 2.11. Three observable zones include a clear liquid at the top, an intermediate sedimentation zone, and a consolidation zone (also known as thickening zone or compaction bed) at the bottom of the thickener. Drainage is allowed only in the upward direction and overflow is collected around the periphery at the top. After the completion of self-weight consolidation, the underflow is removed from the bottom of the thickener at regular intervals of time.

The time requirement for the slurry to remain in the thickener depends on the rate and amount of the solid-liquid separation process. Changing thickener geometry and introducing rakes in the thickener can achieve additional improvement but such redesign is beyond the scope of this research work. Improvement in the solid-liquid separation process is achieved by adding flocculating agents such as synthetic polymers. According to Kynch (1952), the settling rates are not a unique function of the solids content of flocculated slurries. Therefore, it is important to determine the applicability of laboratory test results to the operation of a continuous thickener. The suitability of sedimentation and large-strain consolidation tests to understand and improve the solid-liquid separation of laterite slurries needs to be investigated.

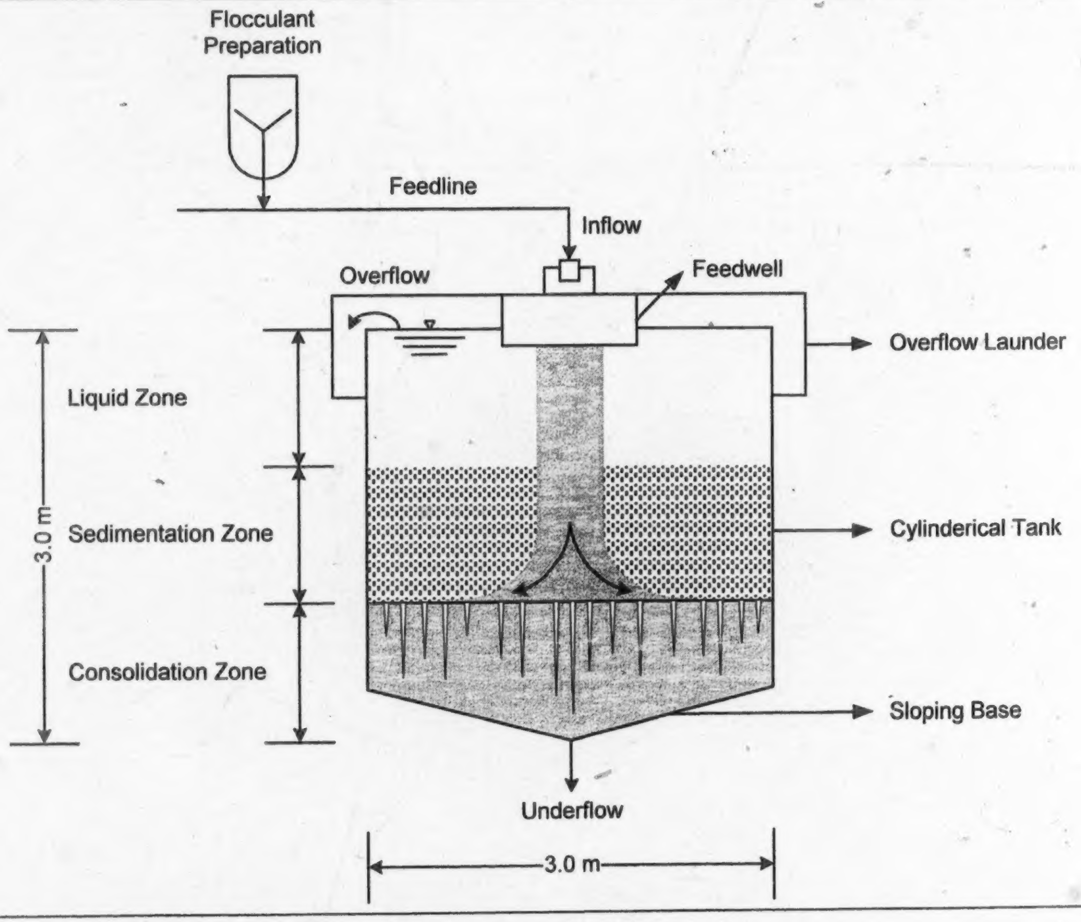
Flocculant Preparation
Feedline
Inflow
Overflow
Feedwell
Overflow Launder
Liquid Zone
3.0 m
Sedimentation Zone
Cylinderical Tank
Consolidation Zone
Sloping Base
Underflow
3.0 m

Figure 3.5: Schematic of a typical thickener used in the metal extraction process

3.6.3 Application

3.6.3.1 General

This section describes the application of computer software to model the sedimentation and consolidation behavior of laterite slurries. For both components of the solid-liquid separation process, the formulation of the numerical models and the use of the software are presented.

3.6.3.2 Sedimentation

The computer program developed by Chan & Masala (1998) was used for modeling the sedimentation behavior of laterite slurries. Based on the classical theory of sedimentation, the model required material properties, initial test conditions and the *log k-e* relationship to generate the sedimentation curve. Therefore, it was used for two purposes; to simulate observed sedimentation curves and to obtain hydraulic conductivity-void ratio relationships for missing data by successive iterations.

3.6.3.3 Consolidation

The computer program SECO, developed by Masala & Chan (2001), was used to model the consolidation behavior of laterite slurries. This program is based on the non-linear finite strain consolidation theory (Masala 1998). To account for non-linearity, the two relationships describing the large-strain consolidation behavior of laterite slurries were approximated to power laws. The parameters A, B and C,D were obtained from the *log k-e* and *e-log* σ' relationships, respectively, as given in the following two equations:

$$k = A\,e^{B} \tag{2.13}$$

$$e = C\,\sigma'^{D} \tag{2.14}$$

Formulated on the finite difference method, the program required material properties, initial test conditions and boundary conditions of the thickeners as inputs. A 15% initial solids content was used in the analysis for a 3.0 m high thickener with no underflow.

The computer software was used to simulate the consolidation behavior of four types of laterite slurries. These included laterite ore and PAL slurries and polymer modified laterite ore and PAL slurries. The output of the computer program was a solids content-time relationship. This output for the polymer modified slurries was compared to the ones obtained for ore and PAL slurries to estimate the improvement due to polymer addition.

3.7 LATERITE SLURRY CHARACTERISTICS DIAGRAM

3.7.1 General

A laterite slurry characteristics diagram (LSCD) is devised to understand the engineering behavior of this class of materials. A similar ternary diagram has been used to select viable tailings disposal alternatives for Alberta oil sands (Scott & Cymermann 1984). Shown in Figure 3.6, the diagram was used to understand the effect of soil structure on the geotechnical behavior of laterite slurries. The main soil characteristics that were studied in this research using the LSCD included consistency, sedimentation-consolidation and hydraulic conductivity.

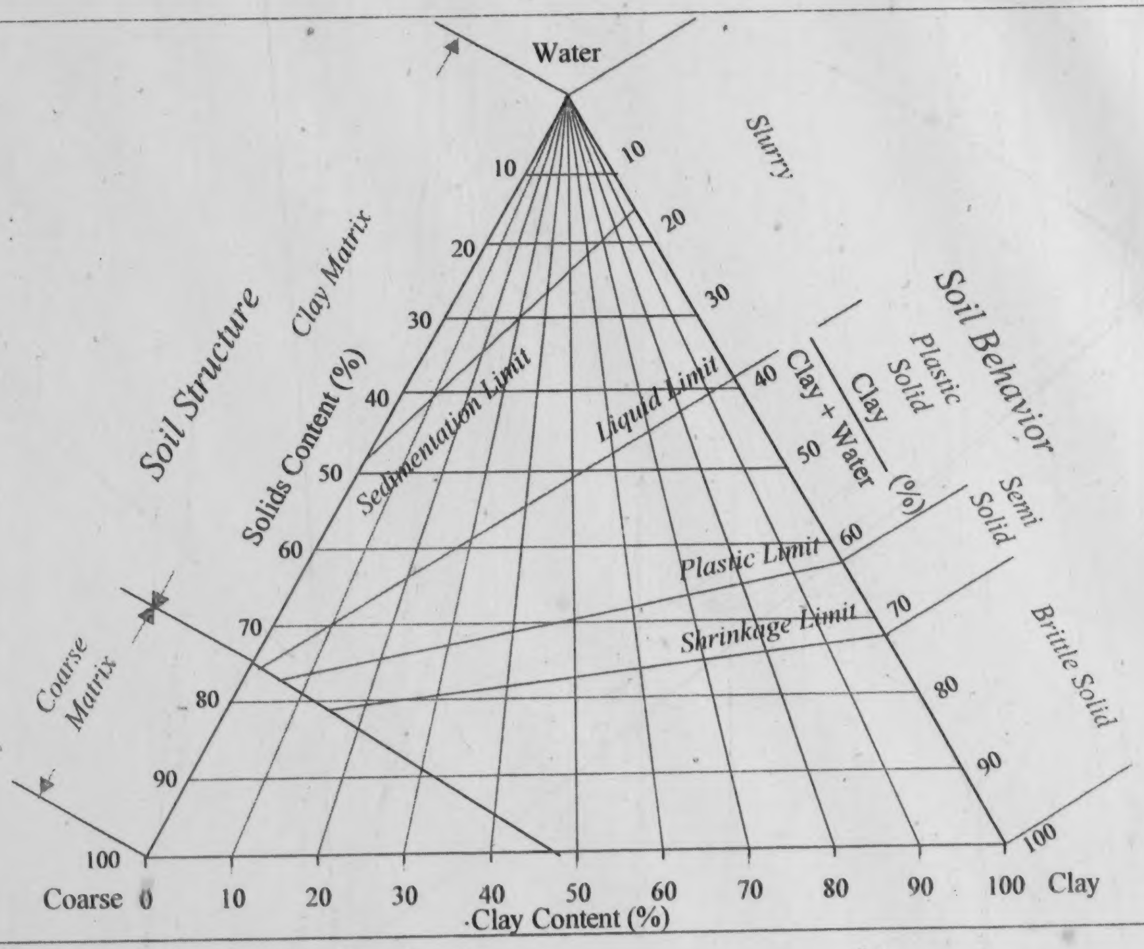
Water
Slurry
Soil Behavior
Plastic Solid
Clay / Clay + Water (%)
Semi Solid
Brittle Solid
Soil Structure
Clay Matrix
Coarse Matrix
Solids Content (%)
Sedimentation Limit
Liquid Limit
Plastic Limit
Shrinkage Limit
10
20
30
40
50
60
70
80
90
100
Coarse 0
10
20
30
40
50
60
70
80
90
100 Clay
Clay Content (%)

Figure 3.6: Laterite slurry characteristics diagram

3.7.2 Construction

Figure 3.6 illustrates that the LSCD is a ternary diagram having three apexes and three axes. The solids content is plotted on the left hand side, the ratio clay divided by clay plus water is given on the right hand side and the clay content is reported along the base; the apexes represent water, coarse and clay. The clay size fraction is defined as material finer than 0.002 mm. Points along the axis line connecting the water-fines apexes denote mixtures of clay and water only. Straight lines drawn from this axis line to the coarse apex signify *constant clay-water ratio lines*. Likewise, straight lines drawn from the base to the water apex describe *constant coarse-clay ratio lines*. These lines represent slurries with constant grain size distribution but varying solids content. Finally, the parallel horizontal lines depict soils with constant solids content.

Figure 3.6 shows that the LSCD presents soil structure on the left. Soil structure differentiates between a coarse matrix and a clay matrix. A coarse matrix is defined as one in which the coarse grains touch one another. The void ratio of the coarse particles can reach a maximum of 0.9 for a simple cubic arrangement of equal spheres. Under such conditions, clay is present in the pore space between the coarse grains. On the contrary, the coarse grains do not touch one another but are suspended in a clay matrix. The boundary between the two types of matrix is estimated according to the following equation (Azam & Al-Shayea 1999):

$$C(\%) = \frac{100\, e_s G_{sc} \quad w G_{sc} G_{ss}}{e_s G_{sc} + G_{ss}} \qquad (2.15)$$

where, C = clay content (by weight) to fill voids of the coarse matrix,

G_{sc} = specific gravity of the clay fraction

G_{ss} = specific gravity of the coarse fraction,

e_s = maximum void ratio of the coarse fraction taken as 0.9, and

w = water content of the entire soil mass

Soil behavior is depicted on the right side of the ternary diagram. Figure 3.6 shows five distinct types of soil behavior that depends on the amount of water present in the soil. These behavior types are separated by five limiting lines, which are based on observed data. The *segregation limit* defines the segregation or settling of particles in suspension. Above this line, coarse grains settle preferentially with respect to clays whereas below it such a phenomena is not observed. The *sedimentation limit* differentiates between sedimentation region (above the line) and consolidation area (below the line). This limit distinguishes a soil suspension from a soil slurry.

Figure 3.6 also gives the consistency limits to highlight the remaining part of soil behavior. The *liquid limit* pertains to an undrained shear strength of 2.5 kPa and denotes the boundary between a soil slurry and a plastic solid. The *plastic limit* means that soils above this limit behave like plastic solids and below this line like semi solids. Similarly, the *shrinkage limit* differentiates between a semi solid (above the line) and a brittle solid (below the line). It is expected that most of the data on laterite slurries obtained during this research would lie above the shrinkage limit.

Figure 3.6 shows that the five limiting lines describing soil behavior are part of the family of constant clay-water ratio lines. This means that the engineering behavior of soils is governed by physico-chemical phenomena between clay and water. Since, colloid-polymer-electrolyte interactions dictate the behavior of laterite slurries, the clay-water ratio lines provide a useful tool to understand the behavior of this class of materials.

3.7.3 Application

3.7.3.1 General

The ternary diagram constructed for Alberta oil sands has been used for the management of large volumes of tailings materials. During the last twenty five years, the diagram provided a design tool to devise alternative slurry disposal methods. In this research, the laterite slurry characteristics diagram was mainly used to understand the engineering behavior in the light of soil fabric. This section describes the application of the LSCD to these two soil characteristics.

3.7.3.2 Soil Structure

A review of the variation of soil morphology with decreasing water content was presented in Chapter Two. The ternary diagram was used to provide a fundamental understanding of the influence of soil microstructure on the solid-liquid separation of laterite slurries. This was achieved by empirically correlating soil fabric with sedimentation and consolidation. It was important to know the subdivision of the clay matrix into smaller units with distinct soil behavior.

3.7.3.3 Soil Behavior

Soil behavior is well documented in the geotechnical engineering literature. The focus of this study was to highlight the significance of clay-water ratio lines for a thorough understanding of the engineering behavior of laterite slurries: ore and PAL materials and their polymer modified versions. In this regard, the variation of hydraulic conductivity was given a special emphasis due to its significance in the solid-liquid separation of laterite slurries.

3.8 SUMMARY

A comprehensive research methodology was followed to understand and improve laterite slurries for the metal extraction process. Dynatec Corporation and Ciba Specialty Chemicals provided slurry materials and synthetic polymers, respectively. Four types of samples were prepared: laterite ore and PAL samples and polymer modified ore and PAL samples. Four laterite ore slurries were selected various from parts of the globe: Cuba, Philippines, Australia and Indonesia. The corresponding laterite PAL slurries were obtained using identical process conditions during pressure acid leaching. Synthetic polymers were used to modify ore and PAL slurries of a selected type representing limonite-saprolite blend from the Philippines. The research program adopted during this study comprised of four stages: laboratory investigations, statistical analysis, numerical simulation and data presentation using the devised laterite slurry characteristics diagram.

Laboratory investigations comprised of five distinct characteristics: geotechnical index properties, mineralogy, pore water chemistry, morphology, and solid-liquid separation. Details of the various testing techniques and modifications to suit laterite slurries were provided. Salient features of this investigation stage include the following:

- Heating was avoided in most cases but where absolutely necessary, an oven temperature of 50 °C was employed.
- Determination of specific gravity involved the use of vacuum for air removal and dry mass calculation after test completion.
- Grain size analyses were conducted on 25 g of dry soil using distilled water. The ores were dispersed with calgon whereas the PALs were not dispersed.
- Segregation tests involved solids content profiling with depth after 24 h in 150 mL graduated cylinders using different initial slurry solids contents.
- Consistency limits were determined by gradual drying of the high water content slurries at 50 °C; mixing time was restricted to five minutes.
- XRD analysis determined mineralogy of randomly oriented powdered samples with grain size distributions identical to those under ambient process conditions.
- Pore water composition was determined using routine methods. Due to negligible flocculant effects, detailed water chemistry was not investigated for polymer modified slurries.
- Morphology was determined using SEM analysis on slurry samples prepared by the cryogenic technique that ensured an intact fabric.

- Sedimentation tests were conducted on 15% initial solids content slurries poured in 8.5 cm diameter graduated cylinders to an initial height of 8.5 cm.
- The solid-liquid interface movement was captured using a camcorder connected to a computer; digital refinement improved accuracy.
- Consolidation test was used due to minimal experimental and theoretical errors and the ability to measure large strains and hydraulic conductivity.
- A 14.0 cm diameter cell that allowed the application of high loads and pore pressure determination during the test was used for ore and PAL slurries.
- A 9.5 cm diameter cell was used for polymer modified slurries because of the preclusion of high loads and pore pressure measurements during the test.

Statistical analysis was conducted for polymer modified samples to understand the significance of various polymer parameters on solid-liquid separation of laterite slurries. The theoretical basis of experimental design and analysis and the use of a statistical program MINITAB were described.

Numerical simulations were conducted to extrapolate laboratory and statistical data for predicting field performance of the storage and CCD thickeners used in the extraction process. The use of separate computer programs to model the sedimentation and consolidation behavior of laterite slurries was presented.

A Laterite Slurry Characteristics Diagram (LSCD) was devised to understand the engineering behavior of these materials. The construction and salient features and utilization of this diagram were presented. This ternary diagram was used to correlate structure and behavior of laterite slurries.

Chapter 4

Characteristics of Laterite Ore Slurries

4.1 GENERAL

Geotechnical characterization of laterite raw ore slurries is obligatory in understanding and improving the solid-liquid separation behavior of this class of materials. This knowledge is also pivotal for an economic assessment of different laterite ores for use in the metal extraction process. This chapter highlights the influence of geology and the environment on the solid-liquid separation behavior of four types of laterite ore slurries. These samples were selected from various parts of the globe: Cuba, Philippines, Australia and Indonesia. The Cuban sample represented a limonite ore whereas the Indonesian sample denoted a saprolite ore; the Philippines and the Australian samples corresponded to two distinct varieties of limonite and saprolite ores blends. For these samples, results of laboratory investigations pertaining to geotechnical index properties, mineralogy, pore water chemistry, morphology and solid-liquid separation characteristics are discussed. This is followed by providing the results of numerical simulation of the laboratory data to predict filed performance of the storage thickener. Next, the laboratory and modeling data is depicted on the laterite slurry characteristics diagram constructed for the ore sample. Finally, a summary and the main conclusions drawn from this chapter are given.

4.2 GEOTECHNICAL INDEX PROPERTIES

4.2.1 General

Geotechnical characterization of laterite ore slurries begins with an investigation of their index properties. These properties are used to classify laterite ores and to evaluate the performance of their slurries. Table 4.1 summarizes the geotechnical index properties of laterite ore slurries. This table indicates similarities and contrasts in samples of different origin. Derived from geology, the color of these samples denotes their composition that controls their distinct set of properties. This section discusses of the geotechnical index properties of laterite ore slurries.

4.2.2 Water Content

Table 4.1 gives the water content of different laterite underflow slurries in the storage thickener. The table indicates that all samples are associated with high water content, which is attributed to the high water requirement for slurry preparation. The amount of water required to convert laterite ores for preparing suitable plant feed depends on the bond strength of particles, size of aggregates and mineral composition (Schramm 1996). Removal of strong sesquioxide coating on soil particles in these ores during wet screening is the key factor contributing to their high water demand (Golightly 1981). Table 4.1 indicates that the water content of the limonite-saprolite ores measures lower than both the limonite and the saprolite ores. This is attributed to the possible presence of clay minerals formed in relatively arid climate. Apart from being easily broken down, these clays adsorbed water that cannot be removed at a temperature of 50 °C (Mackenzie 1957).

Table 4.1: Geotechnical index properties of laterite ore slurries

	Sample Type and Origin			
Property	Limonite Ore	Limonite-Saprolite Ore		Saprolite Ore
	Cuba	Philippines	Australia	Indonesia
Color	Pinkish Red	Pink	Dark Gray	Reddish Brown
w (%)	193	163	173	305
s (%)	34	38	37	25
Gs	2.92	3.16	2.92	2.92
e	5.67	5.16	4.97	8.73
- 0.075 mm (%)	93	93	92	92
- 0.002 mm (%)	20	35	56	19
I_S	14.2	13.5	14.0	13.5
w_L (%)	60	83	95	108
w_P (%)	44	42	48	53
w_s (%)	35	25	29	29
I_P (%)	16	41	46	55

The solids content of laterite underflow ore slurries in the storage thickener gives an insight into their dewatering behavior. Table 4.1 indicates a variable amount of water release for the investigated ore slurries despite the fact that the solids content after slurry preparation is the same for all. The table shows that the limonite-saprolite ore slurries release more water than the other two ore slurries. Thus, the former slurries coalesce the positive characteristics of both ore types. This is attributed to the combined effect of geology that imparted mineralogical composition and environment described by pore water chemistry. Detailed discussion of the influence of these compositional and environmental factors on the solid-liquid separation behavior of laterite ore slurries is discussed latter in this chapter.

4.2.3 Specific Gravity

Table 4.1 indicates that the specific gravity of laterite ores is higher than most sedimentary soils and falls within the range 2.8 to 3.2, common for residual soils. This is attributed to the presence of heavy iron oxides in these ores (Gidigasu 1976). The high values of specific gravity of the raw ores partly contribute in improving the solid-liquid separation behavior of the slurries. Slight improvement is observed for the limonite-saprolite ore slurry from the Philippines that has a specific gravity of 3.16. This value of specific gravity is also responsible for a higher value of void ratio of the Philippines ore slurry despite its low solids content. For all ore slurries, the corresponding void ratios reflect the underflow solids content in the storage thickener due to similar values of specific gravity.

4.2.4 Grain Size Distribution

Figure 4.1 gives the grain size distribution of various laterite ore slurries. Results of the combined hydrometer and wet sieve analyses depict the true grain sizes of the investigated slurries because complete dispersion was achieved during the test (Townsend et al. 1971; Wintermeyer & Kinter 1954). Based on ASTM definitions, the figure distinguishes between three grain sizes for laterite ore slurries. A sand size refers to material coarser than 0.075 mm and a clay size pertains to material finer than 0.002 mm; a silt size is sandwiched between the former two sizes of grains.

Figure 4.1 shows that the amount of sand size material is only 7 to 8% for all of the laterite ores; material finer than 0.075 mm is in the range of 92 to 93% as indicated by Table 4.1. This means that similar slurry preparation procedures are adopted throughout the world and therefore the resulting laterite ore slurries are generally composed of very fine materials. Figure 4.1 further illustrates that bulk of the materials of all of the laterite ore slurries fall in the silt and clay size regions. However, as indicated by this figure and Table 4.1, the amount of clay size material in each of the ore slurry is variable. According to Golightly (1981), the variability in the grain size distribution curves of various types of laterite ore slurries is due to the variable degree of removal of sesquioxide coating from soil particles during wet screening. As stated earlier, such a removal primarily depends upon particle bond strength, aggregate size and mineralogical composition (Schramm 1996).

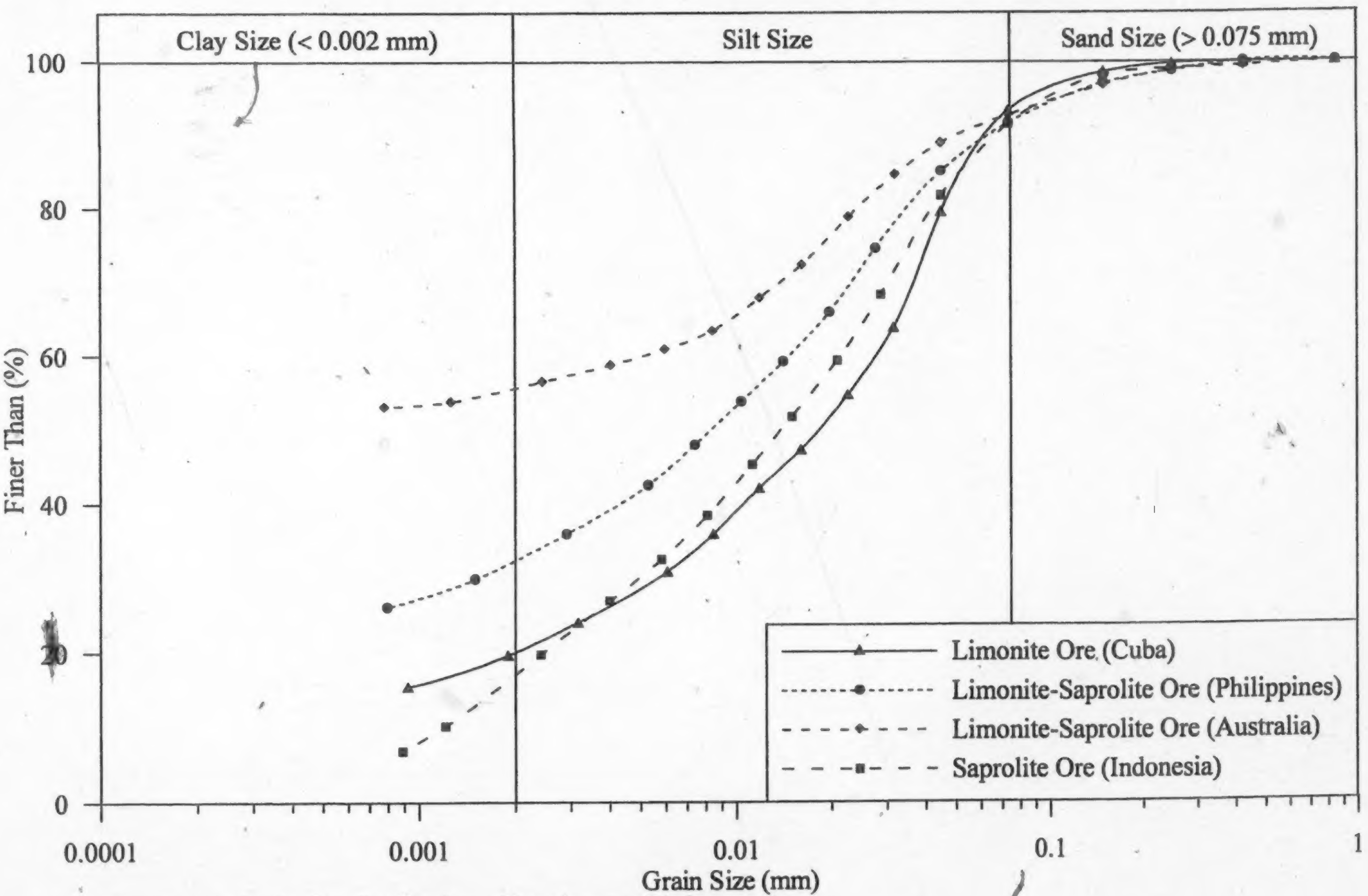

Figure 4.1: Grain size distribution of laterite ore slurries

Figure 4.1 indicates that the limonite ore slurry from Cuba is a slightly gap-graded material (concave upward gradation curve with clearly defined inflection points) containing a clay size fraction of 20%. On the contrary, the limonite-saprolite ore slurry from Philippines is well-graded (relatively linear gradation curve and vague inflection points) with a clay content of 35%. The limonite-saprolite ore from Australia is a poorly-graded slurry as more than half of the material is finer than the clay size. The linear gradation curve of the saprolite ore from Indonesia indicates a well-graded slurry and an amount of the clay size material equal to 18%.

Grain size distribution influences the mechanical and the physico-chemical interactions of laterite ore slurries. First, the very fine gradation of these slurries is partly responsible for the high void ratios in the storage thickeners as indicated in Table 4.1. Second, well-graded materials help minimize segregation of the clay and coarse fractions as discussed in the next section. Third, the clay size fraction of these slurries governs the colloid-electrolyte interactions, which in turn, influence plasticity, volume change and hydraulic conductivity.

4.2.5 Segregation

Figure 4.2 gives the results of the segregation tests on various laterite ore slurries in the form of normalized height versus solids content for different initial solids content. This figure shows that the observed solids content increases with depth and that the profiles tend to reach the vertical with increasing initial solids content. This behavior is attributed to diminishing segregation at high initial solids

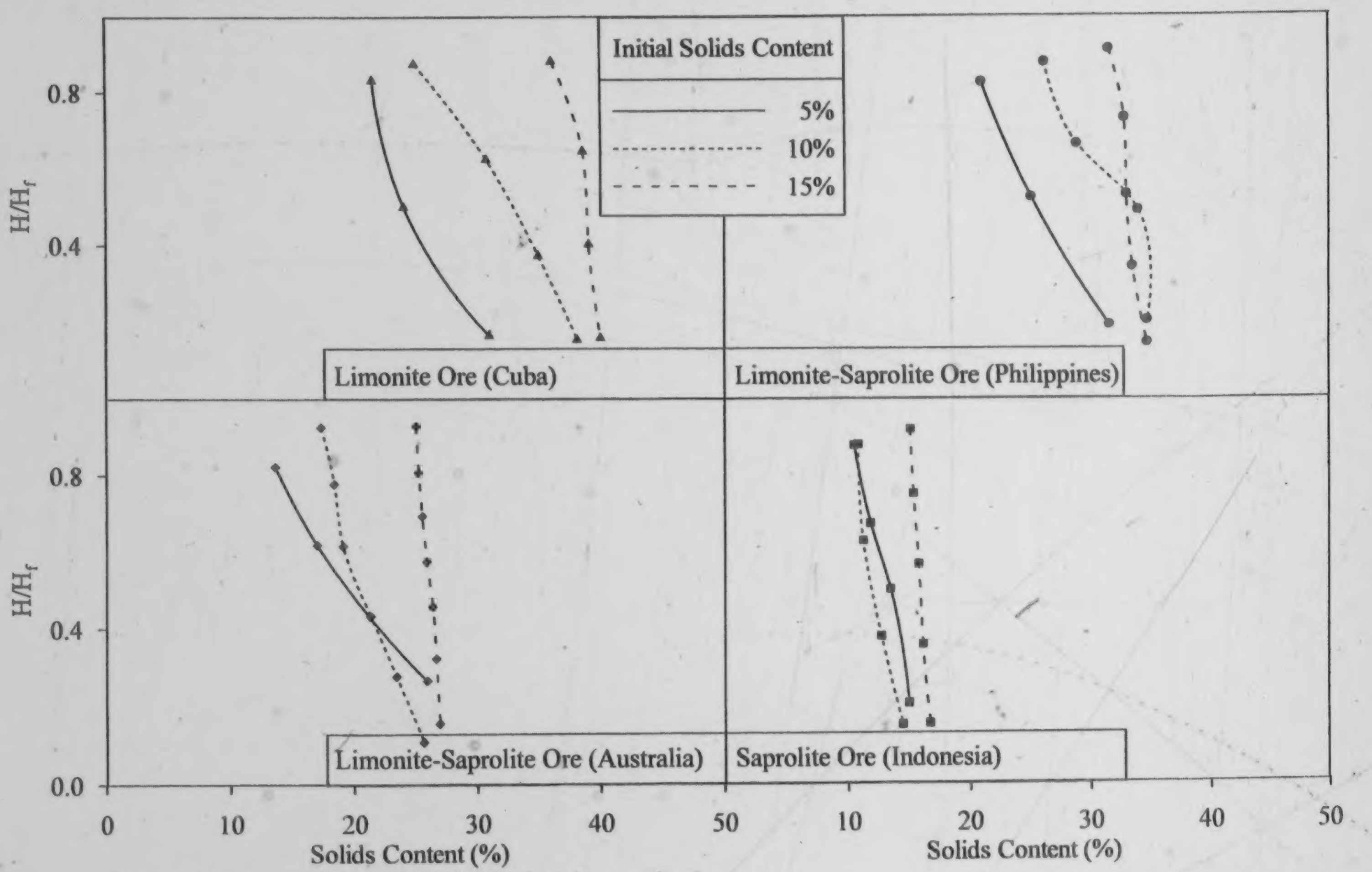

Figure 4.2: Segregation test results for laterite ore slurries

content, which correspond to higher amounts of clay size grains in the samples. These clay size grains tend to create a mesh in which the coarse grains are trapped and hence the latter cannot settle first (Caughill et al. 1993). The entrapment of coarse grains by clay size grains is clearly observed in the limonite-saprolite ore slurries, both of which contain high clay size fractions. Conversely, the gap-graded limonite ore slurry from Cuba with 20% clay size fraction shows greater deviation from the vertical for all values of initial solids content. Despite a low clay size fraction, the saprolite ore slurry from Indonesia exhibits minimum segregation due to its well-graded grain size distribution.

Figure 4.3 gives the percentage of segregation as a function of the initial solids content for various laterite ore slurries. This figure indicates that variation in the segregation characteristics of different slurries is marginal owing to the low and nearly same amount of coarse size material. Most of the laterite slurries are indicated to exhibit 3 to 12% segregation. The only exception is the limonite-saprolite ore slurry from Australia that shows 23% segregation at 5% initial solids content. This single point is attributed to the poor gradation of the slurry or a possible experimental error.

On Figure 4.3, a segregation limit (I_S) is defined as the initial solids content that pertains to 5% segregation with depth measured during the test. Based on this definition, I_S values for the four laterite ore slurries are given in Table 4.1. These values indicate that all of the laterite ore slurries are essentially non-segregating at an initial solids content of 15%.

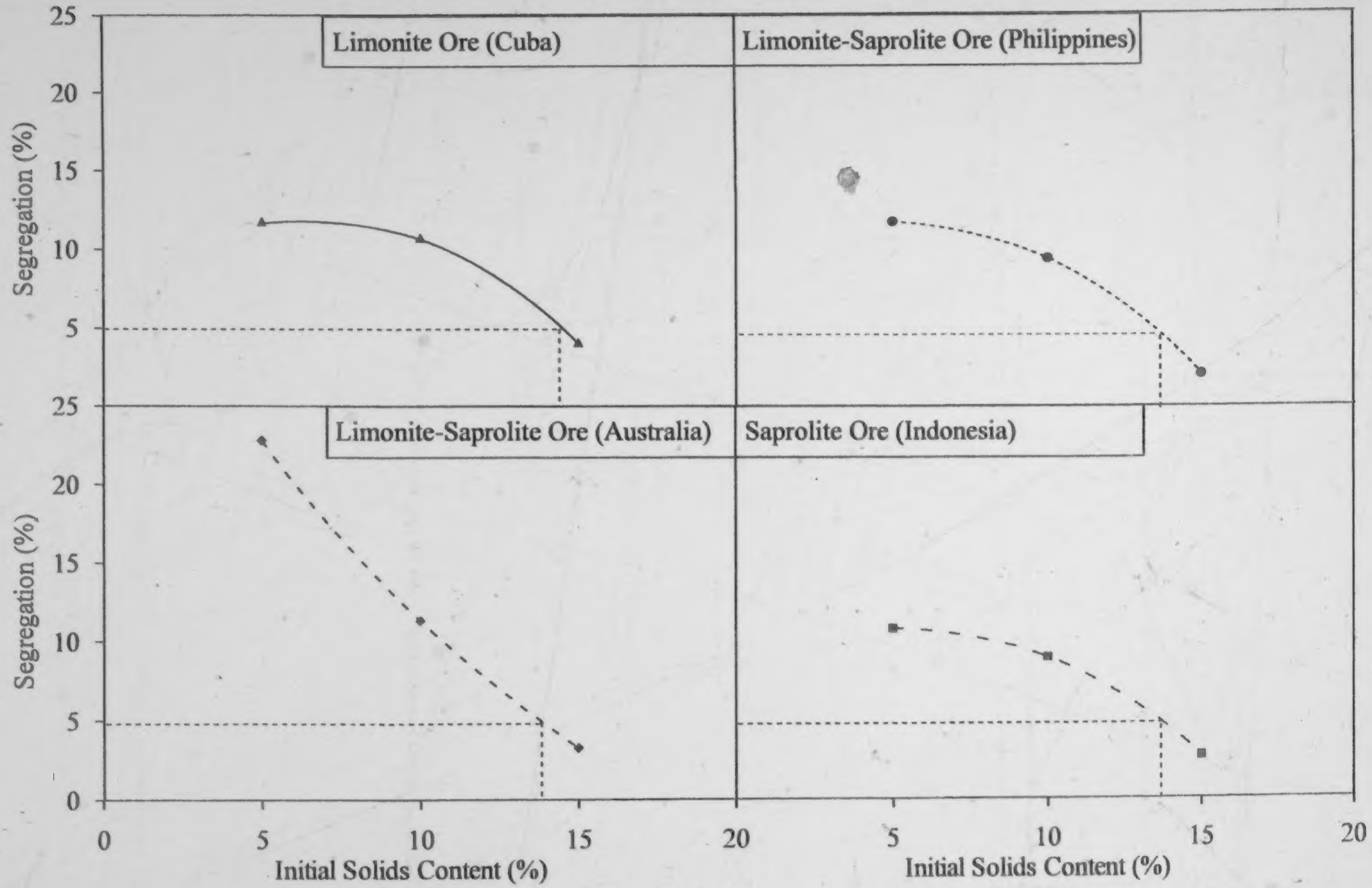

Figure 4.3: Segregation limit for various laterite ore slurries

4.2.6 Consistency Limits

Table 4.1 indicates that laterite ores have variable consistency limits. This is attributed to their distinct mineralogy, which is derived from geology and the environment, as well as chemistry of the pore water used during slurry preparation. The high consistency limits of some of the laterite ores suggest the possible presence of clay mineral species as well as amorphous materials such as iron oxide and silica (Mitchell 1993). Despite the high amount of clay size fraction, the low consistency limits of the limonite-saprolite ore from Australia indicate that the water used for feed preparation contained high concentrations of various electrolytes.

The plasticity chart (Casagrande 1948) gives a preliminary assessment of the mineralogical composition of soils. Figure 4.4 that shows the regions of various clay minerals and sand, plots various laterite ores on such a chart. This figure illustrates that all of the laterite ores fall in the high liquid limit zone and below the A-Line. According to Holtz & Kovacs (1981), soils plotting in this region of the plasticity chart can be classified as micaceous fine sandy and silty clays. Based on their position on the plasticity chart, these laterite ores are expected to contain micaceous clay minerals such as chlorite and hydrous mica as well as kaolinite. However, these minerals will only comprise part of the material in the laterite ores and the bulk is expected to be composed of iron and aluminum oxides. A comprehensive account of the mineralogical composition of different laterite ores is given in the next section.

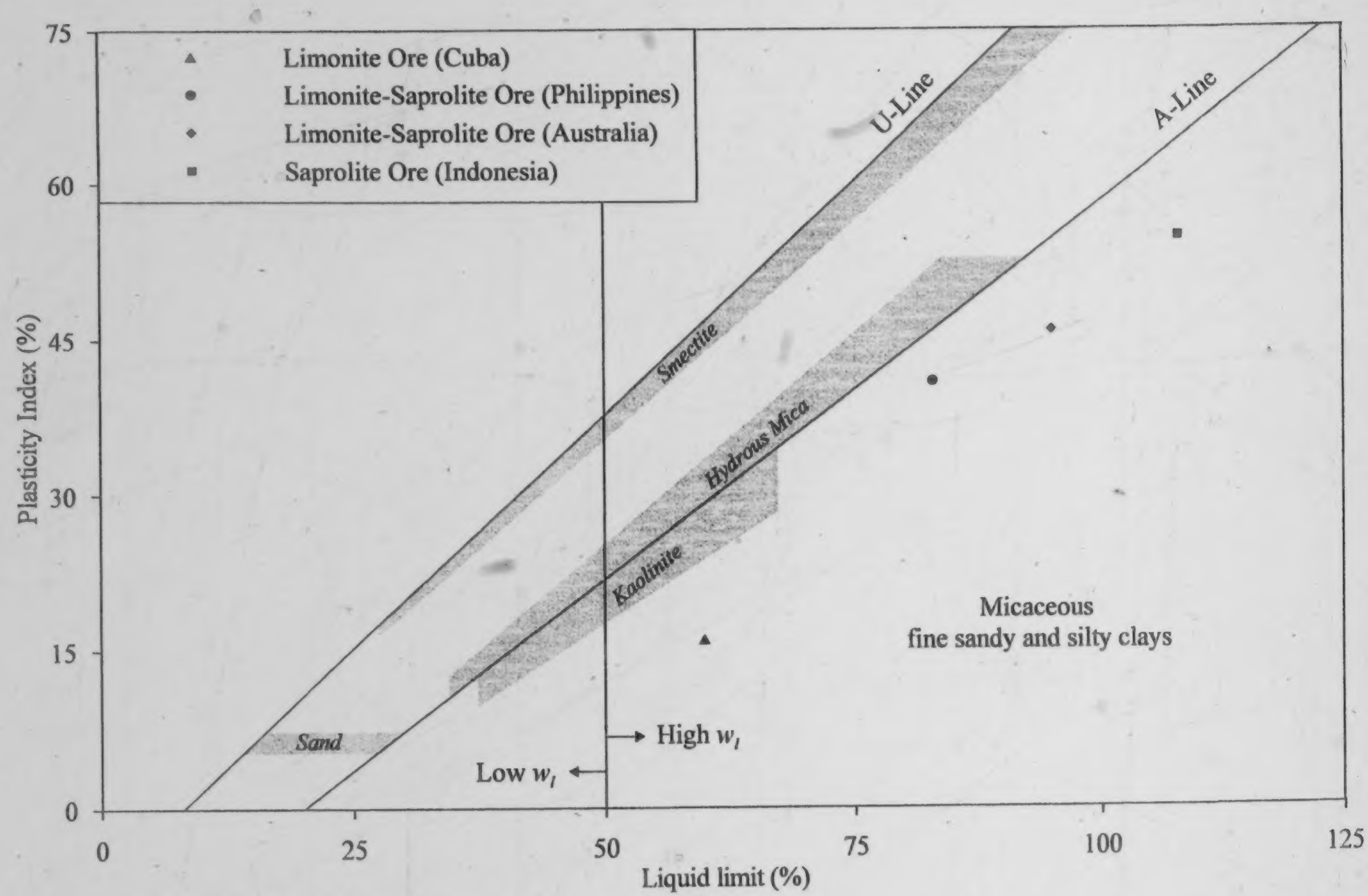

Figure 4.4: Plasticity chart for laterite ores

4.3 MINERALOGY

4.3.1 General

Mineralogical composition governs the size, shape and surface characteristics of soil particles. It determines the interaction of the solid phase with the liquid phase and hence affects sedimentation, consolidation and hydraulic conductivity (Mitchell 1993). Results of x-ray diffraction (XRD) analyses, anion exchange and cation exchange are discussed here.

4.3.2 X-Ray Diffraction

Figure 4.5 highlights the main constituent minerals on the x-ray diffraction patterns of bulk samples of the laterite ores. This figure shows that all of the laterite ores contain goethite (α-FeO.OH), which is derived from the conversion of olivine. According to Burger (1979) and Troly et al. (1979), such mineral transformation can take place under both humid and arid climates, which ensure intense and prolonged weathering under low pH (Mohr & Van Baren 1954). This process of *laterization* involves leaching of silica and accumulation of iron and aluminum oxides ((Loughnan 1969; Pickering 1962).

Figure 4.5 also shows maghemite (Fe_2O_3) and hematite (α-Fe_2O_3) for the limonite ore and both the limonite-saprolite ores; gibbsite ($Al(OH)_3$) is present in the former ore. The presence of maghemite and hematite in these samples is due to goethite *desiccation* that means the conversion of sesquioxide-rich material to secondary minerals (Sherman et al. 1953). Attributed to hot climate, such dehydration

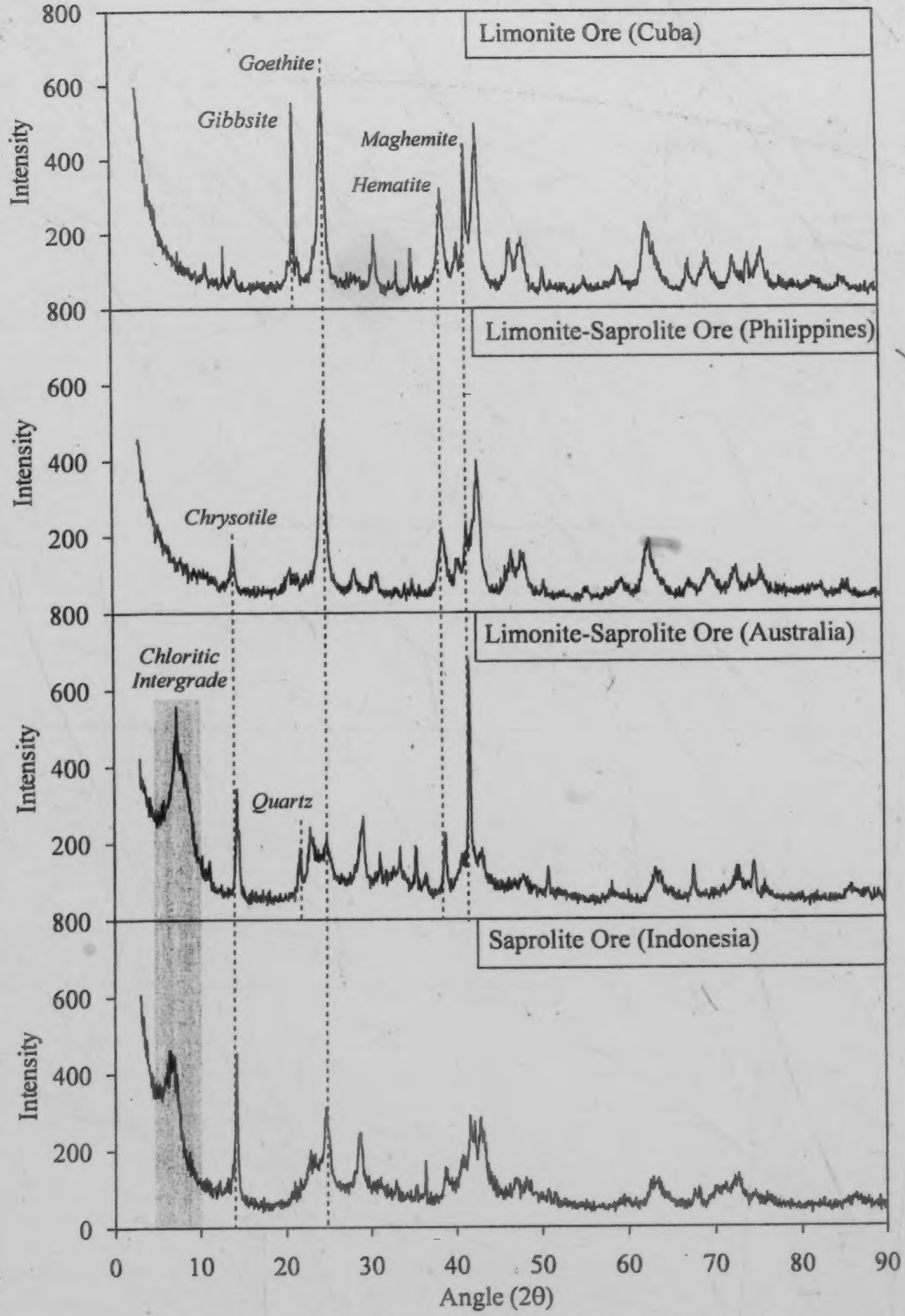

Figure 4.5: X-ray diffraction patterns of bulk samples of laterite ores

of colloidal hydrated iron oxides involves loss of water and crystallization of amorphous iron colloids into dense crystalline iron minerals (Hamilton 1964). However, part of the silica and iron oxides are not completely converted and occur in amorphous form as is shown for both the limonite-saprolite ores and the saprolite ore.

The x-ray diffraction patterns shown in Figure 4.5 for both the limonite-saprolite ores and the saprolite ore indicate the presence of various clay mineral species. All of these samples show the presence of 1:1 phyllosilicate clay having first and second order diffraction peaks at 14° and 28° angle (2θ); the second peak being 60% of the first peak. Having a *d* spacing of 7.05 Å, this clay mineral is identified as chrysotile, which is a member of the kaolinite-serpentine group. Chrysotile results from the oxidation or *serpentinization* of the olivine-rich parent rock known as peridotite and involves alteration of Mg and SiO_2 (Krause et al. 1997). This reaction also causes an increase in Mg^{2+} content in the soil (Golightly1979a).

Figure 4.5 also indicates the presence of indistinguishable 2:1 and/or 2:2 phyllosilicates between 5° and 7° angle (2θ) for the limonite-saprolite ore from Australia and the saprolite ore form Indonesia. Still, the figure reveals poorly crystallized material seen as shoulders on the low side of 7° angle (2θ), which are attributed to the presence of chloritic intergrade in these samples (Grim 1968). This hybrid mineral occurs between mica (*d* spacing of 10 Å) and chlorite (*d* spacing of 14 Å) and is the product of progressive weathering of deeply buried mica. According to Worrall (1968), such a weathering process causes *depotassification* (removal of K^+) in the crystal structure of mica that contains about 9% potassium. The extent of depotassification of mica governs the electro-chemical properties of the resulting intergrade mineral. The chloritic intergrade of the limonite-saprolite ore from Australia is more expandable-collapsible in nature as indicated by the sharp and higher peak at 7^o angle (2θ).

A comprehensive clay mineral identification was not carried out for various laterite ores. This is because of the fact that clay platelets are invariably coated with ultrafine sesquioxide particles thereby inhibiting the electro-chemical activity of the former. This means that clay minerals are less significant and detailed clay mineral identification is redundant for this application. To obtain a tangible bulk mineralogy, grain size distributions identical to ambient process conditions were obtained. The maximum grain size for bulk XRD specimens was 0.85 mm; fine extraction, preheating, and calcium and potassium presaturations were not done.

The amount of each mineral type in various laterite ore samples depends upon local provenance (climate, lithology and topography). Table 4.2 gives a semi-quantitative estimate of x-ray diffraction results for various laterite ores. This table indicates that all of the ores contain variable amount of heavy minerals such as goethite, hematite, maghemite and iron oxides. The presence of these heavy mineral species is the main factor that contributes to the high observed specific gravity of the ore materials depicted in Table 4.1.

Table 4.2. Percent amount of various minerals in laterite ores

Mineral	Sample Type and Origin			
	Limonite Ore	Limonite-Saprolite Ore		Saprolite Ore
	Cuba	Philippines	Australia	Indonesia
Chrysotile		10-15	10-15	15-20
Chloritic Intergrade			40-45	30-35
Goethite	60-65	55-60	10-15	15-20
Gibbsite	15-20			
Hematite	10-15	15-20	5-10	
Maghemite	10-15	10-15	10-15	
Silica and/or Iron oxides			10-20	25-35
Estimated G_s	4.0-4.9	3.9-4.8	3.1-4.7	2.9-3.9

Based on mineralogical composition, an estimate of specific gravity can be made using G_s values of 4.26 for goethite; 5.26 for hematite and maghemite (Gidigasu 1976); and 2.75 for clay minerals and gibbsite (Grim 1968). A comparison of Table 4.1 and Table 4.2 indicates discrepancies between measured and estimated G_s values for various laterite ores. This disagreement is attributed to the semi-quantitative nature of interpreting XRD results. Due to difficulty in quantification, amorphous materials were excluded from G_s calculation of the limonite-saprolite ore from Australia and the saprolite ore from Indonesia. This resulted in an underestimation of specific gravity for these ore samples.

Table 4.2 also explains the consistency behavior (depicted earlier in Table 4.1) of various laterite ores. The table shows that the ores containing high amount of clay minerals such as chrysotile and chloritic intergrade possess higher water holding capacity than those ores with low or no clay minerals. However, these clay minerals are not the only contributors to the high consistency limits of various laterite ores. Amorphous silica also tends to hold water due to adsorption and capillary condensation. The high amount of siliceous materials in the saprolite ore is responsible for providing additional plasticity due to its gelatinous characteristics (Briceno & Osseo-Asare 1995).

The limitations of XRD analyses for laterite specimens must be taken into account to better understand the results. Identification of amorphous materials with x-ray diffraction is not straightforward; non-crystalline materials appear as baseline noise on XRD patterns. The analyses depend on the degree of crystallinity of the material and the grain size. This latter parameter is critical due to coating of soils particles with sesquioxides, which are inconsistently removed during slurry preparation because of the variability in particle bond strength of different ores (Schramm 1996). The use of random samples results in an exposure of the different crystal faces thereby revealing all *d* spacings. This leads to weak diffraction peaks in specimens containing clay minerals, for which basal spacing intensity is reduced. Finally, the use of peak area method for calculating the amount of minerals is semi-quantitative and not suitable for amorphous materials. Despite these limitations, x-ray diffraction technique applied to laterite ores gives invaluable information about soil composition. To compensate for the limitations of the method, results of XRD analyses are supplemented by other tests.

4.3.3 Anion Exchange

Table 4.3 gives the anion exchange of laterite ores. The table indicates that the limonite ore has a marginal TAEC of 2.89 cmol(-)/kg. Derived from equal amounts of Cl^- and SO_4^{2-} ions, this value is attributed to the presence of goethite in the sample. On the other hand, the values of TAEC for all the other ores are much higher and almost equal. The high TAEC values associated with these ores owe their origin to the presence of chrysotile clay mineral, amorphous materials and sesquioxides. At pH values below PZC that ranges from 6.8 to 8.5 (Prafitt 1978), the broken edges of these mineral species facilitate a positively charged double layer (Mitchell 1993). Further, the TAEC of the ores is mainly derived from SO_4^{2-} ion because of the preferential adsorption of the ion (Tan 1998).

Table 4.3. Anion exchange of laterite ores

Exchangeable Anions (cmol(-)/kg)	Sample Type and Origin			
	Limonite Ore	Limonite-Saprolite Ore		Saprolite Ore
	Cuba	Philippines	Australia	Indonesia
Cl^-	1.51	1.36	1.22	3.00
NO_3^-	0.22	0.16	0.20	0.19
SO_4^{2-}	1.17	15.31	15.55	12.67
TAEC	2.89	16.83	16.97	15.86

4.3.4 Cation Exchange

Table 4.4 presents the cation exchange of laterite ores. The table indicates that the limonite ore exhibits a TCEC of 14.52 cmol(+)/kg, which is mainly derived from exchangeable Al^{3+} and Fe^{3+}. The high amount of these high valence cations is responsible for the high liquid limit of this ore, which is devoid of expansive clay minerals (Mitchell 1993). This is also true for the limonite-saprolite ore from Philippines, which has a TCEC of 18.87 cmol (+) / kg and is due to Mg^{2+}, Al^{3+} and Fe^{3+}. The high amount of Mg^{2+} in this latter ore is due to the presence of chrysotile in the specimen (Golightly1979a).

The higher TCEC values of the limonite-saprolite ore from Australia and the saprolite ore from Indonesia portray the type and amount of clay minerals present in these ores. The high amount of Mg^{2+} in both these ores is attributed to the presence of chrysotile clay mineral. Further, the significant amount of Na^{+} and Ca^{2+} in the former ore is associated with a more expandable-collapsible chloritic intergrade. The presence of Na^{+}, Ca^{2+} and Mg^{2+} in both the ores, a common feature of arid region soils (Brady 1990), indicates clay mineral formation.

Table 4.4 also translates the cation exchange of different laterite ores to their microstructure by reporting exchangeable sodium percentage (ESP). According to Mitchell (1993), soils with ESP < 2 possess a flocculated structure whereas those with ESP ≥ 2% are susceptible to dispersion. Therefore, with the exception of the limonite ore slurry from Cuba, slurries prepared from all the other ores are expected to possess dispersed soil morphology.

Table 4.4. Cation exchange of laterite ores

Exchangeable Cations (cmol(+)/kg)	Sample Type and Origin			
	Limonite Ore	Limonite-Saprolite Ore		Saprolite Ore
	Cuba	Philippines	Australia	Indonesia
Na^+	0.21	0.47	1.25	1.13
K^+	0.14	0.09	1.26	0.07
Ca^{2+}	0.13	1.50	8.77	2.73
Mg^{2+}	1.04	6.35	28.29	30.87
Al^{3+}	5.47	4.25	2.91	0.24
Fe^{3+}	7.32	6.11	2.11	1.58
TCEC	14.52	18.87	44.56	36.35
ESP (%)	1.45	2.49	2.81	3.11

4.4 PORE WATER CHEMISTRY

4.4.1 General

The characteristics of the water filling the pores of a soil have a profound effect on the interaction of the solid particles. The electro-chemical forces at the interface of pore water and solid particles govern soil behavior. This section presents the chemical characteristics of the pore water. These include pH and electrical conductivity and electrolyte concentration.

4.4.2 pH and Electrical Conductivity

Table 4.5, which summarizes the pore water chemistry, indicates that the water used in slurry preparation is generally neutral to slightly basic. This means that all materials are close to the PZC for the given mineralogy. Therefore, the conventional double layer theory is applicable to the colloid-electrolyte system of laterite ore slurries.

Table 4.5 indicates that the electrical conductivity (EC) measured for pore fluids of various laterite ore slurries varies significantly. Since, EC strongly correlates with soil composition (Grim 1968), the reported values confirm the mineralogy of various laterite ores. In general, silts have a medium EC of 50 to 300 and clays are associated with a high EC that ranges between 100 and 10,000 μS/cm. In addition to soil composition, the EC values are also affected by the presence of salts in the soil (Rhoades et al. 1990). Therefore, both the limonite-saprolite ore slurries are expected to have high concentrations of salt forming ions such as Na^+, Ca^{2+}, Mg^{2+}, Cl^- and SO_4^{2-}.

Table 4.5. Pore water chemistry of laterite ore slurries

Property	Sample Type and Origin			
	Limonite Ore	Limonite-Saprolite Ore		Saprolite Ore
	Cuba	Philippines	Australia	Indonesia
pH	7.1	7.2	7.5	7.3
EC (μS/cm)	156	744	12500	442
Na^+ (mg/L)	21.1	17.0	2530.0	9.8
K^+ (mg/L)	1.1	1.1	40.0	0.4
Ca^{2+} (mg/L)	3.5	19.5	134.0	2.1
Mg^{2+} (mg/L)	2.8	87.0	381.0	54.1
Mn^{2+} (mg/L)	0.001	0.002	0.007	0.147
Al^{3+} (mg/L)	0.008	0.016	0.120	0.008
Fe^{3+} (mg/L)	0.01	0.12	0.76	0.05
Si^{4+} (mg/L)	1.1	2.2	18.5	11.7
Cl^- (mg/L)	20.5	28.4	4070.0	16.7
NO_3^- (mg/L)	1.9	1.3	34.3	2.1
HCO_3^- (mg/L)	15	24	94	30
SO_4^{2-} (mg/L)	20.2	386.0	1300.0	185.0
TDS (mg/L)	77	550	8500	283

4.4.3 Electrolyte Concentration

Table 4.5 also gives the concentration of individual cations and anions present in the pore water of various laterite ore slurries. The table indicates that the chemical compositions of all these waters have the same trend; Na^+, Ca^{2+}, Mg^{2+}, Cl^- and SO_4^{2-} are present as major ions in all pore waters. It follows that water used during slurry preparation was obtained from identical sources having variable degrees of dilution. This is confirmed by plotting the various cations and anions depicted in Table 4.5 on the Stiff diagram as shown in Figure 4.6. This figures illustrates similar shapes of the Stiff diagrams, which are typical of seawater. It follows that readily available local waters were used for slurry preparation and that the sources of water were located in the proximity of the sea.

Flocculation of colloids results from a thinner double layer and a smaller surface potential (Mitchell 1993). Table 4.5 that also gives the total dissolved solids (TDS), indicates that the TDS values for the pore waters vary by two orders of magnitude. The TDS of pore water in the limonite ore slurry is 77 mg/L that can result in a thick double layer and a dispersed fabric for clay particles (Verwey & Overbeek 1948). However, due to the fact that this ore primarily consists of sesquioxides, which tend to occur in aggregations, a flocculated structure is expected for this slurry. On the contrary, dispersed fabrics are anticipated for all the other ore slurries owing to the presence of high amount of Na^+ ion. For a dispersed fabric, the influence of this ion overcomes that of all of the others ions and can therefore be called as the potential determining ion.

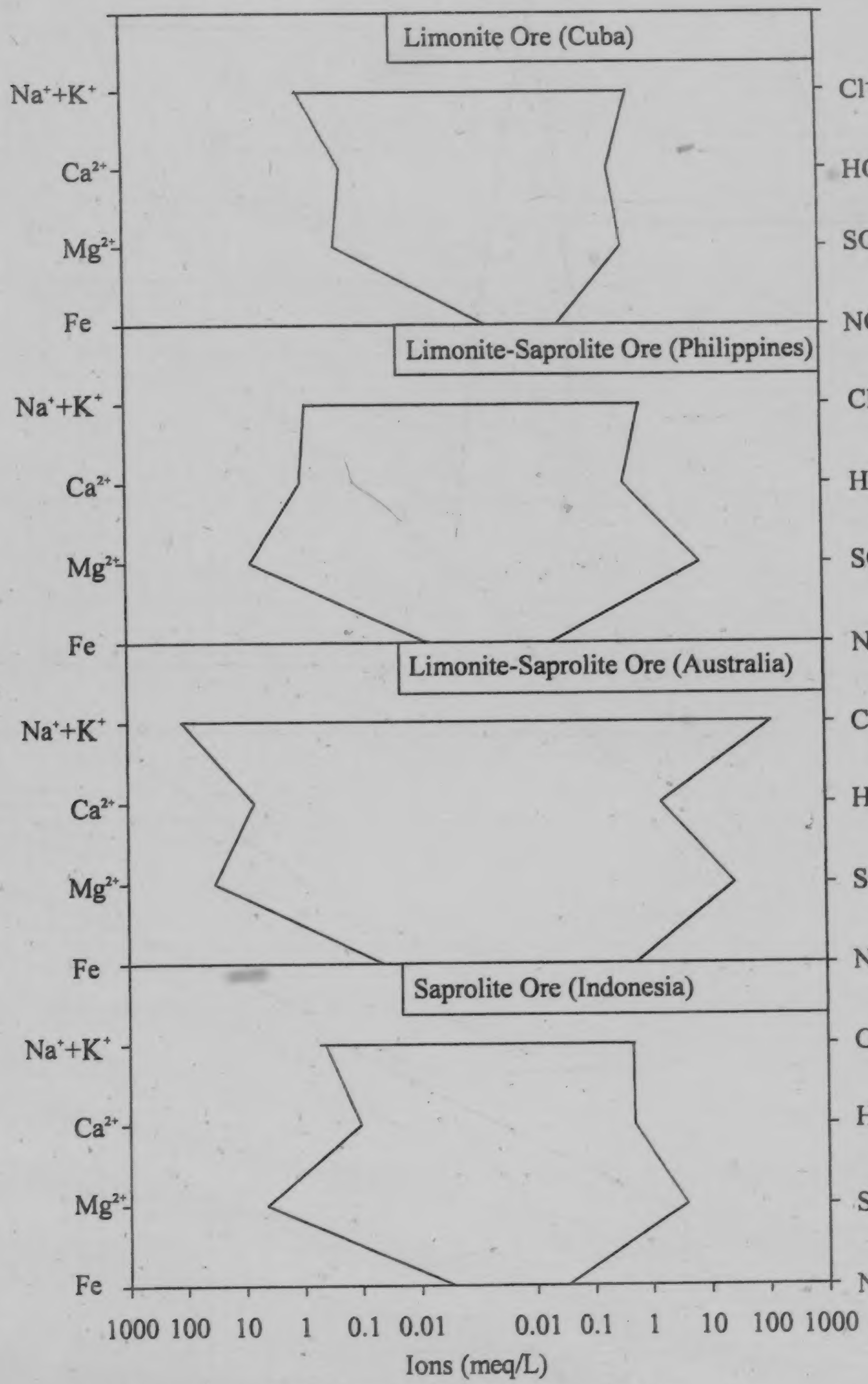

Figure 4.6: Stiff diagrams for laterite ore slurries

4.5 MORPHOLOGY

4.5.1 General

Morphological analyses were used for a qualitative evaluation of laterite ore slurries. This section presents a microstructural assessment of laterite ore slurries obtained from the storage thickener. Therefore, these visual observations pertain to soil fabric after the completion of the sedimentation stage in the solid-liquid separation process. Results of scanning electron microscopy are studied in conjunction with elemental analyses.

4.5.2 Scanning Electron Microscopy

Figure 4.7, 4.8, 4.9 and 4.10 give the morphological details of limonite ore slurry (Cuba), limonite-saprolite ore slurry (Philippines), limonite-saprolite ore slurry (Australia) and saprolite ore slurry (Indonesia), respectively. All of these figures comprise of four micrographs, each with a different magnification and designated by a scale. These enlargements include (a) 20 times, (b) 200 times, (c) 500 times and (d) 2000 times. The first micrograph (a) represents the whole specimen in the 3 mm circular plastic straw. This micrograph was taken to observe the fractured surface during sample preparation. The second micrograph (b) is an enlargement of the selected area on the first micrograph. This location was selected to denote an area that closely represents the entire slurry. The third micrograph (c) and the fourth micrograph (d) show magnified locations on micrograph (b). These two micrographs were taken either to inspect exaggerated portions of the micrograph (b) or to highlight some peculiar features on that micrograph (b).

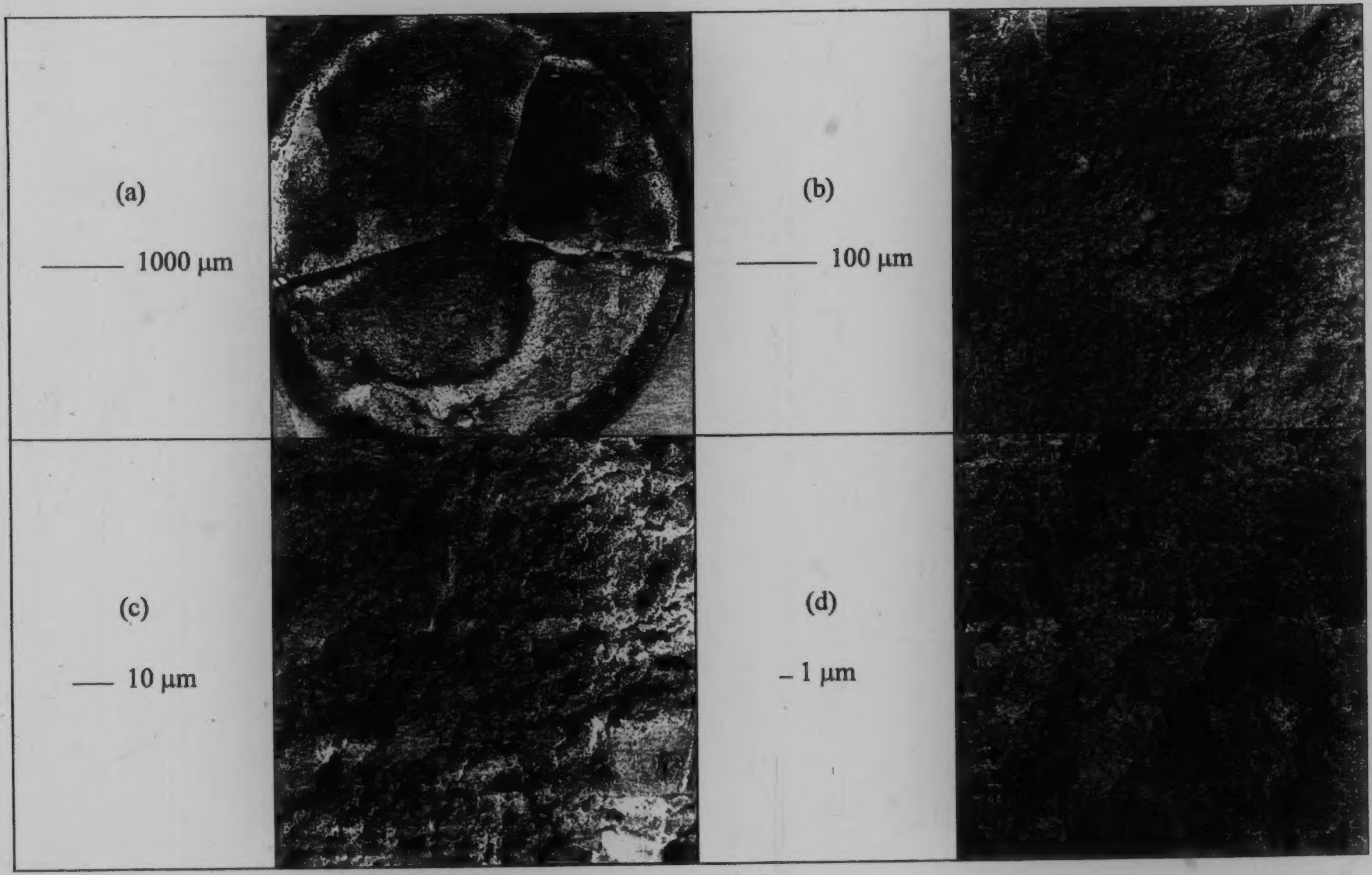
(a)
1000 µm
(b)
100 µm
(c)
10 µm
(d)
1 µm

Figure 4.7: Scanning electron micrographs of limonite ore slurry (Cuba)

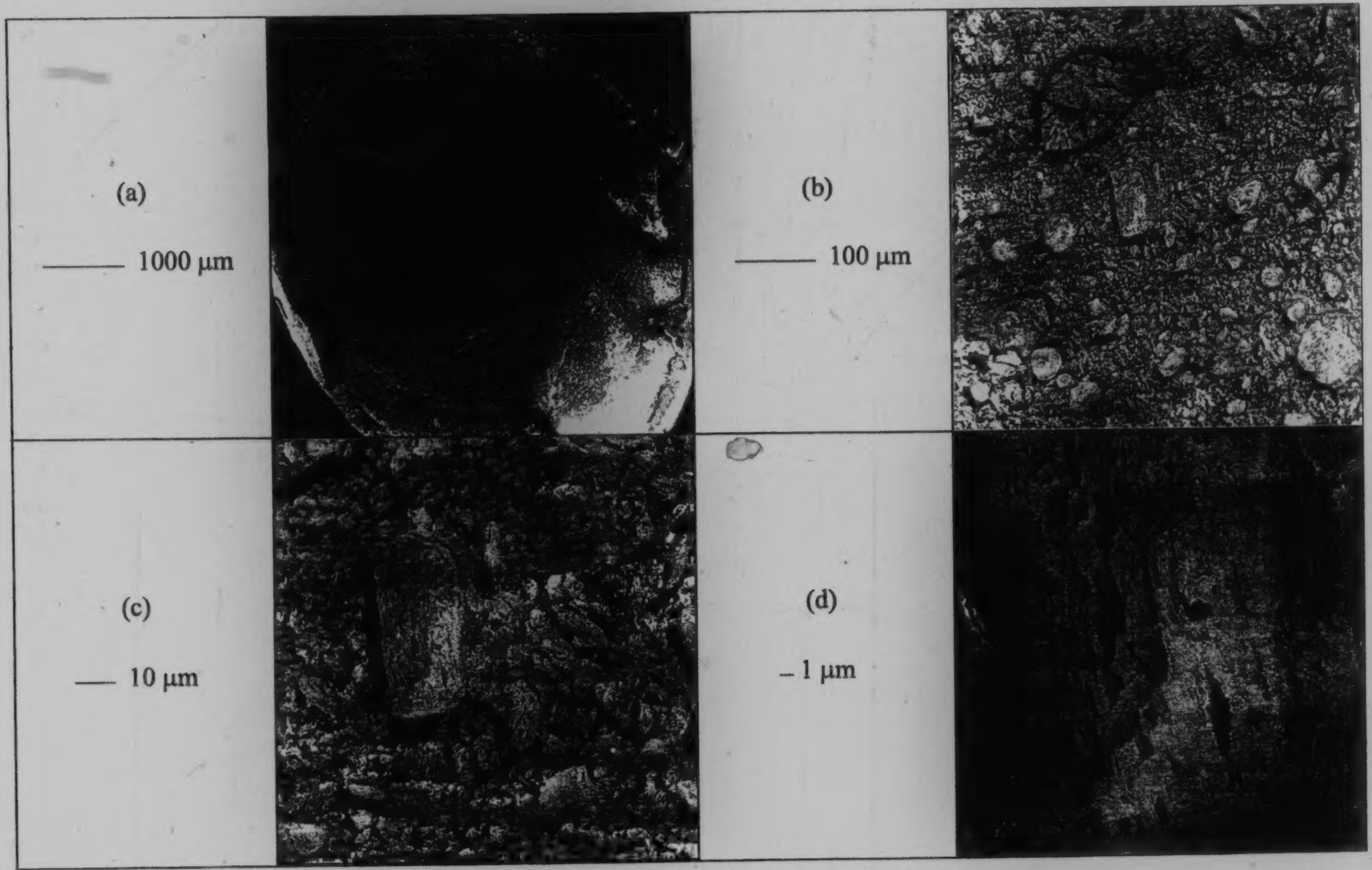
(a)
1000 µm
(b)
100 µm
(c)
10 µm
(d)
1 µm

Figure 4.8: Scanning electron micrographs of limonite-saprolite ore slurry (Philippines)

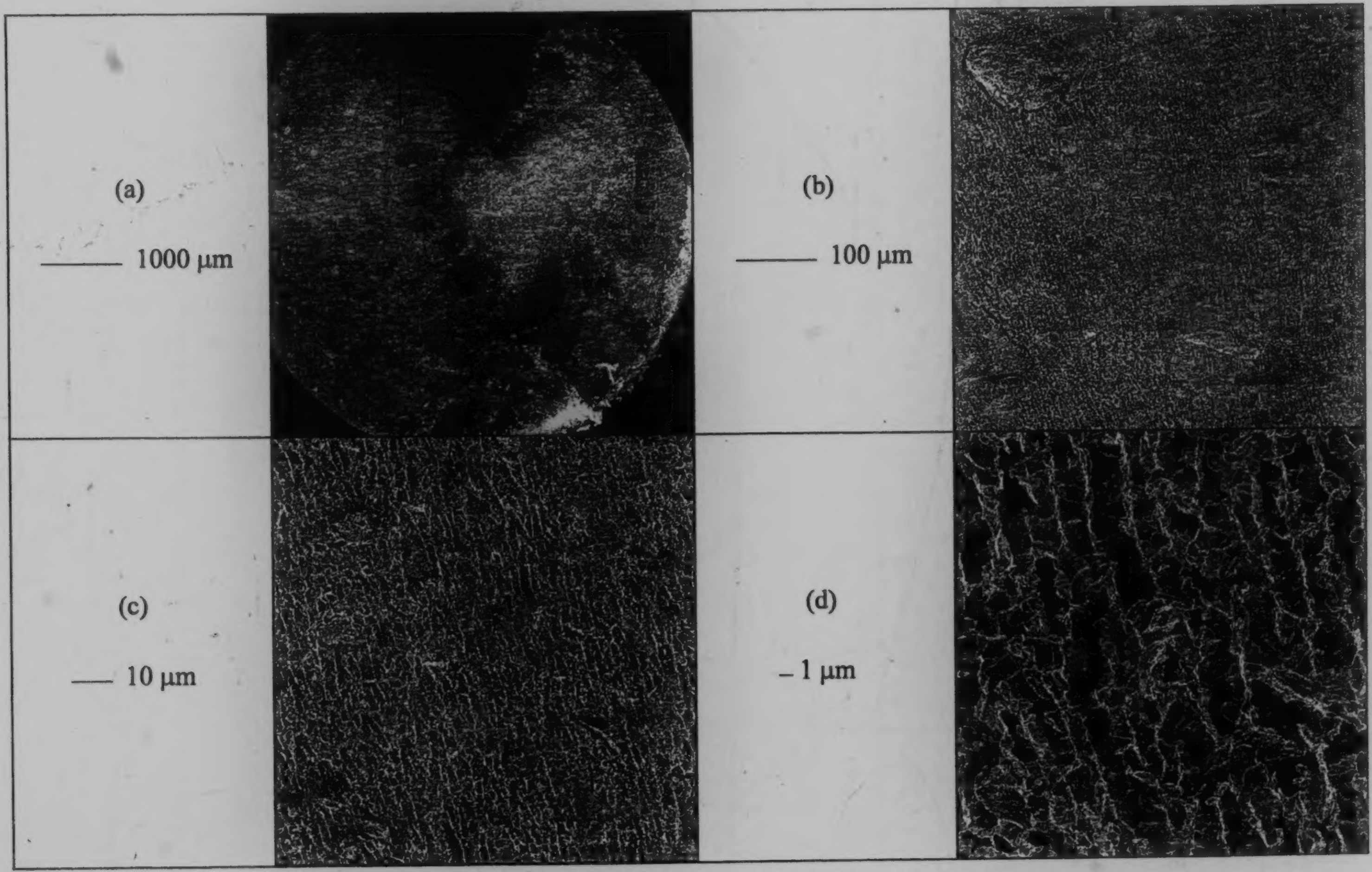
(a)
1000 µm
(b)
100 µm
(c)
10 µm
(d)
1 µm

Figure 4.9: Scanning electron micrographs of limonite-saprolite ore slurry (Australia)

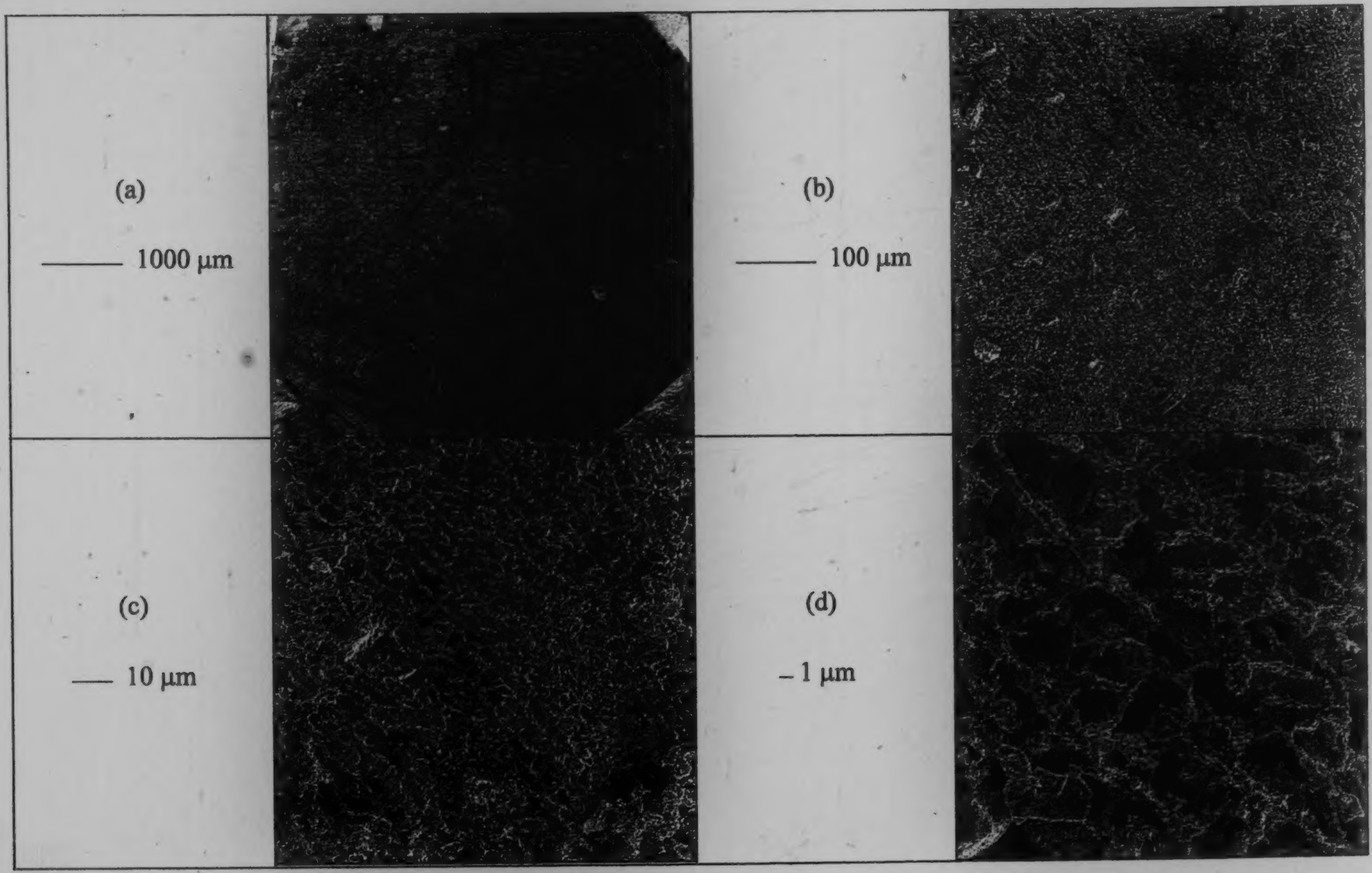
(a)
1000 µm
(b)
100 µm
(c)
10 µm
(d)
1 µm

Figure 4.10: Scanning electron micrographs of saprolite ore slurry (Indonesia)

Figure 4.7 shows the morphology of the limonite ore slurry from Cuba. Micrograph (a) shows the development of cracks during sample preparation. Micrograph (b) illustrates the presence of coarse grains scattered through out the clay matrix. Micrograph (c), which focuses on the clay matrix, shows that this matrix is composed of separate but mutually conjoined colonies. Micrograph (d) shows that these agglomerated colonies are composed of very fine needle-like goethite particles, which are smaller than the clay size particles (2 µm). Confirming the XRD results for the same material, this micrograph shows that the clay matrix is composed of non-clay minerals. Further, these minerals are observed to result in flocculated soil fabric in the given medium of low electrolyte concentration and neutral pH. Therefore, the limonite ore slurry from Cuba is expected to undergo rapid settling.

Figure 4.8 presents the microstructure of the limonite-saprolite ore slurry from Philippines. Micrograph (a) shows a slightly curved (downward at right corner) surface of the specimen. Micrograph (b) shows the presence of evenly distributed coarse grains scattered through out the clay matrix. These grains are either silt size particles or colonies of clay minerals. Micrograph (c) illustrates a morphology similar to that of the limonite ore slurry from Cuba with the additional feature of an occasional clay particle association. Micrograph (d) highlights the clay association and shows platy sheets of chrysotile clay mineral arranged in a cardhouse fashion and coated with needle shaped goethite. Figure 4.8 not only confirms the presence of small amount of clay minerals but also shows their dispersion in the given environment characterized by a neutral pH and a relatively higher electrolyte concentration. However, that environment does not cause a complete dispersion of the entire sample that is composed of goethite, hematite and maghemite. Therefore, the solid-liquid separation behavior of the limonite-saprolite ore slurry from Philippine is expected to be somewhat lower than that of the limonite ore slurry from Cuba.

Figure 4.9 gives the fabric of the limonite-saprolite ore slurry from Australia. Micrograph (a) shows the perfect surface for SEM analysis. Micrograph (b) illustrates the irregular distribution of silt size particles in the clay matrix. Micrograph (c) that presents an enlargement of the clay matrix shows complete dispersion of the clay particles. Micrograph (d) shows that this cardhouse structure has resulted from face-to-face association of the clay particles with spacing of about 2 μm. This figure verifies clay dispersion due to the presence of exchangeable sodium, a slightly basic medium and a high electrolyte concentration. The solid-liquid separation behavior of this material is anticipated to be much slower than both of the above mentioned ore slurries.

Figure 4.10 gives the morphology of the saprolite ore slurry from Indonesia. Micrograph (a) exhibits a good specimen surface with some corrugations and protuberances. Micrograph (b) shows a clay matrix similar to that of the limonite-saprolite ore slurry from Australia. Likewise, Micrograph (c) that magnifies the clay matrix, illustrates complete dispersion. Micrograph (d), which examines the cardhouse fabric, shows a very loose packing for this slurry with inter-particle spacing of the order of 10 to 12 μm. This micrograph also shows the overwhelming presence of amorphous material in the form of small globules (smaller than 1 μm) coating the clay particles. Figure 4.10 confirms clay dispersion in a slightly basic medium and low electrolyte concentration. The voluminous cardhouse structure of clay particles coated by the amorphous materials, as observed in this figure, is attributed to some peculiar feature of the latter material not explained by the classical double layer theory. The important consequence of that fabric is slow sedimentation and consolidation and a reduced hydraulic conductivity for this slurry.

4.5.3 Elemental Analysis

Figure 4.11 gives the elemental analysis of SEM samples (shown in Micrographs (a)) for various laterite ore slurries. For each sample, this figure shows two Au peaks due to gold coating of the specimens and one high Fe peak associated with the presence of goethite, hematite and maghemite. In the limonite ore slurry from Cuba, the low Al peak appears to be associated with gibbsite. Clay forming elements such as Fe, Na, Mg, and Si, appearing in the other three slurries confirm the presence of clay minerals in these samples. The high Si peak appearing in the limonite-saprolite ore slurry (Australia) as well as in the saprolite ore slurry (Indonesia) denotes the presence of amorphous silica and quartz in these samples. Therefore, elemental analysis helped in specimen identification during scanning electron microscopy and in the confirmation of results obtained from x-ray diffraction analysis.

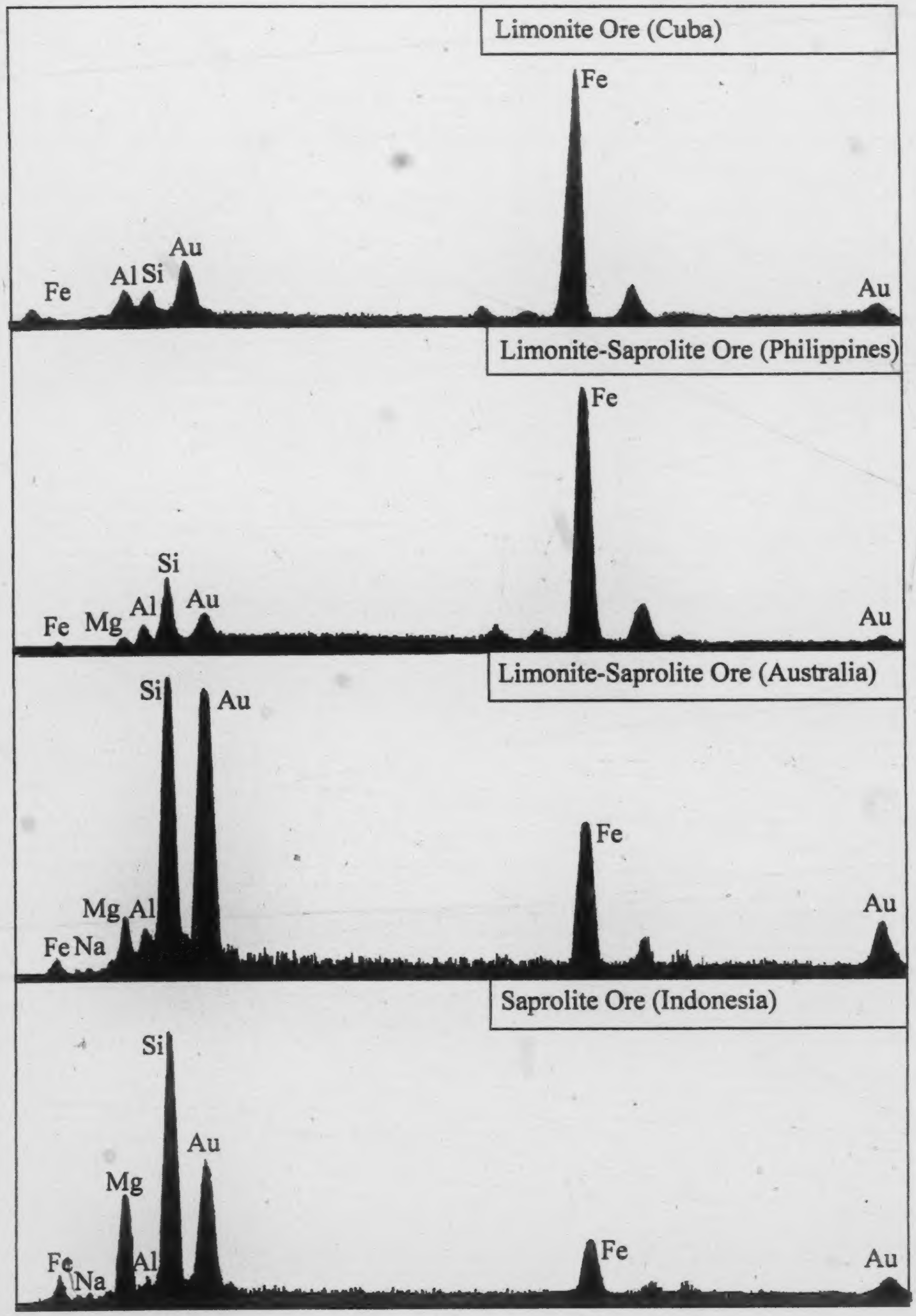

Figure 4.11: Elemental analysis of SEM specimens of laterite ore slurries

4.6 SOLID-LIQUID SEPARATION

4.6.1 General

This section presents the solid-liquid separation behavior of laterite ore slurries. At the outset, the influence of the diameter to height ratio on such a behavior is investigated. The results of sedimentation and consolidation tests are studied in the light of the laboratory characterization given throughout this chapter for various materials. To correlate morphology with consolidation, results of scanning electron microscopy, conducted on specimens cut from the latter test sample, are presented.

4.6.2 Diameter-Height Ratio

The effect of diameter to height ratio on the solid-liquid separation behavior of laterite slurries was investigated by conducting four sedimentation tests with variable D_o/H_o. Figure 4.12 gives the results of these tests conducted on the limonite-saprolite ore slurry from Philippines using identical beakers of 8.3 cm diameter. This figure shows insignificant variation in sedimentation curves for different D_o/H_o ratios and closely matching H/H_o values after 30 minutes of sedimentation. This means that the sedimentation curves are reproducible within experimental error induced by test conditions or observer's bias. Further, this figure illustrates that the limonite-saprolite ore slurry undergoes a rapid sedimentation that allows the determination of the initial hydraulic conductivity from data observed in the initial ten minutes of sedimentation. Such observations are generally applicable to all types of laterite slurries.

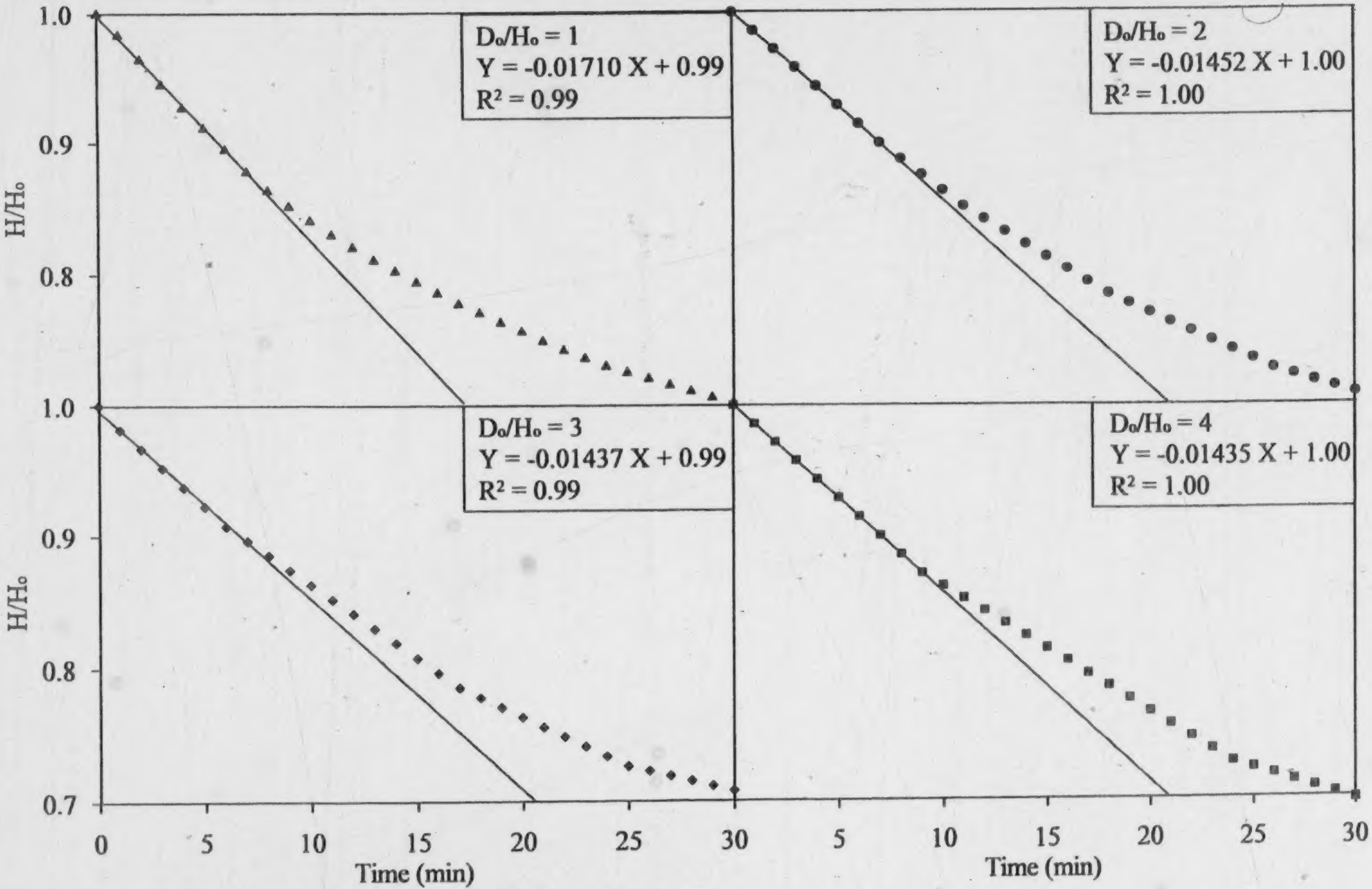

Figure 4.12: Sedimentation test results for various Do/Ho

Figure 4.13 gives the variation in the initial hydraulic conductivity for various D_o/H_o ratios. This figure shows an exponential decrease in the initial hydraulic conductivity with increasing D/H_o. Bulk of this decrease (15%) is observed when the D_o/H_o ratio is changed from 1 to 2 whereas insignificant variation in the initial hydraulic conductivity occurs for D_o/H_o ratios between 2, 3 and 4. These observations are attributed to the formation of channels in the sedimenting materials. Recorded annotations during laboratory experiments suggest an increased tendency of channel formation for higher initial sample height. These channels not only provide paths of least resistance for water flow but also reduce tortuousity thereby further increasing the initial hydraulic conductivity. To facilitate rapid sedimentation and to mimic thickener geometry, a D_o/H_o ratio of 1 was used for all sedimentation tests during this research. The high initial height required to obtain this ratio also allowed the development of a clear solid-liquid interface thereby assisting in reducing the experimental errors. After complete sedimentation, sample height of less than half of H_o was achieved for most of the laterite slurries. This ensured that the influence of D_o/H_o during the consolidation stage of the solid-liquid separation process is negligible.

4.6.3 Sedimentation

Figure 4.14 gives sedimentation test results in the form of interface height, void ratio and solids content as functions of time. Figure 4.15 shows part of the interface height versus time plot for the determination of initial hydraulic conductivity. Table 4.6 summarizes the sedimentation behavior of laterite ore slurries.

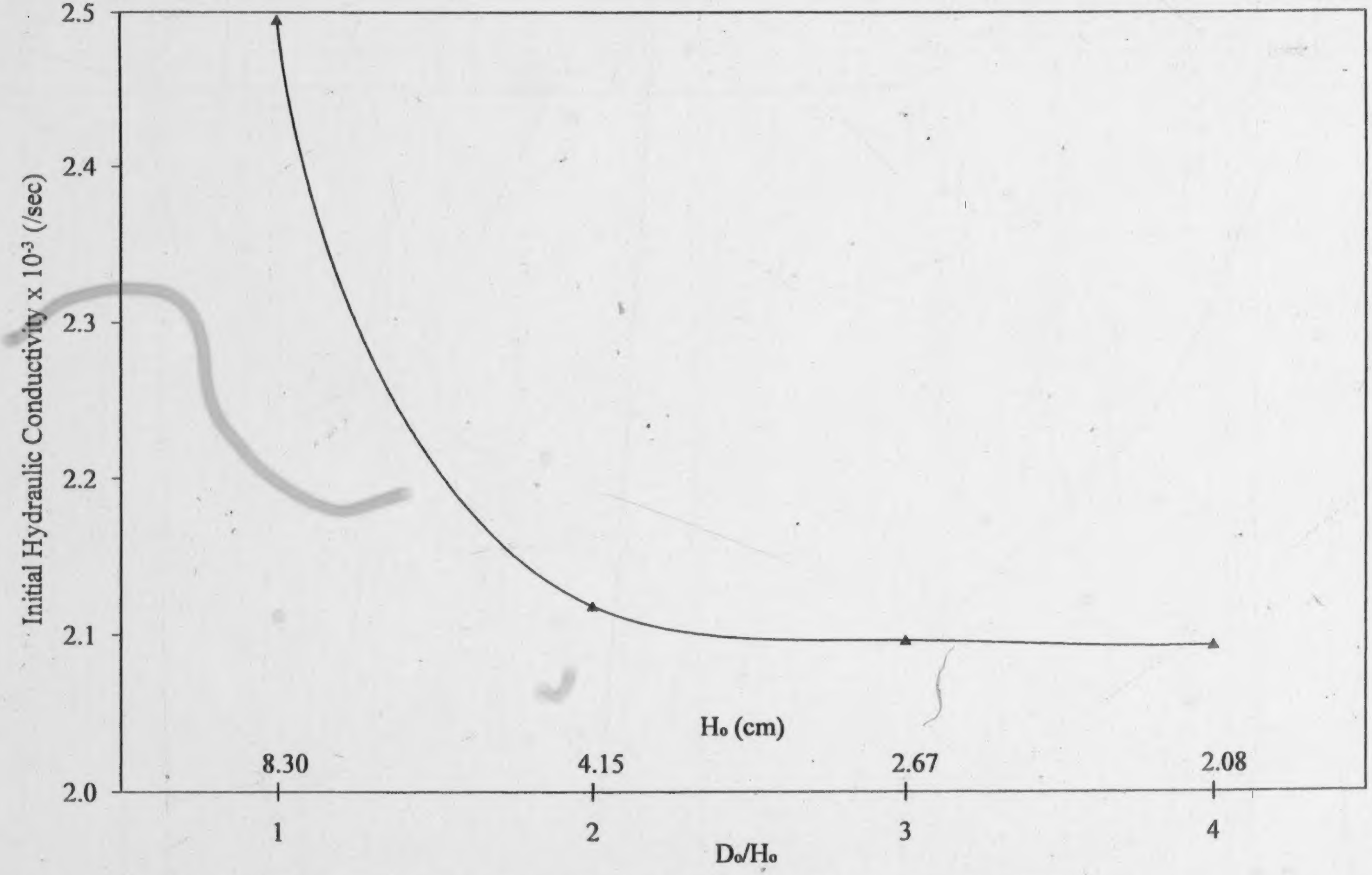

Figure 4.13: Effect of Do/Ho on sedimentation of limonite-saprolite ore slurry from Philippines

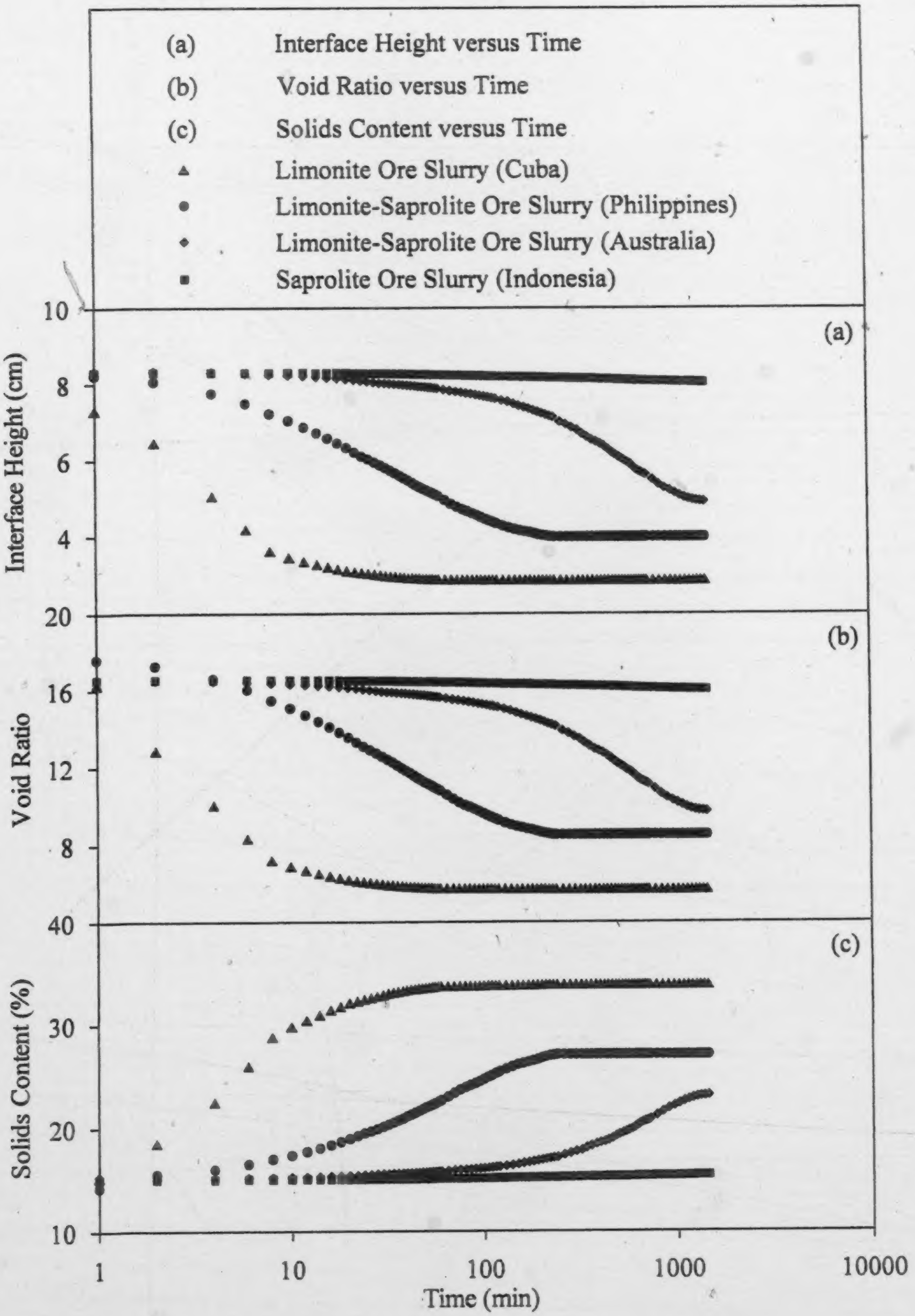

Figure 4.14: Sedimentation test results for laterite ore slurries

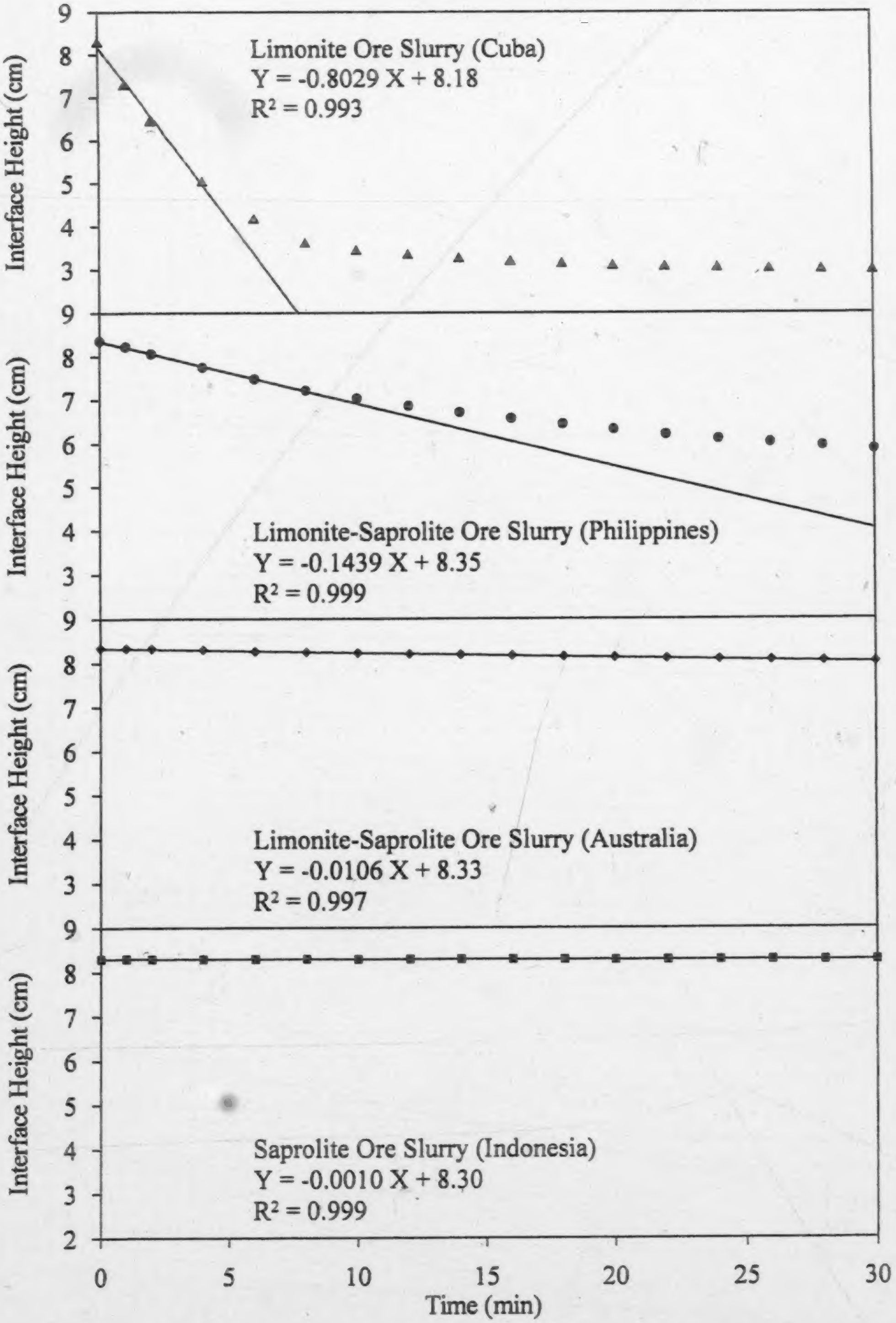

Figure 4.15: Water release rate for various laterite ore slurries

Table 4.6. Summary of sedimentation test results for laterite ore slurries

Property	Sample Type and Origin			
	Limonite Ore	Limonite-Saprolite Ore		Saprolite Ore
	Cuba	Philippines	Australia	Indonesia
	Conditions at the Start of Sedimentation Test			
H_o (cm)	8.30	8.36	8.34	8.30
s_o (%)	15	15	15	15
e_o	16.55	17.91	16.55	16.55
γ_o (kg/m^3)	1109	1114	1109	1109
σ_o' (Pa)	89	94	90	89
	Hydraulic Conductivity During the Sedimentation Test			
Vs (cm/min)	0.8029	0.1439	0.106	0.0010
γ*	1.92	2.16	1.92	1.92
k (cm/s)	1.22×10^{-1}	2.10×10^{-2}	1.61×10^{-3}	1.53×10^{-4}
	Conditions at the End of Sedimentation Test			
H_f (cm)	2.86	3.89	4.90	8.04
s_f (%)	33.87	27.04	23.10	15.41
e_f	5.70	8.53	9.72	16.03
γ_f(kg/m^3)	1287	1227	1179	1113
σ_f' (Pa)	80	89	86	89

The sedimentation behavior of laterite ore slurries is the result of the combined effect of geotechnical index properties, mineralogy and pore water chemistry; all of which result in a specific morphology. Detailed discussions of these material characteristics and the expected solid-liquid separation behavior were provided earlier in this chapter. This section confirms and explains the engineering behavior of laterite ore slurries.

Figure 4.14 shows that the limonite ore slurry from Cuba has the most rapid sedimentation. This is attributed to the mechanical action of coarse particles in this slightly gap-graded material and the presence of high amount of heavy iron oxides in a neutral environment, which result in a flocculated morphology. This is followed by the limonite-saprolite ore slurry from Philippines. The sedimentation behavior of this slurry is due to a well-graded material with 35% clay size content, the presence of clay minerals and reduced amount of iron oxides, and higher amount of electrolytes in the pore water. These material characteristics result in a generally flocculated fabric with localized cardhouses of clay particles. The sedimentation behavior of the limonite-saprolite ore slurry from Australia is dominated by the presence of high amount of clay size fraction including clay minerals and amorphous materials and a high concentration of pore water electrolytes. This causes a completely dispersed soil fabric that is difficult to dewater under self-weight. Although, the amount of clay mineral is lower in the saprolite ore slurry from Indonesia, this material has high amount of amorphous materials. In the given environment, the amorphous materials partially coat a significant amount of the clay platelets. This means that clayey material as well as individual clay platelets can be oppositely charged. Such incomplete coating of clays results in a voluminous cardhouse morphology with an associated slow sedimentation. Therefore, the sedimentation behavior of laterite ore slurries follows a decreasing trend as materials change from limonite though saprolite ore.

Figure 4.15, which is the enlarged version of sedimentation curve of Figure 4.14(a), gives the water release rate for various laterite ore slurries. This figure shows that the slope of the initial straight-line portion of the sedimentation curve decreases from limonite through saprolite ore slurries. Again, this is attributed to the aforementioned reasons.

Table 4.6 that summarizes the sedimentation test results for laterite ore slurries divides the test into three stages. This table indicates approximately constant initial conditions at the start of the sedimentation tests. The slightly higher values for the limonite-saprolite ore slurry are due mainly to the high specific gravity of this material. The table reports that the k_i of all ore slurries is higher than sedimentary clays. This is attributed to the high specific gravity of laterite ores and negligible segregation of their slurries. Further, the initial hydraulic conductivity of various laterite ores follows the same decreasing trend from limonite through saprolite ore slurries. The final conditions at the end of sedimentation tests indicate effective stress lower than at start. This is due to the high time requirement for the completion of the sedimentation stage: the test duration of 24 h is insufficient to completely dissipate the excess pore pressure.

4.6.4 Consolidation

4.6.4.1 General

A comparison of Table 4.1 and Table 4.6 reveals that during sedimentation the limonite ore slurry from Cuba achieves a solids content equal to that of the storage thickener. Conversely, the other three ore slurries do not reach the same under self-weight. Therefore, these latter materials need to undergo consolidation to get the desired solids content in the storage thickener. However, limonite-saprolite ore slurry from Philippines was selected for the consolidation test because of the increasing use of such materials due to their reduced operational cost (Chalkley & Toraic 1997). This section gives the consolidation test results coupled with fabric studies for the limonite-saprolite ore slurry from Philippines.

4.6.4.2 Test Result

Figure 4.16, 4.17 and 4.18 give consolidation test results in the form of sample height, void ratio and solids content versus time for different load increments. These results are summarized in Table 4.7, which indicates that bulk of the solid-liquid separation occurs under self-weight. Under self-weight a 65% dewatering is achieved as the void ratio changes from 17.9 to 8.0 and the solids content changes from 15 to 28%. This is mainly attributed to the high specific gravity (3.16) of the limonite-saprolite ore slurry from Philippines. Up to an effective stress of 8 kPa, an additional 18% dewatering is observed with an associated void ratio change from 8.0 to 5.2 and a solids content increase of about 9%. Increase in σ' beyond 8 kPa results in less than 5% dewatering and increase in solids content.

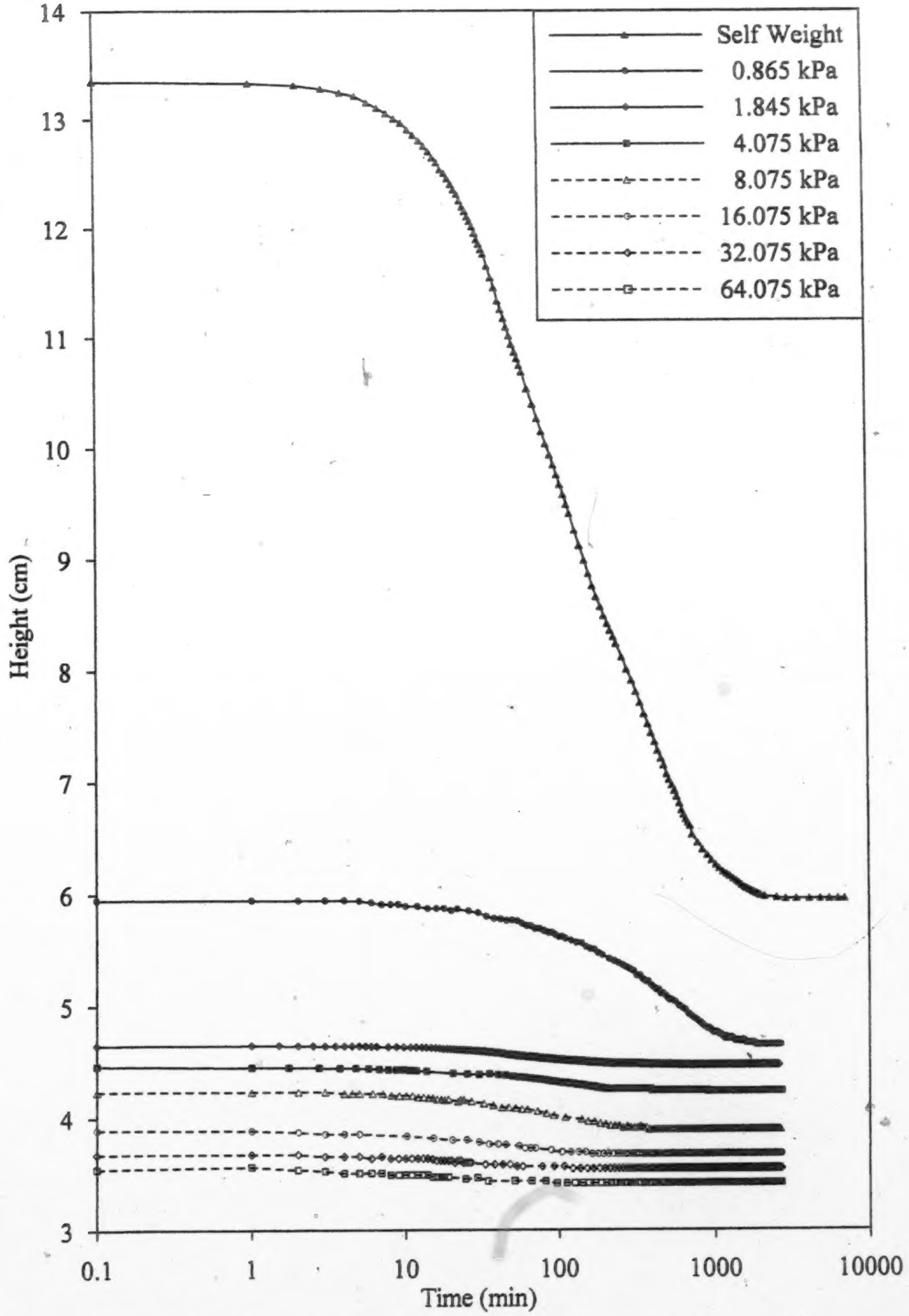

Figure 4.16: Consolidation of limonite-saprolite ore slurry

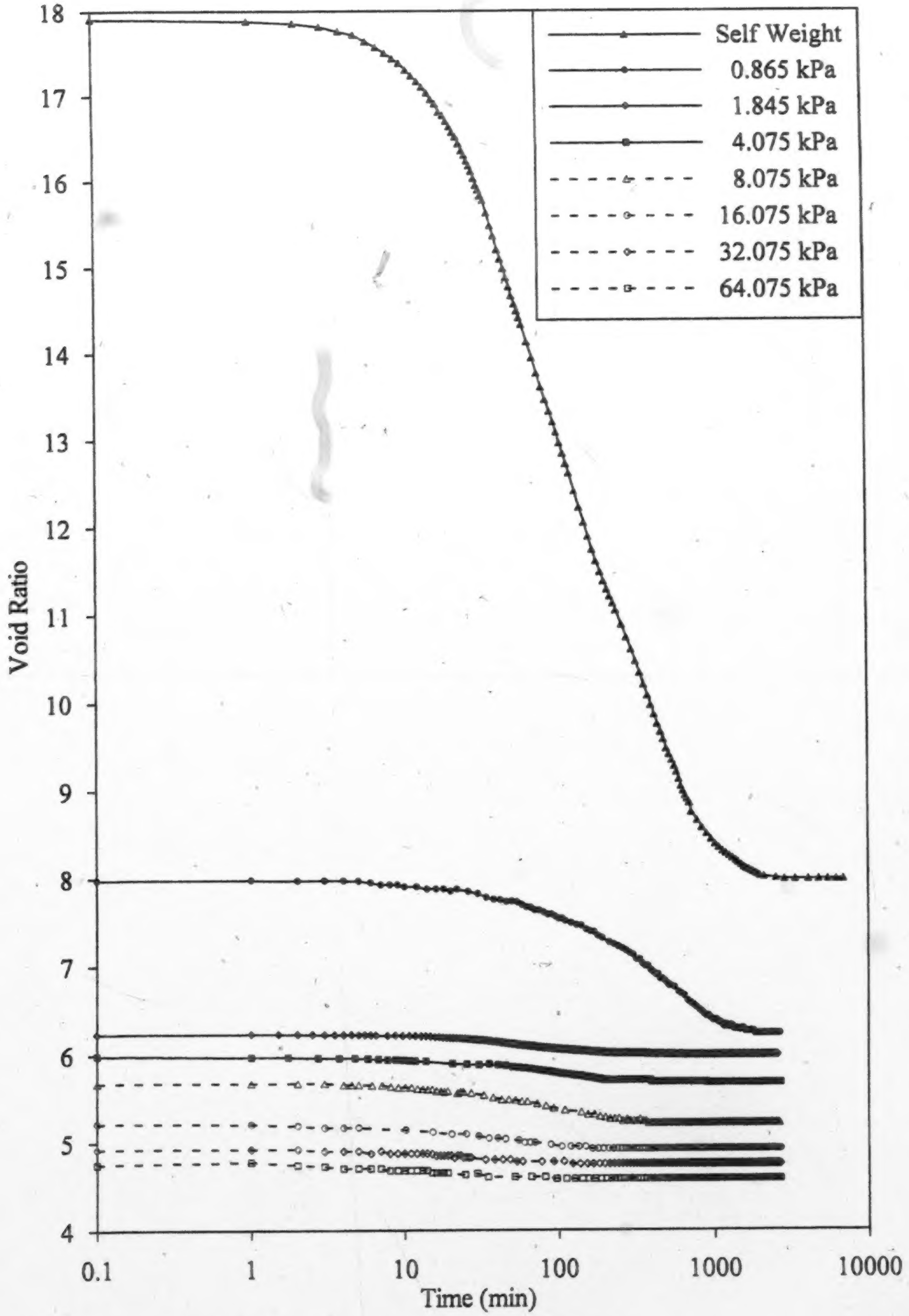

Figure 4.17: Void Ratio of limonite-saprolite ore slurry

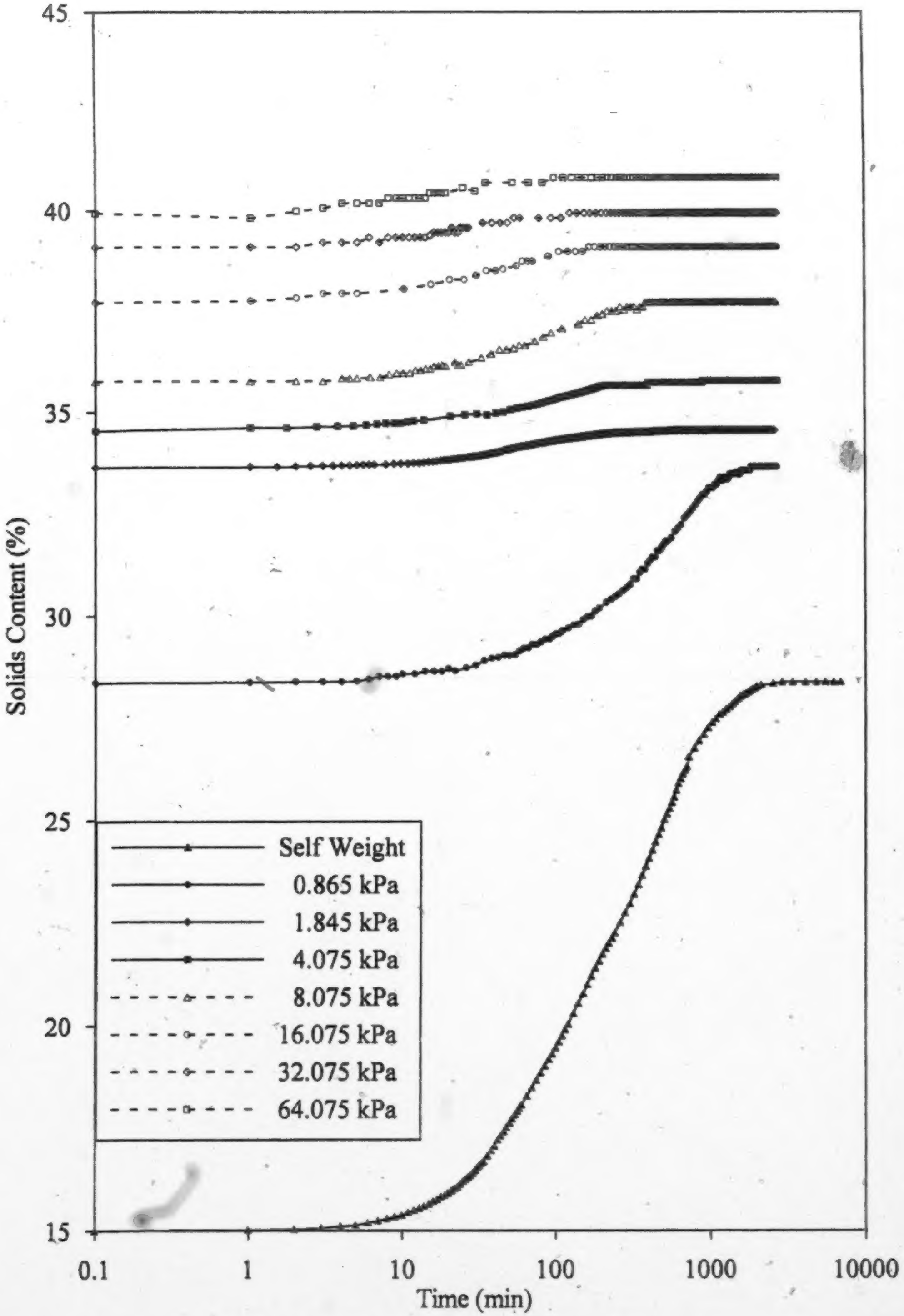

Figure 4.18: Solids Content of limonite-saprolite ore slurry

Table 4.7. Changes during solid-liquid separation of laterite ore slurry

σ' (kPa)	$\Delta H/H$ (%)	e	s (%)	Dewatering (%)*
Initial state	0.0	17.9	15.0	0.0
Self-weight	55.4	8.0	28.4	65.0
0.9	65.2	6.2	33.7	76.4
1.9	66.6	6.0	34.5	78.0
4.1	68.3	5.7	35.8	80.1
8.1	70.9	5.2	37.7	83.1
16.1	72.5	4.9	39.1	85.0
32.1	73.5	4.8	39.9	86.1
64.1	74.4	4.6	40.8	87.3

* Change in water volume divided by initial water volume

Figure 4.19 gives the pore pressure measurements for each load increment. This figure indicates an initial abrupt increase in excess pore pressure with load application and a subsequent steady decrease; high excess pore pressure measured for high load increments. Pore pressure equilibration occurs within the first two hours of load application for all loads.

Figure 4.20 presents the hydraulic conductivity data measured after each load increment in the consolidation test. This figure shows that the variation in hydraulic conductivity is four orders of magnitude for different load increments. Despite the initial scatter in the data points indicated in Figure 4.20, steady state values are observed within about 30 minutes of water flow through the specimen.

The drop in flow from an initial to a steady state value decreased with increasing stress. This is attributed to the diminishing physical changes in the specimen with decreasing void ratio. Olsen et al. (1985), suggested that such time-dependent flow can be due to one or more of the following reasons: (a) undissolved air in the equipment and/or specimen; (b) equipment compliance depending on fabrication material and applied gradients; (c) inertia required to move the pore fluid; and (d) time-dependent changes in pore space distribution. Using identical equipment and test conditions for oil sand tailings, Suthaker & Scott (1996) showed that the last reason is the most likely cause of the observed time-dependent flow. They concluded that transient phenomenon is repeatable and the initial conditions retainable. Therefore, the steady state value was taken as the hydraulic conductivity and used in the analysis during this research.

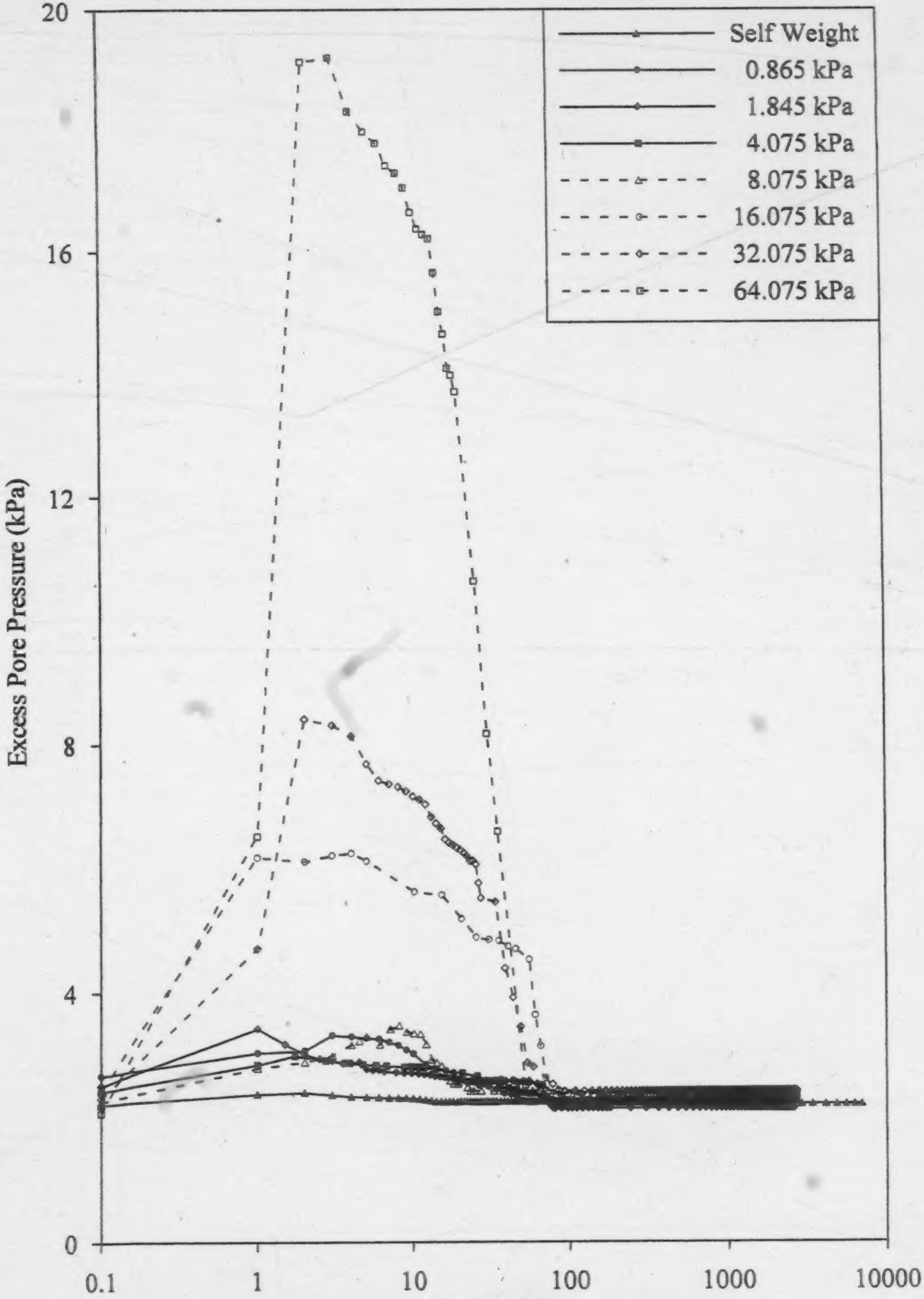

Figure 4.19: Excess Pore pressure of limonite-saprolite ore slurry

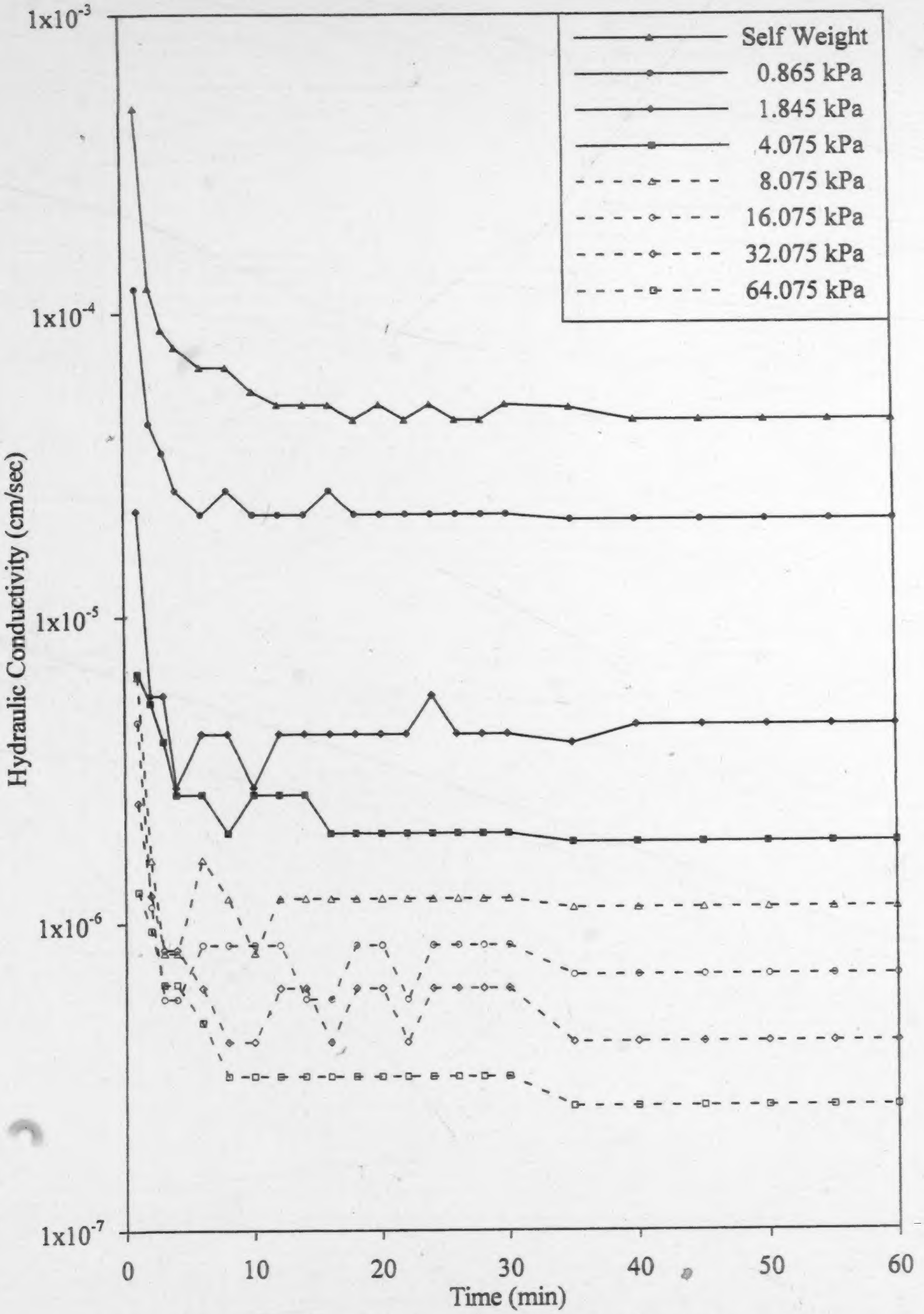

Figure 4.20: Hydraulic conductivity of limonite-saprolite ore slurry

Figure 4.21 and Figure 4.22 summarize the consolidation test results for the limonite-saprolite ore slurry from Philippines. Described as power laws, these two figures give the hydraulic conductivity-void ratio and the void ratio-effective stress relationships, respectively. Data in these two figures is shown in cm/sec and kPa units as well as in m/min and Pa units. Fit parameters obtained from the latter units are used in the numerical analysis, described latter in this chapter. For the two relations, the *A* and *C* parameters denote the intercept or position of the fit whereas the *B* and *D* parameters signify the slope or shape of the curve.

Figure 4.21 indicates that the hydraulic conductivity decreases by more than three orders of magnitude (10^{-4} to 10^{-7} cm/sec) as the void ratio is decreased from 8.0 to 4.0. The investigated ore slurry exhibits a hydraulic conductivity similar to clays ($\leq 10^{-6}$ cm/sec at $e \leq 2.0$) at a higher void ratio of 5.0. This is attributed to the high tortuousity imparted by the ultra-fine, needle-like goethite crystals. The angular nature of these hard sesquioxide particles is also responsible for the low compressibility of limonite-saprolite ore slurry from Philippines. A similar behavior is envisaged for the limonite ore slurry from Cuba. Other laterite ore slurries with high amount of soft clay minerals and rounded amorphous materials should exhibit higher compressibility.

4.6.4.3 Morphology

Figure 4.23 and Figure 4.24 give the sample morphology after the completion of the consolidation test for specimens cut in the vertical (parallel to applied stress) and lateral (perpendicular to applied stress), respectively. These two figures indicate

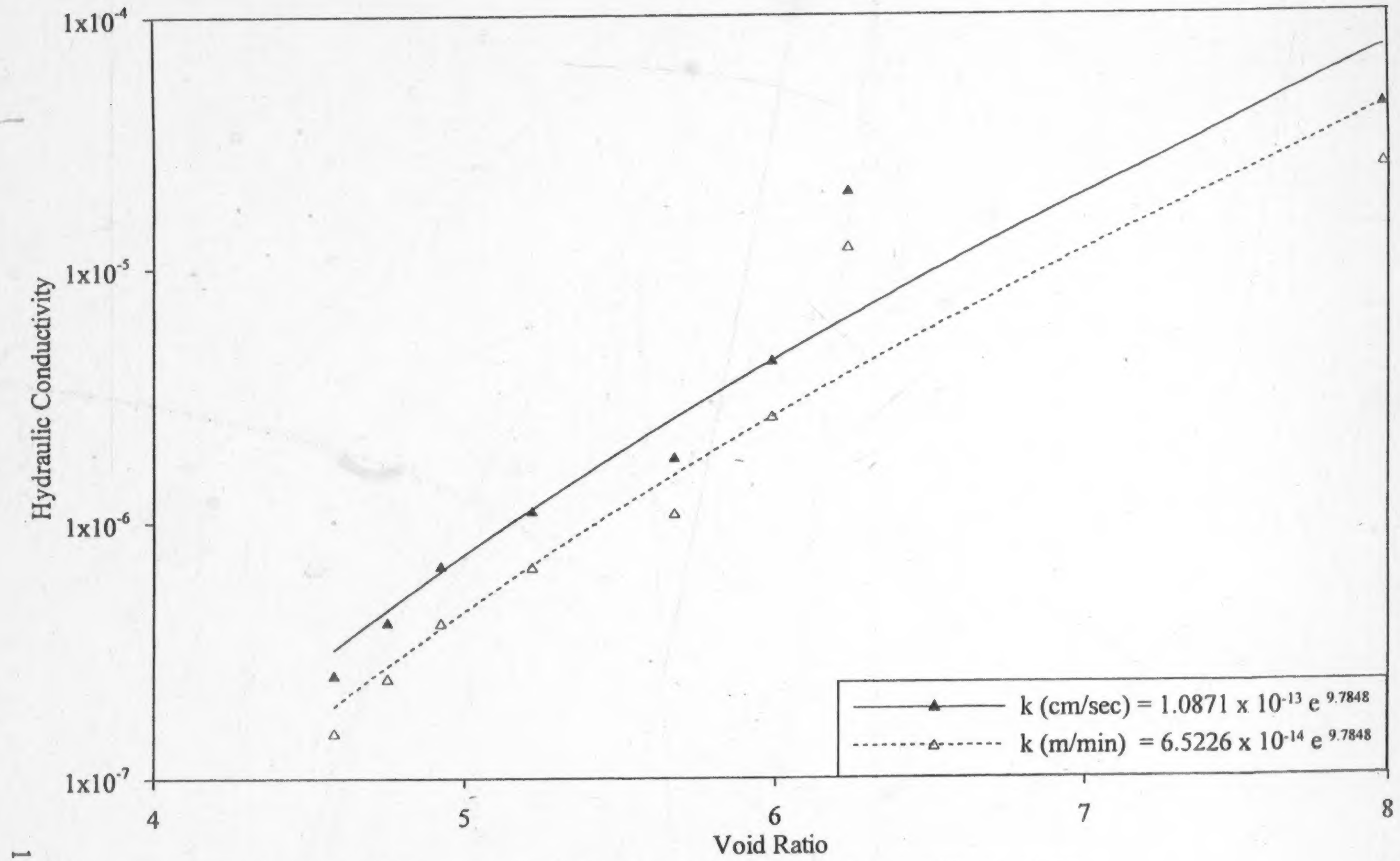

Figure 4.21: Hydraulic conductivity-void ratio relation for limonite-saprolite ore slurry

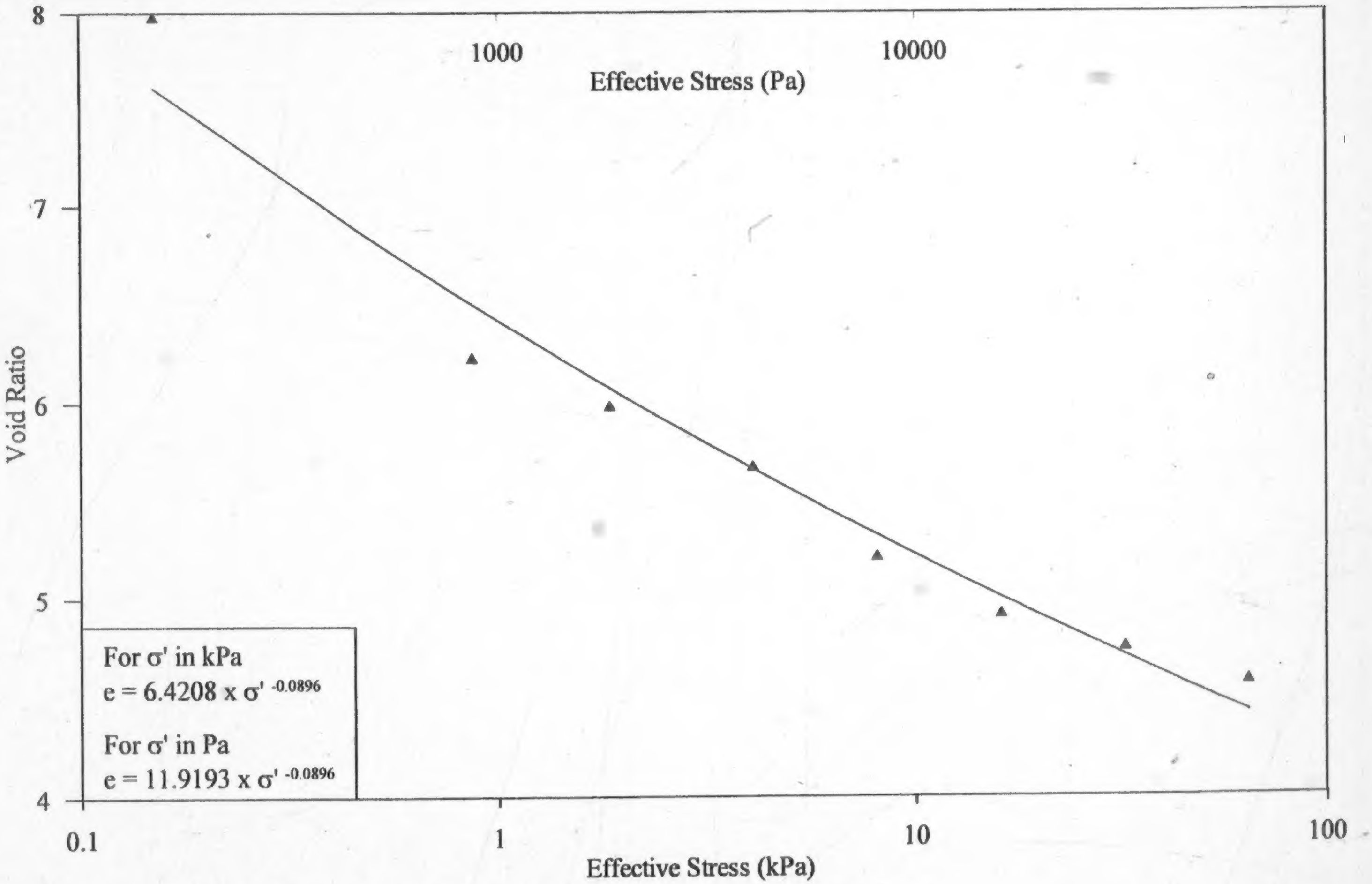

Figure 4.22: Void ratio-effective stress relation for limonite-saprolite ore slurry

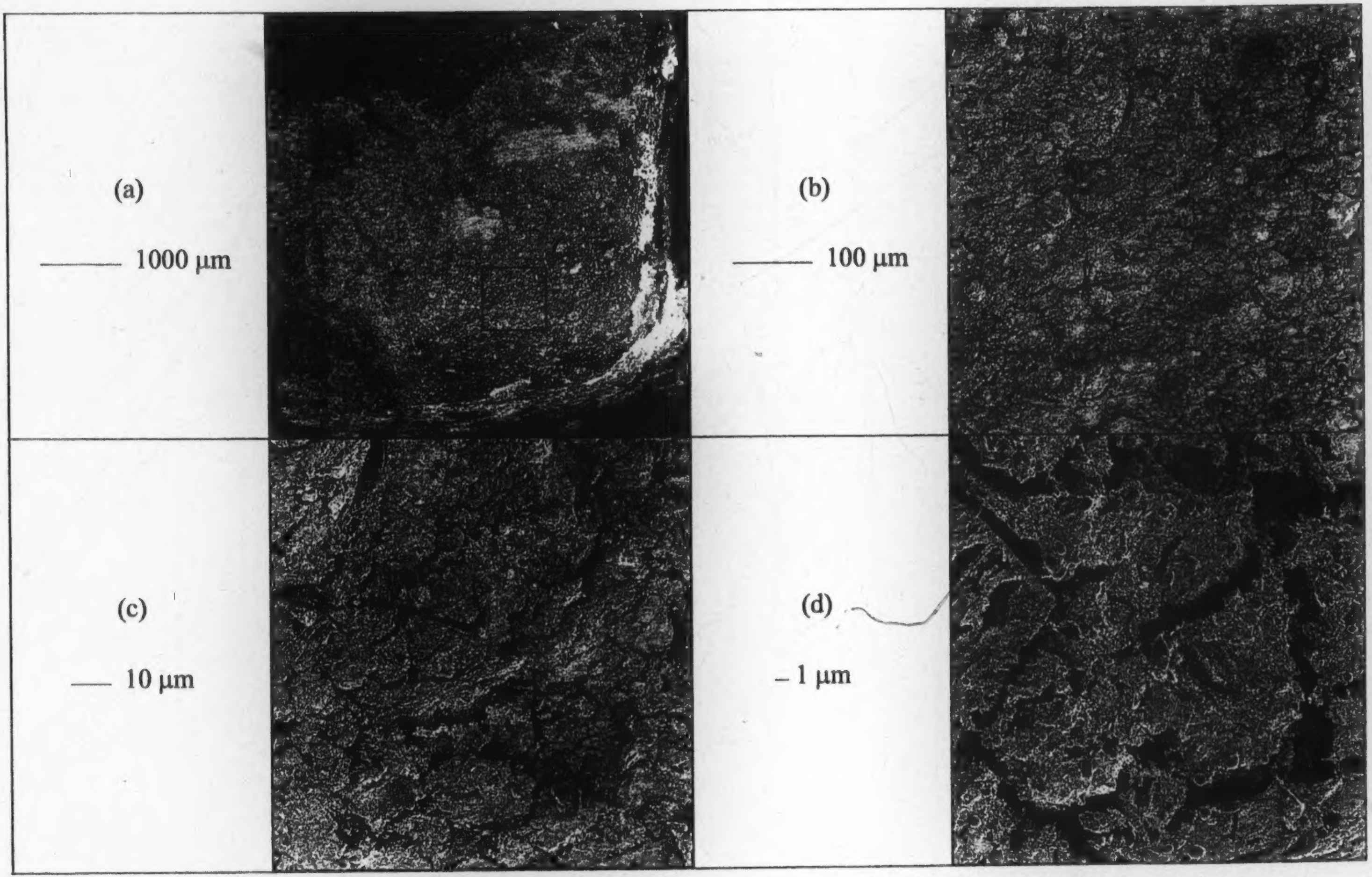
(a)
1000 µm
(b)
100 µm
(c)
10 µm
(d)
1 µm

Figure 4.23: Scanning electron micrographs of limonite-saprolite ore slurry (Philippines) on vertically cut specimen

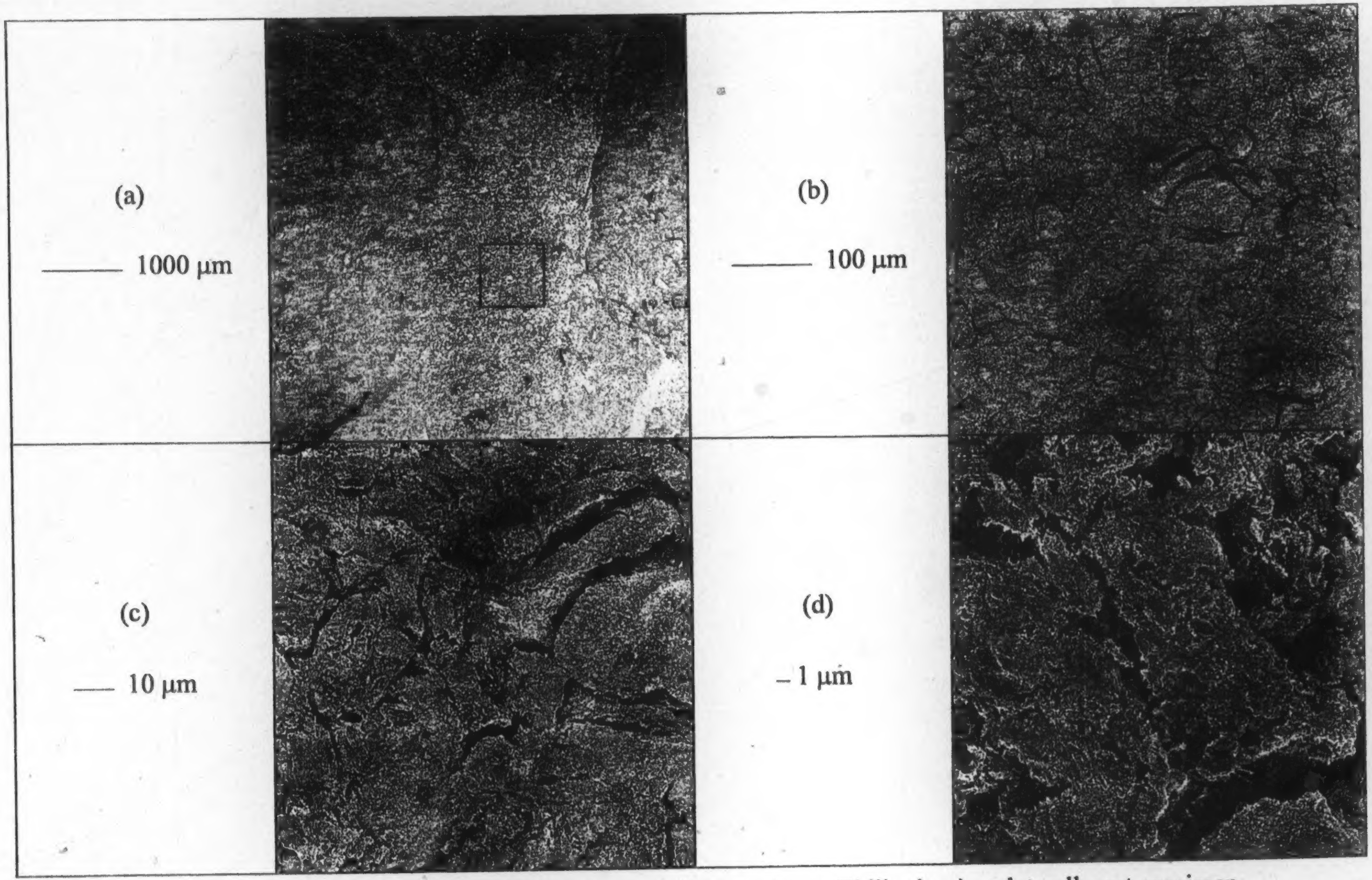
(a)
1000 µm
(b)
100 µm
(c)
10 µm
(d)
1 µm

Figure 4.24: Scanning electron micrographs of limonite-saprolite ore slurry (Philippines) on laterally cut specimen

insignificant differences between soil microstructure in the two perpendicular directions. Micrographs (a) of both of these figures show good fractured surfaces during sample preparation. Micrographs (b) show dense soil fabrics composed of particle assemblages with sizes ranging from 10 to 100 μm. Micrographs (c) indicate the presence of a slightly larger number of pore spaces for the vertically cut specimen when compared with the laterally cut sample. Micrographs (d) illustrate that the size of these inter-assemblage pore spaces are 1 to 5 μm in the vertical direction and 1 to 3 μm in the lateral direction. The size and tortuousity of these inter-assemblage void spaces govern the hydraulic conductivity of the specimen. These voids are affected by particle hardness and angularity, which in turn, control the compressibility of the soil sample.

4.7 NUMERICAL SIMULATION

4.7.1 General

This section describes the performance prediction of various laterite ore slurries. Sedimentation test data was fitted by iterative variation of A and B parameters used in the hydraulic conductivity-void ratio relation; data fitting was checked against the measured initial hydraulic conductivity. Such simulation allowed the determination of hydraulic conductivity-void ratio relationship without conducting the consolidation test. Similarly, the behavior of a storage thickener is modeled using the large-strain consolidation test data for the limonite-saprolite ore slurry from Philippines.

4.7.2 Laboratory Data

Figure 4.25 gives the modeling of sedimentation curves for various laterite ore slurries. This figure shows that, with the exception of the limonite ore slurry from Cuba, the laboratory data fits well to the initial part of the sedimentation curve that was used for the determination of initial hydraulic conductivity. Further, the laboratory determined hydraulic conductivity-void ratio relation of the limonite-saprolite ore slurry from Philippines matches closely with the curve. Using these hydraulic conductivity-void ratio relationships, Figure 4.26 depicts the behavior of various laterite ore slurries. This figure shows that the hydraulic conductivity varies by several orders of magnitude both for various ore slurries and for different void ratios of the same slurry. This is attributed to variation in physico-chemical interactions between the colloidal particles and the electrolyte medium. A detailed discussion of such interactions was given earlier in this chapter. Further, all curves converge at low void ratios at which mechanical phenomena govern soil behavior.

4.7.3 Storage Thickener

Figure 4.27 gives the solids content profiles in a typical 3.0 m storage thickener. This figure was obtained by using the input parameters given earlier in Figures 4.21 and 4.22 in the sedimentation and consolidation program SECO described in Chapter Three. To highlight the solids content variation in the compaction bed of the storage thickener, sediment height is plotted on a logarithmic scale in this figure.

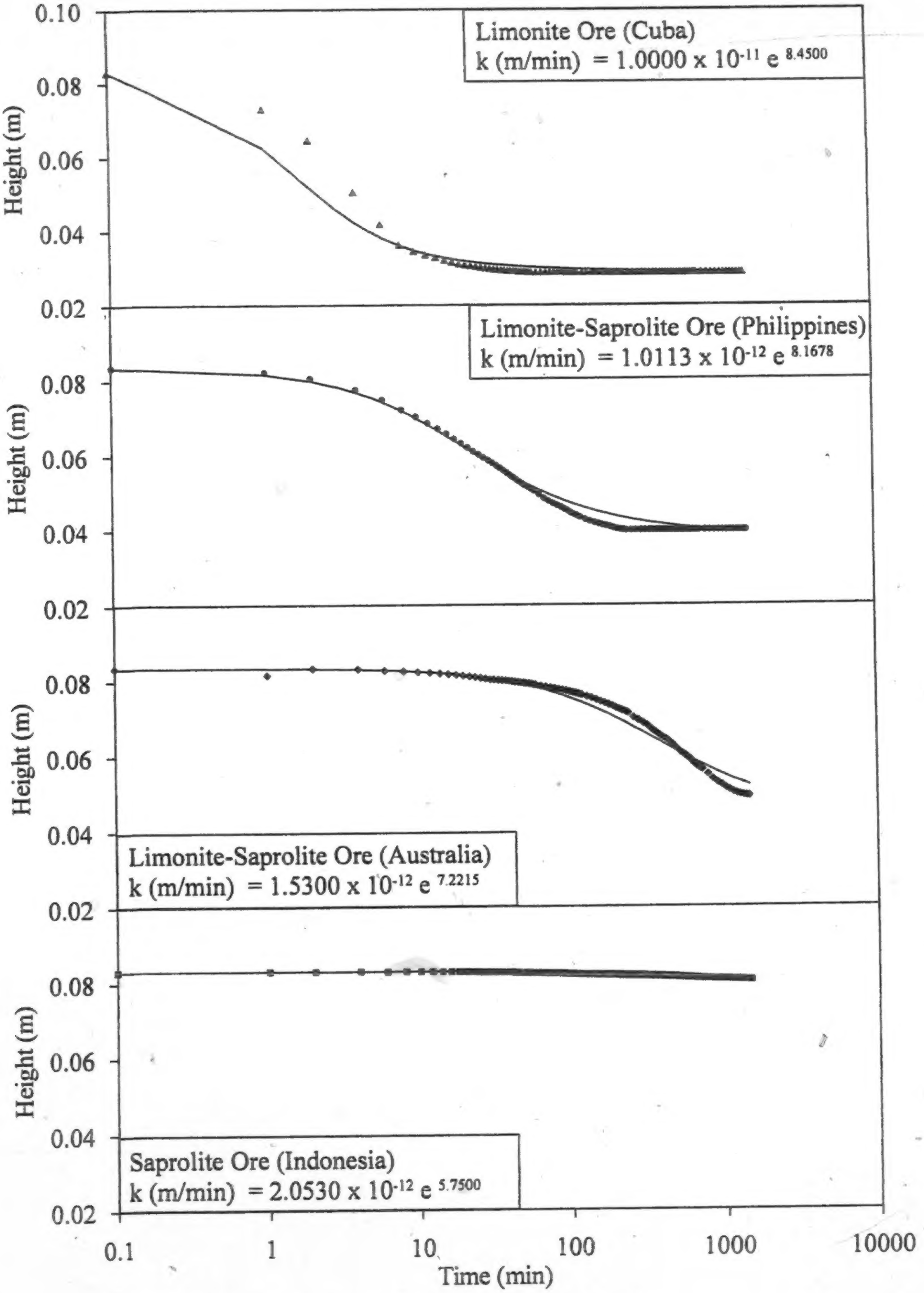

Figure 4.25: Simulation of sedimentation test results

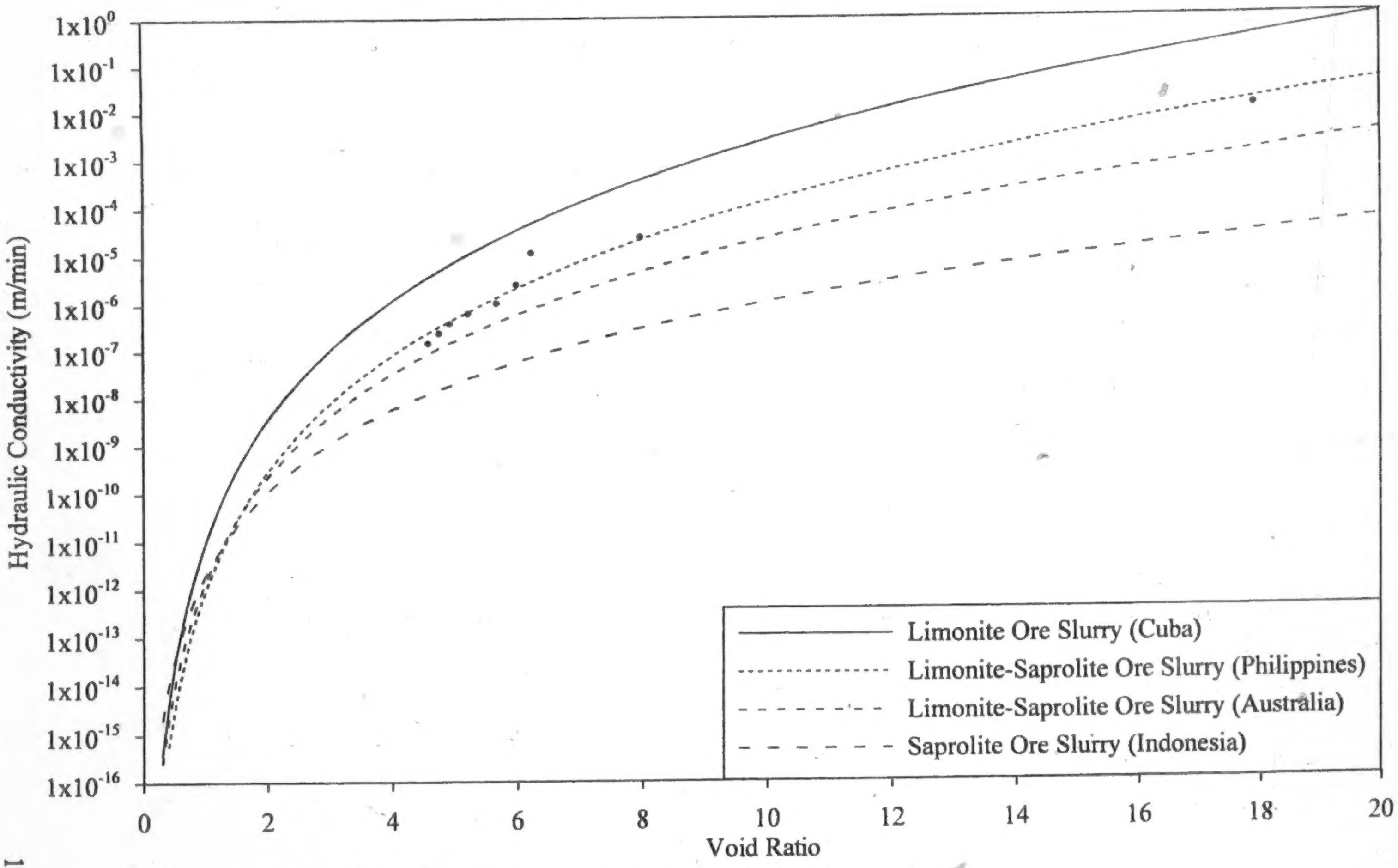

Figure 4.26: Hydraulic conductivity-void ratio relation for laterite ore slurries

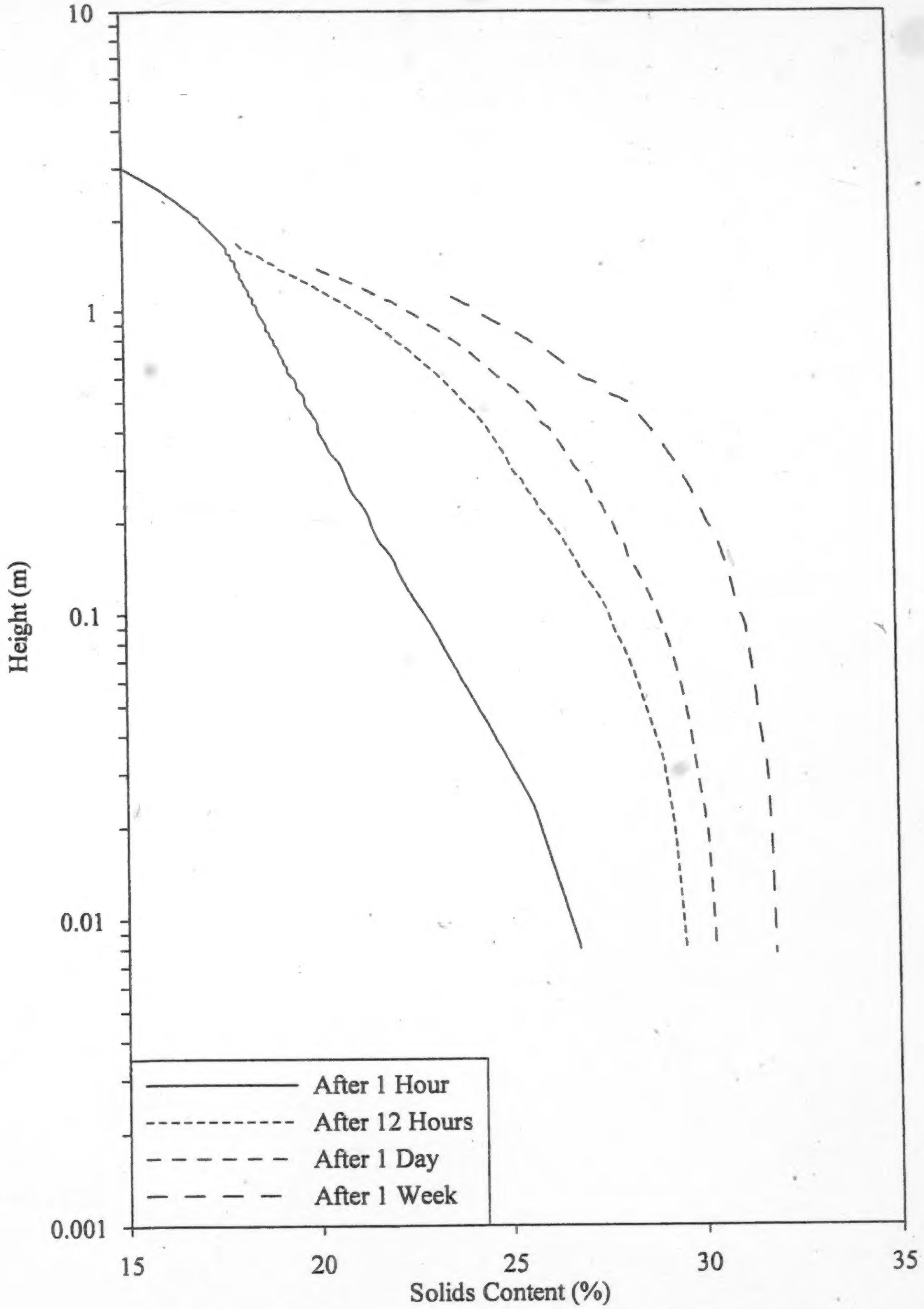

Figure 4.27: Predicted behavior in the storage thickener

Figure 4.27 illustrates that the solids content increases both as a function of time and of depth in the thickener. With increasing time, the decline in surface height of the slurry indicates the gradual commencement of consolidation under self-weight. This consolidation behavior is independent of the filling rate (Suthaker 1995). The figure shows that the profiles converge at low solids content due to the continuation of sedimentation into consolidation. The solids content profile has two smoothly joining straight-line components. The initial straight-line portion portrays rapidly increasing solids content with depth whereas the final straight-line part denotes a slow increase in solids content. The increasing length of this latter straight-line segment with time signifies an increasing compaction bed thickness.

Figure 4.27 indicates that the improvement in solids content of the ore slurry from Philippines is initially high and gradually fades away with time. The solids content increases from 15% to 26.5% after one hour and up to 30% after 12 hours. Under self-weight, a further increase in solids content amounts to a mere 2% after a week in the storage thickener. A similar behavior can be envisaged for all of the other laterite ore slurries.

The computer program modeled the performance of the ore slurry in the storage thickener. This prediction showed that the solids content of the ore slurry can be increased up to 30% in 12 hours. Given the operational constraints of the metal extraction process such as time, thickener geometry, and the preclusion of load application, the solid-liquid separation behavior of laterite ore slurries can be improved using synthetic polymers as will be discussed in Chapter Six.

4.8 LATERITE SLURRY CHARACTERISTICS DIAGRAM

Figure 4.28 depicts the characteristics of various laterite ore slurries on the ternary diagram. The diagram compiles the data presented earlier on sedimentation limit (Table 4.6) and consistency limits (Table 4.1) and shows that all of these limits are part of the family of constant clay-water ratio lines. This is because these lines denote constant physico-chemical interactions between clay particles and the medium. The upward deviation of soil behavior from the constant clay-water ratio lines at low clay content is attributed to the absence of clay minerals in the limonite ore slurry from Cuba and the presence of amorphous material in the saprolite ore slurry from Indonesia. This means that the clay-water ratio lines are sensitive to mineral composition of the materials.

Figure 4.28 also gives the hydraulic conductivity of the laterite ore slurries on the ternary diagram. The figure shows that the hydraulic conductivity is also part of the family of constant clay-water ratio lines. This is because hydraulic conductivity of laterite ore slurries depends on the same interactions described above. The diagram indicates that the hydraulic conductivity of laterite ore slurries varies by two orders of magnitude between the sedimentation limit ($k = 10^{-6}$ cm/sec) and the liquid limit ($k = 10^{-8}$ cm/sec).

It is important to know that separate slurry characteristics diagrams should be developed for different laterite ore materials. However, all of these different materials can be plotted on the same ternary diagram for a convenient comparison of engineering behavior.

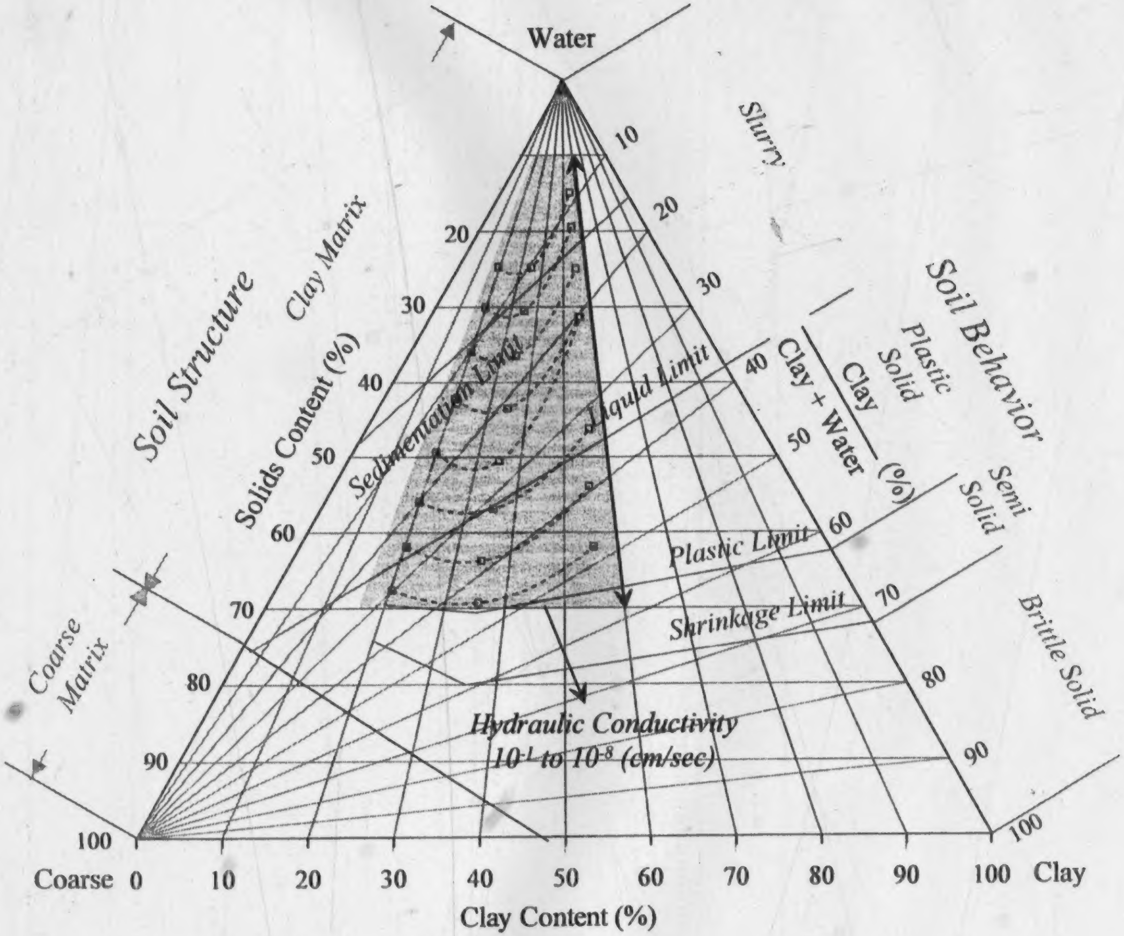

Figure 4.28: LSCD for laterite ore slurries

4.9 SUMMARY AND CONCLUSIONS

This chapter provided a detailed geotechnical characterization of laterite ore slurries. The influence of geological history and the environment on the solid-liquid separation behavior of four laterite ores was investigated. These ore were selected from various parts of the globe; Cuba, Philippines, Australia and Indonesia. Results of laboratory investigations pertaining to geotechnical index properties, mineralogy, pore water chemistry, morphology and solid-liquid separation characteristics were presented. These data was used in the numerical simulation to predict field performance of the storage thickener. The entire data were depicted on the laterite slurry characteristics diagram. The conclusions of this chapter can be summarized as follows:

- Geotechnical characteristics of laterite ore slurries from different origins depend on ore geology and the slurry preparation method. These ores have specific gravities in excess of 2.90 and exhibit high water requirement for conversion to slurries suitable for economic metal extraction.
- More than 90% of the material in such slurries is finer than 0.075 mm. Depending on particle bond strength, aggregate size and mineralogy, the clay size fraction ranges between 20 to 60%. The fine grain size and the presence of clays render these ore slurries nonsegregating at an initial solids content of 15%.
- Classified as micaceous fine sandy and silty clays, these materials are primarily composed of goethite, hematite and maghemite with sizeable amounts of clay minerals and amorphous materials.

- Local slurry preparation practices differ in various parts of the globe but all use tap or groundwater that is influenced by seawater concentration. The pore fluid is neutral to slightly basic with Na^+, Ca^{2+}, Mg^{2+}, Cl^- and SO_4^{2-} as predominant ions.

- Variable mineralogy and pore water chemistry result in variable morphology. Soil fabric ranges from flocculated to dispersed; a partial or complete cardhouse microstructure is associated with limonite-saprolite ore slurries.

- The combined effect of variable material characteristics is vividly expressed during sedimentation under self-weight. The initial hydraulic conductivity of laterite ore slurries ranges between 10^{-1} to 10^{-4} cm/sec.

- The solid-liquid separation process is governed by sedimentation. Under self-weight, 65% dewatering is achieved as the void ratio changes from 17.9 to 8.0 and solids content changes form 15 to 28%. A maximum effective stress of 8 kPa is sufficient to obtain 83% dewatering.

- The hard, ultra-fine and angular sesquioxide particles are associated with high tortuousity and high void ratio. These particle characteristics are responsible for the low hydraulic conductivity and the low compressibility of laterite ore slurry during consolidation.

- The operational constraints of the metal extraction process include time, thickener geometry, preclusion of load application, and minimal changes in process conditions. Using synthetic polymers, improvement in the solid-liquid separation behavior of laterite ore slurries should be investigated.

Chapter 5

Characteristics of Laterite PAL Slurries

5.1 GENERAL

Geotechnical characterization of laterite PAL slurries is pivotal to understand and improve their solid-liquid separation behavior. This knowledge is also useful for an economic assessment of material performance during metal extraction. This chapter studies the effect of environment on the solid-liquid separation behavior of four types of laterite PAL slurries, obtained from consistent process conditions given in Table 3.1. These samples corresponded to the ore samples described in Chapter Four and selected from various parts of the globe: Cuba, Philippines, Australia and Indonesia. The Cuban sample represented a limonite PAL whereas the Indonesian sample denoted a saprolite PAL; the Philippines and the Australian samples corresponded to two distinct varieties of limonite and saprolite PAL blends. Results of laboratory investigations pertaining to geotechnical index properties, mineralogy, pore water chemistry, morphology and solid-liquid separation characteristics are discussed. This is followed by providing the results of numerical simulation of the laboratory data to predict filed performance of the CCD thickener. Next, the laboratory and modeling data is depicted on the laterite slurry characteristics diagram constructed for the PAL samples. Finally, a summary and the main conclusions drawn from this chapter are given.

5.2 GEOTECHNICAL INDEX PROPERTIES

5.2.1 General

Geotechnical characterization of laterite PAL slurries begins with an investigation of their index properties. These properties are used to classify laterite PALs and to evaluate the performance of their slurries. Table 5.1 summarizes the geotechnical index properties of laterite PAL slurries. This table indicates similarities and contrasts in different samples. Derived from the raw ore and the acid leaching environment, the color of these samples denotes their composition that controls their distinct set of properties.

5.2.2 Water Content

Table 5.1 gives the water content of different laterite underflow slurries from the first thickener of the CCD circuit. The table indicates that all samples are associated with high water content, which is attributed to the high water requirement during the acid leaching operation. The amount of water required in the autoclave mainly depends on the economics of the process (Carlson & Simmons 1960). The table also shows that the water content of the PAL slurries is generally higher than their corresponding ore slurries suggesting an improvement in the solid-liquid separation behavior of the latter materials. Table 5.1 also indicates that the water content of the limonite-saprolite PALs measures lower than both the limonite and the saprolite PALs. This is attributed to the possible presence of some mineral types in these PALs containing adsorbed and/or structural water that cannot be removed at a temperature of 50 °C (Mackenzie 1957).

Table 5.1: Geotechnical index properties of laterite PAL slurries

Property	Sample Type and Origin			
	Limonite PAL	Limonite-Saprolite PAL		Saprolite PAL
	Cuba	Philippines	Australia	Indonesia
Color	Brown	Dark Brown	Brown	Light Brown
ω (%)	177	119	131	261
s (%)	36	46	43	28
Gs	3.22	3.56	3.22	3.22
e	5.74	4.24	3.22	8.40
- 0.075 mm (%)	70	71	69	72
- 0.002 mm (%)	6	7	12	19
I_S	13.8	12.3	15.0	10.0
ω_L (%)	26	27	50	83
ω_P (%)	17	16	30	42
ω_s (%)	15	14	18	25
I_P (%)	9	11	20	41

The solids content of laterite underflow PAL slurries in the first CCD thickener gives an insight into their dewatering behavior. Table 5.1 indicates a variable amount of water release for the investigated PAL slurries despite the fact that the solids content at the start of the leaching operation is the same for all. The table shows that the limonite-saprolite PAL slurries release more water than the other two PAL slurries. Thus, the former slurries coalesce the positive characteristics of both PAL types. This is attributed to the combined effect of mineralogical composition and the leaching environment described by pore water chemistry. Detailed discussion of the influence of these compositional and environmental factors on the solid-liquid separation behavior of laterite PAL slurries is discussed latter in this chapter.

5.2.3 Specific Gravity

Table 5.1 indicates that the specific gravity of laterite PALs is higher than their ore counterparts. This is attributed to the presence of heavy iron oxides in these materials (Gidigasu 1976). The high values of specific gravity of the PALs partly contribute in improving the solid-liquid separation behavior of the slurries. Among the two limonite-saprolite PAL slurries, the slight improvement in solids content observed in the Philippines sample is due to its higher specific gravity of 3.56. This value of specific gravity is also responsible for a higher value of void ratio of the Philippines PAL slurry despite its low solids content. For all PAL slurries, the corresponding void ratios reflect the underflow solids content in the first CCD thickener due to identical values of specific gravity.

5.2.4 Grain Size Distribution

Figure 5.1 gives the grain size distribution of various laterite PAL slurries. Results of the combined hydrometer and wet sieve analyses depict the true grain sizes of the investigated slurries because no dispersing agent was used during the test. Based on ASTM definitions, the figure distinguishes between three grain sizes for laterite PAL slurries. A sand size refers to material coarser than 0.075 mm and a clay size pertains to material finer than 0.002 mm; a silt size is sandwiched between the former two sizes of grains.

Figure 5.1 shows that the amount of sand size material is only 28 to 31% for all of the laterite ores; material finer than 0.075 mm is in the range of 69 to 72% as indicated by Table 5.1. A comparison with the corresponding ore slurries (Table 4.1) reveals that the sand size has increased by four to five times. This means that acid leaching has either resulted in grain size growth or dissolution of the fine materials. Based on literature (Tindall & Muir 1998) and observed morphology (given later in this chapter), grain size growth is the most likely phenomenon. Figure 5.1 further illustrates that bulk of the materials of all of the laterite PAL slurries fall in the silt size region with variable clay size fraction. The variability in the grain size distribution curves of various types of laterite PAL slurries is due to the variable ore mineralogy; different initial minerals transform to different final minerals during acid leaching. Further, these various minerals may exhibit different particle bond strength and aggregate size (Schramm 1996) thereby causing variability in grain size distribution.

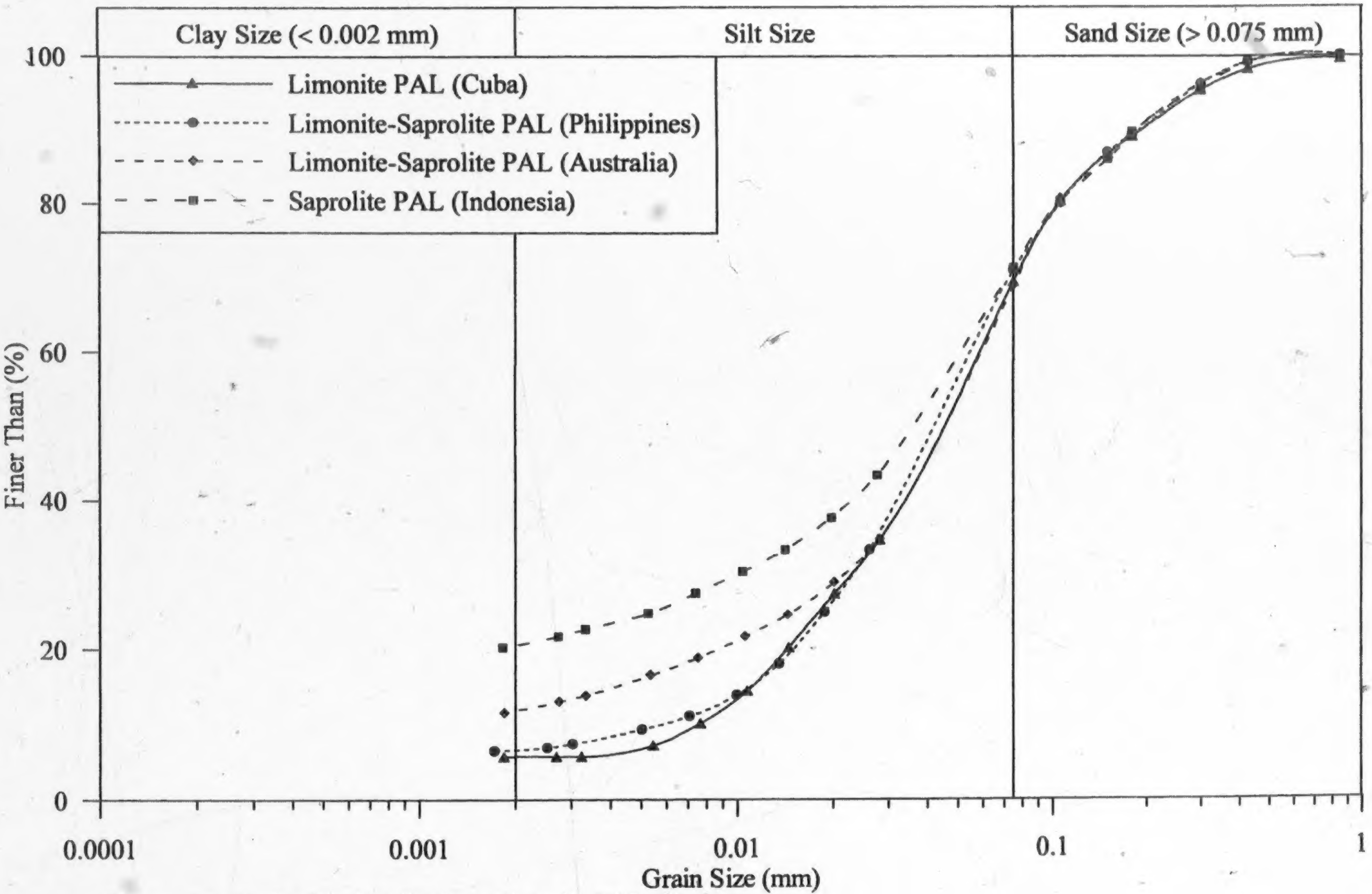

Figure 5.1: Grain size distribution of laterite PAL slurries

Figure 5.1 indicates that all of the laterite PAL slurries are well-graded materials. Still, the limonite PAL slurry from Cuba and the limonite-saprolite PAL slurry from Philippines can be considered slightly poorly-graded as these samples contain a clay size fraction of 7%. On the contrary, the limonite-saprolite PAL from Australia and the saprolite PAL slurry from Indonesia are more well-graded materials having higher clay contents of 12 and 19%, respectively. The latter clay size fraction for the saprolite PAL slurry from Indonesia is identical to the corresponding ore slurry. This suggests that amorphous materials do not transform during acid leaching.

Grain size distribution influences the mechanical and the physico-chemical interactions of laterite ore slurries. First, the high amount of sand size material in these slurries is partly responsible for the lower void ratios in the CCD thickener (Table 5.1) when compared to those of the ore slurries in the storage thickener (Table 4.1). Second, well-graded materials help minimize segregation of the clay and coarse fractions as discussed in the next section. Third, the clay size fraction of these slurries governs the colloid-electrolyte interactions, which in turn, influence plasticity, volume change and hydraulic conductivity.

5.2.5 Segregation

Figure 5.2 gives the results of the segregation tests on various laterite PAL slurries in the form of normalized height versus solids content for different initial solids content. This figure shows that the observed solids content increases with depth and that the profiles tend to reach the vertical with increasing initial solids

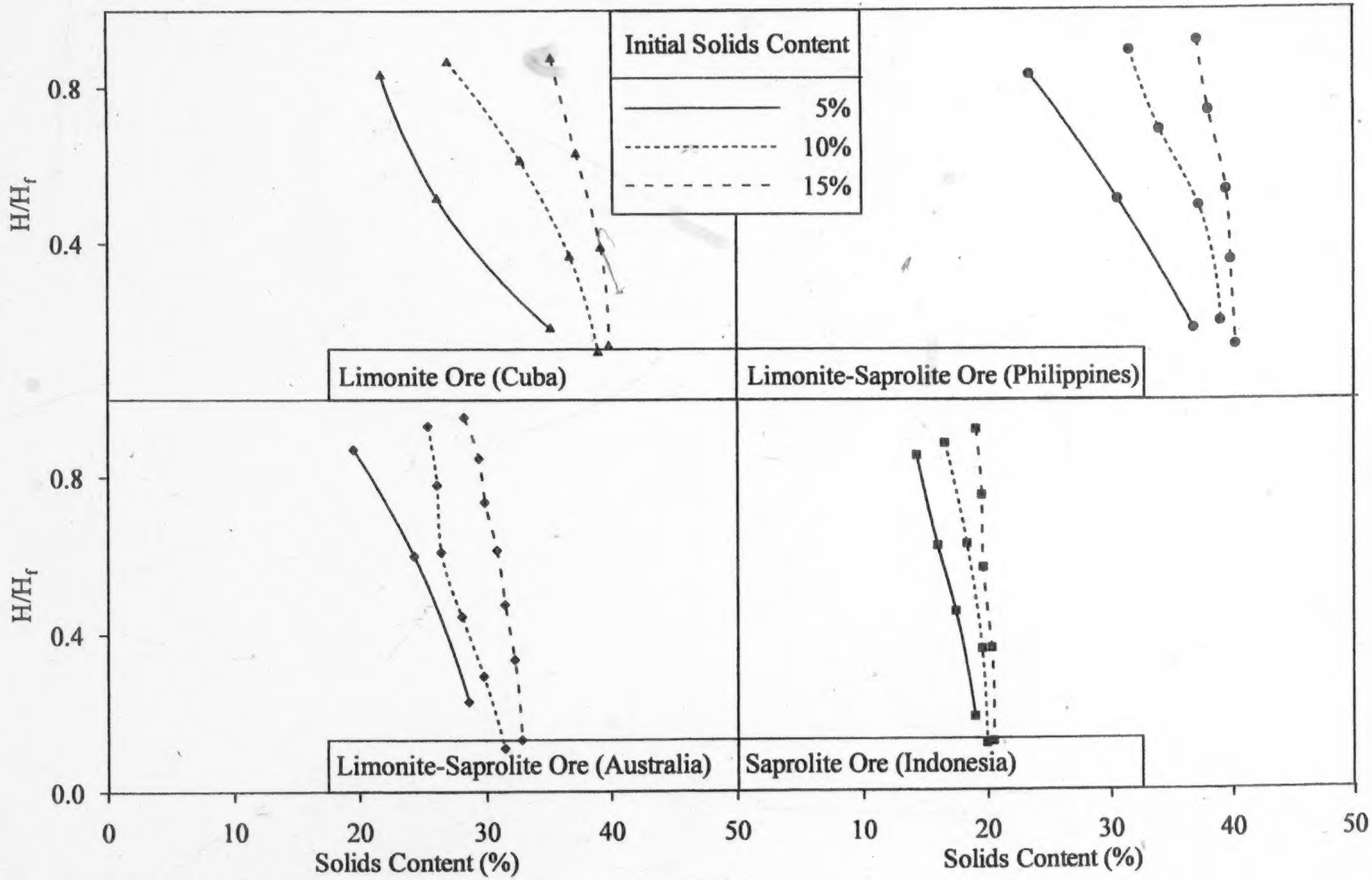

Figure 5.2: Segregation test results for laterite PAL slurries

content. This behavior is similar to the ore slurries and is attributed to diminishing segregation at high initial solids content due entrapment of coarse grains by clay size grains. This is clearly observed in the limonite-saprolite PAL slurry from Australia and the saprolite PAL slurry from Indonesia. Conversely, the limonite PAL slurry from Cuba and the limonite-saprolite PAL slurry from Philippines show greater deviation from the vertical especially at low values of initial solids content. Figure 5.2 also gives an indication of improved sedimentation of PAL slurries by exhibiting higher solids content than their respective ore slurries.

Figure 5.3 gives the percentage of segregation as a function of the initial solids content for various laterite PAL slurries. This figure indicates that variation in the segregation characteristics of different slurries is marginal owing to the nearly same amount of coarse size material. All of the laterite PAL slurries are indicated to exhibit 3 to 15% segregation. On Figure 5.3, a segregation limit (I_S) is defined as the initial solids content that pertains to 5% segregation with depth measured during the test. Based on this definition, I_S values for the four laterite PAL slurries are given in Table 5.1. With the exception of limonite-saprolite ore slurry from Australia, these values indicate that the segregation limits of laterite PAL slurries are lower than the corresponding ore slurries. This is attributed to the interaction of solid particles with sulfuric acid present in the samples. Caughill et al. (1993) reported a similar improvement in the segregation behavior of Alberta oil sand tailings. Based on the Table 5.1, all of the laterite PAL slurries are essentially non-segregating at an initial solids content of 15%.

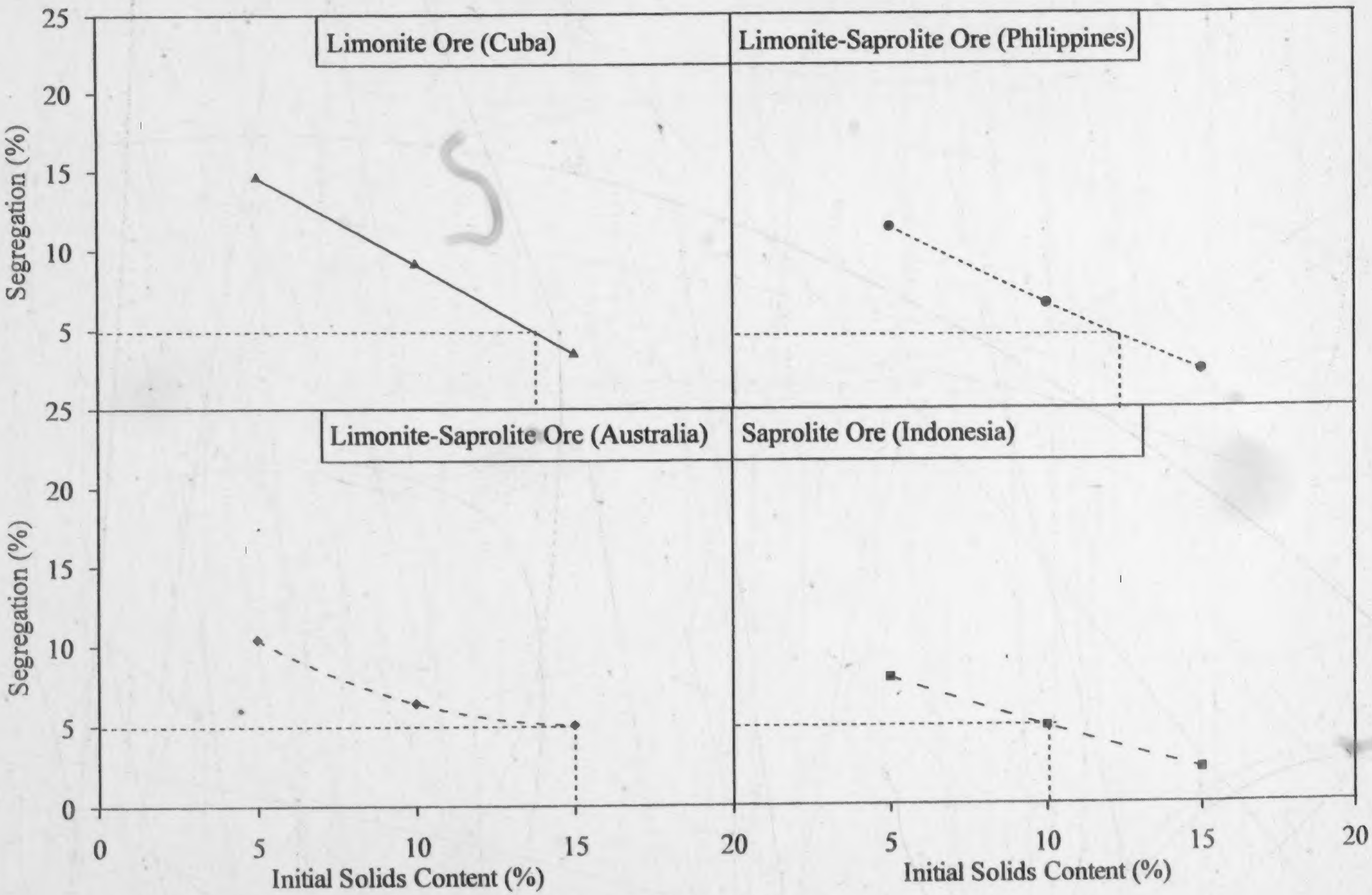

Figure 5.3: Segregation limit for various laterite PAL slurries

5.2.6 Consistency Limits

Table 5.1 indicates that laterite PALs have variable consistency limits. This is attributed to their distinct mineralogy and the chemistry of the pore water during the autoclave operation. The lower consistency limits of all of the laterite PALs than their ore counterparts indicate mineral transformation during acid leaching. Since, such transformation mainly occurs in sesquioxides whereas clay mineral structures collapse, the limonite-saprolite PAL from Australia and the saprolite PAL from Indonesia have higher consistency limits as they contain large amount of amorphous materials. Further, the expected high concentration of various electrolytes in the pore water is also partly responsible for the low consistency limits of the laterite PAL slurries.

The plasticity chart (Casagrande 1948) gives a preliminary assessment of the mineralogical composition of soils. Figure 5.4 that shows the regions of various clay minerals and sand, plots various laterite PALs on such a chart. This figure illustrates that the limonite PAL from Cuba and the limonite-saprolite PAL from Philippines are close to the region designated as *sand*. Similarly, the engineering behavior of the limonite-saprolite PAL from Australia is expected to be similar to that of the kaolinite whereas the saprolite PAL from Indonesia is still classified as micaceous fine sandy and silty clay (Holtz & Kovacs 1981). The plasticity chart reveals little about the mineralogy of these materials. Therefore, a comprehensive account of the mineralogical composition of different laterite PALs is given in the next section.

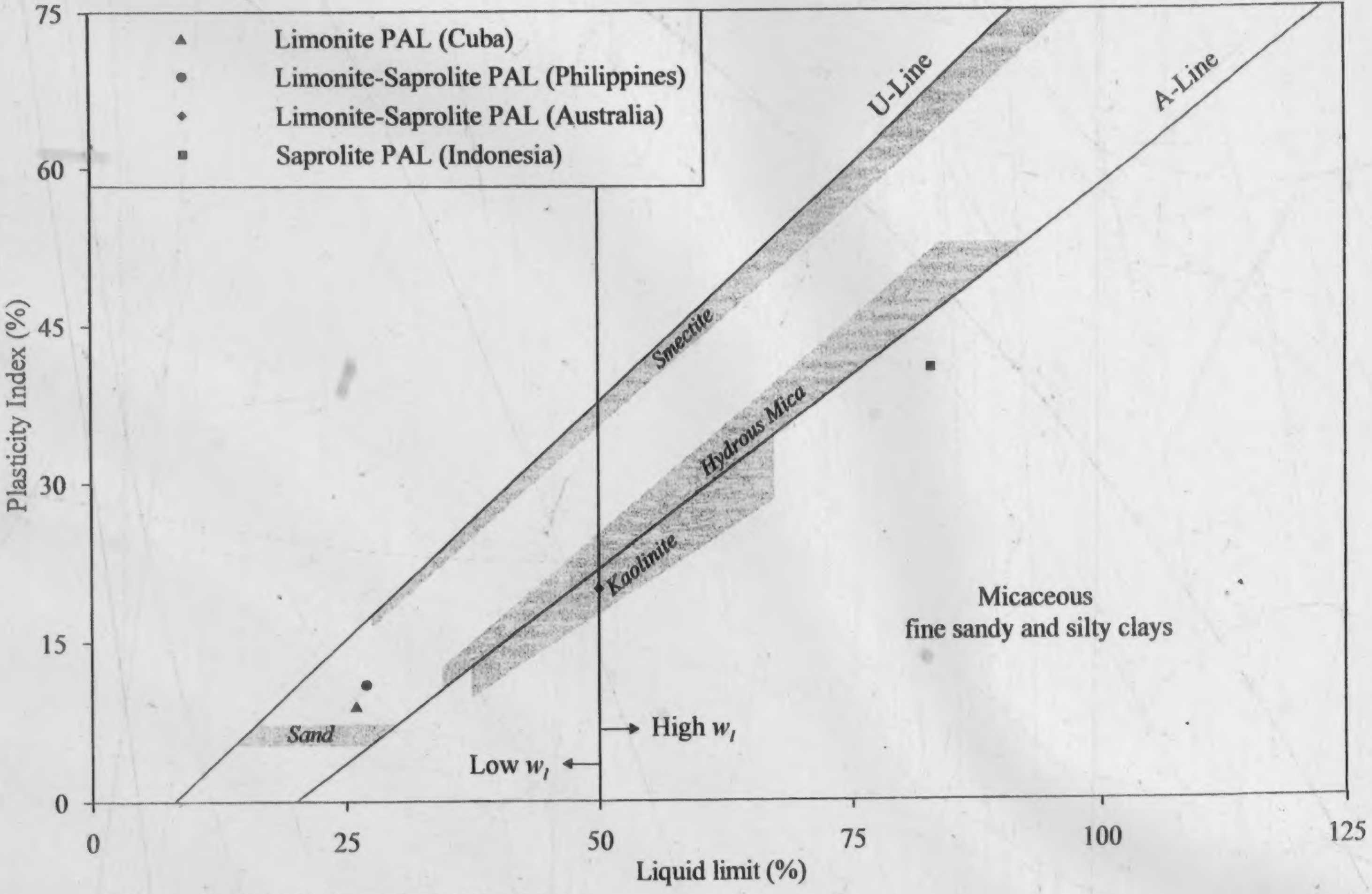

Figure 5.4: Plasticity chart for laterite PALs

5.3 MINERALOGY

5.3.1 General

Mineralogical composition governs the size, shape and surface characteristics of soil particles. It determines the interaction of the solid phase with the liquid phase and hence affects sedimentation, consolidation and hydraulic conductivity (Mitchell 1993). Results of x-ray diffraction (XRD) analyses, anion exchange and cation exchange are discussed in this section.

5.3.2 X-Ray Diffraction

Figure 5.5 highlights the main constituent minerals on the x-ray diffraction patterns of bulk samples of the laterite PALs. This figure shows that all of the laterite PALs contain hematite (Fe_2O_3), which is obtained from the interaction of goethite (α-FeO.OH) with sulfuric acid according to the following two-step reaction (Tindall & Muir 1998):

$$2\ FeO(OH)_{(s)} + 3\ H_2SO_4 \rightarrow 2\ Fe^{3+} + 3\ SO_4^{2-} + 4\ H_2O \qquad (5.1)$$

$$2\ Fe^{3+} + 3\ SO_4^{2-} + 4\ H_2O \rightarrow Fe_2O_{3\ (s)} + 3\ H_2SO_4 + H_2O \qquad (5.2)$$

Figure 5.5 further illustrates that none of the PAL samples have any trace of clay mineral species, which were present in their respective ore samples. Although, the structures of most of the clay mineral species is known to collapse at a temperature of up to 550 °C (Grim 1968), the combined influence of temperature, pressure and sulfuric acid in the autoclave is observed to have produced the same effect.

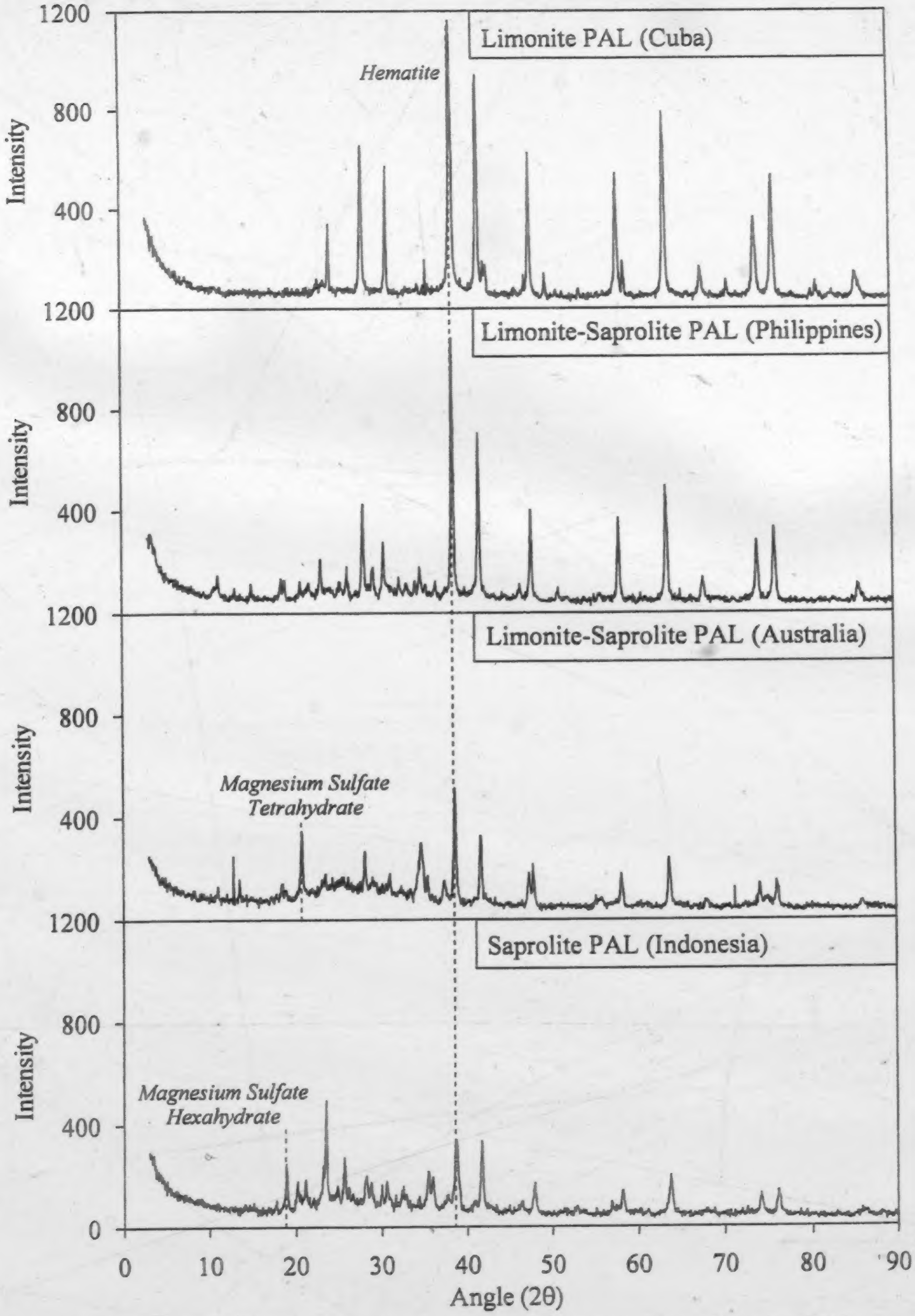

Figure 5.5: X-ray diffraction patterns of bulk samples of laterite PALs

Figure 5.5 also indicates the presence of magnesium sulfate tetrahydrate at 18° angle (2θ) in limonite-saprolite PAL from Australia and magnesium sulfate hexahydrate at 20° angle (2θ) in the saprolite PAL from Indonesia. These two mineral types are characterized by different amounts of water of crystallization. Although, not easily detected by the XRD analyses, the diffraction patterns of these PALs also show the presence of amorphous material such as amorphous silica. The sulfate minerals are obtained during acid leaching by the conversion of magnesium silicates, which constitute an appreciable amount of the corresponding ores. Likewise, amorphous silica is obtained as a byproduct during the conversion of magnesium silicate to magnesium sulfate.

The XRD analyses depend on the degree of crystallinity of the material and grain size. Figure 5.5 shows that the peak intensity of the limonite PAL from Cuba and the limonite-saprolite PAL from Philippines are the highest. On the contrary, the other two PAL materials have much lower degrees of crystallinity. The lower degrees of crystallinity of the limonite-saprolite PAL from Australia and the saprolite PAL from Indonesia are attributed to the presence of amorphous materials in these two samples. The effect of grain size in the XRD analysis of laterite PALs is less important due to the absence of clay mineral species, which are dissolved during the extraction process. Similarly, the iron oxide coatings are invariably removed by identical process conditions during acid leaching. Therefore, the use of x-ray diffraction technique applied to laterite PALs gives credible and invaluable information about soil composition.

The amount of each mineral type in various laterite PALs depends upon ore mineralogy. Table 5.2 gives semi-quantitative estimates of x-ray diffraction results for the former materials. This table indicates that all of the PALs contain high amounts of hematite, which is the main factor that contributes to the high specific gravity of the PAL materials.

Based on mineralogical composition, an estimate of specific gravity can be made using G_s values of 5.26 for hematite (Gidigasu 1976) and 3.80 for magnesium sulfate minerals (Grim 1968). A comparison of Table 5.1 and Table 5.2 indicates discrepancies between measured and estimated G_s values for various laterite PALs. This overestimation is attributed to the semi-quantitative nature of interpreting XRD results, which depend on the degree of crystallinity of the material. Therefore, the percent amount of a mineral given for each sample in Table 5.2 corresponds to the amount of the crystalline phase of that mineral in the specimen. Due to this difficulty in quantification, amorphous materials were excluded from G_s calculation of the limonite-saprolite PAL from Australia and the saprolite PAL from Indonesia.

Table 5.2 also explains the consistency behavior (depicted earlier in Table 5.1) of various laterite PALs. The table shows that the materials containing significant amount of amorphous silica tend to hold water due to adsorption and capillary condensation (Briceno & Osseo-Asare 1995). In addition to siliceous materials, the presence of magnesium sulfate in the limonite-saprolite PAL from Australia and the saprolite PAL from Indonesia resulted in high consistency limits

Table 5.2. Percent amount of various minerals in laterite PALs

Mineral	Sample Type and Origin			
	Limonite PAL	Limonite-Saprolite PAL		Saprolite PAL
	Cuba	Philippines	Australia	Indonesia
Magnesium Sulfate Tetrahydrate			10-15	
Magnesium Sulfate Hexahydrate				15-20
Hematite	100	100	80-85	70-75
Silica and/or Iron oxides			5-10	10-20
G_s	5.3	5.3	4.6 – 5.0	4.3 – 4.7

of these materials. Variation in consistency of these two PALs is attributed either to changes in the gelatinous character of the two mineral types of magnesium sulfate and/or the difficulty in removing crystal water (Yariv & Cross 1979).

The presence of heavy hematite and magnesium sulfate minerals in the laterite PALs is expected to cause an improvement in the solid-liquid separation behavior over their counterpart ore slurries. The occurrence of magnesium sulfates and amorphous materials in both the limonite-saprolite PAL from Australia and the saprolite PAL from Indonesia, it is anticipated that their slurries will exhibit slower and less dewatering during sedimentation and consolidation.

5.3.3 Anion Exchange

Table 5.3 presents the anion exchange characteristics of the laterite PALs. The table indicates that all of the values are less than those of the laterite ores depicted in Table 4.3. This is attributed to the absence of clay minerals with broken edges in these former samples. The TAEC of all of the PAL materials is mainly derived from SO_4^{2-} ion because of the preferential adsorption of the ion (Tan 1998). Further, the somewhat higher TAEC values associated with the limonite-saprolite PAL from Australia and the saprolite PAL from Indonesia owes their origin to the presence of magnesium sulfates and amorphous materials.

The point of zero charge (PZC) for hematite can be as low as 5.0 (Drever 1982). At very low pH values during the acid leaching process, the predominantly hematite minerals, which are positively charged, are expected to result in a negatively charged double layer (Mitchell 1993).

Table 5.3. Anion exchange of laterite PALs

Exchangeable Anions (cmol(-)/kg)	Sample Type and Origin			
	Limonite PAL	Limonite-Saprolite PAL		Saprolite PAL
	Cuba	Philippines	Australia	Indonesia
Cl^-	0.34	0.11	0.51	0.42
NO_3^-	0.02	0.01	0.02	0.01
SO_4^{2-}	1.05	2.79	4.07	5.39
TAEC	1.41	2.91	4.60	5.82

5.3.4 Cation Exchange

Table 5.4 presents the cation exchange of laterite PALs. The table indicates that the TCEC of all of the laterite PALs is mainly derived from exchangeable Mg^{2+}; in case of limonite-saprolite PAL from Australia, some exchangeable Ca^{2+} is also observed. The predominance of Mg^{2+} in these materials is attributed to the release of this ion from collapsed chrysotile clay mineral during acid leaching. The amount of these high valence cations is comparable with the liquid limit of these PALs. According to Mitchell (1993), high amount of high valence cations result in high liquid limit in nonexpansive materials.

The higher TCEC values and high consistency limits of the limonite-saprolite PAL from Australia and the saprolite PAL from Indonesia indicate that the magnesium sulfate minerals are similar to clay minerals. These sulfate minerals partly contribute to the high amount of Mg^{2+} in both of these materials.

Table 5.4 converts cation exchange of laterite PALs to their structure by reporting exchangeable sodium percentage (ESP). Soils with ESP<2 possess a flocculated fabric whereas those with ESP≥2% are susceptible to dispersion (Mitchell 1993). Using this definition, the limonite PAL slurry from Cuba and the limonite-saprolite PAL slurry from Philippines is expected to have a flocculated fabric. Conversely, both the limonite-saprolite PAL slurry from Australia and the saprolite PAL slurry from Indonesia are anticipated to possess a dispersed soil morphology. This analysis also shows that the double layer theory is applicable to laterite PAL materials.

Table 5.4. Cation exchange of laterite PALs

Exchangeable Cations (cmol(+)/kg)	Sample Type and Origin			
	Limonite PAL	Limonite-Saprolite PAL		Saprolite PAL
	Cuba	Philippines	Australia	Indonesia
Na^+	0.05	0.09	0.97	0.86
K^+	0.01	0.02	0.03	0.04
Ca^{2+}	0.00	0.02	6.22	0.22
Mg^{2+}	5.61	12.40	40.29	40.48
Al^{3+}	0.47	0.48	0.51	0.24
Fe^{3+}	0.19	0.21	0.25	0.11
TCEC	6.33	13.22	48.27	41.95
ESP (%)	0.79	0.68	2.01	2.05

5.4 PORE WATER CHEMISTRY

5.4.1 General

The characteristics of the water filling the pores of a soil have a profound effect on the interaction of the solid particles with the liquid phase. In fact, the electro-chemical forces at the interface of pore water and solid particles govern soil behavior. This section presents the chemical characteristics of the pore water associated with laterite PAL slurries. These include pH and electrical conductivity and electrolyte concentration.

5.4.2 pH and Electrical Conductivity

Table 5.5 summarizes the characteristics of the pore water in the first thickener of the CCD circuit. This table indicates the extreme degree of acidity of the pore water by reporting pH values less than 1 for all of the laterite PAL slurries. It follows that all materials are well below the PZC for the given mineralogy. Therefore, the conventional double layer theory is applicable to the colloid-electrolyte system of laterite PAL slurries.

Table 5.5 indicates that the electrical conductivity (EC) measured for pore fluids of various laterite PAL slurries reaches the maximum limit of the measuring device. The reported values of 10,000 μS/cm for all materials suggest the presence of high amount of salt forming ions (Rhoades et al. 1990). Based on the investigated soil mineralogy, all of the laterite PAL slurries are expected to contain high concentrations of cations such as H^+, Ca^{2+}, Mg^{2+}, Mn^{2+}, Al^{3+}, Fe^{3+}, Ni^{3+}, Co^{3+} and SO_4^{2-}.

Table 5.5. Pore water chemistry of laterite PAL slurries

Property	Sample Type and Origin			
	Limonite PAL	Limonite-Saprolite PAL		Saprolite PAL
	Cuba	Philippines	Australia	Indonesia
pH	0.8	0.4	0.5	0.6
EC (μS/cm)	10000	10000	10000	10000
Na^+ (mg/L)	80	80	240	40
K^+ (mg/L)	80	80	80	40
Ca^{2+} (mg/L)	90	220	1060	120
Mg^{2+} (mg/L)	131	3360	4100	2200
Mn^{2+} (mg/L)	514	570	310	119
Al^{3+} (mg/L)	2020	736	302	602
Fe^{3+} (mg/L)	492	670	1520	358
Ni^{3+} (mg/L)	11900	13400	12400	4840
Co^{3+} (mg/L)	1500	1540	874	256
Si^{4+} (mg/L)	768	508	586	103
Cl^- (mg/L)	49	98	10320	36
NO_3^- (mg/L)	81	140	1	1
HCO_3^- (mg/L)	5	5	5	5
SO_4^{2-} (mg/L)	44200	67000	64400	31820
TDS (mg/L)	61910	88407	86910	40540

5.4.3 Electrolyte Concentration

Table 5.5 also gives the concentration of individual cations and anions present in the pore water of various laterite PAL slurries. The table indicates that the chemical compositions of all of these waters have the same trend; Ca^{2+}, Mg^{2+}, Mn^{2+}, Al^{3+}, Fe^{3+}, Ni^{3+}, $Co^{3+}$and SO_4^{2-} are present as major ions in all pore waters. It follows that water the pore fluid chemistry is generally identical for all of the laterite PAL slurries. This is confirmed by plotting the various cations and anions depicted in Table 5.5 on the Stiff diagram as shown in Figure 5.6. This figures illustrates that the shapes of the Stiff diagrams for different pore fluids are similar.

Table 5.5 also reports variations in the concentrations of different ions. These variations are ascribable to the geological origin and the pore fluid chemistry of the different laterite ore slurries. For example, the high amount of Al^{3+} in the limonite PAL from Cuba and that of Mg^{2+} in the other three PALs are due to the dissolution of gibbsite and chrysotile, respectively, during acid leaching. Similarly, the high amount of Cl^- in the limonite-saprolite PAL from Australia is attributed to the high amount of this ion in the pore fluid of the ore slurry. The concentration of SO_4^{2-} is mainly due to the dissociation of sulfuric acid but also depends on the background concentration of this ion in the pore fluid of the ore slurry. From the high concentrations of Ni^{3+} and Co^{3+}, Table 5.5 indicates that the pressure acid leaching process is applicable to all types of laterite ores. However, the yield of these economic metals is the least for the saprolite variety.

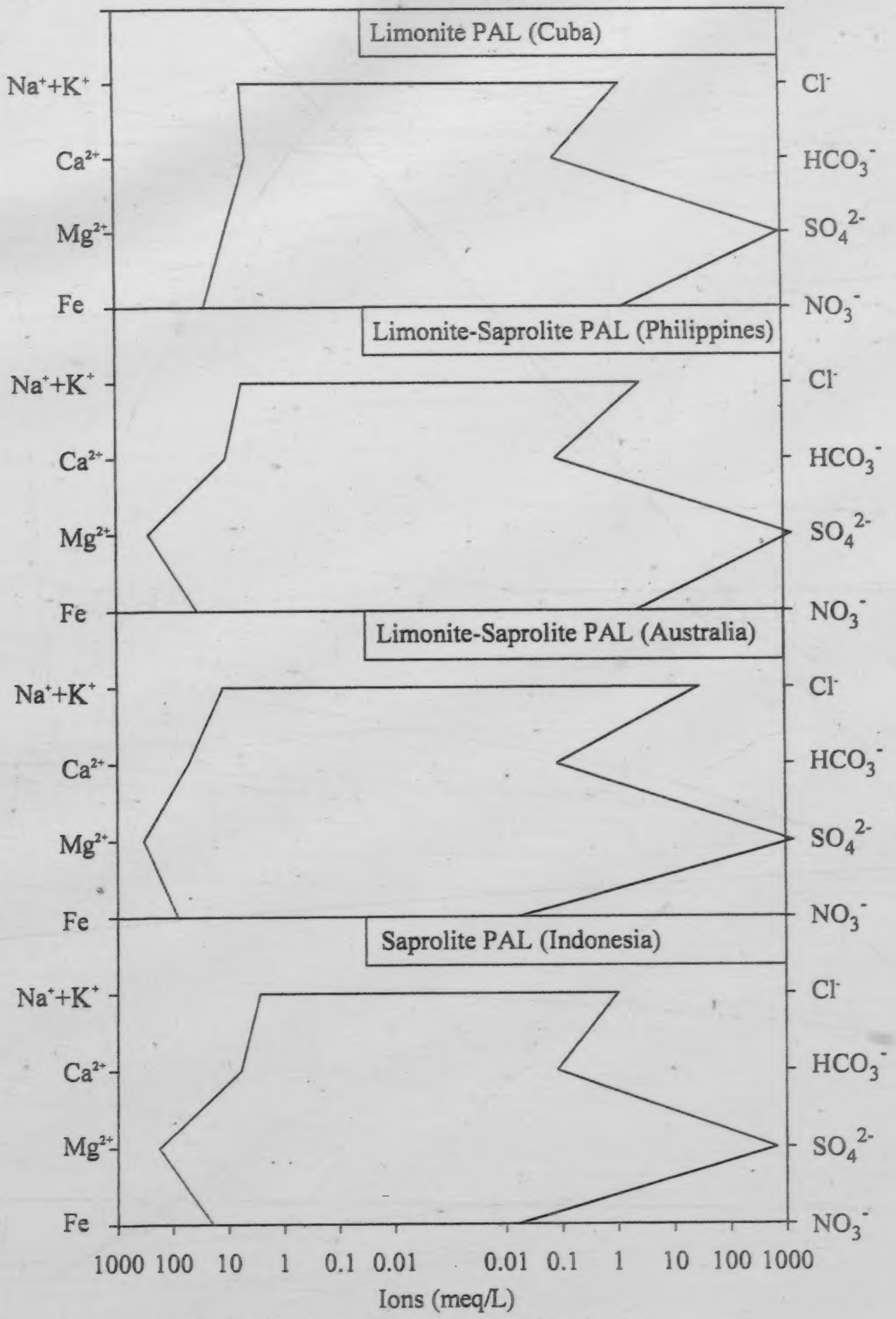

Figure 5.6: Stiff diagrams for laterite PAL slurries

Due to the high values of TDS and the presence of multivalent ions in laterite PAL slurries, as depicted in Table 5.5, flocculated soil microstructures are anticipated. This is because flocculation of colloids is facilitated by a thinner double layer and a reduced surface potential, of which both depend on the presence of a high amount of multivalent electrolytes in the pore fluid (Mitchell 1993). However, soil morphology also depends on the physico-chemical characteristics of the solid phase. Therefore, the above generalization needs to be verified by visual observations of granular interaction in various PAL slurries.

5.5 MORPHOLOGY

5.5.1 General

Morphological analyses were used for a qualitative evaluation of laterite PAL slurries. This section presents a microstructural assessment of laterite PAL slurries obtained from the first CCD thickener. Therefore, these visual observations pertain to soil fabric after the completion of the sedimentation stage in the solid-liquid separation process. Results of scanning electron microscopy are studied in conjunction with elemental analyses.

5.5.2 Scanning Electron Microscopy

Figure 5.7, 5.8, 5.9 and 5.10 give the morphological details of limonite PAL slurry (Cuba), limonite-saprolite PAL slurry (Philippines), limonite-saprolite PAL slurry (Australia) and saprolite PAL slurry (Indonesia), respectively. These figures comprise of four micrographs, each with a different magnification and designated by a scale.

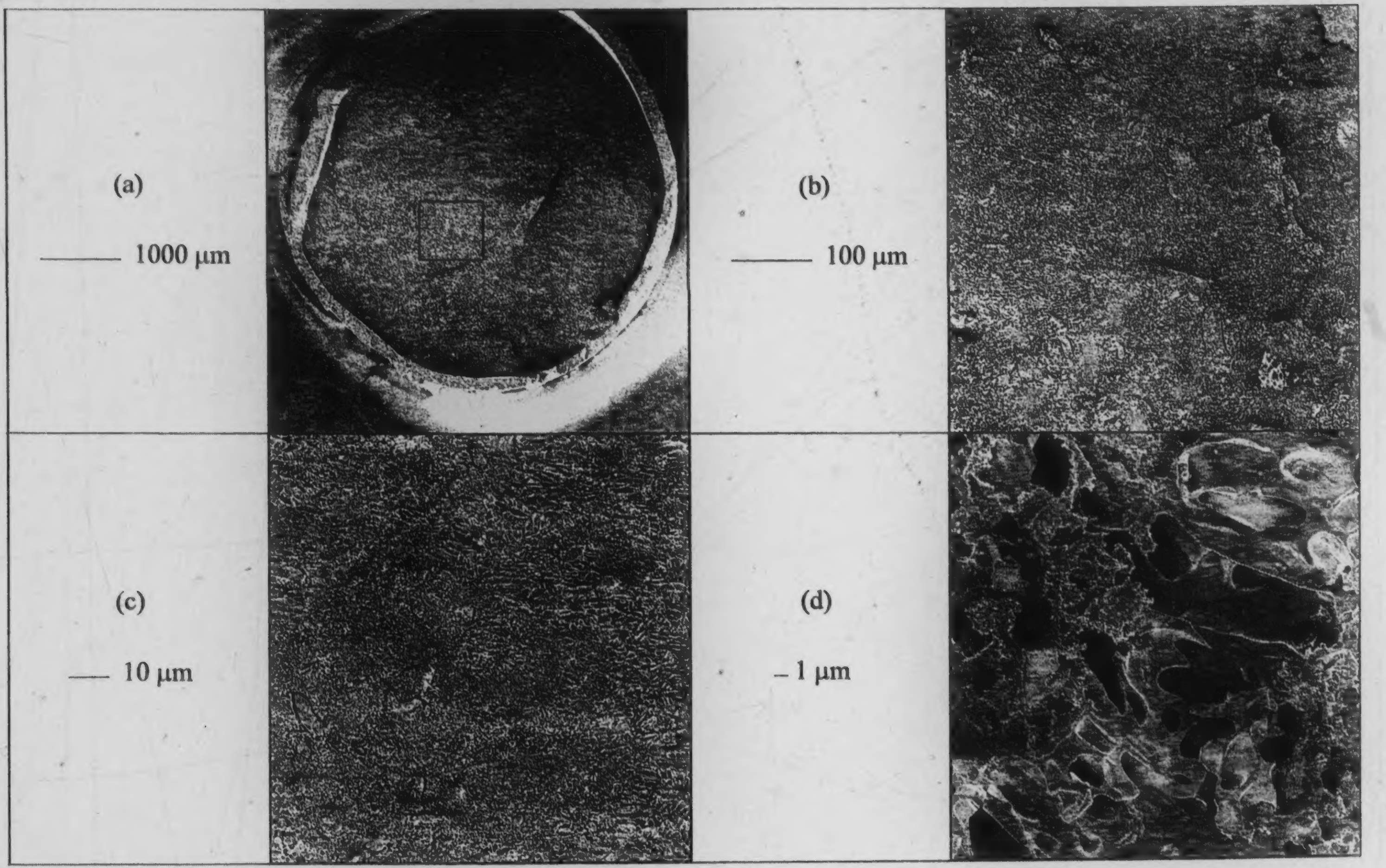
(a)
1000 µm
(b)
100 µm
(c)
10 µm
(d)
1 µm

Figure 5.7: Scanning electron micrographs of limonite PAL slurry (Cuba)

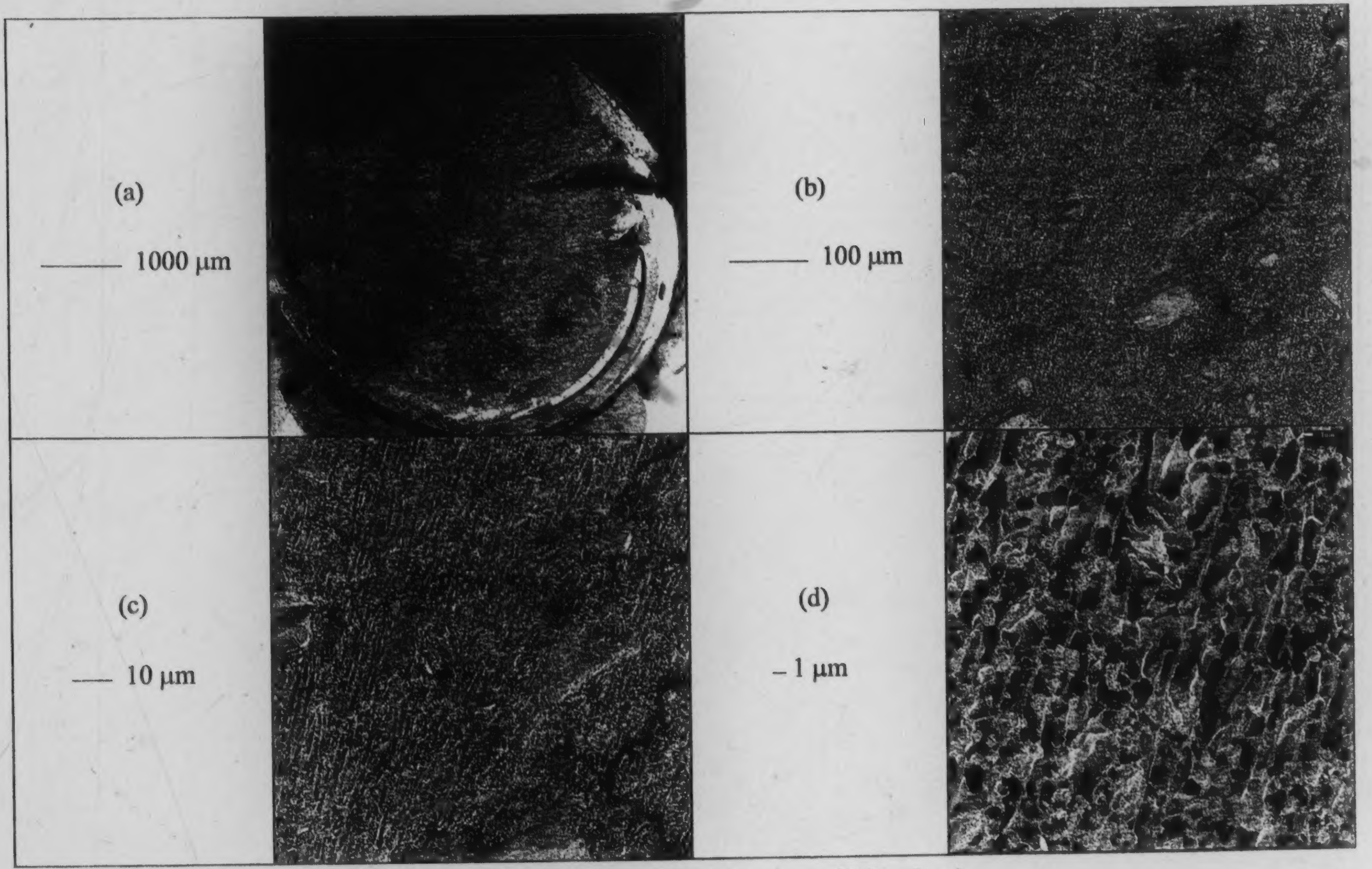
(a)
1000 µm
(b)
100 µm
(c)
10 µm
(d)
1 µm

Figure 5.8: Scanning electron micrographs of limonite-saprolite PAL slurry (Philippines)

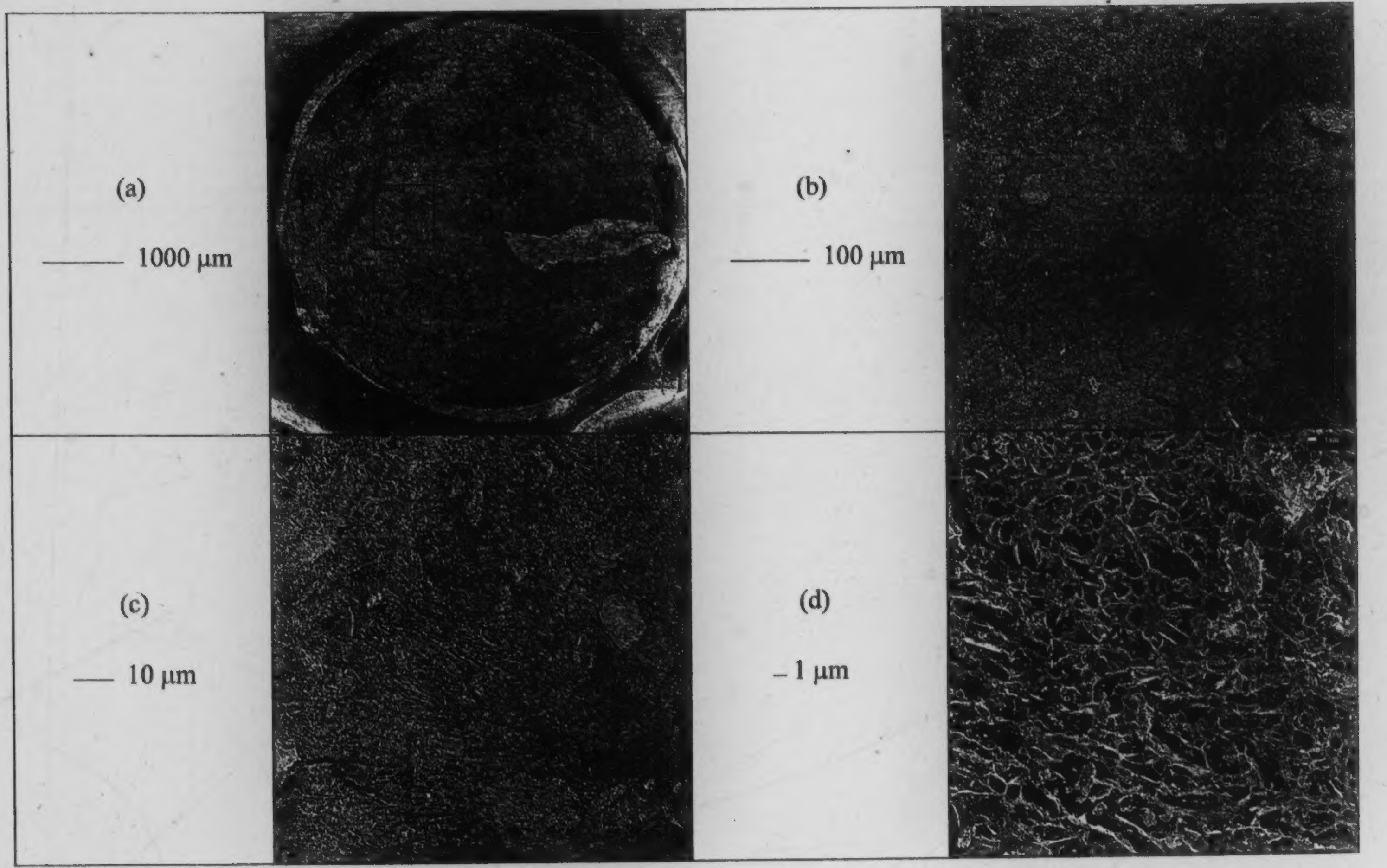
(a)
1000 µm
(b)
100 µm
(c)
10 µm
(d)
1 µm

Figure 5.9: Scanning electron micrographs of limonite-saprolite PAL slurry (Australia)

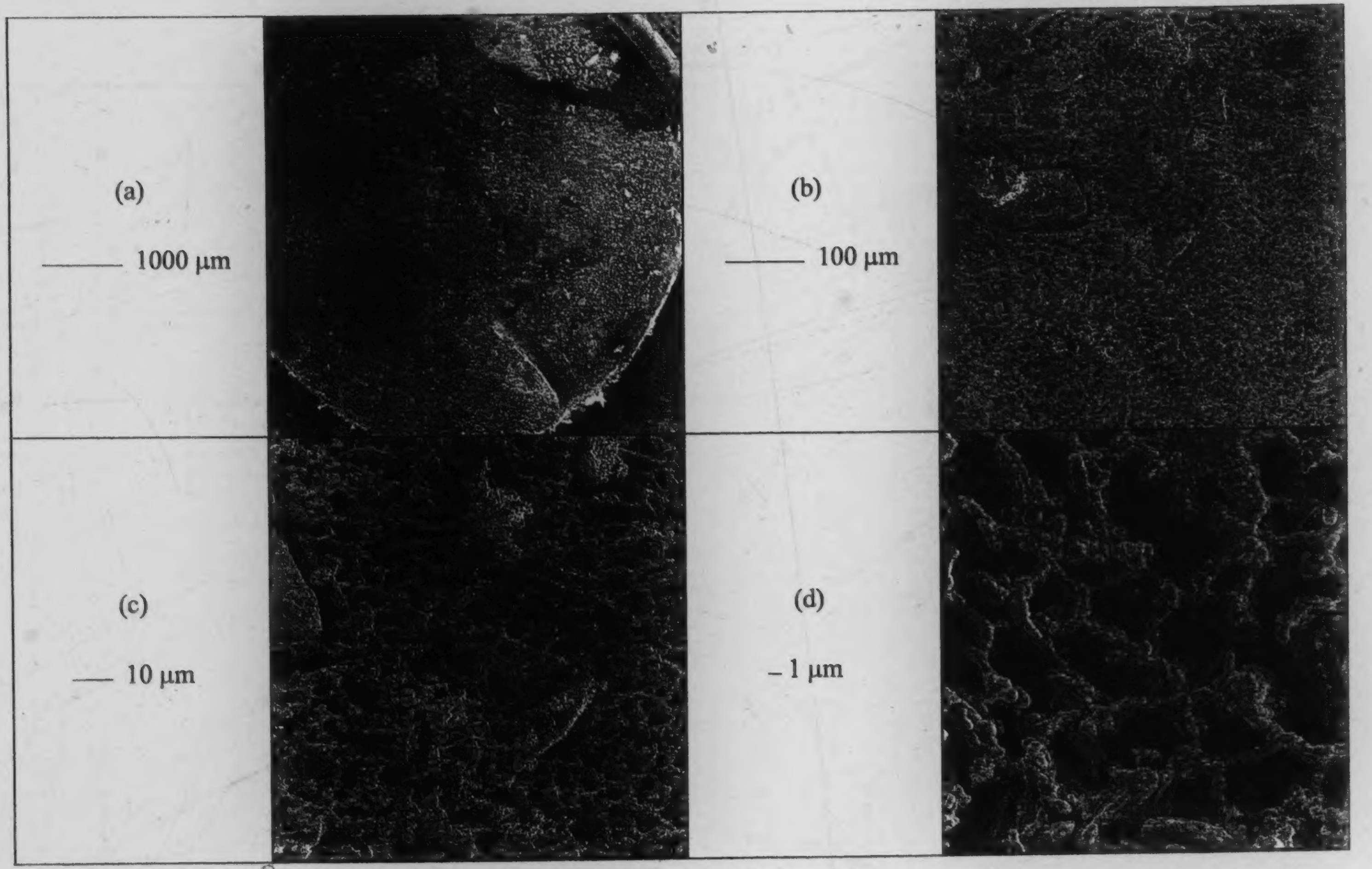
(a)
1000 µm
(b)
100 µm
(c)
10 µm
(d)
1 µm

Figure 5.10: Scanning electron micrographs of saprolite PAL slurry (Indonesia)

The enlargements include (a) 20 times, (b) 200 times, (c) 500 times and (d) 2000 times. The first micrograph (a) represents the whole specimen in the 3 mm circular plastic straw. This micrograph was taken to observe the fractured surface during sample preparation. The second micrograph (b) is an enlargement of the selected area on the first micrograph. This location was selected to denote an area that closely represents the entire slurry. The third micrograph (c) and the fourth micrograph (d) show magnified locations on micrograph (b). These two micrographs were taken either to inspect exaggerated portions of the micrograph (b) or to highlight some peculiar features on that micrograph (b).

Figure 5.7 shows the morphology of the limonite PAL slurry from Cuba. Micrograph (a) shows a good specimen surface with minimal corrugations. Micrograph (b) illustrates the presence of coarse grains scattered through out the clay matrix. Micrograph (c) makes the same observation more clearly due to its higher magnification. Micrograph (d) shows that the clay matrix is composed of fine hematite crystals arranged in separate but mutually conjoined colonies thereby representing a flocculated fabric. Identification of hematite is based on its size that is smaller than the 2 μm clay size and the nearly spherical particles of the mineral (Krause et al. 1998). Confirming the XRD results for the same material, this micrograph shows that the clay matrix is composed of non-clay minerals. Further, these minerals are observed to result in flocculated soil fabric in the given medium of low electrolyte concentration and acidic pH. Therefore, the limonite ore slurry from Cuba is expected to undergo rapid settling.

Figure 5.8 presents the microstructure of the limonite-saprolite PAL slurry from the Philippines. Micrograph (a) shows the development of a crack in the specimen and a rough surface. Despite these limitations, a representative smooth area is observed to be available for detailed morphological assessment. Micrograph (b) shows the presence of evenly distributed coarse silt size grains scattered through out the clay matrix in the enlarged selected area. Micrograph (c) illustrates an apparently cardhouse morphology of the specimen. However, this observation is modified at a higher enlargement. Micrograph (d) shows a morphology identical to that observed for the limonite PAL from Cuba. The observable cardhouse structure is not associated with the clay matrix but with the pore fluid. Such an alignment of the pore water results from freezing artifacts reported to be associated with the cryogenic technique (Mikula 1989). A comparison of the limonite PAL slurry from Cuba and the limonite-saprolite PAL slurry from Philippines reveal a more compressed soil fabric for the latter. Given identical mineralogical composition, the variable fabric of the two materials is attributed to variations in pore fluid chemistry. The limonite-saprolite PAL slurry from Philippines is characterized by a 30% higher electrolyte concentration with significant contributions from multivalent ions. Therefore, the solid-liquid separation behavior of the limonite-saprolite PAL slurry from Philippines is expected to be somewhat higher than that of the limonite ore slurry from Cuba.

Figure 5.9 gives the fabric of the limonite-saprolite PAL slurry from Australia. Micrograph (a) shows a reasonable specimen with scattered protuberances. Micrograph (b) illustrates the irregular distribution of silt size particles in the clay matrix. Micrograph (c) again presents an apparently cardhouse morphology of the specimen. As explained above, this observation is due to freezing artifacts and modified at a higher enlargement. Micrograph (d) shows a soil fabric similar to that of the limonite-saprolite PAL slurry from Philippines. Figure 5.9 does not vividly express either soil mineralogy or the associated fabric. Still, this figure suggests that the solid-liquid separation behavior of limonite-saprolite PAL slurry from Australia is not very different from the above mentioned materials.

Figure 5.10 gives the morphology of the saprolite PAL slurry from Indonesia. Micrograph (a) shows a good surface for half of the specimen with some corrugations and cracking in the other half. Micrograph (b) shows a clay matrix with some silt size particles. Likewise, Micrograph (c) that mainly focuses on the clay matrix, illustrates complete dispersion. Micrograph (d), which examines the cardhouse fabric, shows a very loose packing for this slurry with inter-particle spacing of the order of 10 to 12 μm. This micrograph also shows the overwhelming presence of spherical hematite globules (smaller than 2 μm) coating the soil particles. The platelets formed due to coating of soil particles by hematite grains have dimensions of 5 μm diameter and 1μm thickness. The formation of such a microstructure is typical for saprolite PAL slurries below the PZC of hematite (Rubisov & Papangelakis 1999). Figure 5.10 confirms soil dispersion in an acidic medium with high electrolyte concentration. The voluminous cardhouse structure of soil particles coated by hematite is expected to result in a solid-liquid separation similar to the ore slurry of the same material.

Despite some freezing artifacts, the microstructure of laterite PAL slurries obtained by cryogenic techniques explains several distinct features and can be used to characterize slurries in an empirical way (Scott et al. 1985). Precipitation of hematite is accompanied by an increase in grain size that in turn affects the mechanical response of the PAL slurries. The increased grain size coupled with a flocculated fabric is expected to result in better dewatering of PAL slurries.

5.5.3 Elemental Analysis

Figure 5.11 gives the elemental analysis of SEM samples (shown in Micrographs (a)) for various laterite PAL slurries. This figure shows nearly identical elemental compositions for all specimens. For each sample, this figure shows two Au peaks due to gold coating and one high S peak associated with the presence of sulfuric acid in the specimens. Further, the high Fe peaks associated with the presence of hematite in the figure decrease in intensity from limonite PAL slurry from Cuba through saprolite PAL slurry from Indonesia. This is attributed to the decreasing amount of hematite when the materials change from limonite through saprolite. In contrast, an increasing trend is observed for Mg peaks when the materials are considered in the same order. Finally, the small Si peaks appearing in all of the PAL slurries denote the presence of amorphous silica in some of the samples. Therefore, elemental analyses are in conformity with x-ray diffraction analyses and helped in specimen identification during scanning electron microscopy.

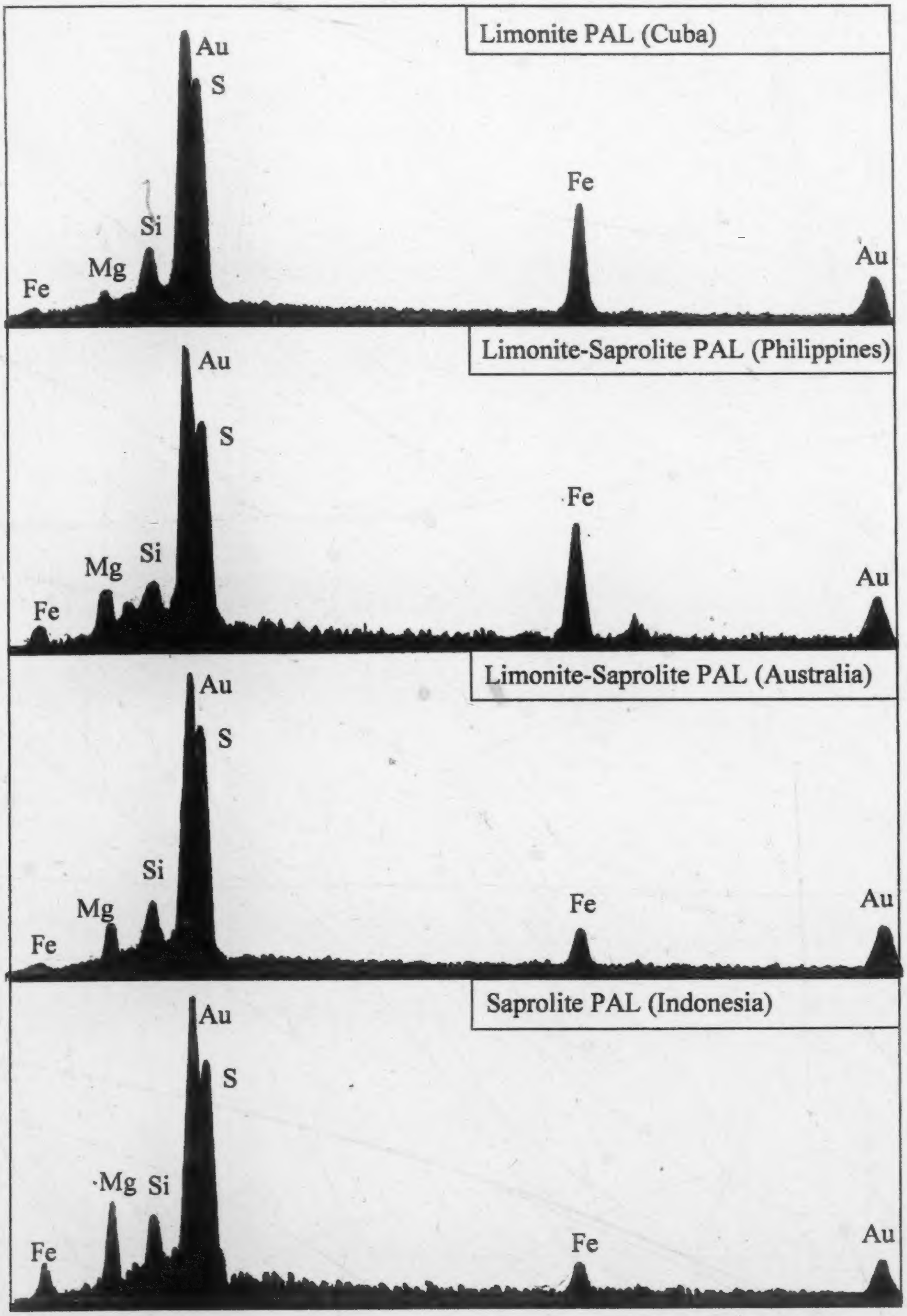

Limonite PAL (Cuba)

Limonite-Saprolite PAL (Philippines)

Limonite-Saprolite PAL (Australia)

Saprolite PAL (Indonesia)

Figure 5.11: Elemental analysis of SEM specimens of laterite PAL slurries

5.6 SOLID-LIQUID SEPARATION

5.6.1 General

This section presents the solid-liquid separation behavior of laterite PAL slurries. First, the influence of the diameter to height ratio on such a behavior is investigated. Results of sedimentation and consolidation tests are studied in conjunction with laboratory characterization. Presenting SEM results of specimens cut from the latter test sample makes a correlation between soil fabric and consolidation.

5.6.2 Diameter-Height Ratio

The effect of diameter to height ratio on the solid-liquid separation behavior of laterite PAL slurries was investigated by conducting four sedimentation tests with variable D_o/H_o. Figure 5.12 gives the results of these tests conducted on the limonite-saprolite PAL slurry from Philippines using identical beakers of 8.3 cm diameter. This figure shows significant variation in sedimentation curves for different D_o/H_o ratios and H/H_o values after 30 minutes of sedimentation are different. This means that the sedimentation curves are highly dependent on the initial sample height. This figure also shows that the limonite-saprolite PAL slurry undergoes a rapid sedimentation thereby allowing the determination of the initial hydraulic conductivity from the observed data in the initial ten minutes.

Figure 5.13 gives the variation in the initial hydraulic conductivity for various D_o/H_o ratios. This figure shows an exponential decrease in the initial hydraulic conductivity with increasing D_o/H_o. More than half of this decrease is observed when the D_o/H_o ratio is changed from 1 to 2 whereas an insignificant variation

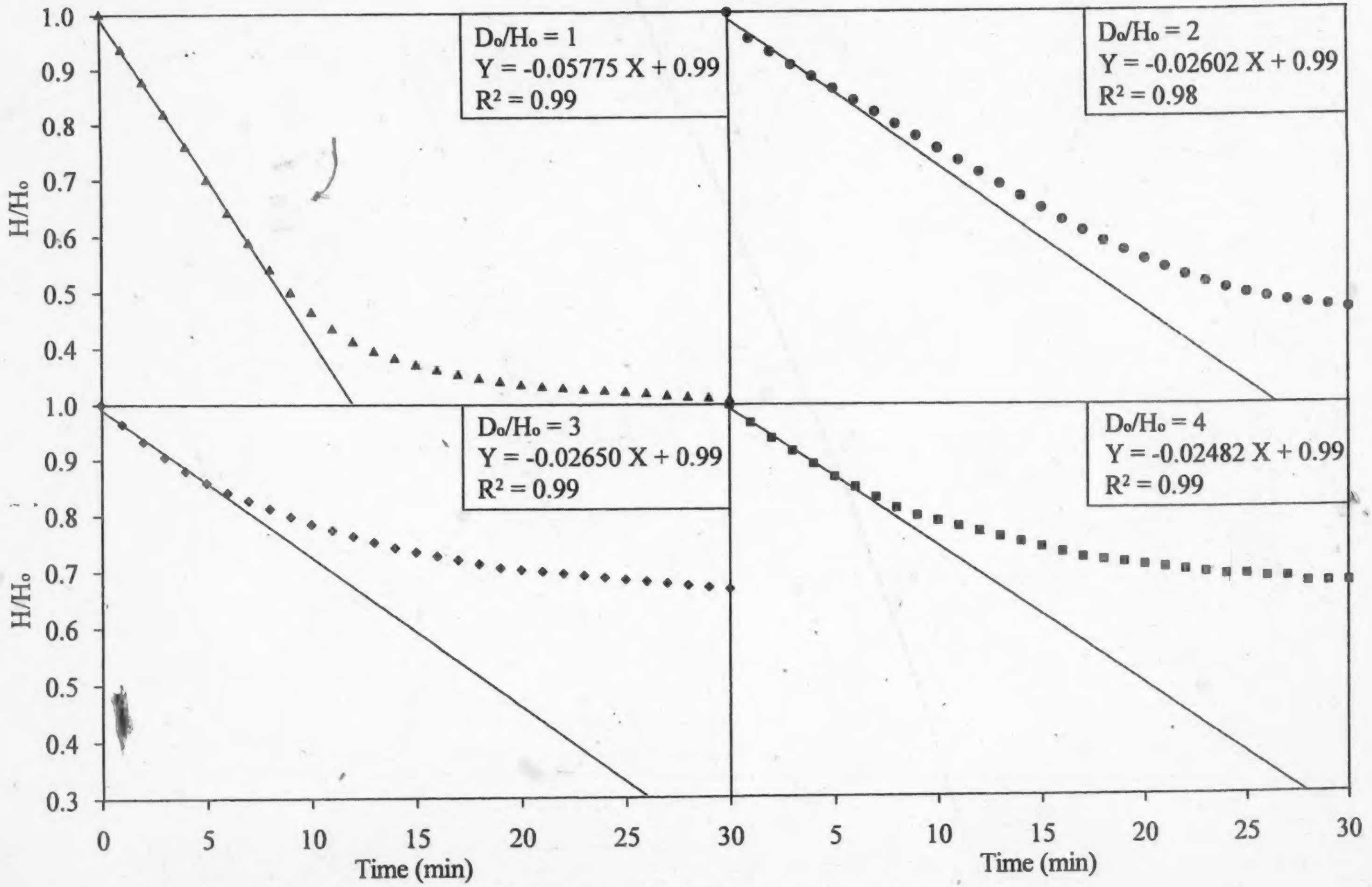

Figure 5.12: Sedimentation test results for various Do/Ho

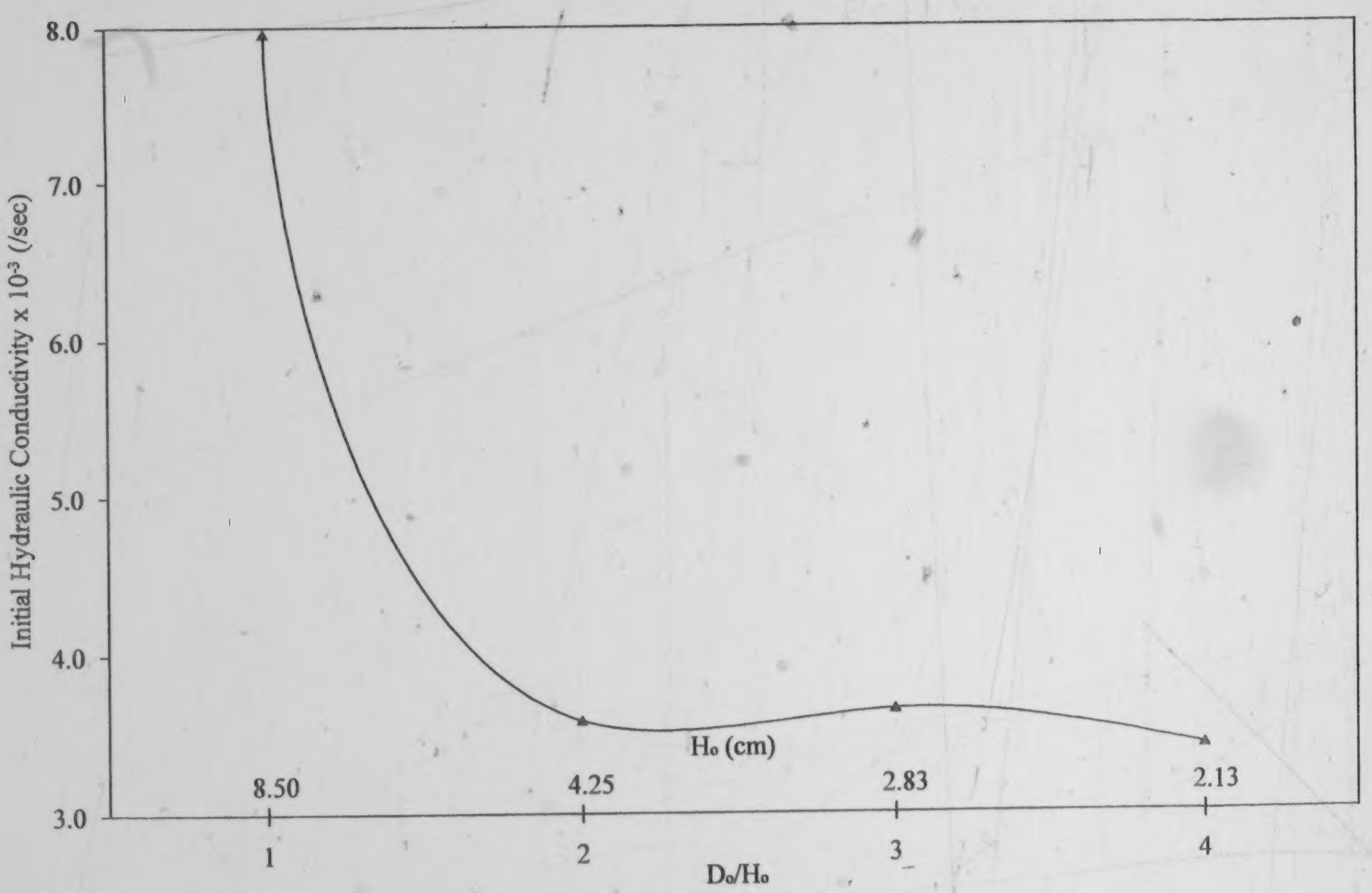

Figure 5.13: Effect of Do/Ho on sedimentation of limonite-saprolite PAL slurry from Philippines

in the initial hydraulic conductivity occurs for D_o/H_o ratios between 2, 3 and 4. These observations are attributed to the formation of channels in the sedimenting materials. Recorded annotations during laboratory experiments suggest an increased tendency of channel formation for higher initial sample height. These channels not only provide paths of least resistance for water flow but also reduce tortuousity thereby further increasing the initial hydraulic conductivity.

To facilitate rapid sedimentation and to mimic thickener geometry, a D_o/H_o ratio of 1 was used for all sedimentation tests on PAL slurries during this research. The high initial height required to obtain this ratio also allowed the development of a clear solid-liquid interface thereby assisting in reducing the experimental errors such observer's bias. After complete sedimentation, sample height of less than half of H_o was achieved for the laterite PAL slurries. This ensured that the influence of D_o/H_o during the consolidation stage of the solid-liquid separation process is negligible.

5.6.3 Sedimentation

The sedimentation behavior of laterite PAL slurries is the result of the combined effect of geotechnical index properties, mineralogy and pore water chemistry. These material characteristics resulted in a specific morphology for each of the laterite PAL slurry. Detailed discussions on all of these characteristics and the expected solid-liquid separation behavior were provided earlier in this chapter. This section aims at confirming and explaining the engineering behavior of laterite PAL slurries.

Figure 5.14 gives sedimentation test results for various laterite PAL slurries in the form of interface height, void ratio and solids content plotted as functions of time. Figure 5.15 shows the initial part of the interface height versus time plot for the determination of initial hydraulic conductivity. Finally, Table 5.6 summarizes the self-weight sedimentation behavior of the four PAL slurries.

Figure 5.14 shows that the limonite-saprolite PAL slurry from Philippines has the most rapid sedimentation followed by the limonite PAL slurry from Cuba. This is attributed to the high specific gravity and the more compressed soil fabric of the former slurry. Given identical mineralogical composition, the compressed soil fabric of the limonite-saprolite PAL slurry from Philippines is due to the high electrolyte concentration in the pore water of this slurry.

The sedimentation behavior of the other two slurries is much slower and is due to the presence of amorphous materials and magnesium sulfate. The observed variation between the limonite-saprolite PAL slurry from Australia and the saprolite PAL slurry from Indonesia is mainly attributed to the more than double electrolyte concentration in the pore water of the former slurry. In addition, the larger amount of amorphous materials and magnesium sulfate in the latter material is also responsible for the faster settling of the saprolite PAL slurry from Indonesia. Finally, the higher amount of structural water associated with magnesium sulfate in the saprolite PAL slurry from Indonesia also results in reduced dewatering. All of the above factors resulted in honey-combed fabric for this material, as shown in Figure 5.10.

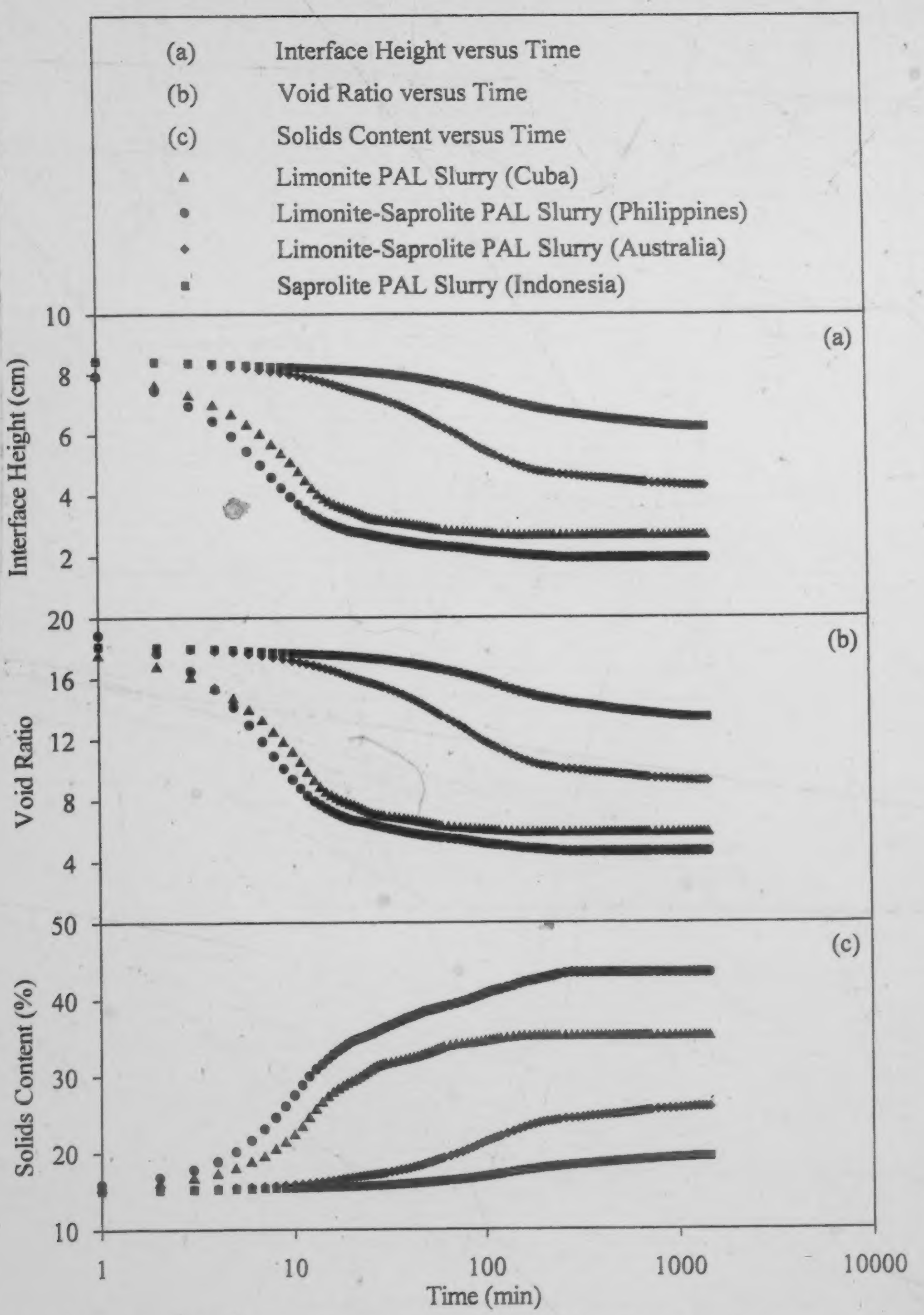

Figure 5.14: Sedimentation test results for laterite PAL slurries

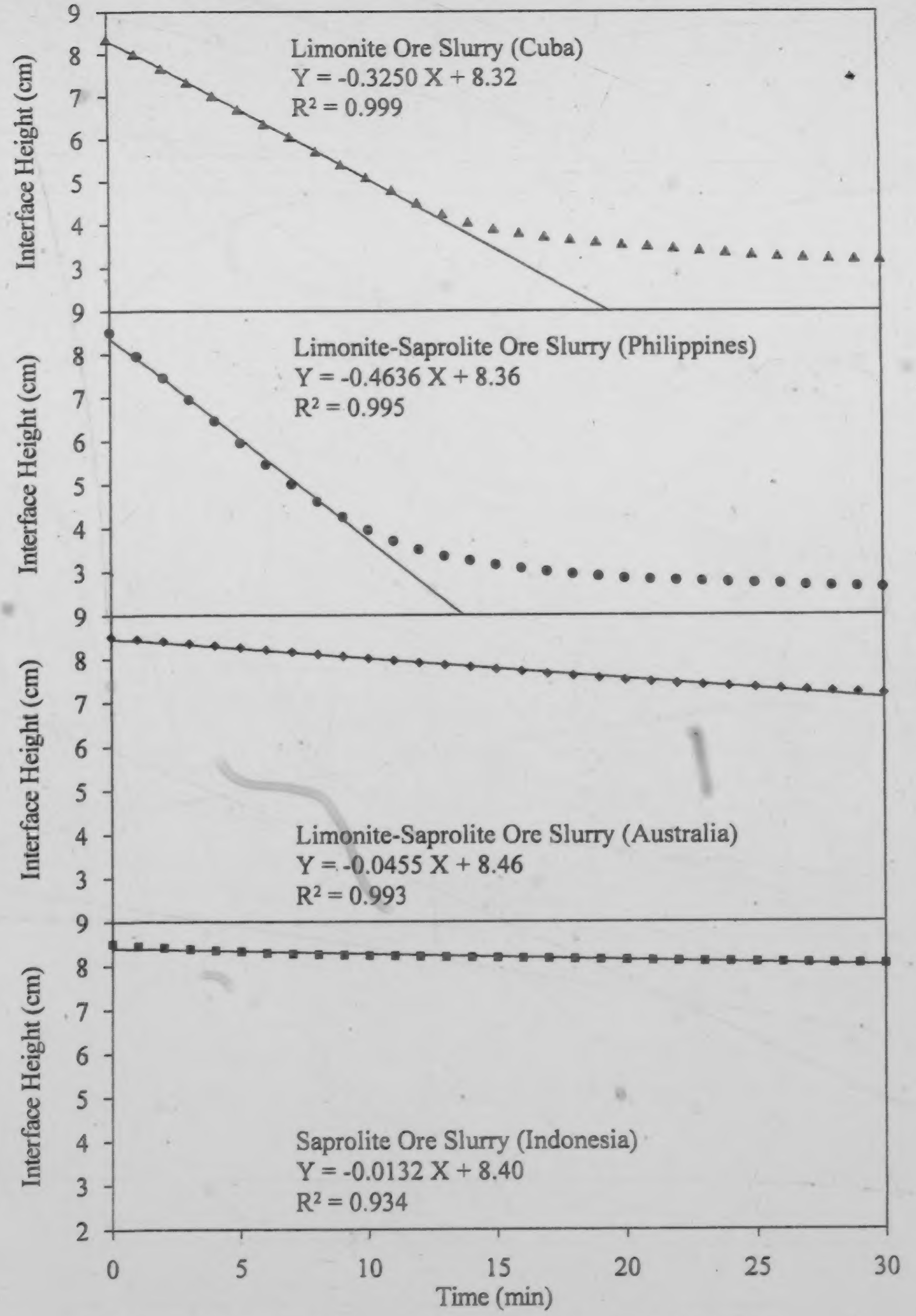

Figure 5.15: Water release rate for various laterite PAL slurries

Table 5.6. Summary of sedimentation test results for laterite PAL slurries

Property	Sample Type and Origin			
	Limonite PAL	Limonite-Saprolite PAL		Saprolite PAL
	Cuba	Philippines	Australia	Indonesia
	Conditions at the Start of Sedimentation Test			
H_o (cm)	8.35	8.50	8.50	8.50
s_o (%)	15	15	15	15
e_o	18.25	20.17	18.25	18.25
γ_o (kg/m^3)	1115	1121	1115	1115
σ_o' (Pa)	94	101	96	96
	Hydraulic Conductivity During the Sedimentation Test			
Vs (cm/min)	0.3250	0.4636	0.0455	0.0132
γ^*	2.22	2.56	2.22	2.22
k (cm/s)	4.70×10^{-2}	6.39×10^{-2}	6.57×10^{-3}	1.91×10^{-3}
	Conditions at the End of Sedimentation Test			
H_f (cm)	2.70	1.95	4.30	6.25
s_f (%)	35.31	43.48	25.86	19.35
e_f	5.90	4.63	9.23	13.42
γ_f (kg/m^3)	1322	1455	1217	1154
σ_f' (Pa)	85	87	92	94

Figure 5.15, which is the enlarged version of the sedimentation curve of Figure 5.14(a), gives the water release rate for various laterite PAL slurries. This figure shows that the slope of the initial straight-line portion of the sedimentation curve is highest for the limonite-saprolite PAL slurry from the Philippines. For other materials, the slope decreases from limonite PAL slurry (Cuba) through limonite-saprolite PAL slurry (Australia) and finally to saprolite PAL slurry (Indonesia).

Table 5.6 that summarizes the sedimentation test results for laterite PAL slurries divides the test into three stages. This table indicates approximately constant initial conditions at the start of the sedimentation tests. The slightly higher values for the limonite-saprolite PAL slurry from Philippines are due mainly to the high specific gravity of this material. The table reports that the initial hydraulic conductivity of all PAL slurries is higher than similar fine tailings such as Alberta oil sands (Suthaker 1995). This is attributed to the high specific gravity of laterite PAL materials and the negligible segregation of their slurries. Further, the initial hydraulic conductivity is highest for the limonite-saprolite PAL slurry from Philippines, whereas for other materials, the initial hydraulic conductivity decreases from limonite through saprolite PAL slurry. The final conditions at the end of sedimentation tests indicate effective stress values higher than at the start. This means that the test duration of twenty-four hours is sufficient to completely dissipate the excess pore pressure generated at the start of the tests.

Studying Table 4.6 in conjunction with Table 5.6 can make a comparison of the sedimentation behavior of ore and PAL slurries. Such an analysis indicates that the initial void ratios of all of the PAL materials are higher than their corresponding ores owing to the high specific gravity of the former. With the exception of the limonite ore from Cuba, all materials exhibit improvement in the initial hydraulic conductivity and final void ratio after acid leaching. Finally, all materials show an increase in final solids content under self-weight when acid leached. This increase amounts to 60% for the limonite-saprolite material from the Philippines.

5.6.4 Consolidation

5.6.4.1 General

A comparison of Table 5.1 and Table 5.6 reveals that during self-weight sedimentation the limonite PAL slurry from Cuba and the limonite-saprolite PAL slurry from Philippines achieve solids content just under those in the CCD thickener. On the contrary, the other two PAL slurries do not reach the same under self-weight sedimentation. Therefore, these latter materials need to undergo consolidation to get the desired solids content in the CCD thickener. However, limonite-saprolite PAL slurry from Philippines was selected for the consolidation test. This selection was based on the increasing use of such materials due to their reduced operational cost (Chalkley & Toraic 1997) and to compare this material with its ore counterpart. This section gives consolidation test results along with morphological studies for the limonite-saprolite PAL slurry from Philippines.

5.6.4.2 Test Result

Figure 5.16, 5.17 and 5.18 give consolidation test results in the form of sample height, void ratio and solids content as functions of time for different load increments. These results are summarized in Table 5.7, which indicates that bulk of the solid-liquid separation occurs during the sedimentation stage under self-weight. Under self-weight a 90% dewatering is achieved as the void ratio changes from 20.0 to 4.3 and the solids content changes from 15 to 46%. This is mainly attributed to the high specific gravity (3.56) of the limonite-saprolite PAL slurry from Philippines. Up to an effective stress of 8 kPa, an additional 2% dewatering is observed with an associated void ratio change from 4.3 to 3.2 and a solids content increase of about 7%. Increase in effective stress beyond 8 kPa results in less than 5% dewatering and increase in solids content.

Figure 5.19 gives the pore pressure measurements for each load increment. This figure indicates an initial abrupt increase in excess pore pressure with load application and a subsequent steady decrease; high excess pore pressure measured for high load increments. Pore pressure equilibration occurs within the first three hours of load application for all loads.

Figure 5.20 presents the hydraulic conductivity data measured after each load increment in the consolidation test. This figure shows that the variation in hydraulic conductivity is less than three orders of magnitude for different load increments. Despite the initial scatter in the data points indicated in Figure 5.20, steady state values are observed within about 30 minutes of water flow through the specimen.

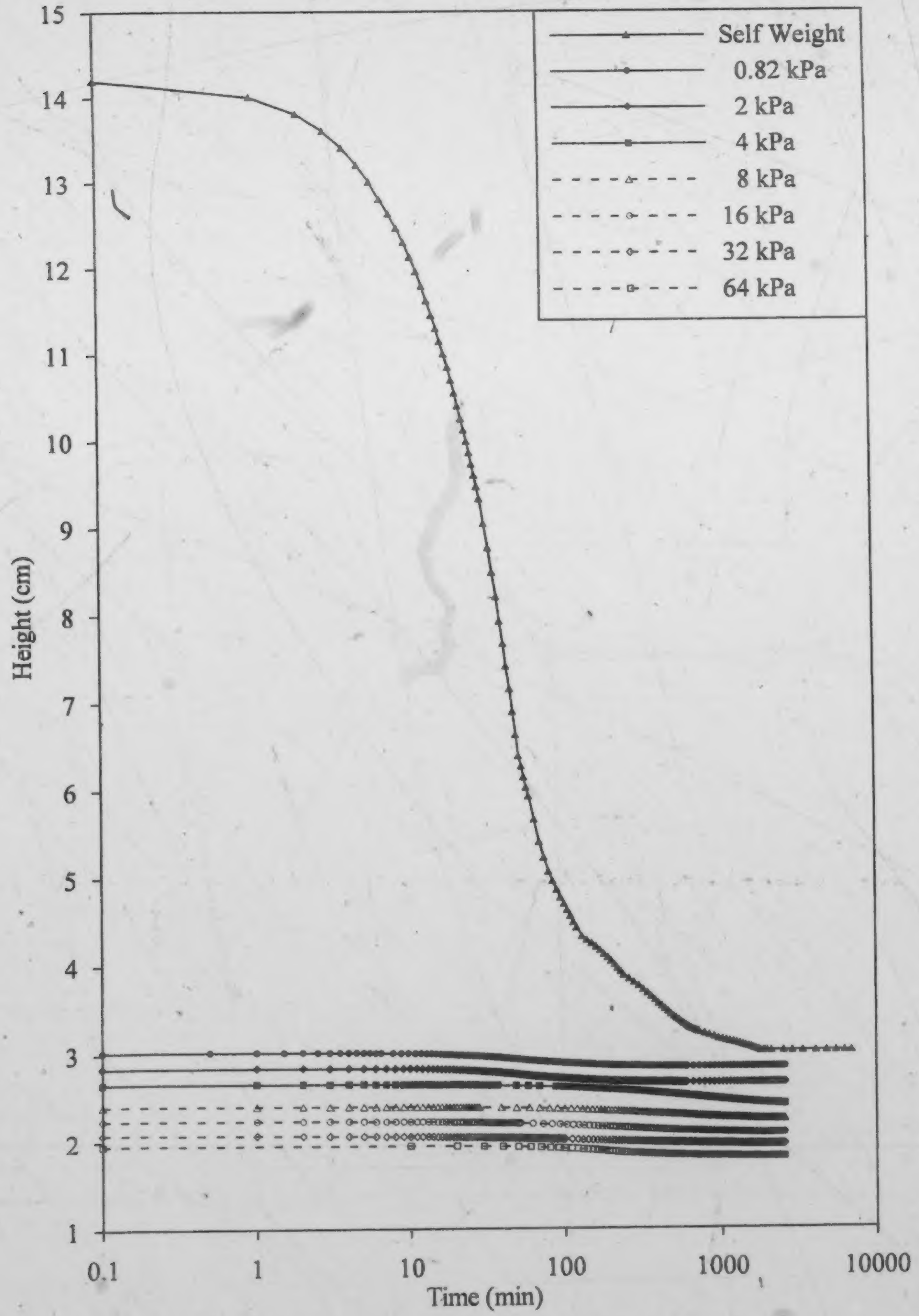

Figure 5.16: Consolidation of limonite-saprolite PAL slurry

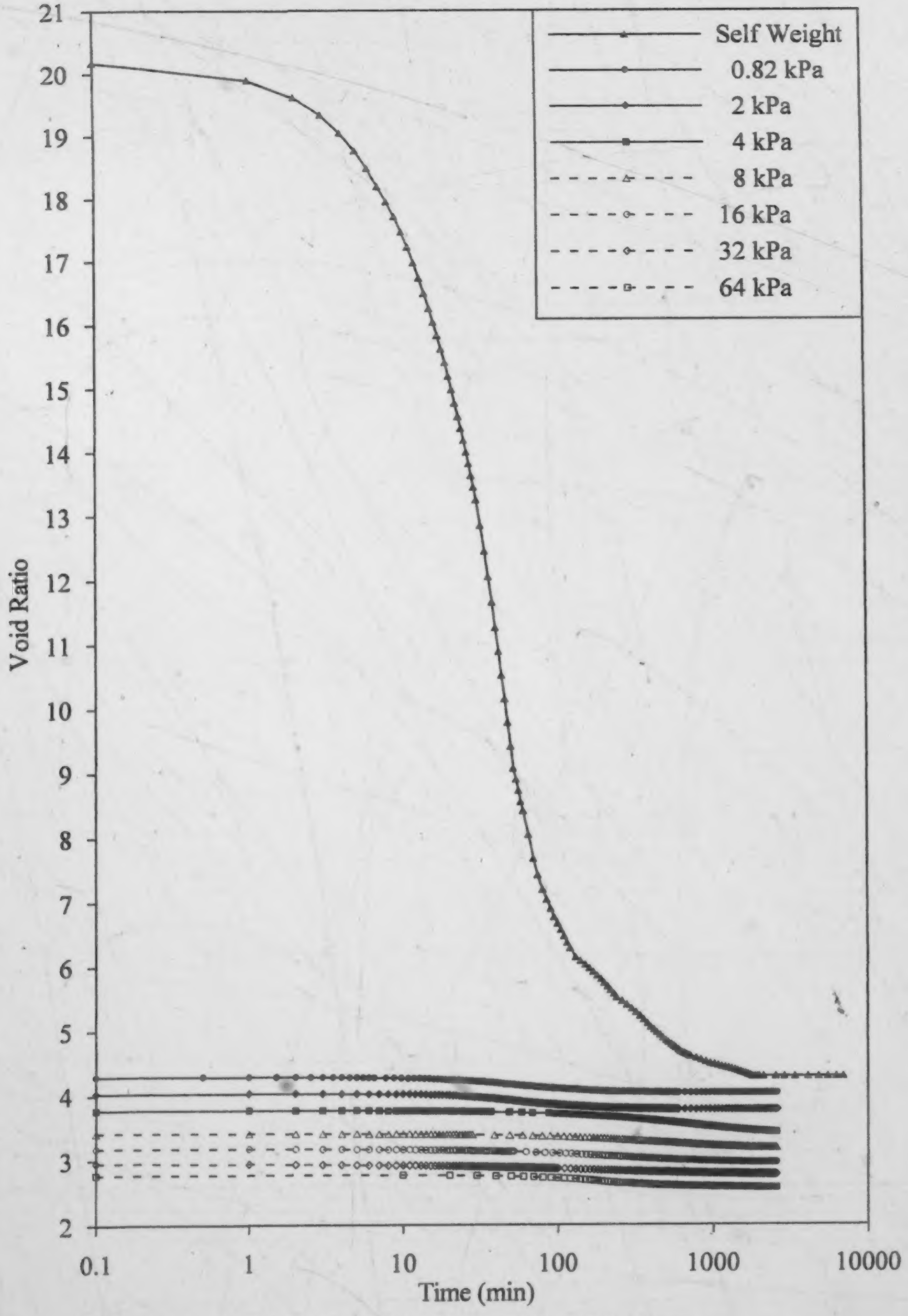

Figure 5.17: Void Ratio of limonite-saprolite PAL slurry

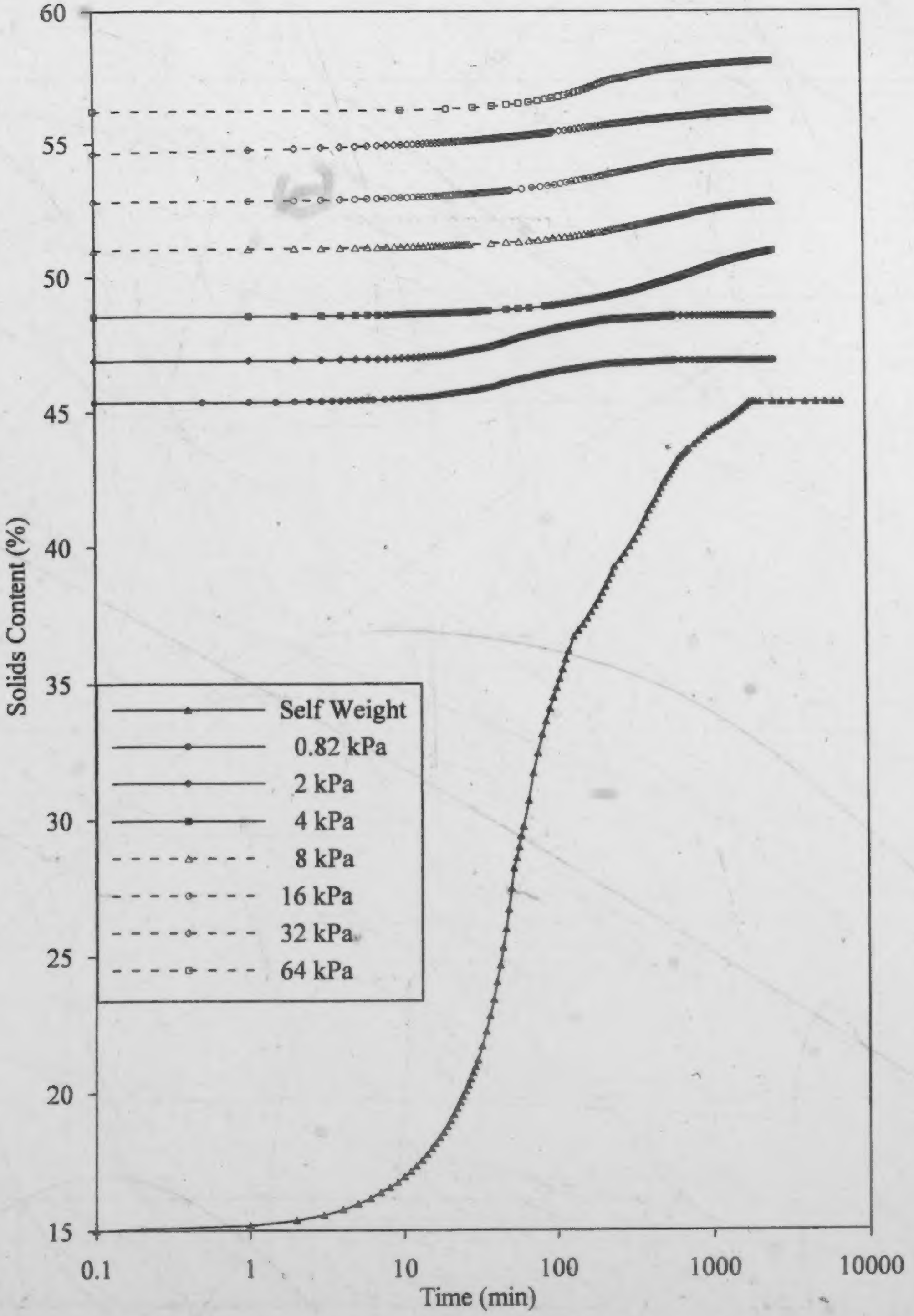

Figure 5.18: Solids Content of limonite-saprolite PAL slurry

Table 5.7. Changes during solid-liquid separation of laterite PAL slurry

σ′ (kPa)	ΔH/H (%)	e	*s* (%)	Dewatering (%)*
Initial State	0.0	20.0	15.0	0.0
Self-Weight	78.7	4.3	45.6	89.5
0.8	80.0	4.0	47.1	86.8
2.0	81.3	3.7	48.8	88.2
4.0	83.0	3.4	51.2	90.1
8.0	84.2	3.2	53.0	91.4
16.0	85.3	2.9	54.8	92.6
32.0	86.2	2.8	56.4	93.6
64.0	87.3	2.6	58.3	94.7

* Change in water volume divided by initial water volume

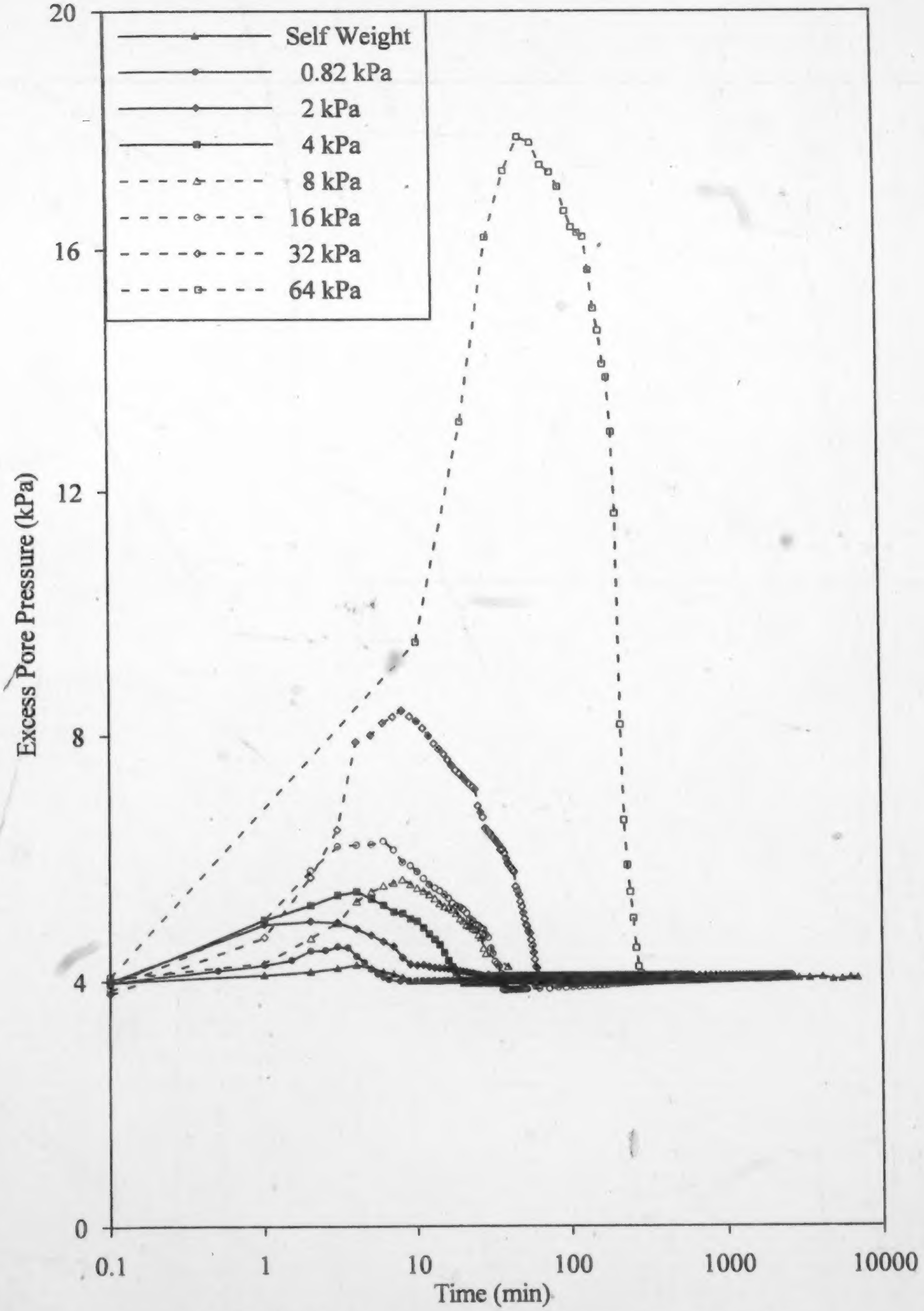

Figure 5.19: Excess Pore pressure of limonite-saprolite PAL slurry

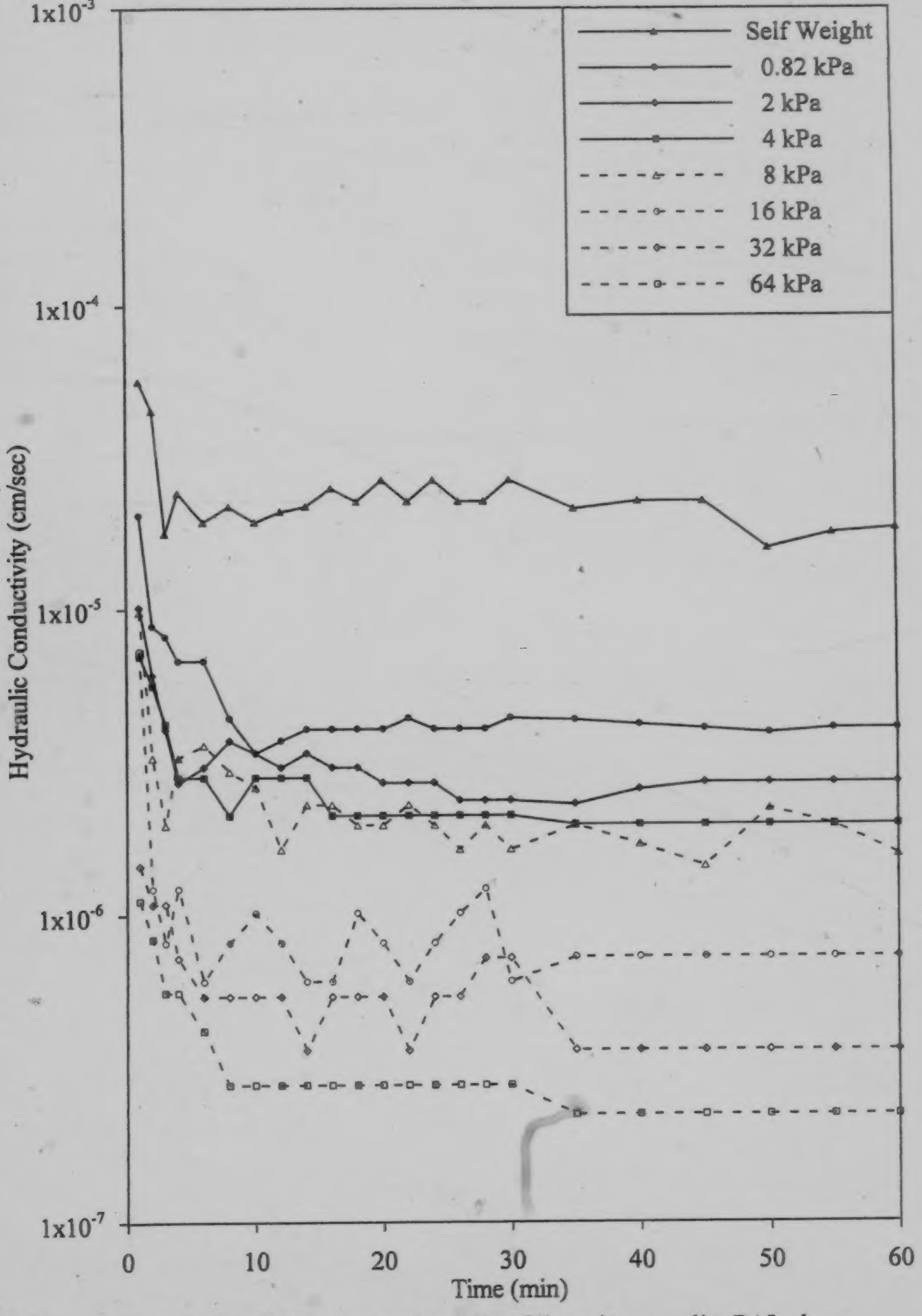

Figure 5.20: Hydraulic conductivity of limonite-saprolite PAL slurry

The drop in flow from an initial to a steady state value decreased with increasing stress. This is attributed to the diminishing physical changes in the specimen with decreasing void ratio. Olsen et al. (1985), suggested that such time-dependent flow can be due to one ore more of the following reasons: (a) undissolved air in the equipment and/or specimen; (b) equipment compliance depending on fabrication material and applied gradients; (c) inertia required to move the pore fluid; and (d) time-dependent changes in pore space distribution. Using identical equipment and test conditions for Alberta oil sand tailings, Suthaker & Scott (1996) showed that the last reason is the most likely cause of the observed time-dependent flow. These authors concluded that this transient phenomenon is repeatable and that the initial conditions are reattainable. Therefore, the steady state value was taken as the hydraulic conductivity and used in the analysis during this research.

Figure 5.21 and Figure 5.22 summarize the consolidation test results for the limonite-saprolite PAL slurry from Philippines. Described as power laws, these two figures give the log k-e and the e-log σ' relationships, respectively. Data in these two figures is shown in cm/sec and kPa units as well as in m/min and Pa units. Fit parameters obtained from the latter units are used in the numerical analysis, described latter in this chapter. For the two relations, the *A* and *C* parameters denote the intercept or position of the fit whereas the *B* and *D* parameters signify the slope or shape of the curve. The parameters obtained for the investigated material are comparable to other fine-grained Alberta oil sand tailings (Suthaker 1995).

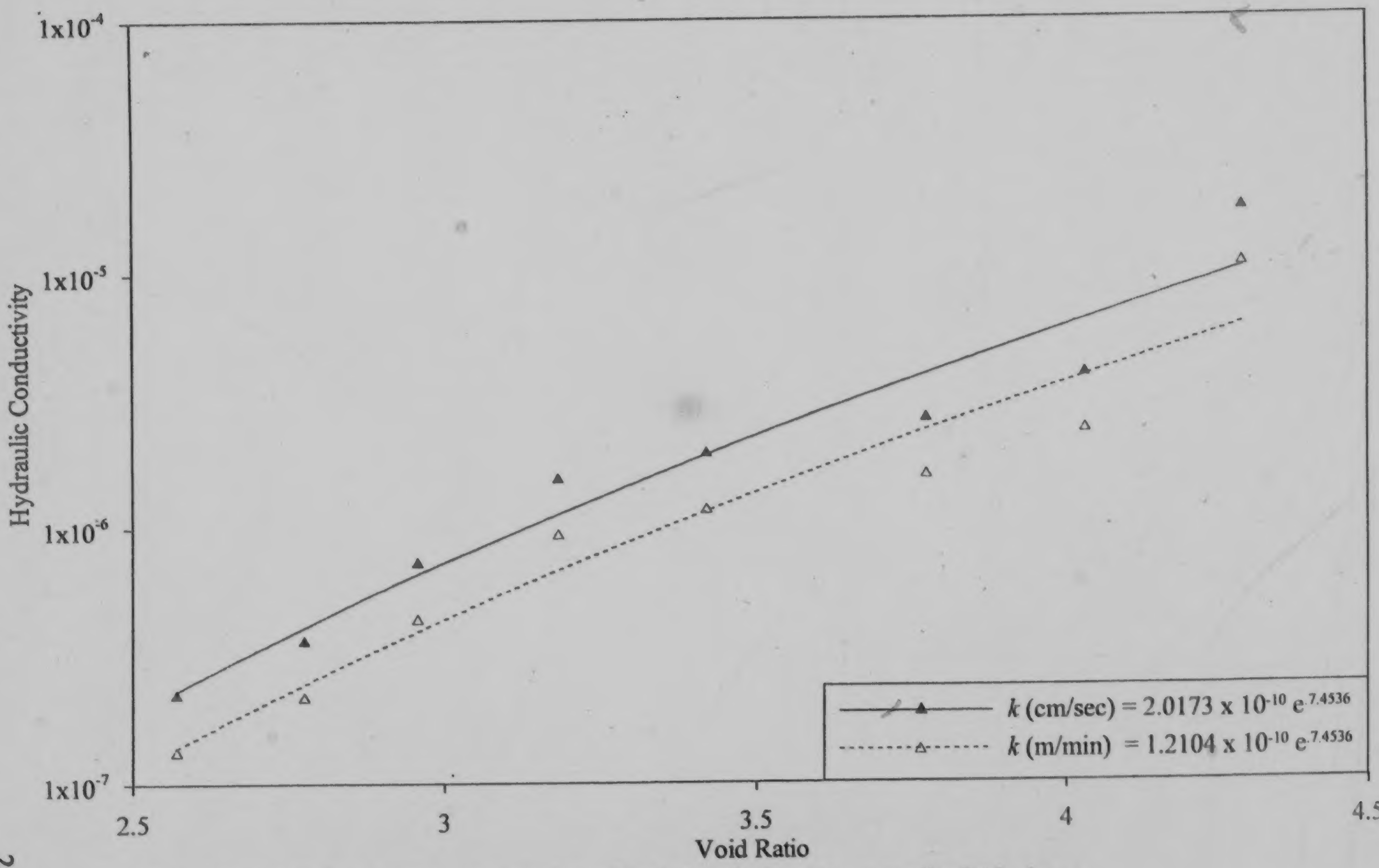

Figure 5.21: Hydraulic conductivity-void ratio relation for limonite-saprolite PAL slurry

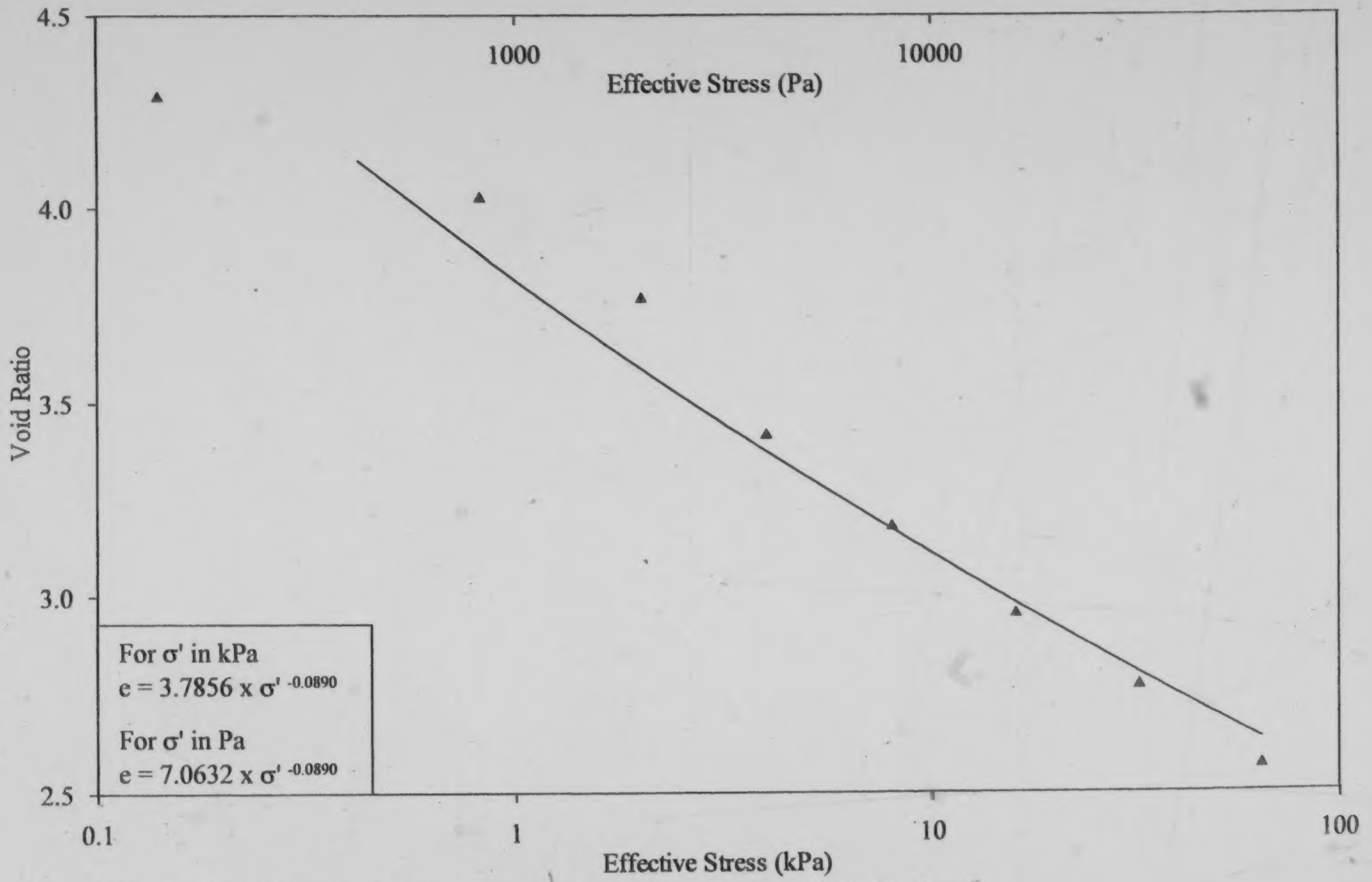

Figure 5.22: Void ratio-effective stress relation for limonite-saprolite PAL slurry

Figure 5.21 indicates that the hydraulic conductivity decreases by about two orders of magnitude (10^{-5} to 10^{-7} cm/sec) as the void ratio is decreased from 4.5 to 2.5. The investigated PAL slurry exhibits a hydraulic conductivity similar to clays ($\leq 10^{-6}$ cm/sec at $e \leq 2.0$) at a void ratio of 3.0. This is attributed to the high tortuousity imparted by the ultra-fine, rounded hematite crystals. These spherical iron oxide particles are also responsible for the relatively higher compressibility of the PAL slurry compared to the ore slurry; limonite-saprolite from Philippines. Due to closely matching material characteristics, a similar behavior is envisaged for all of the other PAL slurries.

5.6.4.3 Morphology

Figure 5.23 and Figure 5.24 give the sample morphology after the completion of the consolidation test for specimens cut in the vertical (parallel to applied stress) and lateral (perpendicular to applied stress) directions, respectively. These figures indicate that there is channelization in the vertical direction only. Such a soil fabric facilitates the flow of water along the sample.

Figure 5.23 indicates the presence of large voids in the vertical direction. Micrograph (a) of this figure shows a slight cleavage towards the right end of the specimen. Micrograph (b) shows a dense soil fabric composed of assemblages with sizes ranging from 10 to 20 μm. Micrograph (c) indicates the presence of a large number of pore spaces for the this specimen. Micrograph (d) illustrates that the size of these inter-assemblage pore spaces are 1 to 5 μm. Therefore, the hydraulic conductivity of this material is mainly in the vertical direction.

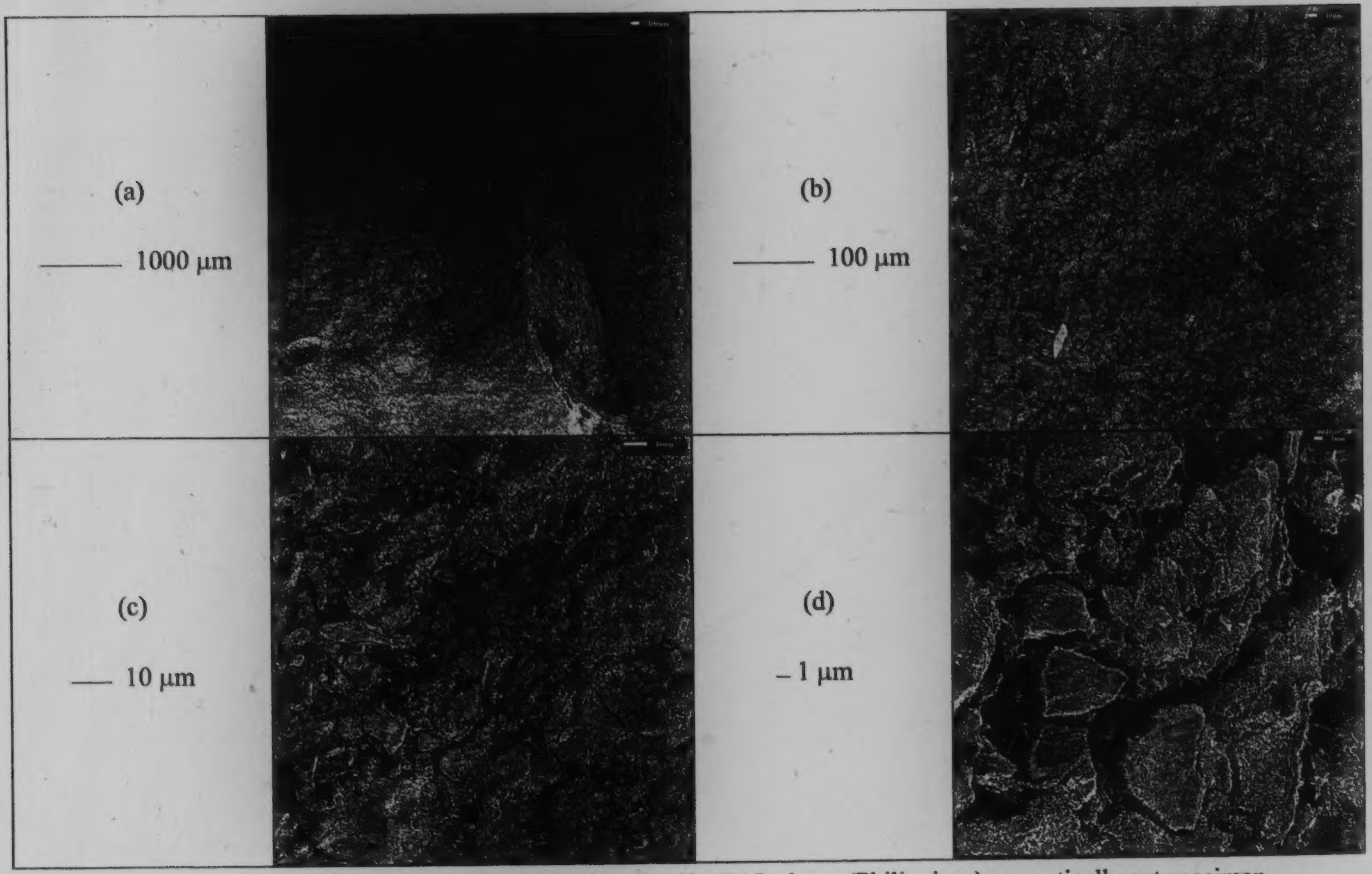
(a)
1000 µm
(b)
100 µm
(c)
10 µm
(d)
1 µm

Figure 5.23: Scanning electron micrographs of limonite-saprolite PAL slurry (Philippines) on vertically cut specimen

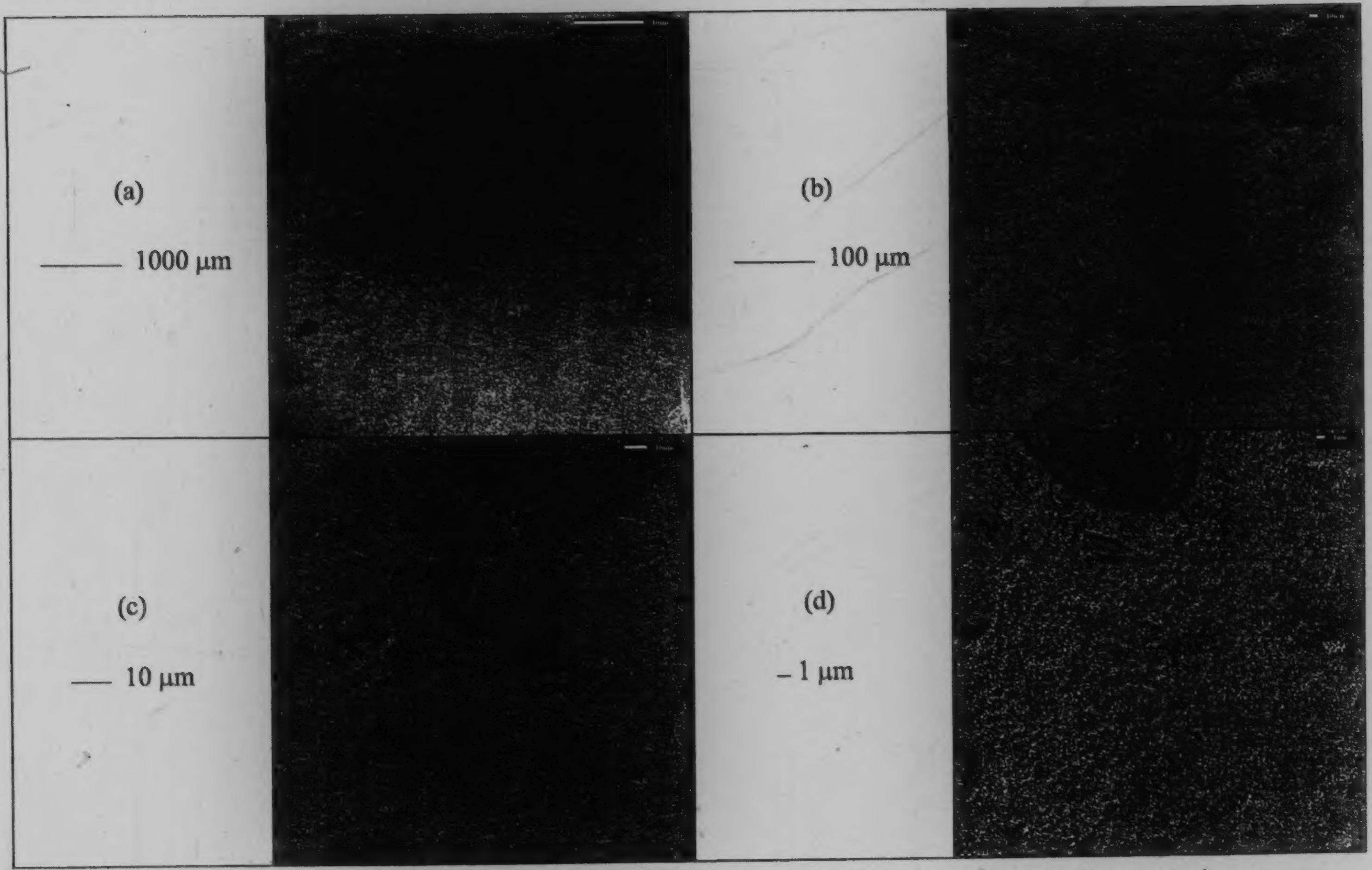
(a)
1000 µm
(b)
100 µm
(c)
10 µm
(d)
1 µm

Figure 5.24: Scanning electron micrographs of limonite-saprolite PAL slurry (Philippines) on laterally cut specimen

Figure 5.24 indicates a reduced void ratio in the lateral direction compared to the previous sample. Micrograph (a) of this figure shows a good fractured surface for the specimen. Micrograph (b) shows a dense soil fabric that is devoid of any assemblages. Micrograph (c) indicates the presence of occasional slit size particles in the dense soil microstructure. Micrograph (d) illustrates that this fabric is primarily composed of interconnected hematite particles having equally spaced voids of less than 1 μm size. Collectively, the soil fabric shows a markedly reduced channeling of the specimen in the lateral direction in contrast to the sample in the vertical direction. This ensures negligible water flow in the lateral direction. These micrographs also confirm the reduced void ratio of the PAL slurry compared to the ore slurry.

5.7 NUMERICAL SIMULATION

5.7.1 General

This section describes performance prediction of laterite PAL slurries. Sedimentation test data was fitted by iterative variation of *A* and *B* parameters used in the hydraulic conductivity-void ratio relation; data fitting was checked against measured initial hydraulic conductivity. Such simulation allowed the determination of hydraulic conductivity-void ratio relation without conducting the consolidation test. Similarly, the behavior of a Counter Current Decantation (CCD) thickener is modeled using the consolidation test data for the limonite-saprolite PAL slurry from Philippines.

5.7.2 Laboratory Data

Figure 5.25 gives the modeling of sedimentation curves for various laterite PAL slurries. This figure illustrates that the laboratory data fits reasonably well to the initial part of the sedimentation curve that was used for the determination of initial hydraulic conductivity. Further, this figure also indicates that the laboratory determined hydraulic conductivity-void ratio relation for the limonite-saprolite PAL slurry from Philippines matches closely with the measured sedimentation curve for the same material.

Figure 5.26 depicts the behavior of laterite PAL slurries. This figure, which uses the above-mentioned hydraulic conductivity-void ratio relations, shows that the hydraulic conductivity varies by several orders of magnitude for different void ratios. However, at high void ratios, variation among different PAL slurries is only two orders of magnitude in contrast to six orders of magnitude for the different ore slurries. Such a convergence of behavior is attributed to the environmental conditions in the acid leaching process that yields identical mineralogical composition and high electrolyte concentration. In other words, variation in physico-chemical interactions between colloids and the electrolyte medium is less significant for various PAL materials than for the corresponding ore materials. This figure also shows that similar to the laterite ore slurries, all relationships for the PAL materials converge at low void ratios. Again, such an identical behavior is attributed to the governing influence of mechanics rather than physico-chemistry.

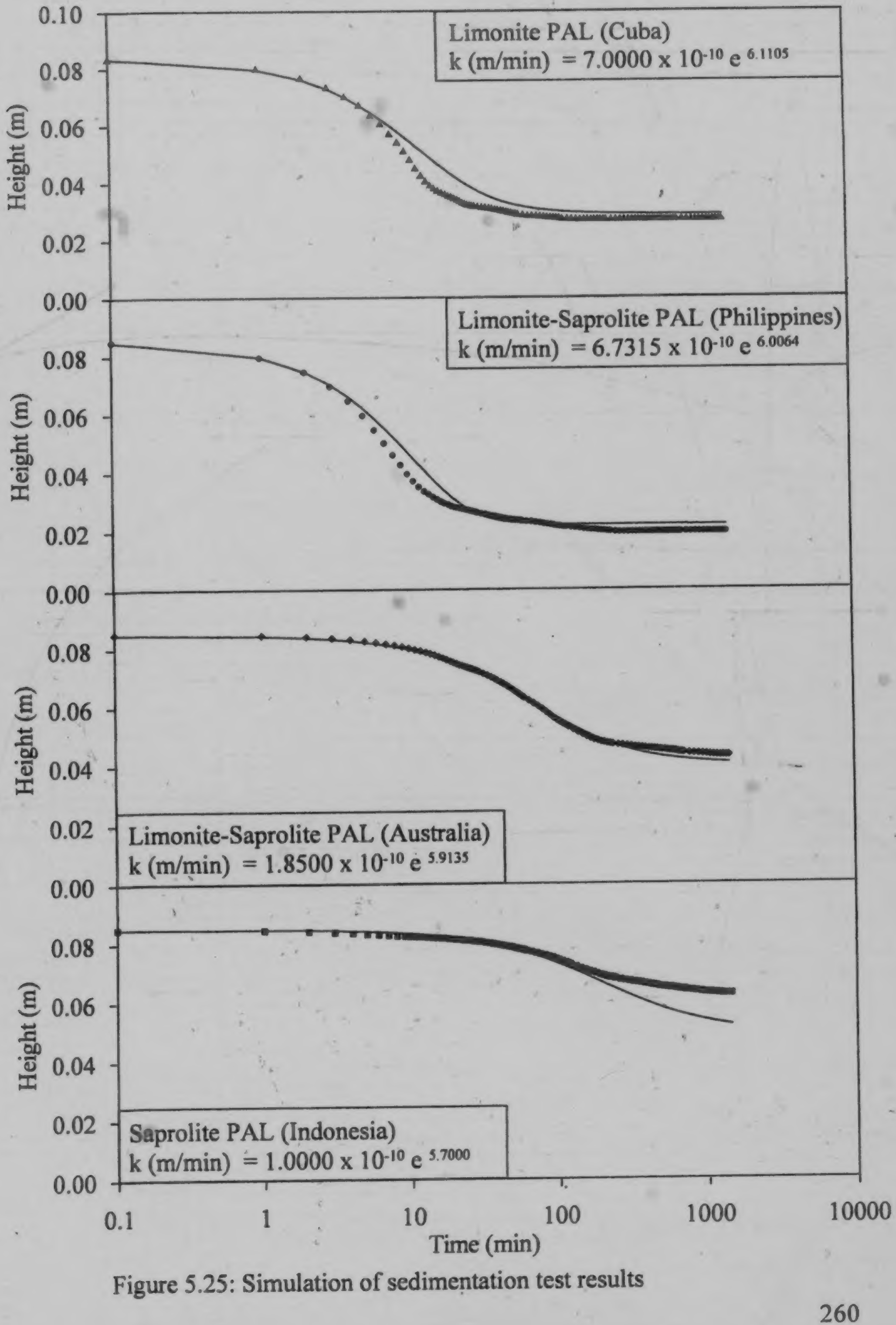

Figure 5.25: Simulation of sedimentation test results

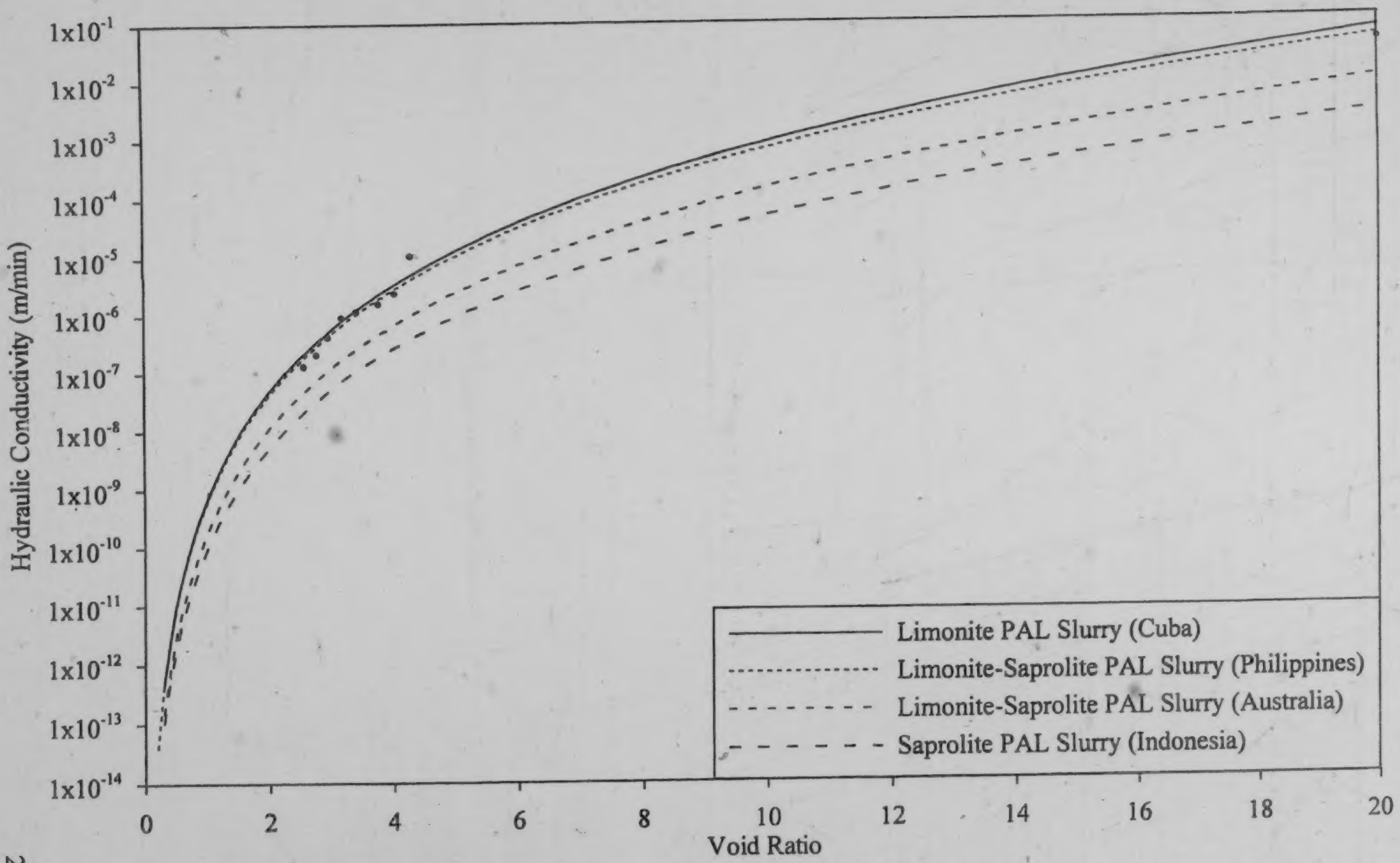

Figure 4.26: Hydraulic conductivity-void ratio relation for laterite PAL slurries

5.7.3 CCD Thickener

Figure 5.27 gives the solids content profile in a 3.0 m CCD thickener. This figure was obtained by using the input parameters given in Figures 5.21 and 5.22 in the sedimentation and consolidation program SECO described in Chapter Three. To highlight the solids content variation in the compaction bed of the storage thickener, sediment height is plotted on a logarithmic scale in the figure.

Figure 5.27 illustrates that the solids content increases both as a function of time and of depth in the thickener. Further, the solids content profile has two smoothly joining straight-line components. The initial straight-line portion portrays rapidly increasing solids content with depth whereas the final straight-line part denotes a slow increase in solids content. The increasing length of this latter straight-line segment with time signifies an increasing compaction bed thickness.

Figure 5.27 indicates that the improvement in solids content of the PAL slurry from Philippines is initially high and gradually fades away with time. The solids content increases from 15% to 39% after one hour and up to 44% after 12 hours. Under self-weight, a further increase in solids content amounts to a mere 2% after a week in the CCD thickener. A similar behavior can be envisaged for all of the other laterite PAL slurries.

Given the operational constraint of the metal extraction process such as time, thickener geometry, and the preclusion of load application, the solid-liquid separation behavior of laterite PAL slurries can be effectively improved using synthetic polymers as will be discussed in Chapter Seven.

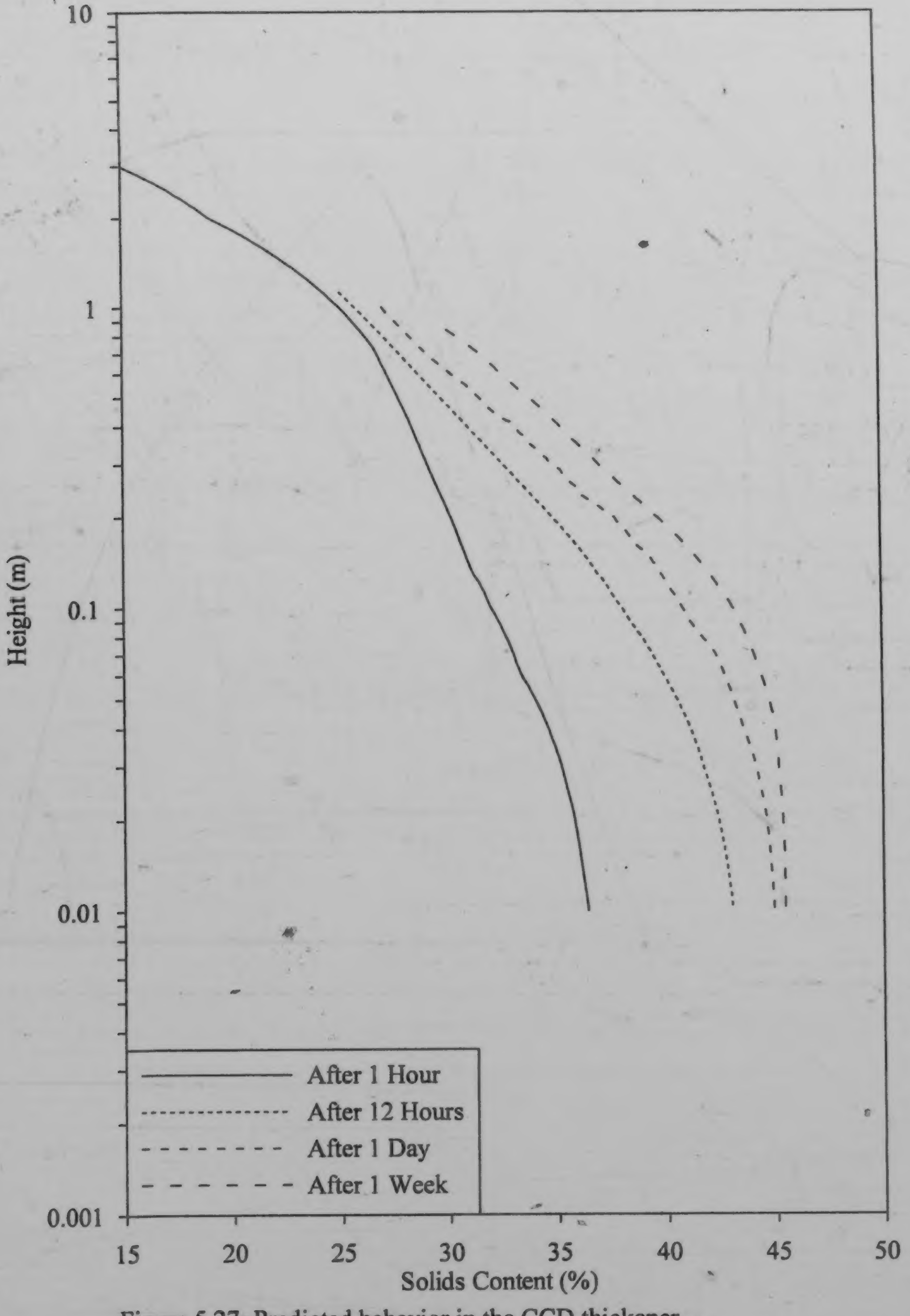

Figure 5.27: Predicted behavior in the CCD thickener

5.8 LATERITE SLURRY CHARACTERISTICS DIAGRAM

Figure 5.28 depicts the characteristics of various laterite PAL slurries on the ternary diagram. The diagram compiles the data presented earlier on sedimentation limit (Table 5.6) and consistency limits (Table 5.1) and shows that all of these limits are part of the family of constant clay-water ratio lines. This is because these lines denote constant physico-chemical interactions between colloidal particles and the medium. The deviation of soil behavior from the constant clay-water ratio lines at low clay content is attributed to the absence of clay minerals in the limonite PAL slurries and the presence of amorphous material in the saprolite PAL slurry from Indonesia. This means that the clay-water ratio lines are sensitive to mineral composition of the materials.

Figure 5.28 also gives the hydraulic conductivity of the laterite PAL slurries on the ternary diagram. The figure shows that the hydraulic conductivity is also part of the family of constant clay-water ratio lines. This is because hydraulic conductivity of laterite PAL slurries depends on the same interactions described above. The diagram indicates that the hydraulic conductivity of laterite PAL slurries varies by one order of magnitude between the sedimentation limit ($k = 10^{-5}$ cm/sec) and the liquid limit ($k = 10^{-6}$ cm/sec).

A comparison between the ore and the PAL slurries indicate an improved behavior of the latter materials. Such amelioration is attributed to mineral and environmental changes in the material characteristics during pressure acid leaching process.

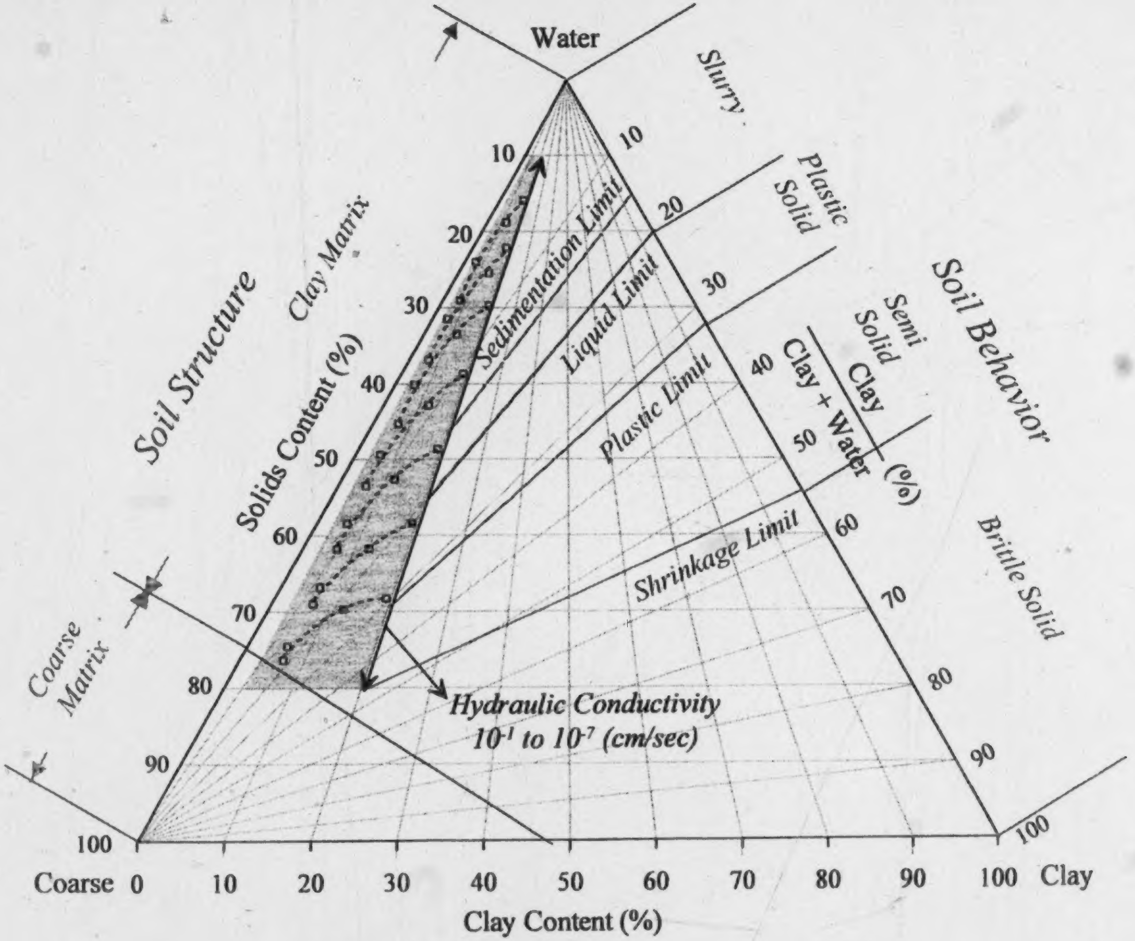

Figure 5.28: LSCD for laterite PAL slurries

5.9 SUMMARY AND CONCLUSIONS

This chapter provided a detailed geotechnical characterization of laterite PAL slurries. The influence of the acid leaching environment on the solid-liquid separation behavior of four laterite PAL material was investigated. These materials were selected from various parts of the globe; Cuba, Philippines, Australia and Indonesia. Results of laboratory investigations pertaining to geotechnical index properties, mineralogy, pore water chemistry, morphology and solid-liquid separation characteristics were presented. These data was used in the numerical simulation to predict filed performance of the CCD thickener. The entire data were depicted on the laterite slurry characteristics diagram. The conclusions of this chapter can be summarized as follows:

- Geotechnical characteristics of laterite PAL slurries from different origins are generally improved during pressure acid leaching. These materials have specific gravities above 3.20 and exhibit high water requirement during the autoclave operation for economic metal extraction.
- Materials undergo grain size growth during acid leaching. About 70% of the material is finer than 0.075 mm whereas the amount of clay size fraction ranges between 5 to 20%. The fine grain size and the presence of clay size fraction render these PAL slurries nonsegregating at an initial solids content of 15%.
- Converted to materials similar to sand or less active clays, laterite PALs are primarily composed of hematite. In some varieties, magnesium sulfates and amorphous materials are present in sizeable amounts.

- Autoclave operations generally use the required amount of sulfuric acid that influences the concentration of the pore water. The pore fluid is highly acidic (pH $\leq$ 1) with H^+, Ca^{2+}, Mg^{2+}, Mn^{2+}, Al^{3+}, Fe^{3+}, Ni^{3+}, $Co^{3+}$and SO_4^{2-} as predominant ions.
- Similar mineralogy and pore water chemistry result in identical morphology. Still, soil fabric ranges from flocculated to dispersed; a cardhouse microstructure is associated with saprolite PAL slurry.
- Improvement in material characteristics is clearly identified during sedimentation under self-weight. The initial hydraulic conductivity of laterite PAL slurries ranges between 10^{-2} to 10^{-3} cm/sec.
- The solid-liquid separation process is governed by sedimentation. Under self-weight a 90% dewatering is achieved as the void ratio changes from 20.0 to 4.3 and the solids content changes from 15 to 46%. A maximum effective stress of 8 kPa is sufficient to obtain about 95% dewatering.
- The hard, ultra-fine and spherical iron oxide particles are associated with high tortuousity and high void ratio. These particle characteristics result in the low hydraulic conductivity and compressibility of laterite PAL slurry during consolidation. Still, both of these parameters are improved compared to the ore slurry.
- The operational constraints of the metal extraction process include time, thickener geometry, preclusion of load application, and minimal changes in process conditions. Using synthetic polymers, improvement in the solid-liquid separation behavior of laterite PAL slurries should be investigated.

Chapter 6

Polymer Modification of Laterite Ore Slurries

6.1 GENERAL

Geotechnical investigation of polymer modified laterite ore slurries is pivotal in understanding the improvement or deterioration of solid-liquid separation behavior. This knowledge is useful for an assessment of the performance of various synthetic polymers in the metal extraction process. This chapter highlights the influence of polymer parameters on the solid-liquid separation behavior of the limonite-saprolite ore slurry from the Philippines. Denoted as laterite ore slurry in this chapter, characteristics of this material were described in chapter four. The various polymer parameters include polymer type, charge, molecular weight (MW) and dosage. Results of laboratory investigations pertaining to geotechnical index properties, sedimentation (in conjunction with morphology) and consolidation are discussed. Statistical analyses are used to develop and validate models describing each of these stages of the solid-liquid separation process. This is followed by providing the results of numerical simulation of the statistically analyzed data to predict field performance of the storage thickener. Next, the laboratory and modeling data is depicted on the laterite slurry characteristics diagram constructed for the laterite ore sample. Finally, a summary and the main conclusions drawn from this chapter are given.

6.2 GEOTECHNICAL INDEX PROPERTIES

6.2.1 General

Geotechnical characterization of polymer modified laterite ore slurries begins with an investigation of their index properties. These properties are used to classify the materials and to evaluate the performance of the synthetic polymers.

6.2.2 Segregation

Figure 6.1 gives the results of the segregation tests on laterite ore slurry modified with 4 ppm of selected polymers. Results are given in the form of normalized height versus solids content for different initial solids content. This figure shows that the observed solids content increases with depth and that the profiles tend to reach a constant solids content with increasing initial solids content. This behavior is similar to the ore slurry without polymer modification and is attributed to diminishing segregation at high initial solids content. Reduced segregation is attributed to the formation of a mesh due to the interaction of solid particles and synthetic polymers in the given medium.

Figure 6.2 gives the percentage of segregation as a function of the initial solids content for laterite ore slurry modified with the above polymers. This figure indicates that variation in the segregation characteristics of the ore slurry using different polymers is not significant. The segregation limit (I_S), which is defined as the initial solids content that pertains to 5% segregation with depth, closely matches for all polymers. Therefore, the investigated laterite ore slurry modified with polymers is non-segregating at an initial solids content of 15%.

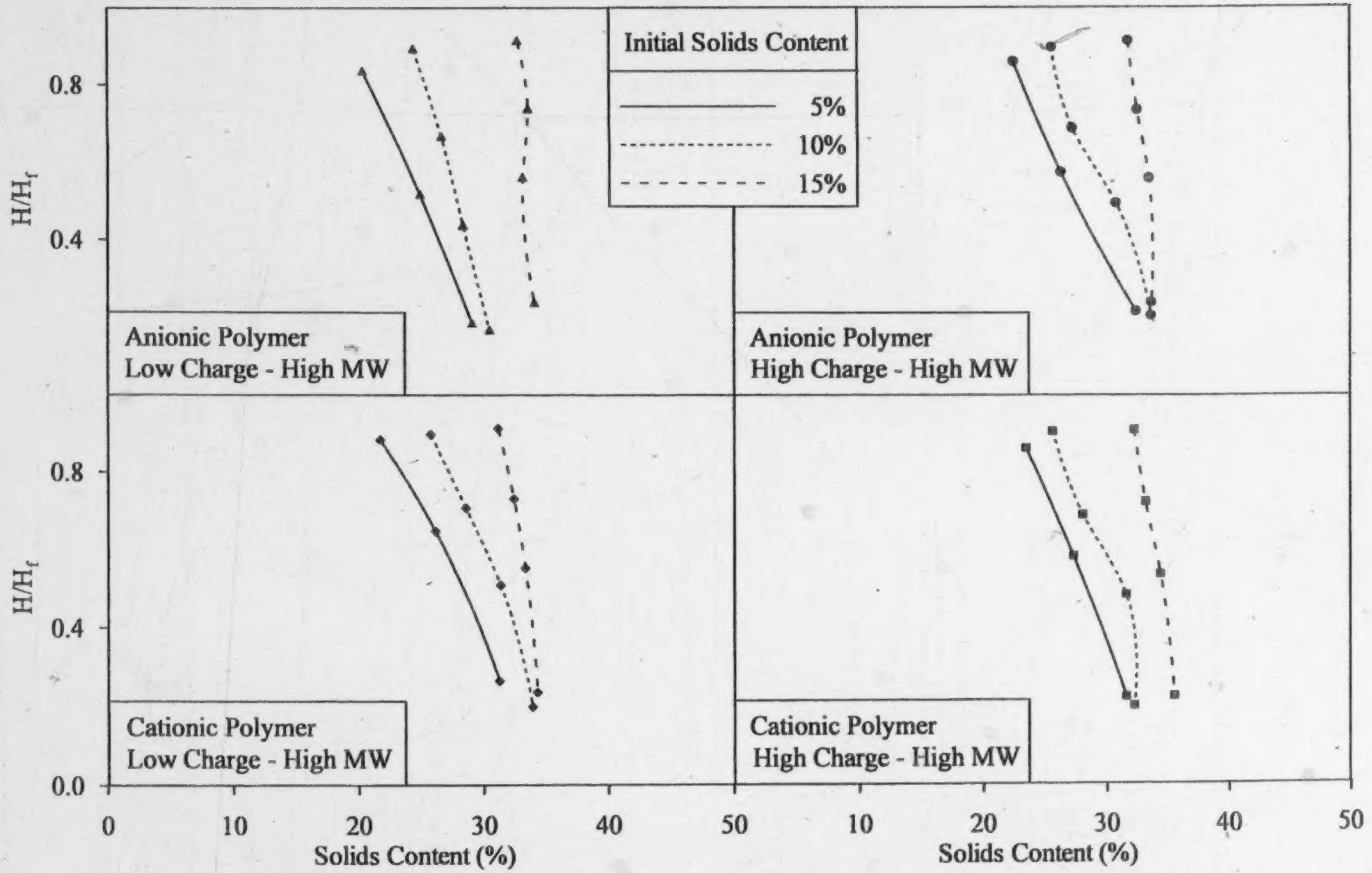

Figure 6.1: Segregation test results for laterite ore slurry modified with 4 ppm of diffrerent polymers

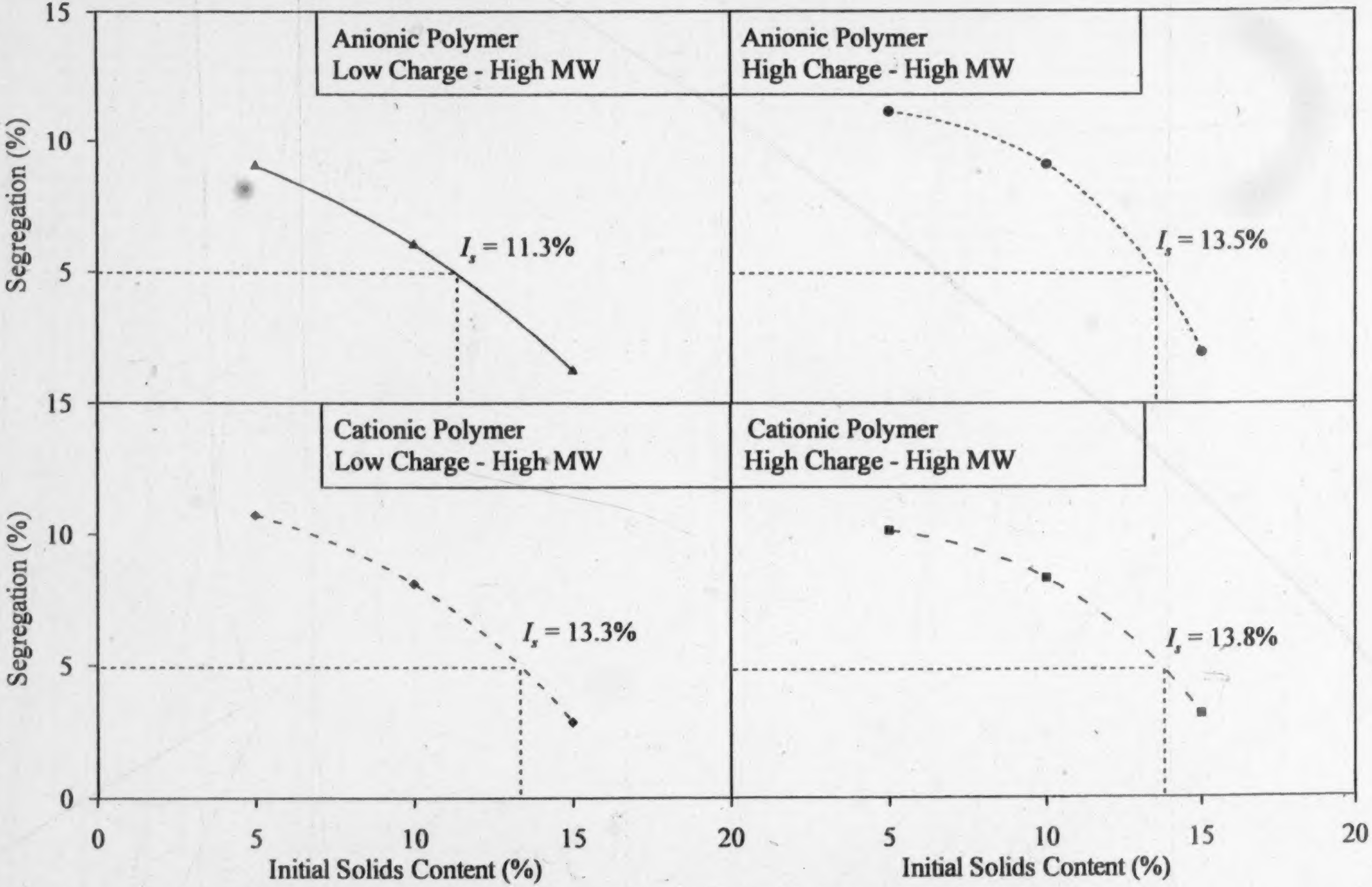

Figure 6.2: Segregation limit for laterite ore slurry modified with 4 ppm of various polymers

6.2.3 Consistency Limits

Table A.1 and A.2, presented in Appendix A, give the consistency limits of laterite ore modified with various ionic and nonionic polymers, respectively. Figure 6.3 summarizes test data in the plasticity chart (Casagrande 1948). This figure shows that all of the polymer modified materials plot in the area designated as *micaceous fine sandy and silty clays*. This suggests that the behavior of these materials is similar to that of clay particles with variable electro-chemical activity.

Figure 6.3 also compares polymer modified ore slurries with the laterite ore without polymer. This comparison illustrates that polymer modification of laterite ore results in considerable variation in the engineering characteristics. Materials modified with nonionic polymers plot close to the laterite ore without polymer, whereas considerable variation is observed among both anionic and cationic polymer modification. The figure shows that some of the polymer modified ore slurries are associated with large amount of water in the newly formed flocs. Described later in this chapter, the entrapped water results in an increase in the consistency limits of the polymer modified ore slurries.

The variation in plasticity characteristics among different polymers is mainly attributed to the variable interaction of synthetic polymers with the ore material in the given medium. This indicates that the solid-liquid separation behavior of this class of materials is governed by the parameters of synthetic polymers (type, charge, MW and dosage). The relative significance of these parameters is highlighted later in this chapter.

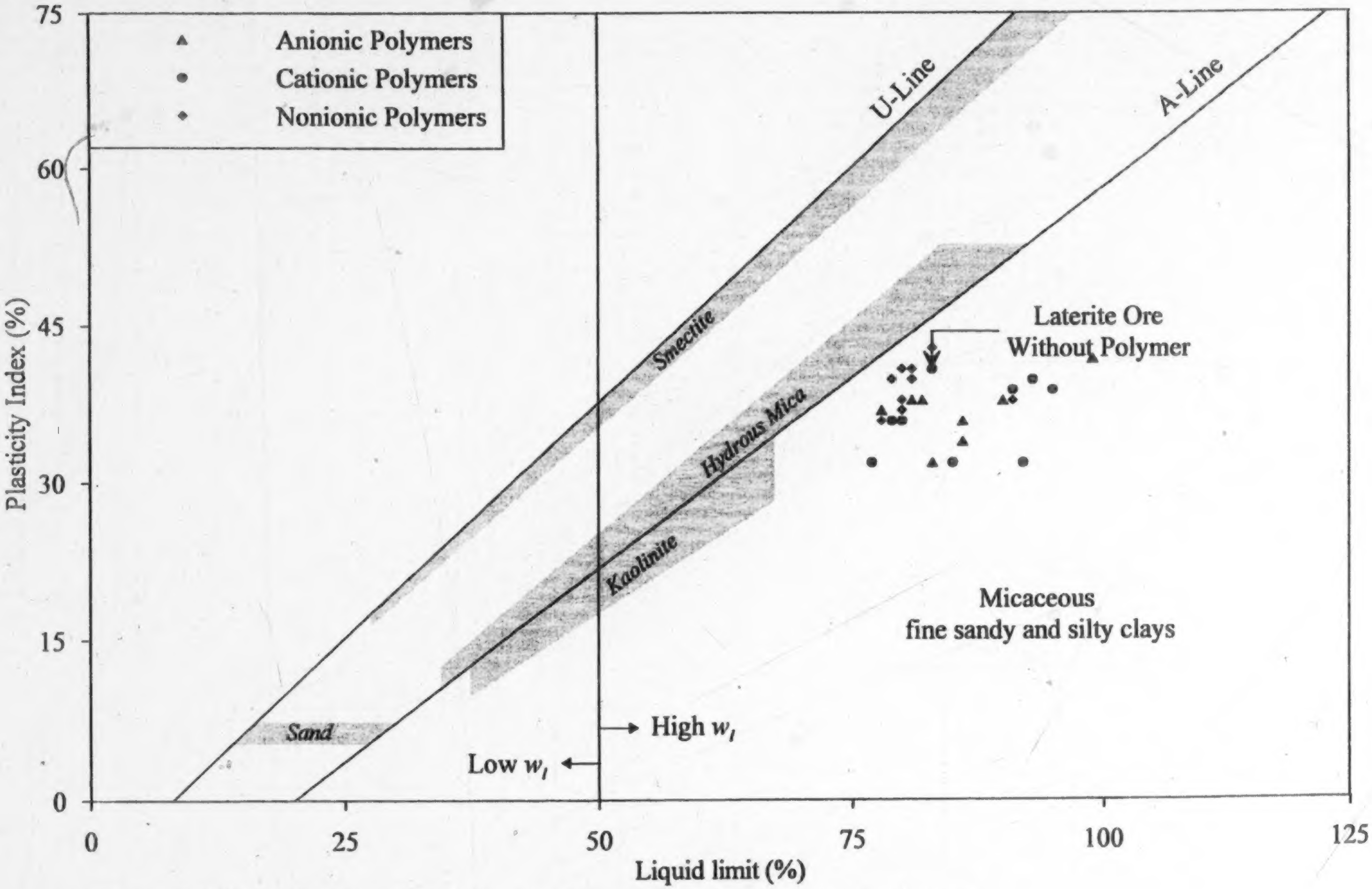

Figure 6.3: Plasticity chart for laterite ore slurry modified with various polymers

6.3 SEDIMENTATION

6.3.1 General

This section gives the self-weight sedimentation behavior of laterite ore slurry using various polymers; ionic and nonionic polymers are described separately. The initial hydraulic conductivity is obtained from the initial straight-line portions of the sedimentation curves. The effects of polymer parameters on the initial hydraulic conductivity are highlighted. Morphological observations are used to understand the observed behavior from a fundamental standpoint. Statistical analyses are used to assess the relative significance of various polymer parameters.

6.3.2 Ionic Polymers

6.3.2.1 General

Figure 6.4 gives the sedimentation test results for laterite ore slurry modified with various anionic polymers. This figure shows that similar to the ore slurry without polymer modification, the self-weight sedimentation is essentially completed within the first 180 minutes when the same slurry is modified with various anionic polymers. This figure further shows that with 30 minutes from the start of the test, most of the sedimentation curves start converging and curves for 4 and 12 ppm merge by the end of 180 minutes. The only exception to this general behavior is that of the 10% charge (low)-7.5 x 10^6 g/mol MW (low) polymer. Further, among the two polymer dosages, an increase in the rate of sedimentation is observed with an increase in polymer dosage. Detailed discussion of the behavior of these materials will be given in the next sub-section.

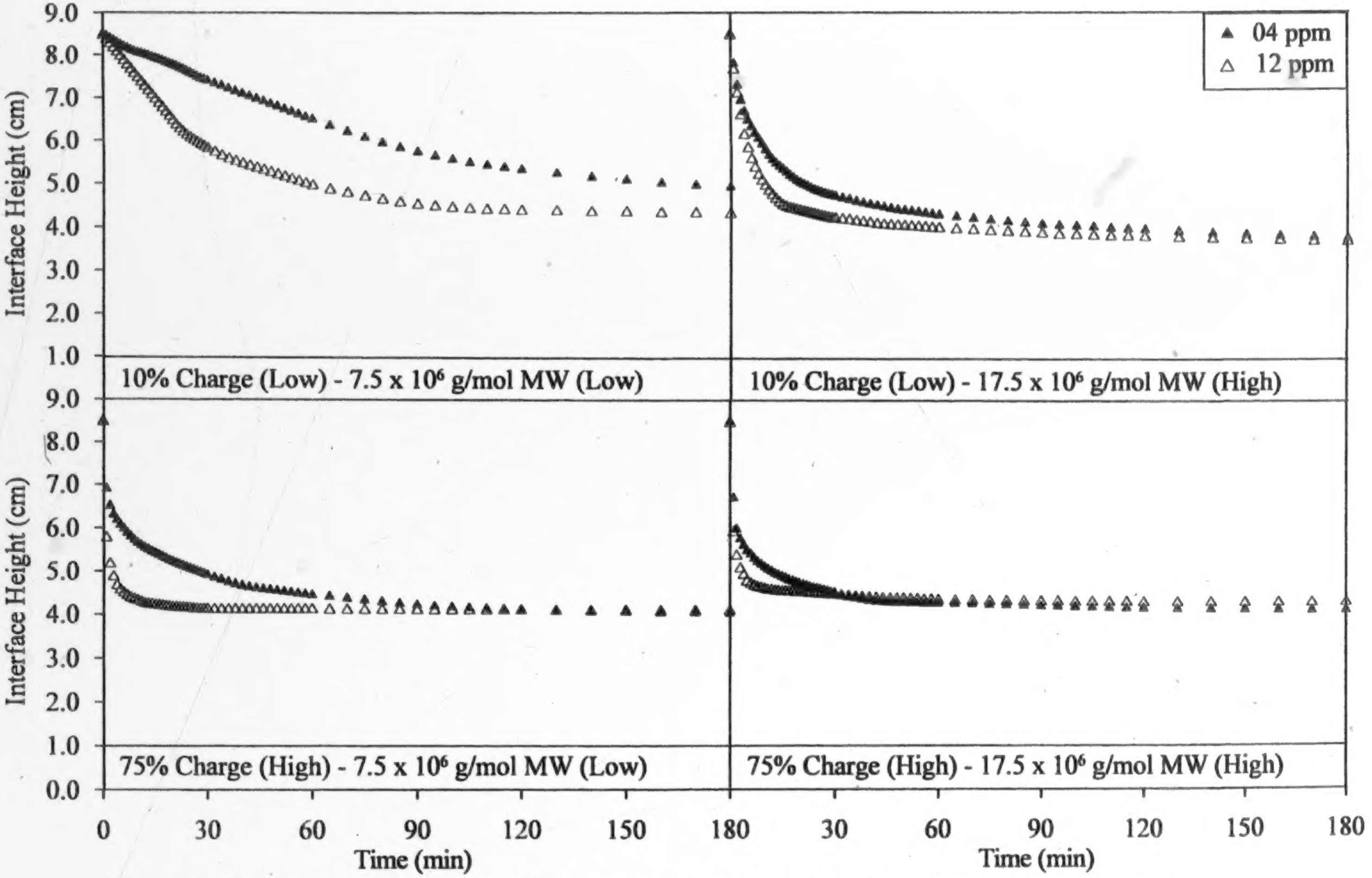

Figure 6.4: Sedimentation test results for laterite ore slurry modified with various anionic polymers

Figure 6.5 gives the sedimentation test results for laterite ore slurry modified with various cationic polymers. This figure indicates that although the self-weight sedimentation is essentially completed in the first 180 minutes, no two curves for 4 and 12 ppm dosages merge. With the exception of the 10% charge (low)-17.5 x 10^6 g/mol MW (high) polymer, an increase in the rate of sedimentation with an increase in polymer dosage is observed between the two polymer dosages.

A comparison of Figures 6.4 and 6.5 indicates that colloid-polymer-electrolyte interactions are much more variable for cationic polymers than for anionic polymers. These interactions govern the sedimentation behavior of the laterite ore slurry in the given neutral medium, which is comprised of low concentration of ions and a TDS of 550 mg/L. A comprehensive discussion of the variation during the sedimentation stage of the solid-liquid separation process is given next.

6.3.2.2 Initial Hydraulic Conductivity

Figures A.1 through A.4 give the sedimentation test result for the first 30 minutes for laterite ore slurry modified with various ionic polymers. The slope of the initial straight-line portion is used to obtain the initial hydraulic conductivity (k_i). Derived from Figure A.1 though A.4, Table 6.1 gives k_i for laterite ore slurry modified with various ionic polymers. Likewise, Figure 6.6 highlights the effect of polymer charge, molecular weight (MW) and dosage on the k_i of laterite ore slurry.

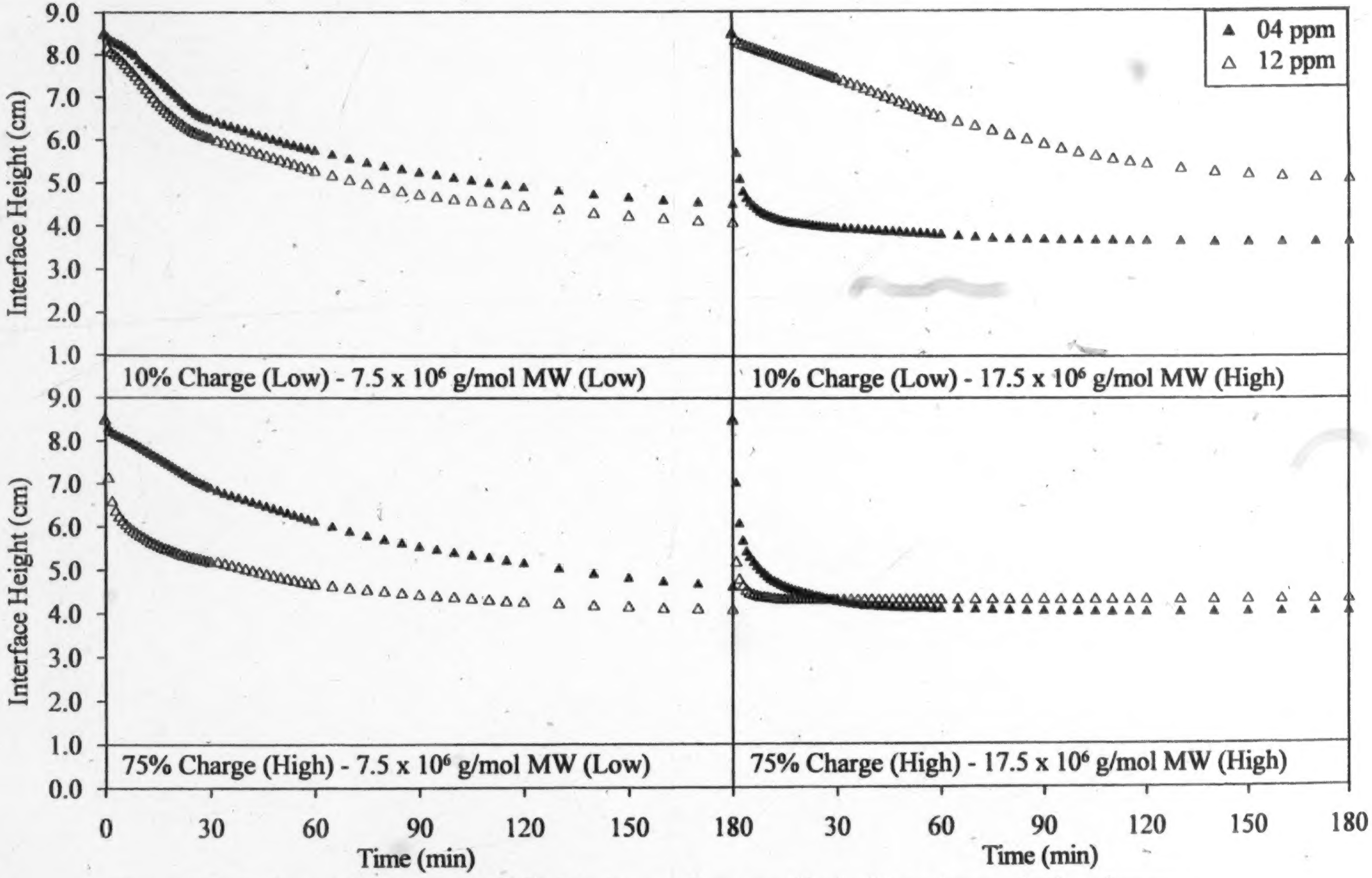

Figure 6.5: Sedimentation test results for laterite ore slurry modified with various cationic polymers

Table 6.1: k_i of laterite ore slurry modified with various ionic polymers

Polymer Parameters				k_i x 10^{-3} (cm/sec)	
Type	Charge	MW x 10^6 (g/mol)	Dose (ppm)	Sedimentation	Consolidation
Anionic	10% (Low)	7.5 (Low)	4	7	7
			12	15	15
		17.5 (High)	4	88	85
			12	99	102
	75% (High)	7.5 (Low)	4	234	234
			12	394	423
		17.5 (High)	4	263	292
			12	372	409
Cationic	10% (Low)	7.5 (Low)	4	11	12
			12	14	14
		17.5 (High)	4	409	445
			12	5	5
	75% (High)	7.5 (Low)	4	7	8
			12	197	204
		17.5 (High)	4	179	182
			12	394	438

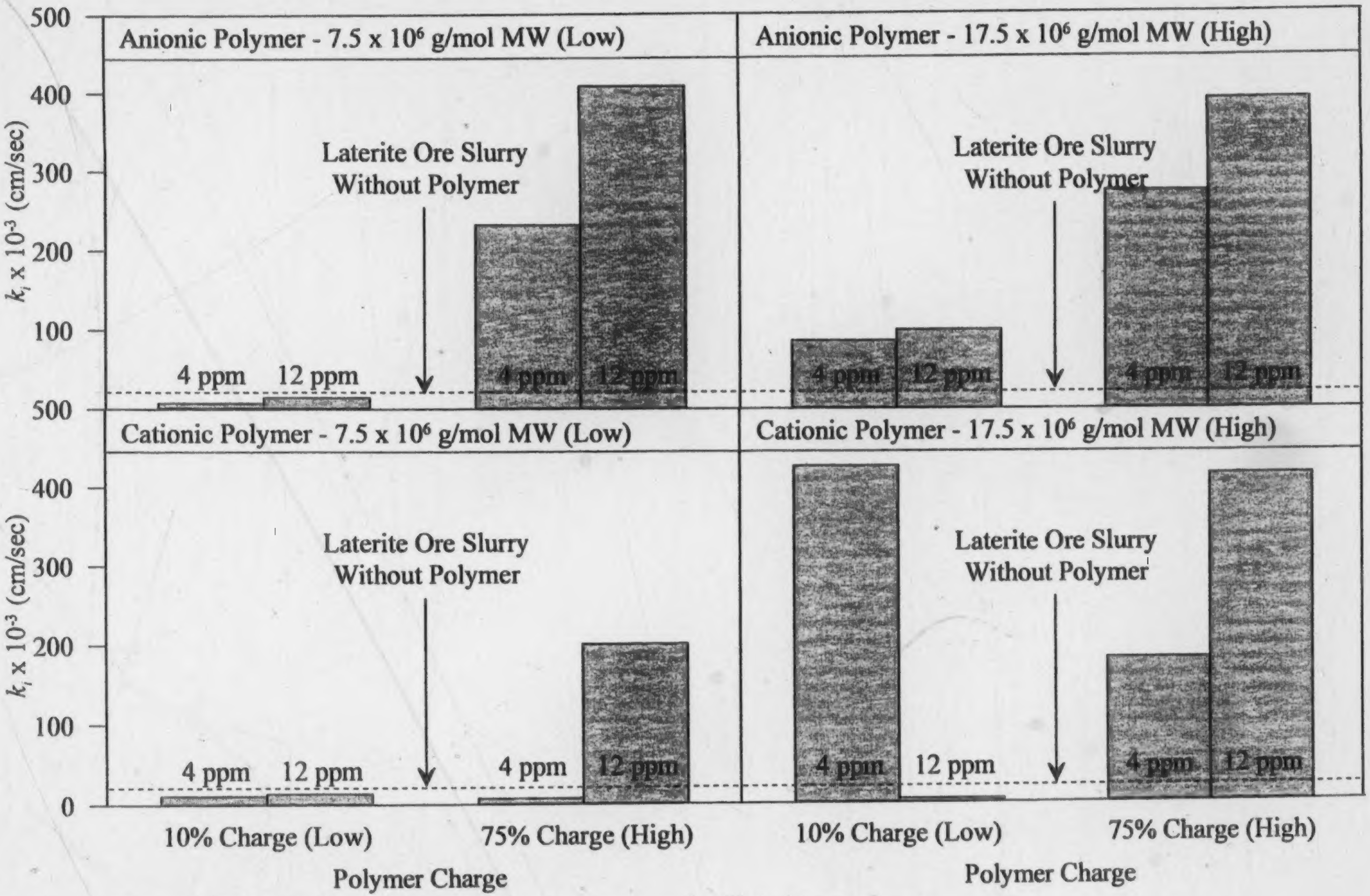

Figure 6.6: Effect of various polymer parameters on k_i of laterite ore slurry

Table 6.1 indicates variation in the k_i of identical samples measured during the sedimentation test and the initial part of the consolidation test. Large variations are observed for high k_i due to the fact that for these materials, a maximum of two data points were available for curve fitting of the initial straight-line portion of the sedimentation curve. The cloudy solid-liquid interface did not allow the observer to clearly determine the data points during the initial stages of the test. Therefore, the resulting fit equation and hence k_i partly depended on observer's bias. It is noteworthy that the cloudiness reduced at lower rates of sedimentation suggesting a flocculation mechanism that also includes the smaller solid particles in the slurry. The reduced cloudiness in the vicinity of the solid-liquid interface permitted the observer to ascertain the data points and make a better judgment about measured k_i. Therefore, variations in the k_i between the two identical samples gradually diminish with a decrease in k_i.

The k_i of laterite ore slurry without polymer modification measured 21 x 10^{-3} (cm/sec) as reported in Chapter Four. A comparison of this value with the data depicted in Table 6.1 reveals that polymer modification changes k_i of the laterite ore slurry to variable extent. Considering the sedimentation test data, an improvement of about 20 times and a decrease of four times are observed for the investigated materials. Such a large variability in the observed k_i is mainly attributed to the variable colloid-polymer-electrolyte interactions.

Figure 6.6 shows that for the conducted tests, polymer modification improves k_i of laterite ore slurry on ten occasions out of a total of sixteen tests. A higher k_i for the polymer modified slurry compared to that without polymer modification is generally observed for either 75% charge (high) and/or 17.5 x 10^6 g/mol MW (high) polymers. On the other hand, a lesser k_i for the polymer modified slurry compared to that without polymer modification is mainly observed for 10% charge (low) and 7.5 x 10^6 g/mol MW (low) polymers.

Figure 6.6 also indicates that for anionic polymers, increase in polymer charge results in an increase in k_i for all polymer MW and dosages. On the contrary, an increase in polymer charge does not necessarily result in a k_i increase for laterite ore slurry modified with cationic polymers. For these polymers, charge increase at 4 ppm dosage (low) results in a marginal k_i decrease whereas at 12 ppm dosage (high) a substantial increase in k_i is observed with an increase in polymer charge.

The higher k_i for the polymer modified slurry compared to that without polymer modification is attributed to increased polymer adsorption either at 75% charge (high) and/or 17.5 x 10^6 g/mol MW (high), thereby resulting in increased flocculation. Two exceptions to this generalization are observed in cationic polymers: (i) 75% charge (high)-7.5 x 10^6 g/mol MW (low)-4 ppm dosage (low) and (ii) 10% charge (low)- 17.5 x 10^6 g/mol MW (high)-12 ppm dosage (high). The former is attributed to electrostatic repulsion between the positively charged particle surfaces of sesquioxides and the cationic polymer possessing an identical charge. Such repulsion is known to hinder polymer adsorption and hence the development of flocs (Gregory 1973). This is also supported by the fact that a lesser k_i is observed for the same polymer MW and dosage even at 10% polymer charge (low). Conversely, the latter exception is explained by the possible development of bimodal size distribution consisting of individual particles and flocs in the slurry (Hogg 1999). The individual dispersed particles obstruct the settling of flocculated material thereby resulting in a reduced k_i. This is substantiated by the fact that at 75% charge (high), electrostatic repulsion overcomes the effect of dispersed particles, thereby resulting in a higher k_i for the same MW and dosage.

The smaller k_i for the polymer modified slurry compared to that without polymer modification is observed for polymers with 10% charge (low) and 7.5 x 10^6 g/mol MW (low). This is attributed to depleted polymer adsorption and flocculation due to the combined effect of polymer charge and MW (Alonso & Laskowski 1999). The smaller chain length associated with 7.5 x 10^6 g/mol MW (low) cannot accommodate a large number of solid particles. This is supported by the fact that at 17.5 x 10^6 g/mol MW (high), higher k_i is generally observed for all but one test. For anionic polymers, the 10% polymer charge (low) is insufficient for hydrolysis and in fact causes dispersion similar to Na^+ addition to clays. For cationic polymers, electrostatic repulsion causes additional reduction in the amount of flocculation. This is in accordance with recorded observations during various sedimentation tests, which indicated reduced floc size.

The increase in k_i for anionic polymers, with increasing polymer charge, polymer MW and dosage, is due to increasing flocculation. For the eight tests, an increase in k_i is observed when any of the polymer parameter is increased from a low to a high value. The relative significance of these parameters will be described later in this chapter. Here, a comparison between the low and the high dosages is highlighted. Such a comparison indicates a minor increase in k_i when the dosage is increased from 4 ppm to 12 ppm. This indicates that the optimum dosage for anionic polymers is just above the latter dosage used in this research.

For cationic polymers, charge increase at 4 ppm dosage (low) results in a marginal k_i decrease. This is attributed to an increase in electrostatic repulsion between sesquioxides and cationic polymers at low dosages (Gregory 1973). The same phenomenon is responsible for the low k_i at 10% polymer charge (low) and high dosage of 12 ppm (Hogg 1999). At 12 ppm dosage (high), such repulsion is overcome by flocculation when the charge is increased from 10% (low) to 75% (high). Further, for both 10% charge (low) and 75% charge (high), an increase in polymer dosage results in a k_i increase in all but one case. Therefore, an optimum dosage for cationic polymers is also in the vicinity of 12 ppm for most cases studied during this investigation.

The influence of various polymer parameters can be combined in a single term to be called the *polymer factor*. Mathematically, this term is equal to polymer charge divided by the product of polymer MW and polymer dosage and has the units mol/g-ppm.

Figure 6.7 gives the variation of the polymer factor with the initial hydraulic conductivity of the polymer modified laterite ore slurries. This figure shows a cyclic k_i variation with polymer factor and the relationships hold for both anionic and cationic polymers. Based on colloid-polymer-electrolyte interactions, the relationships show three zones of behavior, in which the first and the third zones match closely. These zones include: (a) dispersion, (b) uniform flocculation and (c) bimodal flocculation.

The various zones depicted in Figure 6.7 are explained by the mechanism governing colloid-polymer electrolyte interactions. It was established in Chapter Four that the laterite ore slurry is predominantly composed of iron oxides and some clay minerals in a near neutral pH and low electrolyte concentration thereby resulting in large double large thickness. This allows the synthetic polymers to experience electrostatic forces due to the colloidal particles. As a result, the positively charged iron oxide surfaces attract anionic polymers and clay surfaces cationic polymers. However, the magnitude of these forces is generally small as the double layer of oppositely charged ions surrounds the colloids (Mitchell 1993). Therefore, flocculation of both types of colloidal particles takes place as a result of polymer addition to the slurry. The type of flocculation or dispersion depends on bond strength and floc size. In general, high charge synthetic polymers result in a stronger bond between the polymer and the colloid as well as between various flocs. Similarly, a high polymer molecular weight leads to a large floc size (Hogg 1999).

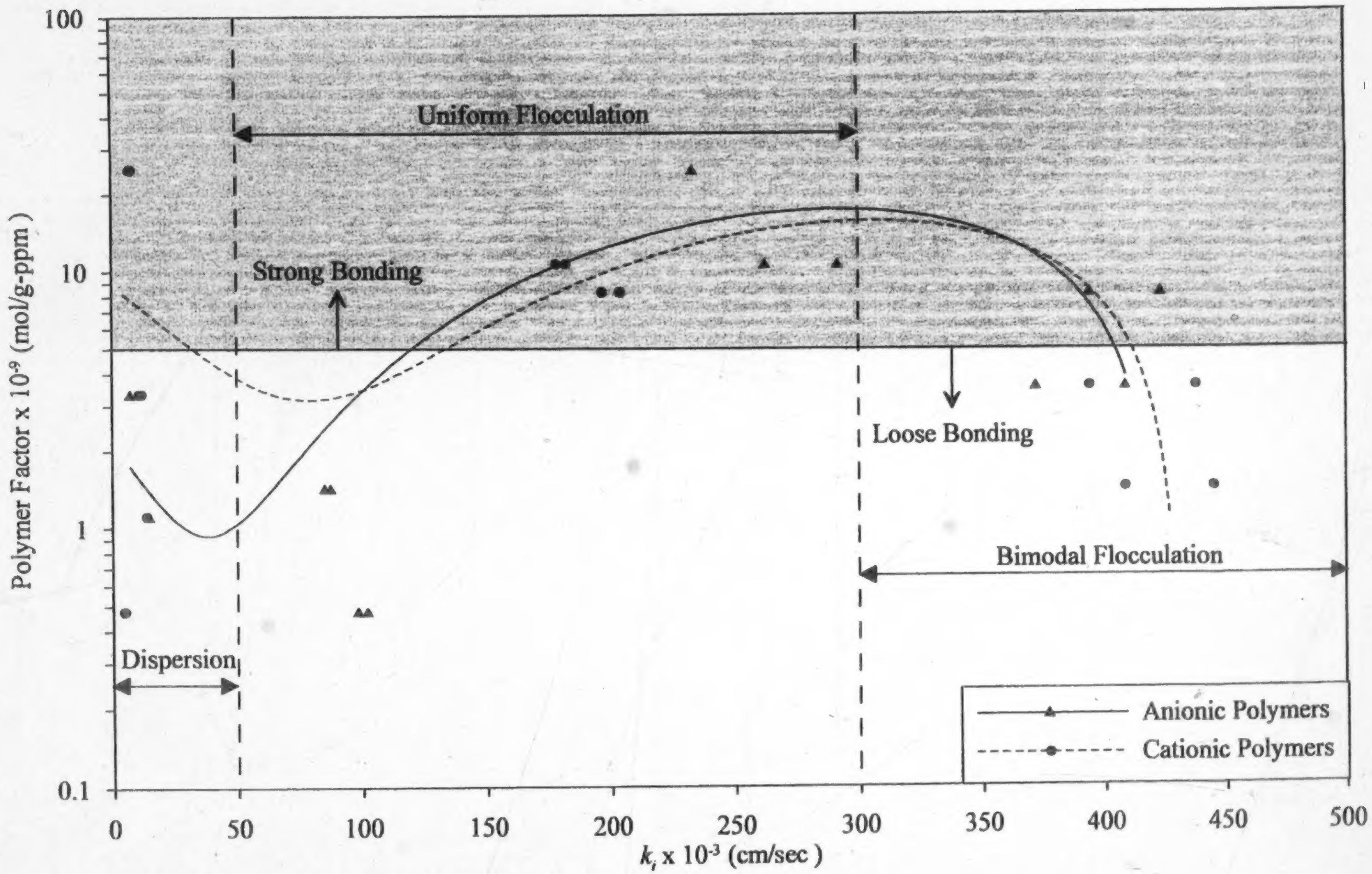

Figure 6.7: Variation of k_i with polymer factor

Combining the various polymer parameters, a polymer factor around 5.0 x 10^{-9} mol/g-ppm is chosen to be the boundary between the strong and the loose bonding. Similarly, the inflexion points of the fitting curves are the limits between various kinds of colloid-polymer-electrolyte interactions. These arbitrary limits on Figure 6.7 allow a better understanding of the sedimentation behavior of laterite ore slurries.

Up to an initial hydraulic conductivity of about 50 x 10^{-3} cm/sec, a dispersion zone occurs. All of the observed data that fall below the ore slurry without polymer (21 x 10^{-3} cm/sec) is located in this zone. Likewise, most of the observed data in this zone falls in the area designated as loose bonding. The partly dispersed laterite ore slurry without polymers is rendered completely dispersed by the low charge anionic polymers leading to a k_i reduction. This is analogous to the dispersion of negatively charged clay particles by the addition of Na^+. Similarly, electrostatic repulsion between the positive colloids and the cationic polymers also results in dispersion and a k_i reduction.

Between a k_i of 50 and 300 x 10^{-3} cm/sec, a flocculation zone is found. In this zone, the high charge anionic polymers do not disperse but flocculate the solid particles. This is similar to a flocculated clay fabric due to the addition of high charge cations. Likewise, electrostatic repulsion is negligible for high charge cationic polymers, which interact with the negatively charged double layer causing flocculation. The high charge of the synthetic polymers results in strong colloid-polymer and floc-floc bonds. This leads to a narrow size distribution of the flocs. Most of the observed data in this zone falls above a polymer factor of 5.0 x 10^{-9} mol/g-ppm.

Beyond a k_i of 300 x 10^{-3} cm/sec, a zone of bimodal flocculation exists. In this region, most of the observed data falls in the area designated as loose bonding, which occurs due to the low polymer factor. Such bonding results in floc breakage and bimodal size distribution that comprises of both large and small flocs. This creates channels or flow paths of least resistance in the flocculated slurry matrix. These channels result in an increase in the initial hydraulic conductivity of the material.

This discussion is supported by extensive annotations taken during the laboratory testing of the polymer modified laterite ore slurries and illustrates that the combined effect of polymer parameters is efficiently explained by the term polymer factor.

6.3.2.3 Morphology

The observed behavior given above is explained in the light of morphological examinations of some of the samples taken after the sedimentation tests. Results of scanning electron microscopy are studied in conjunction with elemental analyses. Figure 6.8 and 6.9 give the morphological details of laterite ore slurry modified with anionic polymers having 10% charge (low)-17.5 x 10^6 g/mol (high) MW and 75% charge (high)-17.5 x 10^6 g/mol (high) MW, respectively. Similarly, Figure 6.10 and 6.11 give the microstructural details of laterite ore slurry modified with cationic polymers and the above designation, respectively. All observations pertain to a polymer dosage of 4 ppm (low). All of these figures are comprised of four micrographs, similar to those described in Chapters Four, Five and Six.

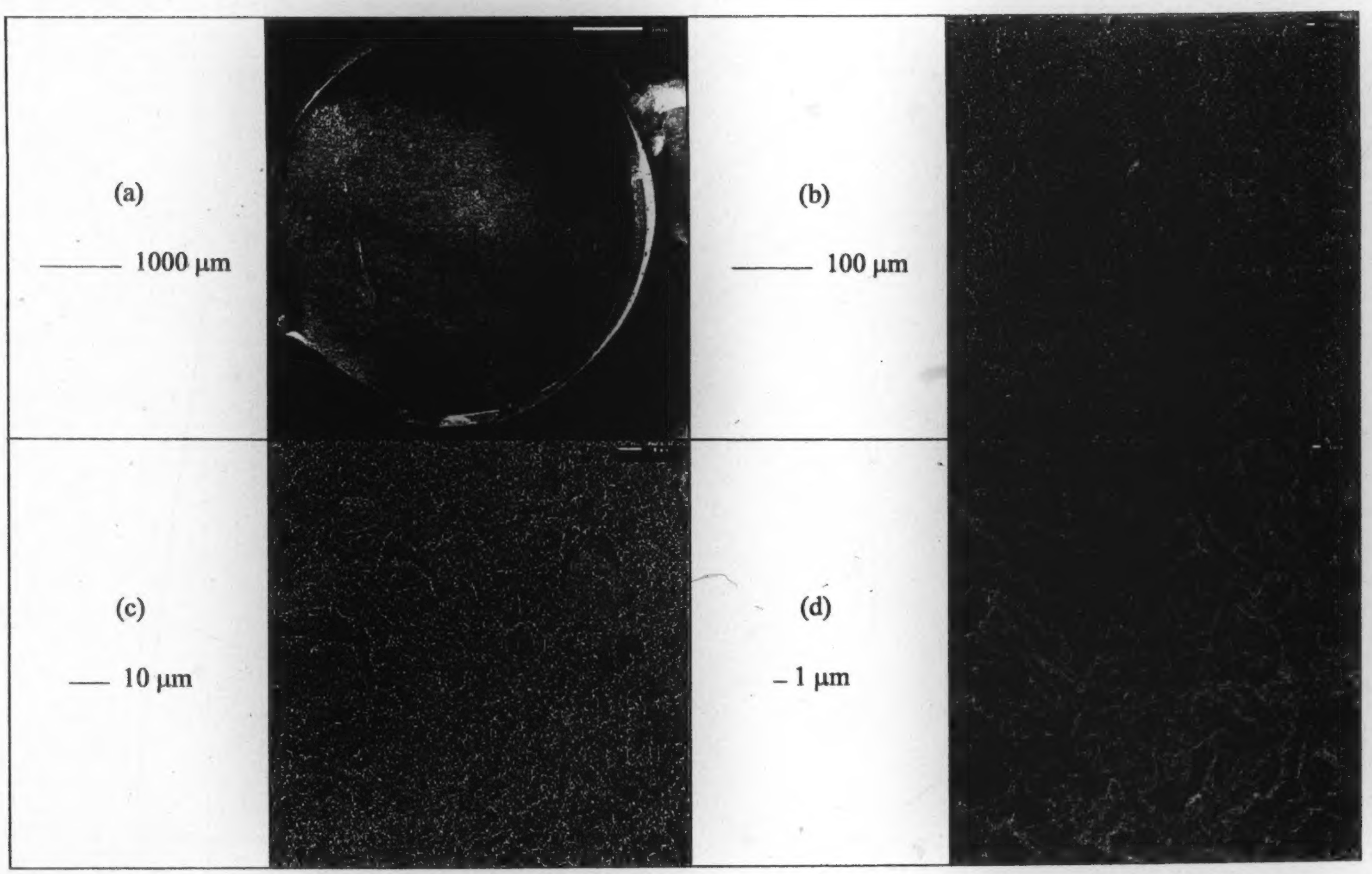
(a)
1000 μm
(b)
100 μm
(c)
10 μm
(d)
1 μm

Figure 6.8: SEM of laterite ore slurry modified with 10% charge (low)-17.5 x 10^6 g/mol MW (high)-04 ppm (low) anionic polymer

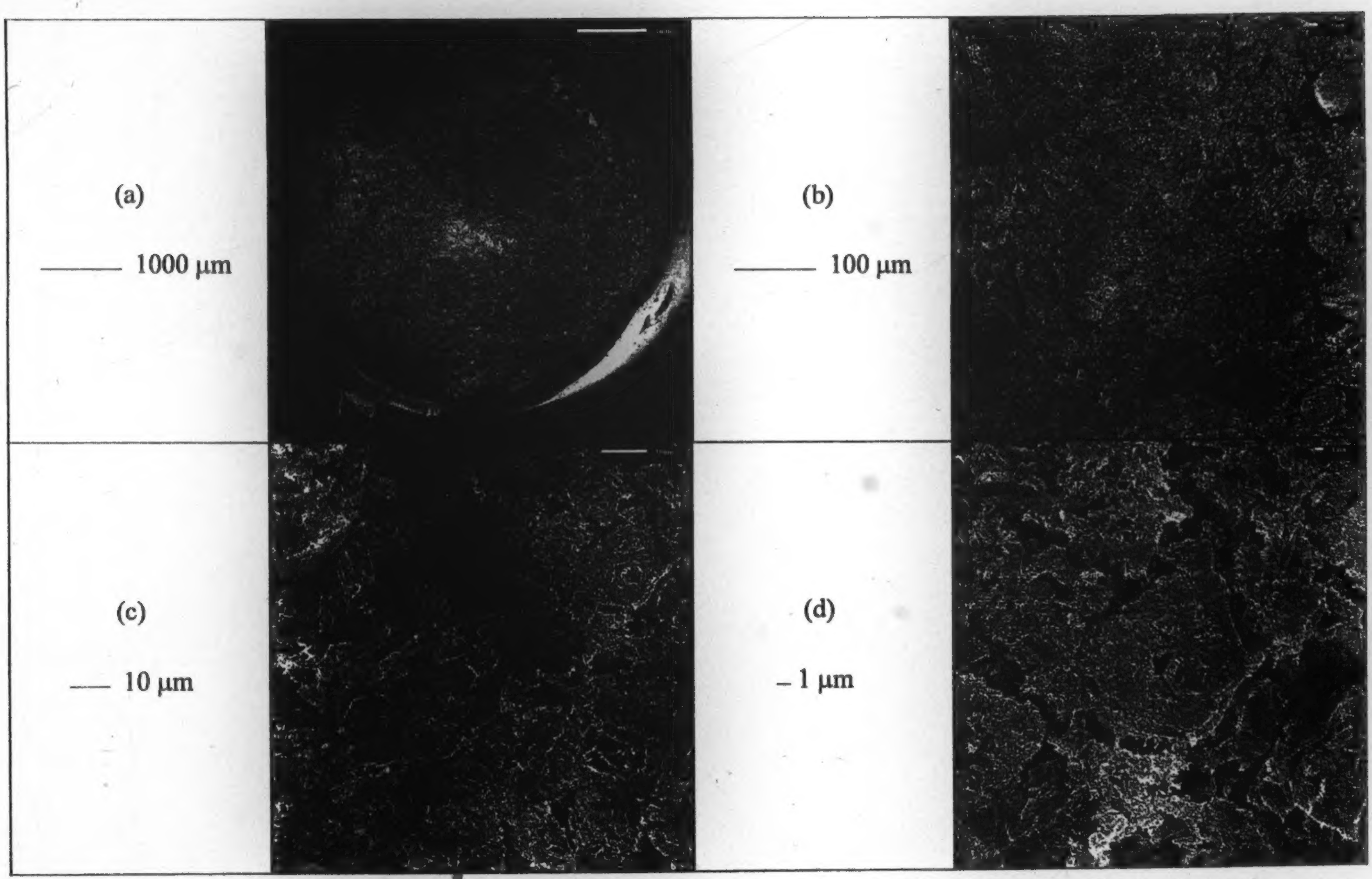
(a)
1000 μm
(b)
100 μm
(c)
10 μm
(d)
1 μm

Figure 6.9: SEM of laterite ore slurry modified with 75% charge (high)-17.5 x 10^6 g/mol MW (high)-04 ppm (low) anionic polymer

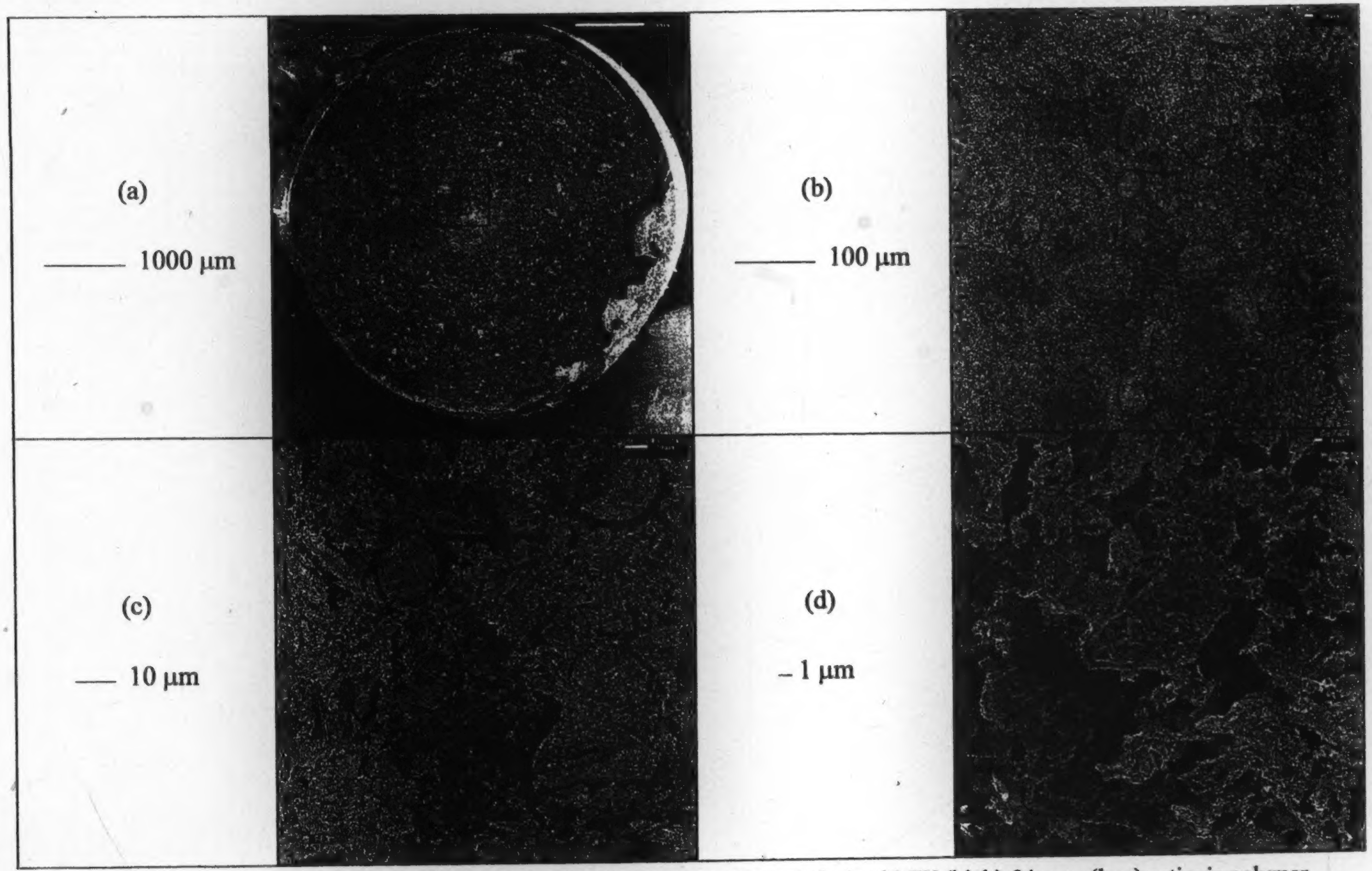
(a)
1000 µm
(b)
100 µm
(c)
10 µm
(d)
1 µm

Figure 6.10: SEM of laterite ore slurry modified with 10% charge (low)-17.5 x 10^6 g/mol MW (high)-04 ppm (low) cationic polymer

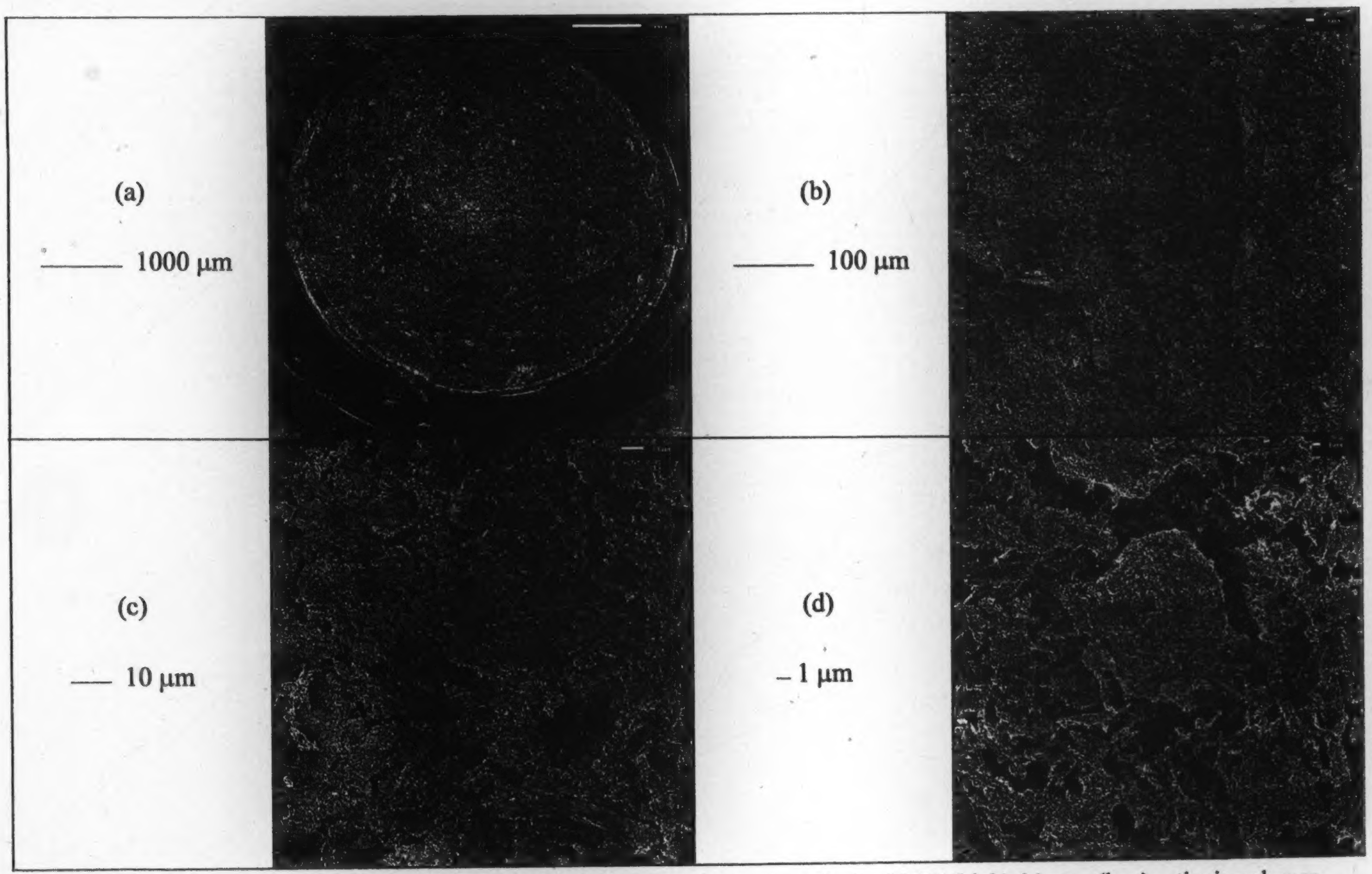
(a)
1000 µm
(b)
100 µm
(c)
10 µm
(d)
1 µm

Figure 6.11: SEM of laterite ore slurry modified with 75% charge (high)-17.5 x 10^6 g/mol MW (high)-04 ppm (low) cationic polymer

Figure 6.8 shows the morphology of the laterite ore slurry modified with 10% charge (low)-17.5 x 10^6 g/mol MW (high)-04 ppm (low) anionic polymer. Micrograph (a) shows a good specimen surface with some corrugations. Micrograph (b) shows the presence of evenly distributed coarse grains scattered through out the clay matrix. Micrograph (c) shows that these grains are mainly silt size particles. Micrograph (d) illustrates that the clay fabric is flocculated but does not vividly show any flocs with distinct boundaries. Collectively, the entire morphology is devoid of any definite structural motif and channeling is minimal. Therefore, the hydraulic conductivity is considered to be entirely dependent on the microfabric, which is composed of particle assemblages and interassemblage pore spaces. The higher resistance offered to the flow of water through these small pores is responsible for the low increase in hydraulic conductivity due to polymer modification. The average k_i of 86 x 10^{-3} cm/sec measured for this sample is four times that of the ore slurry without polymer.

Figure 6.9 shows the morphology of the laterite ore slurry modified with 75% charge (high)-17.5 x 10^6 g/mol MW (high)-04 ppm (low) anionic polymer. Micrograph (a) shows a reasonable specimen surface with some corrugations. Micrograph (b) shows evenly distributed coarse grains scattered through out the clay size matrix. Micrograph (c) depicts that most of these grains are comprised of flocculated clay particles. Micrograph (d) illustrates that these flocs can be as large as 15 μm. The morphology of this specimen is flocculated with hydraulic conductivity governed by the pore spaces between the flocs. The larger pore size is resulted in an average k_i of 277 x 10^{-3} cm/sec measured for this sample. This hydraulic conductivity is about three times that of the previous sample and thirteen times that of the ore slurry without polymer.

Figure 6.10 shows the morphology of the laterite ore slurry modified with 10% charge (low)-17.5 x 10^6 g/mol MW (high)-04 ppm (low) cationic polymer. Micrograph (a) shows an excellent specimen surface for microscopy. Micrograph (b) shows coarse silt grains scattered through out the clay matrix. Micrograph (c) gives a flocculated clay size structure with abundant pore spaces between the flocculated materials. Micrograph (d) illustrates large floc size, a low apparent tortuousity and large pore size, all of which result in a high initial hydraulic conductivity of this sample. The measured average k_i is 427 x 10^{-3} cm/sec, which is a twenty times increase compared with the ore slurry without polymer modification.

Figure 6.11 shows the morphology of the laterite ore slurry modified with 75% charge (high)-17.5 x 10^6 g/mol MW (high)-04 ppm (low) cationic polymer. Micrograph (a) shows a good specimen surface with minimal disturbance. Micrograph (b) shows a compact clay size structure with evenly distributed silts size grains. Micrograph (c) illustrates even-sized flocs with uniform pore spaces between the flocs. Micrograph (d) shows that these pore spaces are smaller than those in the previous sample. This has resulted in a lower value of average k_i of 180 x 10^{-3} cm/sec compared with the previous sample. Still, this measured value is about nine times that of the ore slurry without polymer.

6.3.2.4 Statistical Analysis

Based on the 2^k factorial design of experiments described in Chapter Three, a statistical analysis was conducted for ionic polymers. Using the measured k_i as input, an estimate of k_i resulted according to the following model:

$$k_i = 0.17963 - 0.01616\,T_p + 0.09401\,C_p + 0.06511\,MW_p + 0.0215\,D_p \quad (6.1)$$

where,

T_p = Polymer type

C_p = Polymer charge

MW_p = Polymer MW

D_p = Polymer dosage

Using –1 for low and +1 for high values of the above polymer parameters, equation (6.1) estimated the k_i depicted in Figure 6.12. Despite the scatter, this figure shows a reasonable correlation between the observed and the estimated values for the given set of data.

The analysis showed that the most significant factors are polymer charge (p-value of 0.03) followed by polymer MW (p-value of 0.10). Conversely, polymer dosage (p-value of 0.57) and polymer type (p-value of 0.67) are less significant. This is in accordance with observations depicted in Figure 6.7. This figure showed that variations in polymer charge and MW result in significant alterations in observed k_i, whereas marginal changes in k_i occur due to variations in polymer dosage and type. Therefore, the observed solid-liquid separation of laterite PAL slurries modified with ionic polymers is in accordance with statistical analysis.

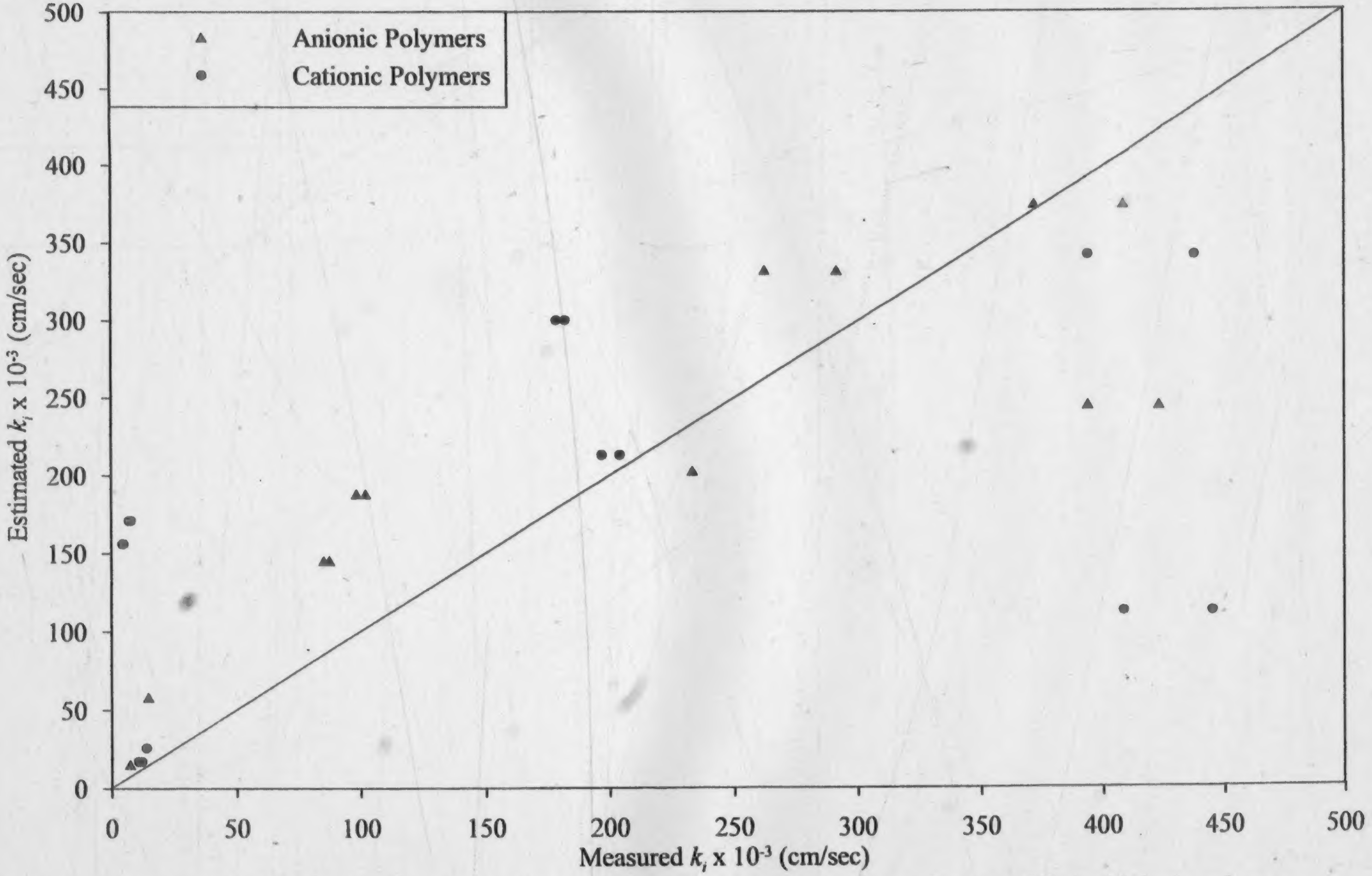

Figure 6.12: Relationship between measured and predicted k_i of laterite ore slurry modified with ionic polymers

6.3.3 Nonionic Polymers

6.3.3.1 General

Figure 6.13 gives the sedimentation test results for laterite ore slurry modified with various nonionic polymers. This figure shows that similar to the ore slurry without polymer modification, the self-weight sedimentation is essentially complete within the first 180 minutes when the same slurry is modified with various nonionic polymers. After about 30 minutes, all of the sedimentation curves for various dosages start converging and curves for 4, 8 and 12 ppm merge by the end of 180 minutes. Among the three polymer dosages, an increase in the rate of sedimentation is generally observed with an increase in polymer dosage. The only exception to this generalization is observed for the high MW at 12 ppm dosage. The sedimentation behavior of laterite ore slurry modified with nonionic polymers is explained in this section.

6.3.3.2 Initial Hydraulic Conductivity

Figures A.5 through A.7 give the sedimentation test result for the first 30 minutes for laterite ore slurry modified with various nonionic polymers. The slope of the initial straight-line portion is used to obtain the initial hydraulic conductivity (k_i). Derived from Figure A.5 though A.7, Table 6.2 gives k_i for laterite ore slurry modified with various nonionic polymers. Likewise, Figure 6.14 highlights the effect of polymer molecular weight (MW) and polymer dosage on the initial hydraulic conductivity of laterite ore slurry, when modified with nonionic polymers.

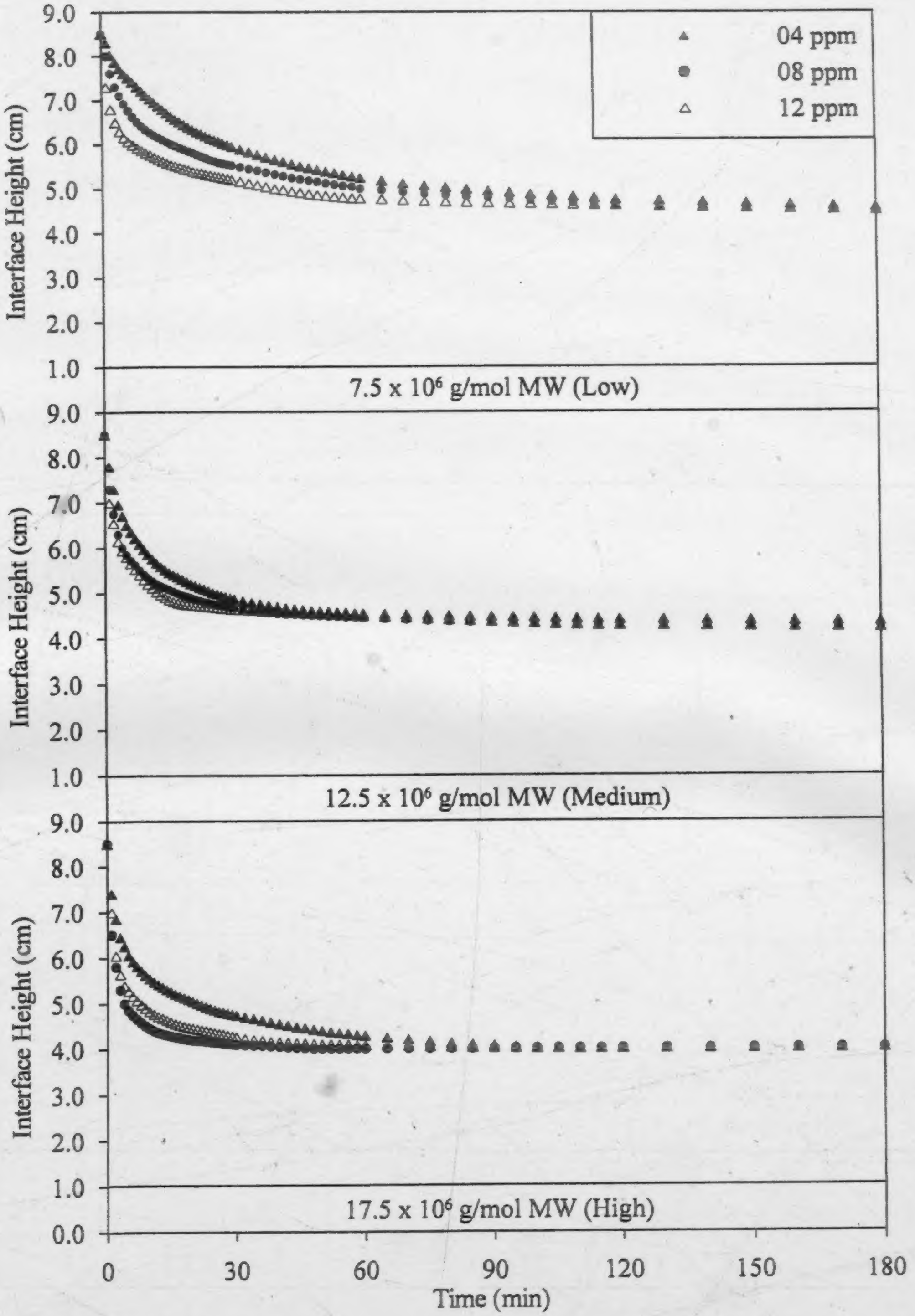

Figure 6.13: Sedimentation test results using nonionic polymers

Table 6.2: k_i of laterite ore slurry modified with various nonionic polymers

Polymer Parameters				k_i x 10^{-3} (cm/sec)
Type	Charge	MW x 10^6 (g/mol)	Dose (ppm)	
Nonionic	NA	7.5 (Low)	4	35
			8	66
			12	175
		12.5 (Medium)	4	88
			8	175
			12	219
		17.5 (High)	4	161
			8	292
			12	219

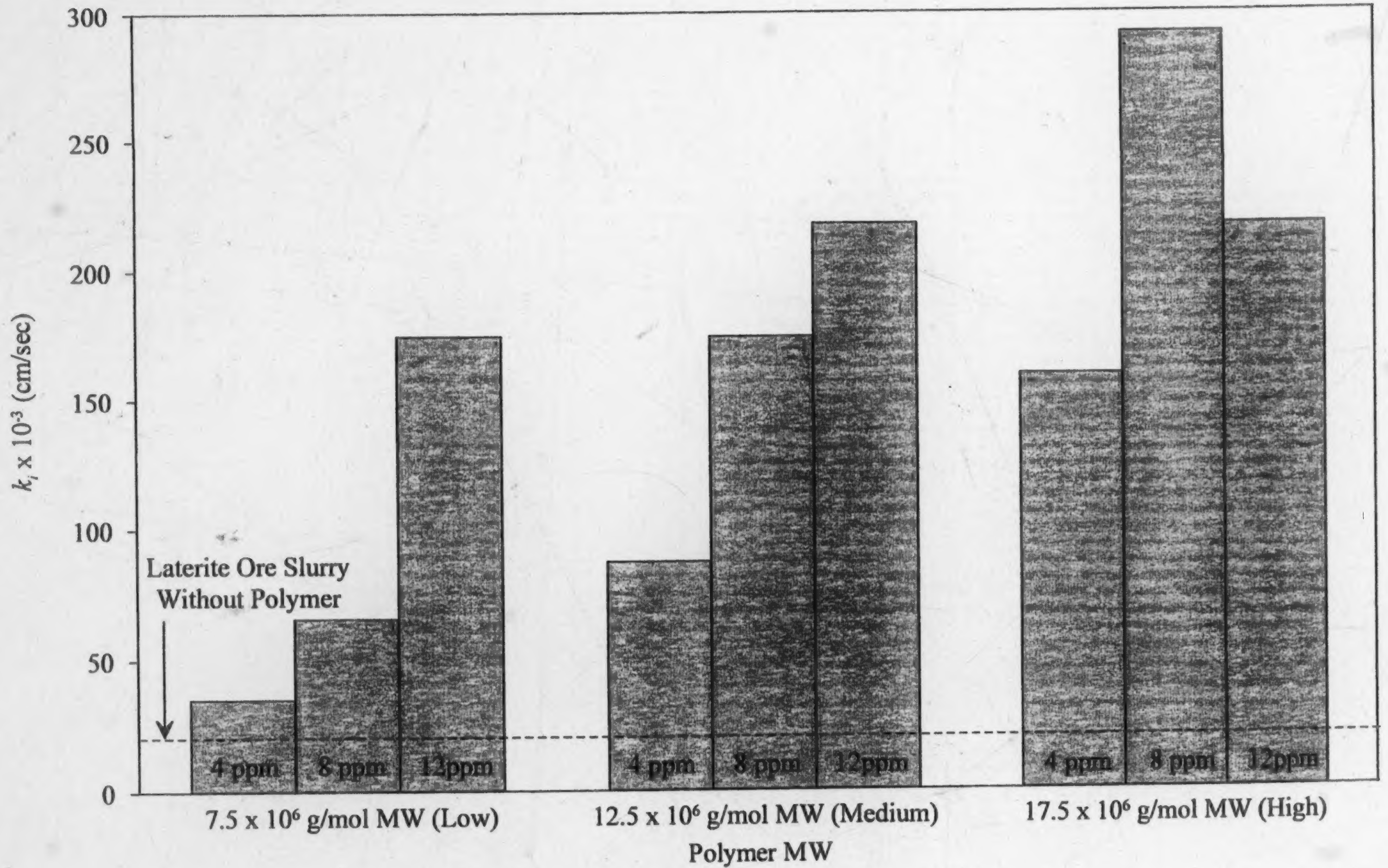

Figure 6.14: Effect of nonionic polymer parameters on k_i of laterite ore slurry

The k_i of laterite ore slurry without polymer modification measured 21 x 10^{-3} (cm/sec). A comparison of this value with the data depicted in Table 6.2 reveals that modification of laterite ore slurry with nonionic polymer always improve k_i of the material. Although, a maximum improvement of about fourteen times is obtained, variability among various observed values is not as extensive as for the ionic polymers and is attributed to colloid-polymer-electrolyte interactions.

Figure 6.14 shows that a higher k_i for the polymer modified slurry compared to that without polymer modification is always observed for the conducted tests. This is attributed to the polymer adsorption leading to flocculation of the ore slurry due to the addition of nonionic polymers. Adsorption is always facilitated because of the absence of polymer charge for nonionic polymers. This precludes the phenomenon of dispersion and electrostatic repulsion that led to k_i reduction described earlier for low charge ionic polymers.

Figure 6.14 indicates that an increase in either the molecular weight (MW) and/or dosage of the nonionic polymers improves k_i of laterite ore slurry. This is due to the increased adsorption and flocculation due to one or both of the polymer characteristics. The only exception to this generalization is for 17.5 x 10^6 g/mol MW (high)-12 ppm dosage (high) test, which shows a 25% decrease compared with that for the 8 ppm dosage (medium) test. This is attributed to the development of bimodal size distribution that causes a k_i reduction when channeling is absent because of low amount of unflocculated material (Hogg 1999). These phenomena occur due to overdosing that causes the formation of polymer brush configuration.

6.3.3.3 Morphology

Figure 6.15 shows the morphology of the limonite-saprolite ore slurry modified with 12.5 x 10^6 g/mol MW (medium)-08 ppm dosage (medium) of nonionic polymer. Micrograph (a) shows a specimen with two surfaces separated by a cut. Micrograph (b) shows a compact clay microstructure with evenly distributed silts size grains. Micrograph (c) illustrates some of these grains and a flocculated clay structure. Micrograph (d) shows that the pore spaces in the clay fabric have uniform size and distribution. This micrograph also indicates some tortuousity, which is responsible for the moderate increase in the initial hydraulic conductivity (175 x 10^{-3} cm/sec) of this specimen. It is noteworthy to mention that this fabric is not very different from that depicted in Figure 6.11 for the 75% charge (high)-17.5 x 10^6 g/mol (high) MW-04 ppm (low) dosage of cationic polymer for which k_i measured 180 x 10^{-3} cm/sec.

6.3.3.4 Statistical Analysis

Using 0 for no charge in nonionic polymers; –1 for 7.5 x 10^6 g/mol (low), 0 for 12.5 x 10^6 g/mol (medium) and +1 for 17.5 x 10^6 g/mol (high) polymer MW; and –1 for 4 ppm, 0 for 8 ppm and +1 for 12 ppm polymer dosage, equation (6.1) estimated the k_i depicted in Figure 6.16. This figure gives the results for nonionic polymers superimposed on those of the ionic polymers, given earlier in Figure 6.12. The current figure shows that the results of statistical analysis for nonionic polymers correlate well with those of the ionic polymers.

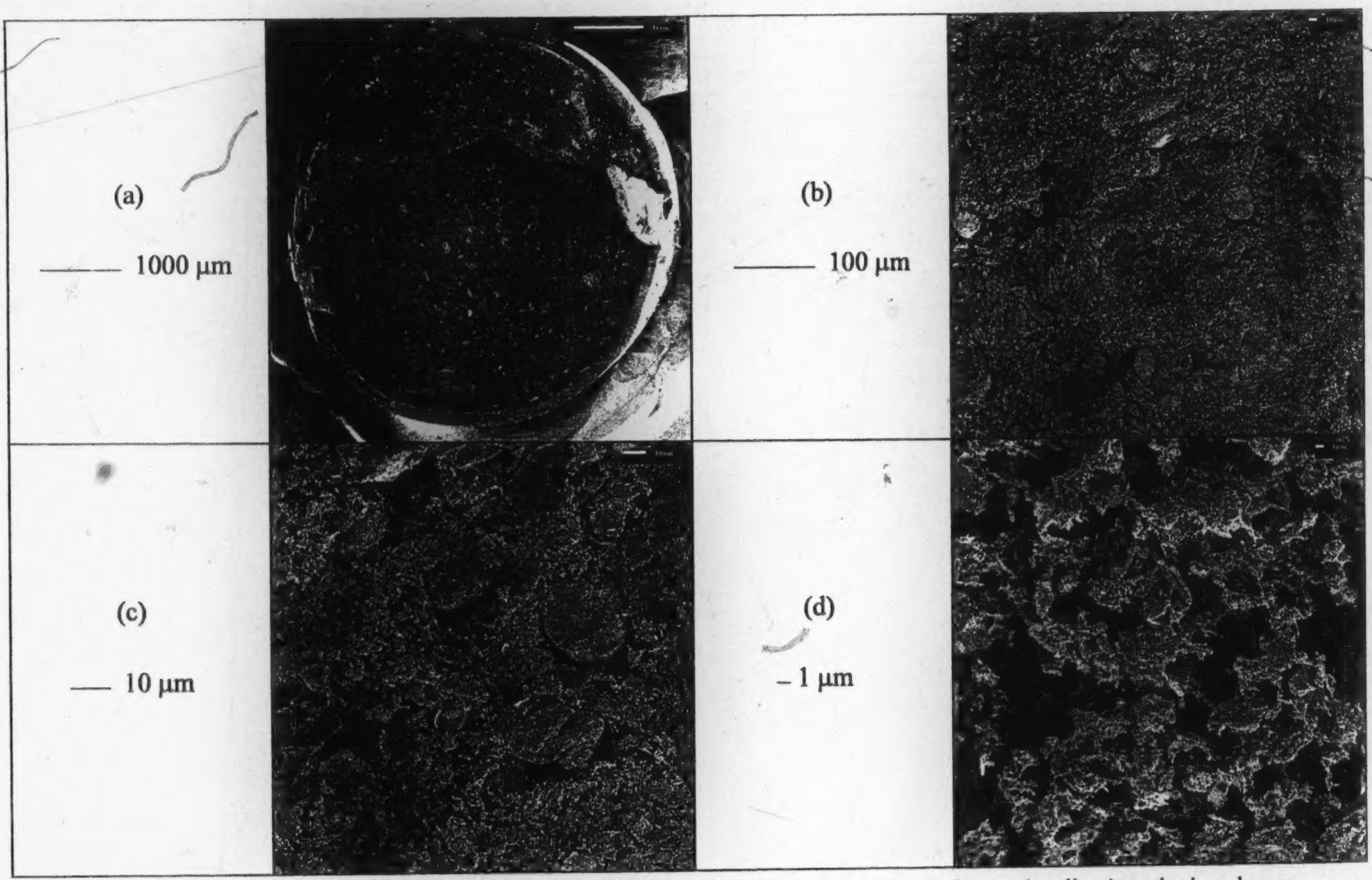
(a)
1000 μm
(b)
100 μm
(c)
10 μm
(d)
1 μm

Figure 6.15: SEM of laterite ore slurry modified with 12.5 x 10^6 g/mol MW (medium)-08 ppm dosage (medium) nonionic polymer

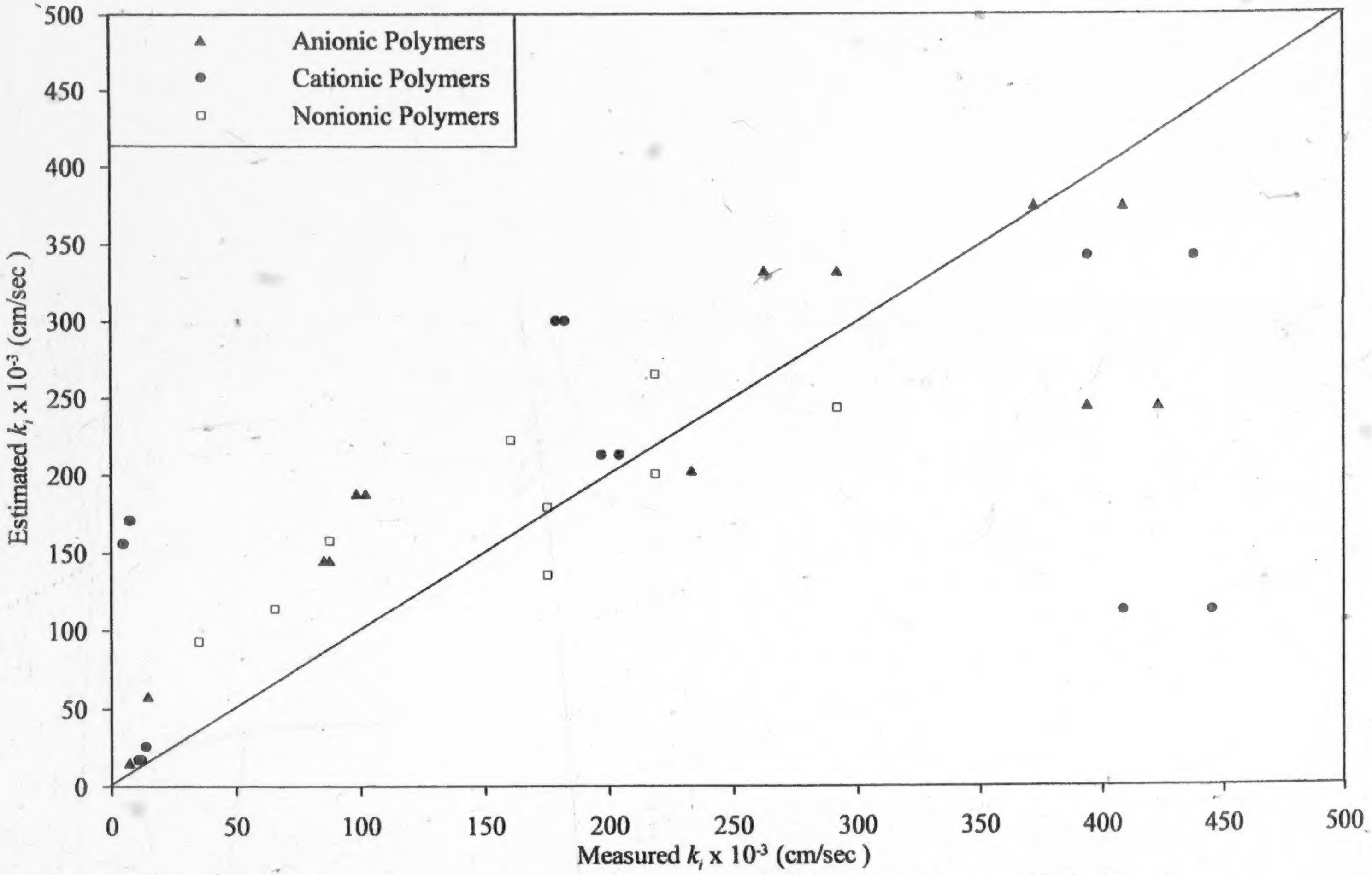

Figure 6.16: Relationship between measured and estimated k_i of laterite ore slurry modified with polymers

6.4 CONSOLIDATION

6.4.1 General

The interaction between synthetic polymers, soil particles and the pore fluid was highlighted in the section on sedimentation. This section aims at understanding the significance of such interactions during load application. First, the solid-liquid separation behavior of laterite ore slurry modified with ionic polymers is described. These results are then combined with those of the nonionic polymer modification. In each case, consolidation test results are depicted in the form of *log k-e* and *e-log* σ' relationships; both relations are then statistically analyzed.

6.4.2 Ionic Polymers

6.4.2.1 General

Sixteen consolidation tests were conducted on laterite ore slurry modified with ionic polymers. Results of these tests are depicted in Figures A.8 through A.39 given in Appendix A. For each test, results are depicted in the form of interface height versus elapsed time and hydraulic conductivity versus elapsed time. Table A.5 gives the solids content at the start and the end of the various consolidation tests.

Consolidation test results indicate that the solid-liquid separation of laterite ore slurries modified with ionic polymers ~~is~~ predominantly composed of sedimentation. For all tests, the solid-liquid interface moved from an initial height of 9.5 cm to a final height ranging from 5.5 to 4.5 cm under self-weight and between 3.0 and 1.5 cm under a maximum stress of 9.0 kPa. This means that in a total height variation of 6.5 to 8.0 cm during the tests, the part due to sedimentation amounts to about 60% and that due to consolidation is 40%. The higher solid-liquid separation during sedimentation is mainly attributed to the high specific gravity (3.16) of the laterite ore material, discussed in Chapter Five.

Polymer modification results in flocculation of laterite ore materials thereby causing additional dewatering due to the development of large and heavy flocs. In the section on sedimentation, it was observed that modification of laterite ore slurries with ionic polymers does not necessarily result in k_i increase. In the current section, it is observed that such modification invariably results in a higher amount of dewatering under self-weight. Therefore, polymer selection should be based on both the rate and the amount of solid-liquid separation.

The improved dewatering under self-weight is attributed to the development of soil morphology during sedimentation. At the initial part of sedimentation (used for k_i determination), soil morphology undergoes minimal variation and the soil containing entrapped water settles as one mass (Pane & Schiffman 1997). During the transition stage, soil morphology undergoes considerable changes as colloid-polymer-electrolyte interactions are progressively overcome by effective stresses. A dense morphology is envisaged when the slurry is converted to a soil sediment. Such a morphology is characterized by channels and/or hairline cracks between adjacent dense soil minifabrics. These discontinuities allow an easy and generally identical water escape during the latter part of sedimentation.

Hydraulic conductivity test results (given in Appendix A) indicate that flow through the samples was not constant but decreased with time and reached a steady state within 30 minutes. The drop in flow from an initial to a steady state value decreased with increasing stress. This is attributed to the diminishing physical changes in the specimen with decreasing void ratio. Olsen et al. (1985), suggested that such time-dependent flow can be due to one ore more of the following reasons: (a) undissolved air in the equipment and/or specimen; (b) equipment compliance depending on fabrication material and applied gradients; (c) inertia required to move the pore fluid; and (d) time-dependent changes in pore space distribution. Using identical equipment and test conditions for Alberta oil sand tailings, Suthaker & Scott (1996) showed that the last reason is the most likely cause of the observed time-dependent flow. These authors concluded that this transient phenomenon is repeatable and that the initial conditions are reattainable. Therefore, the steady state value was taken as the hydraulic conductivity and used in the analysis during this research.

6.4.2.2 Hydraulic Conductivity-Void Ratio

Figure 6.17 and 6.18 give the *log k-e* relationships for anionic and cationic polymer modification, respectively. Table 6.3 summarizes the A and B parameters obtained from these relationships. Figure 6.19 combines *log k-e* relationships for all ionic polymer modification and compare these with the laterite ore slurry without polymer. Figure 6.20 explains the results by highlighting the effect of hydraulic gradient (*i*) on the hydraulic conductivity.

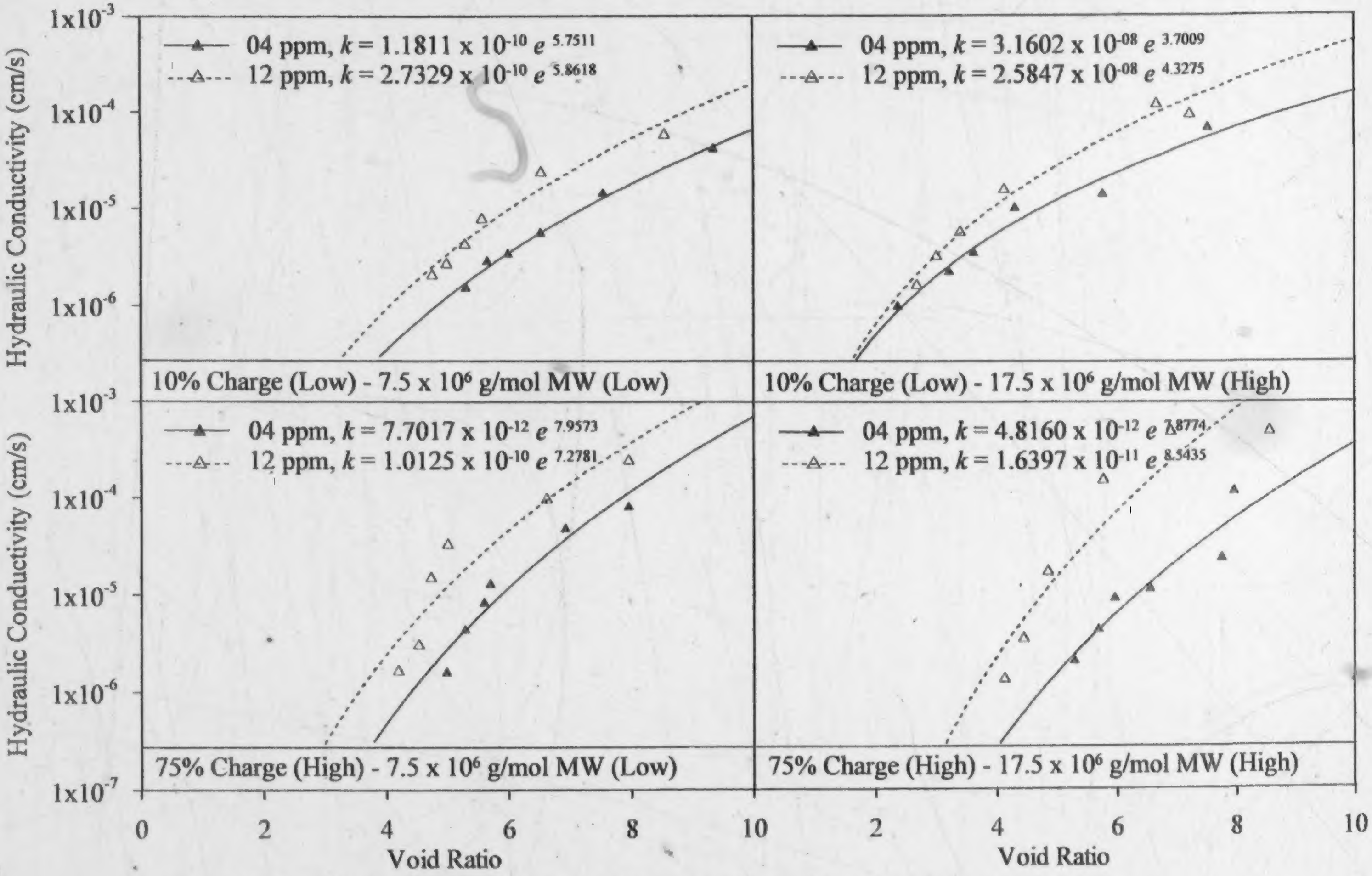

Figure 6.17: *k-e* relationships for laterite ore slurry modified with various anionic polymers

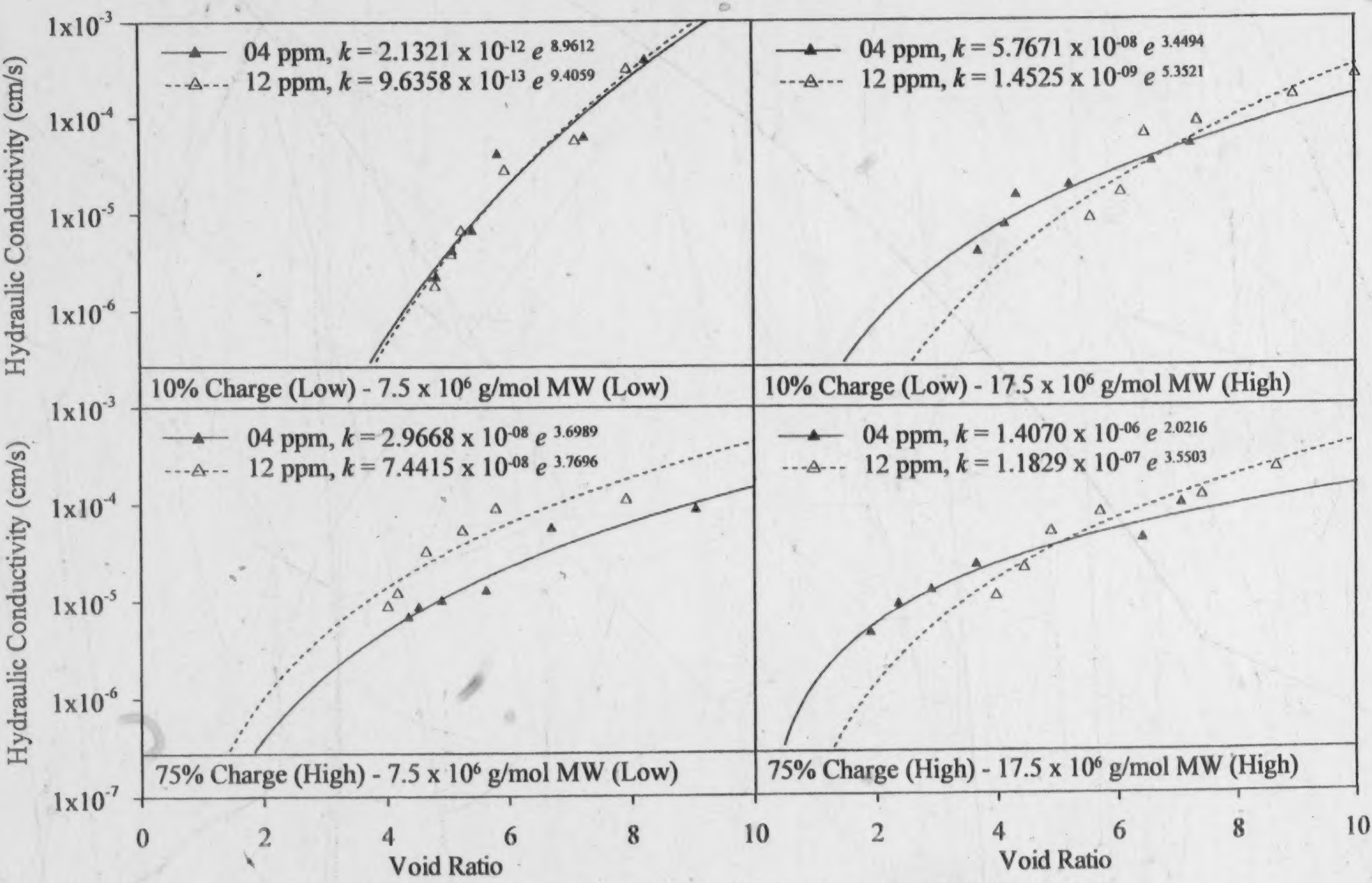

Figure 6.18: *k-e* relationships for laterite ore slurry modified with various cationic polymers

Table 6.3: *log k-e* parameters for laterite ore slurry modified with ionic polymers

Polymer Parameters				A	B
Type	Charge	MW x 10^6 (g/mol)	Dose (ppm)		
Anionic	10% (Low)	7.5 (Low)	4	1.2×10^{-10}	5.8
			12	2.7×10^{-10}	5.8
		17.5 (High)	4	3.2×10^{-08}	3.7
			12	2.6×10^{-08}	4.3
	75% (High)	7.5 (Low)	4	7.7×10^{-12}	8.0
			12	1.0×10^{-10}	7.3
		17.5 (High)	4	4.8×10^{-12}	7.9
			12	1.6×10^{-11}	8.5
Cationic	10% (Low)	7.5 (Low)	4	2.1×10^{-12}	9.0
			12	1.0×10^{-12}	9.4
		17.5 (High)	4	5.8×10^{-08}	3.5
			12	1.5×10^{-09}	5.4
	75% (High)	7.5 (Low)	4	3.0×10^{-08}	3.7
			12	7.4×10^{-08}	3.8
		17.5 (High)	4	1.4×10^{-06}	2.0
			12	1.2×10^{-07}	3.6

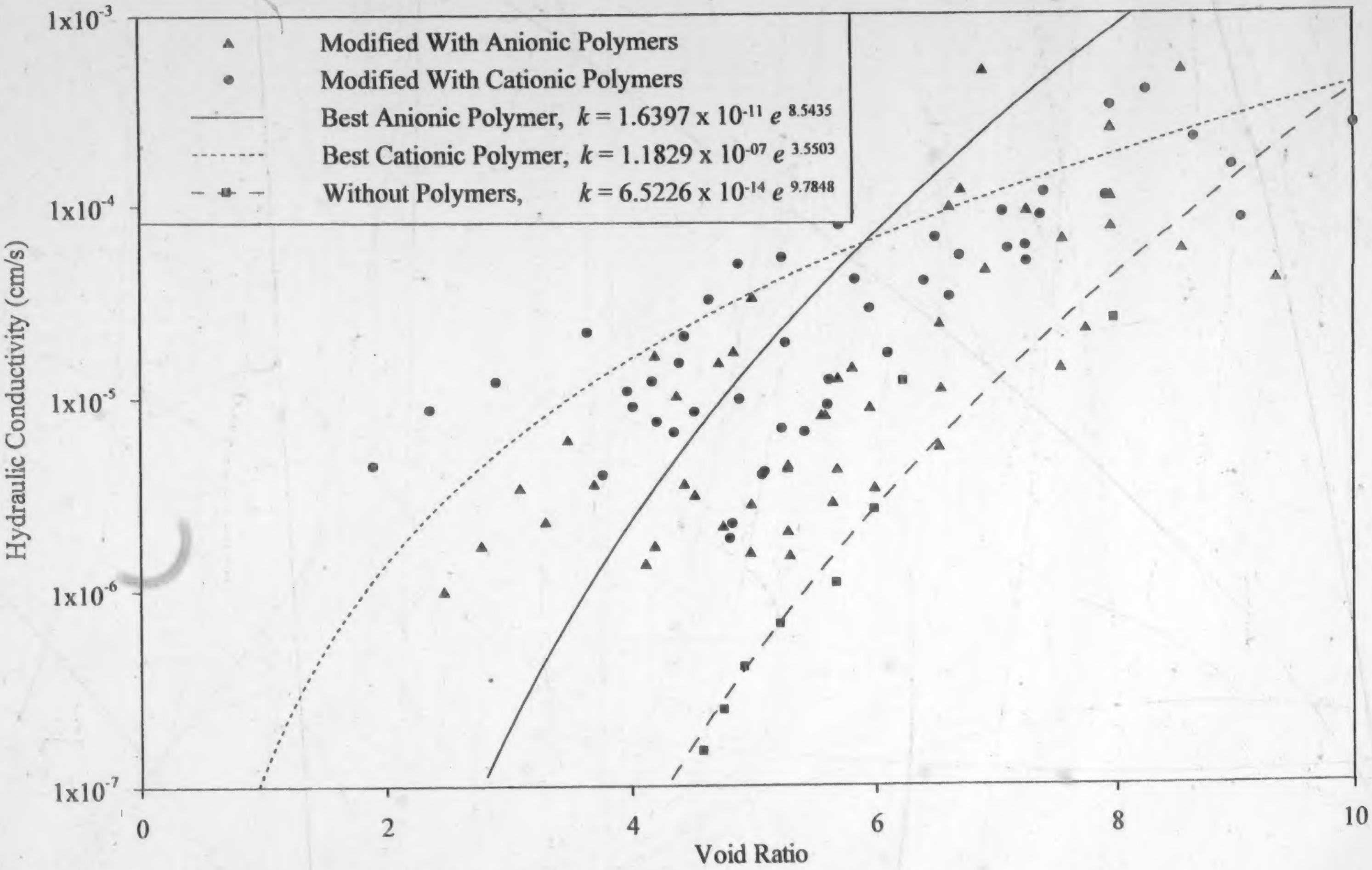

Figure 6.19: *k-e* relationship for laterite ore slurry modified with various ionic polymers

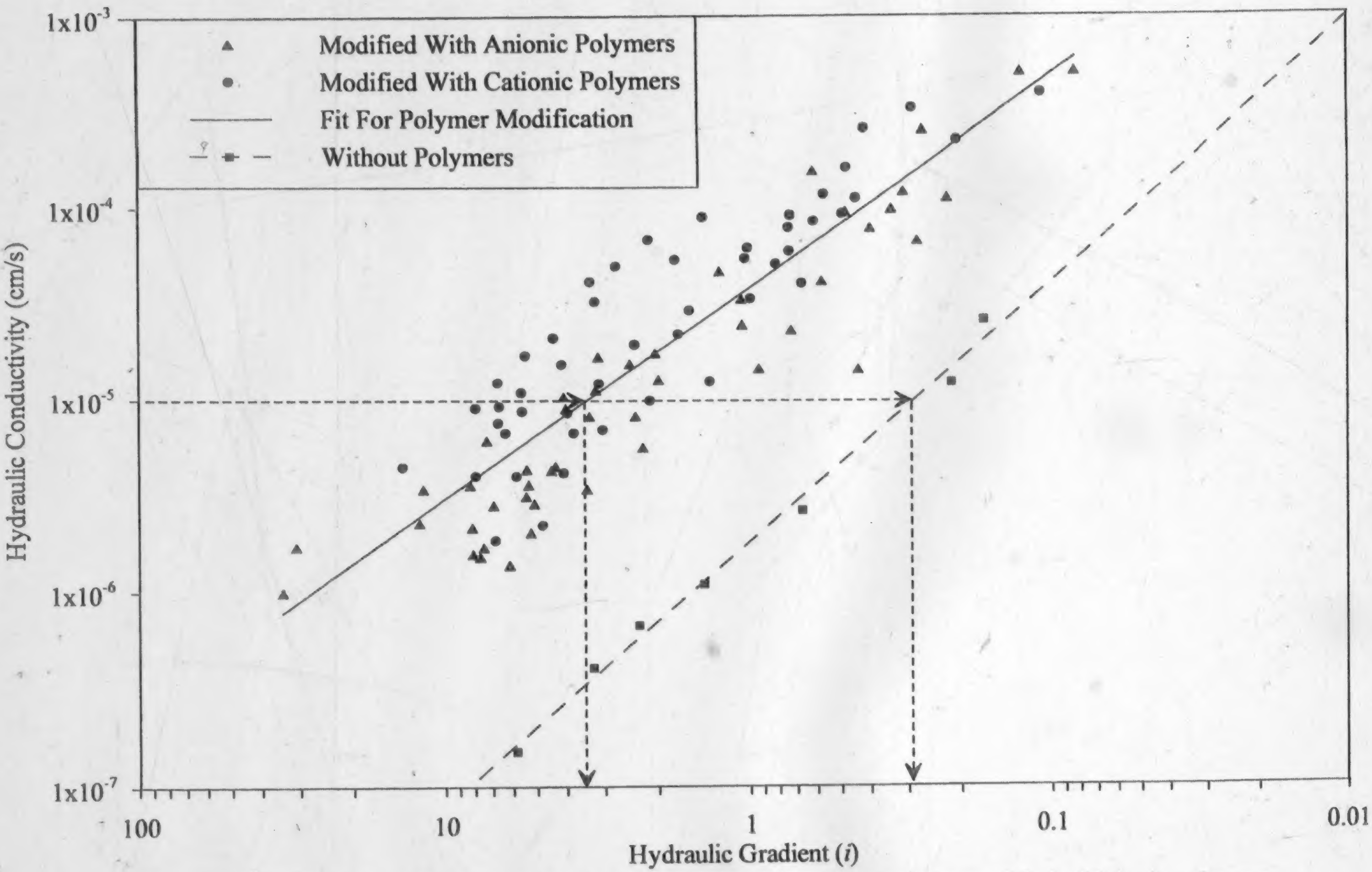

Figure 6.20: Effect of gradient on hydraulic conductivity of laterite ore slurry modified with ionic polymers

Figure 6.17 indicates that the hydraulic conductivity-void ratio relationships of laterite ore slurry modified with 12 ppm dosage (high) of anionic polymers plots above that using the 4 ppm dosage (low). This means that at a given void ratio, the hydraulic conductivity for the former dosage is always higher than that at the latter dosage. Therefore, the variation of hydraulic conductivity during consolidation follows the same pattern of the k_i during sedimentation for laterite ore slurry modified with anionic polymers.

Figure 6.18 depicts a similar behavior for the laterite ore slurry modified with cationic polymers with 7.5 x 10^6 g/mol MW (low) and a reverse behavior for the same polymers with 17.5 x 10^6 g/mol MW (high) for both values of polymer charge. This reversal in behavior is attributed to the type of flocculation developed during sedimentation. The size of the floc and the floc assemblage increase with an increase in polymer MW and this increase is more pronounced at low MW. Due to the size increase with polymer dosage for the former polymer MW, the hydraulic conductivity follows the same trend as for both anionic polymers. Conversely, stronger bonds between the flocs and floc assemblages at 12 ppm dosage (high) of the latter polymer MW lead to a limited bond breakage and water release and a hence a reversal in behavior.

A comparison of anionic and cationic polymer modification of laterite ore slurry indicates that in addition to polymer charge, the bond strength between the particle and the polymer depends on the sign of the charge. For the given near neutral pore fluid with low electrolyte concentration, a stronger bond is formed between the positive sesquioxides and the anionic polymer. Further, the opposite sign of the colloid and the polymer leads to a small size floc and low tendency of floc assemblage for anionic polymers. Although, the flocs grow and floc assemblages are increased with polymer dosage, little bond breakage occurs up to the investigated void ratios. A similar behavior is observed for the laterite ore slurry modified with cationic polymers at 7.5 x 10^6 g/mol MW (low). The reversal in behavior for the same polymers with 17.5 x 10^6 g/mol MW (high) for both values of polymer charge is discussed above. It is noteworthy that the same sign of colloid and polymer results in loose bonds, large size flocs and floc assemblages for cationic polymers.

Table 6.3 summarizes the A and B parameters of the *log k-e* relationships for all ionic polymer modifications. This table indicates that variations in parameter A (intercept or position) amount to six orders of magnitude whereas parameter B (shape or slope) varies between 2 and 10. This means that the *log k-e* relationships for the laterite ore slurry modified with both anionic and cationic polymers depend on parameter A. Further, the A and B parameters for the laterite ore slurry without polymer were 6.5226 x 10^{-14} and 9.7848, respectively. This A value for the laterite ore slurry without polymer is less than all of the A values obtained for the polymer modified materials depicted in Table 6.3. This means that ionic polymer modification of laterite ore slurry invariably results in an improvement in the hydraulic conductivity of the material during consolidation.

Figure 6.19 combines the results of both anionic and cationic polymer modification and compares these with the ore slurry without polymer. This figure shows that almost the entire data plots above the ore slurry without polymer. Therefore, all ionic polymers improve the hydraulic conductivity of laterite ore slurry during consolidation. Such improvement in hydraulic conductivity varies by one order of magnitude (10^{-3} to 10^{-4} cm/sec) at a void ratio of 9.0 and by two orders of magnitude (10^{-5} to 10^{-7} cm/sec) at a void ratio of 4.0. This means that at the start of consolidation, hydraulic conductivity depends on the type of flocculation attained during the initial stages of the solid-liquid separation process. The effect of flocculation type is narrowed towards the end of sedimentation under self-weight. During consolidation under applied loads, breakage and redistribution of these flocs results in the release of pore water and the escape of entrapped floc water through channels. As expected, these phenomena are more conspicuous at low void ratios.

The effect of hydraulic gradient on hydraulic conductivity was studied by performing constant head tests after each load increment during consolidation. The gradient for each test was kept less than the critical gradient at which piping of the sample occurs. Figure 6.20 gives the variation of hydraulic conductivity with hydraulic gradient. This figure shows that the hydraulic conductivity of polymer modified laterite ore slurry decreases with an increase in the hydraulic gradient. Further, a change in the behavior between the laterite ore slurry modified with ionic polymers and the one without polymers is observed. A hydraulic conductivity of say 10^{-5} cm/sec requires a gradient of 3.2 for the former materials and only 0.3 for the latter. This more than one order of magnitude difference in gradient to achieve the same hydraulic conductivity is attributed to the development of flocs due to polymer modification. These flocs contain entrapped water that can only be extracted at elevated hydraulic gradients. For polymers resulting in lower flocculation or bimodal size distribution, migration of fine un-flocculated soil particles occurs into pore throats (Suthaker & Scott 1996). This results in the development of channels thereby offering paths of least resistance to water flow. The same phenomenon controls the hydraulic conductivity of the ore slurry without polymer.

Since, no distinguishable trend in the hydraulic conductivity for the two polymer types is observed in Figure 6.19, polymer selection should be based on examining their performance independently. This requires that the sedimentation data depicted in Figure 6.6 and consolidation data given in Figures 6.17 and 6.18, be studied in conjunction. Based on this assessment, polymer parameters for best anionic and cationic performers include 75% charge (high), 17.5 x 10^6 g/mol MW (high) and 12 ppm dosage. These selected polymers are shown in Figure 6.19.

6.4.2.3 Void Ratio-Effective Stress

Figure 6.21 and 6.22 give the *e-log* σ' relationships for anionic and cationic polymer modification, respectively. Table 6.4 summarizes the C and D parameters obtained from these relationships. Figure 6.23 combines *e-log* σ' relationships for all ionic polymer modification and compare the results with the ore slurry without polymer.

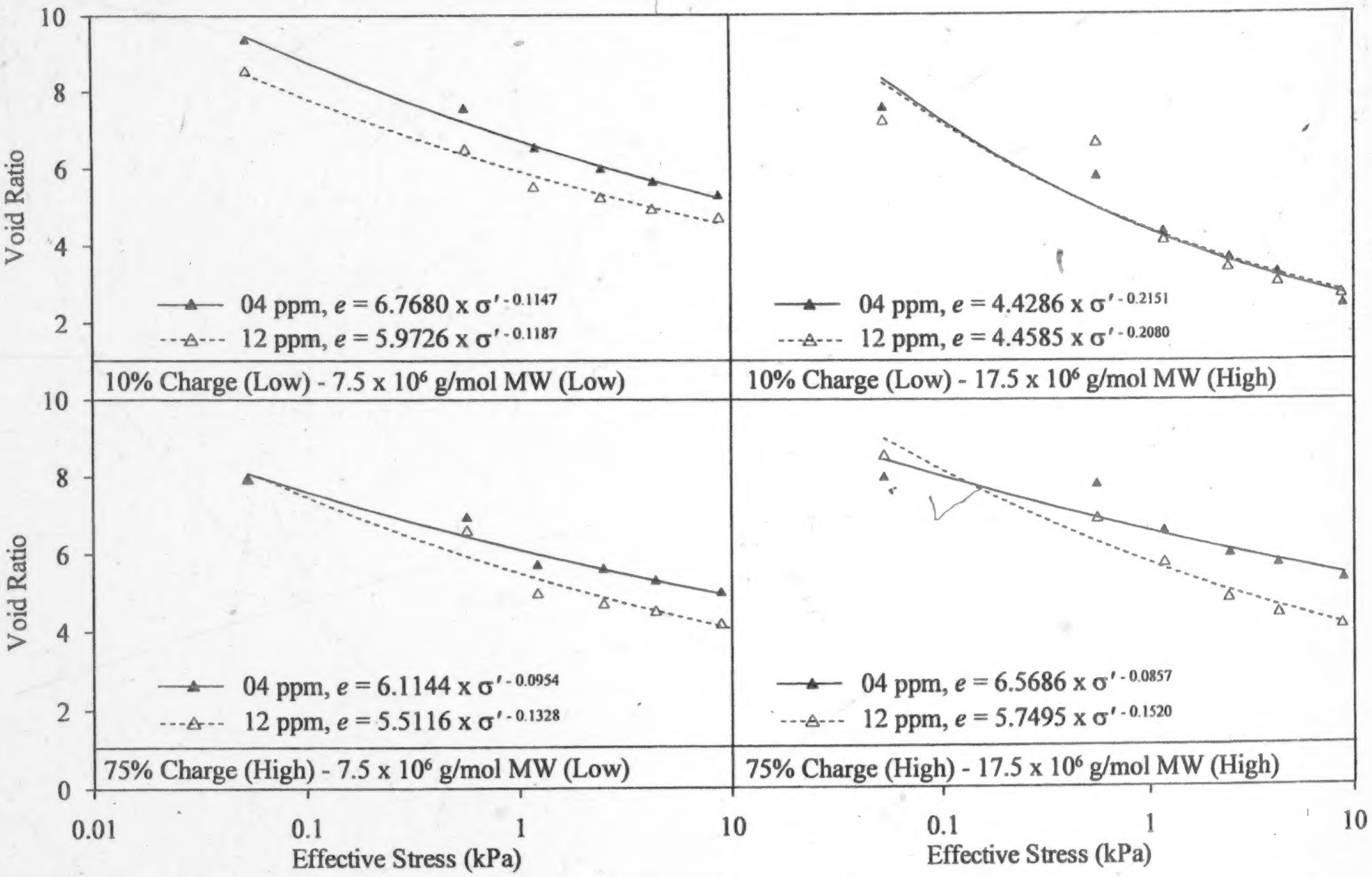

Figure 6.21: e-σ' relationships for laterite ore slurry modified with various anionic polymers

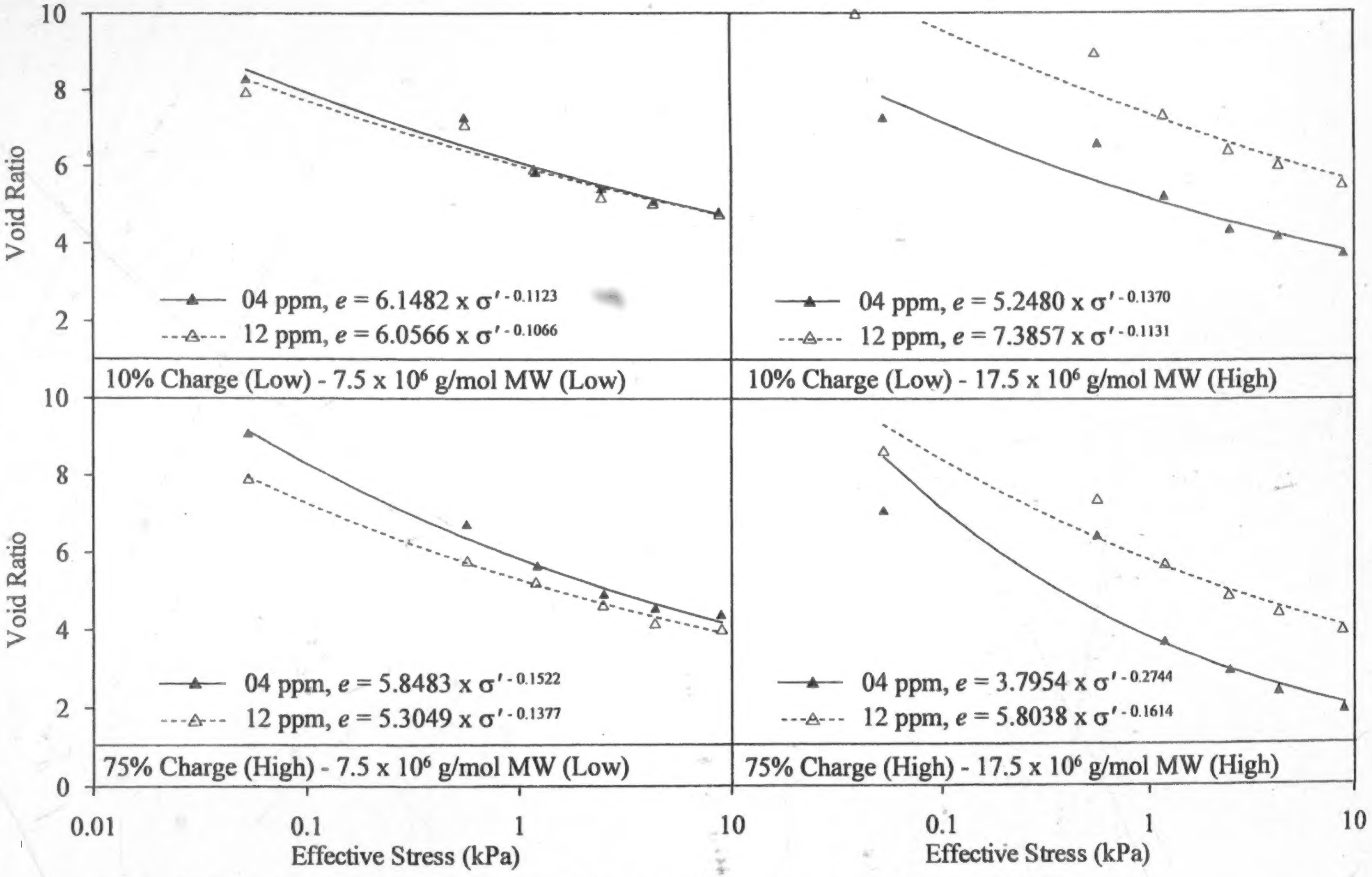

Figure 6.22: e-σ' relationships for laterite ore slurry modified with various cationic polymers

Table 6.4: *e-log* σ' parameters for laterite ore slurry modified with ionic polymers

Polymer Parameters				C	D
Type	Charge	MW x 10^6 (g/mol)	Dose (ppm)		
Anionic	10% (Low)	7.5 (Low)	4	6.8	- 0.12
			12	6.0	- 0.12
		17.5 (High)	4	4.4	- 0.22
			12	4.5	- 0.21
	75% (High)	7.5 (Low)	4	6.1	- 0.10
			12	5.5	- 0.13
		17.5 (High)	4	6.6	- 0.09
			12	5.8	- 0.15
Cationic	10% (Low)	7.5 (Low)	4	6.2	- 0.11
			12	6.1	- 0.11
		17.5 (High)	4	5.3	- 0.14
			12	7.4	- 0.11
	75% (High)	7.5 (Low)	4	5.9	- 0.15
			12	5.3	- 0.14
		17.5 (High)	4	3.8	- 0.27
			12	5.8	- 0.16

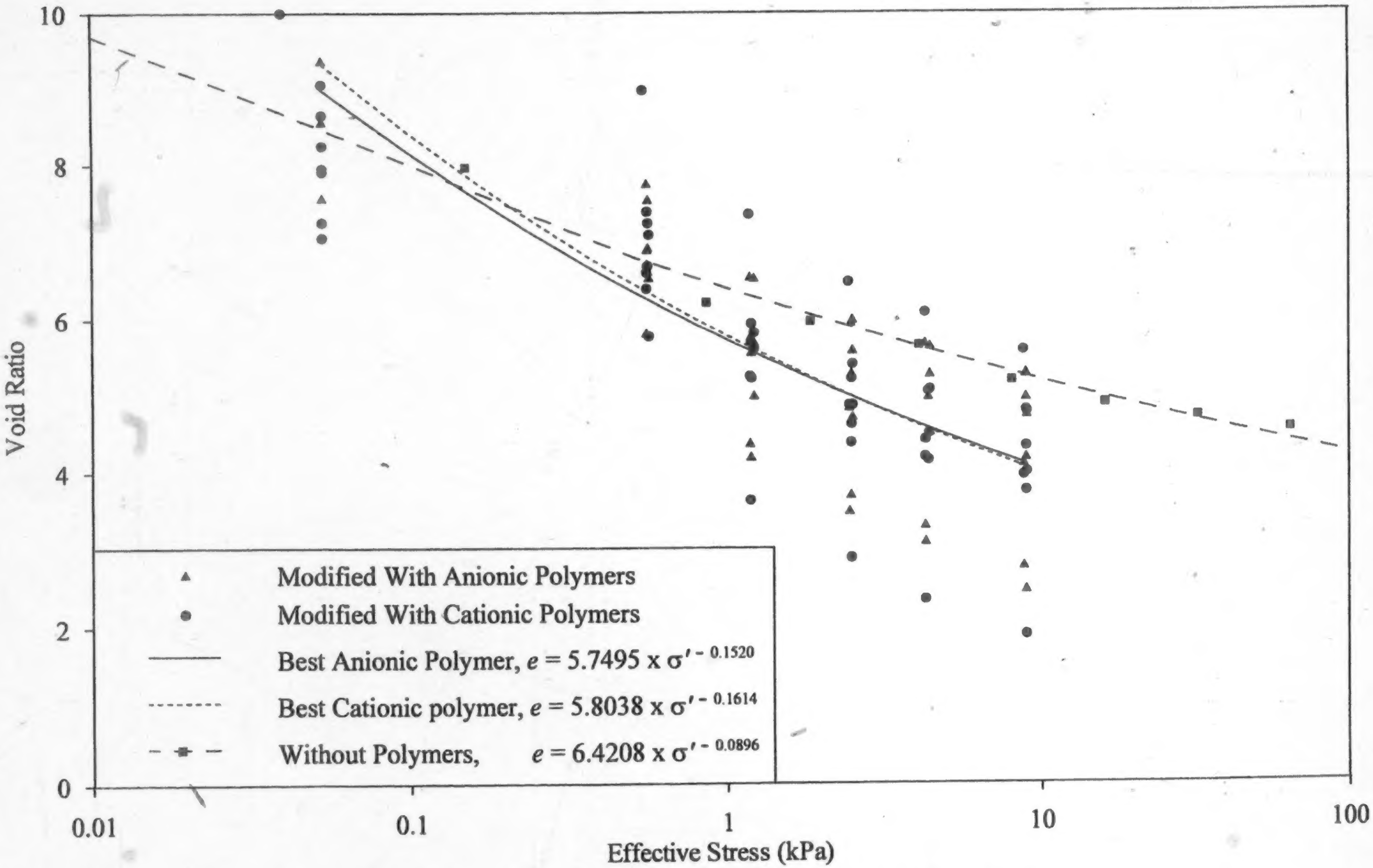

Figure 6.23: e-σ' relationship for laterite ore slurry modified with various ionic polymers

Figure 6.21 indicates that the void ratio-effective stress relationships of laterite ore slurry modified with 12 ppm dosage (high) of anionic polymers plots above that of the 4 ppm dosage (low) for both polymer charges and both polymer MW. This means that at a given effective stress, the void ratio of the former dosage is always lower than that at the latter dosage. This is attributed to the breakage and redistribution of the larger flocs formed at the higher dosage of anionic polymers.

Figure 6.22 depicts a similar behavior for the laterite ore slurry modified with cationic polymers with 7.5 x 10^6 g/mol MW (low) and a reverse behavior for the same polymers with 17.5 x 10^6 g/mol MW (high) for both values of polymer charge. This reversal in behavior is attributed to the type of flocculation developed during the early stages of the solid-liquid separation process. As would be expected, the size of the floc and the floc assemblage increase with an increase in polymer MW. Further, a size increase with increasing polymer MW is eminent for 7.5 x 10^6 g/mol MW (low) but negligible for 17.5 x 10^6 g/mol MW (high). Due to the size increase with polymer dosage for the former polymer MW, the compressibility behavior is similar to anionic polymers (Figure 6.21). Conversely, stronger bonds between the flocs and floc assemblages at 12 ppm dosage (high) of the latter polymer MW lead to a limited bond breakage. Alternatively, bond breakage and the associated redistribution of flocs are not much pronounced at the high dosage of 12 ppm. Therefore, a reversal in compressibility behavior is observed for 17.5 x 10^6 g/mol MW (high) cationic polymers

Table 6.4 summarizes the C and D parameters of the e-$\log\sigma'$ relationships for all ionic polymer modifications. This table indicates that parameter C (intercept or position) is in the range of 3.8 and 7.4 whereas parameter D (slope or shape) varies between - 0.09 and - 0.27. This indicates that e-$\log\sigma'$ relationships for the laterite ore slurry modified with ionic polymers depends mainly on parameter C. For comparison, the C and D parameters for the laterite ore slurry without polymer, were reported as 6.4208 and - 0.0896, respectively.

Figure 6.23 combines the results of both anionic and cationic polymer modification and compares these with the ore slurry without polymer. This figure shows that at effective stresses above 1.0 kPa, most of data for polymer modified materials plot below the ore slurry without polymer. However, the ore slurry without polymer bisects this data at effective stresses below 1.0 kPa. This means that modification of the laterite ore slurry modified with ionic polymers can have a favorable or adverse effect on compressibility. Therefore, polymer selection should be based on optimizing both hydraulic conductivity (efficiency) and compressibility (yield) in the storage thickener. Choosing the most efficient anionic and cationic polymers (Figure 6.19), Figure 6.23 illustrates that these polymers perform well for compressibility. At effective stresses of more than 0.2 kPa, both polymers improve compressibility and the void ratio of the laterite ore slurry without polymers at 9.0 kPa is reduced from 5.0 to about 4.0 due to modification with ionic polymer. There is essentially no difference in the compressibility behavior of the two polymers.

6.4.2.4 *Statistical Analysis*

The data given Table 6.3 was used to obtain hydraulic conductivity at different void ratios. Corresponding to each test, this generated a set of sixteen hydraulic conductivity values, which were statistically analyzed as before. Using the statistical equation obtained for each void ratio, estimated hydraulic conductivity values were obtained. The data is shown in Figure 6.24, which indicates that the relationship between the estimated and measured values is linear. Similarly, using the data given in Table 6.4 and conducting the above exercise for the void ratio-effective stress relationships yields Figure 6.25. Again, a linear relationship is obtained between the estimated and measured values.

The statistical equations were associated with P-values for each of the polymer parameter. Figure 6.26 gives the statistical significance of various polymer parameters on the solid-liquid separation of laterite ore slurry. This figure shows that the effect of polymer parameters is more significant for hydraulic conductivity than for compressibility. For hydraulic conductivity, the significance of various polymer parameters is high for high void ratios and decreases as the void ratio is decreased. In this case, the significance of polymer charge is highest followed by polymer MW; polymer type and dosage are less significant. For compressibility, the significance of various polymer parameters is high at low effective stresses and either decreases or remains constant as the effective stress is increased. In this case, the significance of polymer MW is highest and all other factors are much lower and identical.

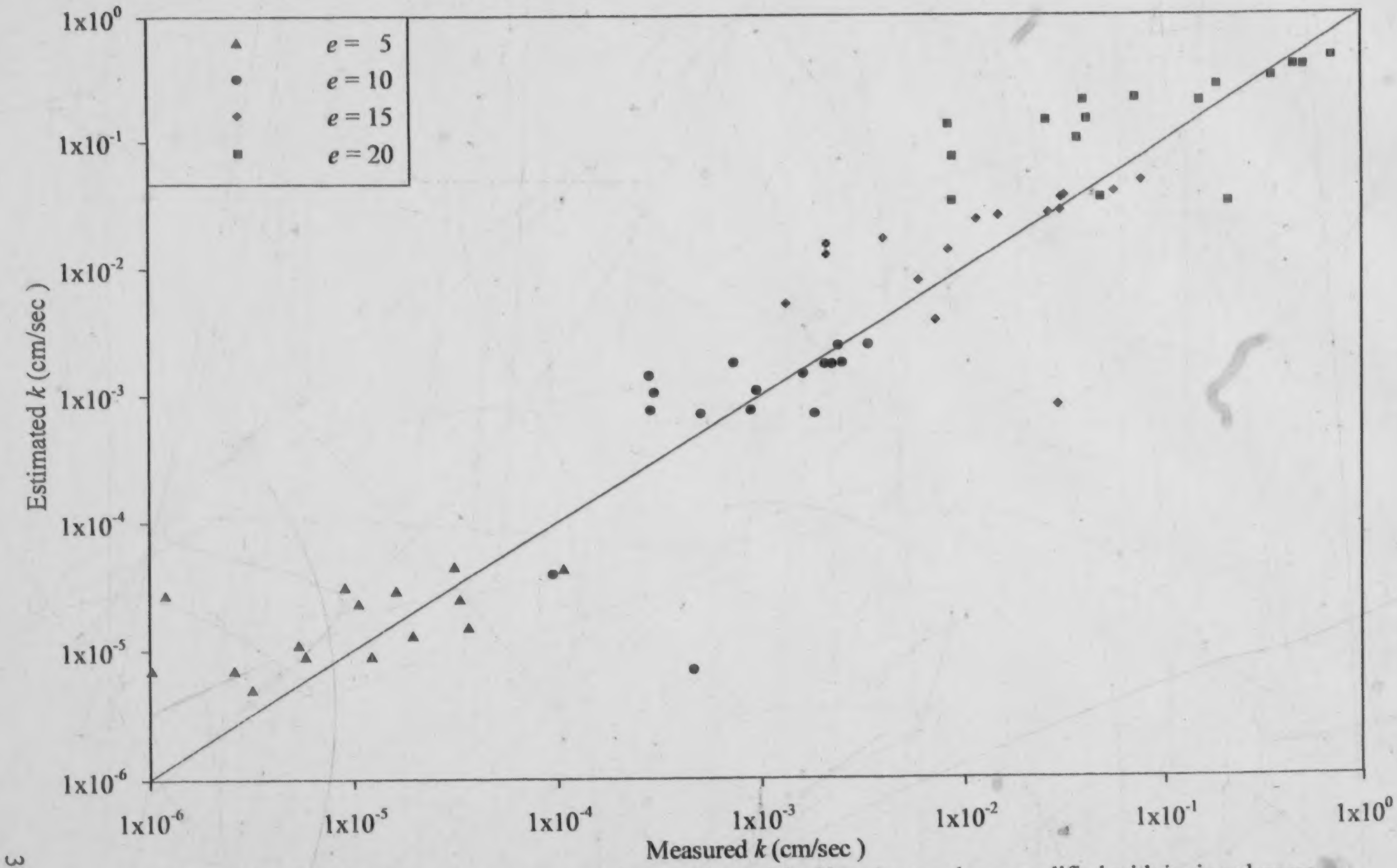

Figure 6.24: Relationship between measured and estimated k of laterite ore slurry modified with ionic polymers

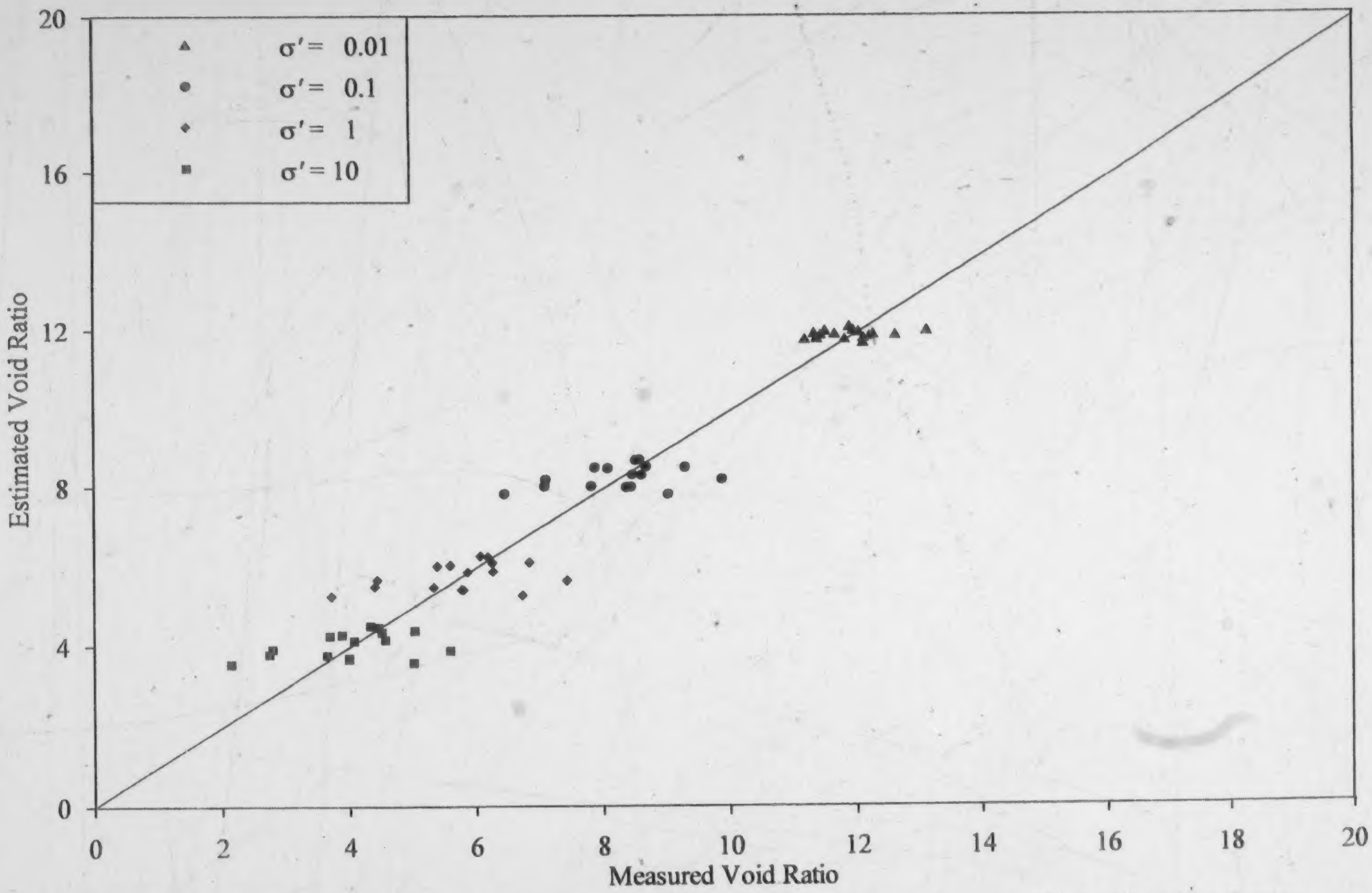

Figure 6.25: Relationship between measured and estimated *e* of laterite ore slurry modified with ionic polymers

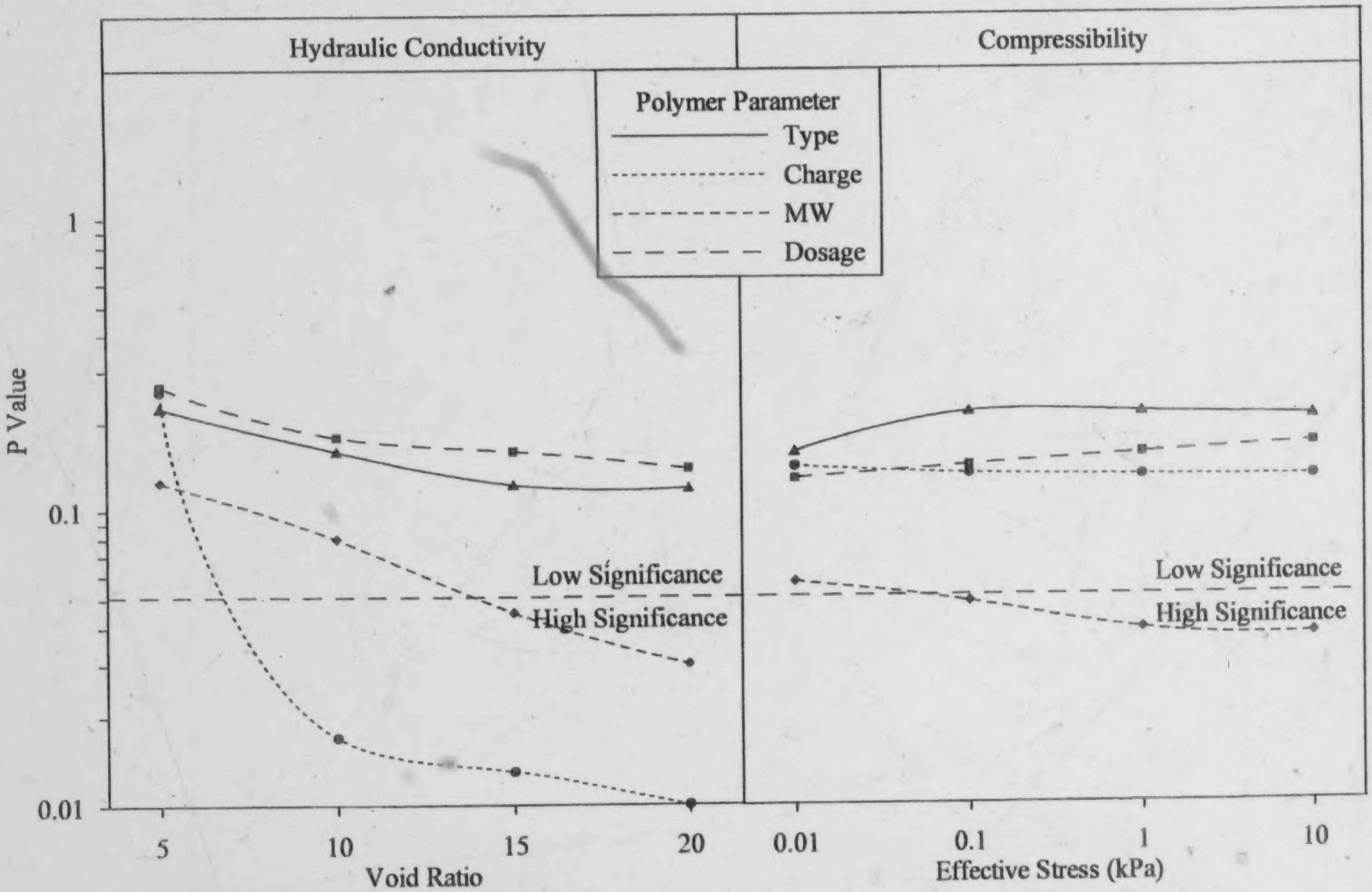

Figure 6.26: Significance of polymer characteristics on solid-liquid separation of laterite ore slurry

6.4.3 Nonionic Polymers

6.4.3.1 General

One consolidation test was conducted on laterite ore slurry modified with nonionic polymer. The polymer parameters for the selected polymer were 12.5 x 10^6 g/mol MW (medium) and 8 ppm dosage (medium). Results of this test are depicted in Figure A.40 and Figure A.41, given in Appendix A. These results are depicted in the form of interface height versus elapsed time and hydraulic conductivity versus elapsed time, respectively. Table A.6 gives the solids content at the start and the end of the consolidation test.

Consolidation test results of Figure A.40 indicate that the solid-liquid separation of laterite ore slurries modified with nonionic polymers is predominantly composed of sedimentation. The solid-liquid interface moved from an initial height of 9.5 cm to a final height of up to 4.6 cm under self-weight and up to 2.8 under a maximum stress of 9.0 kPa. This means that in a total height variation of 6.7 cm during the tests, the part due to sedimentation amounts to 75% and that due to consolidation is only 25%. Similarly, hydraulic conductivity test results given in Figure A.41 indicate that although flow through the sample decreased with time, a steady state was achieved well before 30 minutes. This means that the investigated nonionic polymer is more efficient than both anionic and cationic polymers. In general, the test data of laterite PAL slurry modified with nonionic polymer follows the same trends of those modified with ionic polymers.

6.4.3.2 Hydraulic Conductivity-Void Ratio

Figure 6.27 give the hydraulic conductivity-void ratio relationship for nonionic polymer modification of laterite ore slurry. A comparison of this material with ionic polymer modification and the ore slurry without polymer is also given in this figure. This figure shows that the nonionic polymer results in a lower hydraulic conductivity during consolidation. This is attributed to the preclusion of polymer charge that was observed to be the most significant influencing factor for ionic polymer modification. The absence of polymer charge leads to the formation of loosely bonded flocs, which are easy to break upon load application. This liberates the previously entrapped water in the flocs thereby results in a high hydraulic conductivity during consolidation.

6.4.3.3 Void Ratio-Effective Stress

Figure 6.28 give the void ratio-effective stress relationship for nonionic polymer modification and compares this relationship with those obtained for ionic polymer modification and the ore slurry without polymer. This figure indicates that the curve for nonionic polymer modification plots below that of the ionic polymer modification and the ore slurry without polymer. The higher compressibility of the nonionic polymer modified material is attributed to the phenomenon of floc separation discussed above. Such floc breakage results in floc and grain readjustment upon loading during consolidation.

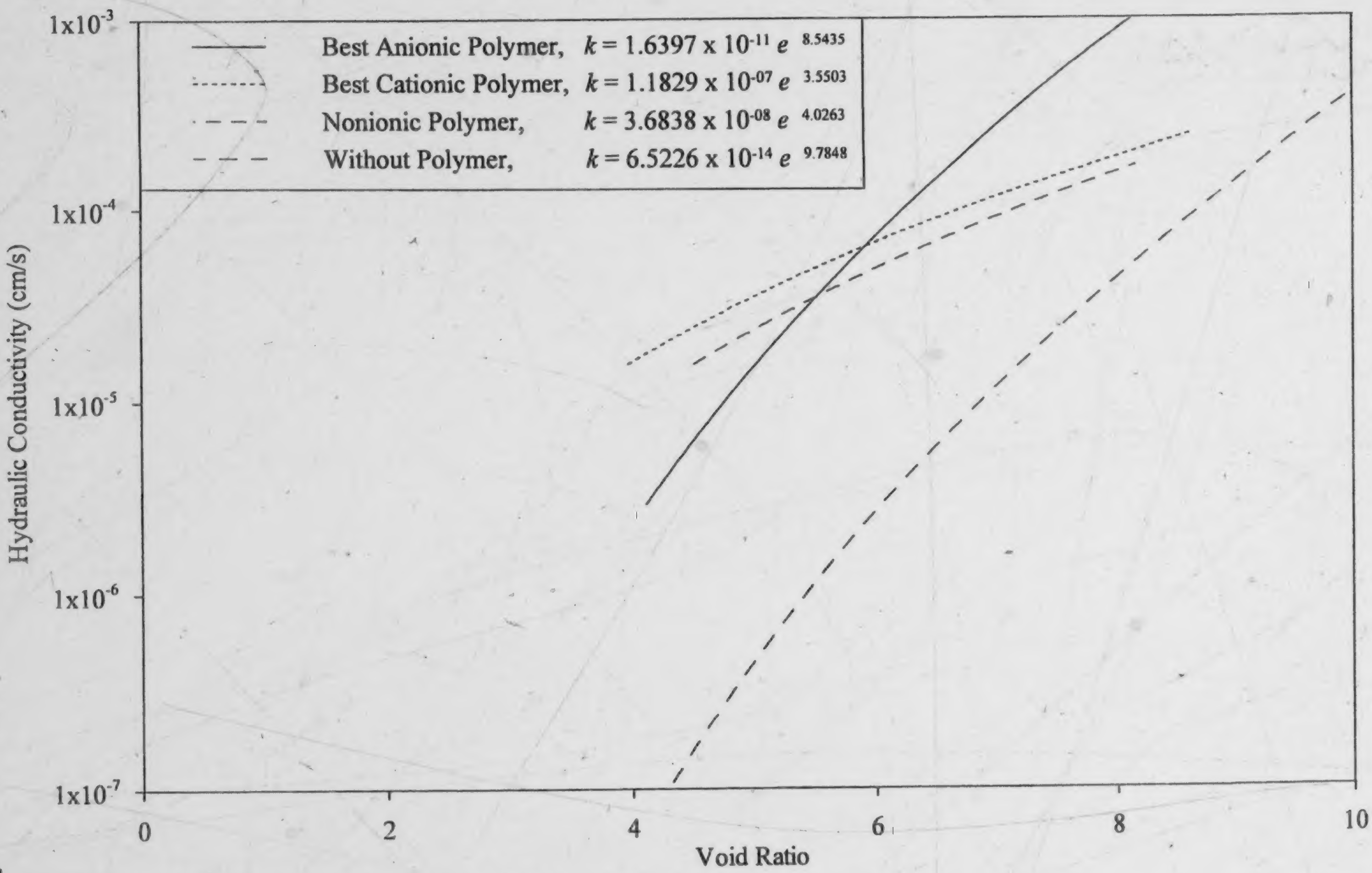

Figure 6.27: *k-e* relationships for laterite ore slurry

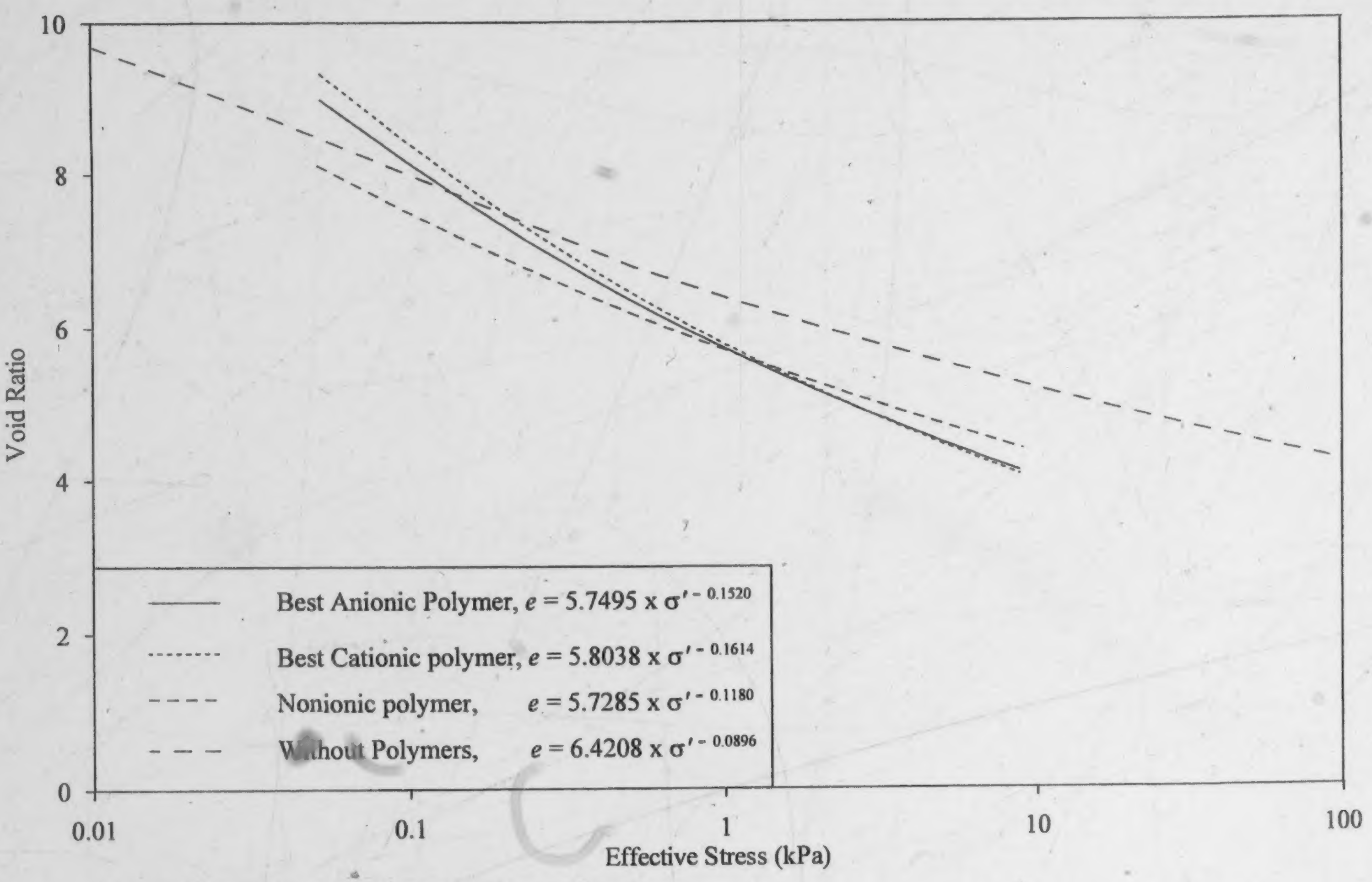

Figure 6.28: e-σ' relationship for laterite ore slurry

Based on consolidation, nonionic polymer is not the most appropriate candidate for modifying the hydraulic conductivity of laterite ore slurry. However, the high compressibility of the material due to this polymer makes it useful for the storage thickener. Therefore, the three contenders for the laterite ore slurry include anionic and cationic polymers with 75% charge (high), 17.5 x 10^6 g/mol MW (high) at 12 ppm dosage and nonionic polymer with 12.5 x 10^6 g/mol MW (medium) at 8 ppm dosage. Due to variation in material characteristics, this conclusion should be verified for specific processes.

6.4.3.4 Statistical Analysis

The *log k-e* and the *e-log* σ' relationships for the nonionic polymer modified laterite ore slurry and the statistical equations obtained for ionic polymer modifications were used for the analysis described in this section. In the statistical equations, all of the variables were give a value of zero that corresponded to polymer parameters falling between the boundary values for ionic polymers. Figure 6.29 gives the relationships between the measured and estimated hydraulic conductivity for polymer modified laterite ore slurry. Similarly, Figure 6.30 presents the relationship between the measured and estimated void ratio for polymer modified laterite ore slurry. Both of these figures show that the curves for nonionic polymer modification follow those of the ionic polymer modification. Therefore, the solid-liquid separation behavior of this class of materials can be estimated with a reasonable degree of confidence.

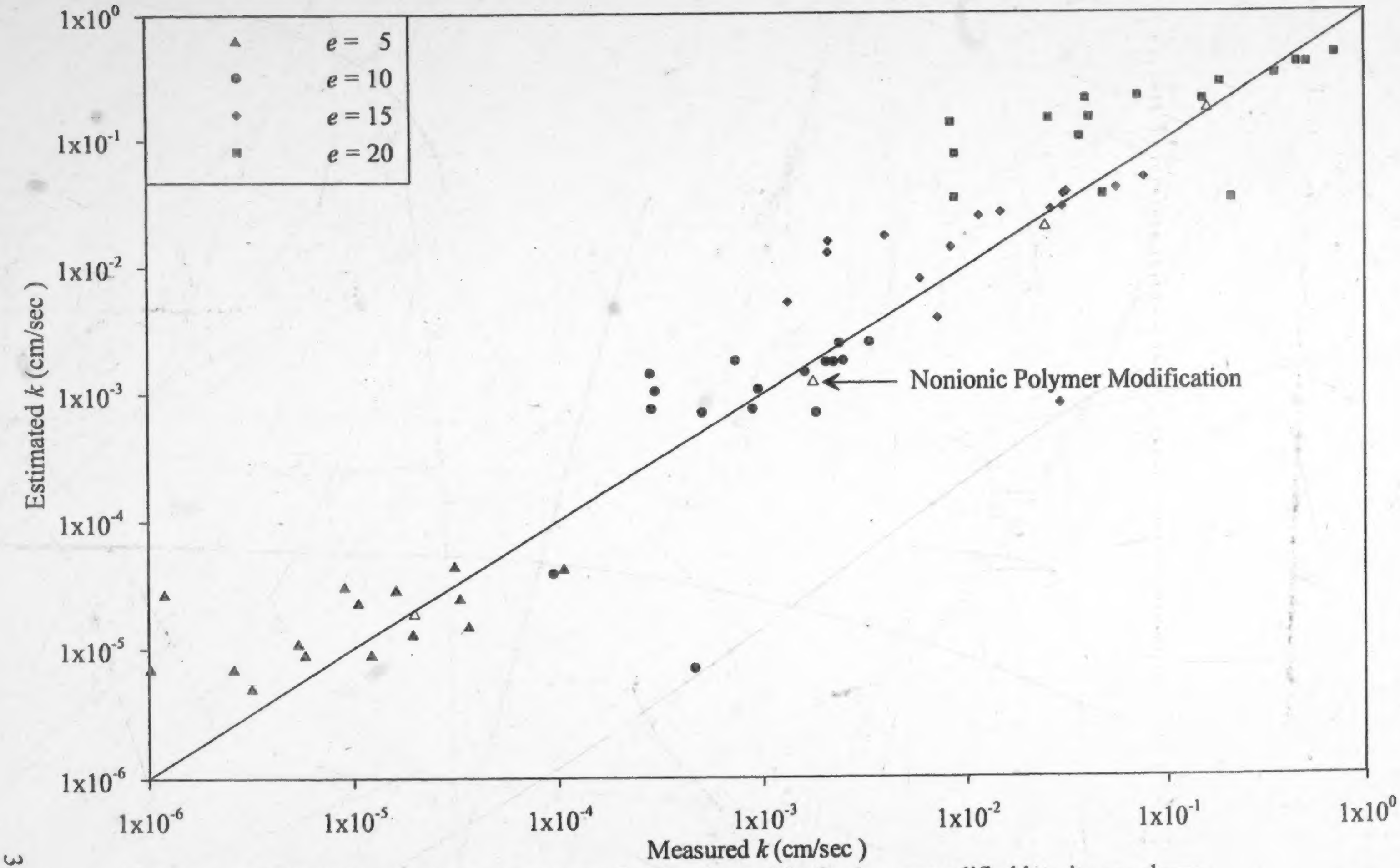

Figure 6.29: Relationship between measured and estimated k of polymer modified laterite ore slurry

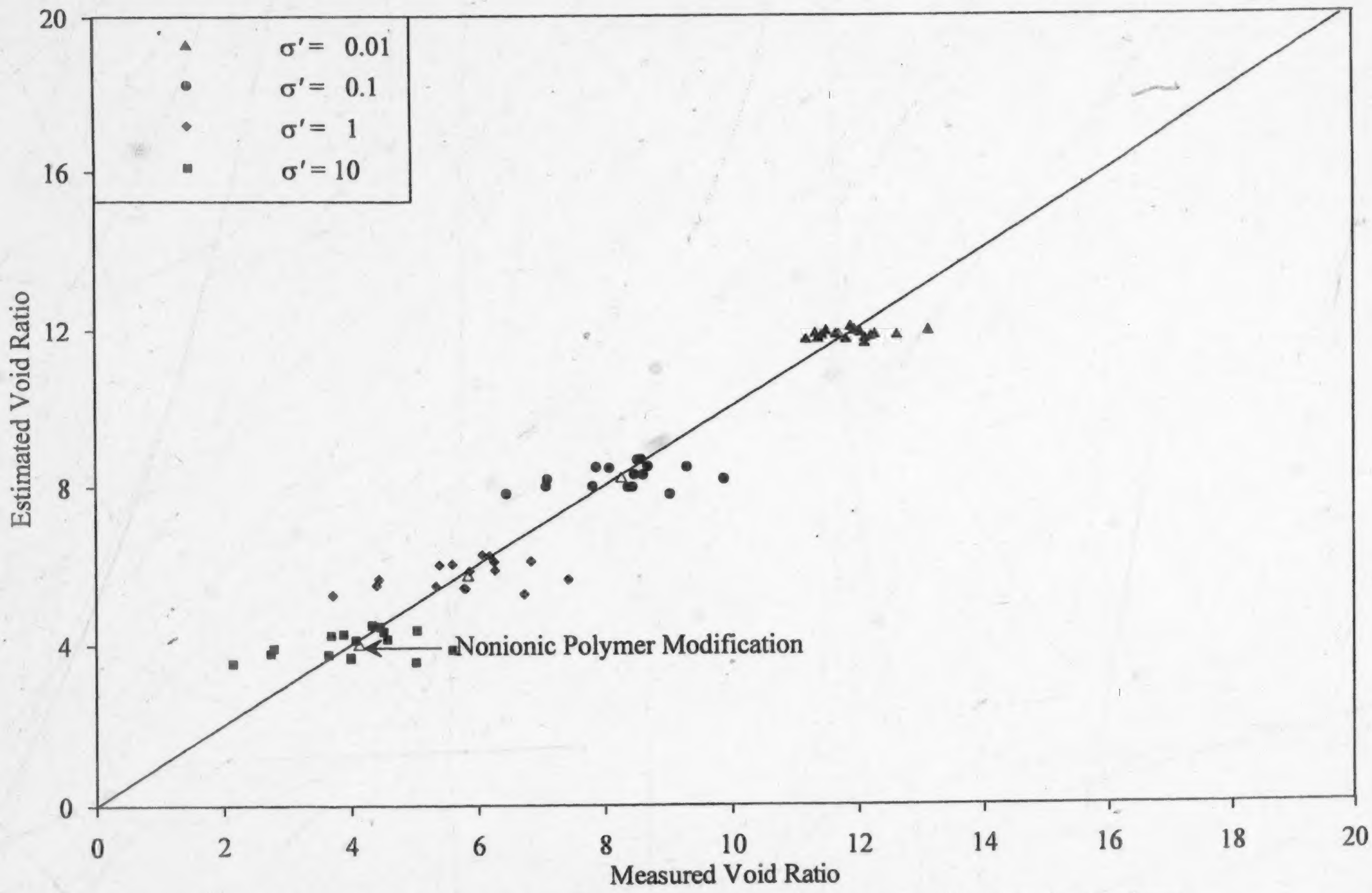

Figure 6.30: Relationship between measured and estimated *e* of polymer modified laterite ore slurry

6.5 NUMERICAL SIMULATION

6.5.1 General

This section describes the performance prediction of laterite ore slurry modified with synthetic polymers. The consolidation data depicted in previous sections are used to predict the solid-liquid separation behavior of laterite ore slurry for a hypothetical storage thickener. A comparison of the behavior of laterite ore slurry without polymer is made with that modified with anionic, cationic and nonionic polymers.

6.5.2 Analyzed Data

The *log k-e* and the *e-log* σ' relationships summarized in Figures 6.27 and Figure 6.28 are used to extrapolate the behavior of laterite ore slurry. For use in the consolidation program, data depicted in these two figures is converted to commensurate units and the transformed data was plotted to obtain the new fit parameters; the new units being m/min and Pa for *log k-e* and the *e-log* σ' relationships, respectively. Table 6.5 summarizes the parameters derived for these transformed units.

6.5.3 Storage Thickener

Figure 6.31 gives the predicted behavior of polymer modified laterite ore slurry in a storage thickener using the consolidation program SECO. Similarly, Figure 6.32 compares the predicted consolidation data with data predicted by the sedimentation program. For use in both of these programs, a 3.0 m height was chosen for the storage thickener.

Table 6.5: Summary of analyzed data for laterite ore slurry

Material	A	B	C	D
Without Polymer	7.0×10^{-14}	9.79	11.9	-0.09
Modified With Best Anionic Polymer	1.0×10^{-11}	8.54	16.4	-0.15
Modified With Best Cationic Polymer	7.0×10^{-08}	3.55	17.7	-0.16
Modified With Nonionic Polymer	2.0×10^{-08}	4.03	12.9	-0.12

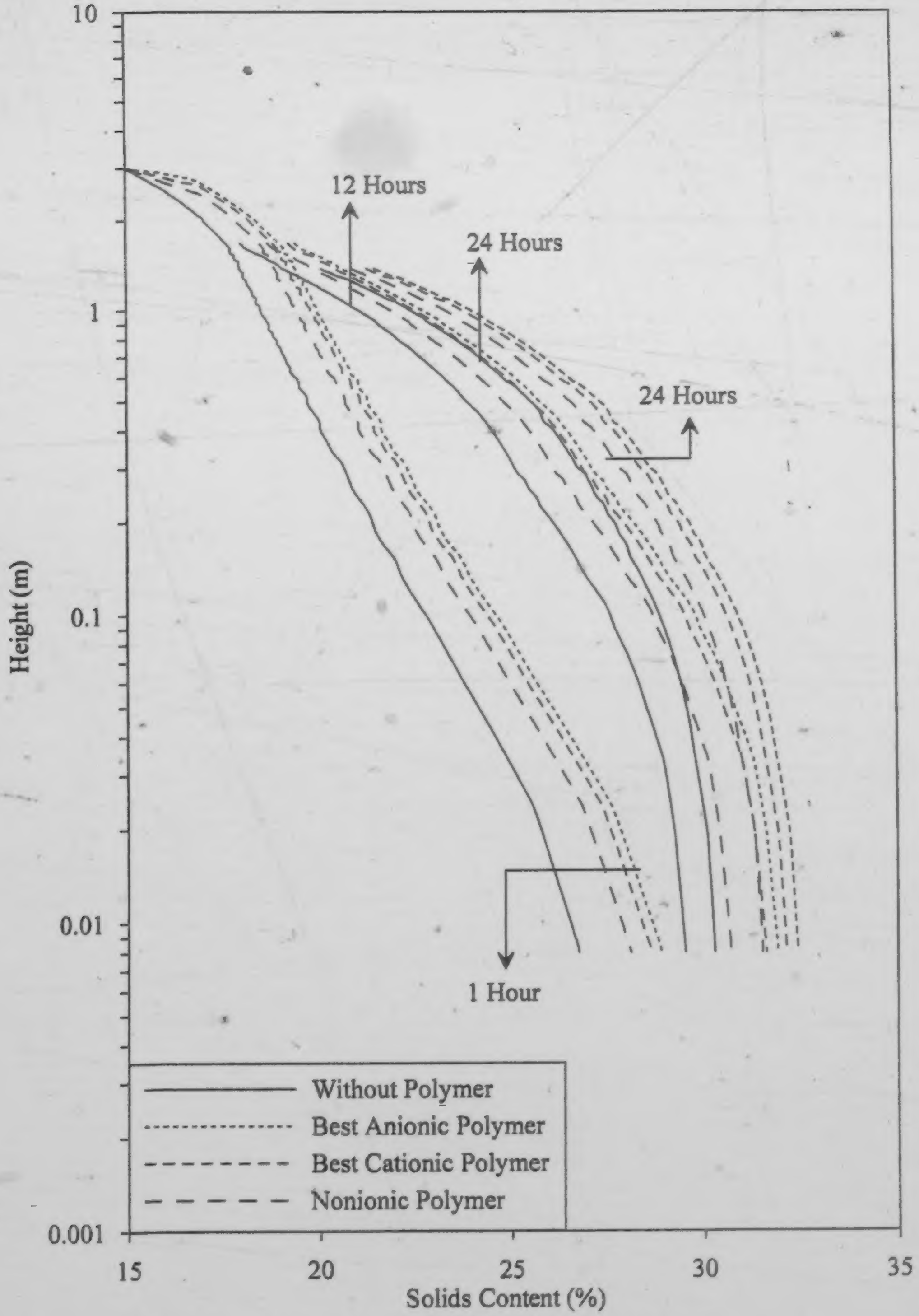

Figure 6.31: Predicted behavior in the storage thickener

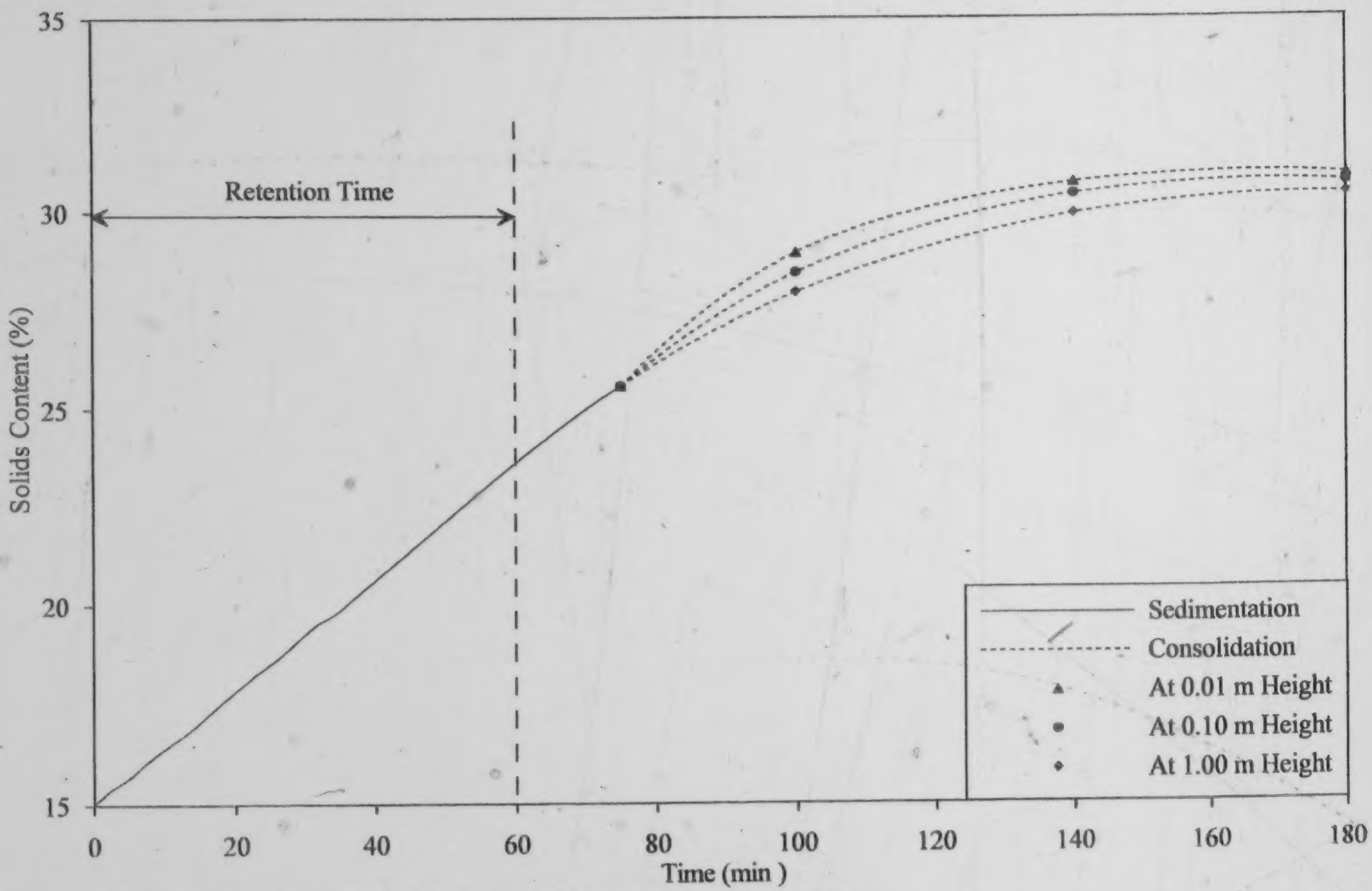

Figure 6.32: Performance of the selected polymer in the storage thickener

Figure 6.31 gives the solids content profile in a 3.0 m storage thickener at three points in time: 1, 12 and 24 hours. This figure was obtained by using the input parameters given in Table 6.5 in the sedimentation and consolidation program SECO described in Chapter Three. To highlight the solids content variation in the compaction bed of the storage thickener, sediment height is plotted on a logarithmic scale in the figure.

Figure 6.31 indicates that the improvement in solids content of the ore slurry due to polymer modification is initially high and gradually fades away with time. This is attributed to enhanced colloid-polymer-electrolyte interactions during the sedimentation stage of the solid-liquid separation process. Using consolidation parameters given in Table 7.5, improvement is highest for anionic polymers followed by cationic polymers and then nonionic polymers. After 1 hour, the solids content increases from 26.8% for the ore slurry without polymer to 28.9, 28.6, and 28.1% for modification with anionic, cationic and nonionic polymers, respectively.

Improvement in the solids content between the ore slurry and the polymer modified materials increases with time and the difference among various polymers gradually diminish with time. After 12 hours, the solids content increase from 29.5% for the ore slurry to a maximum of 31.9% for polymer modified materials. After one day, these values amount to 30.3% and 32.4% for the same two materials: ore slurry and its polymer modified version. Therefore, a solids content increase of 21% and 27% are estimated at the two points in time for the laterite ore slurry modified with the selected anionic polymer.

Figure 6.31 shows that the solids content profiles are similar to the ore slurry without polymer; solids content increases both as a function of time and of depth in the thickener. The solids content profile has two smoothly joining straight-line components. The initial straight-line portion portrays a high increase in solids content with depth whereas the final straight-line part denotes a slow solids content increase. Although the sediment starts developing during the initial stages of the solid-liquid separation process, a distinct compaction bed is observed in the storage thickener.

Figure 6.32 depicts the performance of the selected polymer for optimum results during both sedimentation and consolidation. The chosen anionic polymer had 75% charge (high), 17.5 x 10^6 g/mol MW (high) and 12 ppm dosage (low). This figure compares the predictions of the two programs: (a) sedimentation and (b) sedimentation and consolidation. Since, parameters based on consolidation data were used, the latter program only predicted the consolidation behavior. The figure shows a straight-line increase in solids content during sedimentation that is complete in 75 minutes. Taking this time as the start of consolidation, the predictions of the latter program indicate a slow increase in solids content. This procedure minimizes the *weak link* between sedimentation and consolidation reported by the developers (Masala & Chan 2001) and makes the predictions of the two programs in close conformity. The figure illustrates that at a typical retention time of 60 minutes, sedimentation is the dominant phenomenon during the solid-liquid separation process. Some additional improvement in solids content can be achieved during consolidation.

6.6 LATERITE SLURRY CHARATERISTICS DIAGRAM

Figure 6.33 gives the hydraulic conductivity of the polymer modified laterite ore slurry on the ternary diagram and compares the same with data for the ore slurry without polymer. The figure shows that similar to the laterite ore slurry without polymer, the hydraulic conductivity of polymer modified materials is part of the family of constant clay-water ratio lines. This is because these lines denote colloid-polymer-electrolyte interactions.

The diagram indicates that the hydraulic conductivity of polymer modified laterite ore slurries varies by two orders of magnitude between the sedimentation limit ($k = 10^{-6}$ cm/sec) and the liquid limit ($k = 10^{-8}$ cm/sec). Earlier, it was observed that in comparison to the laterite ore slurry without polymer, identical values of hydraulic conductivity for the polymer modified materials are obtained at higher solids content (low void ratio). Preceding discussions attributed this to variations in colloid-polymer-electrolyte interactions and the resulting fabric during the various stages of the solid-liquid separation process.

Given the operational constraints of the metal extraction process such as time, thickener geometry, and the preclusion of load application, the solid-liquid separation behavior of laterite ore slurry is improved using synthetic polymers. Effective improvement depends upon the choice of polymer for the given mineralogy and pore water chemistry. Under self-weight, improvement due to polymer modification is highest initially and gradually diminishes. Sedimentation is the governing phenomenon during the solid-liquid separation process of polymer modified laterite ore slurries.

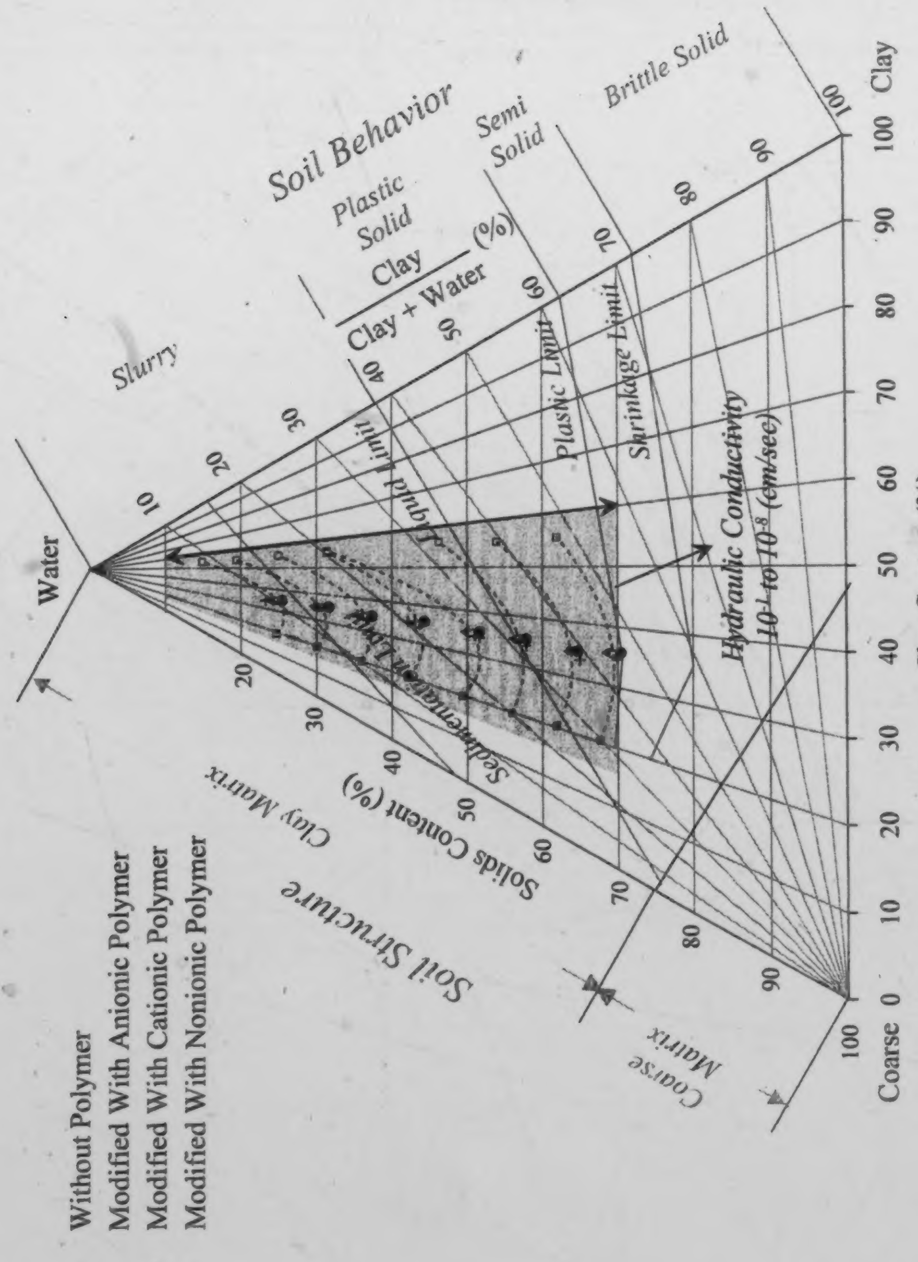

Figure 6.33: LSCD for polymer modified laterite ore slurry

6.7 SUMMARY AND CONCLUSIONS

This chapter provided a detailed characterization of polymer modified laterite ore slurries. The influence of various polymer parameters (type, charge, molecular weight and dosage) on the solid-liquid separation behavior of selected laterite ore slurry was investigated. Results of laboratory investigations pertaining to geotechnical index properties, sedimentation in conjunction with soil morphology and consolidation were presented. These data were statistically analyzed and used in the numerical simulation to predict field performance of the storage thickener. The entire data were depicted on the laterite slurry characteristics diagram. The conclusions of this chapter can be summarized as follows:

- Polymer modification of laterite ore slurry causes subtle variations in geotechnical characteristics. These materials generally adsorb large amount of water and are essentially nonsegregating.
- Both anionic and cationic polymers can increase or decrease k_i of laterite ore slurry during sedimentation. An increase of 20 times and a decrease of four times were observed. Optimum polymer parameters for both anionic and cation polymers include a 75% charge (high), 17.5 x 10^6 g/mol MW (high) and 12 ppm dosage (high).
- Although, nonionic polymers always improve k_i, this increase is lower than ionic polymers; a maximum of 14 times k_i is observed. Generally, k_i increases with an increase in polymer MW from 7.5 x 10^6 g/mol (low) though 17.5 x 10^6 g/mol (high) or dosage from 4 ppm (low) through 12 ppm (high).

- The initial hydraulic conductivity of polymer modified PAL slurry strongly depends on soil morphology. Good flocculation, reduced tortuousity and the presence of channels are associated with high k_i.
- The type of flocculation attained during the initial stages of sedimentation governs both stages of the solid-liquid separation process. For anionic polymers, tightly bonded small flocs develop whereas loosely attached large flocs characterize cationic polymers; floc size decreases with increasing polymer charge.
- The performance of various synthetic polymers during consolidation depends on floc breakage and grain redistribution. These phenomena control the escape of water from the pores or void spaces between grains and the release of entrapped water from the flocs.
- Hydraulic conductivity during consolidation depends on the imposed hydraulic gradient. A high gradient is required to extract water entrapped in the flocs whereas a low gradient is associated with flow through channels and low tortuousity.
- Polymer selection depends on optimizing efficiency (hydraulic conductivity) and yield (compressibility) of the extraction process. An anionic polymer with 75% charge (high), 17.5 x 10^6 g/mol MW (high) and 12 ppm dosage (high) is the most suitable one for an improved solid-liquid separation of laterite ore slurries.
- Sedimentation is the governing phenomenon for the solid-liquid separation of polymer modified laterite ore slurries. During this stage, there is a maximum chance for colloid-polymer-electrolyte interactions to be displayed. Additional improvement can be achieved during consolidation.

Chapter 7

Polymer Modification of Laterite PAL Slurries

7.1 GENERAL

Geotechnical investigation of polymer modified laterite PAL slurries is pivotal in understanding the improvement or deterioration of solid-liquid separation behavior. This knowledge is useful for an assessment of the performance of various synthetic polymers in the metal extraction process. This chapter highlights the influence of polymer characteristics on the solid-liquid separation behavior of the limonite-saprolite PAL slurry from the Philippines. Denoted as laterite PAL slurry in this chapter, characteristics of this material were described in chapter five. The various polymer parameters include polymer type, charge, molecular weight (MW) and dosage. Results of laboratory investigations pertaining to geotechnical index properties, sedimentation (in conjunction with morphology) and consolidation are discussed. Statistical analyses are used to develop and validate models describing both stages of the solid-liquid separation process. This is followed by providing the results of numerical simulation of the statistically analyzed data to predict field performance of the CCD thickener. Next, the laboratory and modeling data is depicted on the laterite slurry characteristics diagram constructed for the laterite PAL sample. Finally, a summary and the main conclusions drawn from this chapter are given.

7.2 GEOTECHNICAL INDEX PROPERTIES

7.2.1 General

Geotechnical characterization of polymer modified laterite PAL slurries begins with an investigation of their index properties. These properties are used to classify the materials and to evaluate the performance of the synthetic polymers.

7.2.2 Segregation

Figure 7.1 gives the results of the segregation tests on laterite PAL slurry modified with 4 ppm of selected polymers. Results are given in the form of normalized height versus solids content for different initial solids content. This figure shows that the observed solids content increases with depth and that the profiles tend to reach a constant solids content with increasing initial solids content. This behavior is similar to the PAL slurry without polymer modification and is attributed to diminishing segregation at high initial solids content. Reduced segregation is attributed to the formation of a mesh due to the interaction of solid particles and synthetic polymers in the given medium.

Figure 7.2 gives the percentage of segregation as a function of the initial solids content for laterite ore slurry modified with the above polymers. This figure indicates that variation in the segregation characteristics of the ore slurry using different polymers is not significant. The segregation limit (I_S), which is defined as the initial solids content that pertains to 5% segregation with depth, closely matches for all polymers. Therefore, the investigated laterite PAL slurry modified with polymers is non-segregating at an initial solids content of 15%.

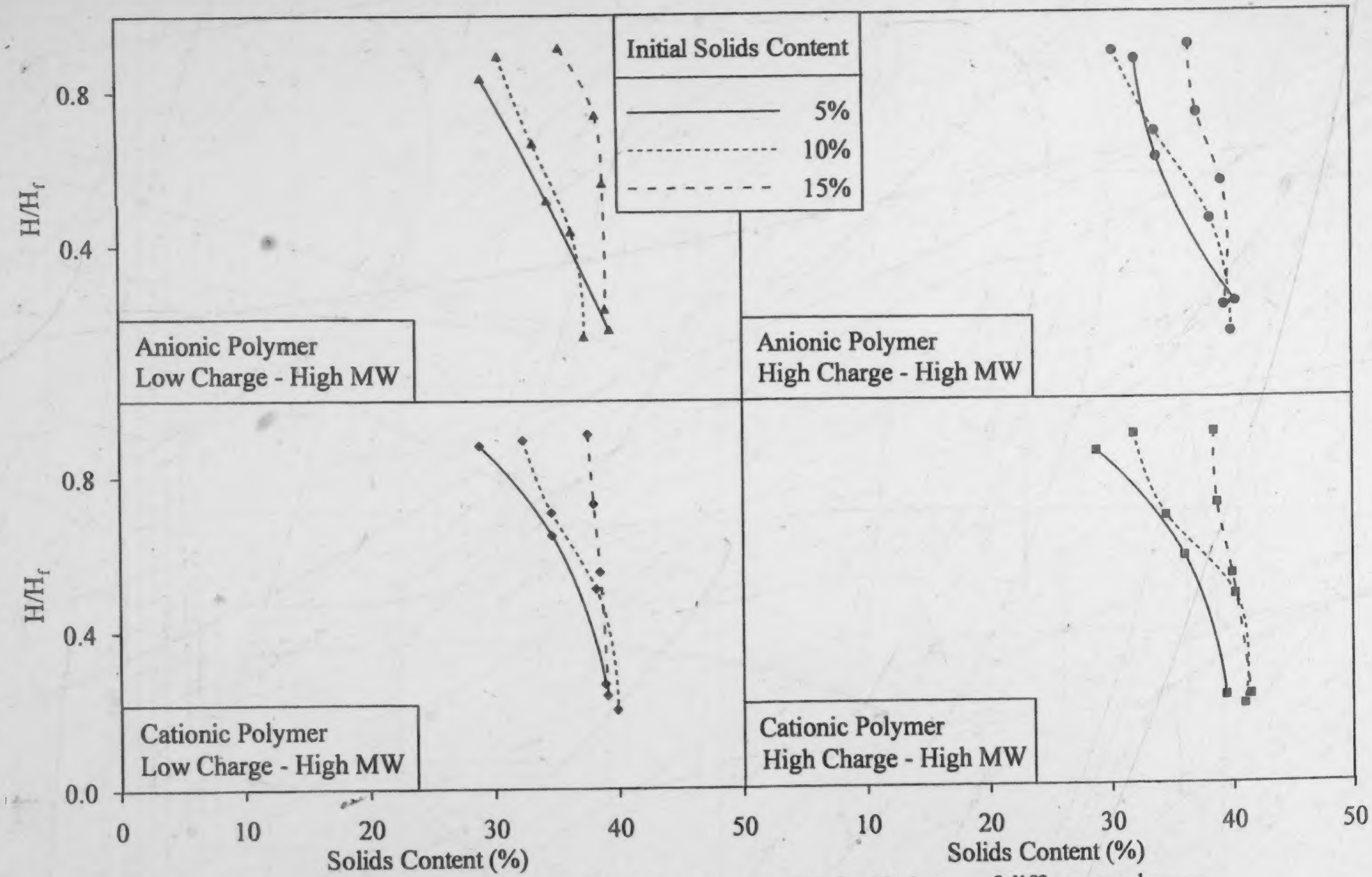

Figure 7.1: Segregation test results for laterite PAL slurry modified with 4 ppm of diffrerent polymers

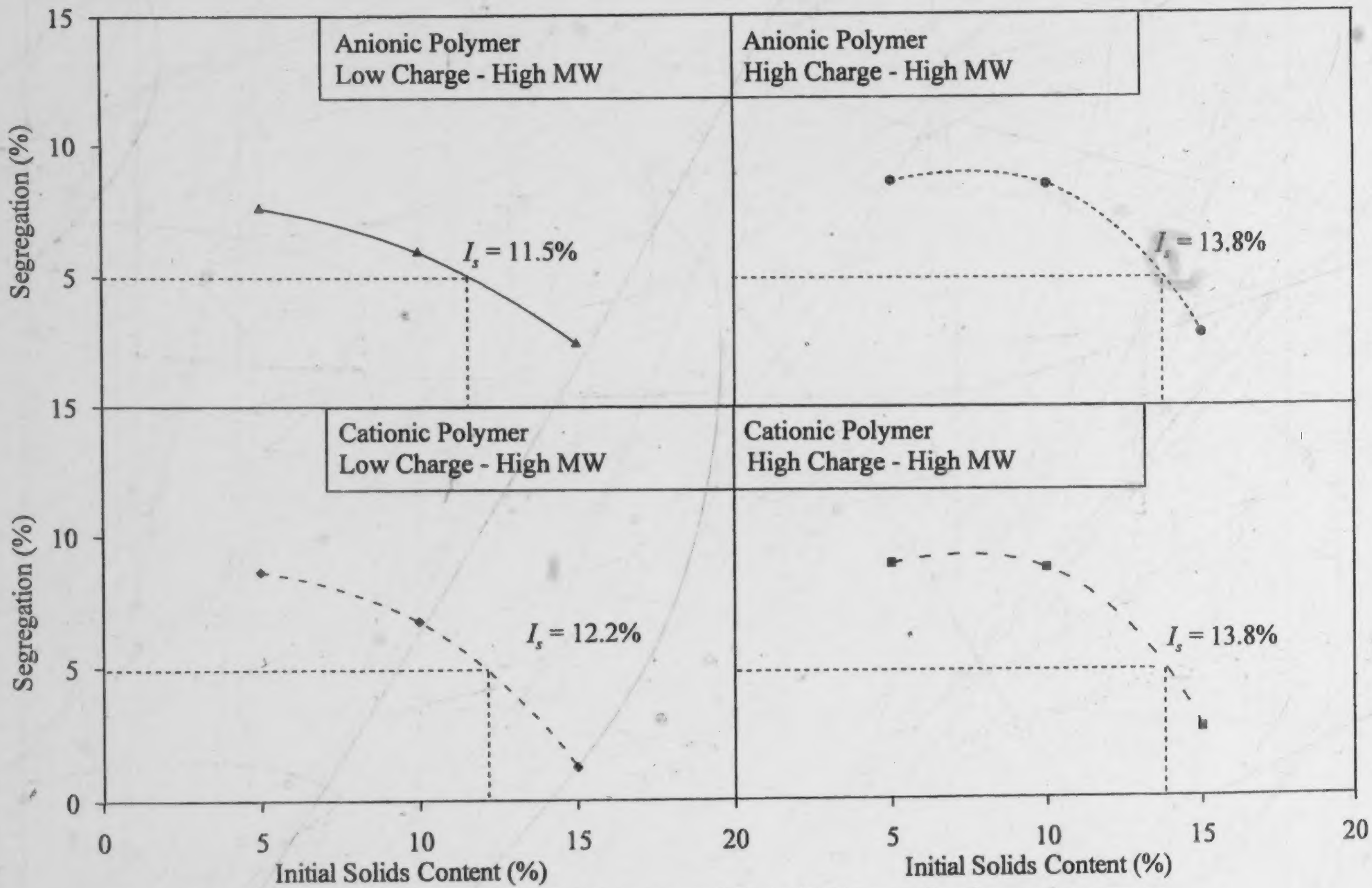

Figure 7.2: Segregation limit for laterite PAL slurry modified with 4 ppm of various polymers

7.2.3 Consistency Limits

Table B.1 and B.2 give the consistency limits of laterite ore modified with various ionic and nonionic polymers, respectively. Figure 7.3 summarizes test data in the plasticity chart (Casagrande 1948). This figure shows that the polymer modified laterite PAL materials plot close to kaolinite clay mineral. This suggests that the behavior of these materials is anticipated to be similar to that of clay particles with low electro-chemical activity.

Figure 7.3 also compares polymer modified PAL slurries with the laterite PAL without polymer. This comparison illustrates that polymer modification of laterite PAL results in considerable variation in the engineering characteristics; a material not very different from *sand* is converted to one similar to *clays*. In contrast to laterite PAL without polymer, polymer modified PAL slurries are associated with a large amount of entrapped water in the newly formed flocs. This entrapped water results in an increase in the consistency limits of the polymer modified PAL slurries. The transformation in material properties is expected to change the solid-liquid separation behavior of the laterite PAL slurry.

The variation in plasticity characteristics among different polymers is mainly attributed to the variable interaction of synthetic polymers with the PAL material in the given medium. This indicates that the solid-liquid separation behavior of this class of materials is governed by the parameters of synthetic polymers (type, charge, MW and dosage). The relative significance of these parameters is highlighted later in this chapter.

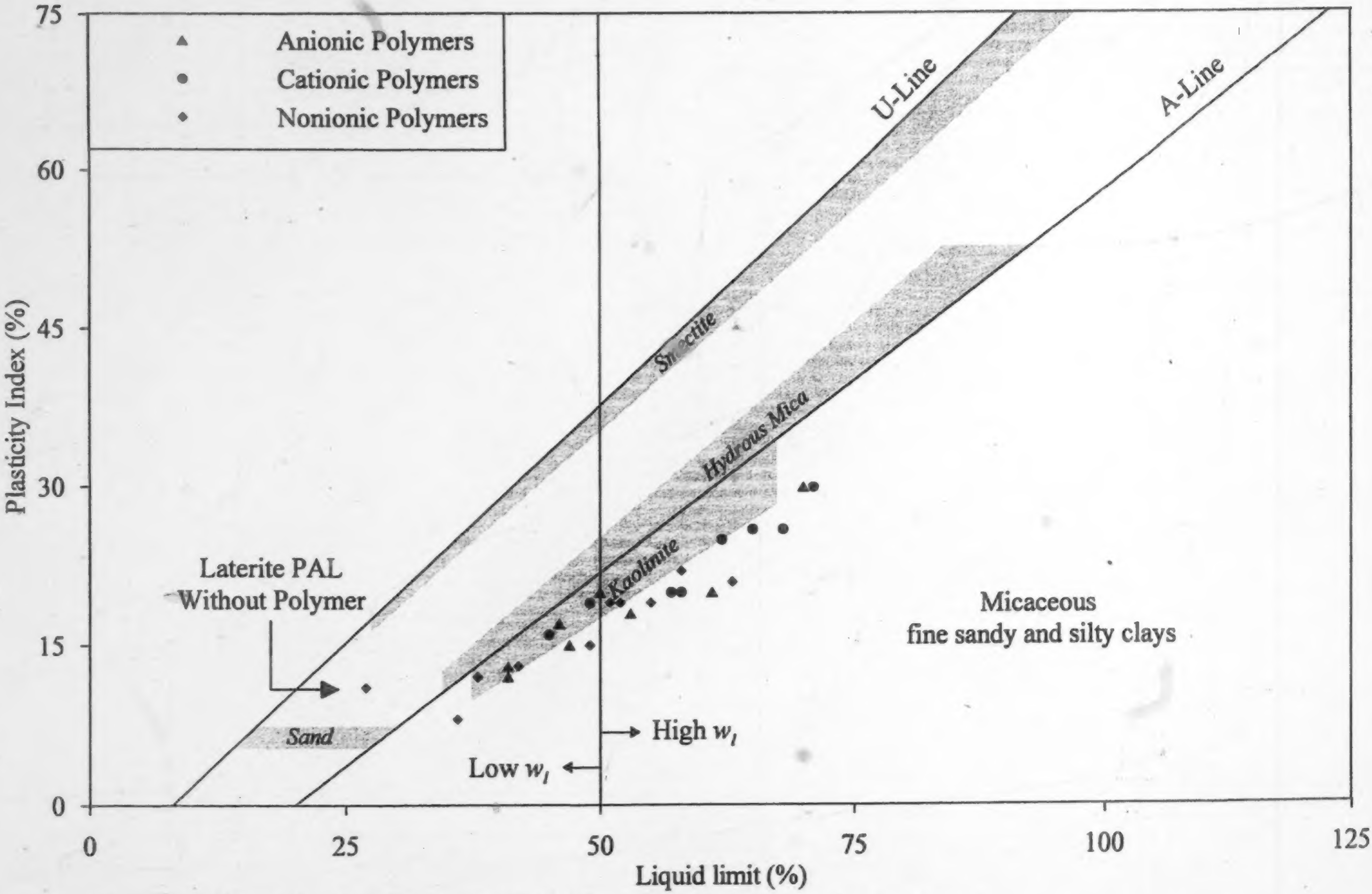

Figure 7.3: Plasticity chart for laterite PAL slurry modified with various polymers

7.3 SEDIMENTATION

7.3.1 General

This section gives the self-weight sedimentation behavior of laterite PAL slurry using various polymers; ionic and nonionic polymers are described separately. The initial hydraulic conductivity is obtained from the initial straight-line portions of the sedimentation curves. The effects of polymer parameters on the initial hydraulic conductivity are highlighted. Morphological observations are used to understand the observed behavior from a fundamental standpoint. Statistical analyses are used to assess the relative significance of various polymer parameters.

7.3.2 Ionic Polymers

7.3.2.1 General

Figure 7.4 and Figure 7.5 give the sedimentation test results for laterite PAL slurry modified with various anionic and cationic polymers, respectively. Both of these figures show that similar to the PAL slurry without polymer modification, the self-weight sedimentation is essentially completed within the first 180 minutes when the same slurry is modified with various polymers. These figures further show that within 30 minutes from the start of the tests, all of the sedimentation curves start converging and curves for 4 and 12 ppm merge well before the end of 180 minutes. Furthermore, both figures indicate an L-shaped sedimentation curve, which highlights a distinct point of inflection between the sedimentation and the consolidation zones. This is attributed to the high specific gravity of the soil particles and the improved flocculation of these particles due to polymer modification.

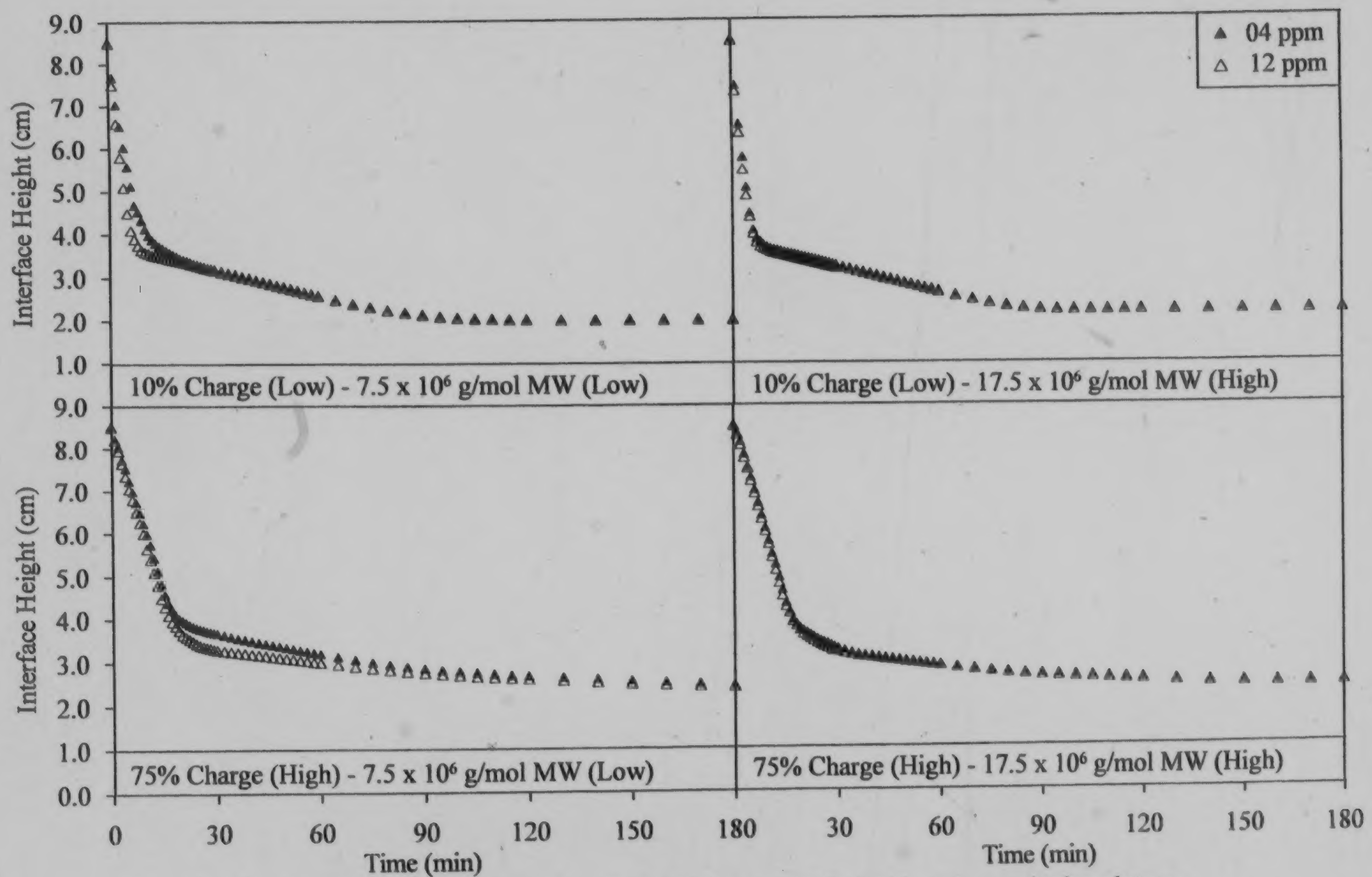

Figure 7.4: Sedimentation test results for laterite PAL slurry modified with various anionic polymers

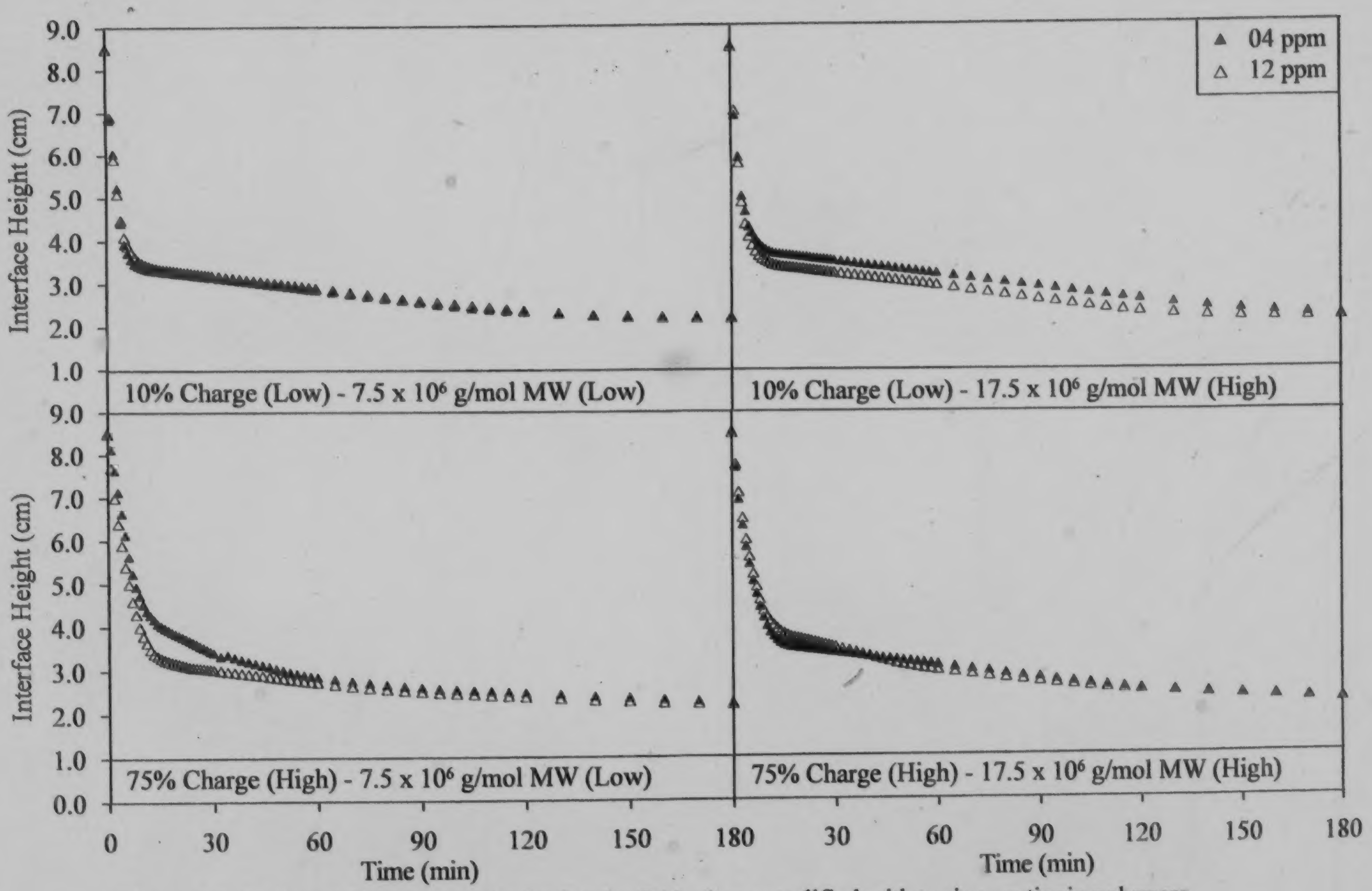

Figure 7.5: Sedimentation test results for laterite PAL slurry modified with various cationic polymers

A comparison of Figure 7.4 and Figure 7.5 indicates that among the two polymer dosages, a slight increase in the rate of sedimentation is observed with an increase in polymer dosage. Further, colloid-polymer-electrolyte interactions appear to be consistent for both anionic and cationic polymers. These interactions govern the sedimentation behavior of the laterite PAL slurry in the highly acidic electrolyte medium comprised of large amount of multivalent ions. Detailed discussion about subtle variations in the sedimentation behavior is given later in this chapter.

7.3.2.2 Initial Hydraulic Conductivity

Figures B.1 through B.4 give the sedimentation test result for the first 30 minutes for laterite PAL slurry modified with various ionic polymers. The slope of the initial straight-line portion is used to obtain the initial hydraulic conductivity (k_i). Derived from Figure B.1 though B.4, Table 7.1 gives k_i for laterite PAL slurry modified with various ionic polymers. Like wise, Figure 7.6 highlights the effect of polymer charge, molecular weight (MW) and dosage on the k_i of laterite PAL slurry.

The k_i of laterite PAL slurry without polymer modification measured 64 x 10^{-3} (cm/sec) as reported in Chapter Five. A comparison of this value with the data depicted in Table 7.1 reveals that polymer modification changes k_i of the laterite PAL slurry to variable extent. An improvement of more than two times and a depletion of less than two times are observed for the investigated materials. This variability is mainly attributed to the variable colloid-polymer-electrolyte interactions in an acidic medium.

Table 7.1: k_i of laterite PAL slurry modified with various ionic polymers

Polymer Parameters				$k_i \times 10^{-3}$ (cm/sec)
Type	Charge	MW x 10^6 (g/mol)	Dose (ppm)	
Anionic	10% (Low)	7.5 (Low)	4	76
			12	110
		17.5 (High)	4	118
			12	124
	75% (High)	7.5 (Low)	4	36
			12	39
		17.5 (High)	4	39
			12	40
Cationic	10% (Low)	7.5 (Low)	4	148
			12	154
		17.5 (High)	4	158
			12	165
	75% (High)	7.5 (Low)	4	67
			12	85
		17.5 (High)	4	85
			12	86

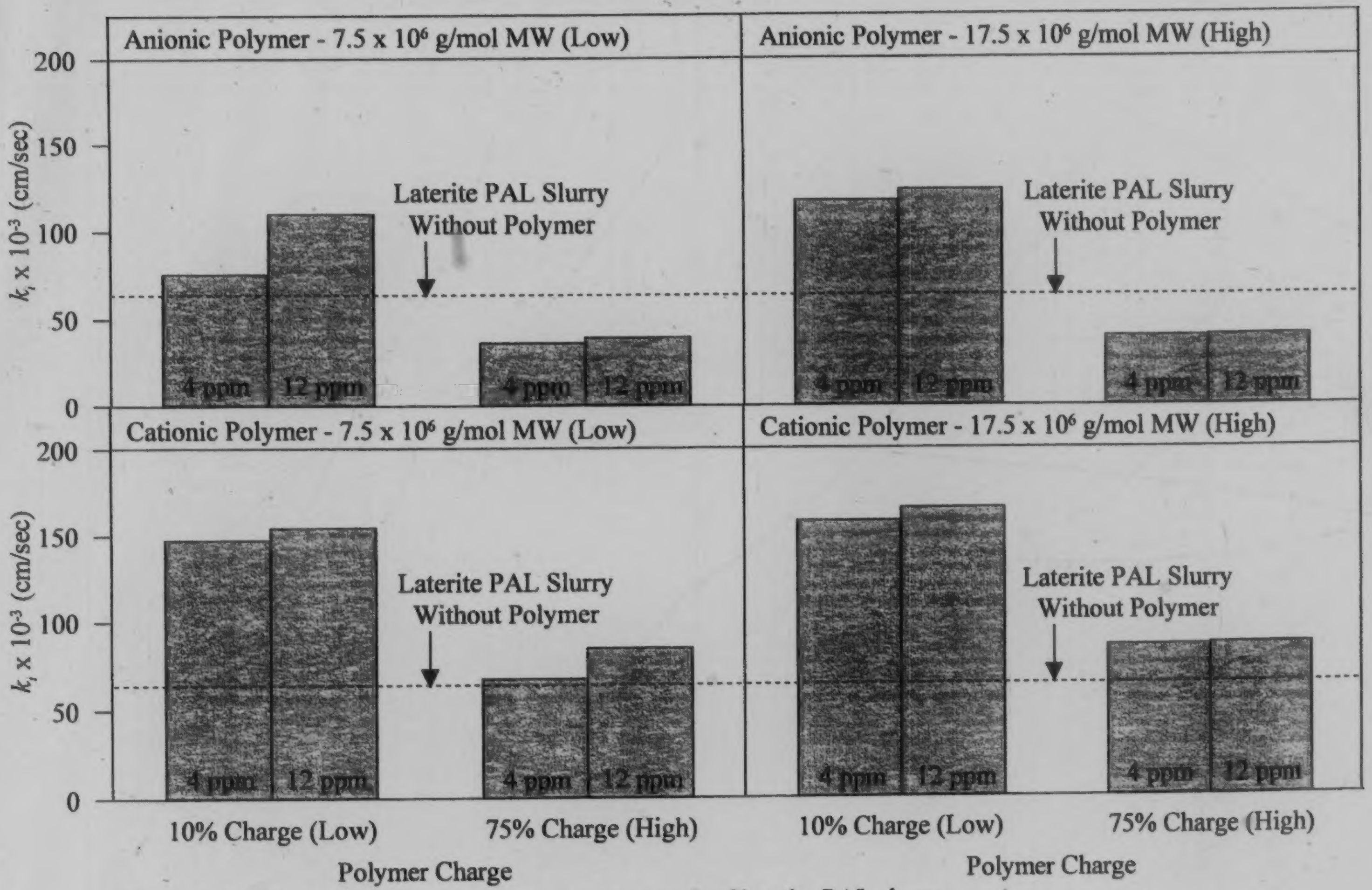

Figure 7.6: Effect of various polymer parameters on k_i of laterite PAL slurry

Figure 7.6 shows that for the conducted tests, polymer modification improves k_i of laterite PAL slurry on twelve occasions out of a total of sixteen tests. A higher k_i for the polymer modified slurry compared to that without polymer modification is generally observed for all but 75% charge (high) anionic polymers. Improvement in the initial hydraulic conductivity is highest for 10% charge (low) cationic polymers, followed by 10% charge (low) anionic polymers and then 75% charge (high) cationic polymers.

Figure 7.6 also illustrates that an increase in polymer charge from 10% to 75% results in a decrease in k_i. Similarly, an increase in k_i is observed with increasing polymer MW from 7.5×10^6 g/mol to 12.5×10^6 g/mol and polymer dosage from 4 ppm to 12 ppm; variations in k_i due to polymer MW and polymer dosage are marginal. The influence of polymer parameters can be combined in one term to be called the *polymer factor*. Mathematically, this newly devised term is equal to polymer charge divided by the product of polymer MW and polymer dosage and has the units mol/g-ppm.

Figure 7.7 gives the variation of the initial hydraulic conductivity with the polymer factor. This figure shows that decreasing the polymer factor due to an increase in polymer MW and/or polymer dosage results in an increase in k_i. The polymer factor varies by more than three orders of magnitude and has exponential relationships with k_i for ionic polymers. These relationships clearly illustrates that the combined effect of polymer parameters is efficiently explained by the term polymer factor.

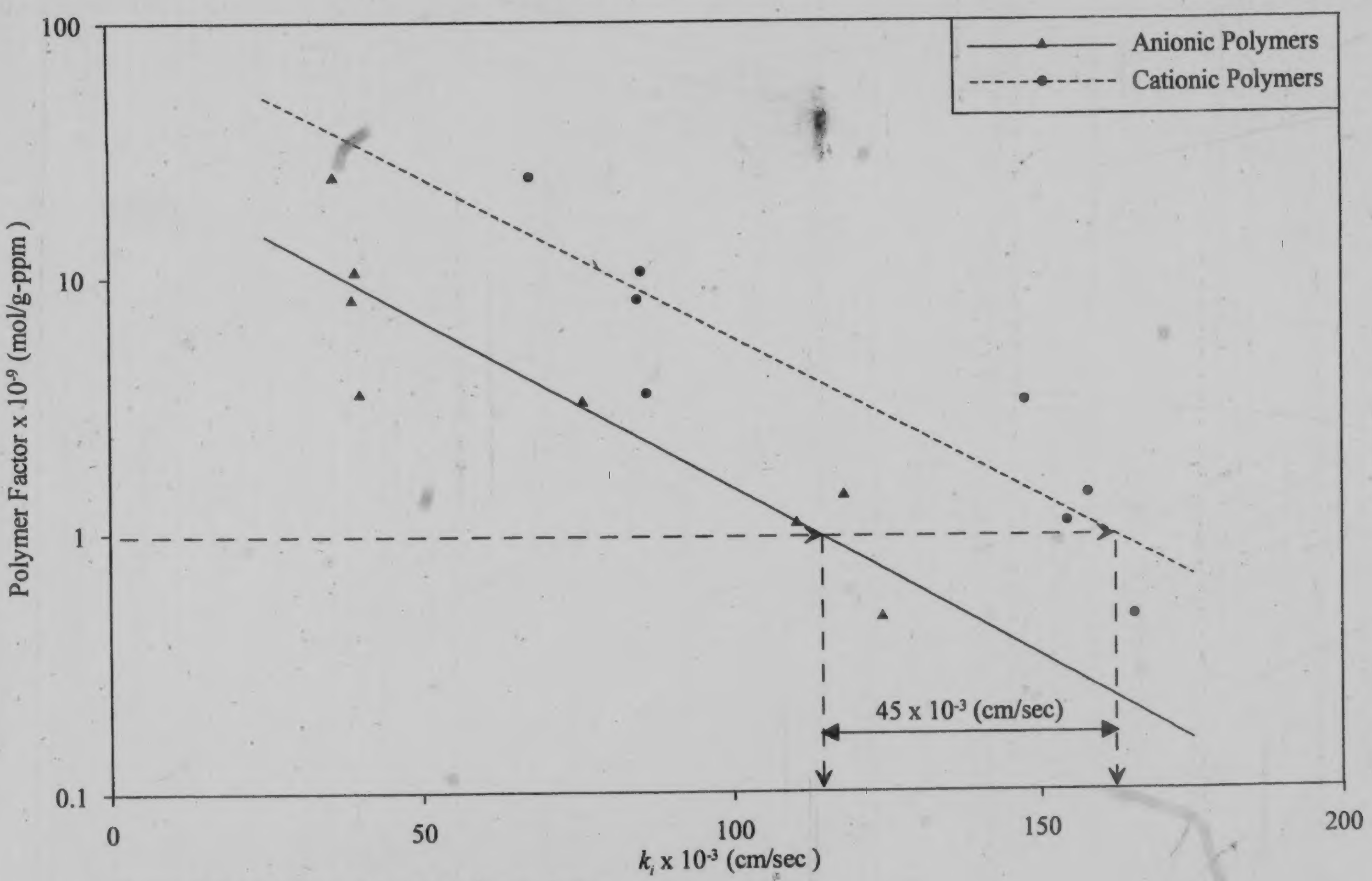

Figure 7.7: Variation of k_i with polymer factor

Figure 7.7 shows that the relationships between polymer factor and k_i for both polymer types are parallel. This highlights the influence of the severe environmental conditions of the laterite PAL slurry. The pore fluid is highly acidic with Ca^{2+}, Mg^{2+}, Mn^{2+}, Al^{3+}, Fe^{3+}, Ni^{3+}, $Co^{3+}$and SO_4^{2-} as predominant ions. This figure further shows that cationic polymers are more effective than anionic polymers in k_i improvement of the laterite PAL slurry. The figure demonstrates that at a polymer factor of say 1 x 10^{-9} mol/g-ppm, k_i for anionic polymer modification is 115 x 10^{-3} cm/sec whereas k_i for cationic polymer modification is 160 x 10^{-3} cm/sec. This amounts to a 40% k_i increase for the latter polymer type.

The above observations are explained on the basis of the following mechanism. The positively charged hematite particles and the acidic medium that is characterized by an excess of H^+ ions, help create a negatively charged double layer in the vicinity of the particles. The cationic polymers containing the methyl chloride functional group remain positively charged under acidic conditions. These positive polymer chains become loosely attached to several negatively charged double layers around the particles thereby causing flocculation of the latter. On the contrary, the sodium acrylate functional group of anionic polymers undergoes protonation (exchange of Na^+ by H^+) in the acidic medium. This results in significant charge neutralization of the anionic polymer thereby rendering it less effective for flocculation. Still, the nonprotonated sites on these polymers interact with the positive charges in the double layer thereby resulting in some flocculation. Therefore, cationic polymers are more effective in k_i improvement of the laterite PAL slurries.

Figure 7.6 shows that for both polymer types, 10% polymer charge (low) results in a higher k_i increase than the 75% polymer charge (high). This is attributed to the higher degree of flocculation due to the inhibited electro-chemical activity between the 10% charge (low) polymers and the pore fluid electrolytes beyond the double layers of the solid particles. These depleted interactions allow the synthetic polymers to reach the electrical double layer and cause the above flocculation mechanism to occur. Recorded observations during various sedimentation tests using 10% charge (low) polymers indicated large flocs with unobservable variation in floc size. The resulting behavior depicted in Figure 7.6 is in accordance with other published data. Using anionic polymers for laterite acid leach residues, Briceno & Osseo-Asare (1995c) reported a decrease in settling rate with increasing polymer charge.

A smaller k_i for the polymer modified slurry compared to that without polymer modification is observed for 75% charge (high) anionic polymers. This is attributed to the possible development of bimodal size distribution consisting of individual particles and flocs of variable sizes in the slurry (Hogg 1999). The individual dispersed particles obstruct the settling of the flocculated material that is already impeded by the variable floc size. The same phenomenon occurs for 75% charge (high) cationic polymers but because of the favorable polymer-electrolyte interactions, its intensity is reduced. Consequently, k_i due to modification of these latter polymers is not less than that of the laterite PAL slurry without polymers.

The marginal increase in the initial hydraulic conductivity due to polymer MW and dosage is attributed to the effect of pressure acid leaching on the colloid-polymer-electrolyte interactions. Particle size growth during the process results in reducing the particle surface area available for adsorption. The addition of polymers causes flocculation that further reduces the available surface area (Hogg 1999). Further, the long chain length associated with 17.5 x 10^6 g/mol (high) MW causes intermingling of the chains thereby leading to an insignificant increase in flocculation (Alonso & Laskowski 1999). Therefore, a 7.5 x 10^6 g/mol (low) MW and/or 4 ppm (low) dosage is required to provide sufficient surface coverage for effective bridging phenomenon to occur. Both of these lower values reduce the polymer factor thereby increasing the initial hydraulic conductivity of the laterite PAL slurry.

7.3.2.3 Morphology

The observed behavior given above is explained in the light of morphological examinations of some of the samples taken after the sedimentation tests. Results of scanning electron microscopy are studied in conjunction with elemental analyses. Figure 7.8 and 7.9 give the morphological details of laterite PAL slurry modified with anionic polymers having 10% charge (low)-17.5 x 10^6 g/mol (high) MW and 75% charge (high)-17.5 x 10^6 g/mol (high) MW, respectively. Similarly, Figure 7.10 and 7.11 give the microstructural details of laterite PAL slurry modified with cationic polymers and the above designation, respectively. All observations pertain to a polymer dosage of 4 ppm (low). All of these figures are comprised of four micrographs, similar to those described in Chapters Four, Five and Six.

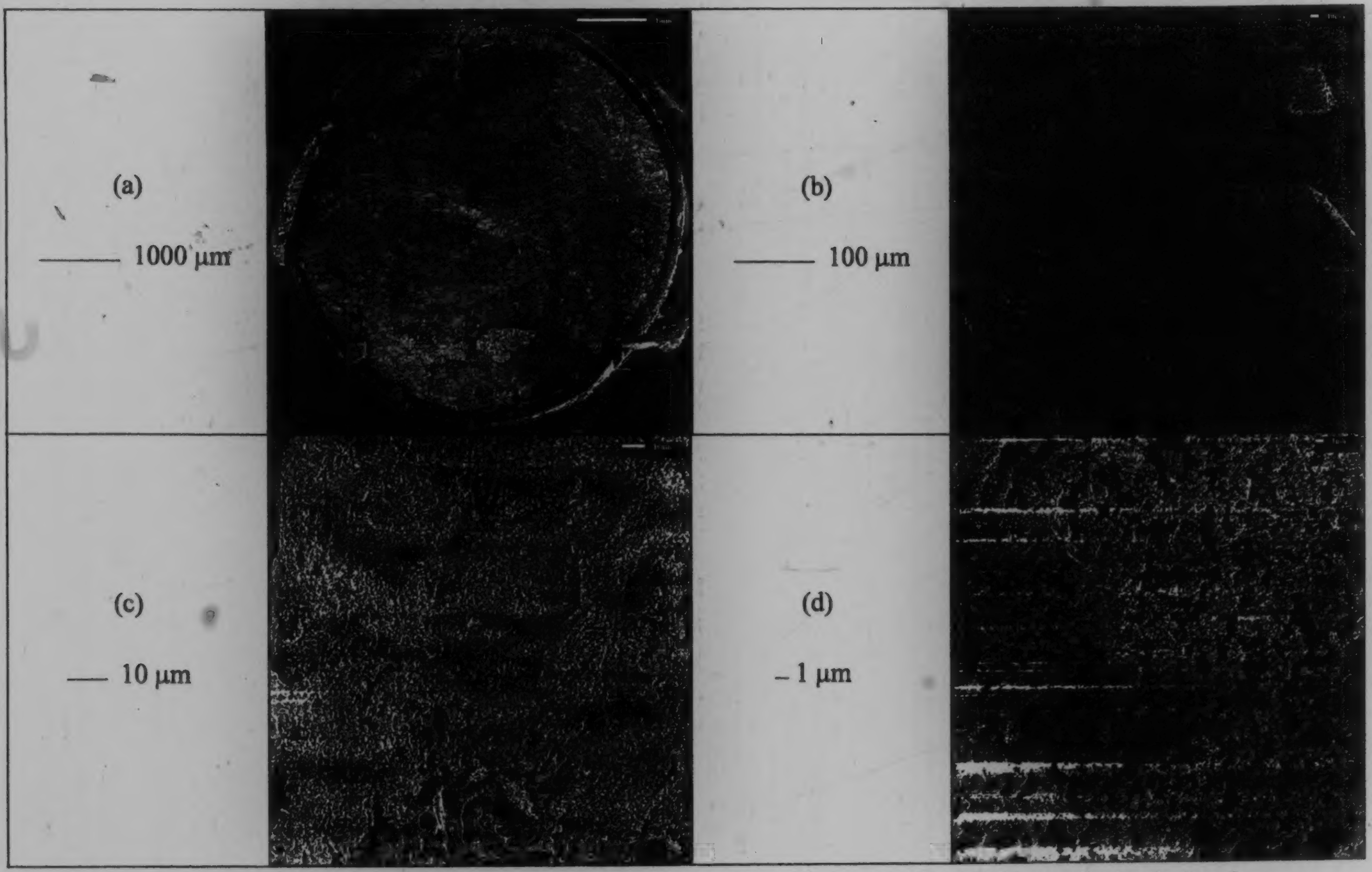
(a)
1000 µm
(b)
100 µm
(c)
10 µm
(d)
1 µm

Figure 7.8: SEM of laterite PAL slurry modified with 10% charge (low)-17.5 x 10^6 g/mol (high) MW-04 ppm (low) anionic polymer

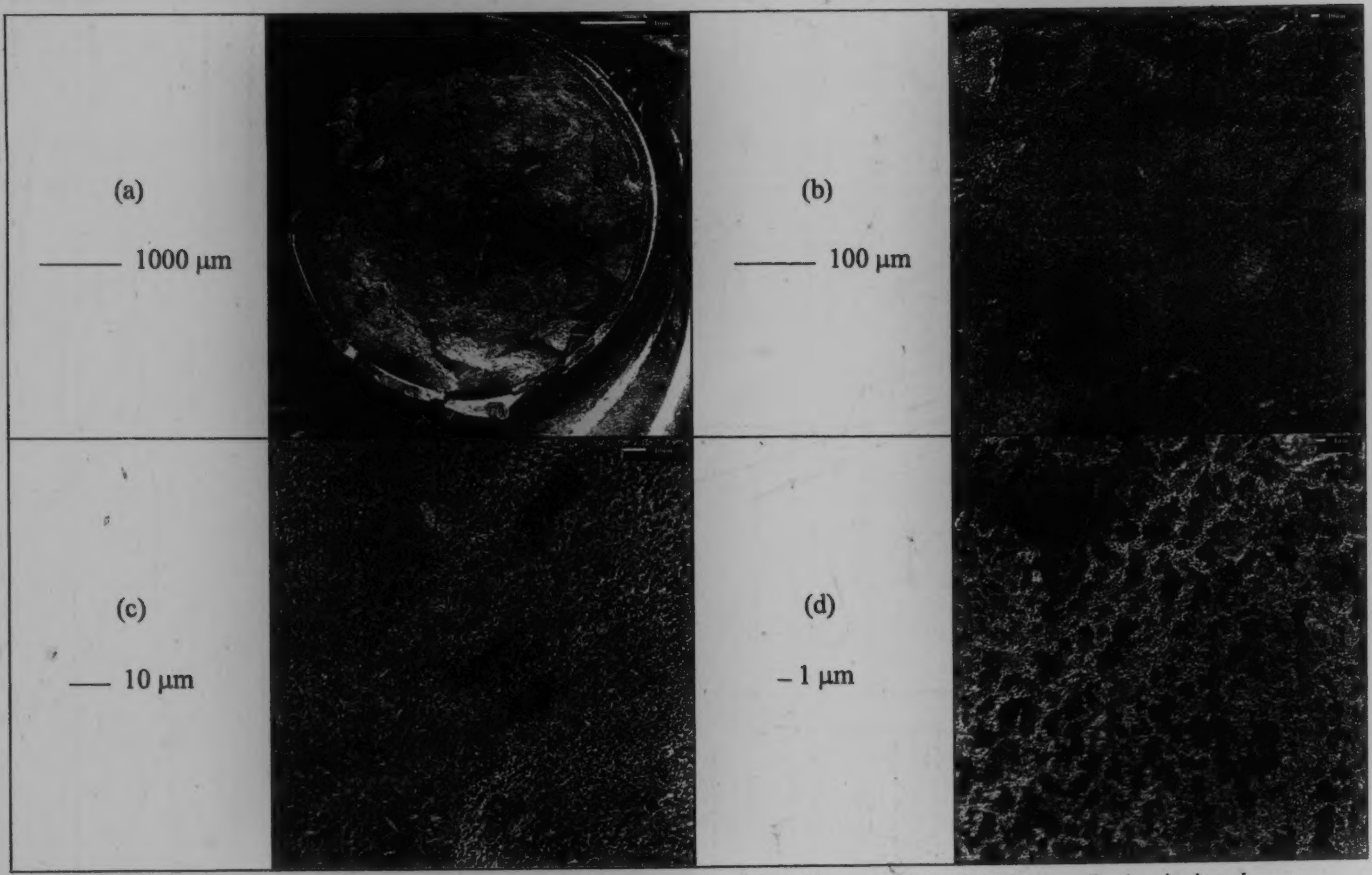
(a)
1000 µm
(b)
100 µm
(c)
10 µm
(d)
1 µm

Figure 7.9: SEM of laterite PAL slurry modified with 75% charge (high)-17.5 x 10^6 g/mol (high) MW-04 ppm (low) anionic polymer

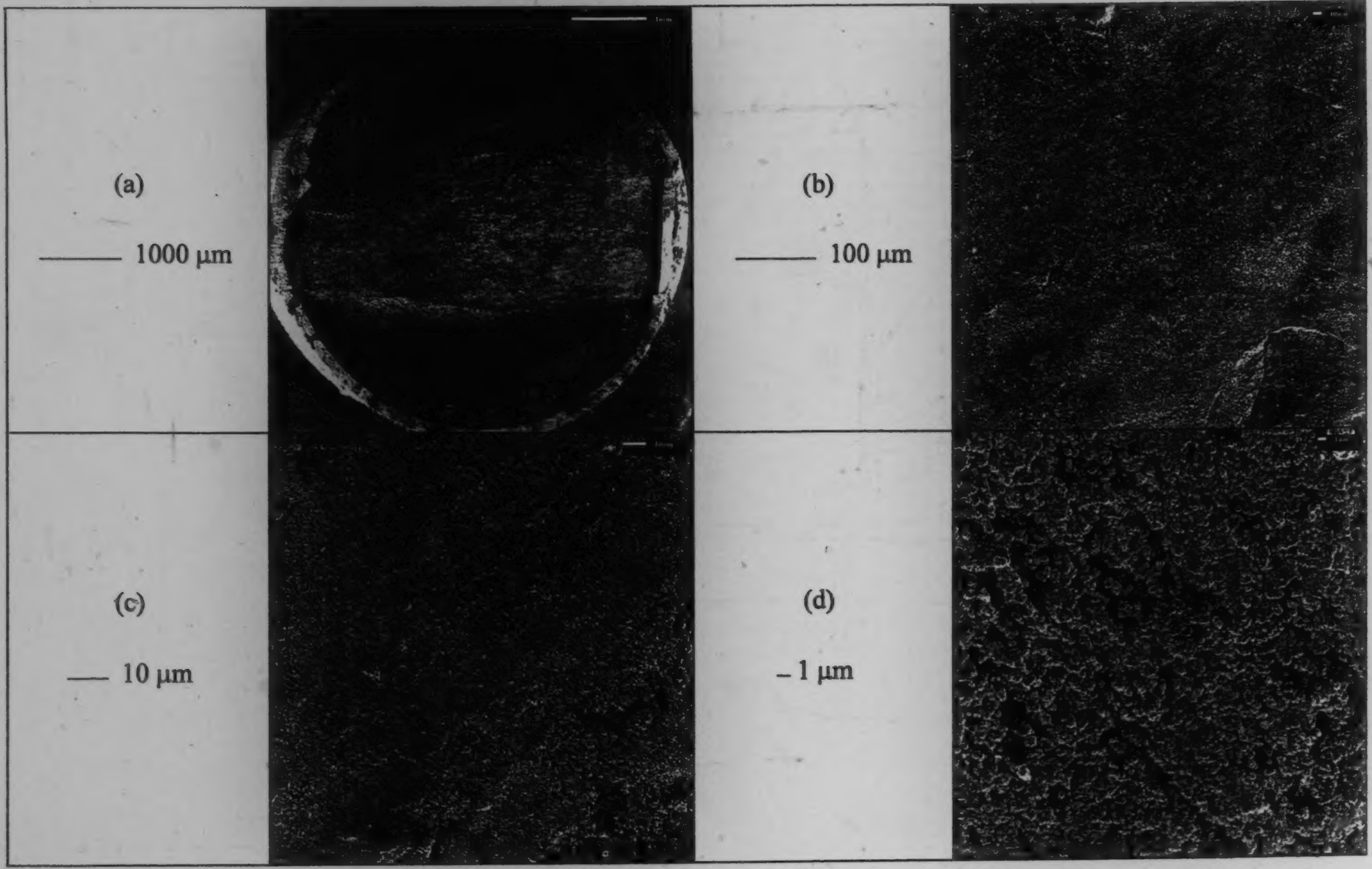
(a)
1000 µm
(b)
100 µm
(c)
10 µm
(d)
1 µm

Figure 7.10: SEM of laterite PAL slurry modified with 10% charge (low)-17.5 x 10^6 g/mol (high) MW-04 ppm (low) cationic polymer

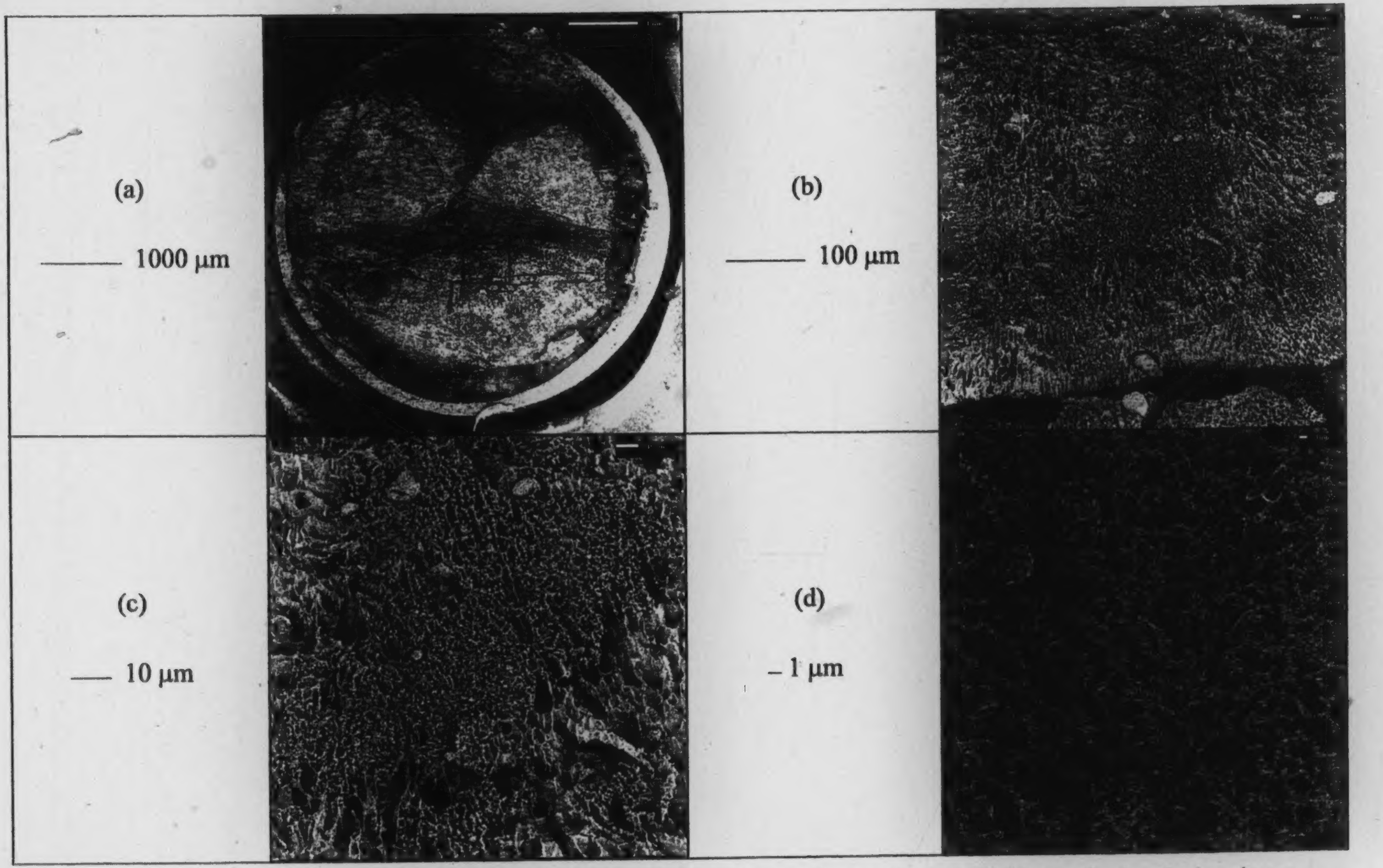
(a)
1000 µm
(b)
100 µm
(c)
10 µm
(d)
1 µm

Figure 7.11: SEM of laterite PAL slurry modified with 75% charge (low)-17.5 x 10^6 g/mol (high) MW-04 ppm (low) cationic polymer

Figure 7.8 shows the morphology of the limonite-saprolite PAL slurry modified with 10% charge (low)-17.5 x 10^6 g/mol (high) MW-04 ppm (low) dosage of anionic polymer. Micrograph (a) shows a good specimen surface with some protuberances. Micrograph (b) shows the presence of occasional coarse grains in the clay matrix. Micrograph (c) shows that the clay fabric consists of vaguely defined clusters, which are separated by interassemblage pore spaces. Micrograph (d) illustrates that the clay fabric that consists of globular hematite is flocculated. However, this clay fabric does not show distinct floc boundaries although channels partly separate these large aggregations. Therefore, the k_i depends on both the microfabric and on the minifabric. The k_i of 118 x 10^{-3} cm/sec measured for this sample is twice that of the PAL slurry without polymer.

Figure 7.9 shows the morphology of the limonite-saprolite PAL slurry modified with 75% charge (high)-17.5 x 10^6 g/mol (high) MW-04 ppm (low) dosage of anionic polymer. Micrograph (a) shows a very rough specimen surface with a large diametrical bisector. Micrograph (b) shows some coarse grains in the predominantly clay matrix. Micrograph (c) depicts that the clay matrix is devoid of distinctly observable channeling. Micrograph (d) illustrates that the hematite particle aggregations are arranged in a tubular fashion with 2 μm diameter tubes. Although, the morphology of this specimen is flocculated, k_i is governed by the small tube size in the flocs. The k_i of 39 x 10^{-3} cm/sec measured for this sample is three times less than that of the previous sample and two-thirds of that of the PAL slurry without polymer.

Figure 7.10 shows the morphology of the limonite-saprolite PAL slurry modified with 10% charge (low)-17.5 x 10^6 g/mol (high) MW-04 ppm (low) dosage of cationic polymer. Micrograph (a) shows a good specimen surface with negligible sample disturbance at the bottom. Micrograph (b) shows the occasional presence of coarse size grains in the clay matrix. Micrograph (c) gives a flocculated clay structure with some channeling. Micrograph (d) illustrates a clay fabric that consists of flocculated hematite particles with evenly distributed pore spaces. This morphology is not very different from that shown in Figure 7.8; a sample with similar k_i. The measured k_i of the current sample is 158 x 10^{-3} cm/sec, which is more than twice that of the PAL slurry without polymer modification.

Figure 7.11 shows the morphology of the limonite-saprolite PAL slurry modified with 75% charge (high)-17.5 x 10^6 g/mol (high) MW-04 ppm (low) dosage of cationic polymer. Micrograph (a) shows a bad specimen surface with extensive disturbance. Micrograph (b) shows a compact clay structure with some coarse grains. Micrograph (c) illustrates a flocculated clay fabric composed of circularly arranged spherical hematite particles, which engulf vaguely defined tubes. Micrograph (d) shows that the pore spaces are 2 to 5 μm in this sample. This resulted in a k_i of 85 x 10^{-3} cm/sec, which is twice that of the specimen depicted in Figure 7.9.

The morphology of polymer modified PAL slurries reveal that all polymers cause a flocculated clay fabric. This flocculation is more pronounced for 10% charge (low) polymers compared with 75% charge (high) polymers. Further, channeling is evident for the former polymers whereas tubulation is observed for the latter polymers.

7.3.2.4 Statistical Analysis

Based on the 2^k factorial design of experiments described in Chapter Three, a statistical analysis was conducted for ionic polymers. Using the measured k_i as input, an estimate of k_i resulted according to the following model:

$$k_i = 0.0957 + 0.0229\, T_p - 0.0359\, C_p + 0.0063\, MW_p + 0.0048\, D_p \qquad (7.1)$$

where,

T_p = Polymer type

C_p = Polymer charge

MW_p = Polymer MW

D_p = Polymer dosage

Using –1 for low and +1 for high values of the above polymer parameters, equation (7.1) estimated the k_i depicted in Figure 7.12. This figure shows a good correlation between the observed and the estimated values for the given set of data; none of the observed data need to be neglected as an outlier.

The analysis showed that the most significant factors are polymer type and charge (p-value of 0.001) followed by polymer MW (p-value of 0.02) and then polymer dosage (p-value of 0.05). This is in accordance with observations depicted in Figure 7.7. This figure showed that variations in polymer type and polymer charge result in significant alterations in observed k_i, whereas marginal changes in k_i occur due to variations in polymer MW and dosage. Therefore, the observed solid-liquid separation of laterite PAL slurries modified with ionic polymers is in accordance with statistical analysis.

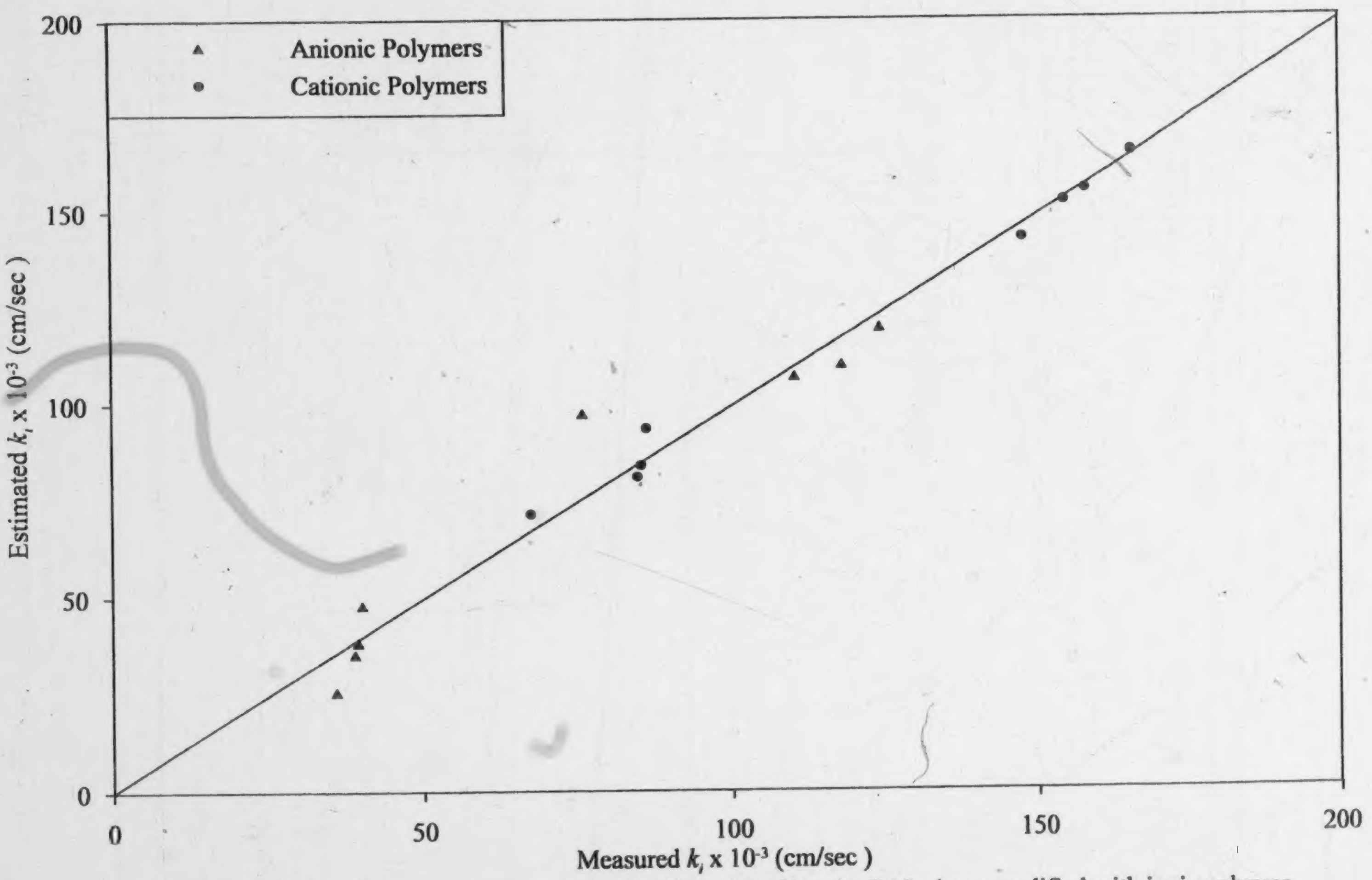

Figure 7.12: Relationship between measured and estimated k_i of laterite PAL slurry modified with ionic polymer

7.3.3 Nonionic Polymers

7.3.3.1 General

Figure 7.13 gives the sedimentation test results for laterite PAL slurry modified with various nonionic polymers. This figure shows that similar to the PAL slurry without polymer modification, the self-weight sedimentation is essentially complete within the first 180 minutes when the same slurry is modified with various nonionic polymers. After about 30 minutes, all of the sedimentation curves for various dosages start converging and curves for 4, 8 and 12 ppm merge by the end of 180 minutes. Among the three polymer dosages, an increase in the rate of sedimentation is generally observed with an increase in polymer dosage. The only exception to this generalization is observed for the 17.5 x 10^6 g/mol (high) polymer MW at 12 ppm dosage. The sedimentation behavior of laterite PAL slurry modified with nonionic polymers is explained in this section.

7.3.3.2 Initial Hydraulic Conductivity

Figures B.5 through B.7 give the sedimentation test result for the first 30 minutes for laterite PAL slurry modified with various nonionic polymers. The slope of the initial straight-line portion is used to obtain the initial hydraulic conductivity (k_i). Derived from Figure B.5 though B.7, Table 7.2 gives k_i for laterite PAL slurry modified with various nonionic polymers. Likewise, Figure 7.14 highlights the effect of polymer molecular weight (MW) and polymer dosage on the initial hydraulic conductivity of laterite PAL slurry, when modified with nonionic polymers.

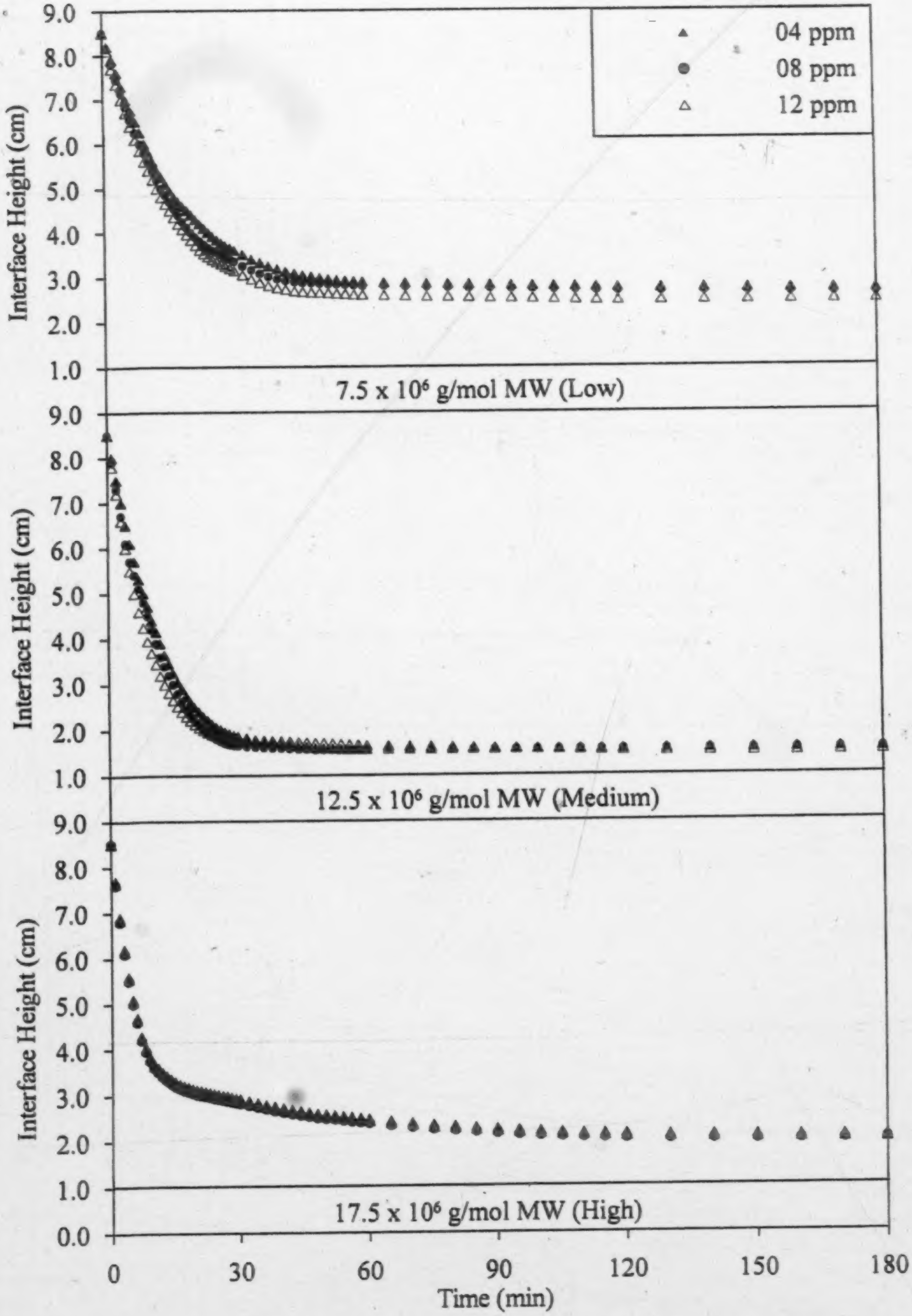

Figure 7.13: Sedimentation test results using nonionic polymers

Table 7.2: k_i of laterite PAL slurry modified with various nonionic polymers

Polymer Parameters				$k_i \times 10^{-3}$ (cm/sec)
Type	Charge	MW x 10^6 (g/mol)	Dose (ppm)	
Nonionic	NA	7.5 (Low)	4	41
			8	48
			12	55
		12.5 (Medium)	4	69
			8	83
			12	90
		17.5 (High)	4	110
			8	117
			12	114

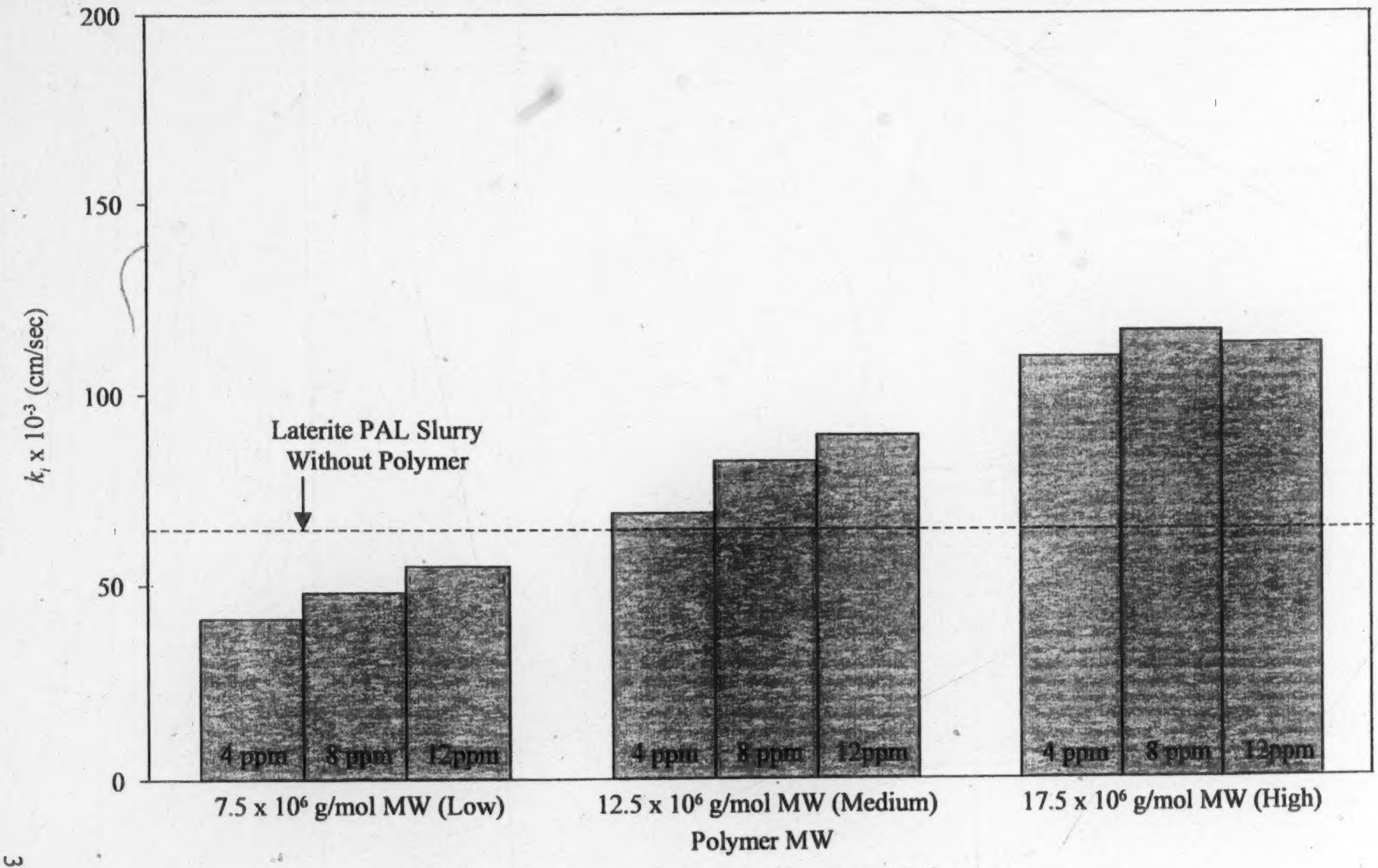

Figure 7.14: Effect of nonionic polymer parameters on k_i of laterite PAL slurry

The k_i of laterite PAL slurry without polymer modification measured 64 x 10^{-3} (cm/sec) as reported in Chapter Five. A comparison of this value with the data depicted in Table 7.2 reveals that nonionic polymer modification does not necessarily improve k_i of the material. Due to electrostatic charge repulsion, 7.5 x 10^6 g/mol MW (low) polymer results in k_i reduction. Although, an improvement of almost two times is obtained, variability among measured values of various polymer MW is not as extensive as observed earlier for ionic polymers.

The operative mechanism for nonionic polymer flocculation is hydrogen bonding. Under acidic conditions, nonionic polymers display a slight cationic charge due to partial protonation of the amide group, which is the basic building block of these polymers. According to Briceno & Osseo-Asare (1995c), acrylamides attract protons in acidic media due to the fact that these polymers display weak base properties. Such partial positivity of the nonionic polymer results in hydrogen bonding between the negatively charged double layer around the particles and the polymer. Further, mutual electrostatic repulsion between adjacent protonated amide groups results in stretching out of the polymer into solution. This results in enhanced flocculation as the polymer chain length is increased with increasing polymer MW.

Figure 7.14 indicates that an increase in either the molecular weight (MW) and/or dosage of the nonionic polymers improves k_i of laterite PAL slurry. This is due to increased adsorption and flocculation according to the above mechanism. Conversely, the k_i reduction is attributed to the development of bimodal size distribution occurring at high MW polymers (Hogg 1999).

7.3.3.3 Morphology

Figure 7.15 shows the morphology of the laterite PAL slurry modified with 12.5 x 10^6 g/mol (medium) polymer MW-08 ppm of nonionic polymer. Micrograph (a) shows a rough specimen with two surfaces separated by a cut. Micrograph (b) shows a compact clay microstructure with some silts size grains. Micrograph (c) illustrates the presence of some channeling and a flocculated clay structure. Micrograph (d) shows that the pore spaces in the clay fabric have uniform size and distribution. This micrograph also indicates some tortuousity, which is responsible for the moderate k_i increase (83 x 10^{-3} cm/sec) of this specimen. Although, no tubular arrangement is observed, the apparent porosity depicted in this fabric is not very different from that given in Figure 7.11 for the 75% charge (high)-17.5 x 10^6 g/mol (high) MW-04 ppm (low) dosage of cationic polymer. The k_i of that sample measured 85 x 10^{-3} cm/sec.

7.3.3.4 Statistical Analysis

Using –1 for 7.5 x 10^6 g/mol (low), 0 for 12.5 x 10^6 g/mol (medium) and +1 for 17.5 x 10^6 g/mol (high) polymer MW and –1 for 4 ppm, 0 for 8 ppm and +1 for 12 ppm polymer dosage, equation (7.1) estimated the k_i depicted in Figure 7.16. This figure shows that the results of statistical analysis for nonionic polymers correlate reasonably well with those of the ionic polymers for measured data above 70 x 10^{-3} cm/sec. Although, a positive slope is obtained for the nonionic polymer relationship, this relationship is almost flat compared with the 45° slope for ionic polymer modification.

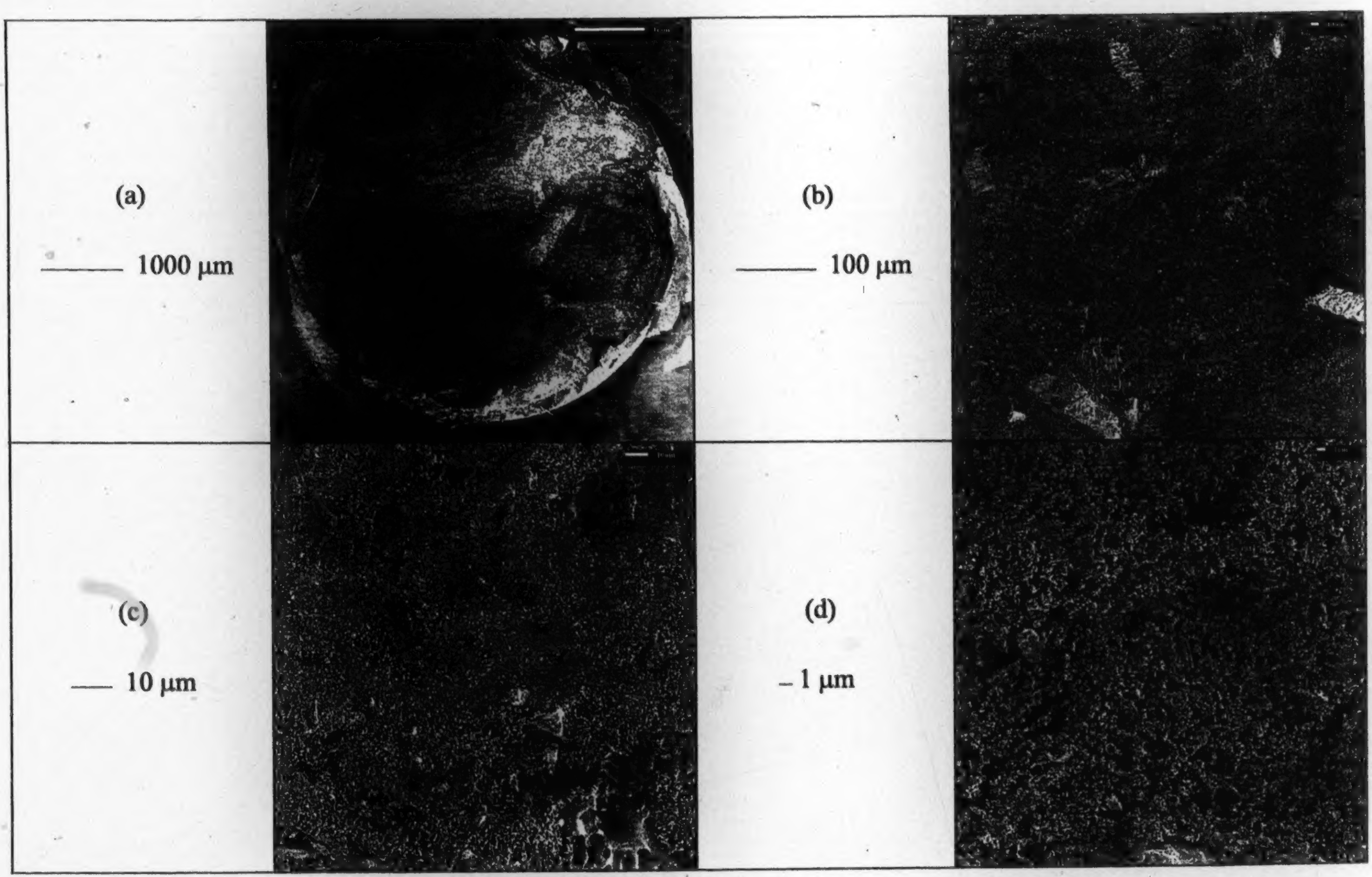
(a)
1000 µm
(b)
100 µm
(c)
10 µm
(d)
1 µm

Figure 7.15: SEM of laterite PAL slurry modified with 12.5 x 10^6 g/mol (medium) MW-08 ppm (medium) nonionic polymer

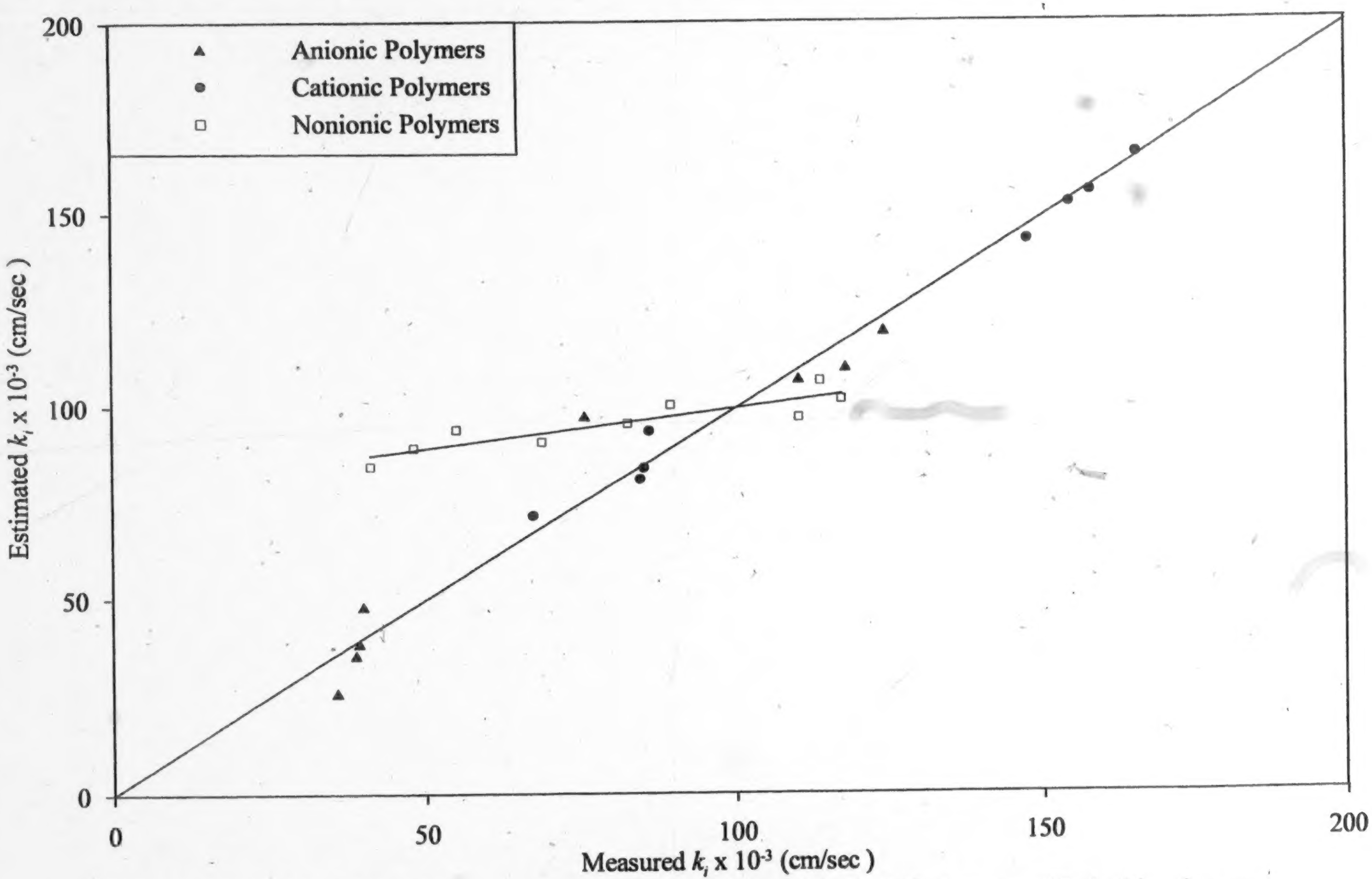

Figure 7.16: Relationship between measured and estimated k_i of laterite PAL slurry modified with polymers

7.4 CONSOLIDATION

7.4.1 General

The interaction between synthetic polymers, solid particles and the pore fluid was highlighted in the section on sedimentation. This section aims at understanding the significance of such interactions during load application. First, the solid-liquid separation behavior of laterite PAL slurry modified with ionic polymers is described. These results are then combined with those of the nonionic polymer modification. In each case, consolidation test results are depicted in the form of *log k-e* and *e-log* σ' relationships; both relations are then statistically analyzed.

7.4.2 Ionic Polymers

7.4.2.1 General

Four consolidation tests were conducted on laterite PAL slurry modified with ionic polymers. Results of these tests are depicted in Figures B.8 through B.15 given in Appendix B. For each test, results are depicted in the form of interface height versus elapsed time and hydraulic conductivity versus elapsed time. Table B.5 gives the solids content at the start and the end of the various consolidation tests.

Consolidation test results indicate that the solid-liquid separation of laterite PAL slurries modified with ionic polymers is predominantly composed of sedimentation. For all tests, the solid-liquid interface moved from an initial height of 9.5 cm to a final height of up to 2.6 cm under self-weight and up to 2.2 under a maximum stress of 9.0 kPa. This means that in a total height variation of 7.3 cm during the tests, the part due to sedimentation amounts to 95% and that due to consolidation is only 5%. Such a high solid-liquid separation during sedimentation is mainly attributed to the high specific gravity of the laterite PAL material, discussed in Chapter Five.

Polymer modification results in flocculation of laterite PAL materials thereby causing additional dewatering due to the development of large and heavy flocs. In the section on sedimentation, it was observed that modification of laterite PAL slurries with ionic polymers does not necessarily result in k_i increase. In the current section, it is observed that such modification invariably results in a higher amount of dewatering under self-weight. Therefore, polymer selection should be based on both the rate and the amount of solid-liquid separation.

The improved dewatering under self-weight is attributed to the development of soil morphology during sedimentation. At the initial part of sedimentation (used for k_i determination), soil morphology undergoes minimal variation and the soil containing entrapped water settles as one mass (Pane & Schiffman 1997). During the transition stage, soil morphology undergoes considerable changes as colloid-polymer-electrolyte interactions are progressively overcome by effective stresses. A dense morphology is envisaged when the slurry is converted to a soil sediment. Such a morphology is characterized by channels and/or hairline cracks between adjacent dense soil minifabrics. These discontinuities allow an easy and generally identical water escape during the latter part of sedimentation.

Hydraulic conductivity test results (given in Appendix B) indicate that flow through the samples was not constant but decreased with time and reached a steady state within 30 minutes. The drop in flow from an initial to a steady state value decreased with increasing stress. This is attributed to the diminishing physical changes in the specimen with decreasing void ratio. Olsen et al. (1985), suggested that such time-dependent flow can be due to one ore more of the following reasons: (a) undissolved air in the equipment and/or specimen; (b) equipment compliance depending on fabrication material and applied gradients; (c) inertia required to move the pore fluid; and (d) time-dependent changes in pore space distribution. Using identical equipment and test conditions for Alberta oil sand tailings, Suthaker & Scott (1996) showed that the last reason is the most likely cause of the observed time-dependent flow. These authors concluded that this transient phenomenon is repeatable and that the initial conditions are reattainable. Therefore, the steady state value was taken as the hydraulic conductivity and used in the analysis during this research.

7.4.2.2 Hydraulic Conductivity-Void Ratio

Figure 7.17 gives the *log k-e* relationships for both anionic and cationic polymer modification. Table 7.3 summarizes the A and B parameters obtained from these relationships. Figure 7.18 combines *log k-e* relationships for all ionic polymer modification and compare these with the laterite PAL slurry without polymer. Figure 7.19 explains the results by highlighting the effect of hydraulic gradient (*i*) on the hydraulic conductivity.

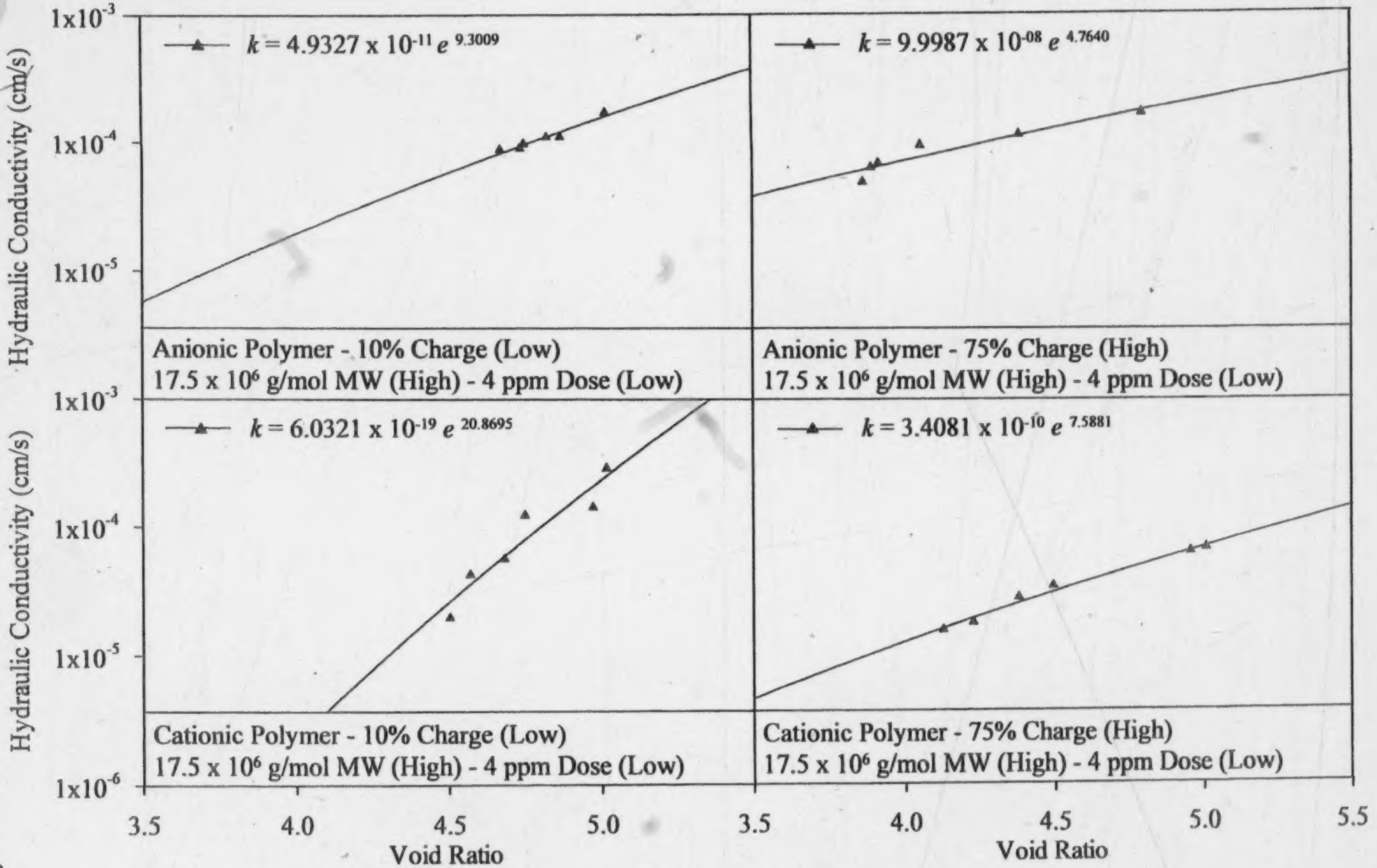

Figure 7.17: *k-e* relationships for laterite PAL slurry modified with ionic polymers

Table 7.3: *log k-e* parameters for laterite PAL slurry modified with ionic polymers

Polymer Parameters				A	B
Type	Charge	MW x 10^6 (g/mol)	Dose (ppm)		
Anionic	10% (Low)	7.5 (Low)	4	-----	-----
			12	-----	-----
		17.5 (High)	4	4.9×10^{-11}	9.3
			12	-----	-----
	75% (High)	7.5 (Low)	4	-----	-----
			12	-----	-----
		17.5 (High)	4	1.0×10^{-07}	4.8
			12	-----	-----
Cationic	10% (Low)	7.5 (Low)	4	-----	-----
			12	-----	-----
		17.5 (High)	4	6.0×10^{-19}	20.9
			12	-----	-----
	75% (High)	7.5 (Low)	4	-----	-----
			12	-----	-----
		17.5 (High)	4	3.4×10^{-10}	7.6
			12	-----	-----

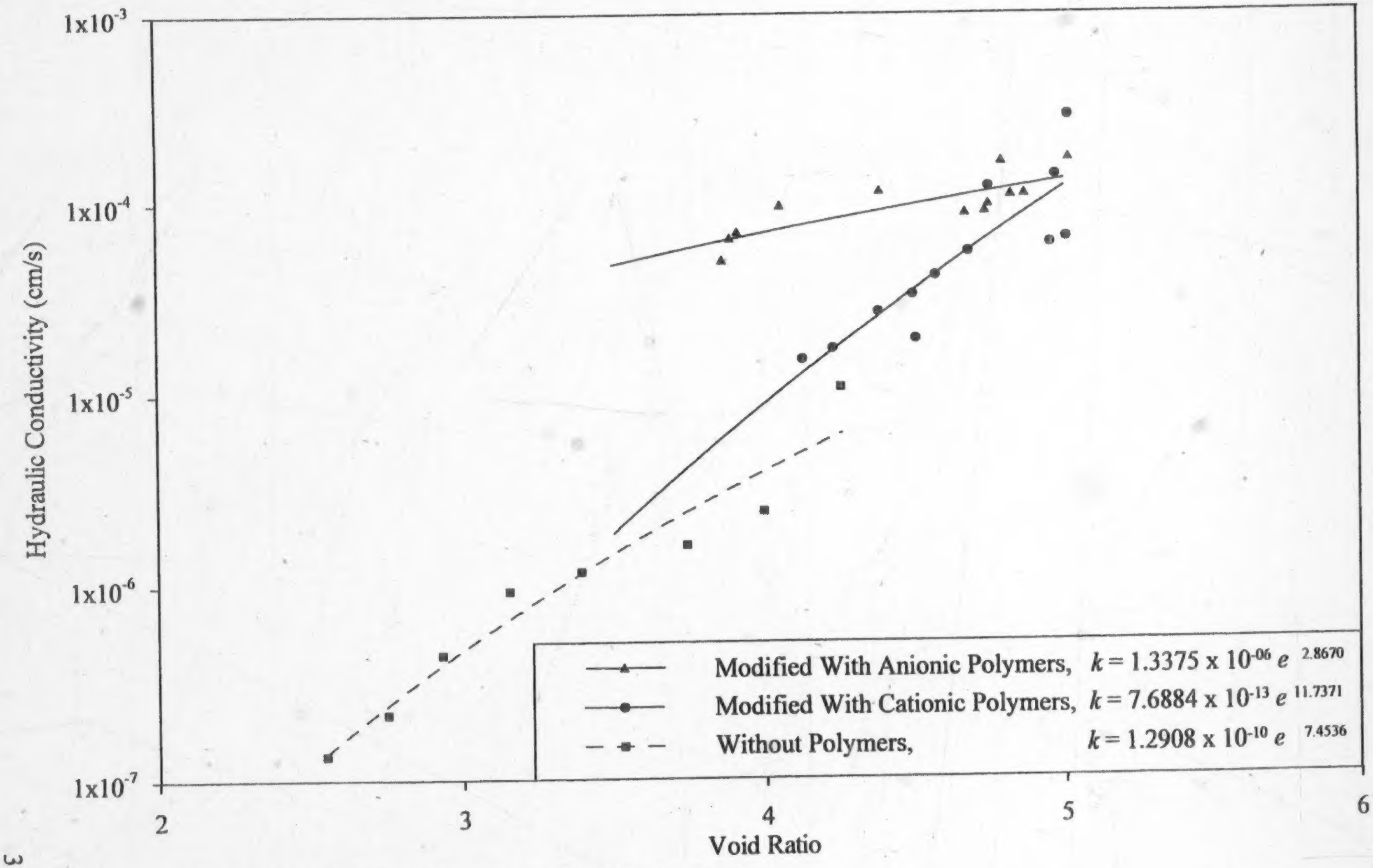

Figure 7.18: *k-e* relationships for laterite PAL slurry

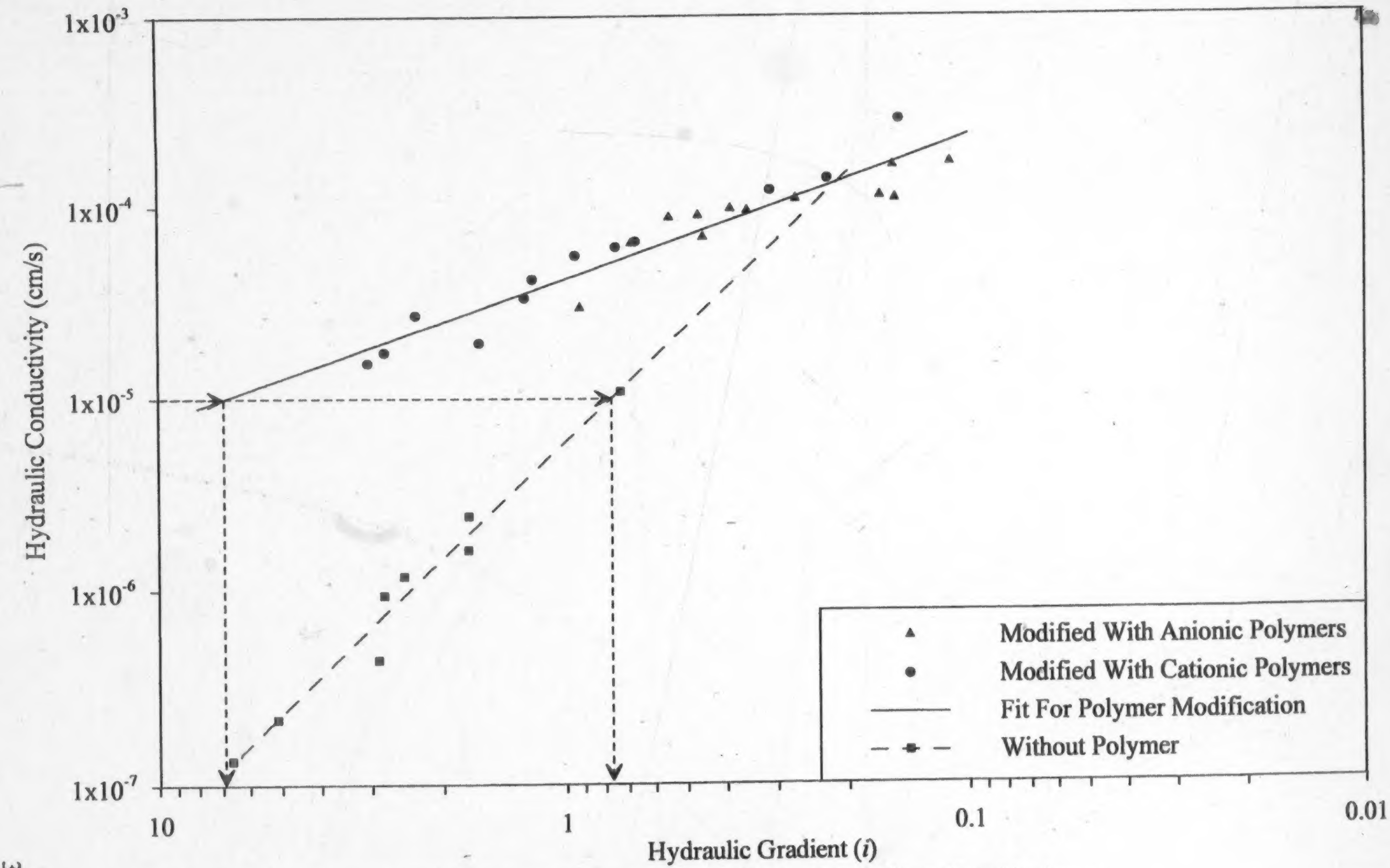

Figure 7.19: Effect of hydraulic gradient on hydraulic conductivity of laterite PAL slurry

Figure 7.17 gives the hydraulic conductivity-void ratio relationships of laterite PAL slurry modified with variable charge but identical polymer MW and dosage. The constant polymer MW and dosage were 17.5 g/mol (high) and 4 ppm (low), respectively; polymer charges were 10% (low) and 75% (high). The figure shows that polymer modification affects the hydraulic conductivity during the consolidation stage. This means that although colloid-polymer-electrolyte interactions decrease as the slurry is converted to a sediment, these interactions still govern the solid-liquid separation behavior of laterite PAL materials.

Table 7.3 summarizes the A and B parameters of the *log k-e* relationships for all ionic polymer modifications. The large variation in parameter A depicted in this table shows that the *log k-e* relationships for the laterite PAL slurry modified with ionic polymers mainly depend on this parameter This table indicates difference between anionic and cationic polymers. For the former polymers, variations in parameter A amounts to four orders of magnitude whereas parameter B varies between 4 and 10. Similarly, for cationic polymers, parameter A and B varies by nine orders of magnitude and between 7 and 21, respectively. Further, the A and B parameters for the laterite PAL slurry without polymers, were 1.2908×10^{-10} and 7.4536, respectively. These values for the laterite PAL slurry without polymers appear to be not very different from the data depicted in this table. However, a comparison of the different materials has to be made to identify the variation in behavior.

Figure 7.18 combines the results of both anionic and cationic polymer modification and compares these with the PAL slurry without polymer. This figure shows that ionic polymer modification results in an increase in the hydraulic conductivity of laterite PAL slurry. For these polymers, hydraulic conductivity is the same at a void ratio of about 5.0. However, as the void ratio is reduced, the hydraulic conductivity of the two materials varies and one order of magnitude difference is noted at a void ratio of 4.0. In general, the hydraulic conductivity of the laterite PAL slurry modified with ionic polymers is higher than that modified with cationic polymers. Further, the laterite PAL slurry modified with cationic polymers is a continuation of the laterite PAL slurry without polymers.

The observed behavior of laterite PAL slurry modified ionic polymers during consolidation is opposite to that observed during sedimentation. This is attributed to channel formation in the former slurries. Such channels are more pronounced in anionic polymer modified laterite PAL slurries due to a lower degree of flocculation achieved by these materials during the initial stages of sedimentation. This means that the loosely bonded small flocs get detached under small loads and develop channels and hairline cracks, which govern the hydraulic conductivity of these materials. On the contrary, laterite PAL slurry modified with cationic polymers is characterized by tightly bonded large flocs. Hydraulic conductivity of these latter materials is governed by the release of entrapped water in the flocs; a slower process than flow through channels.

The continuation of the laterite PAL slurry modified with cationic polymers with that without polymers signifies identical pore distribution and tortuousity of the two materials. Hence, their hydraulic conductivity at a given void ratio is the same despite differing grain or floc distributions.

The effect of hydraulic gradient on hydraulic conductivity was studied by performing constant head tests after each load increment during consolidation. The gradient for each test was kept less than the critical gradient at which piping of the sample occurs. Figure 7.19 gives the variation of hydraulic conductivity with hydraulic gradient. This figure shows that the hydraulic conductivity of laterite PAL slurry decreases with an increase in the hydraulic gradient. At a gradient of less than 0.2, all materials have the same hydraulic conductivity in the range of 10^{-4} cm/sec. As the gradient is increased from 0.2, there is a change in the behavior between the laterite PAL slurry modified with ionic polymers and the one without polymers. Despite a nonuniform effective stress distribution at high gradients, this change explains the behavior of the two material types. A hydraulic conductivity of say 10^{-5} cm/sec requires a gradient of 7.0 for the former materials and only 0.75 for the latter. This is mainly attributed to the development of flocs due to polymer modification. These flocs contain entrapped water that can only be extracted at elevated hydraulic gradients. For polymers resulting in lower flocculation or bimodal size distribution, migration of fine un-flocculated soil particles occurs into pore throats (Suthaker & Scott 1996). This results in the development of channels thereby offering paths of least resistance to water flow.

Combining the results of sedimentation and consolidation help in selecting appropriate polymers for improving the hydraulic conductivity of laterite PAL slurries. Although anionic polymers result in a higher dewatering during consolidation, these polymers do not necessarily improve k_i during sedimentation. Conversely, cationic polymers result in good flocculation causing an increase in k_i during sedimentation but the newly developed flocs do not easily release the entrapped water during consolidation. In both cases, 10% charge (low) polymers are more effective in improving k_i than 75% charge (high) polymers. Therefore, 10% charge (low) cationic polymers are suitable candidates for optimizing the rate and the yield in the CCD thickeners. Based on the results given in the section on sedimentation, the two 10% charge (low) cationic polymers result in improving the k_i by more than twice. Based on economic considerations, a decision between the 7.5 x 10^6 g/mol MW (low) polymer and 17.5 x 10^6 g/mol MW (high) polymer can be made. For both of these polymers, the effect of polymer dosage on k_i improvement is not highly significant and hence, 4 ppm (low) of the selected polymer may be enough for desired results.

7.4.2.3 Void Ratio-Effective Stress

Figure 7.20 gives the void ratio-effective stress relationships for ionic polymer modification of laterite PAL slurries. Table 7.4 summarizes the C and D parameters obtained from these relationships. Figure 7.21 combines $e\text{-}\log \sigma'$ relationships for all ionic polymer modification and compares the results with PAL slurry without polymer.

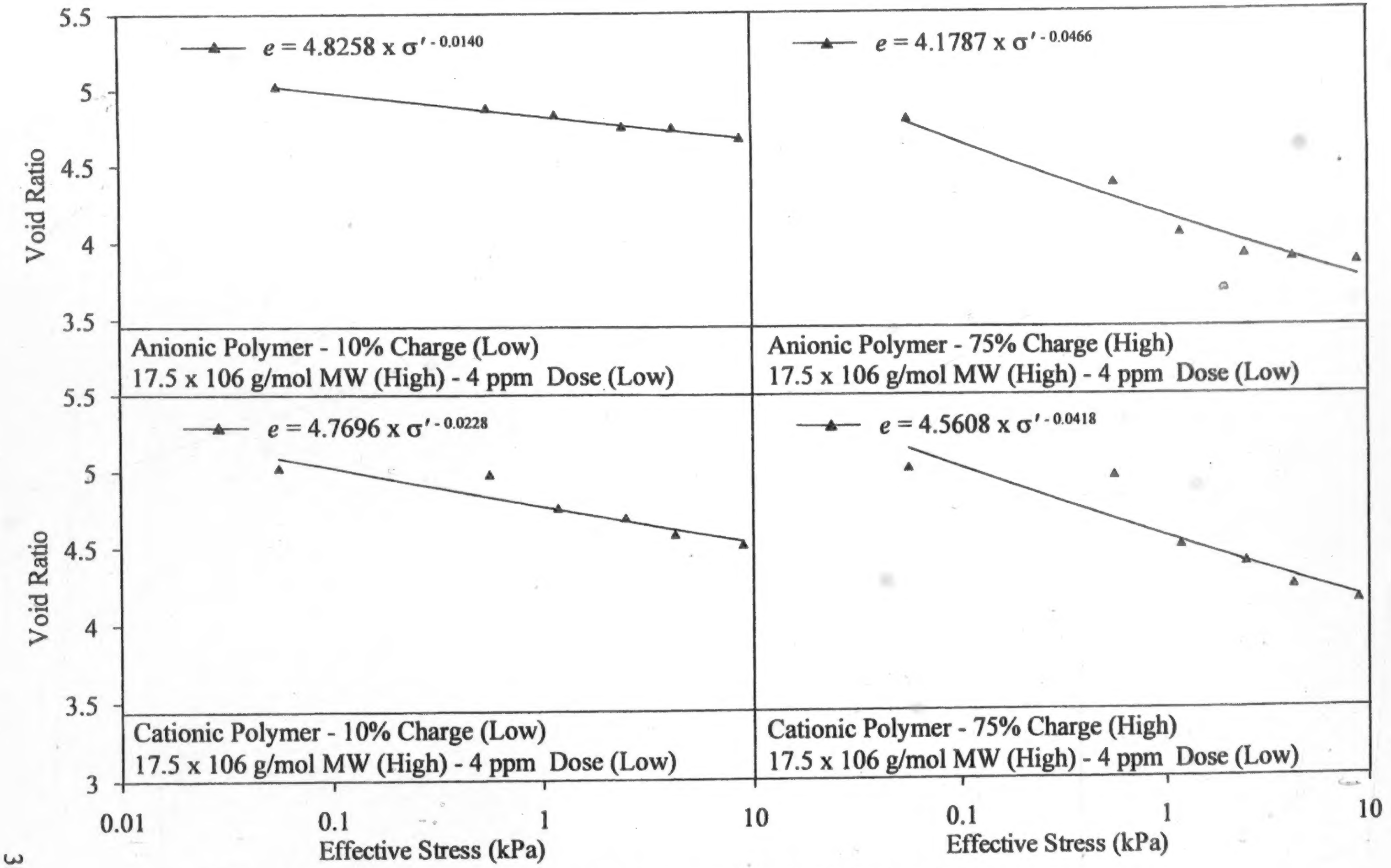

Figure 7.20: e-σ' relationships for laterite PAL slurry modified with ionic polymers

Table 7.4: *e-log* σ' parameters for laterite PAL slurry modified with ionic polymers

Polymer Parameters				C	D
Type	Charge	MW x 10^6 (g/mol)	Dose (ppm)		
Anionic	10% (Low)	7.5 (Low)	4	-----	-----
			12	-----	-----
		17.5 (High)	4	4.8	- 0.01
			12	-----	-----
	75% (High)	7.5 (Low)	4	-----	-----
			12	-----	-----
		17.5 (High)	4	4.2	- 0.05
			12	-----	-----
Cationic	10% (Low)	7.5 (Low)	4	-----	-----
			12	-----	-----
		17.5 (High)	4	4.8	- 0.02
			12	-----	-----
	75% (High)	7.5 (Low)	4	-----	-----
			12	-----	-----
		17.5 (High)	4	4.7	- 0.04
			12	-----	-----

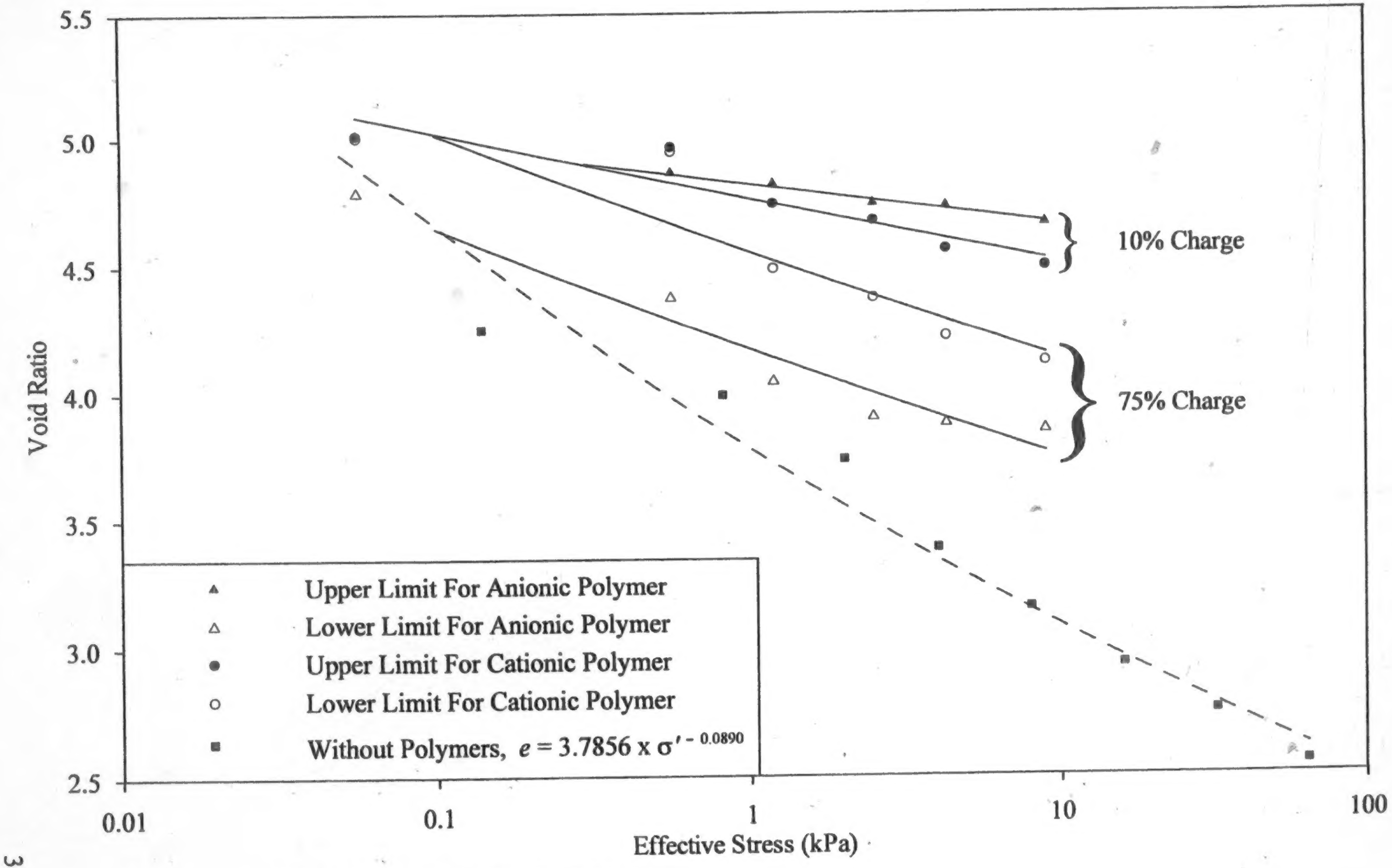

Figure 7.21: e-σ' relationships for laterite PAL slurry

Figure 7.20 gives the void ratio-effective stress relationships of laterite PAL slurry modified with variable charge but identical polymer MW and dosage. The constant polymer MW and dosage were 17.5 g/mol (high) and 4 ppm (low), respectively; polymer charges were 10% (low) and 75% (high). The figure shows that polymer modification affects the compressibility of the material during the consolidation stage. This means that although colloid-polymer-electrolyte interactions decrease as the slurry is converted to a sediment, these interactions still affect the solid-liquid separation behavior of laterite PAL materials.

Figure 7.20 shows that polymers with 10% charge (low) are less compressible than those with 75% charge (high). The former materials decrease from a void ratio of 5.0 at an effective stress of 0.05 kPa to a maximum of about 4.5 at 9.0 kPa. For identical values of effective stress, the void ratio changes from 5.0 to just under 4.0 for polymers with 75% charge (high). This means that the polymers with 75% charge (high) are twice compressible than those with 10% charge (low) under the low effective stress of 9.0 kPa.

The compressibility of the polymer modified laterite PAL slurries is attributed to the type of flocculation. For the 10% charge (low) polymers, equal size flocs are formed during the initial stages of sedimentation resulting in a higher k_i. Conversely, bimodal size distribution and the associated lower k_i was observed for the 75% charge (high) polymers during sedimentation. The smaller flocs fit between the larger flocs thereby leading to a reduced void ratio. Further, this type of flocculation has the shortcoming of leaving behind a significant amount of unflocculated material. In the laterite PAL slurry, such materials are mainly hematite grains, which by virtue of their spherical nature slide past one another and lead to a further volume reduction.

Figure 6.20 indicates that the power law fits the observed data reasonably well and therefore explains the compressibility behavior of polymer modified laterite PAL slurries. Among all possible equations, this law was found to be the closest match with measured data. For similar fine-grained slurries such as the mature fine tails of Alberta oil sands, Suthaker (1995) showed that the power law is most appropriate.

Table 7.4 summarizes the C and D parameters of the *e-log*σ' relationships for all ionic polymer modifications. This table indicates that parameter C (intercept or position) is in the range of 4.2 and 4.8 whereas parameter D (slope or shape) varies between - 0.02 and - 0.05. This suggests that the position of the various polymer modified laterite PAL slurries is close but their shapes are different. For comparison, the C and D parameters for the laterite PAL slurry without polymer, were reported as 3.8 and - 0.09, respectively.

Figure 7.21 combines the results of both anionic and cationic polymer modification and compares these with the PAL slurry without polymer. This figure shows that all of the polymer modified slurries are less compressible than the PAL slurry without polymer. This is attributed to the difficulty in removing entrapped water from the flocculated materials at low effective stress. Figure 7.21 further indicates that instead of fits for anionic and cationic polymers, an upper and lower limit was obtained in each case. For both polymers, these limits occur at 10% charge (low) and 75% charge (high), respectively. It is interesting to note that most of the fits converge at an effective stress of 0.1 kPa. This is attributed to minimal changes in morphology during sedimentation. Significant morphological changes occur during the transition stage between sedimentation and consolidation. This highlights the influence of transition state on the solid-liquid separation behavior of laterite PAL slurries. Increasing the effective stress causes a redistribution of the flocs thereby decreasing the void ratio. The variation among different polymers portrays the degree (large flocs versus small flocs) and type (equal size flocs versus bimodal size flocs) of flocculation, and the effect of unflocculated spherical particles discussed, earlier in this section.

Figure 7.21 is used to assist in selecting appropriate polymers for improving the solid-liquid separation behavior of laterite PAL slurries. Based on hydraulic conductivity during sedimentation and consolidation, 10% charge (low) cationic polymers were selected. Although, these polymers result in a low compressibility (difficult water removal) during consolidation, these should still be selected. This selection is made because of two considerations: (a) the low expected effective stress in the CCD thickener, and (b) the negligible variation in compressibility at low effective stresses.

7.4.2.4 Statistical Analysis

The data given Table 7.3 was used to obtain hydraulic conductivity at different void ratios. Based on the results of sedimentation tests, it was assumed that the fit equations remain the same for the given polymer charge. Corresponding to each test, this generated a set of sixteen hydraulic conductivity values, which were statistically analyzed as before. Using the statistical equation obtained for each void ratio, estimated hydraulic conductivity values were obtained. The data is shown in Figure 7.22, which indicates that the relationship between the estimated and measured values is linear. Similarly, using the data given in Table 7.4 and conducting the above exercise for the void ratio-effective stress relationships yields Figure 7.23. Again, a linear relationship is obtained between the estimated and measured values.

The statistical equations were associated with P-values for each of the polymer parameters. Figure 7.24 gives the statistical significance of various polymer parameters on the solid-liquid separation of polymer modified laterite PAL slurry. This figure shows that the effect of polymer parameters is equally significant for both hydraulic conductivity and compressibility. The significance of various polymer parameters is high under initial conditions (high void ratios or low effective stress) and decreases with load application. For both cases, the significance decrease is highest for polymer type followed by polymer charge; molecular weight and dosage are insignificant factors in the solid-liquid separation behavior of laterite PAL slurries.

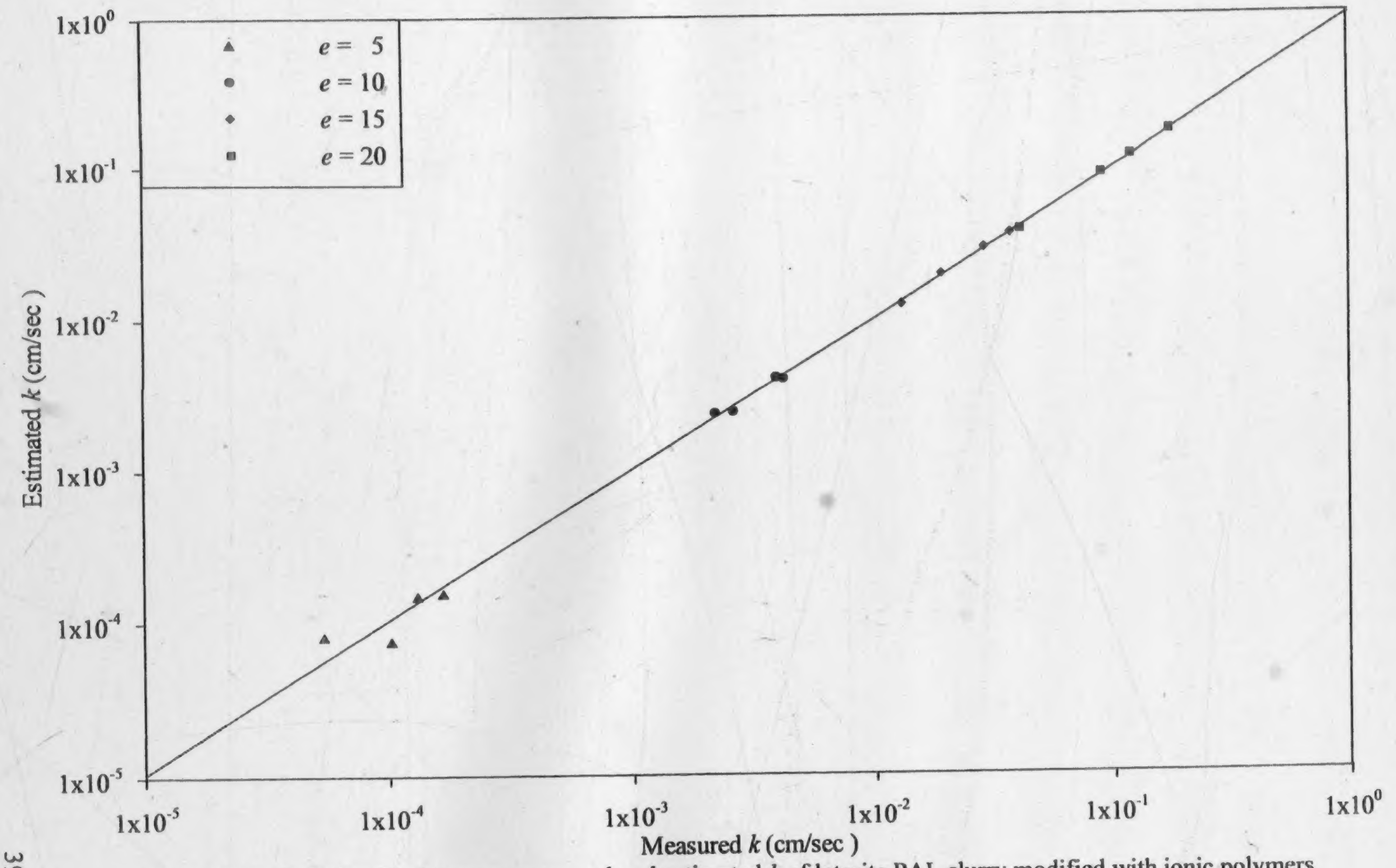

Figure 7.22: Relationship between measured and estimated k of laterite PAL slurry modified with ionic polymers

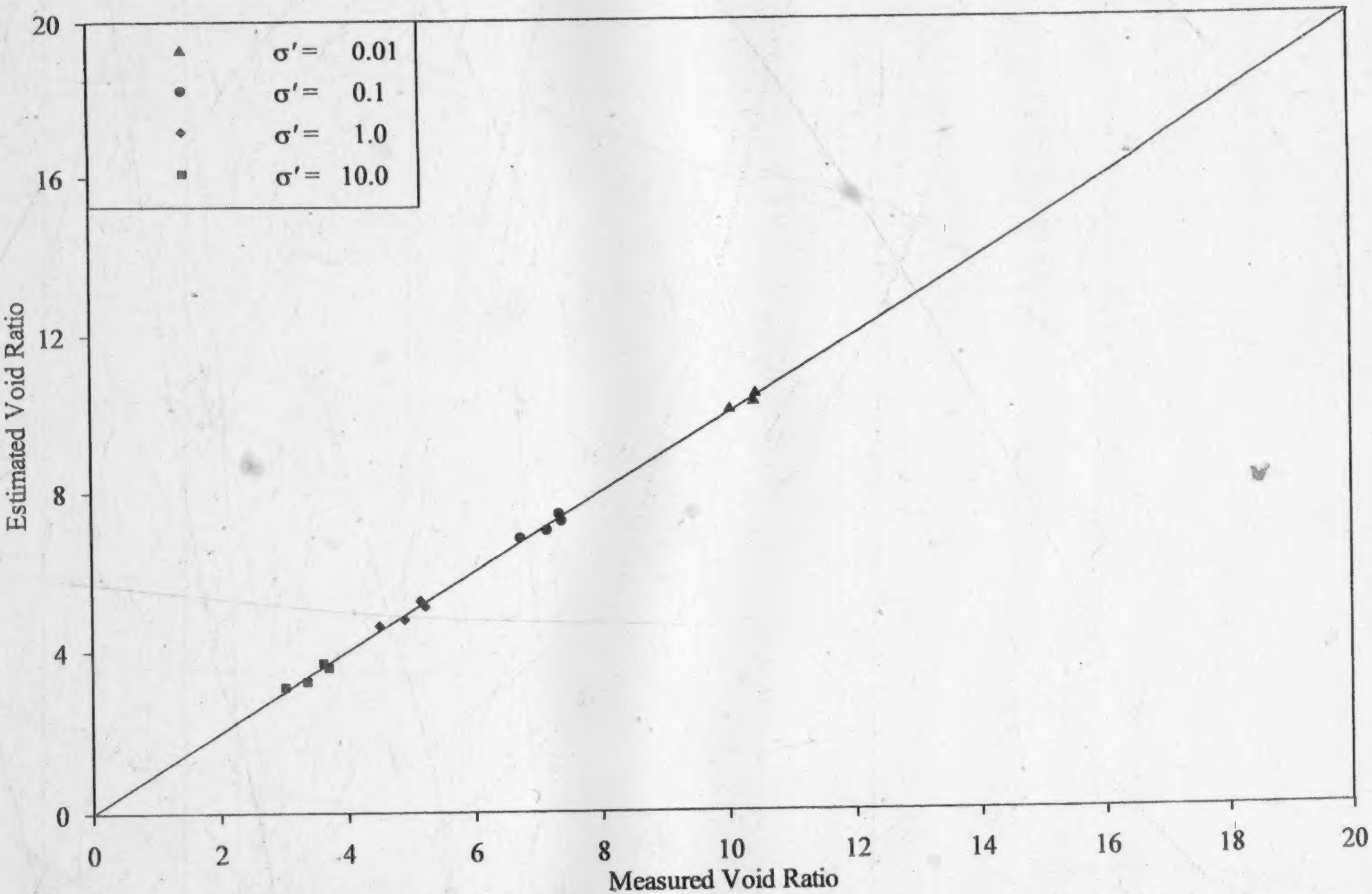

Figure 7.23: Relationship between measured and estimated *e* of laterite PAL slurry modified with ionic polymers

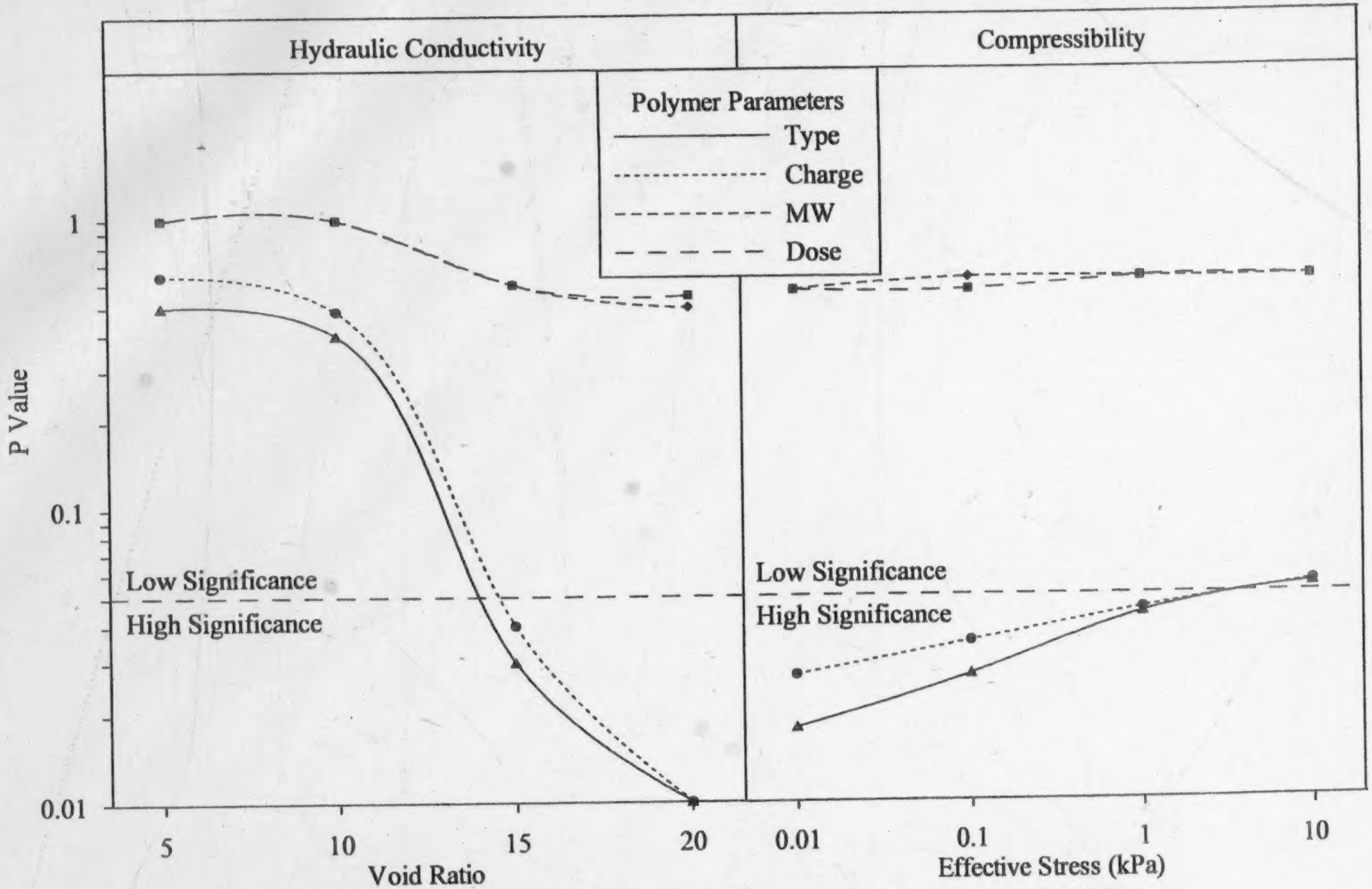

Figure 7.24: Significance of polymer parameters on solid-liquid separation of laterite PAL slurry

7.4.3 Nonionic Polymers

7.4.3.1 General

One consolidation test was conducted on laterite PAL slurry modified with nonionic polymer. The polymer parameters for the selected polymer were 12.5 x 10^6 g/mol MW (medium) and 8 ppm dosage (medium). Results of this test are depicted in Figure B.16 and Figure B.17, given in Appendix B. These results are depicted in the form of interface height versus elapsed time and hydraulic conductivity versus elapsed time, respectively. Table B.6 gives the solids content at the start and the end of the consolidation test.

Consolidation test results of Figure B.16 indicate that the solid-liquid separation of laterite PAL slurries modified with nonionic polymers is predominantly composed of sedimentation. The solid-liquid interface moved from an initial height of 9.5 cm to a final height of up to 1.8 cm under self-weight and up to 1.6 under a maximum stress of 9.0 kPa. This means that in a total height variation of 7.9 cm during the tests, the part due to sedimentation amounts to 97% and that due to consolidation is only 3%. Similarly, hydraulic conductivity test results given in Figure B.17 indicate that although flow through the sample decreased with time, a steady state was achieved well before 30 minutes. This means that the investigated nonionic polymer is more efficient than both anionic and cationic polymers. In general, the test data of laterite PAL slurry modified with nonionic polymer follows the same trends of those modified with ionic polymers.

7.4.3.2 Hydraulic Conductivity-Void Ratio

Figure 7.25 give the hydraulic conductivity-void ratio relationship for nonionic polymer modification of laterite PAL slurry. A comparison of this material with ionic polymer modification and the PAL slurry without polymer is also given in this figure. This figure shows that the nonionic polymer results in a higher hydraulic conductivity during consolidation. This is attributed to the preclusion of polymer charge that was observed to be one of the two significant influencing factors for ionic polymer modification. The absence of polymer charge leads to the formation of loosely bonded flocs, which are easy to break upon load application. This liberates the previously entrapped water in the flocs thereby results in a high hydraulic conductivity during consolidation.

7.4.3.3 Void Ratio-Effective Stress

Figure 7.26 give the void ratio-effective stress relationship for nonionic polymer modification and compares this relationship with those obtained for ionic polymer modification and the PAL slurry without polymer. This figure indicates that the curve for nonionic polymer modification plots below that of the ionic polymer modification and the PAL slurry without polymer. The higher compressibility of the nonionic polymer modified material is attributed to the phenomenon of floc separation discussed above. Such floc breakage results floc and grain readjustment upon loading during consolidation.

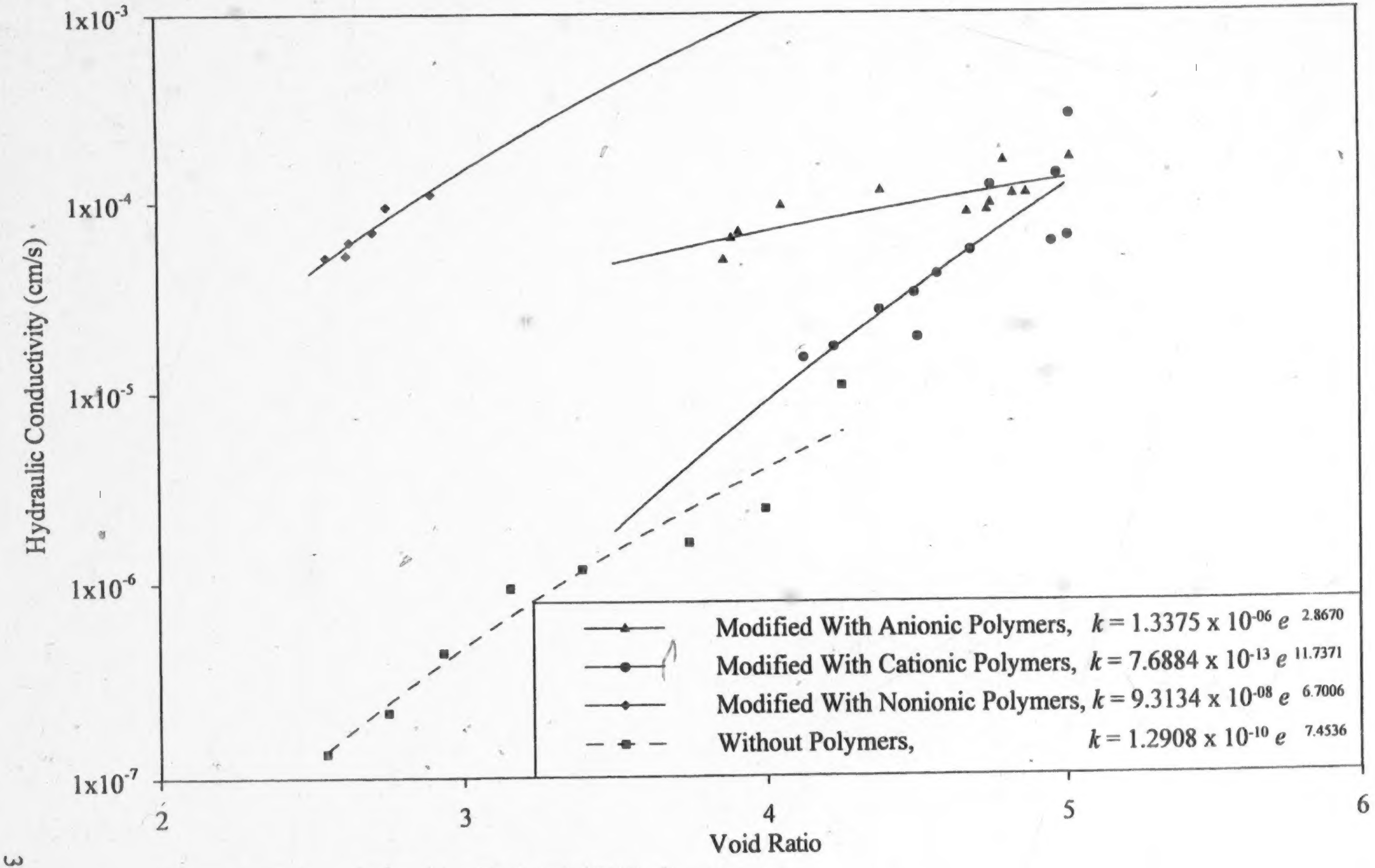

Figure 7.25: *k-e* relationships for laterite PAL slurry

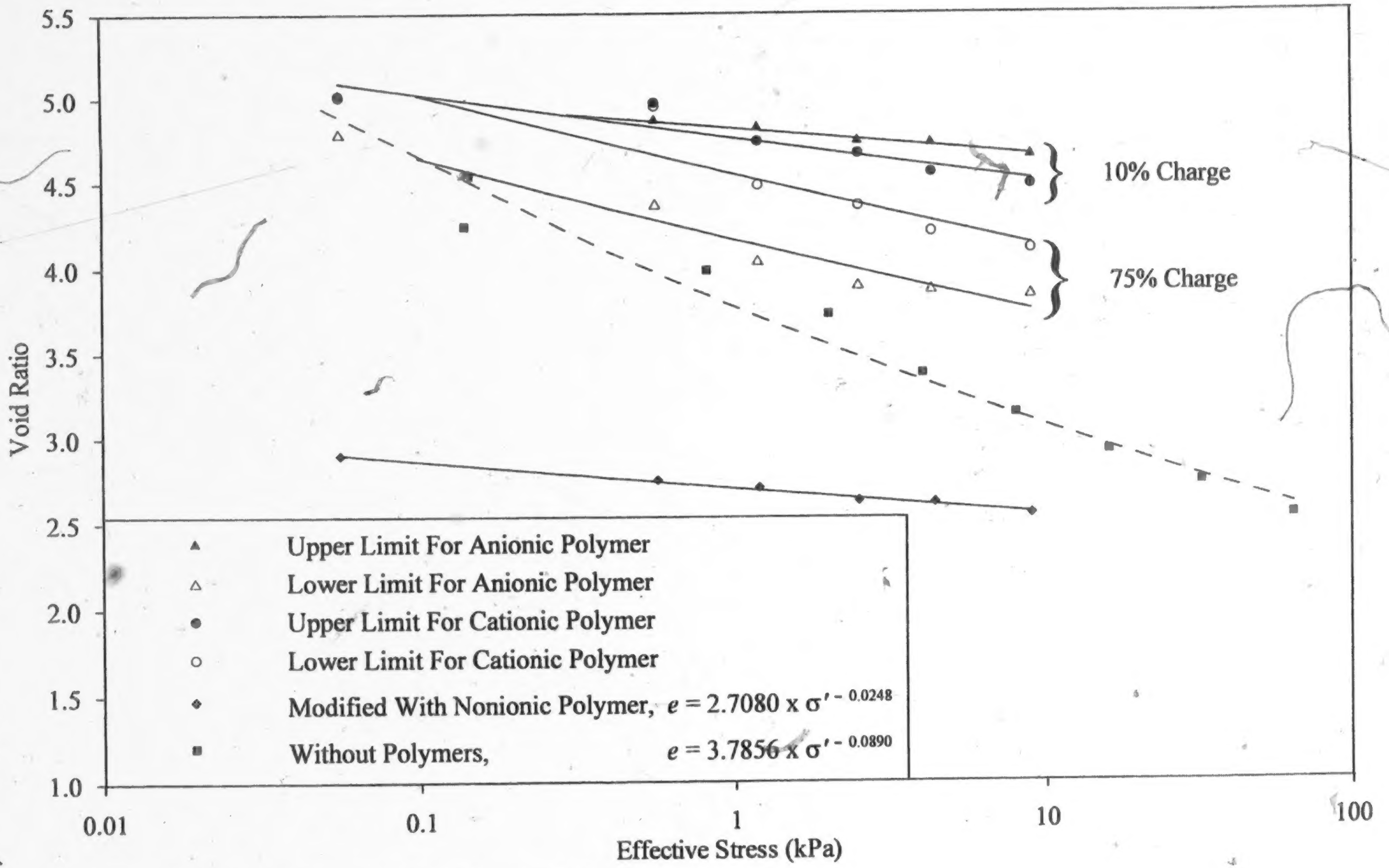

Figure 7.26: e-σ' relationships for laterite PAL slurry

Based on consolidation, nonionic polymer is the most appropriate candidate for modifying laterite PAL slurry. However, the k_i due to this polymer during sedimentation is only 83 x 10^{-3} cm/sec, which is about 30% higher than the PAL slurry without polymer. Such a low increase in k_i due to this polymer renders it less suitable for this application. Still, nonionic polymers with 17.5 x 10^{6} g/mol MW (high) may prove to be more promising owing to their better performance during sedimentation. Therefore, 10% charge (low) cationic polymers are best suited for laterite PAL slurry. Due to little variation in material characteristics, this conclusion is valid for most processes due to identical conditions in the CCD circuit.

7.4.3.4 Statistical Analysis

The *log k-e* and the *e-log σ'* relationships for the nonionic polymer modified laterite PAL slurry and the statistical equations obtained for ionic polymer modifications were used for the analysis described in this section. In the statistical equations derived for ionic polymers, all of the variables were given a value of zero corresponding to polymer parameters falling between the boundary values for ionic polymers. Figure 7.27 gives the relationships between the measured and estimated hydraulic conductivity for polymer modified laterite PAL slurry. Similarly, Figure 7.28 presents the relationship between the measured and estimated void ratio for polymer modified laterite PAL slurry. Both of these figures show that the fits for nonionic polymer modification are not very different from those of the ionic polymer modification.

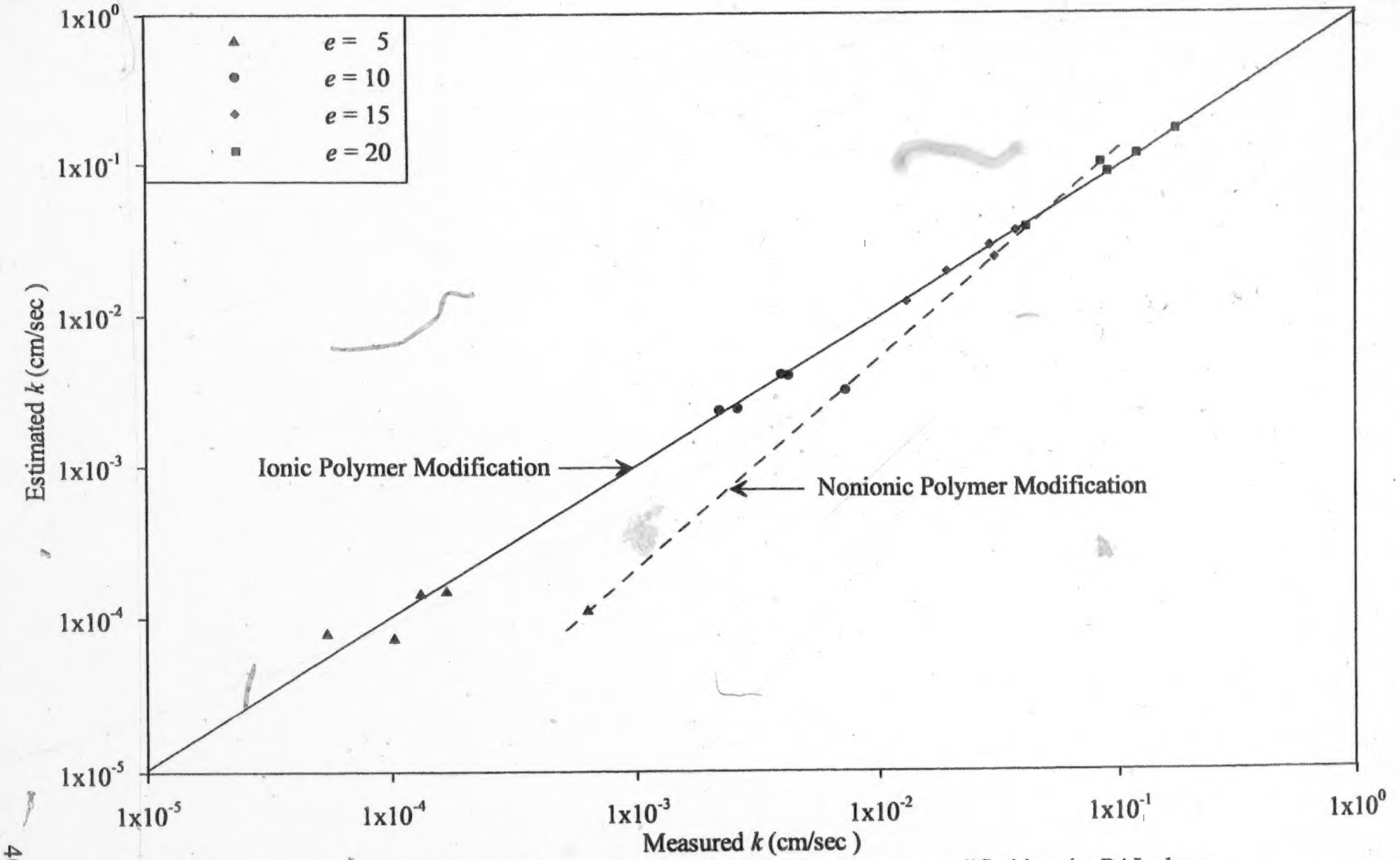

Figure 7.27: Relationship between measured and estimated *k* for polymer modified laterite PAL slurry

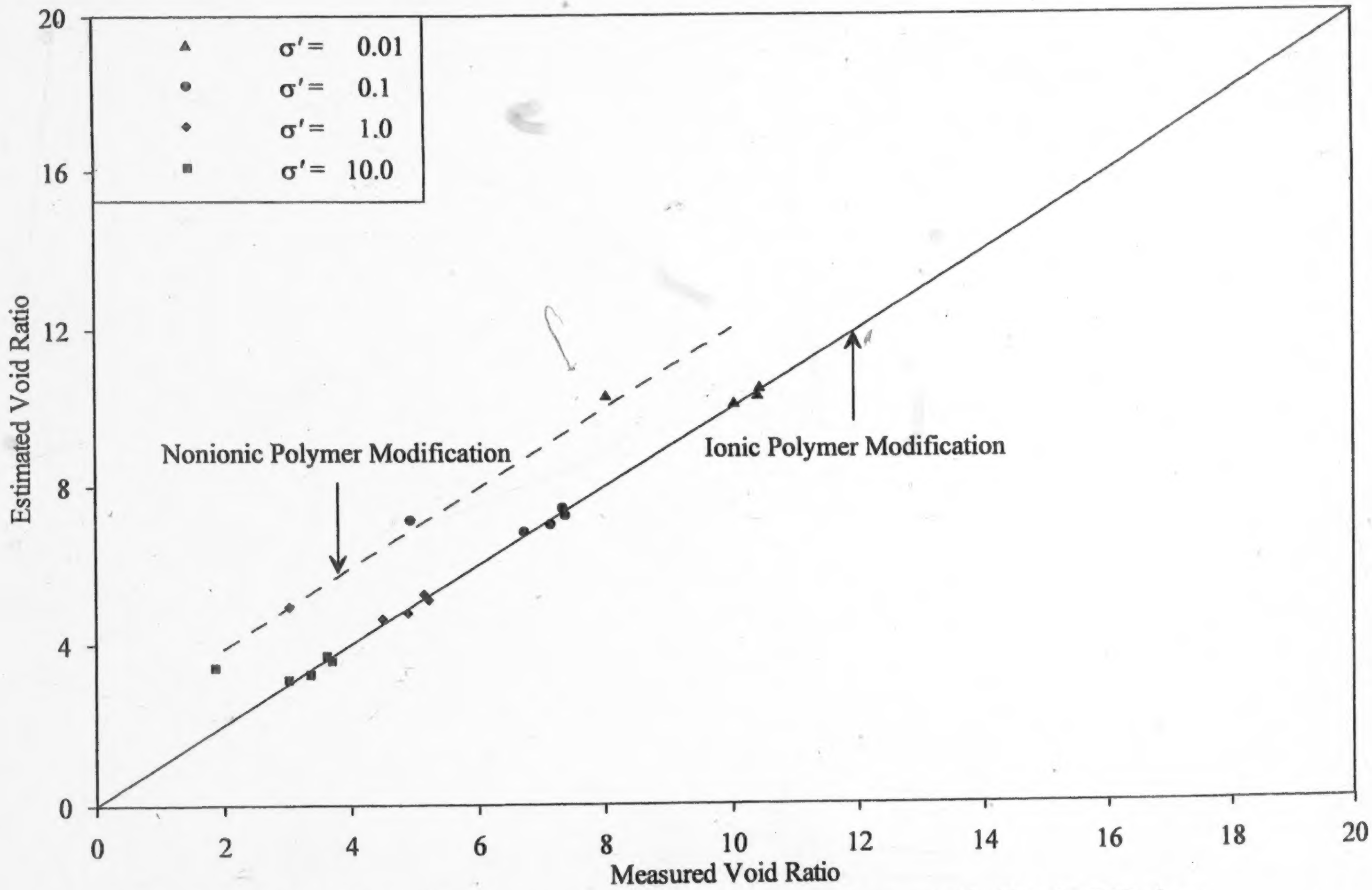

Figure 7.28: Relationship between measured and estimated *e* for polymer modified laterite PAL slurry

7.5 NUMERICAL SIMULATION

7.5.1 General

This section describes the performance prediction of laterite PAL slurry modified with synthetic polymers. The sedimentation and consolidation data depicted in previous sections are used to predict the solid-liquid separation behavior of laterite PAL slurry for a hypothetical CCD thickener. A comparison of the behavior of laterite PAL slurry without polymer is made with that modified with anionic, cationic and nonionic polymers.

7.5.2 Analyzed Data

The *log k-e* and the *e-log* σ' relationships summarized in Table 7.3 and Table 7.4 are used to extrapolate the behavior of laterite PAL slurry. For use in the consolidation program, data depicted in these two tables was converted to commensurate units and the transformed data was plotted to obtain the new fit parameters; the new units being m/min and Pa for *log k-e* and the *e-log* σ' relationships, respectively. Table 7.5 summarizes the parameters derived for these new units.

7.5.3 CCD Thickener

Figure 7.29 gives the predicted behavior of polymer modified laterite PAL slurry in a CCD thickener using the consolidation program SECO. Similarly, Figure 7.30 compares the predicted consolidation data with data predicted by the sedimentation program. For use in both of these programs, a 3.0 m height was chosen for the CCD thickener.

Table 7.5: Summary of analyzed data for laterite PAL slurry

Material	A	B	C	D
Without Polymer	1.0×10^{-10}	7.45	7.0	-0.09
Modified With Anionic Polymer (UL)*	3.0×10^{-11}	9.30	5.3	-0.01
Modified With Cationic Polymer (UL)*	4.0×10^{-19}	20.9	5.6	-0.02
Modified With Nonionic Polymer	6.0×10^{-08}	6.7	3.2	-0.03

* UL stands for Upper Limit

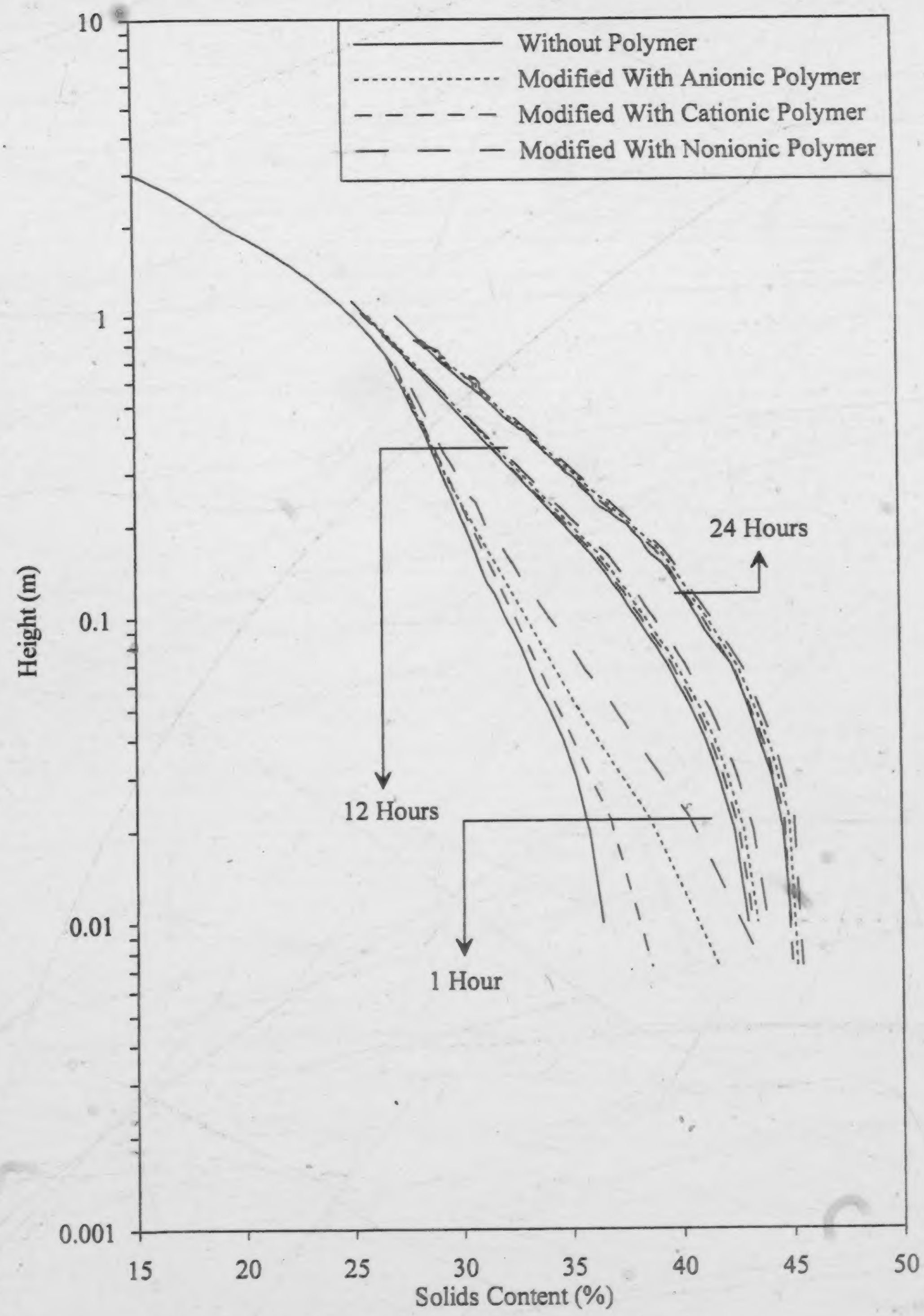

Figure 7.29: Predicted behavior in the CCD thickener

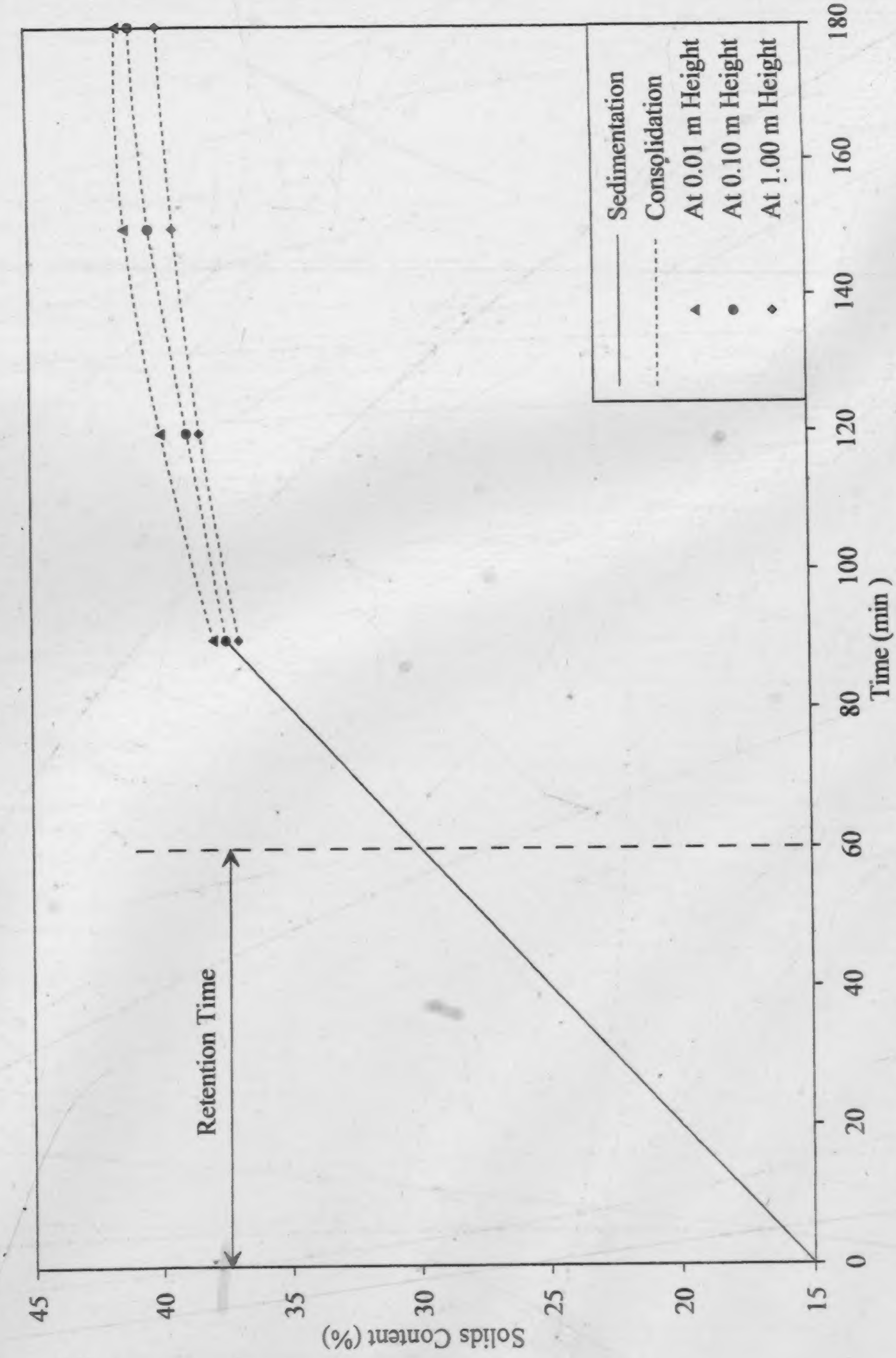

Figure 7.30: Performance of the selected polymer in the CCD thickener

Figure 7.29 gives the solids content profile in a 3.0 m CCD thickener at three points in time: 1, 12 and 24 hours. This figure was obtained by using the input parameters given in Table 7.5 in the sedimentation and consolidation program SECO described in Chapter Three. To highlight the solids content variation in the compaction bed of the CCD thickener, sediment height is plotted on a logarithmic scale in the figure.

Figure 7.29 indicates that the improvement in solids content of the PAL slurry due to polymer modification is initially high and gradually fades away with time. This is attributed to enhanced colloid-polymer-electrolyte interactions during the sedimentation stage of the solid-liquid separation process. Using consolidation parameters given in Table 7.5, improvement is highest for nonionic polymers, followed by anionic polymers and then cationic polymers. After 1 hour, the solids content increases from 35.4% for the PAL slurry without polymer to 43.6, 41.6, and 38.6% for modification with nonionic, anionic and cationic polymers, respectively. These values amount to 18, 9% and 23% improvements for the above selected polymers.

Figure 7.29 shows that the solids content profiles are similar to the PAL slurry without polymer; solids content increases both as a function of time and of depth in the thickener. The solids content profile has two smoothly joining straight-line components. The initial straight-line portion portrays increasing solids content with depth whereas the final straight-line part denotes constant solids content. Although the sediment starts developing during the initial stages of the solid-liquid separation process, a distinct compaction bed is observed only after 12 hours. The thickness of this compaction bed increases from 0.1 m after 12 hours to 0.2 m after 24 hours. This suggests the presence of a consolidation zone in the CCD thickener at prolonged durations.

Figure 7.30 depicts the performance of the selected polymer for optimum results during both sedimentation and consolidation. The chosen cationic polymer had 10% charge (low), 17.5 x 10^6 g/mol MW (high) and 4 ppm dosage (low). This figure compares the predictions of the two programs: (a) sedimentation and (b) sedimentation and consolidation. Since, parameters based on consolidation data were used, the program only predicted the consolidation behavior. The figure shows a straight-line increase in solids content during sedimentation that is complete in 90 minutes. Taking this time as the start of consolidation, the predictions of the latter program indicate a slow increase in solids content. This procedure minimizes the *weak link* between sedimentation and consolidation reported by the developers (Masala & Chan 2001) and makes the predictions of the two programs in close conformity. The figure illustrates that at a typical retention time of 60 minutes, sedimentation is the dominant phenomenon during the solid-liquid separation process. Some additional improvement in solids content can be achieved during consolidation.

The predicted behavior gives a idea about the range of possible improvement. Given the operational constraints of the metal extraction process such as time, thickener geometry, and the preclusion of load application, the solid-liquid separation behavior of laterite PAL slurry can be improved using synthetic polymers. Effective improvement depends upon the choice of polymer parameters for the given mineralogy and pore water chemistry. Under self-weight, improvement due to polymer modification is highest initially and gradually diminishes. Sedimentation is the governing phenomenon during the solid-liquid separation process of polymer modified laterite PAL slurries.

7.6 LATERITE SLURRY CHARATERISTICS DIAGRAM

Figure 7.31 gives the hydraulic conductivity of the polymer modified laterite PAL slurry on the ternary diagram and compares the same with data for the PAL slurry without polymer. The laterite slurry characteristics diagram shows that similar to the laterite PAL slurry without polymer, the hydraulic conductivity of polymer modified materials is part of the family of constant clay-water ratio lines. This is because these lines denote colloid-polymer-electrolyte interactions.

The diagram indicates that the hydraulic conductivity of polymer modified laterite PAL slurries varies by one order of magnitude between the sedimentation limit ($k = 10^{-5}$ cm/sec) and the liquid limit ($k = 10^{-6}$ cm/sec). Earlier, it was observed that in comparison to the laterite PAL slurry without polymer, identical values of hydraulic conductivity for the polymer modified materials are obtained at higher solids content (low void ratio). Preceding discussions attributed this to variations in colloid-polymer-electrolyte interactions and the resulting morphology during the various stages of the solid-liquid separation process. Therefore, the ternary diagram highlights the significance of the constant clay-water ratio lines on the behavior of polymer modified laterite PAL slurries.

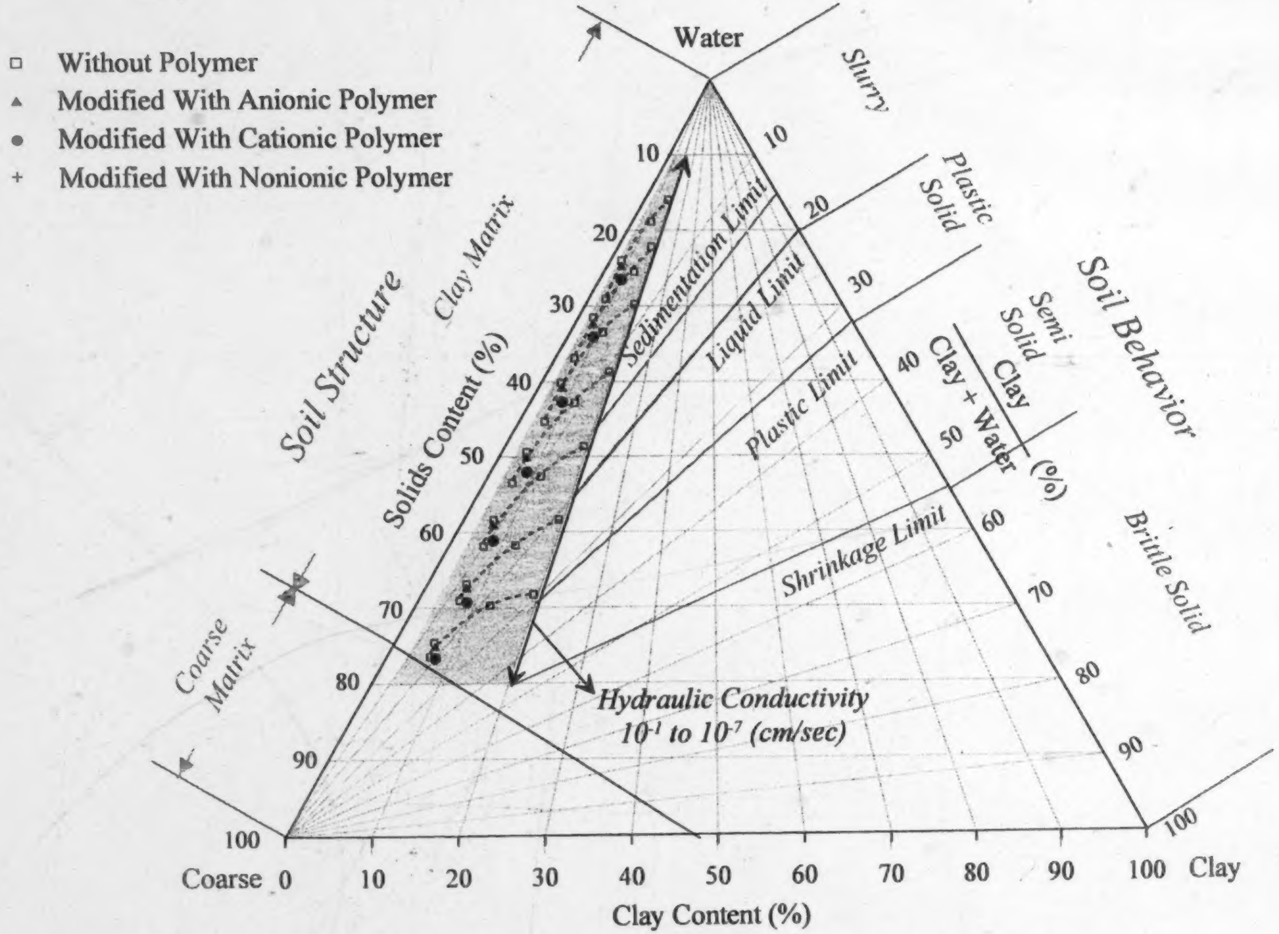

Figure 7.31: LSCD for polymer modified laterite PAL slurries

7.7 SUMMARY AND CONCLUSIONS

This chapter provided a detailed investigation of the polymer modified laterite PAL slurries. The influence of various polymer parameters (type, charge, MW and dosage) on the solid-liquid separation behavior of the selected laterite PAL slurry was investigated. Results of laboratory investigations pertaining to geotechnical index properties, sedimentation in conjunction with soil morphology and consolidation were presented. These data were statistically analyzed and used in two numerical simulation programs to predict the performance of the CCD thickener. The entire data were depicted on the laterite slurry characteristics diagram. The conclusions of this chapter can be summarized as follows:

- Polymer modification of laterite PAL slurries converts a *sand* like material to one similar to *clays*. These transformed materials generally adsorb a significant amount of water and are essentially nonsegregating.
- Anionic polymers generally k_i improve the hydraulic c 10% charge (low) results in k_i increase of two times for anionic polymers and 2½ times for cationic polymers. Conversely, a 75% charge (high) results in about 45% k_i decrease for the former and a 30% k_i increase for the latter polymers. Variations in polymer MW and dosage are less significant.
- For nonionic polymers, a 7.5 x 10^6 g/mol MW (low) results in k_i decrease of up to 35%. At elevated MW of 12.5 x 10^6 g/mol (medium) and 17.5 x 10^6 g/mol (high), increase in k_i amounts to 40% and 80%, respectively. Increasing polymer dosage from 4 ppm (low) to 12 ppm (high) results in a k_i increase of up to 30%.

- The initial hydraulic conductivity of polymer modified PAL slurry strongly depends on soil morphology. Good flocculation, reduced tortuousity and the presence of channels or tubules are associated with high k_i.
- The performance of various synthetic polymers during consolidation is the opposite of that during sedimentation. High k_i polymers have lower hydraulic conductivity and compressibility during consolidation and vice versa. This is due the difficulty in removing the entrapped water from the flocs.
- Hydraulic conductivity during consolidation depends on the imposed hydraulic gradient as opposed to Darcy's law. A high gradient is required to extract water entrapped in the flocs whereas a low gradient is associated with flow through channels and low tortuousity.
- Compressibility during consolidation depends on the type of flocculation. Strong attachment between large and equal size flocs result in low compressibility and the reverse is true for loose bonding and bimodal size distribution.
- Polymer selection depends on optimizing efficiency (hydraulic conductivity) and yield (compressibility) of the extraction process. A cationic polymer with 10% charge (low), 17.5 x 10^6 g/mol MW (high) and 4 ppm dosage (low) is best suited to improve the solid-liquid separation of laterite PAL slurries.
- Sedimentation is the governing phenomenon for the solid-liquid separation of polymer modified laterite PAL slurries. During this stage, there is a maximum chance for colloid-polymer-electrolyte interactions to be displayed.

Chapter 8

Conclusions, Application, Recommendations

8.1 GENERAL

The pressure acid leaching process is the most widely used method for extracting economic metals from laterites. The solid-liquid separation of the laterite ore slurries prepared prior to leaching influences the efficiency of this method. Likewise, the solid-liquid separation of the laterite PAL slurries in the counter current decantation (CCD) circuit affects the yield. Given the increasing demand of Ni and Co, there was an exigent need to conduct a comprehensive and fundamental study of this class of materials. The main objective of this work was to understand and improve the solid-liquid separation of laterite slurries. The specific objectives included the following:

- To determine geotechnical index properties for preliminary soil assessment
- To study the effect of mineralogy and pore water chemistry on solid-liquid separation
- To investigate the influence of microstructure on solid-liquid separation
- To study solid-liquid separation behavior by determining sedimentation, consolidation and hydraulic conductivity properties

These objectives were achieved using the following framework:

- Understanding laterite slurry behavior under ambient process conditions
- Devising a polymer amelioration method for improved solid-liquid separation
- Developing a detailed laboratory characterization protocol
- Predicting field performance from laboratory data

This chapter first summarizes the methodology adopted during the current research that was described in detail earlier in Chapter Three. Then, it gives an account of the main observations and conclusions given earlier in Chapters Four through Seven. This is followed by highlighting the geotechnical significance as well as the field application of this research work. As is the case with many research undertakings, new venues for future work related to laterite ore and laterite PAL materials were discovered during the course of the current study. Some of the major discoveries are given as recommendations towards the end of this chapter.

8.2 RESEARCH METHODOLGY

- The research program comprised of laboratory investigations, statistical analysis, numerical simulation and data presentation using LSCD.
- Four types of samples were prepared: laterite ore and PAL samples and polymer modified ore and PAL samples.
- Four ore slurries were selected from various parts of the globe: Cuba, Philippines, Australia and Indonesia. The corresponding PAL slurries were obtained using identical process conditions during pressure acid leaching.
- Synthetic polymers were used to modify ore and PAL slurries of a selected type representing limonite-saprolite blend from the Philippines.
- Laboratory investigations comprised of geotechnical index properties, mineralogy, pore water chemistry, morphology, and solid-liquid separation.

- During laboratory investigations, significant modifications were adopted in testing techniques to suit laterite slurries.
- Heating was avoided in most cases but where absolutely necessary, an oven temperature of 50 °C was employed.
- Determination of specific gravity involved the use of vacuum for air removal and dry mass calculation after test completion.
- Grain size analyses were conducted on 25 g of dry soil using distilled water. The ores were dispersed with calgon whereas the PALs were not dispersed.
- Segregation tests involved solids content profiling with depth after 24 h in 150 mL graduated cylinders using different initial slurry solids contents.
- Consistency limits were determined by gradual drying of the high water content slurries at 50 °C; mixing time was restricted to five minutes.
- XRD analysis determined mineralogy of randomly oriented powdered samples with grain size distributions identical to those under ambient process conditions.
- Pore water composition was determined using routine methods. Due to negligible flocculant effects, detailed water chemistry was not investigated for polymer modified slurries.
- Morphology was determined using SEM analysis on slurry samples prepared by the cryogenic technique that ensured an intact fabric.
- Sedimentation tests were conducted on 15% initial solids content slurries poured in 8.5 cm diameter graduated cylinders to an initial height of 8.5 cm.
- The solid-liquid interface movement was captured using a camcorder

connected to a computer; digital refinement improved accuracy.

- Consolidation test was used due to minimal experimental and theoretical errors and the ability to measure large strains and hydraulic conductivity.
- A 14.0 cm diameter cell that allowed the application of high loads and pore pressure determination during the test was used for ore and PAL slurries.
- A 9.5 cm diameter cell was used for polymer modified slurries because of the preclusion of high loads and pore pressure measurements during the test.

8.3 OBSERVATIONS AND CONCLUSIONS

8.3.1 General For All Laterite Slurries

8.3.1.1 Observations

- Laterite slurries constitute a distinct class of materials with geotechnical characteristics depending on ore geology and the metal extraction process.
- Laterite ores are primarily composed of sesquioxides in a neutral environment whereas the hematite-rich PAL materials interact with a highly acidic medium.

8.3.1.2 Conclusions

- The engineering behavior of laterite slurries ameliorates by using synthetic polymers; anionic for ore slurries and cationic for PAL slurries.
- Effective flocculation during the initial stages of the solid-liquid separation process improves sedimentation, consolidation and hydraulic conductivity.
- Sedimentation is the governing phenomenon during the solid-liquid separation process of laterite slurries.

- Hydraulic conductivity and compressibility during consolidation depend on efficient removal of both pore water and water entrapped in flocs.
- The polymer factor that combines the various parameters of synthetic polymers, correlates with solid-liquid separation behavior of polymer modified laterite slurries.

8.3.2 Laterite Ore Slurries

8.3.2.1 Observations

- Geotechnical characteristics of laterite ore slurries from different origins depend on geology and the slurry preparation method. These ores have specific gravities of 2.90 and exhibit high water requirement for conversion to slurries.
- Classified as micaceous fine sandy and silty clays, these materials are primarily composed of goethite, hematite and maghemite with sizeable amounts of clay minerals and amorphous materials.
- Local slurry preparation practices differ in various parts of the globe but most use tap water that is influenced by seawater concentration. The pore fluid is neutral to slightly basic with Na^+, Ca^{2+}, Mg^{2+}, Cl^- and SO_4^{2-} as predominant ions.

8.3.2.2 Conclusions

- More than 90% of the material in such slurries is finer than 0.075 mm. Depending on particle bond strength, aggregate size and mineralogy, the clay size fraction ranges between 20 to 60%. The fine grain size and the presence of clays render these ore slurries nonsegregating at an initial solids content of 15%.

- Variable mineralogy and pore water chemistry result in variable morphology. Soil fabric ranges from flocculated to dispersed; a partial or complete cardhouse microstructure is associated with limonite-saprolite ore slurries.
- The combined effect of variable material characteristics is vividly expressed during sedimentation under self-weight. The initial hydraulic conductivity of laterite ore slurries ranges between 10^{-1} to 10^{-4} cm/sec.
- The solid-liquid separation process is governed by sedimentation. Under self-weight, 65% dewatering is achieved as the void ratio changes from 17.9 to 8.0 ands solids content changes form 15 to 28%. A maximum effective stress of 8 kPa is sufficient to obtain 83% dewatering.
- The hard, ultra-fine and angular sesquioxide particles are associated with high tortuousity and high void ratio. These particle characteristics are responsible for the low hydraulic conductivity and compressibility of laterite ore slurry during consolidation.

8.3.3 Laterite PAL Slurries

8.3.3.1 Observations

- Geotechnical characteristics of laterite PAL slurries from different origins are generally improved during pressure acid leaching. These materials have specific gravities above 3.20 and exhibit high water requirement during the autoclave operation for economic metal extraction.
- Converted to materials similar to sand or less active clays, laterite PALs are primarily composed of hematite. In some varieties, magnesium sulfates and amorphous materials are present in sizeable amounts.

- Autoclave operations generally use the required amount of sulfuric acid that influences the pore water concentration. The pore fluid is highly acidic (pH ≤ 1) with Ca^{2+}, Mg^{2+}, Mn^{2+}, Al^{3+}, Fe^{3+}, Ni^{3+}, Co^{3+} and SO_4^{2-} as predominant ions.

8.3.3.2 Conclusions

- Materials undergo grain size growth during acid leaching. About 70% of the material is finer than 0.075 mm whereas the amount of clay size fraction ranges between 5 to 20%. The fine grain size and the presence of clay size fraction render these PAL slurries nonsegregating at an initial solids content of 15%.
- Similar mineralogy and pore water chemistry result in identical morphology. Still, soil fabric ranges from flocculated to dispersed; a cardhouse microstructure is associated with saprolite PAL slurry.
- Improvement in material characteristics is clearly identified during sedimentation under self-weight. The initial hydraulic conductivity of laterite PAL slurries ranges between 10^{-2} to 10^{-3} cm/sec.
- The solid-liquid separation process is governed by sedimentation. Under self-weight a 90% dewatering is achieved as the void ratio changes from 20.0 to 4.3 and the solids content changes from 15 to 46%. A maximum effective stress of 8 kPa is sufficient to obtain about 95% dewatering.
- The hard, ultra-fine and spherical iron oxide particles are associated with high tortuousity and high void ratio. These particle characteristics result in the low hydraulic conductivity and compressibility of laterite PAL slurry during consolidation. Still, both of these parameters are improved compared to the ore slurry.

8.3.4 Conclusions For Polymer Modified Laterite Ore Slurries

- Both anionic and cationic polymers can increase or decrease k_i of laterite ore slurry during sedimentation. An increase of 20 times and a decrease of four times were observed. Optimum polymer parameters for both anionic and cation polymers include a 75% charge (high), 17.5 x 10^6 g/mol MW (high) and 12 ppm dosage (high).

- Although, nonionic polymers always improve k_i, this increase is lower than ionic polymers; a maximum of 14 times k_i is observed. Generally, k_i increases with an increase in polymer MW from 7.5 x 10^6 g/mol (low) though 17.5 x 10^6 g/mol (high) or dosage from 4 ppm (low) through 12 ppm (high).

- The initial hydraulic conductivity of polymer modified PAL slurry strongly depends on soil morphology. Good flocculation, reduced tortuousity and the presence of channels are associated with high k_i.

- The type of flocculation attained during the initial stages of sedimentation governs both stages of the solid-liquid separation process. For anionic polymers, tightly bonded small flocs develop whereas loosely attached large flocs characterize cationic polymers; floc size decreases with increasing polymer charge.

- Based on the polymer factor, the performance of various synthetic polymers during consolidation depends on floc breakage and grain redistribution. These phenomena control the escape of pore water and the release of entrapped water from the flocs.

- Hydraulic conductivity during consolidation depends on the imposed hydraulic gradient and the void ratio. A high gradient is required to extract water entrapped in flocs whereas a low gradient is associated with flow through channels and low tortuousity.

- Polymer selection depends on optimizing efficiency (hydraulic conductivity) and yield (compressibility) of the extraction process. An anionic polymer with 75% charge (high), 17.5 x 10^6 g/mol MW (high) and 12 ppm dosage (high) is the most viable for improving the solid-liquid separation of laterite ore slurries.
- Sedimentation is the governs the solid-liquid separation of polymer modified laterite ore slurries. During this stage, colloid-polymer-electrolyte interactions are maximized. Additional improvement can be achieved during consolidation.

8.3.5 Conclusions For Polymer Modified Laterite PAL Slurries

- Polymer modification of laterite PAL slurries converts a *sand* like material to one similar to *clays*. These transformed materials generally adsorb a significant amount of water and are essentially nonsegregating.
- A 10% charge (low) results in k_i increase of two times for anionic polymers and 2½ times for cationic polymers. Conversely, a 75% charge (high) results in about 45% k_i decrease for the former and a 30% k_i increase for the latter polymers. Variations in polymer MW and dosage are less significant.
- For nonionic polymers, a 7.5 x 10^6 g/mol MW (low) results in k_i decrease of up to 35%. At elevated MW of 12.5 x 10^6 g/mol (medium) and 17.5 x 10^6 g/mol (high), increase in k_i amounts to 40% and 80%, respectively. Increasing polymer dosage from 4 ppm (low) to 12 ppm (high) results in a k_i increase of up to 30%.
- The initial hydraulic conductivity of polymer modified PAL slurry strongly depends on soil morphology. Good flocculation, reduced tortuousity and the presence of channels or tubules are associated with high k_i.

- The performance of various synthetic polymers during consolidation is the opposite of that during sedimentation. High k_i polymers have lower hydraulic conductivity and compressibility during consolidation and vice versa. This is due to the difficulty in removing the entrapped water from the flocs.
- Hydraulic conductivity during consolidation depends on the imposed hydraulic gradient and the void ratio. A high gradient is required to extract water entrapped in the flocs whereas a low gradient is associated with flow through channels and low tortuousity.
- Compressibility during consolidation depends on the type of flocculation. Strong attachment between large and equal size flocs result in low compressibility and the reverse is true for loose bonding and bimodal size distribution.
- Polymer selection depends on optimizing efficiency (hydraulic conductivity) and yield (compressibility) of the extraction process. A cationic polymer with 10% charge (low), 17.5 x 10^6 g/mol MW (high) and 4 ppm dosage (low) is best suited to improve the solid-liquid separation of laterite PAL slurries.
- Sedimentation is the governing phenomenon for the solid-liquid separation of polymer modified laterite PAL slurries. During this stage, there is a maximum chance for colloid-polymer-electrolyte interactions to be displayed.

8.4 SIGNIFICANCE AND APPLICATION

The field of geoenvironmental engineering focuses on the management of solid wastes. Engineers benefit from the knowledge of soil scientists, geologists, hydrologists, and environmental scientists. This research is an excellent example of the multi-disciplinary nature of geoenvironmental engineering. The solid-liquid separation of laterite slurries was studied and improved using sedimentation, consolidation and hydraulic conductivity principles. The successful application of basic soil mechanics concepts to a hydrometallurgical process has broadened the scope of geotechnical engineering.

This research showed that sedimentation governs the dewatering behavior of laterite slurries. Improved solid-liquid separation necessitated maximum colloid-polymer-electrolyte interactions during initial stages. In comparison to PAL slurries, these interactions were more profound for ore slurries due to their ultrafine grain sizes and large surface areas. Anionic polymers were found to be best suited for ore slurries because these materials were primarily composed of positively charged sesquioxides in a neutral environment. The presence of large amount of multivalent ions in a highly acidic medium helped in the development of a negatively charged double layer in the hematite-rich PALs. Therefore, cationic polymers proved most viable for these latter slurries.

The amount of nickel in mineable laterites ores varies from 1.0% (minimum for limonite) to 3.0% (maximum for saprolite). The sulfuric acid pressure leaching process is the method of choice for metal extraction from most laterite ores. The estimated volume of the generated waste slurries is usually twice that of the mine. In addition to improving the efficiency and productivity of the extraction technology, the devised polymer amelioration methods are expected to reduce the amount of waste slurries deposited in the tailings ponds.

8.5 RECOMMENDATIONS

- The data generated by this research work should be validated under actual process conditions of elevated temperature and pressure. The economic feasibility of the polymer amelioration methods should be evaluated.
- The devised polymer amelioration methods should be tested and verified in pilot scale thickeners to improve efficiency and productivity of the metal extraction process.
- Multi-disciplinary studies should be conducted to investigate the autoclave performance of ore slurries modified with anionic polymers and the long term behavior of waste slurries modified with cationic polymer in the tailings ponds.
- A comparative study of the two polymer amelioration methods should be undertaken to use the data generated by this research for other types of laterite ore and PAL materials.
- Results of this study can be utilized for an assessment of alternative slurry disposal methods. The usefulness of the devised polymer amelioration methods on the rheological behavior of laterite slurries should be investigated.
- The data generated by this research are applicable to the management of solid wastes. An assessment of the devised polymer amelioration methods for reducing the volume of waste slurries deposited in the tailings ponds should be made.
- A comprehensive environmental impact study should be conducted to investigate the influence of dissociated synthetic polymers on aquatic life in the tailings ponds.

References

Aboshi, H., H. Yoshikuni, & S. Maruyama (1979). Constant loading rate consolidation test. *Soils & Foundations*. 10(1):43-56.

Ahlrichs, J.L. (1962). Bonding of organic polyanions to clay minerals. *Dissertation Abstracts*. 22:2121.

Alexander, L.T. & J.G. Caddy (1962). Genesis and hardening of laterite in soils. *United States Department of Agriculture Technical Bulletin*. 1282:90.

Allen, T. (1981). *Particle Size Measurement*. 3rd ed. Chapman & Hall & Methuen, New York, USA.

Atkins, P. W. (1988). *Physical Chemistry*. 3rd ed. Chapman & Hall & Methuen, New York, USA.

Avotins, P.V., S.S. Ahlschlager, & G.R. Wicker (1979). The rheology and handling of laterite slurries. *Proceedings, International Laterite Symposium*, New Orleans, USA. 1:610-635.

Azam, S. & N.A. Al-Shayea (1999). Clayey behavior of calcareous soils. *Proceedings, 2nd International Conference on Engineering for Calcareous Sediments*, Bahrain. 1:199-208.

Azam, S., R. Chalaturnyk, J.D. Scott & J. Stiksma (2000). Characteristics of laterite slurry tailings from acid leach metal extraction process. *Proceedings, 53rd Canadian Geotechnical Conference*, Montreal, QC, Canada. 1:657-664.

Azam, S., S.N. Abduljauwad, N.A. Al-Shayea, & O.S.B. Al-Amoudi (1998). Expansive characteristics of gypsiferous/anhydritic soil formations. *Engineering Geology*. 5:89-107.

Babcock, K.L. (1963). Theory of the chemical aspects of soil colloidal systems at equilibrium. *Hilgardia*. 34(11):25-37.

Baghala, M. & V.G. Papangelakis (1998a). Pressure acid leaching of laterites at 250 °C: a solution chemical model and its application. *Metallurgical and*

Materials Transactions B. 29B:945-952.

Baghala, M. & V.G. Papangelakis (1998b). The ion association interaction approach as applied to aqueous H_2SO_4-$(Al_2SO_4)_3$-$MgSO_4$ solutions at 250 °C. *Metallurgical and Materials Transactions B*. 29B:1021-1030.

Bascomb, C.L. (1964). Rapid method for the determination of cation exchange capacity of calcareous and non-calcareous soils. *Journal of Science Food Agriculture*. 15:821-823.

Been K. & G.C. Sills (1981).Self-weight consolidation of soft soils-an experimental and theoretical study. *Geotechnique*. 31(4):519-535.

Bidwell, J.I., W.B. Jepson, G.L. Toms (1970). The interaction of kaolinite with polyphosphate and polyacrylate in aqueous solutions-some preliminary results. *Clay Minerals*. 8:445-459.

Bishop, A.W. (1977). The stability of tips and spoil heaps. *Quarterly Journal of Engineering Geology*. 6:335-376.

Blakey, B.C. & V.G. Papngelakis (1995). A study of solid-aqueous equilibria by the speciation approach in the hydronium alunite-sulfuric acid-water system at high temperatures. *Metallurgical and Materials Transactions B*. 27B:555-566.

Bolt, G.H. (1956). Physico-chemical analysis of the compressibility of pure clays. *Geotechnique*. 6(2):86-93.

Brady, N.C. (1990). *The Nature and Properties of Soils*. 10th Edition, Macmillan, New York.

Briceno, A., & K. Osseo-Asare (1995a). Particulates in hydrometallurgy: Part I. Characterization of laterite acid leach residues. *Metallurgical & Materials Transactions B*. (26)6:1123-1131.

Briceno, A., & K. Osseo-Asare (1995b). Particulates in hydrometallurgy: Part II. Dewatering behavior of unflocculated laterite acid leach residues. *Metallurgical & Materials Transactions B*. (26)6:1133-1138.

Briceno, A., & K. Osseo-Asare (1995c). Particulates in hydrometallurgy: Part III. Dewatering behavior of flocculated laterite acid leach residues.

Metallurgical & Materials Transactions B. (26)6:1139-1145.

Buchanan, F. (1807). *A Journey from Madras through the Countries of Mysore, Canara and Malabar*. East Indian Company, London, United Kingdom.

Burger, P.A. (1995). Ni/Co laterite deposits: geology, evaluation and mining. *Nickel/Cobalt Laterites,* Alta Metallurgical Services, Melbourne, Australia.

Burger, P.A. (1979). The Greenvale nickel laterite ore body. *Proceedings, International Laterite Symposium*, New Orleans, USA. 1:24-37.

Carlson, E.T. & C.S. Simons (1960). Acid leaching, Moa Bays nickel. *Journal of Metals*, March, 206-213

Casagrande, A. (1948). Classification and identification of soils. *Transactions,* ASCE. 113:901-930.

Caughill, D.L., N.R. Morgenstern & J.D. Scott (1993). Geotechnics of non-segregating oil sand tailings. *Canadian Geotechnical Journal,* (30)5:801-811.

Chalkley M.E. & I.L. Toirac (1997). The acid pressure leach process for nickel and cobalt laterite. Part I: Review of operations at Moa. *Proceeding, Nickel-Cobalt International Syposium.* Sudbury, Ontario, Canada. 1:341-353.

Chapman, D.L. (1913). A contribution to the theory of electro-capillarity. *Philosophical Magazine*. 25(6):475-481.

Chou, E.C., P.B. Queneau & R.S. Rickard (1977). Sulfuric acid pressure leaching of nickeliferous limonites. *Metallurgical Transactions B.* 8B:547-554.

Collis-George, N. & J.M. Bozeman (1970). A double layer theory for mixed ion systems as applied to the moisture content of clays under restraint. *Australian Journal of Soil Research.* 8(3):239-258.

Cruz, P. (1969). Engineering properties of some residual compacted soils. *Proceedings, 7th International Conference on Soil Mechanics & Foundation Engineering*, Mexico. 1:91-100.

Dempsey, B.A., H. Sheu & T.M.T. Ahmed (1985). Polyaluminum chloride and alum coagulation of clay-fulvic acid suspensions. *Journal of the American Water Works Association.* 77(3):74-80.

Dixon, J.B. & S.B. Weed (1989). *Minerals in Soil Environment (2^{nd} edition)*. Soil Science Society of America, Madison, Wisconsin.

D'Hoore, J.L. & J.J. Fripiat (1954). Tropical clays and their iron oxide coverings. *Proceedings, 2^{nd} International African Soil Conference,*. Leopoldville. 256-266.

Dusseault M.B. & J.D. Scott (1983). Tailings pond behavior and characterization of oil sand tailings sludge. *Particulate Science and Technology*. 1:295-309.

Duyvesteyn, W.P.C, G.R. Wicker & R.E. Doane (1979). Omnivorous process for laterite deposits. *International Laterite Symposium*, New Orleans, LA. 253-270.

Erol, 0., R.A. Lohnes & T. Demirel (1976). Preparation of clay-type, moisture containing samples for scanning electron microscopy. *Proceedings, Workshop on Techniques for Particulate Matter Studies in SEM,* IIT Research Institute, Chicago, Illinois, USA. 769-776.

Farinato, R.S., S.Y. Huang & P. Hawkins (1999). Polyelectrolyte assisted dewatering. *Colloid-Polymer Interaction-From Theory to Practice*. John Wiley & Sons Inc. New York.

Frisch, H.L. (1955). Polymer chain configuration near a boundary exerting force. *The Journal of Chemical Physics*. 59:633-636.

Frisch, H.L. & R. Simha (1957). Statistical mechanics of flexible high polymers at surfaces. *The Journal of Chemical Physics*. 27:702-706.

Fourie, A.B. (1997). Classification and index tests. *Mechanics of Residual Soils, (Blight ed.)*. ISSMFE Technical Committee 25. Balkema, Rotterdam, The Netherlands. 57-63.

Frost, R.J. (1976). Importance of correct pretesting preparation of some tropical soils. *Proceedings, 1^{st} South East Asian Conference on Soil Engineering,* Bangkok, Thailand.

Georgio, D. & V.G. Papangelakis (1998). Sulfuric acid pressure leaching of a limonitic laterite: chemistry and kinetics. *Hydrometallurgy*. 49:23-46.

Gibson, R.E., G.L. England & M.J.L. Hussey. (1967). The theory of one dimensional consolidation of saturated clays: Finite strain consolidation of thick homogeneous layers. *Geotechnique*. 17:261-273.

Gidigasu, M.D. (1976). *Laterite Soil Engineering-Pedogenesis and Engineering Principles*. Elsevier Amsterdam, The Netherlands.

Gidigasu, M.D. (1974). Degree of weathering in the identification of laterite materials for engineering purposes-A review. *Engineering Geology*. 8(3):213-266.

Gidigasu, M.D. (1972). Mode of formation and geotechnical characteristics of laterite materials of Ghana in relation to soil forming factors. *Engineering Geology*. 6(2):79-150.

Gidigasu, M.D. (1971). The importance of soil genesis in the engineering classification of Ghana soils. *Engineering Geology*. 5: 117-161.

Gidigasu, M.D. & H.S. Bhatia (1971). Importance of soil profile in the engineering studies of laterite soils. *Proceedings, 5th Regional Conference on Soil Mechanics and Foundation Engineering*, Luanda. 1:255-260.

Gillman, G.P. (1979). A proposed method for the measurement of exchange properties of highly weathered soils. *Australian Journal of Soil Research*. 17:129-139.

Grim, R.E. (1968). *Clay Mineralogy*. McGraw-Hill, New York.

Goldschmidt, V.M. (1926). Undersokelser ved Lersedimenter, Nordisk fordbruskning, Kongress 3, Kobenhavn.434-445. (in Mitchell 1993).

Golightly, J.P. (1981). Nilckeliferous laterite deposits. *Economic Geology*. 75: 710-735.

Golightly, J.P. (1979a). Nilckeliferous laterites-a general description. *Proceedings, International Laterite Symposium*, New Orleans, USA. 1:3-23.

Golightly, J.P. (1979b). Geology of Saroako nilckeliferous laterite deposits. *Proceedings, International Laterite Symposium*, New Orleans, USA. 1:38-56.

Grant, K. (1974). Laterites, Ferricretes, Bauxites, and Silcretes. *Proceedings, 2nd International Congress of the International Association of Engineering Geology*, Sao Paulo, Brazil. 1:

Greenland, D.J., J.M. Oades & T.W. Sherwin (1968). Electron microscope observations of iron oxide in some red soils. *Journal of Soil Science*.

19:123-126.

Haldemann, E.G., R. Buchan, J.H. Blowes, & T. Chandler (1979). Geology of lateritic nickel deposits, Dominican Republic. *Proceedings, International Laterite Symposium*, New Orleans, USA. 1:57-84.

Hamilton, R. (1964). Microscopic study of laterite formation. *Soil Micromorphology,* (Jungerius edition), Elsevier Amsterdam, The Netherlands. 269-278.

Holtz, W.G. & W.D. Kovacs (1981). *An Introduction to Geotechnical Engineering*, Englewood Cliffs, New Jersey, Prentice Hall.

Hunter, R.J. (1981). *Zeta Potential in Colloidal Science*. Academic Press Inc. Orlando, Florida.

Imai, G. (1981). Experimental studies on sedimentation mechanism and sediment formation of clay materials. *Soils and Foundations.* 21(1):7-20.

Imai, G. (1979). Development of a new consolidation test procedure using seepage force. *Soils & Foundations*. 19(3):45-60.

Janbu, N., O. Tokheim, & K. Senneset (1981). Consolidation test with continuous loadinu. *Proceedings, 10th International Conference on Soil Mechanics & Foundation Engineering.* 1:645-654.

Jankovics, L. (1965). Effect of agitation and molecular weight on polymer adsorption and deflocculation. *Journal of Applied Science*. 9:545-552.

Jones, R.A.L & R.W. Richards (1999). *Polymers at Surfaces and Interfaces.* Cambridge University Press., London, UK.

Joyace, I.H. & W.E. Worrall (1970). The adsorption of polyanions by clay and its effect on their physical properties. *Transactions of the British Ceramic Society*. 69:211-216.

Kavanagh, B.V., A.M. Posner & J.P. Quirk (1975). Effect of polymer adsorption on the properties of electrical double layer. *Faraday Discussions of the Chemical Society*. 59:242-249.

Kilmer, V.J. & L.T. Alexander (1949). Methods of making mechanical analysis of soils. *Soil Science*. 68:15-24.

Kinter, E.B. & S. Diamond (1956). A new method for preparation and treatment of oriented aggregate specimens of soil clays for X-ray diffraction analysis. *Soil Science*. 81:111-120.

Kitchener, J.A. (1972). Principles of action of polymeric flocculants. *British Polymer Journal*. 4:217-229.

Klotz, I.M. (1950). *Chemical Thermodynamics*. Prentice-Hall, Englewood Cliffs, N.J.

Kohl, R.A. & S.A. Taylor (1961). Hydrogen bonding between the carbonyl group and Wyoming bentonite. *Soil Science*. 91:223-227.

Krause, E., A. Singhal, B.C. Blakey, V.G. Papangelakis & D. Georgiou (1997). Sulfuric acid leaching of nickeliferous laterites. *Proceeding, Nickel-Cobalt International Syposium*. Sudbury, Ontario, Canada. 1:441-458.

Krause, E., B.C. Blakey & V.G. Papangelakis (1998). Pressure acid leaching of nickeliferous laterite ores. *Nickel/Cobalt Pressure Leaching & Hydrometallurgy Forum*. ALTA Metallurgical Services, Perth, Australia.

Küpper A.A., N.R. Morgenstern & D.C. Sego (1992). Laboratory tests to study hydraulic fill. *Canadian Geotechnical Journal*. 29:405-417.

Kuzkin, S.F., V.P. Nebera & S.N. Zolin (1964). Aspects of the theory of suspension flocculation by polyacrylamides. *Proceedings, 7th International Mineral Processing Congress*. New York. 7:347-357.

Kynch, E.J. (1952). A theory of sedimentation. *Transactions of Faraday Society*. 48:168-176.

Lamb, T.W. (1951). *Soil Testing for Engineers*. John Wiley & Sons, New York, USA.

La Mer, V.K. & R.H. Smellie (1962). Theory of flocculation, subsidence and refiltration rates of colloidal dispersions flocculated by polyelectrolytes, *Clays & Clay Minerals. 9:295-314.*

Lee, K. (1981). Consolidation with constant rate of deformation. *Geotechnique*. 31:295-329.

Li, C.T.C. (1994). *Comparison Between CDTA and Extension Method for Acid*

Determination in the Presence of Metal Ions. B.A.Sc. Thesis. University of Toronto, Toronto, Canada.

Linke, W.F. & R.B. Booth (1960). Physical chemical aspects of flocculation by polymers. *Transactions of the American Institute of Mining, Metallurgical and Petroleum Engineers.* 217:364-371.

Lohnes, R.A., R.O. Fish & T. Demirel (1971). Geotechnical properties of selected Puerto Rican soils in relation to climate and parent rock. *Geological Society of America Bulletin*. 82:2617-2624.

Loughnan, F.C. (1969). *Chemical Weathering of the Silicate Minerals.* Elsevier, New York, USA.

Lowe, J., E. Jonas, & V. Obrician (1969). Controlled gradient consolidation test. ASCE *Journal of Soil Mechanics and Foundation Division*, 95(SM 1):77-97.

Lyklema, J. (1976). Inference of polymer adsorption from electrical double layer measurements. *Pure & Applied Chemistry.* 46:149-156.

Mackenzie, R.C. (1957). The differential thermal investigation of clays. *Mineralogical Society*, Clay Minerals group, London.

Maignien, R. (1966). *Review of Research on Laterites*. Natural Resources Research IV, UNESCO, Paris, France.

Matheson, P.J. (1996). Development of nickel/cobalt laterites in the South West Pacific. *Mineral to Market Conference Series, Australian Institute of Mining & Metallurgy.* Carlton, Australia. (6):59-60.

McCabe, W.L., J.C. Smith & P. Harriott (1985). *Unit Operations of Chemical Engineering.* McGraw Hill Inc. Toronto, Canada.

McMahone, D. (1989). *Properties of Sodium Sulfate Attack, Salt Heave, Lime Sulfate Heave on Earthening.* Master Independent Project. University of California, Berkeley, USA.

McRoberts, E.C. & J.F. Nixon (1976). A theory of soil sedimentation. *Canadian Geotechnical Journal*. 13:294-310.

Michaels, A.S. (1954). Aggregation of suspensions by polyelectrolytes. *Industrial*

& Engineering Chemistry. 46:1485-1490.

Mikula, R.J. (1988). Chemical characterization of an oil/water emulsion interface via electron microscope observation of a frozen hydrated sample. *Journal of Colloid and Interface Science*. 121(1):273-277.

Mikula, R.J., V.A. Munoz & W.W. Lam (1989). Microscopic charcterization of oil sands processing emulsions. *Fuel Science and Technology International*. 7(5-6):727-749.

Mitchell, J.K. (1993). *Fundamentals of Soil Behavior*, 2nd edition, John Wiley & Sons, Inc. New York, USA.

Mitchell, J.K. (1993). *Fundamentals of Soil Behavior*, 2nd edition, John Wiley & Sons, Inc. New York, USA.

Mitchell, J.K. & N. Sitar (1982). Engineering properties of tropical residual soils. *Proceedings, ASCE Conference on Engineering & Construction in Tropical Residual Soils*. Honolulu, Hawai. 30-57.

Mohr, E.C.J. & F.A. Van Baren (1954). *Tropical Soils*. Inter-Science, London, UK.

Morgenstern N.R. & J.D. Scott (1995). Geotechnics of fine tailings management. *Proceedings, Geo-Environment 2000,* ASCE, New Orleans, Louisiana, USA. 2:1663-1673.

Morin, W.J. & P.C. Todor (1975). Laterite and lateritic soils and other problem soils of the tropics. *An Engineering Evaluation and Highway Design Study for the U.S. Agency for International Development*. Lyon Associates Inc. Baltimore, MD.

Morin, W.J. & W.T. Parry (1969). Mineralogy and index properties of some African lateritic residual soils. *Proceedings, 7th International Conference on Soil Mechanics and Foundation Engineering,* Mexico. 1:53-63.

Mortensen, J.L. (1962). Adsorption of hydrolyzed polyacrylonitrile on kaolinite. *Clays & Clay Minerals*. 9:530-545.

Mortland, M.M. (1970). Clay organic complexes and interactions. *Advances in Agronomy*. 22:75-117.

Motteram, G., M. Ryan, R. Berezowsky, & R. Raudsepp (1996). Murrin Murrin nickel cobalt project. *Nickel/Cobalt Pressure leaching & Hydrometallurgy Forum*, Perth, Australia.

Muthukumar, M. (1999). Polyelectrolyte adsorption: theory and simulation. *Colloid-Polymer Interaction-From Theory to Practice*. John Wiley & Sons Inc. New York.

Neal, J.A., J.M.L. Zdybak & W.G. Bannerman (1985). Lignodulfonate copolymer stabilizes lime mud. *Oil & Gas Journal*. 3:118-124.

Nixon, I.K. & B.O. Skipp (1957). Airfield construction on overseas soils. *Proceeding, British Institute for Civil Engineering*. London, United Kingdom. 8:253-292.

Olsen, H.W. (1966). Darcy's law in saturated kaolinite. *Water Resources Research*. 2(6):287-295.

Ozberk, E., S.A. Gendron & G.H. Kaiura (1986). Review of nickel smelters-responses to questionnaire. *Proceedings, 25th Annual Conference of Metallurgists, Nickel Metallurgy*. 1:304-319.

Pane, V. & R.L. Schiffman (1997). The permeability of clay suspensions. *Geotechnique*. 47:273-288.

Pane, V. & R.L. Schiffman (1985). A note on sedimentation and consolidation. *Geotechnique*. 35:69-72.

Petzold, G. & K. Lukwitz (1998). The interaction between polyelectrolyte complexes made from poly(dimethyldiallyammonium chloride) (PDMDAAC) poly(maleic acid-co-α-methylstyrene) (P(MS-α-MeSty)) and cellulosic materials. *Colloids & Surfaces A: Physicochemical & Engineering Aspects*. (1995):225-233.

Pickering, R.L. (1962). Some leaching experiments on three quartz-free silicate rocks and their contribution to the understanding of laterization. *Economic Geology*. 57:1185-1206.

Pollock, G.W. (1988). *Consolidation of Oil Sand Tailings Sludge*. M.Sc. Thesis, University of Alberta, Edmonton, Alberta, Canada.

Prado, F.G. & J.P. Dempsey (1986). Indigenous solids reductants in caron type nickel plants. *Proceedings, 25th Annual Conference of Metallurgists, Nickel Metallurgy.* 1:320-333.

Prafitt, R.L. (1978). Anion adsorption by soils and soil materials. *Advances in Agronomy.* 30:1-50.

Queneau, P.B., R.E. Doane, M.W. Cooperrider, M.H. Berggren & P. Rey (1984). Control of autoclave scaling during acid pressure leaching of nickeliferous laterite ores. *Metallurgical Transactions B.* 15B: 433-440.

Reid, J.G. (1996). Laterite ores-nickel and cobalt resources for the future. *Mineral to Market Conference Series, Australian Institute of Mining & Metallurgy.* Carlton, Australia. (6):11-16.

Rhoades, J.D., P.J. Shouse, W.J. Alves, N.A. Manteghi, & S.M. Lesch (1990). Determining soil salinity from soil electrical conductivity using different models and estimates. *Soil Science Society of America Journal.* 54:46-54.

Richardson, J.F. & W.N. Zaki (1954). Sedimentation and fluidization: part I. *Transactions of the Institute of Chemical Engineers.* 32:35-53.

Robinsky, E.I. (1982). *Thickened Tailings Disposal Feasibility Study: Laboratory Tests for Determination of Thickened Tailings Properties.* Syncrude Research Department, Progress Report. 1-4.

Rouse, W.C., A.J. Reading & R.P.D. Walsh (1986). Volcanic soil properties in Dominica, West Indies. *Engineering Geology.* 23:1-28.

Rubisov, D.H. & V.G. Papangelakis (1999). The effect of acidity 'at temperature' on the morphology of precipitates and scale during sulfuric acid pressure leaching of laterites. 29th Annual Hydrometallurgical Meeting, Montreal, Canada. 1:185-203.

Ruehrwein, R.A. & D.W. Ward (1952). Mechanism of clay aggregation by polyelectrolytes. *Soil Science.* 73:485-492.

Ruhe, R.V. (1954). Erosion surfaces of Central African interior high plateau. *Institute of Natural and Economic Agriculture*, Bruxelles. 59:38.

Sakaguchi, K. & K. Nagase (1966). The flocculation of kaolin and precipitated calcium carbonate by polymers. *Bulletin of the Chemical Society of Japan.* 39:88-91.

Saunders, M.K. & P.G. Fookes (1970). A review of the relationship of rock weathering and climate and its significance to foundation engineering. *Engineering Geology.* 4:289-325.

Sawyer, C.N., P.L. McCarty & G.F. Perkin. (1994). *Chemistry for Environmental Engineering.* 4th ed. McGraw-Hill Inc. New York.

Schamp, N. & J. Huylebroeck (1973). Adsorption of polymers on clays. *Journal of Polymer Science.* 42:553-562.

Schramm, L.L. (1996). Suspensions: basic principles. *Suspensions: Fundamentals and Applications in Petroleum Industry* (Schramm ed.), American Chemical Society. 3-44.

Scott, J.D. & G.J. Cymermann (1984). Prediction of viable tailings disposal methods. *Proceedings, Symposium on Sedimentation Consolidation Models*, ASCE, San Francisco. CA. 522-544.

Scott, J.D., M.B. Dusseault & W.D. Carrier III (1985). Behavior of the clay/bitumen/water sludge system from oil sands extraction plants. *Applied Clay Science.* 1:207-218.

Sergeev, J.M., V.L. Osipov & V.N. Sokolov (1985). Quantitative analysis of soil structure with the microcomputer system. *Bulletin of the Association of Engineering Geology.* 31: 13 1-136.

Sherman, G.D., Y. Kanehiro & Y. Matsu Saka (1953). Role of dehydration in the development of laterite crust. *Pacific Science.* 7:438-446.

Slater, R.W., J.P. Clark & J.A. Kitchener (1969). Chemical factors in the flocculation of mineral slurries with polymeric flocculants. *Proceedings, British Ceramic Society.* 13:1-12.

Smart, P. & X. Leng (1993). Present developments in image analysis. *Scanning Microscopy.* 7:5-16.

Somogyi, F. (1980). Large strain consolidation of grained slurries. *Presentation, Canadian Society of Civil Engineering.* Winnipeg, Manitoba.

Sposito, G. (1989). *The Chemistry of Soils*. Oxford University Press, New York.

Sposito, G. (1984). *The Surface Chemistry of Soils*. Oxford University Press, New York.

Suthaker, N.N. (1995). *Geotechnics of Oil Sand Fine Tailings*, Ph.D. Dissertation, University of Alberta, Edmonton, Canada.

Suthaker, N.N. & J.D. Scott (1994). Large scale consolidation testing of oil sand fine tails. Proceedings, *1st International Congress on Environmental Geotechnics,* Edmonton, Alberta, Canada. 557-562.

Svarovsky, L. (1981). *Solid-Liquid Separation.* 2nd ed. Butterworth & Co. London, UK.

Tabor, D. (1991). *Gases, Liquids and Solids and Other States of Matter.* Cambridge University Press, London, UK.

Tan, K.H. (1998). *Principles of Soil Chemistry.* 3rd ed. Marcel Dekker Inc., New York.

Terzaghi, K. (1958). The design and performance of the Sasumua dam. *Proceedings, British Institute of Civil Engineers*, London, United Kingdom. 9:369-394.

Terzaghi, K. (1943). *Theoretical Soil Mechanics.* John Wiley & Sons, Inc. New York.

Theng, B.K.G. (1979). *Formation and Properties of Clay-Polymer Complexes.* Elsevier, Amsterdam, The Netherlands.

Theng, B.K.G. (1974). *The Chemistry of Clay-Organic Reactions.* Adam Hilger Ltd., London.

Tindall, G.P. & D.M. Muir (1998). Effect of E_h on the rate and mechanism of the transformation of goethite into hematite in a high temperature acid leach process *Hydrometallurgy.* (47)2-3:377-381.

Tourtelot, H.A. 1973. Geologic origin and distribution of swelling clays.

Proceedings, Workshop on Expansive Clay & Shale in Highway Division & Construction. 1:

Townsend, F.C. (1985). Geotechnical characteristics of residual soils. *ASCE, Journal of Geotechnical Engineering.* 1:77-94.

Townsend, F.C., P.G. Manke, J.V. Parcher (1971). The influence of sesquioxides on lateritc soil properties. *Highway Research Record,* Highway Research Board. Washington, D.C. USA. 374:80-92.

Troly, G., M. Esterle, B. Pelletier, & W. Reibell (1979). Nickel deposits in New Caledonia, some factors influencing their formation. *Proceedings, International Laterite Symposium*, New Orleans, USA. 1:85-119.

Tsuchida, T., M. Koba yashi J. Mizukami (1991). Effect of ageing of marine clay and its duplication by high temperature consolidation. *Soils & Foundations.* 31(4):133-147.

Tuovinen O.H. & C.H. Jason (1984). Effect of pH, iron concentration, and pulp density on the solubilization of uranium from ore material in chemical and microbiological acid leach solutions: regression equation and confidence band analysis. *Hydrometallurgy.* 12(2):141-149.

Ueda, T. & S. Harada (1968a). Adsorption of cationic polysulfone on bentonite. *Journal of Applied Polymer Science.* 12:2395-2401.

Ueda, T. & S. Harada (1968b). Effect of the structure of cationic polysulfone on the flocculation of kaolinite. *Journal of Applied Polymer Science.* 12:2383-23931.

van Olphen, H. (1977). *An Introduction to Clay Colloidal chemistry.* 2nd ed. Wiley Interscience, New York.

Verwey, E.J.W. & J.T.G. Overbeek (1948). *Theory of the Stability of Lyophobic Colloids*. Elsevier, Amsterdam, The Netherlands.

Vincent, B. (1974). The effect of adsorbed polymer on dispersion stability. *Advances in Colloid and Interface Science.* 4:193-277.

Vitton, S.J. & L.Y. Sadler (1997). Particle size analysis of soils using laser light scattering and x-ray absorption technology. *ASTM Geotechnical Testing Journal*. 20:63-73.

Warkentin, B.P. & R.D. Miller (1958). Conditions affecting formation of the montmorillonite-polyacrylic acid bond. *Soil Science*. 85:14-18.

Wesley L.D. & T. Matuschika (1988). Geotechnical engineering in volcanic ash soils. *Proceedings, 2nd International Conference on Geomechanics in Tropical Soils*, Singapore. 1:333-342.

Wilemon, G.M., R.G. Swanton, J.G. Davis & B.J. Scheiner (1990). Phosphate from wastes via acid leaching in the presence of methanol. *Minerals & Metallurgical Processes. 7(4):201-205.*

Winterkorn, F.H. (1948). Engineering uses and limitations of pedology for regional exploration of soils. *Proceeding, 2nd International Conference on Soil Mechanics & Foundation Engineering*, Rotterdam, The Netherlands. 1:8-12.

Winterkorn, F.H. & R.B. Moorman (1941). A study of changes in physical properties of Putnam soils induced by ionic substitution. *Proceeding, Highway Research Board*. 21:415-434.

Wintermeyer, A.M. & E.B. Kinter (1954). Dispersing agents for the particle size analysis of soils. *Highway Research Board Bulletin*. 95:1-14.

Wood, D.M. (1992). *Soil Behavior and Critical State Soil Mechanics*. Cambridge University Press, London..

Worrall, W.E. (1968). *Clays, Their Origin and General Properties*. Transatlantic Arts Inc. New York.

Yariv, S. & H. Cross (1979). *Geochemistry of Colloid Systems for Earth Scientists*. Springer-Verlag, Berlin, Germany.

Znidarcic, D., P. Croce, V. Pane, H.W. Ko, H.W. Olsen, & R.L. Schiffman (1984). The theory of one-dimensional consolidation of saturated clays, III, existing testing procedures and analyses. *Geotechnical Testing Journal*. 7(3): 123-1 33.

Appendix A

Test Data of Chapter 6

A.1 GENERAL

This appendix provides the test data in the form of tables and figures. The test data was analyzed and discussed in Chapter Six.

Table A.1: Consistency limits of laterite ore modified with various ionic polymers

Polymer Parameters				w_l (%)	w_p (%)	w_s (%)	I_p (%)
Type	Charge	MW x 10^6 (g/mol)	Dose (ppm)				
Anionic	10% (Low)	7.5 (Low)	4	81	43	27	38
			12	82	44	27	38
		17.5 (High)	4	86	52	34	34
			12	78	41	25	37
	75% (High)	7.5 (Low)	4	83	51	34	32
			12	90	52	33	38
		17.5 (High)	4	86	50	32	36
			12	99	57	36	42
Cationic	10% (Low)	7.5 (Low)	4	77	45	30	32
			12	85	53	36	32
		17.5 (High)	4	92	60	41	32
			12	95	56	36	39
	75% (High)	7.5 (Low)	4	79	43	27	36
			12	80	44	28	36
		17.5 (High)	4	93	53	33	40
			12	91	52	33	39

Table A.2: Consistency limits of laterite ore modified with various nonionic polymers

Polymer Parameters							
Type	Charge	MW x 10^6 (g/mol)	Dose (ppm)	w_l (%)	w_p (%)	w_s (%)	I_p (%)
Nonionic	NA	7.5 (Low)	4	78	42	26	36
			8	80	43	27	37
			12	81	41	25	40
		12.5 (Medium)	4	80	39	23	41
			8	81	40	24	41
			12	80	42	26	38
		17.5 (High)	4	79	39	23	40
			8	83	40	23	43
			12	91	53	34	38

Table A.3: Solids content at start and end of sedimentation tests for laterite ore slurry modified with various ionic polymers

Polymer Parameters				*s* (%) Test Start	*s* (%) Test End
Type	Charge	MW x 10^6 (g/mol)	Dose (ppm)		
Anionic	10% (Low)	7.5 (Low)	4	15.0	23.2
			12	15.1	25.5
		17.5 (High)	4	15.0	28.3
			12	15.1	28.5
	75% (High)	7.5 (Low)	4	14.9	27.2
			12	15.1	26.7
		17.5 (High)	4	15.0	26.9
			12	15.1	25.9
Cationic	10% (Low)	7.5 (Low)	4	15.1	25.0
			12	15.2	26.7
		17.5 (High)	4	14.9	29.1
			12	15.1	22.6
	75% (High)	7.5 (Low)	4	15.2	24.6
			12	15.1	26.8
		17.5 (High)	4	15.0	27.3
			12	15.0	25.7

Table A.4: Solids content at start and end of sedimentation tests for laterite ore slurry modified with various nonionic polymers

Polymer Parameters					
Type	Charge	MW x 10^6 (g/mol)	Dose (ppm)	*s* (%) Test Start	*s* (%) Test End
Nonionic	NA	7.5 (Low)	4	15.1	24.7
			8	15.0	25.0
			12	15.2	25.0
		12.5 (Medium)	4	15.1	25.6
			8	15.1	26.2
			12	14.9	26.2
		17.5 (High)	4	15.2	27.3
			8	15.1	27.3
			12	15.0	27.3

Table A.5: Solids content at start and end of consolidation tests for laterite ore slurry modified with various ionic polymers

Polymer Parameters				*s* (%)	*s* (%)
Type	Charge	MW x 10^6 (g/mol)	Dose (ppm)	Test Start	Test End
Anionic	10% (Low)	7.5 (Low)	4	15.1	37.3
			12	15.2	39.9
		17.5 (High)	4	15.0	56.1
			12	15.1	53.2
	75% (High)	7.5 (Low)	4	15.0	38.8
			12	15.1	43.0
		17.5 (High)	4	14.9	37.4
			12	15.0	43.4
Cationic	10% (Low)	7.5 (Low)	4	15.1	39.5
			12	15.1	39.6
		17.5 (High)	4	14.8	45.6
			12	15.1	36.0
	75% (High)	7.5 (Low)	4	15.1	42.1
			12	15.0	44.0
		17.5 (High)	4	15.0	62.5
			12	15.1	44.3

Table A.6: Solids content at start and end of consolidation test for laterite ore slurry modified with nonionic polymer

Polymer Parameters					
Type	Charge	MW x 10^6 (g/mol)	Dose (ppm)	s (%) Test Start	s (%) Test End
Nonionic	NA	7.5 (Low)	4	-----	-----
			8	-----	-----
			12	-----	-----
		12.5 (Medium)	4	-----	-----
			8	15.1	41.2
			12	-----	-----
		17.5 (High)	4	-----	-----
			8	-----	-----
			12	-----	-----

Table A.7: pH and EC after sedimentation and consolidation tests for laterite ore slurry modified with various ionic polymers

Polymer Parameters				Sedimentation Test		Consolidation Test	
Type	Charge	MW x 10^6 (g/mol)	Dose (ppm)	pH	EC (μS/cm)	pH	EC (μS/cm)
Anionic	10% (Low)	7.5 (Low)	4	7.2	743	7.2	753
			12	7.2	744	7.1	740
		17.5 (High)	4	7.1	752	7.2	742
			12	7.2	741	7.2	748
	75% (High)	7.5 (Low)	4	7.1	750	7.1	752
			12	7.1	752	7.2	756
		17.5 (High)	4	7.2	740	7.2	743
			12	7.2	757	7.2	751
Cationic	10% (Low)	7.5 (Low)	4	7.1	745	7.1	745
			12	7.2	758	7.1	753
		17.5 (High)	4	7.2	750	7.2	751
			12	7.2	751	7.2	747
	75% (High)	7.5 (Low)	4	7.2	743	7.2	748
			12	7.1	742	7.2	746
		17.5 (High)	4	7.1	753	7.1	750
			12	7.2	752	7.1	750

Table A.8: pH and EC after sedimentation and consolidation tests for laterite ore slurry modified with various nonionic polymers

Polymer Parameters				Sedimentation Test		Consolidation Test	
Type	Charge	MW x 10^6 (g/mol)	Dose (ppm)	pH	EC (μS/cm)	pH	EC (μS/cm)
Nonionic	NA	7.5 (Low)	4	7.1	742	-----	-----
			8	7.1	740	-----	-----
			12	7.2	741	-----	-----
		12.5 (Medium)	4	7.2	743	-----	-----
			8	7.1	742	7.1	741
			12	7.1	742	-----	-----
		17.5 (High)	4	7.2	745	-----	-----
			8	7.1	741	-----	-----
			12	7.2	748	-----	-----

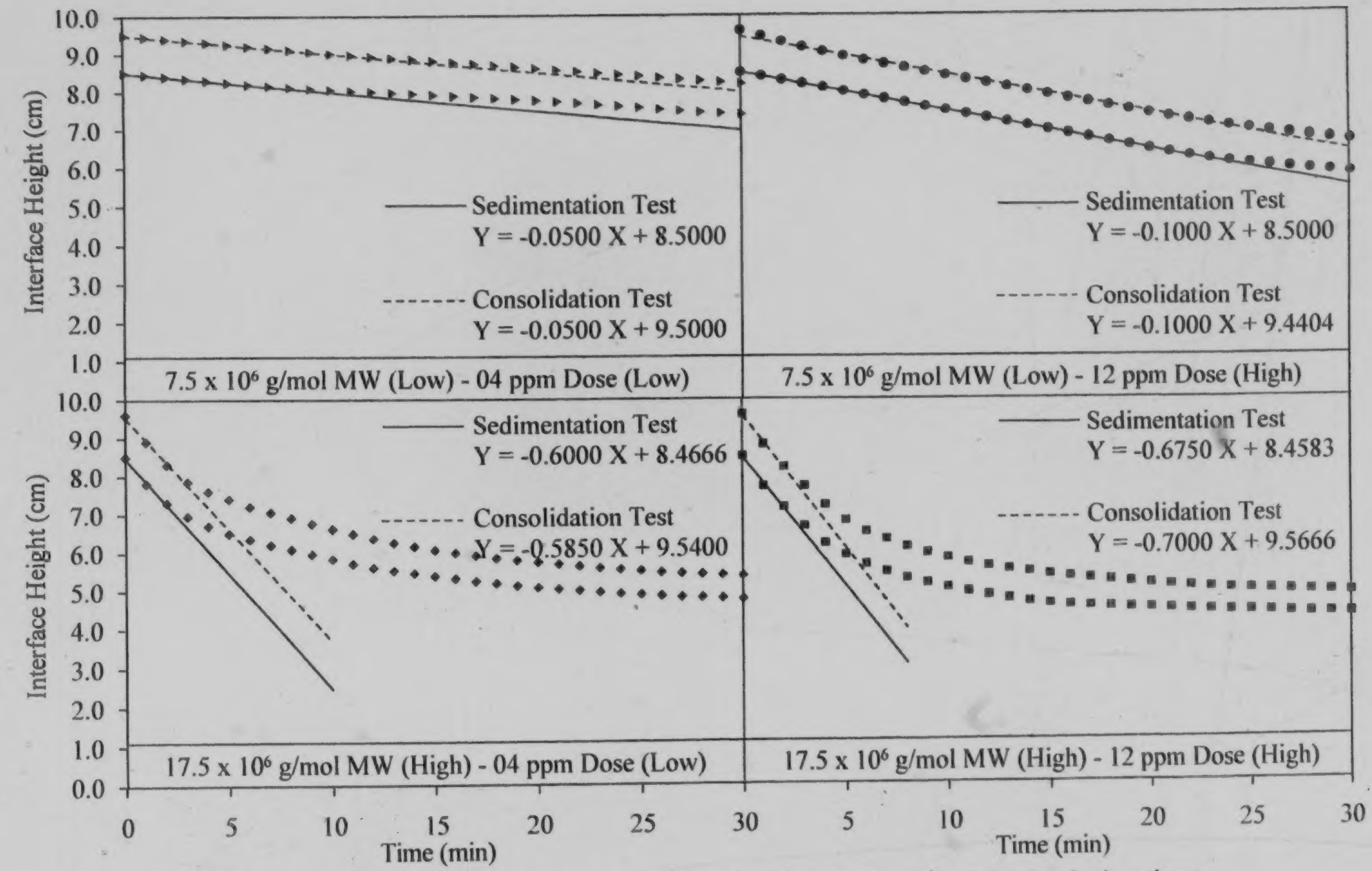

Figure A.1: Determination of k_i for laterite ore slurry modified with 10% charge (low) anionic polymers

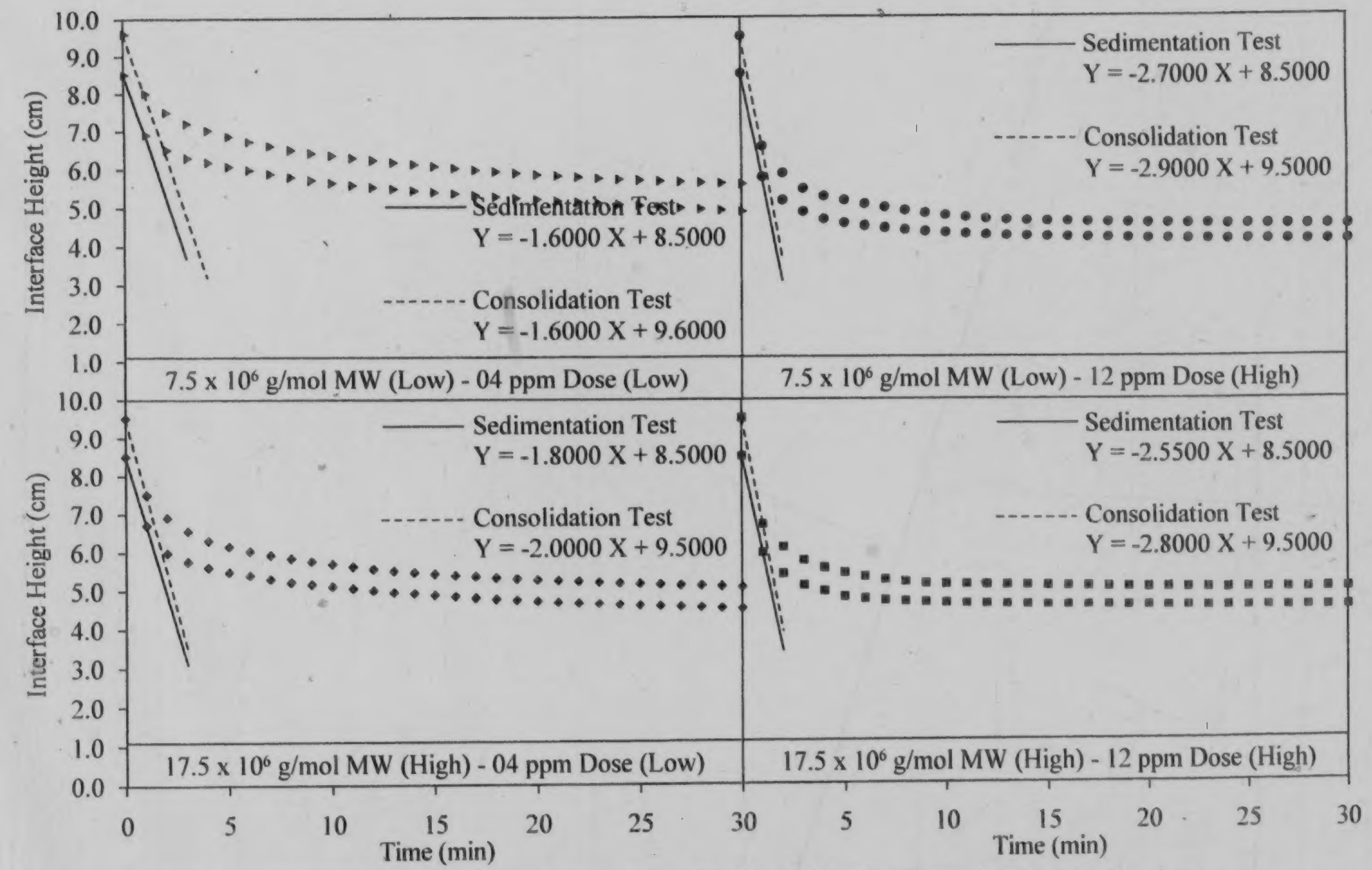

Figure A.2: Determination of k_i for laterite ore slurry modified with 75% charge (high) anionic polymers

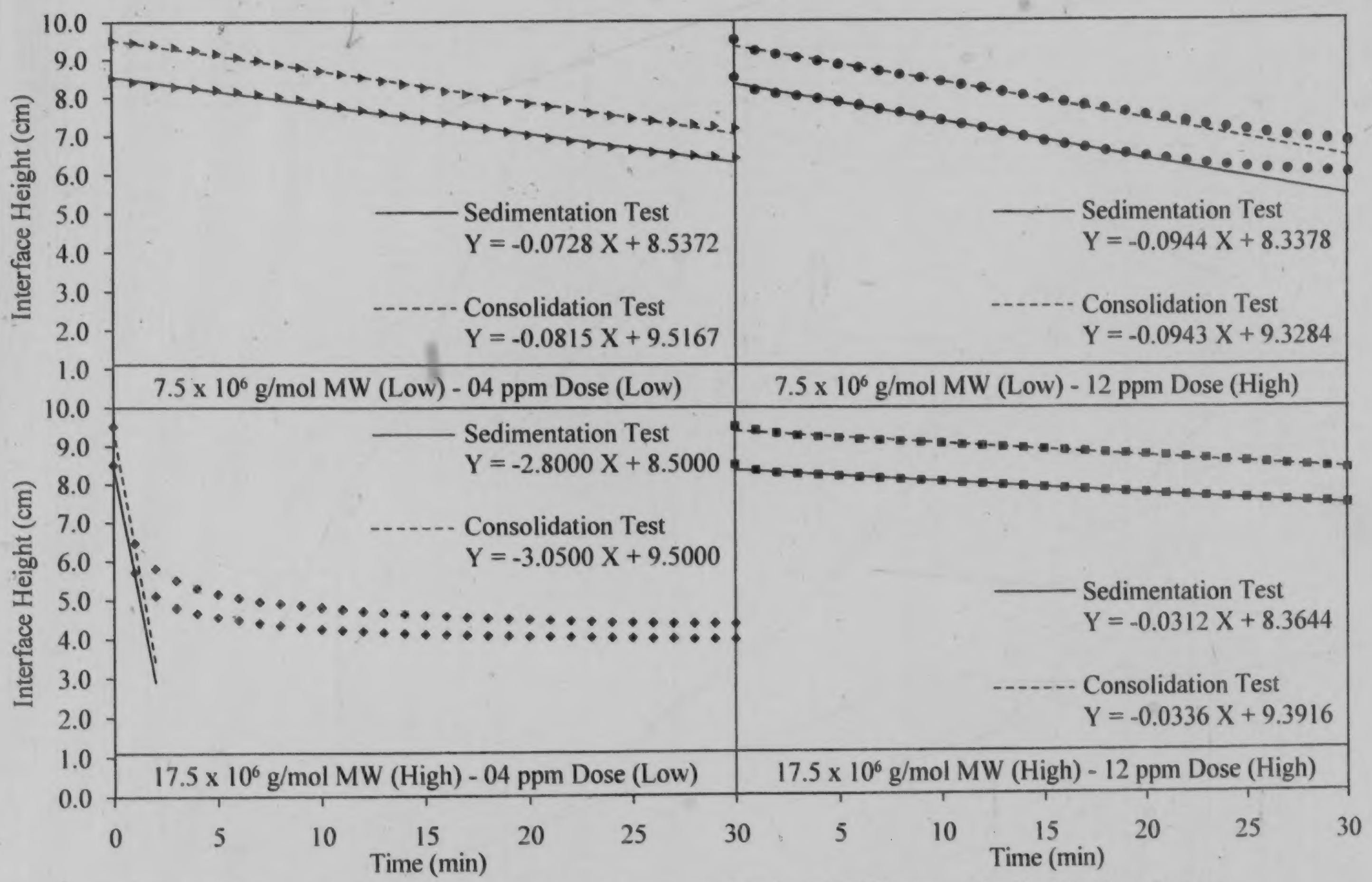

Figure A.3: Determination of k_i for laterite ore slurry modified with 10% charge (low) cationic polymers

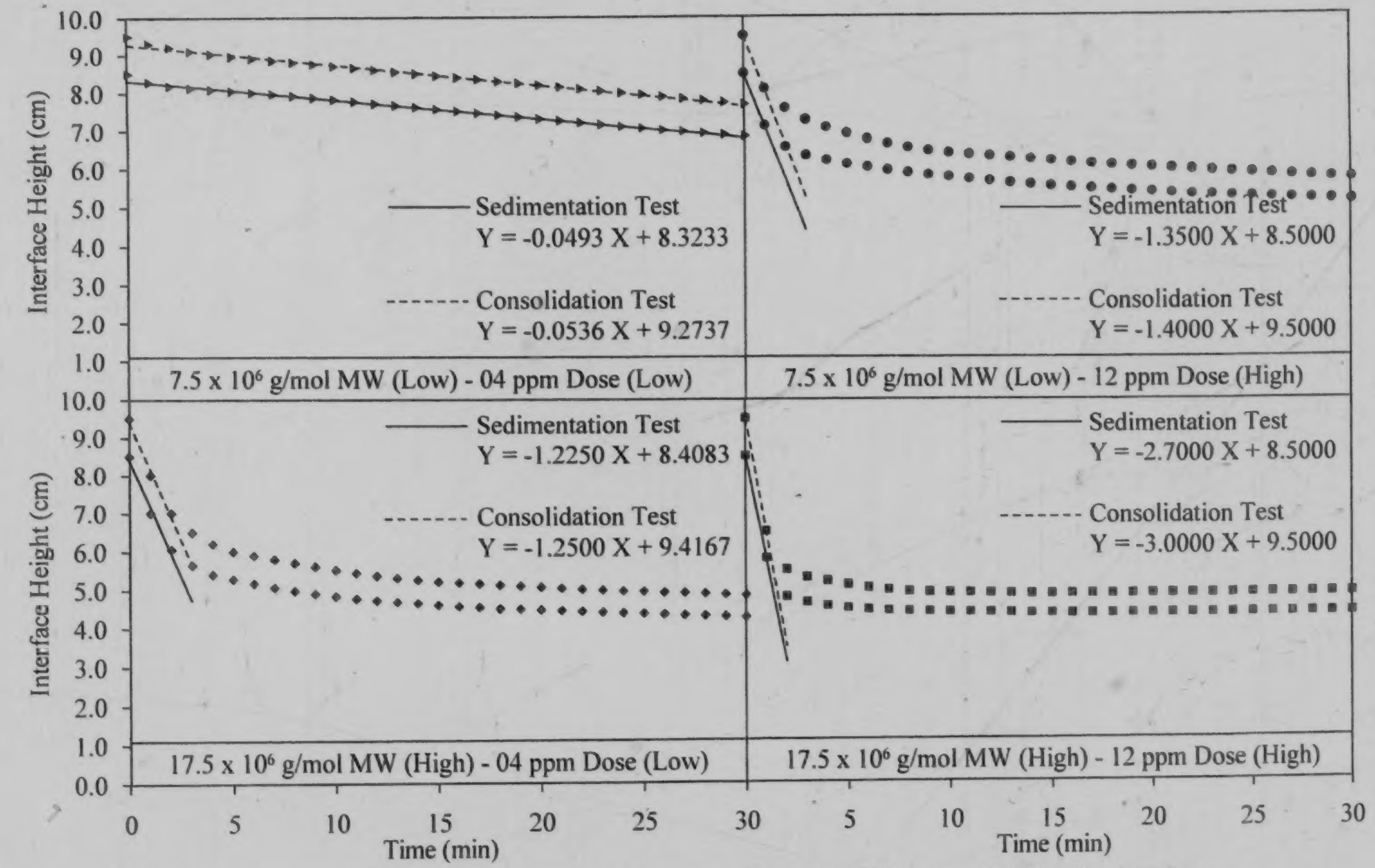

Figure A.4: Determination of k_t for laterite ore slurry modified with 75% charge (high) cationic polymers

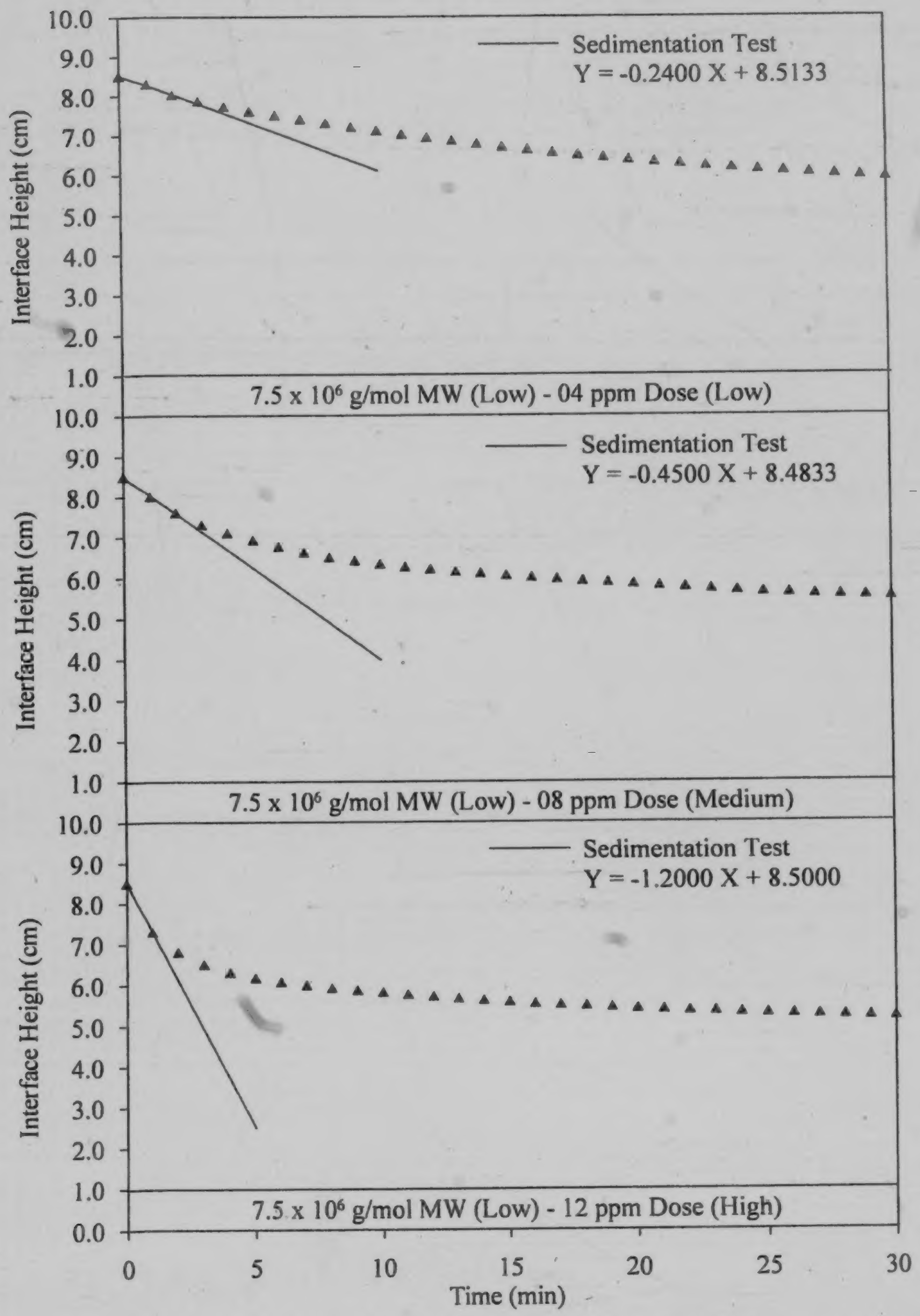

Figure A.5: Determination of k_i using low MW nonionic polymer

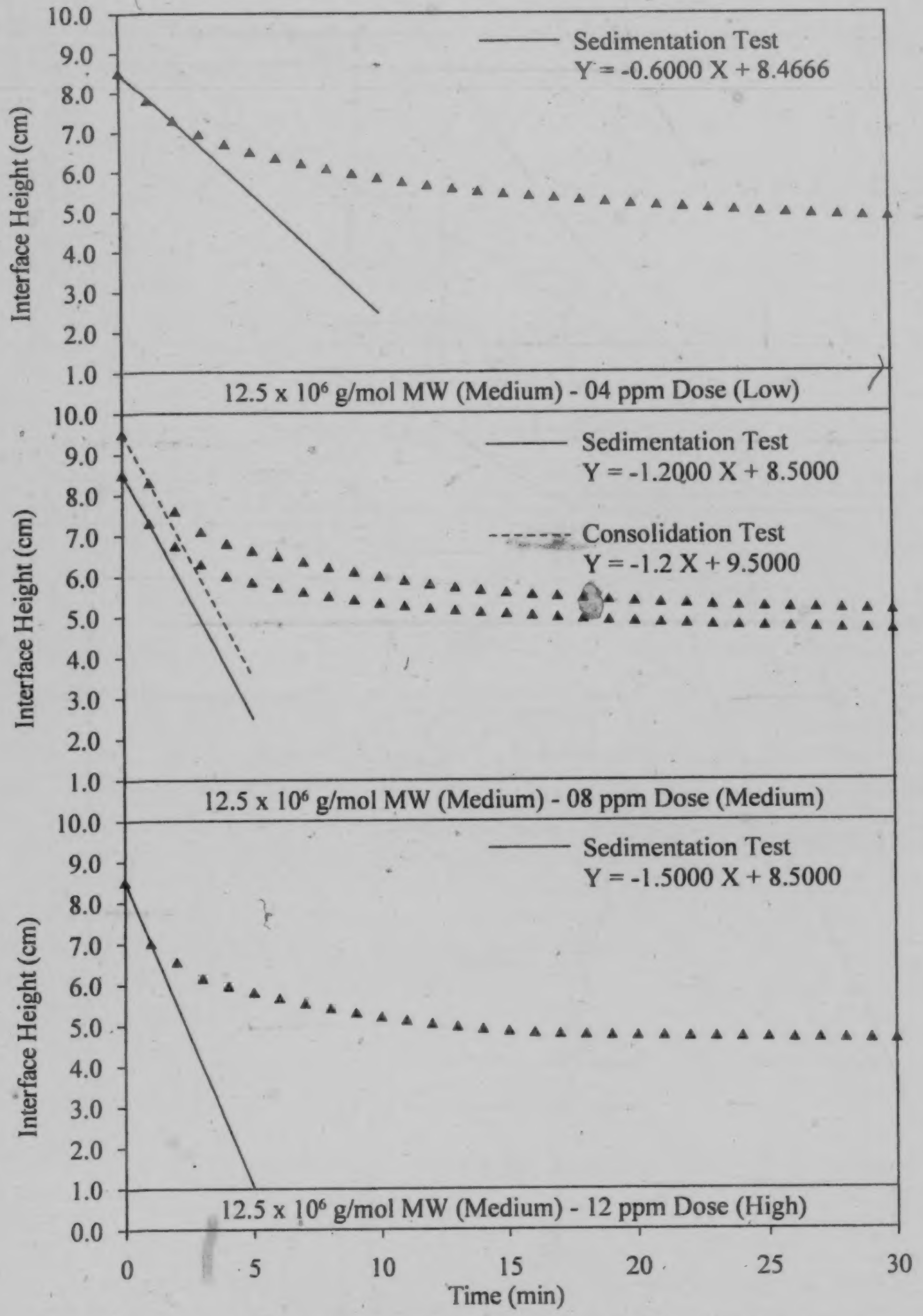

Figure A.6: Determination of k_i using medium MW nonionic polymer

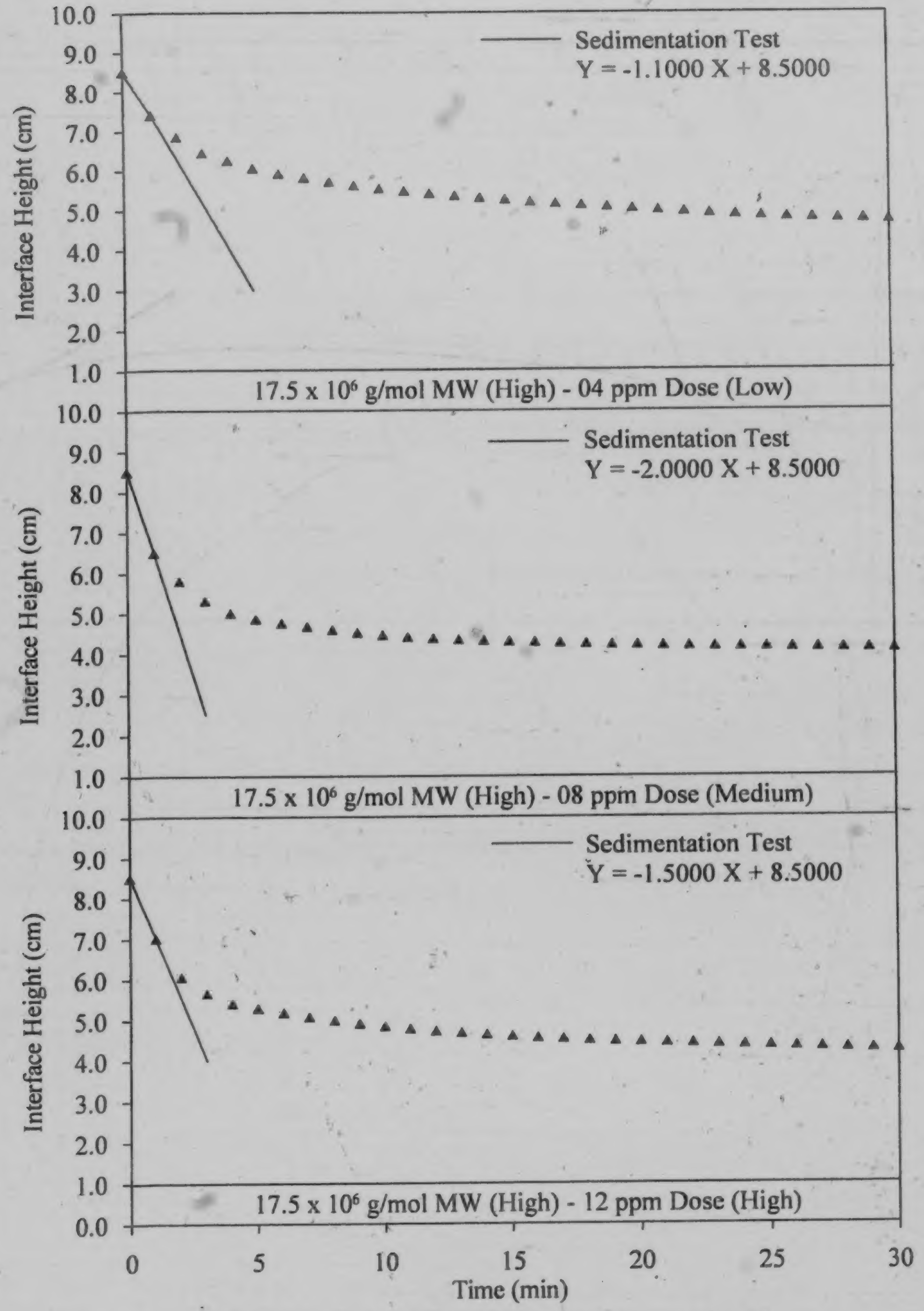

Figure A.7: Determination of k_i using high MW nonionic polymer

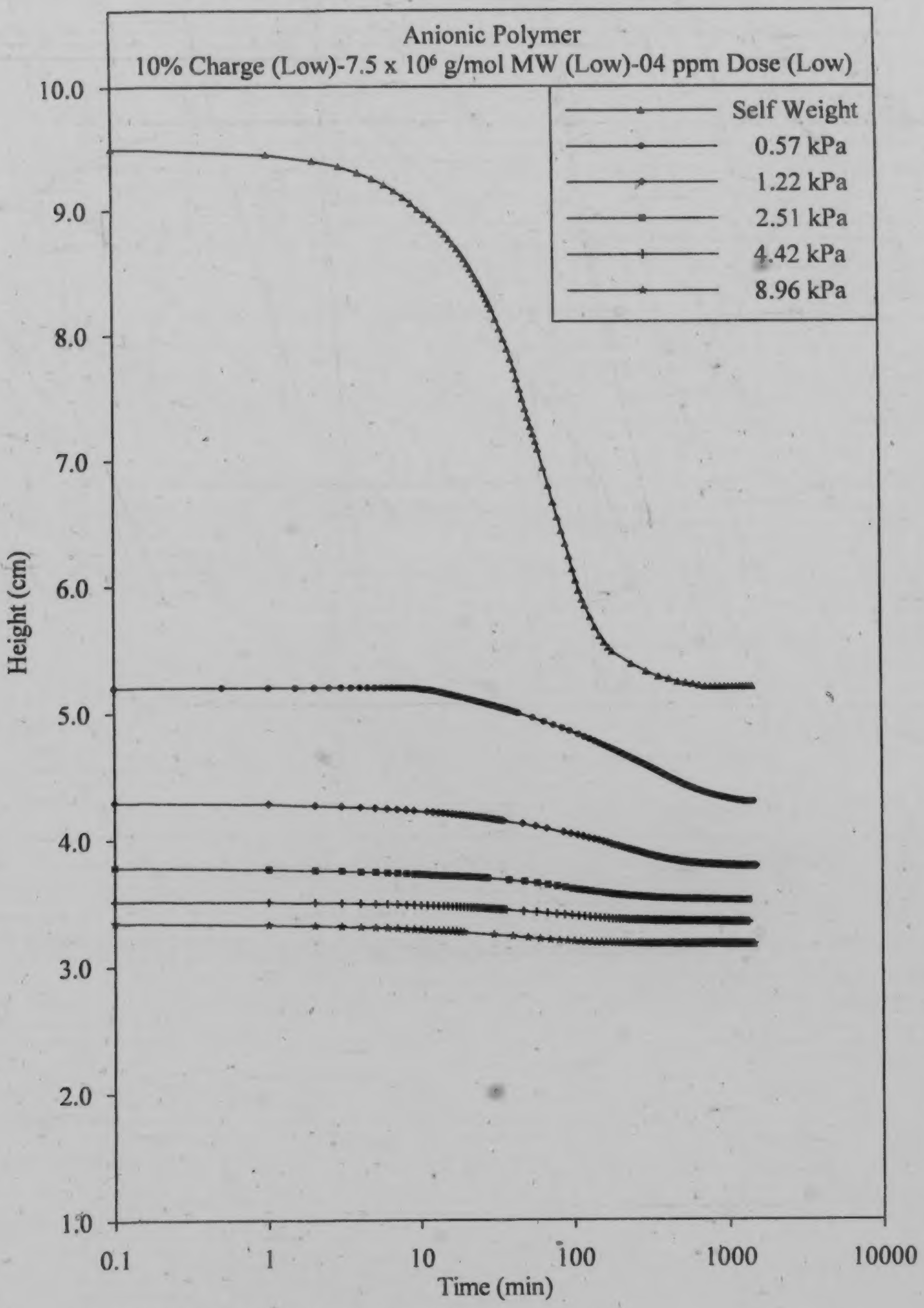

Figure A.8: Consolidation Test#1

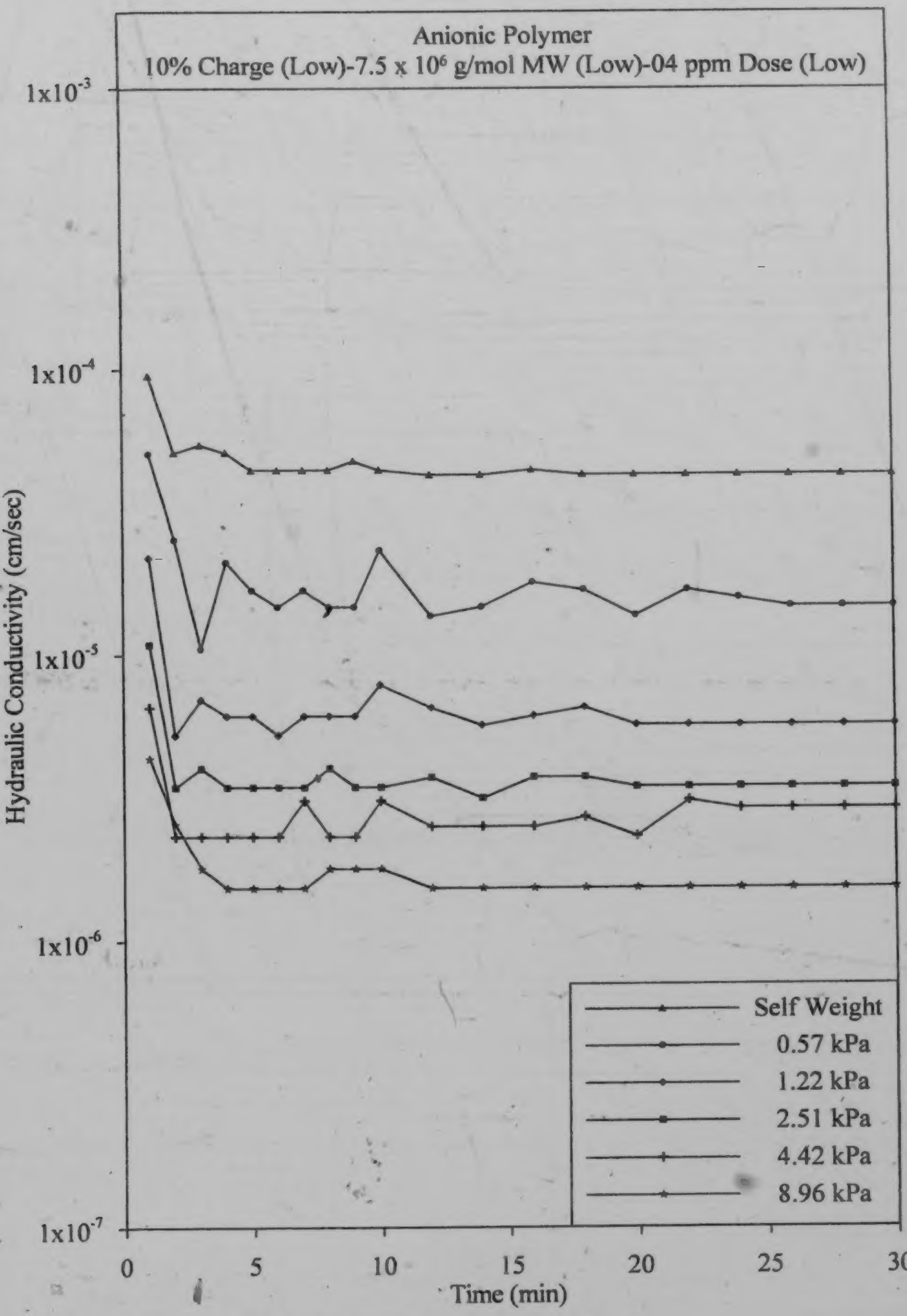

Figure A.9: Hydraulic conductivity during Test#1

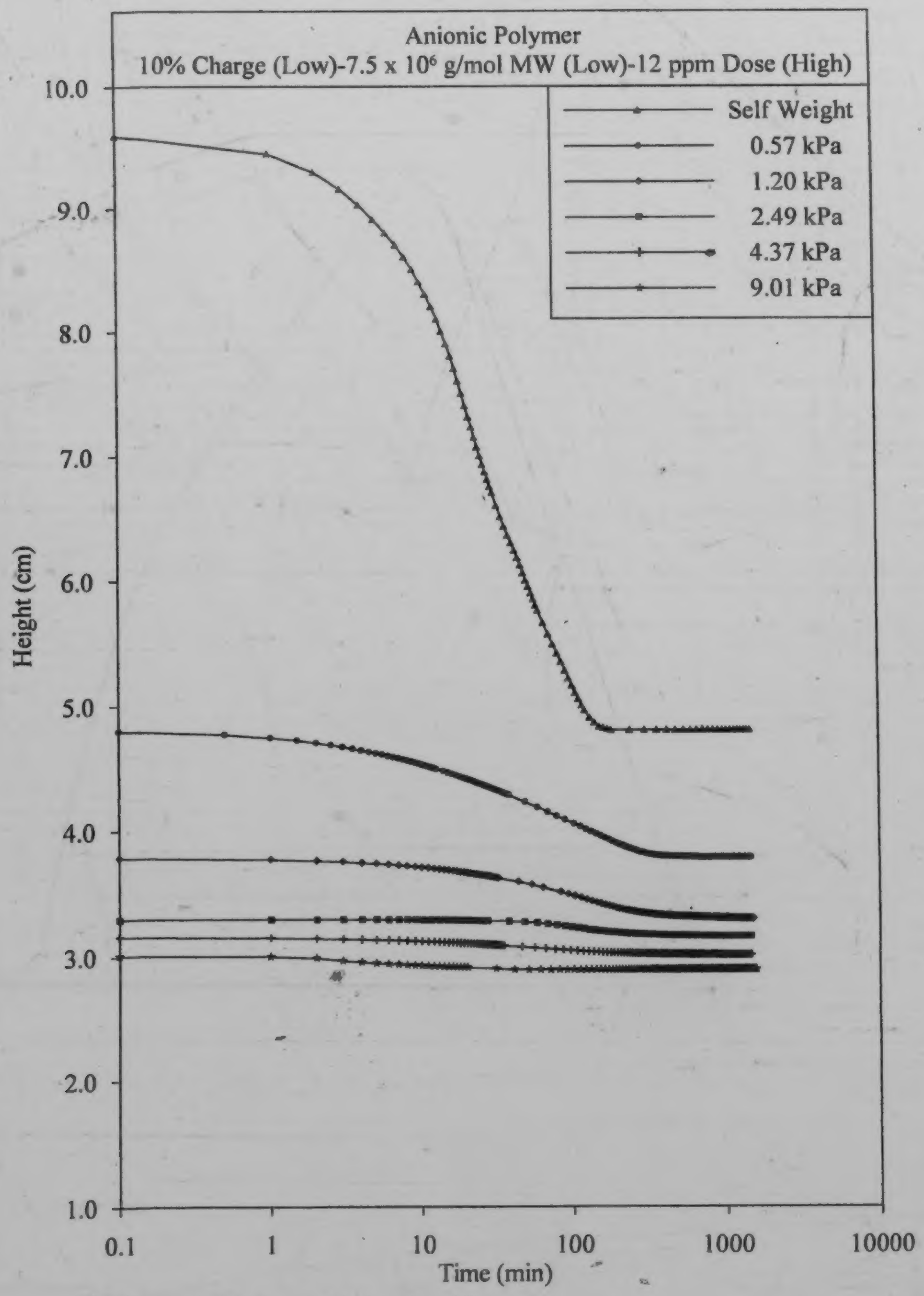

Figure A.10: Consolidation Test#2

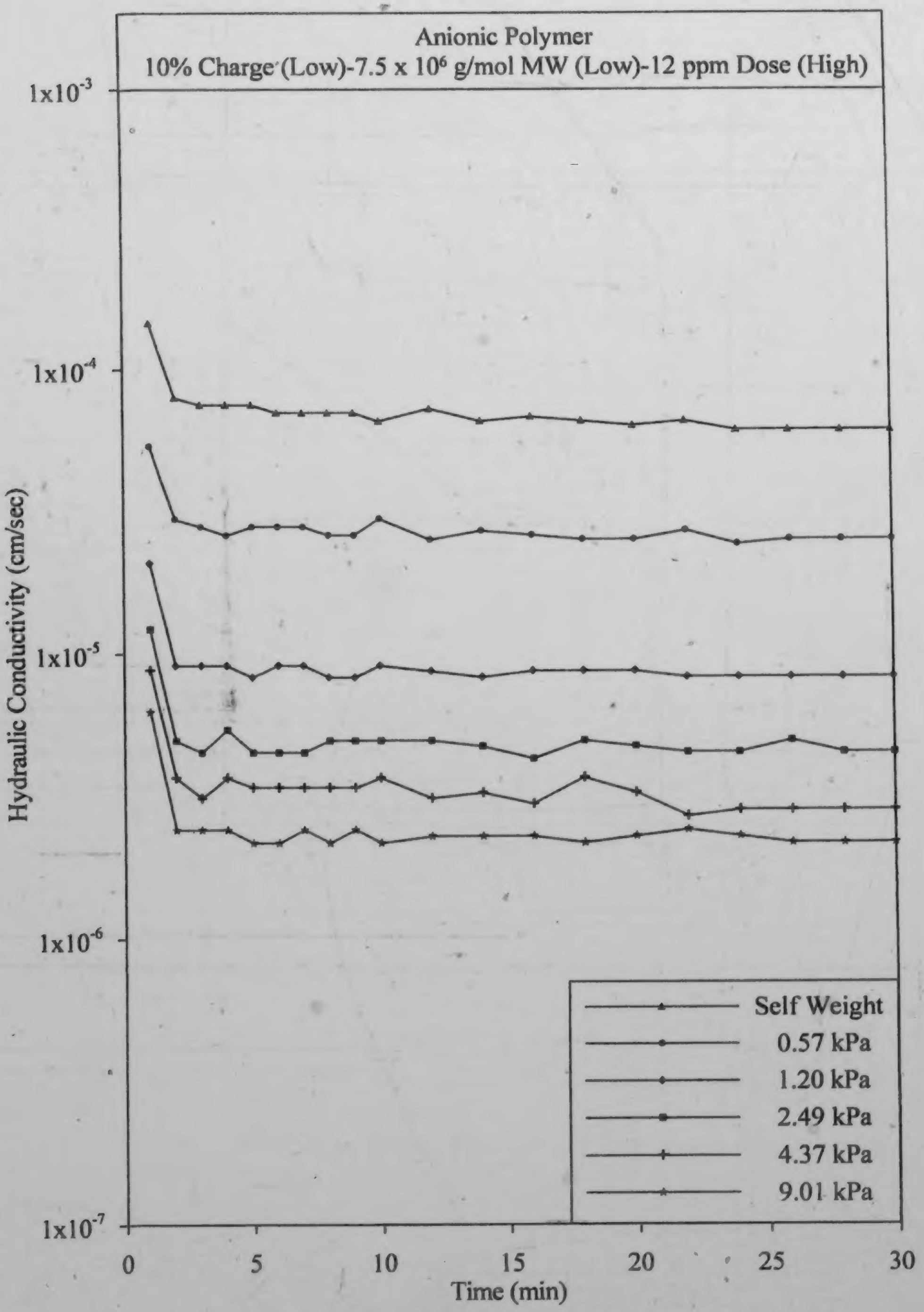

Figure A.11: Hydraulic conductivity during Test#2

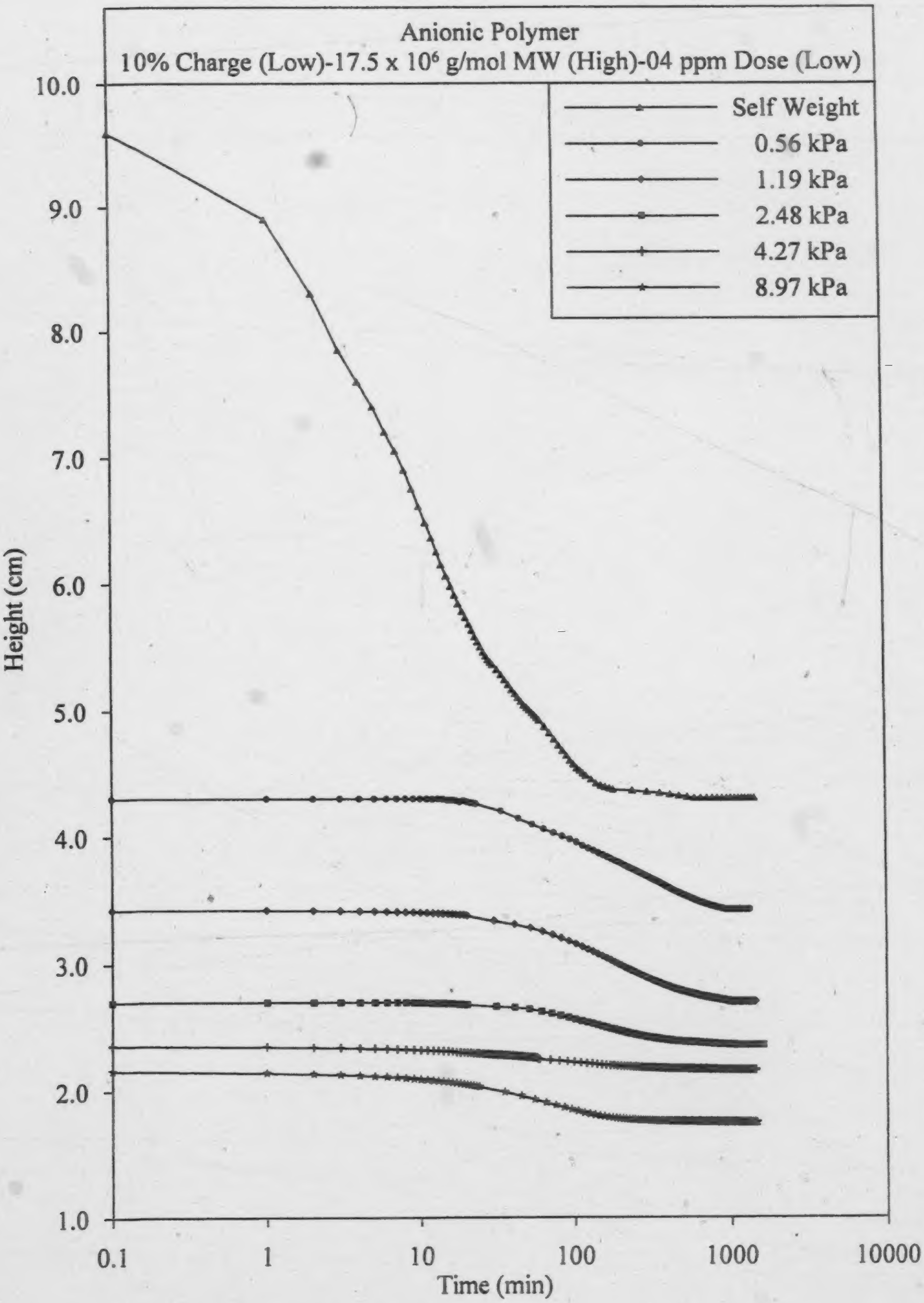

Figure A.12: Consolidation Test#3

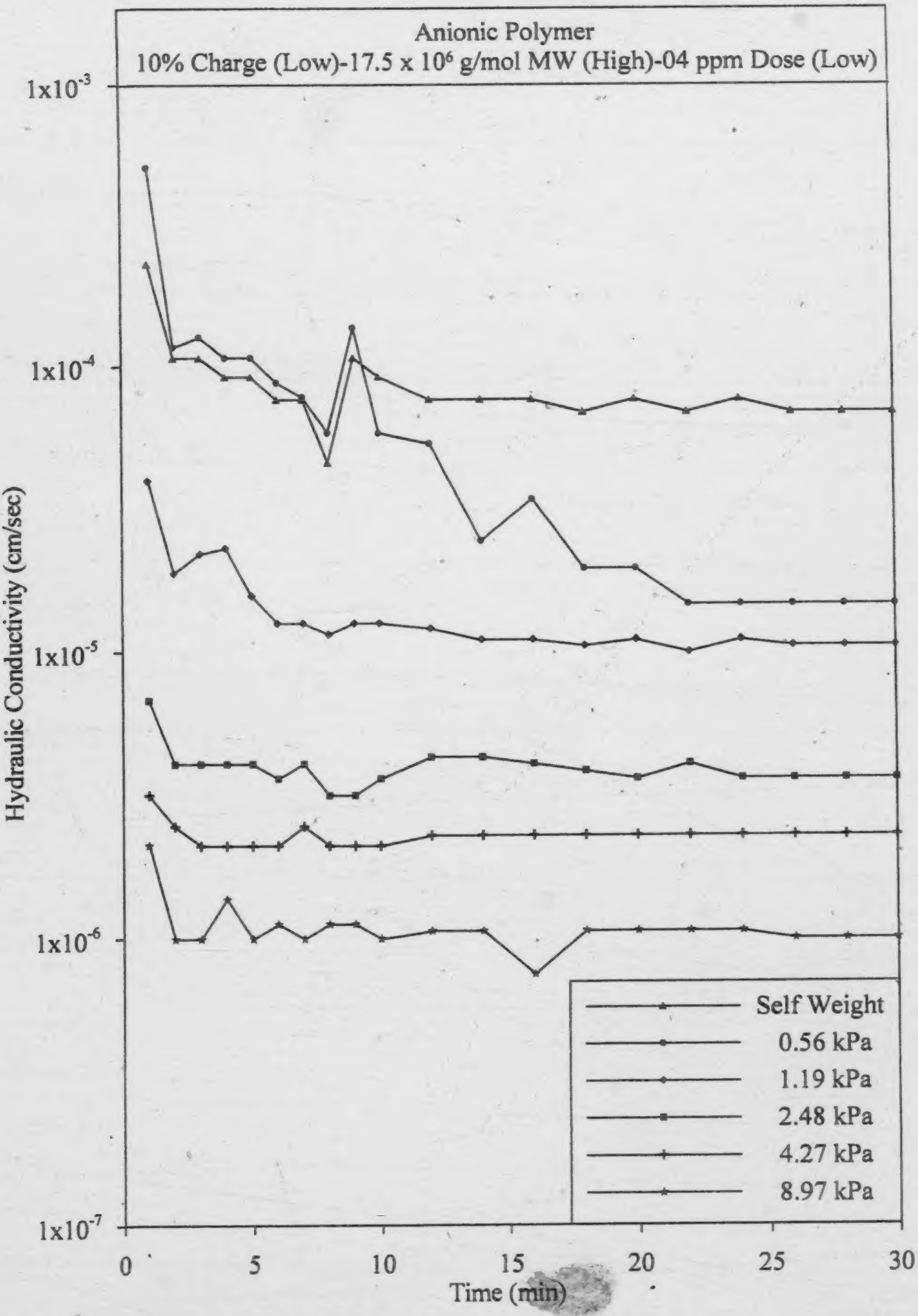

Figure A.13: Hydraulic conductivity during Test#3

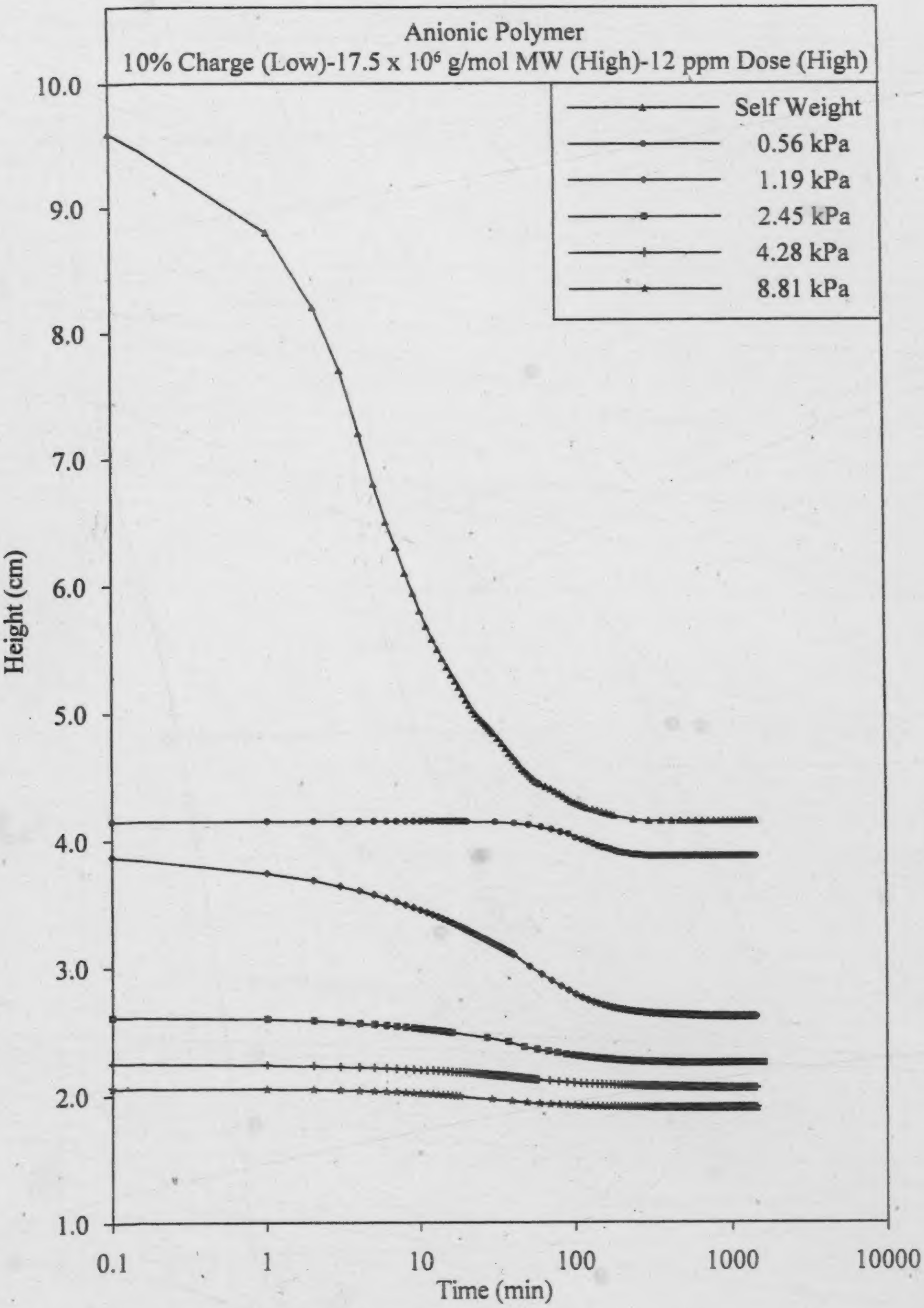

Figure A.14: Consolidation Test#4

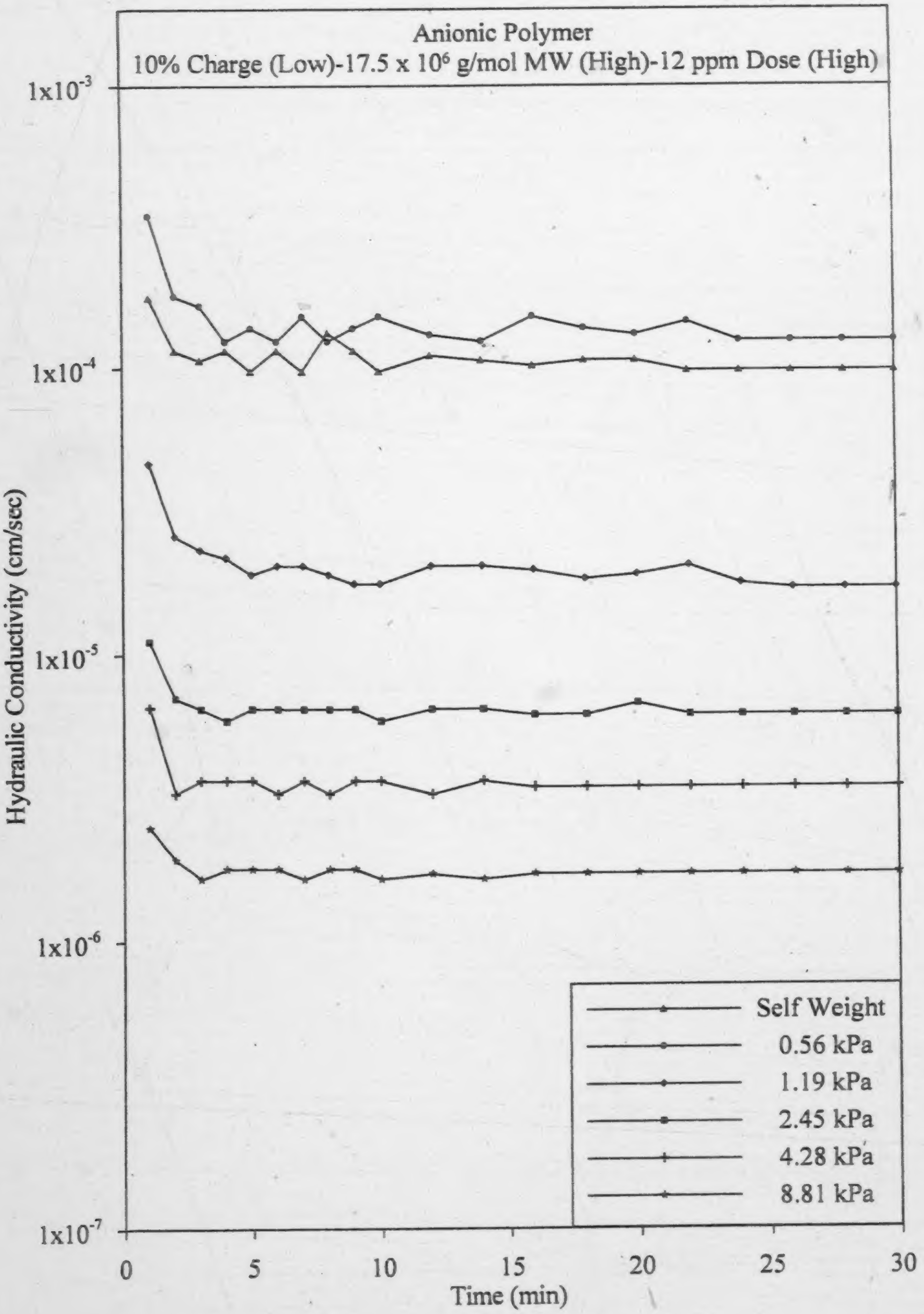

Figure A.15: Hydraulic conductivity during Test#4

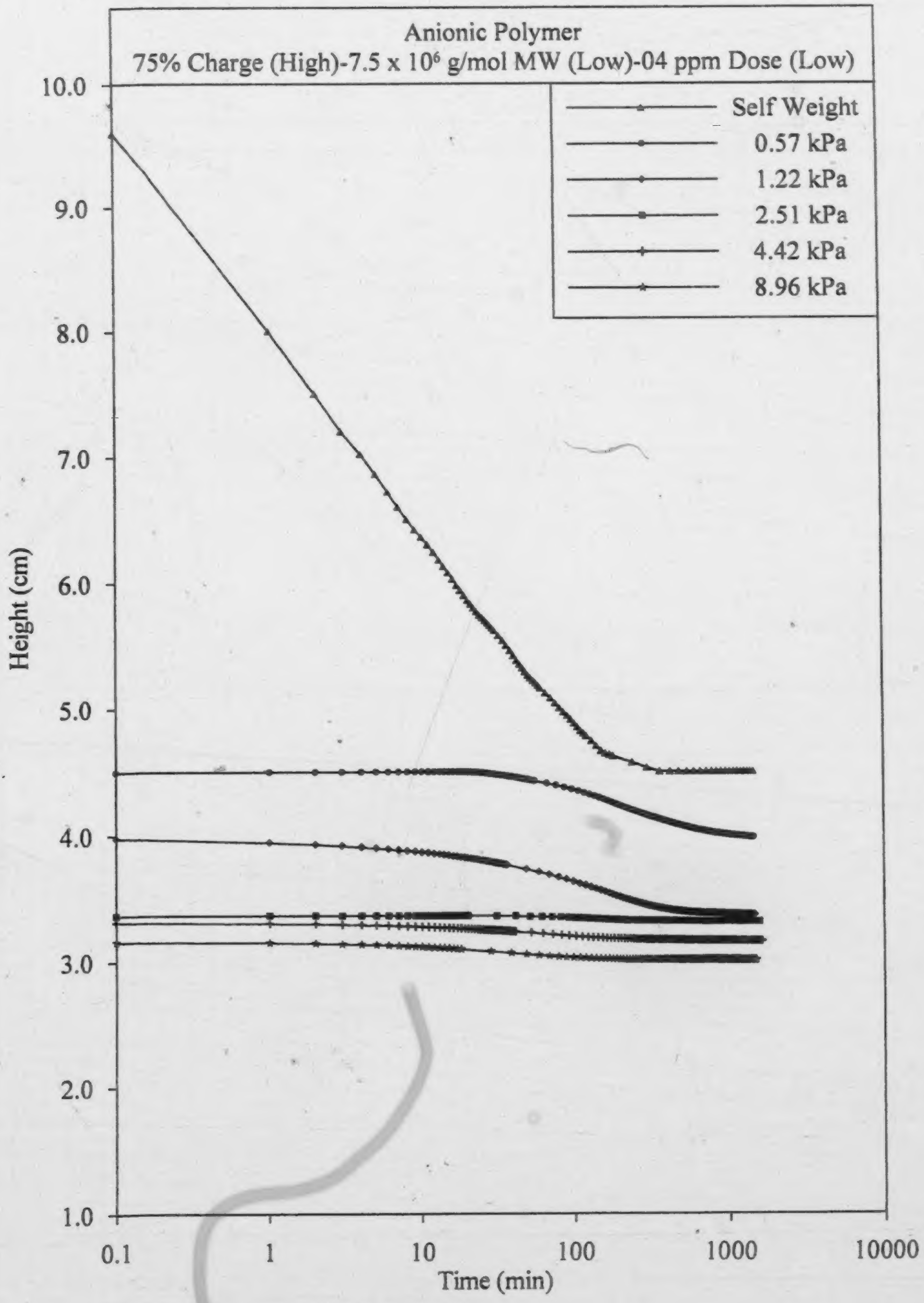

Figure A.16: Consolidation Test#5

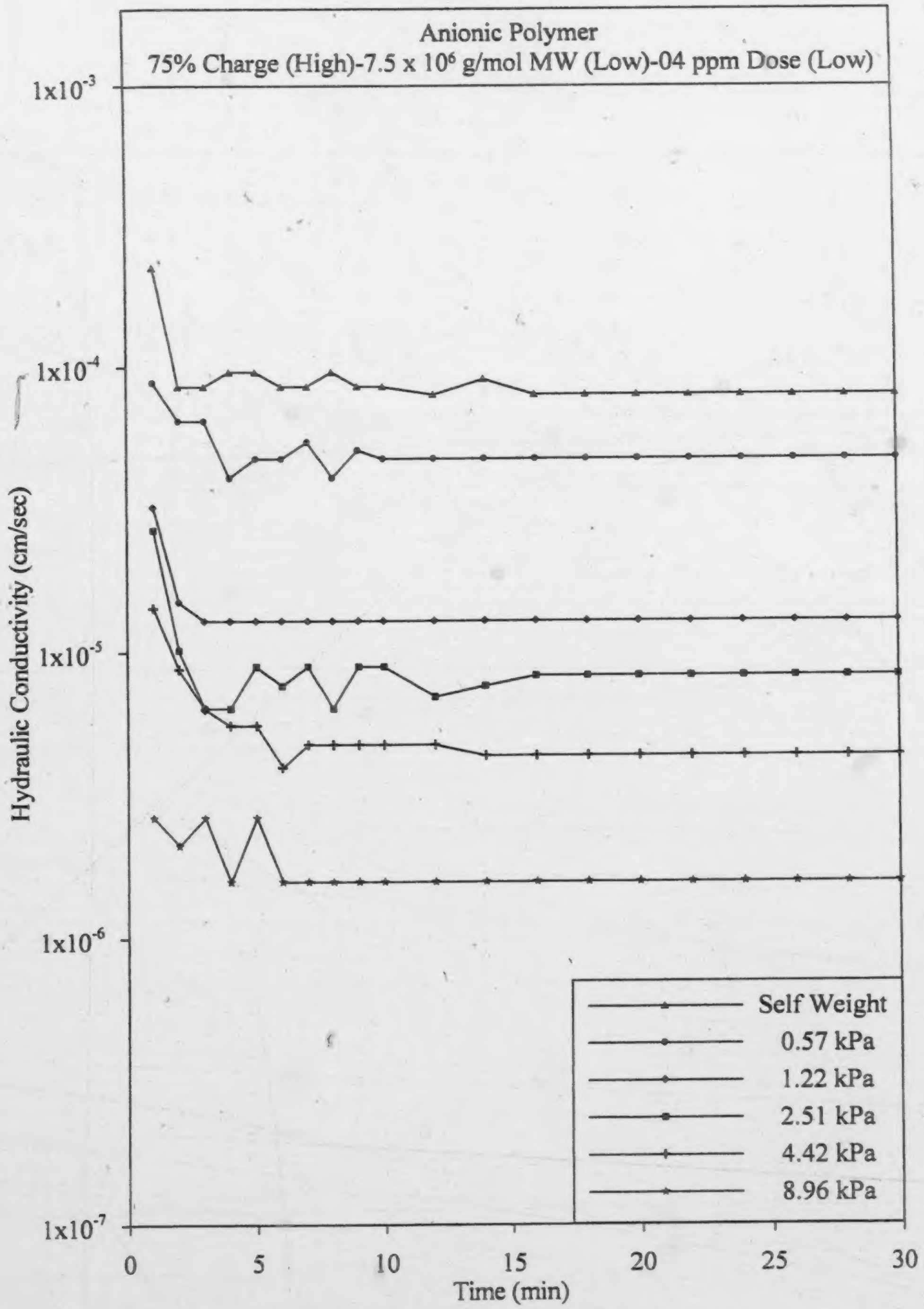

Figure A.17: Hydraulic conductivity during Test#5

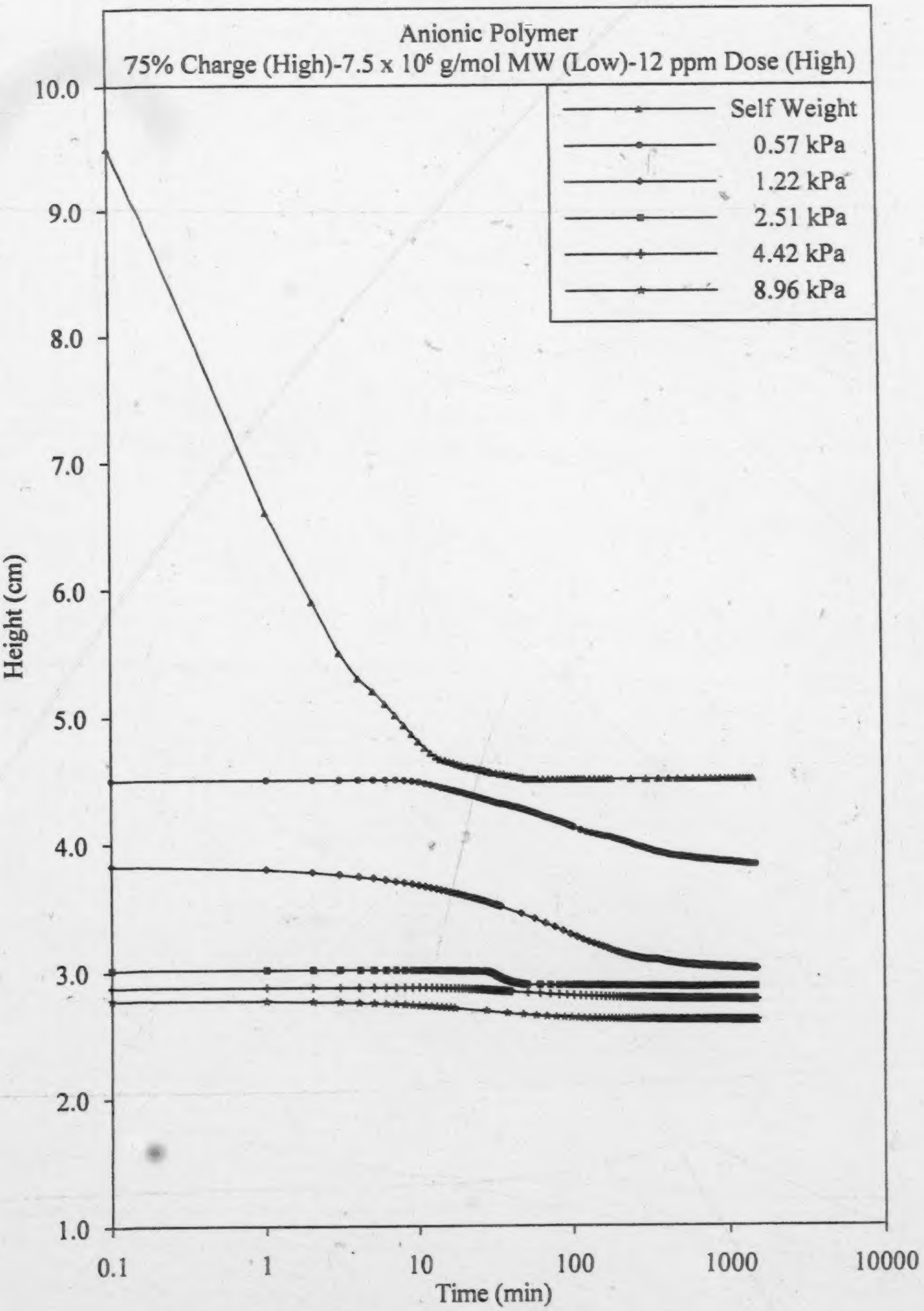

Figure A.18: Consolidation Test#6

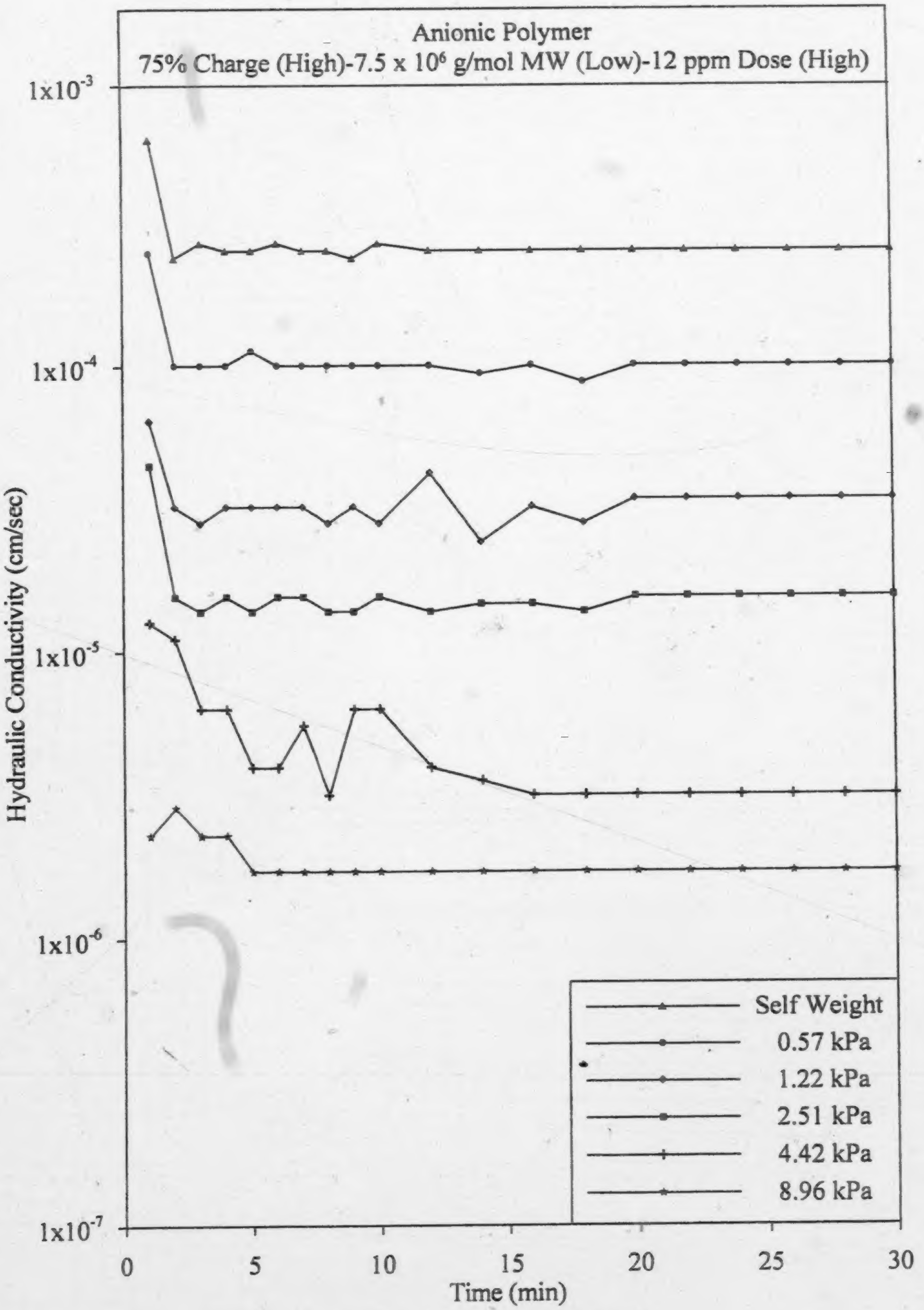

Figure A.19: Hydraulic conductivity during Test#6

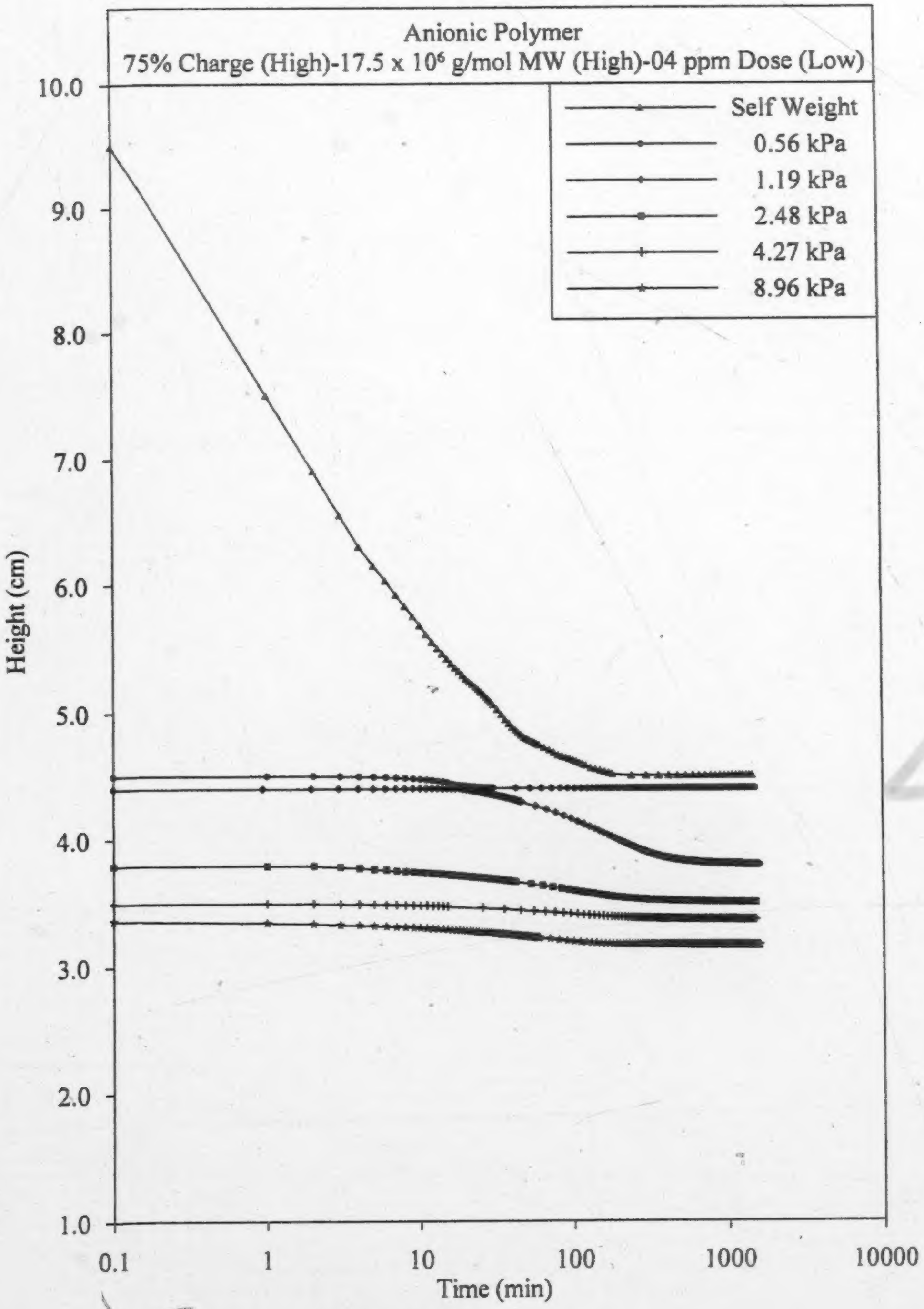

Figure A.20: Consolidation-Test#7

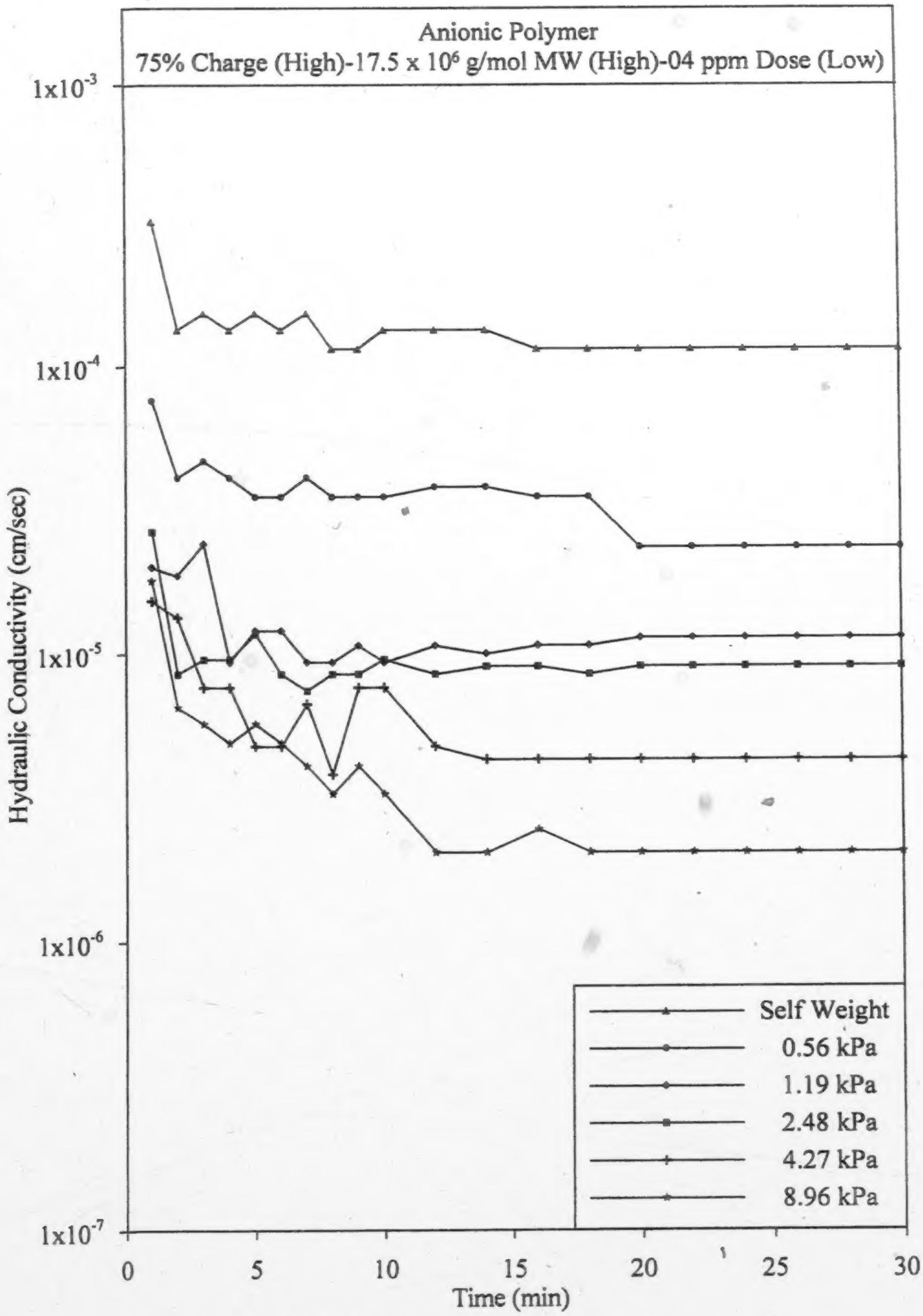

Figure A.21: Hydraulic conductivity during Test#7

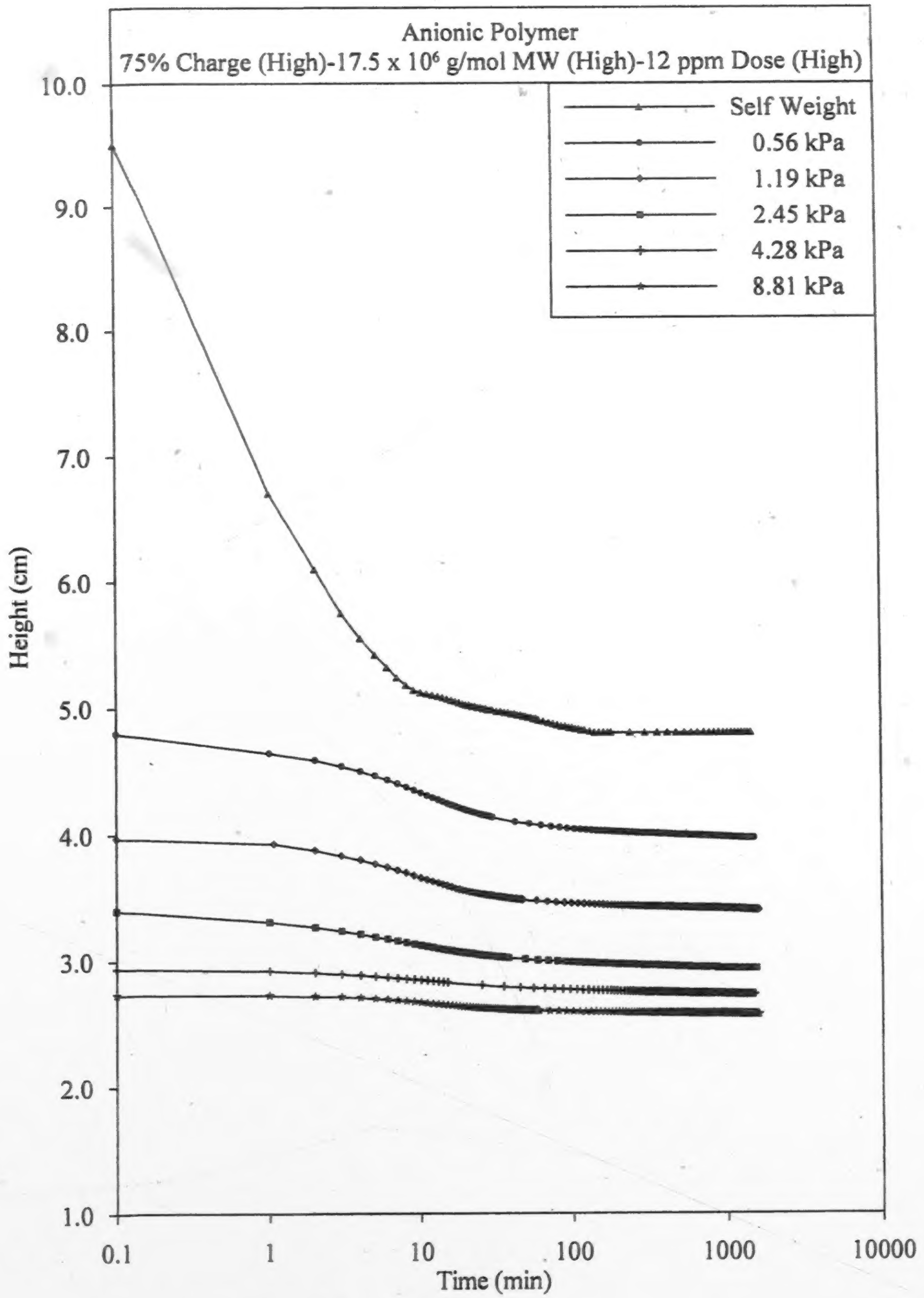

Figure A.22: Consolidation Test#8

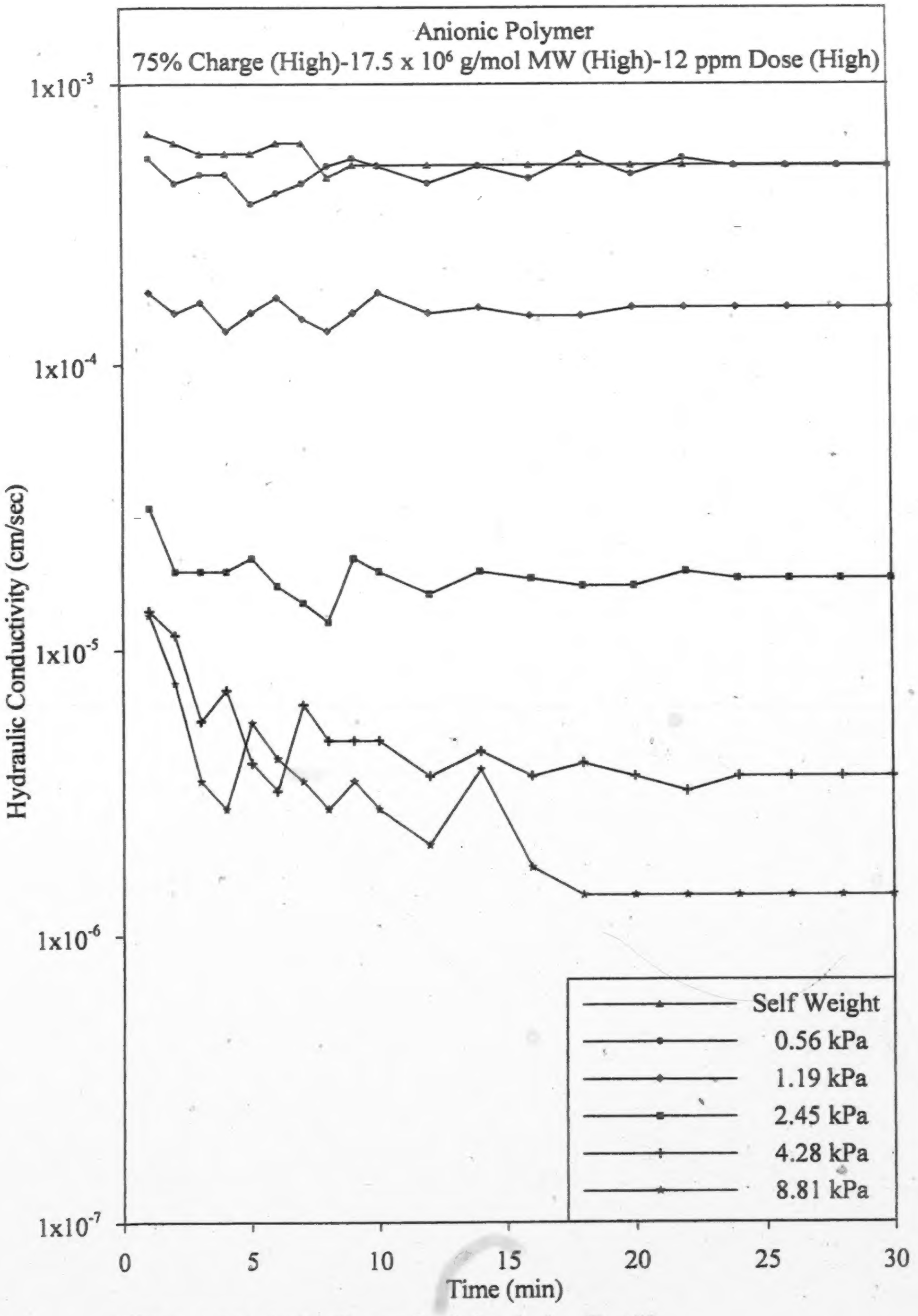

Figure A.23: Hydraulic conductivity during Test#8

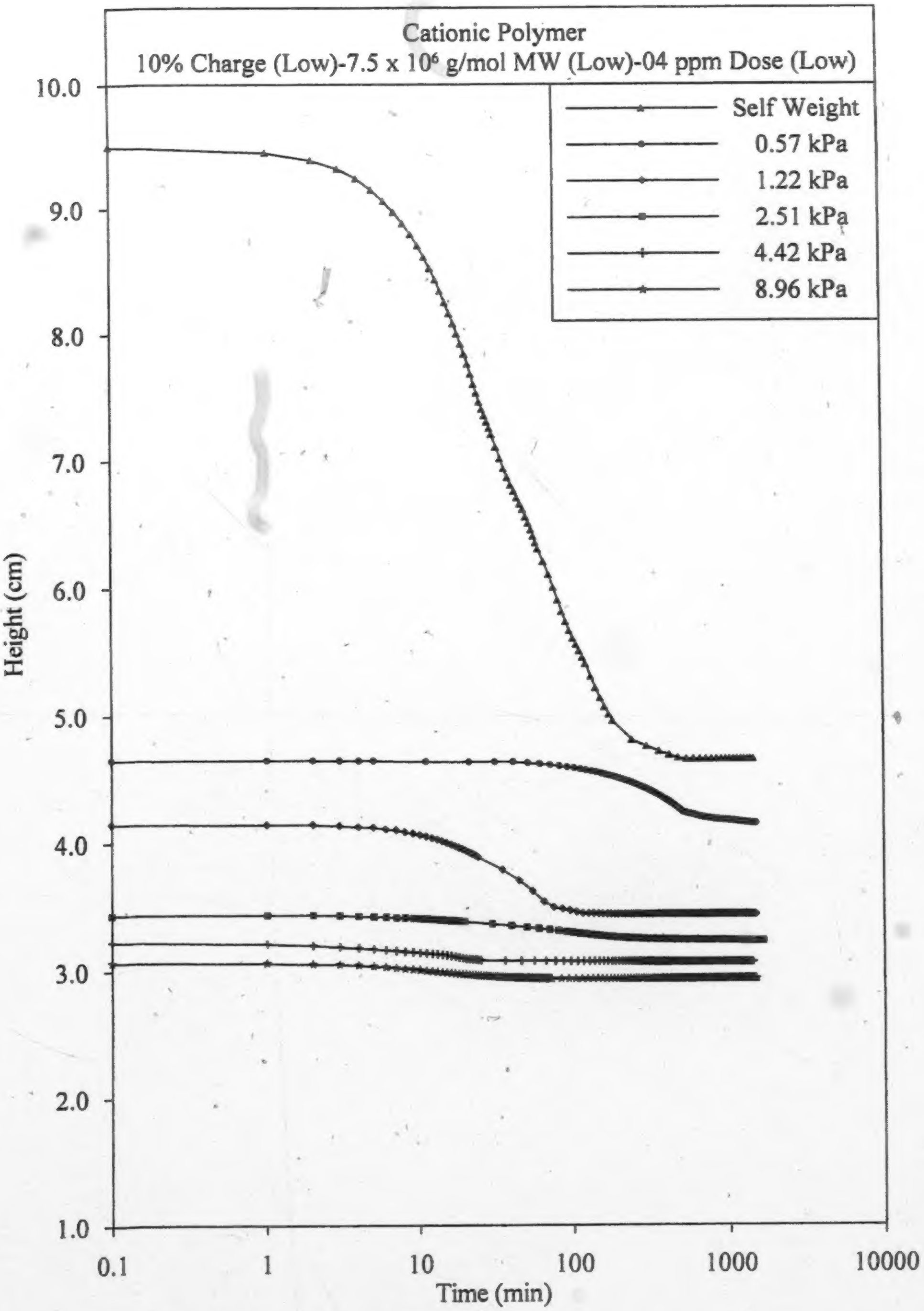

Figure A.24: Consolidation Test#9

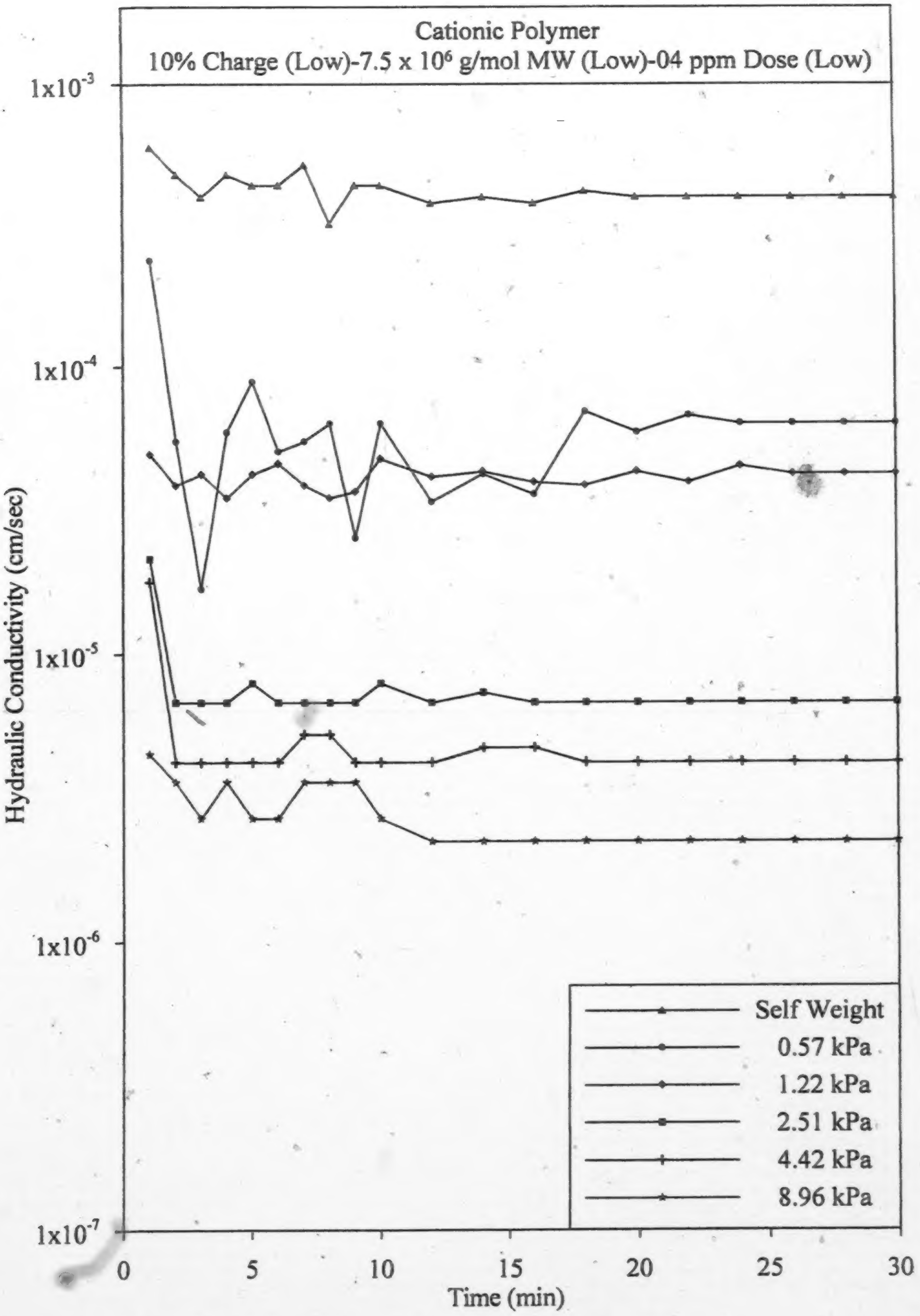

Figure A.25: Hydraulic conductivity during Test#9

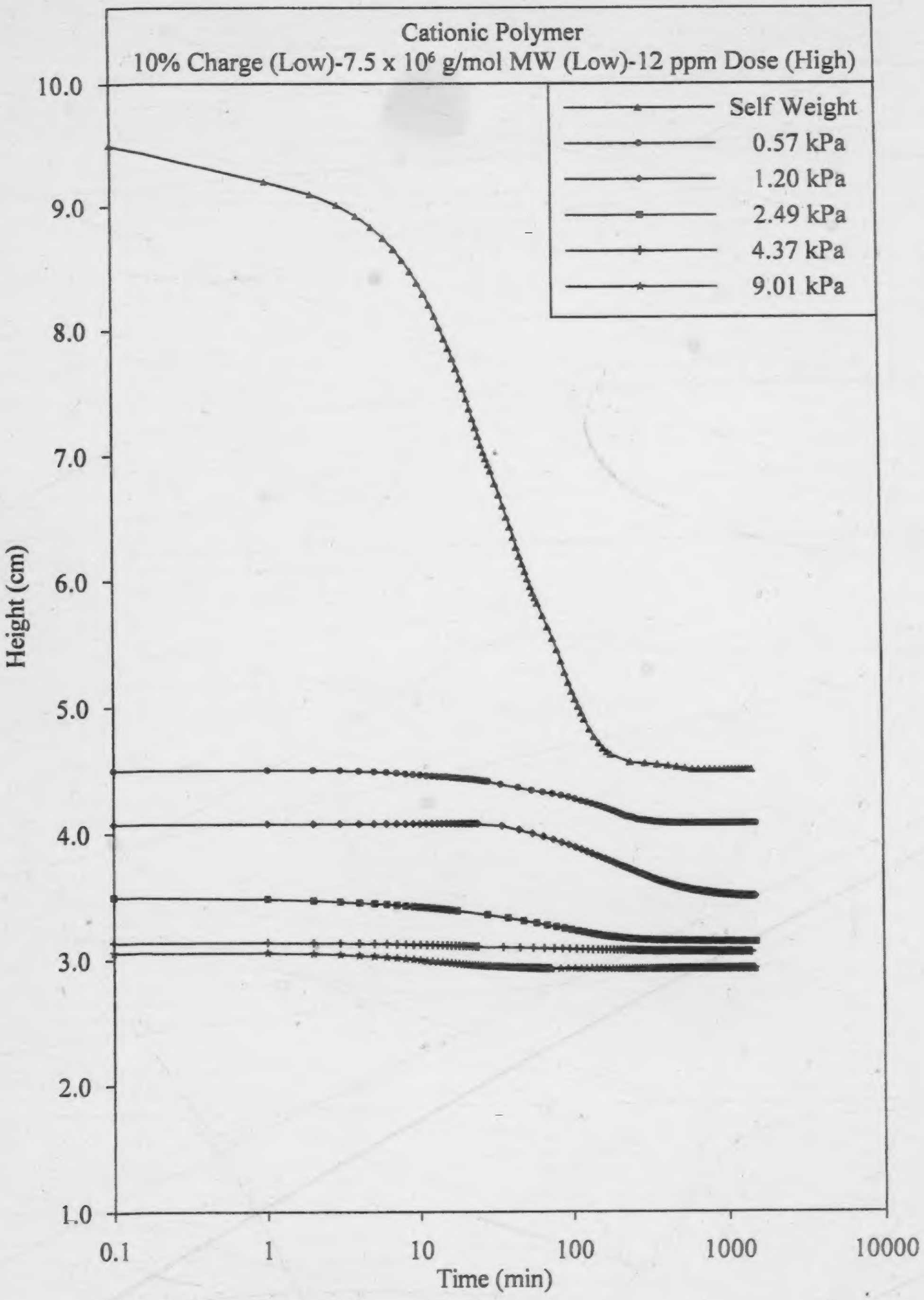

Figure A.26: Consolidation Test#10

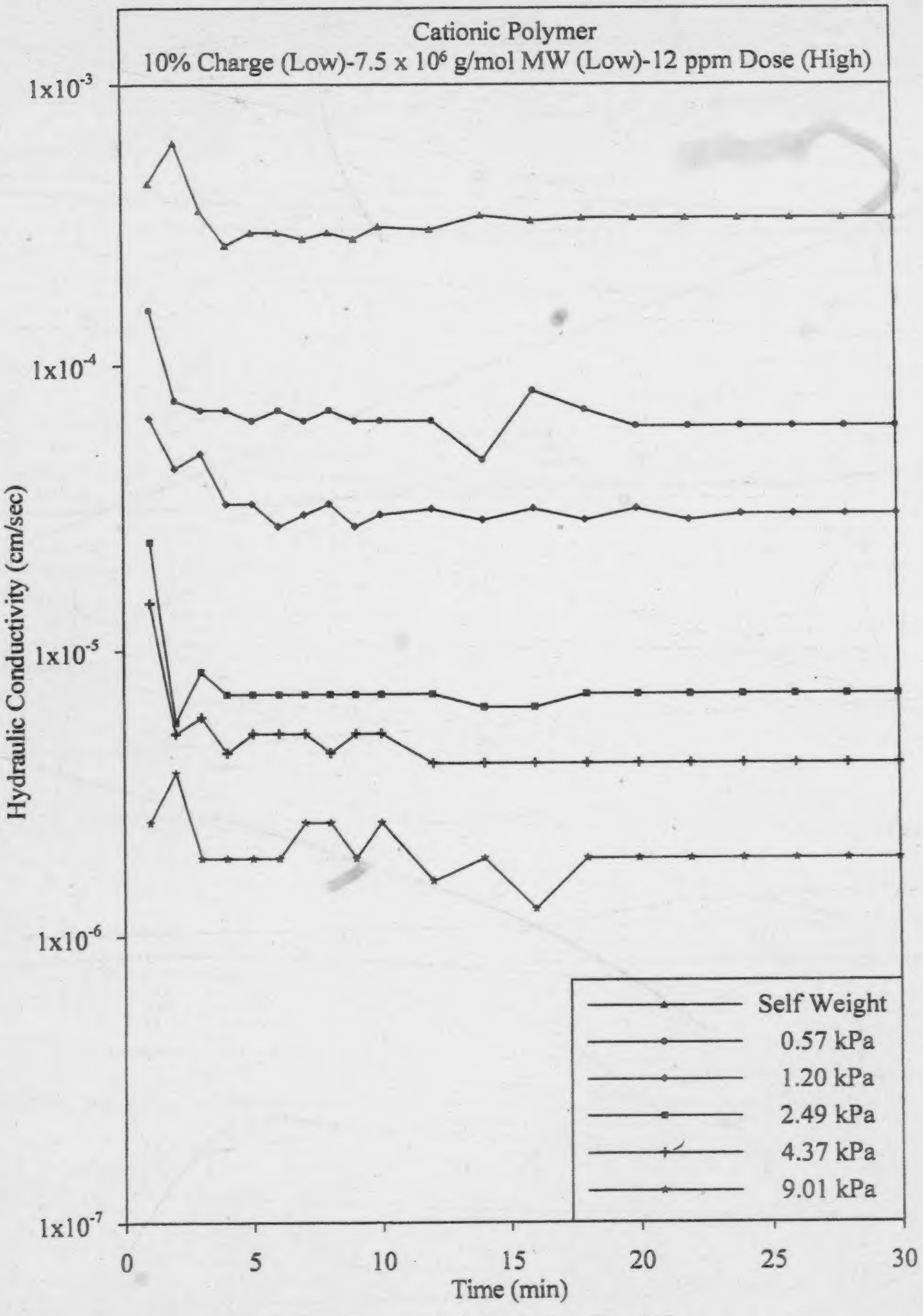

Figure A.27: Hydraulic conductivity during Test#10

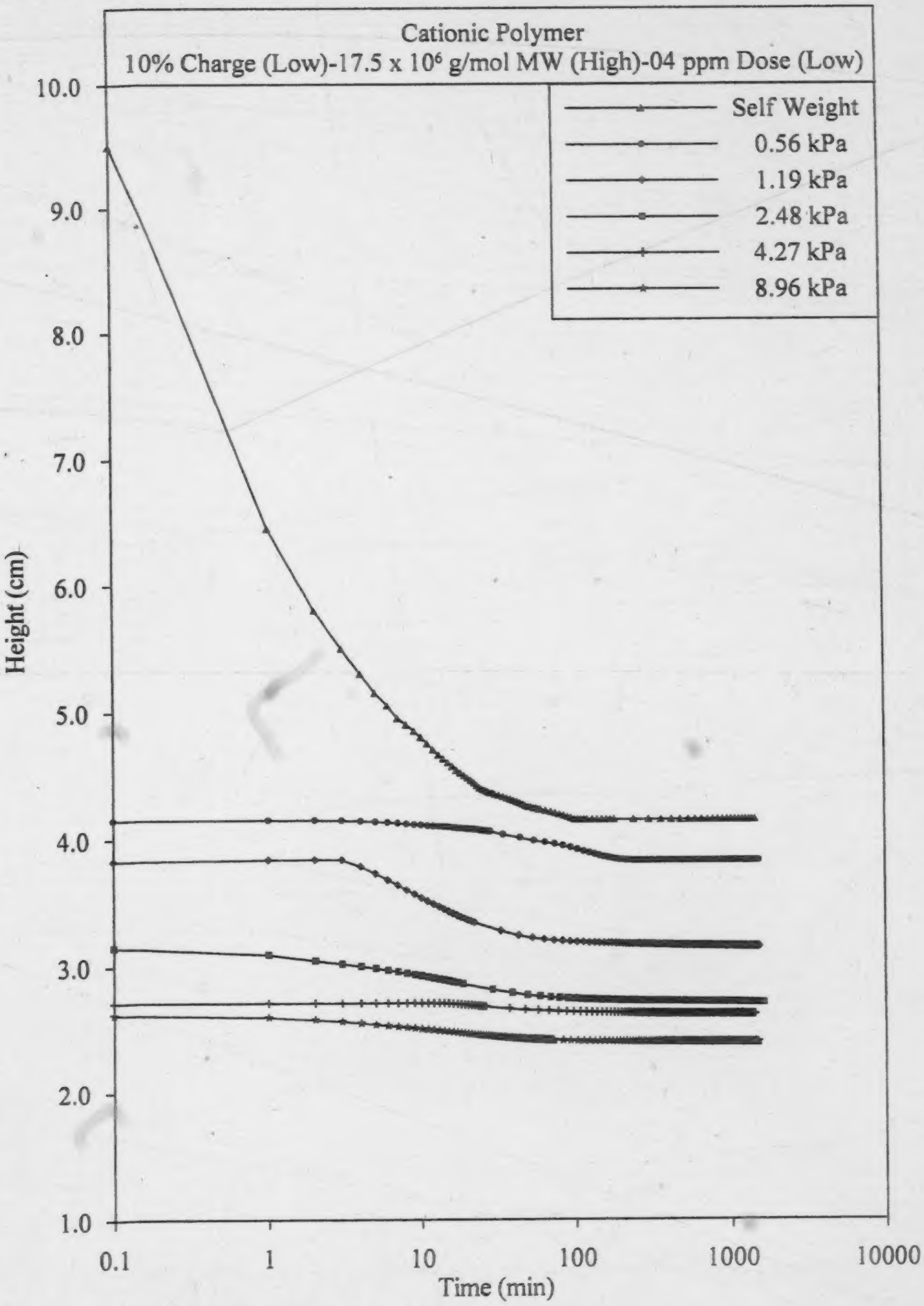

Figure A.28: Consolidation Test#11

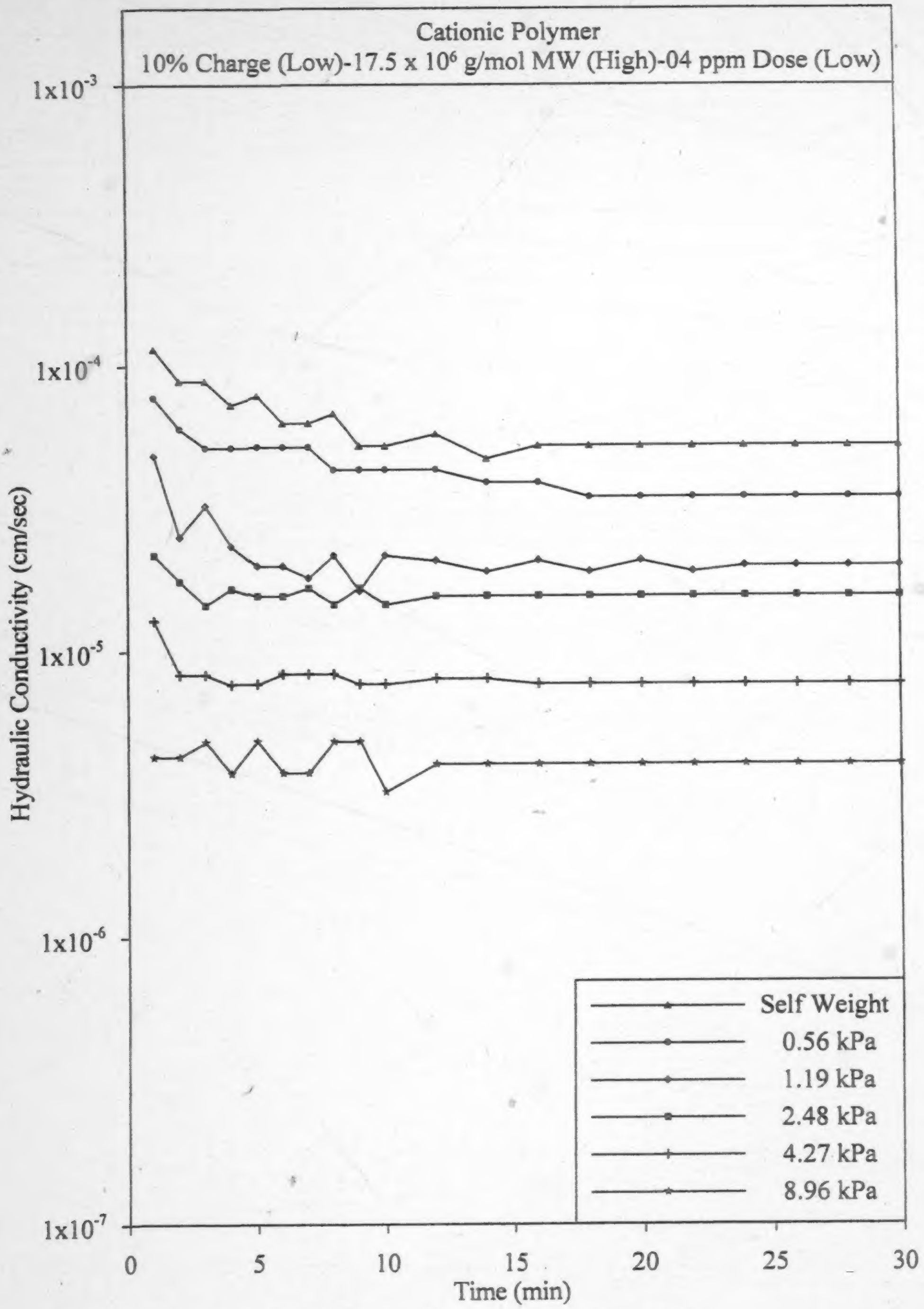

Figure A.29: Hydraulic conductivity during Test#11

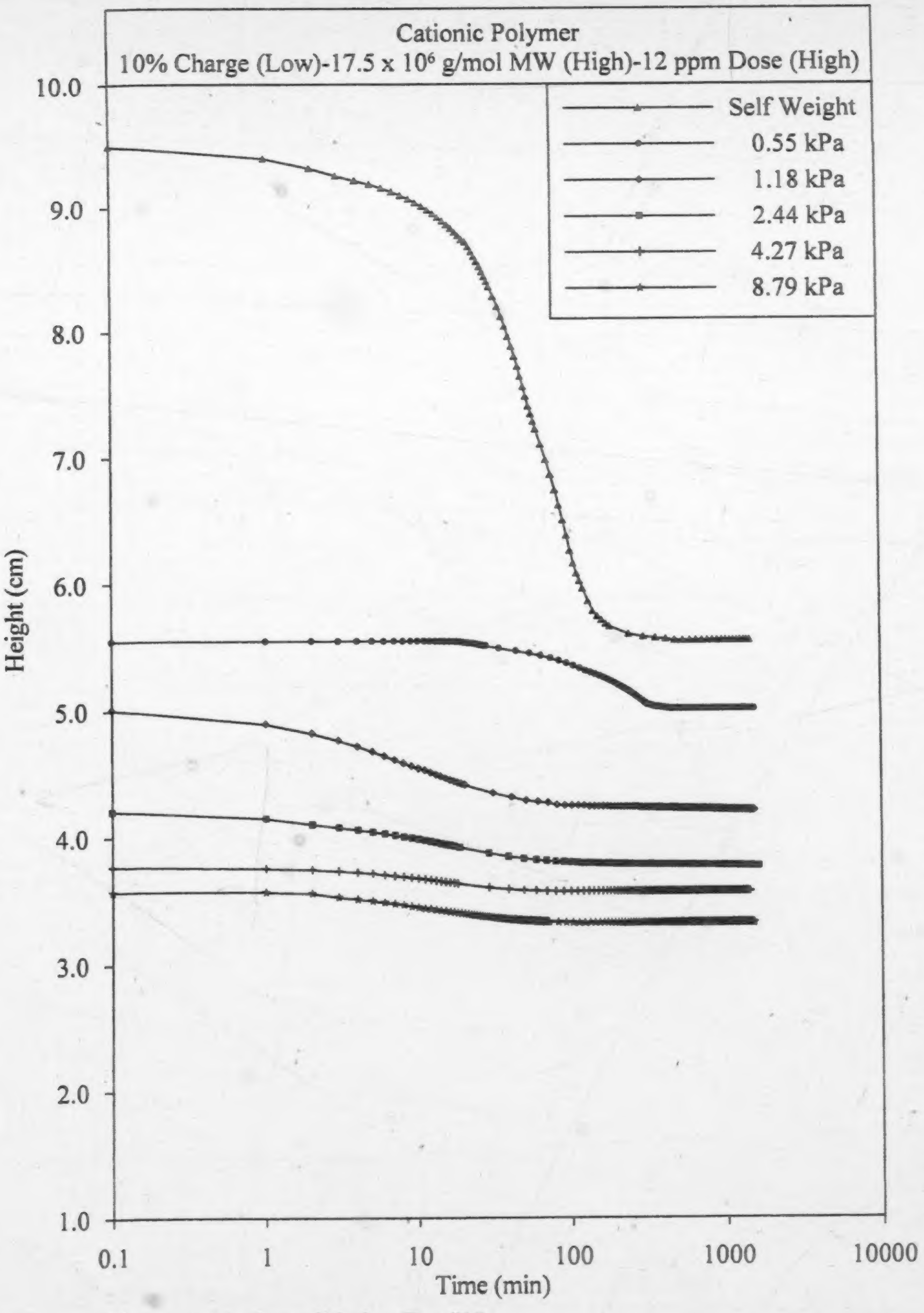

Figure A.30: Consolidation Test#12

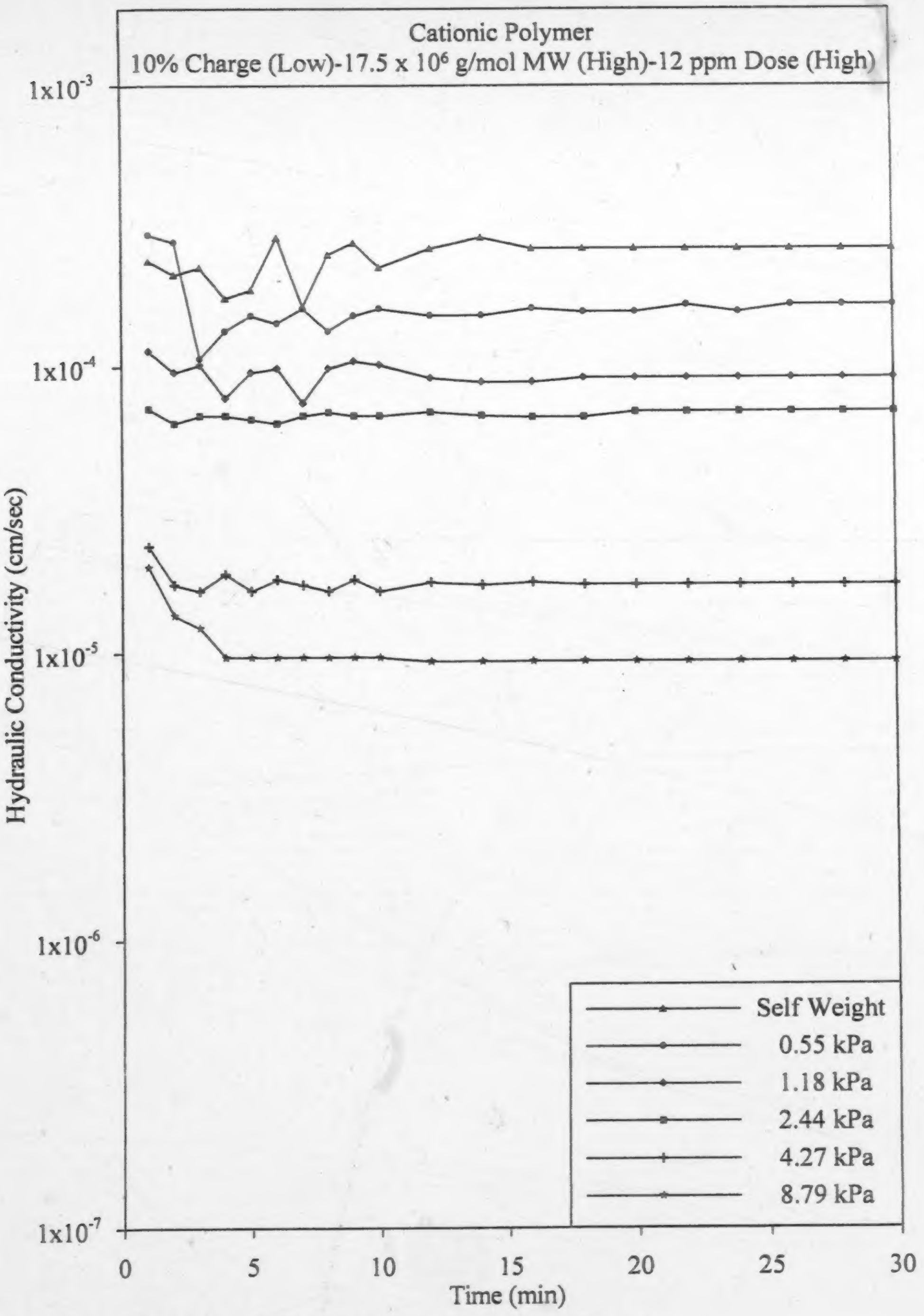

Figure A.31: Hydraulic conductivity during Test#12

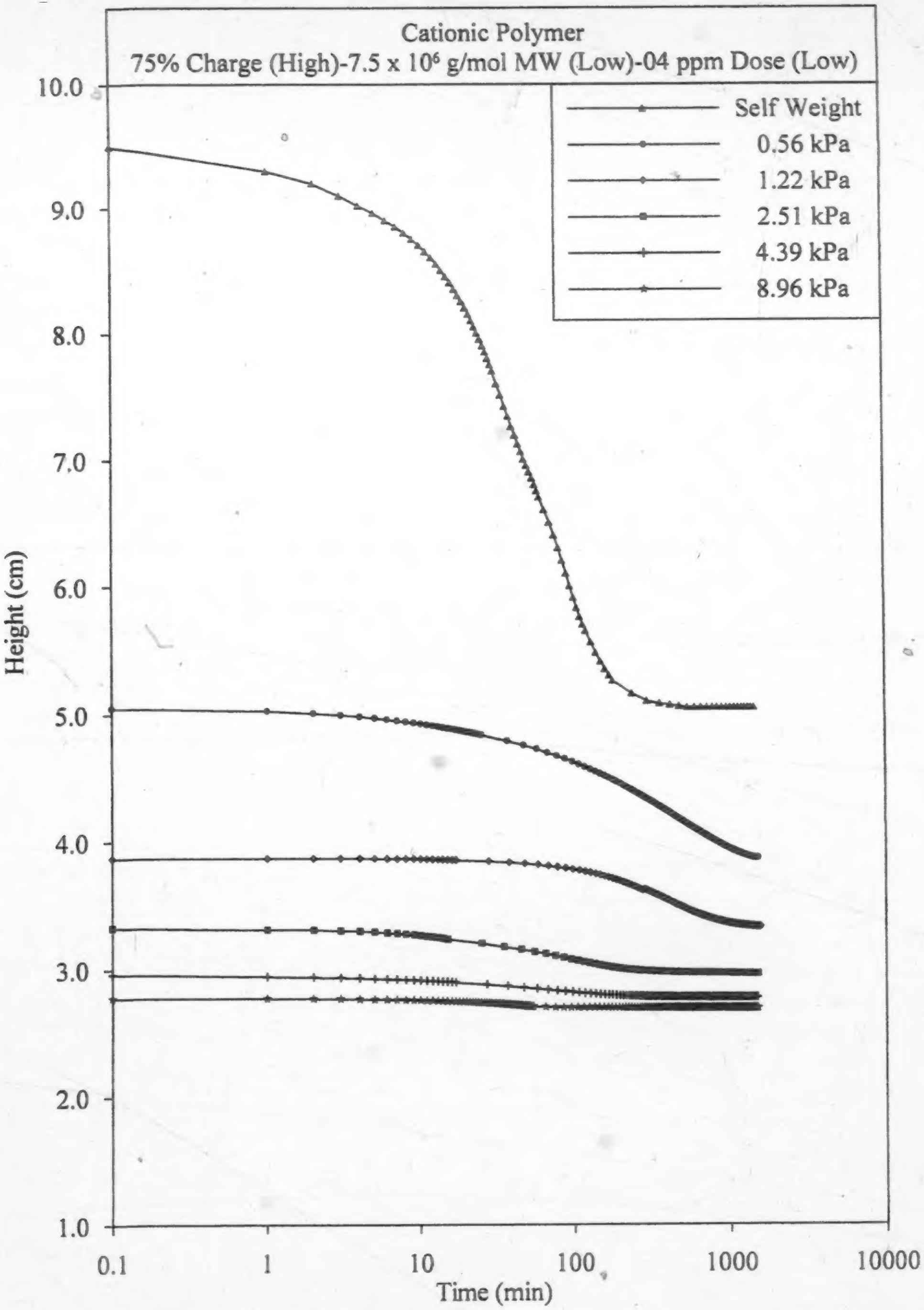

Figure A.32: Consolidation Test#13

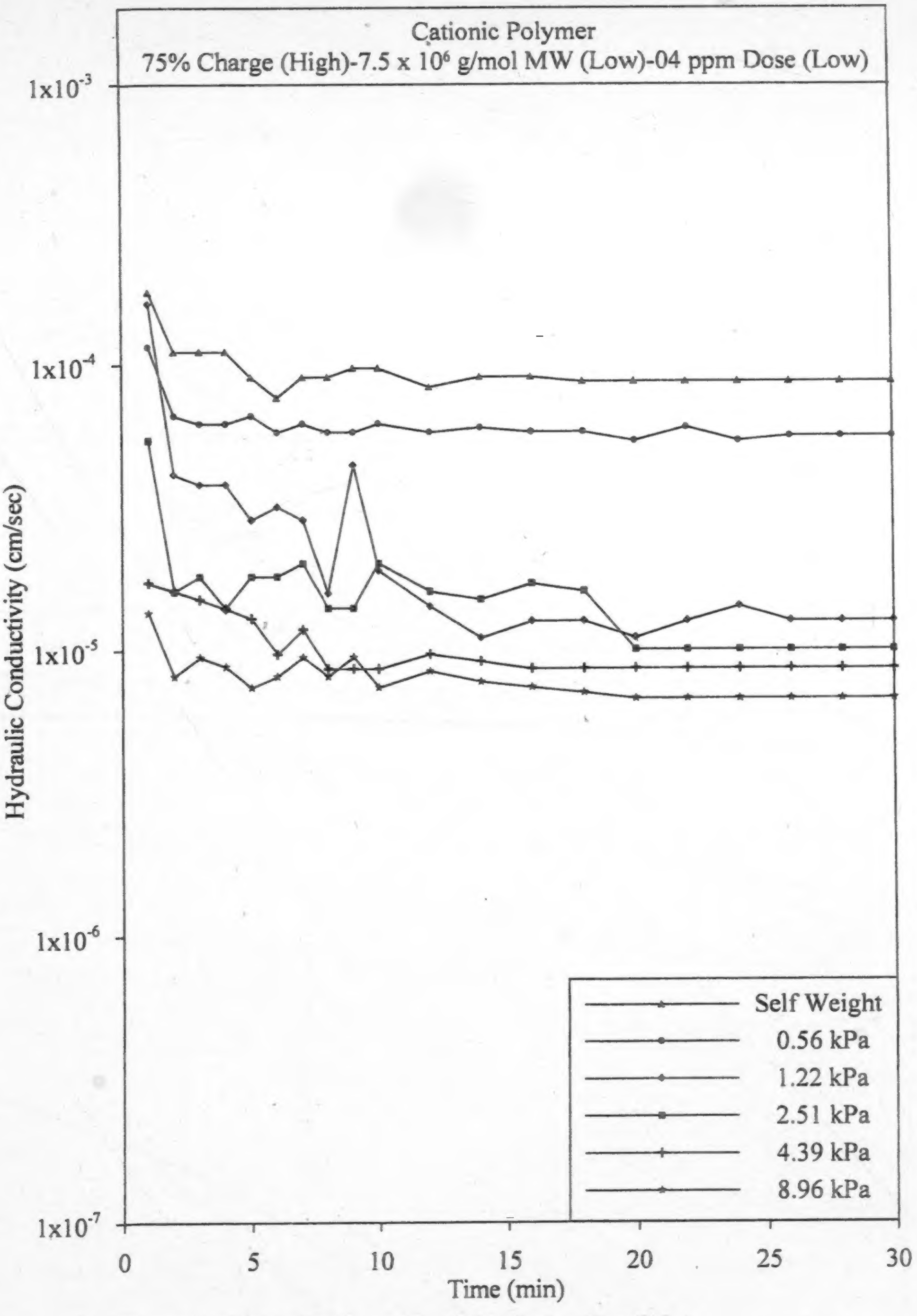

Figure A.33: Hydraulic conductivity during Test#13

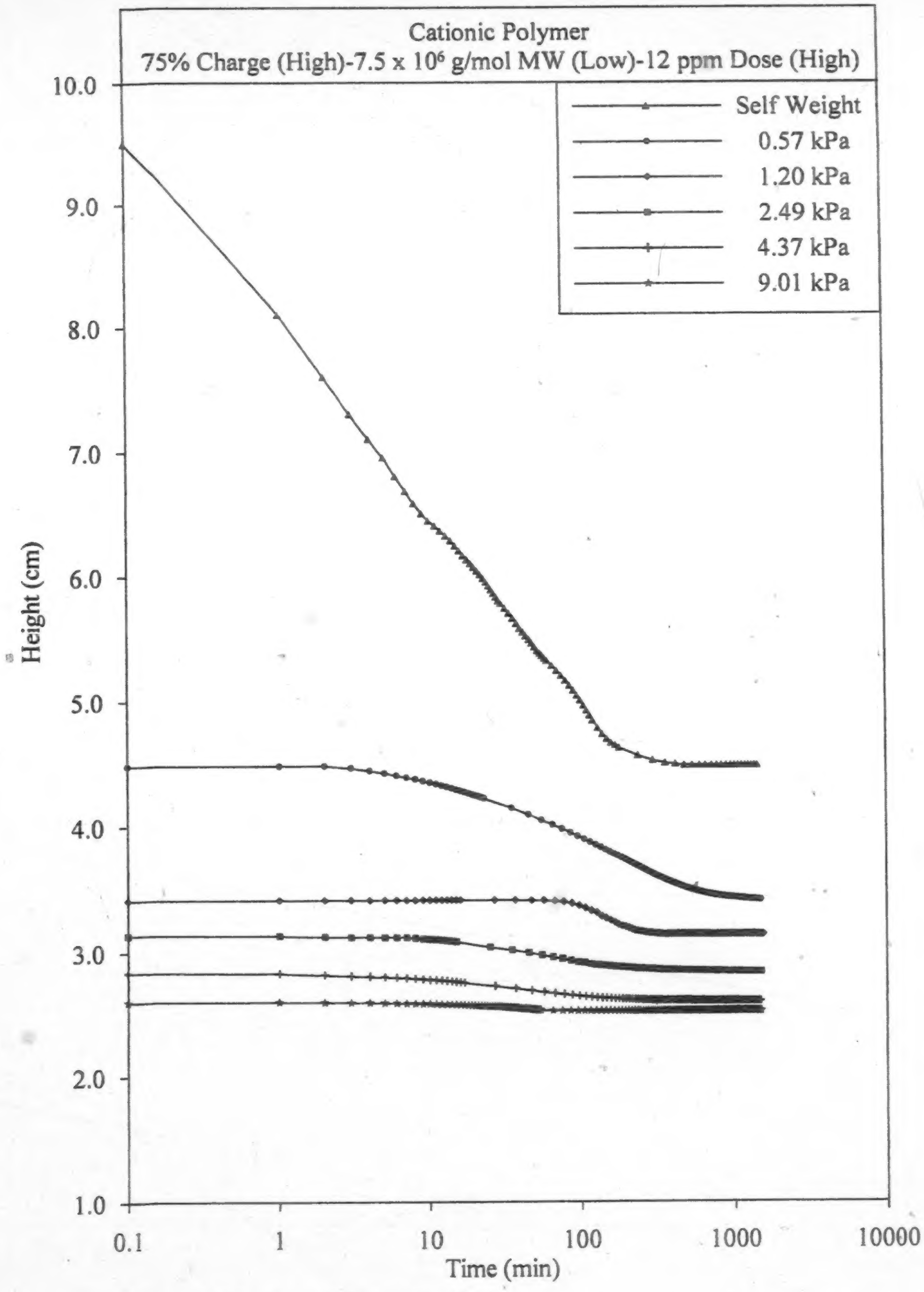

Figure A.34: Consolidation Test#14

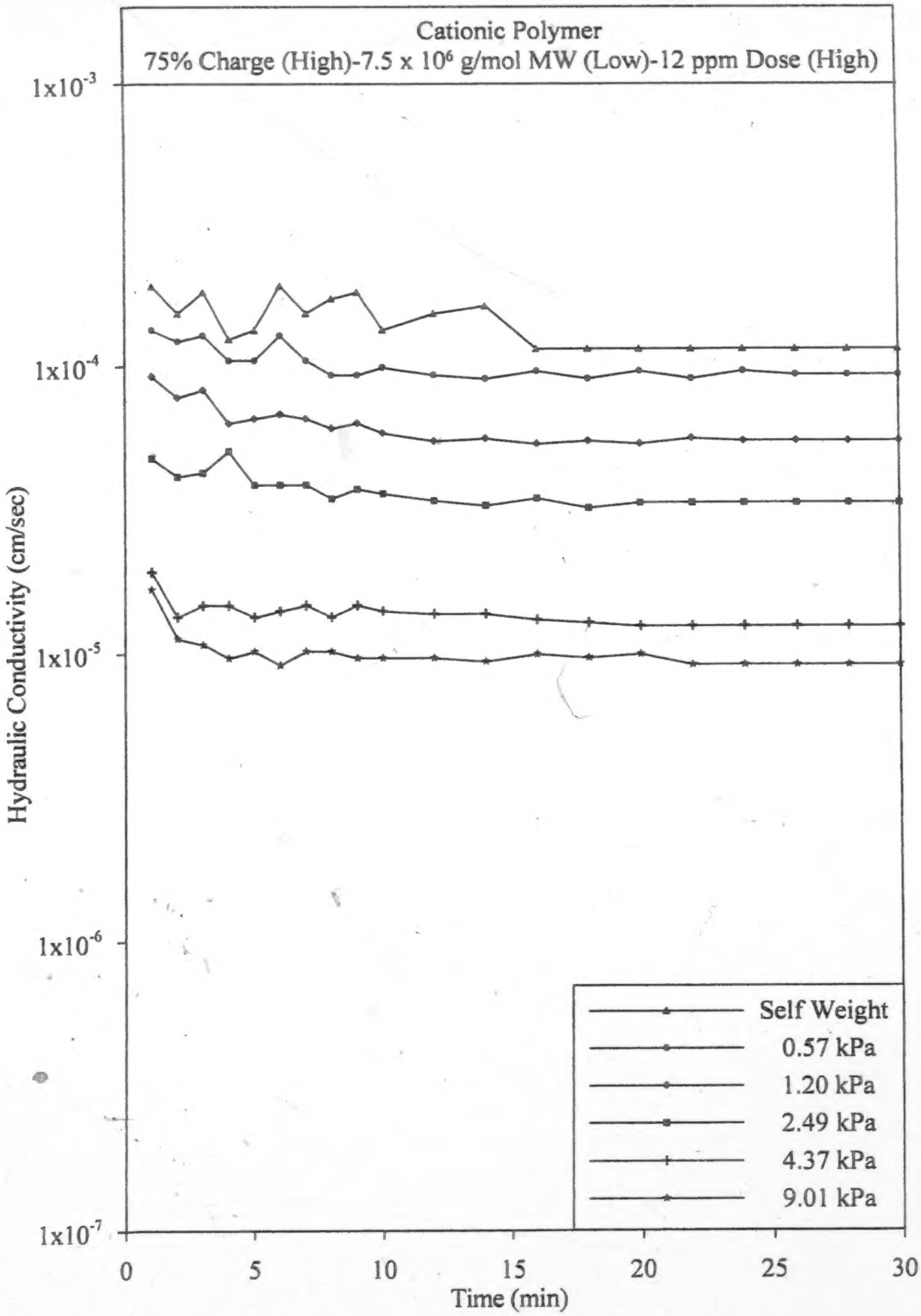

Figure A.35: Hydraulic conductivity during Test#14

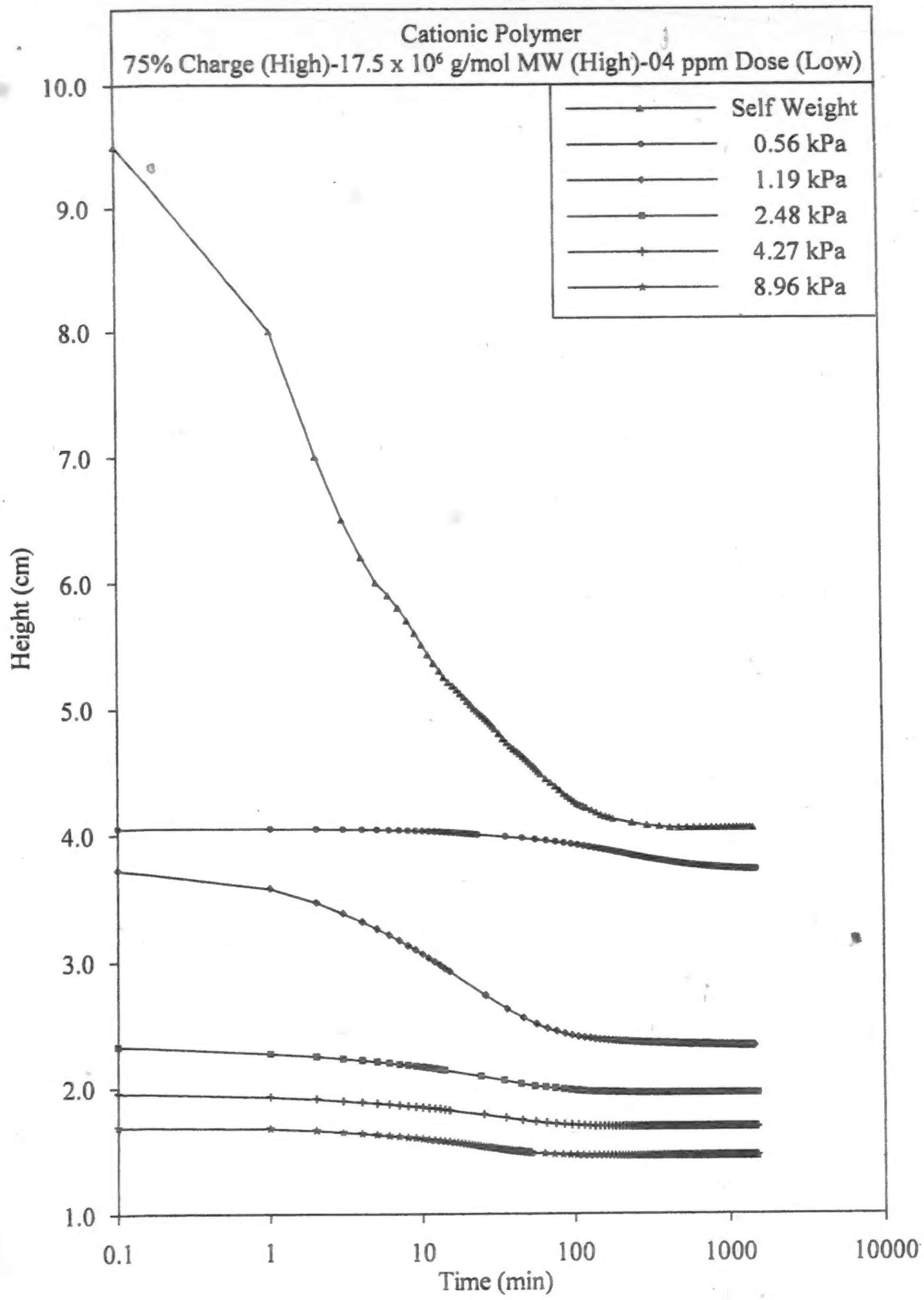

Figure A.36: Consolidation Test#15

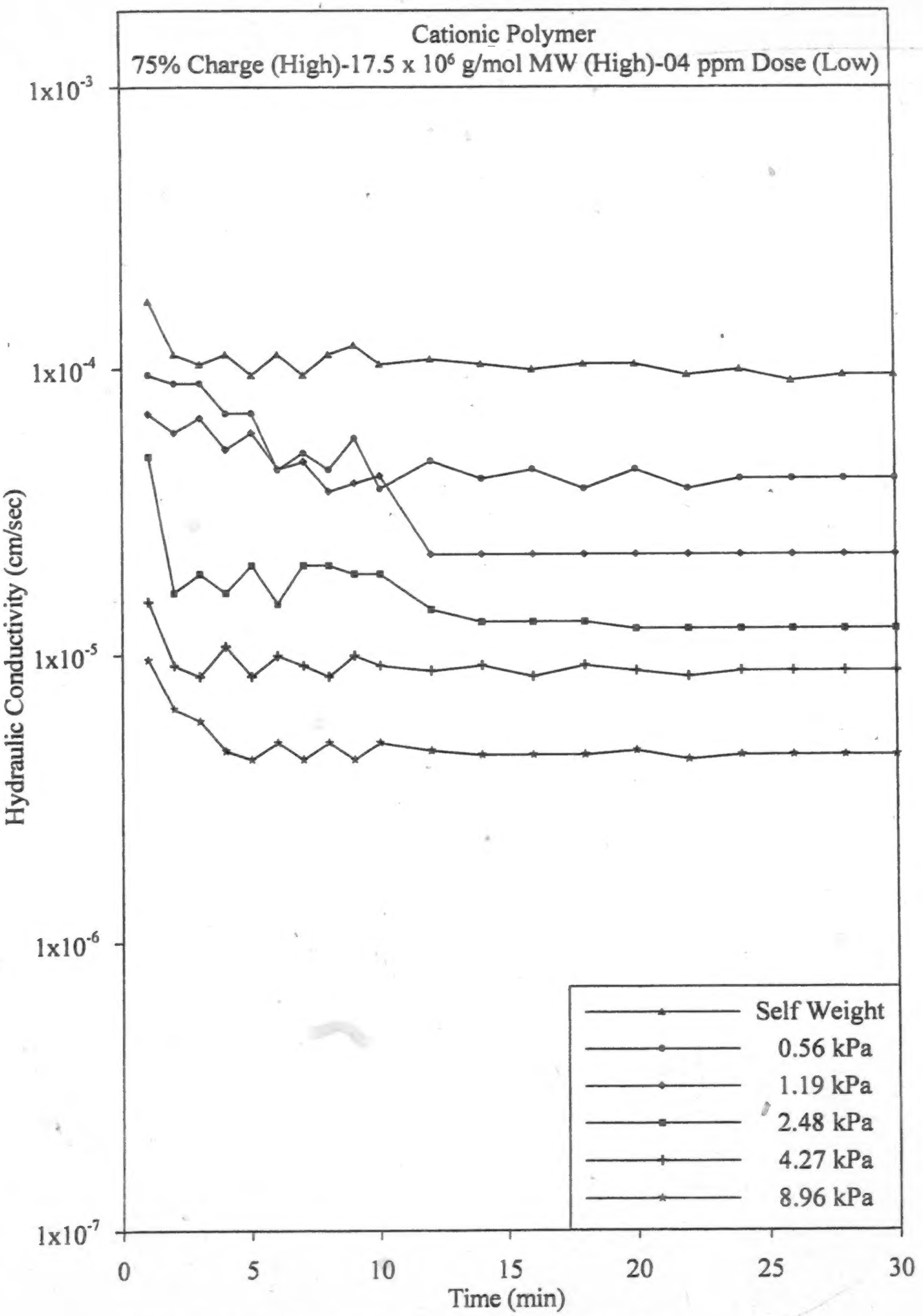

Figure A.37: Hydraulic conductivity during Test#15

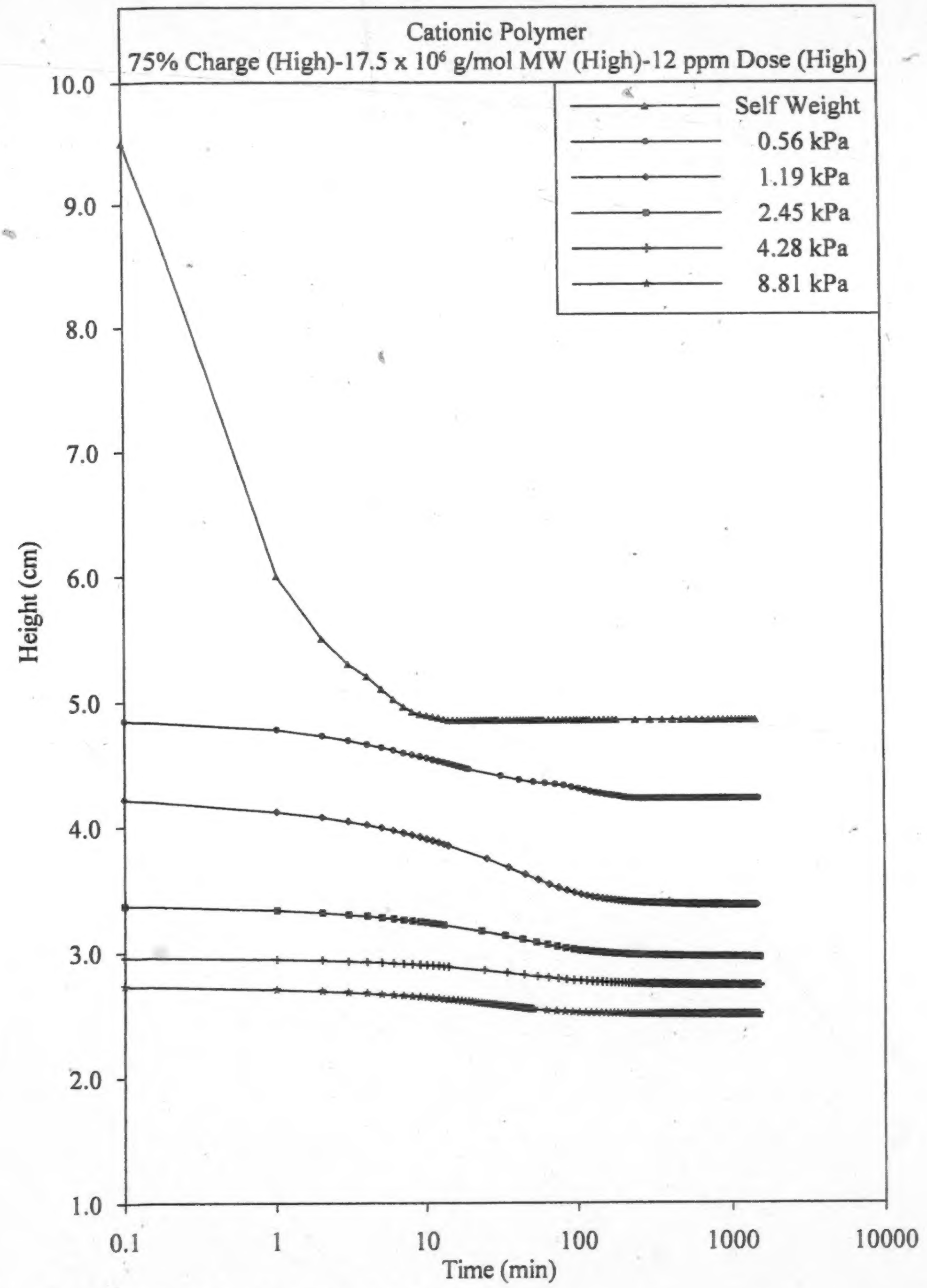

Figure A.38: Consolidation Test#16

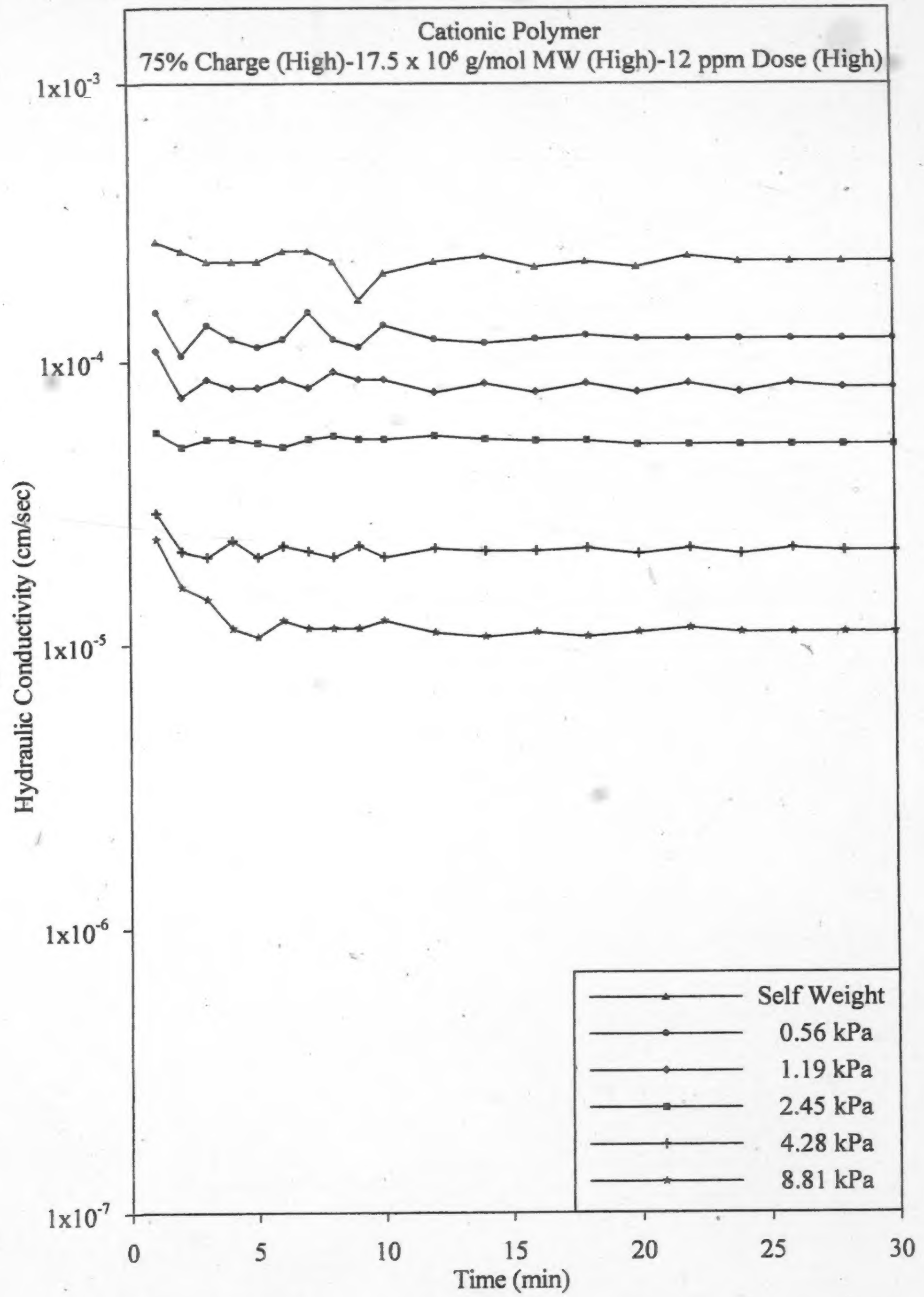

Figure A.39: Hydraulic conductivity during Test#16

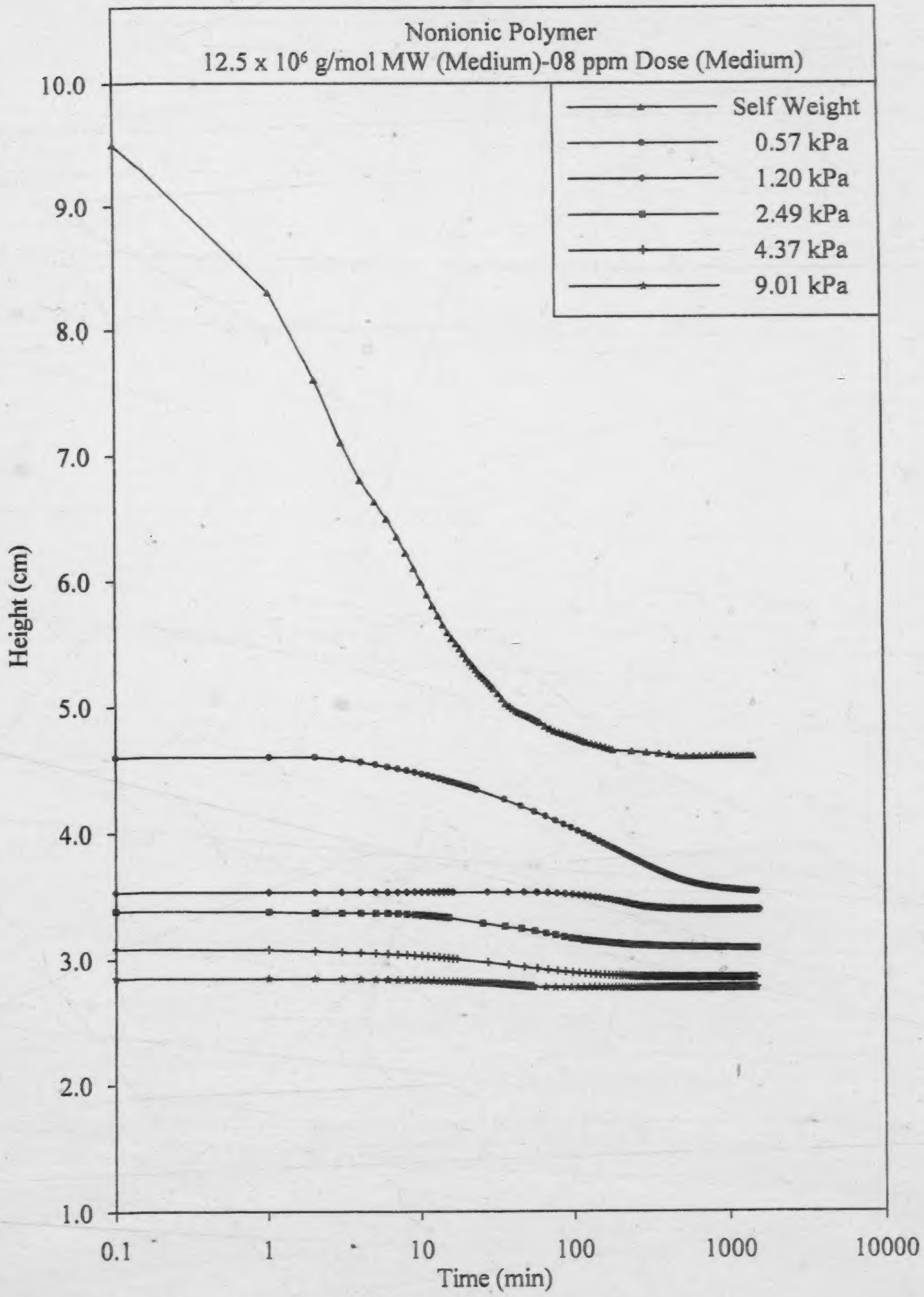

Figure A.40: Consolidation Test#17

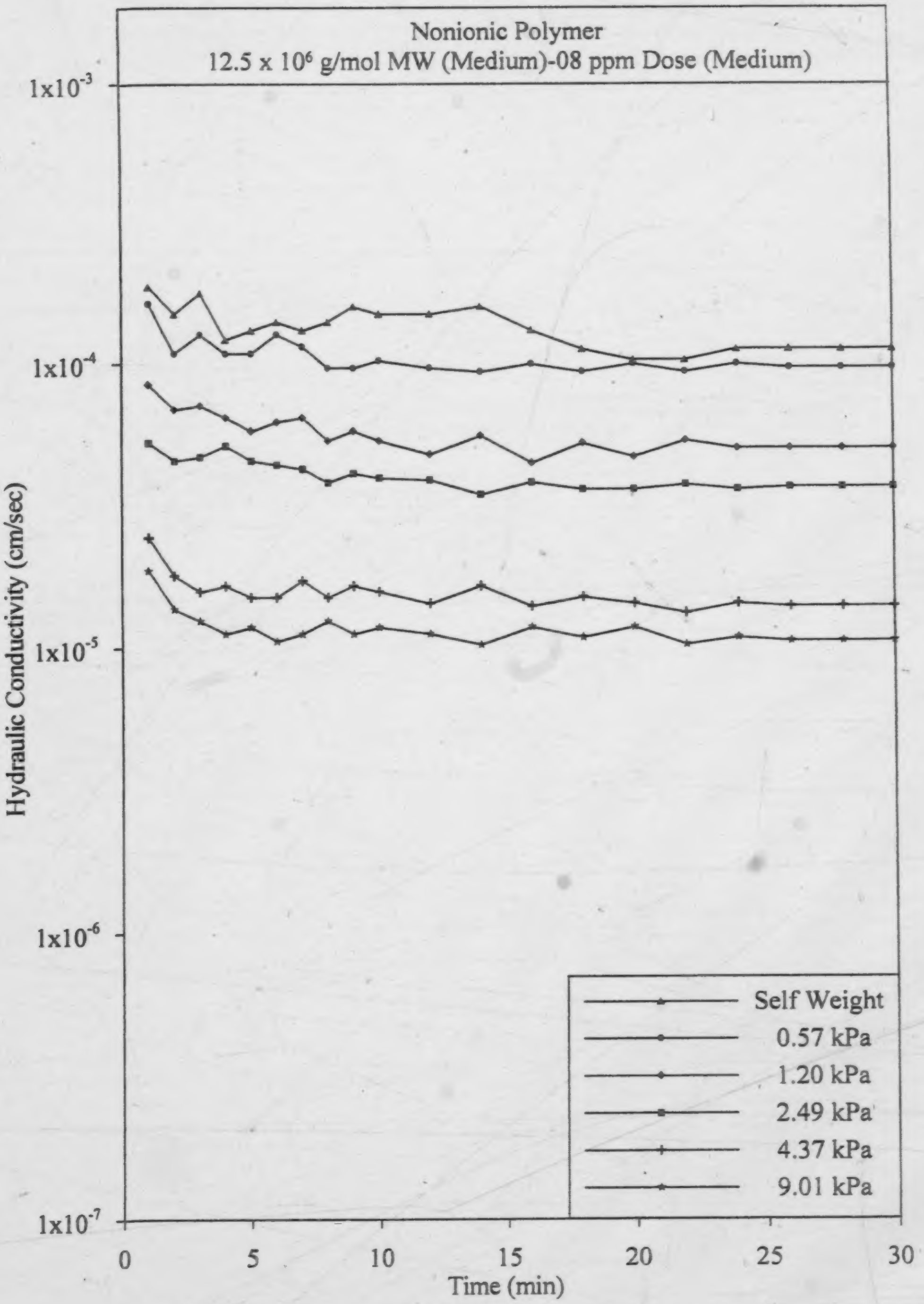

Figure A.41: Hydraulic conductivity during Test#17

Appendix B

Test Data of Chapter 7

B.1 GENERAL

This appendix provides the test data in the form of tables and figures. The test data was analyzed and discussed in Chapter Seven.

Table B.1: Consistency limits of laterite PAL modified with various ionic polymers

Polymer Parameters							
Type	Charge	MW x 10^6 (g/mol)	Dose (ppm)	w_l (%)	w_p (%)	w_s (%)	I_p (%)
Anionic	10% (Low)	7.5 (Low)	4	41	29	23	12
			12	53	35	26	18
		17.5 (High)	4	61	41	30	20
			12	70	40	27	30
	75% (High)	7.5 (Low)	4	46	29	22	17
			12	50	30	22	20
		17.5 (High)	4	41	28	22	13
			12	47	32	25	15
Cationic	10% (Low)	7.5 (Low)	4	49	30	22	19
			12	45	29	22	16
		17.5 (High)	4	71	41	27	30
			12	68	42	29	26
	75% (High)	7.5 (Low)	4	58	38	28	20
			12	62	37	26	25
		17.5 (High)	4	65	39	27	26
			12	57	37	27	20

Table B.2: Consistency limits of laterite PAL modified with various nonionic polymers

Polymer Parameters							
Type	Charge	MW x 10^6 (g/mol)	Dose (ppm)	w_l (%)	w_p (%)	w_s (%)	I_p (%)
Nonionic	NA	7.5 (Low)	4	36	28	24	8
			8	38	26	21	12
			12	52	33	24	19
		12.5 (Medium)	4	51	32	24	19
			8	63	42	30	21
			12	55	36	27	19
		17.5 (High)	4	42	29	23	13
			8	49	34	26	15
			12	58	36	26	22

Table B.3: Solids content at start and end of sedimentation tests for laterite PAL slurry modified with various ionic polymers

Polymer Parameters				s (%) Test Start	s (%) Test End
Type	Charge	MW x 10^6 (g/mol)	Dose (ppm)		
Anionic	10% (Low)	7.5 (Low)	4	15.1	43.0
			12	15.0	42.9
		17.5 (High)	4	15.1	40.5
			12	15.1	40.5
	75% (High)	7.5 (Low)	4	15.0	38.5
			12	15.1	38.5
		17.5 (High)	4	14.9	39.2
			12	15.2	38.5
Cationic	10% (Low)	7.5 (Low)	4	15.1	40.5
			12	15.0	40.5
		17.5 (High)	4	14.9	40.4
			12	15.0	40.5
	75% (High)	7.5 (Low)	4	15.1	40.8
			12	15.2	40.5
		17.5 (High)	4	15.1	40.5
			12	15.0	40.1

Table B.4: Solids content at start and end of sedimentation tests for laterite PAL slurry modified with various nonionic polymers

Polymer Parameters					
Type	Charge	MW x 10^6 (g/mol)	Dose (ppm)	*s* (%) Test Start	*s* (%) Test End
Nonionic	NA	7.5 (Low)	4	15.0	35.7
			8	15.1	36.4
			12	15.2	37.7
		12.5 (Medium)	4	15.1	49.0
			8	15.0	49.2
			12	15.1	50.0
		17.5 (High)	4	14.9	42.0
			8	15.2	42.9
			12	15.1	42.6

Table B.5: Solids content at start and end of consolidation tests for laterite PAL slurry modified with various ionic polymers

Polymer Parameters				s (%) Test Start	s (%) Test End
Type	Charge	MW x 10^6 (g/mol)	Dose (ppm)		
Anionic	10% (Low)	7.5 (Low)	4	-----	-----
			12	-----	-----
		17.5 (High)	4	15.0	43.2
			12	-----	-----
	75% (High)	7.5 (Low)	4	-----	-----
			12	-----	-----
		17.5 (High)	4	15.1	48.0
			12	-----	-----
Cationic	10% (Low)	7.5 (Low)	4	-----	-----
			12	-----	-----
		17.5 (High)	4	14.9	44.1
			12	-----	-----
	75% (High)	7.5 (Low)	4	-----	-----
			12	-----	-----
		17.5 (High)	4	15.0	46.3
			12	-----	-----

Table B.6: Solids content at start and end of consolidation test for laterite PAL slurry modified with nonionic polymer

Polymer Parameters				s (%)	s (%)
Type	Charge	MW x 10^6 (g/mol)	Dose (ppm)	Test Start	Test End
Nonionic	NA	7.5 (Low)	4	-----	-----
			8	-----	-----
			12	-----	-----
		12.5 (Medium)	4	-----	-----
			8	15.0	58.2
			12	-----	-----
		17.5 (High)	4	-----	-----
			8	-----	-----
			12	-----	-----

Table B.7: pH and EC after sedimentation and consolidation tests for laterite PAL slurry modified with various ionic polymers

Polymer Parameters				Sedimentation Test		Consolidation Test	
Type	Charge	MW x 10^6 (g/mol)	Dose (ppm)	pH	EC (μS/cm)	pH	EC (μS/cm)
Anionic	10% (Low)	7.5 (Low)	4	0.4	10000	-----	-----
			12	0.4	10000	-----	-----
		17.5 (High)	4	0.4	10000	0.4	10000
			12	0.4	10000	-----	-----
	75% (High)	7.5 (Low)	4	0.4	10000	-----	-----
			12	0.4	10000	-----	-----
		17.5 (High)	4	0.4	10000	0.4	10000
			12	0.4	10000	-----	-----
Cationic	10% (Low)	7.5 (Low)	4	0.4	10000	-----	-----
			12	0.4	10000	-----	-----
		17.5 (High)	4	0.4	10000	0.4	10000
			12	0.4	10000	-----	-----
	75% (High)	7.5 (Low)	4	0.4	10000	-----	-----
			12	0.4	10000	-----	-----
		17.5 (High)	4	0.4	10000	0.4	10000
			12	0.4	10000	-----	-----

Table B.8: pH and EC after sedimentation and consolidation tests for laterite PAL slurry modified with various nonionic polymers

Polymer Parameters				Sedimentation Test		Consolidation Test	
Type	Charge	MW x 10^6 (g/mol)	Dose (ppm)	pH	EC (µS/cm)	pH	EC (µS/cm)
Nonionic	NA	7.5 (Low)	4	0.4	10000	-----	-----
			8	0.4	10000	-----	-----
			12	0.4	10000	-----	-----
		12.5 (Medium)	4	0.4	10000	-----	-----
			8	0.4	10000	0.4	10000
			12	0.4	10000	-----	-----
		17.5 (High)	4	0.4	10000	-----	-----
			8	0.4	10000	-----	-----
			12	0.4	10000	-----	-----

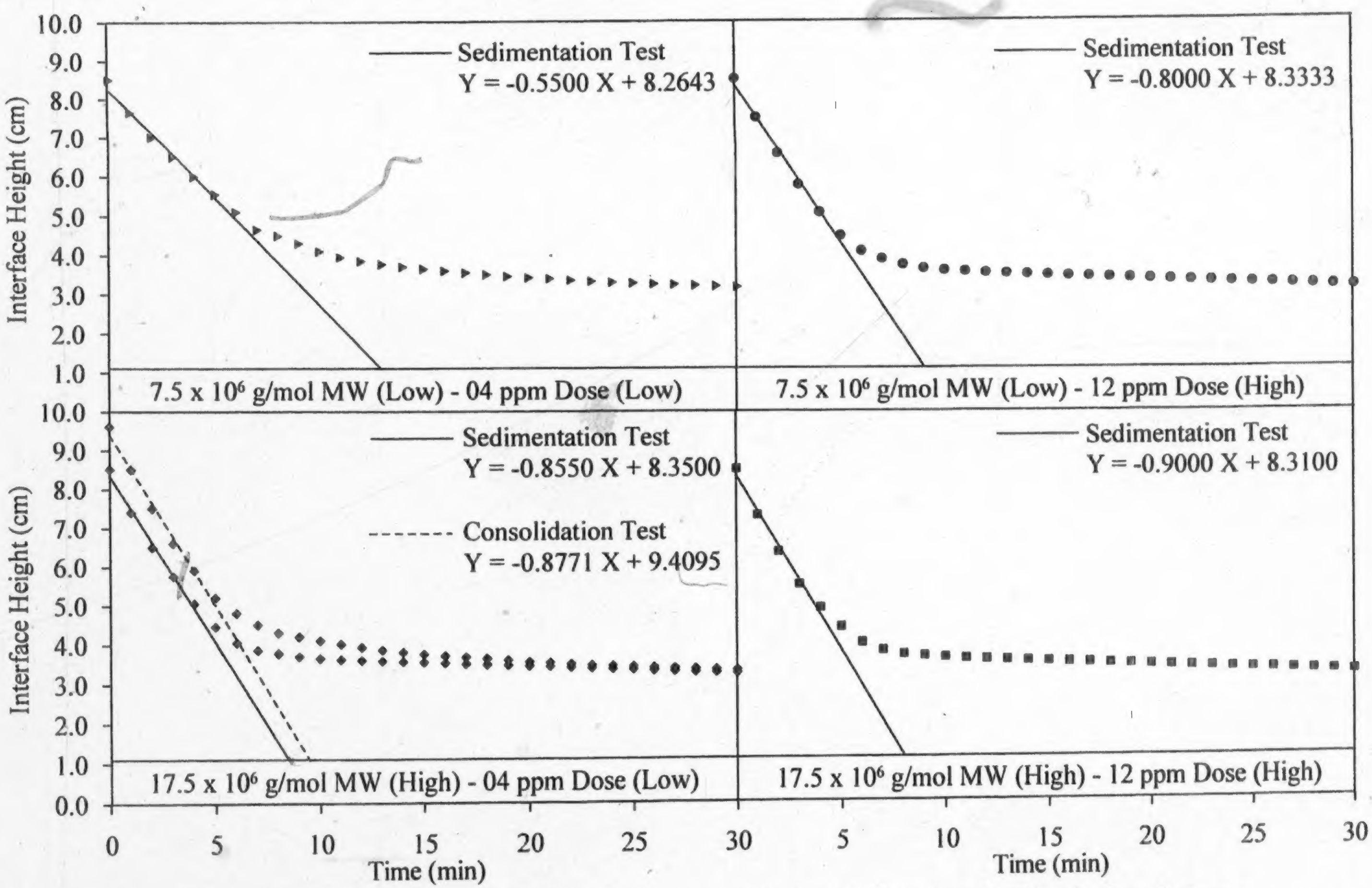

Figure B.1: Determination of k_i for laterite PAL slurry modified with 10% charge low) anionic polymers

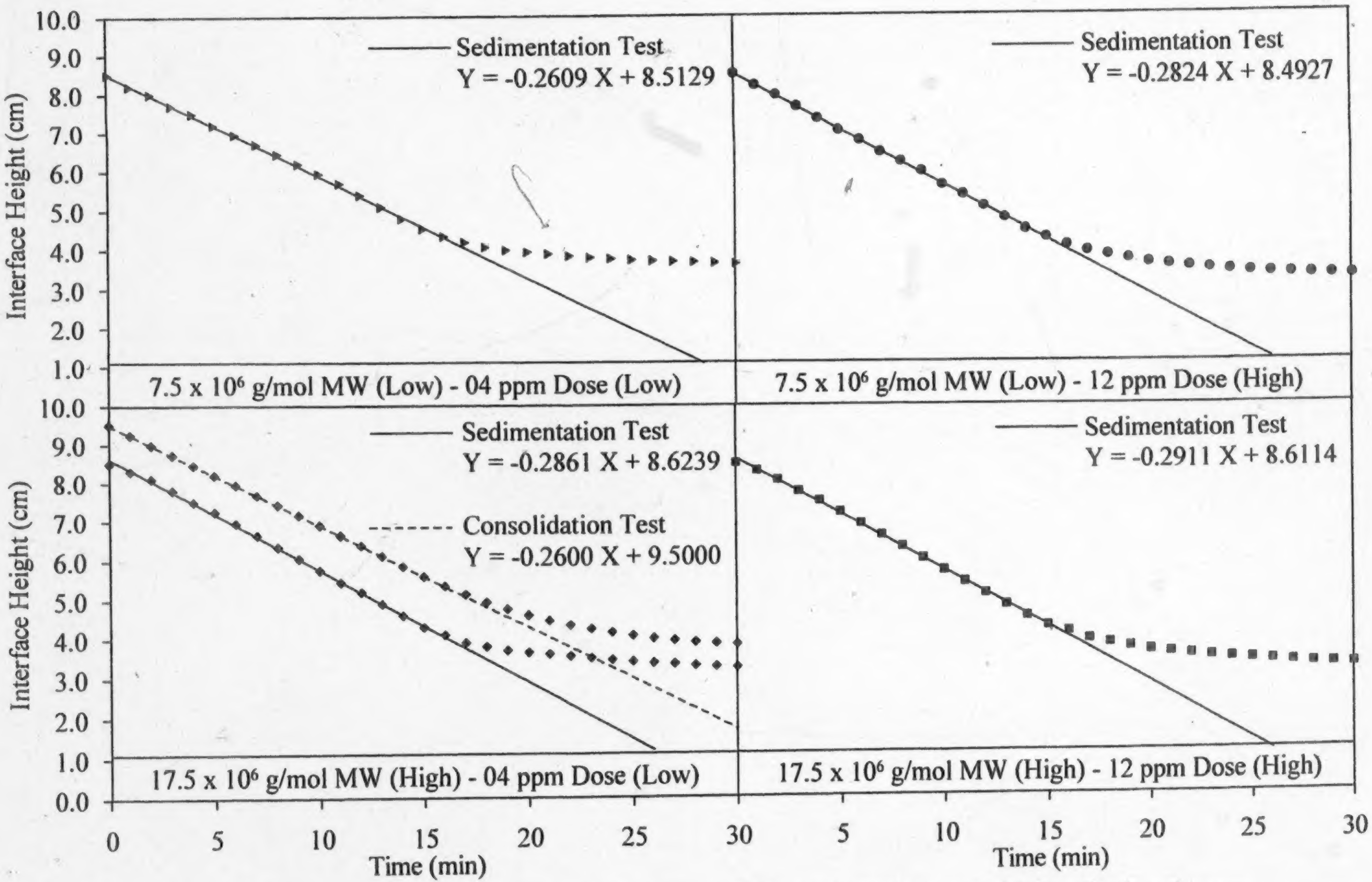

Figure B.2: Determination of k_i for laterite PAL slurry modified with 75% charge (high) anionic polymers

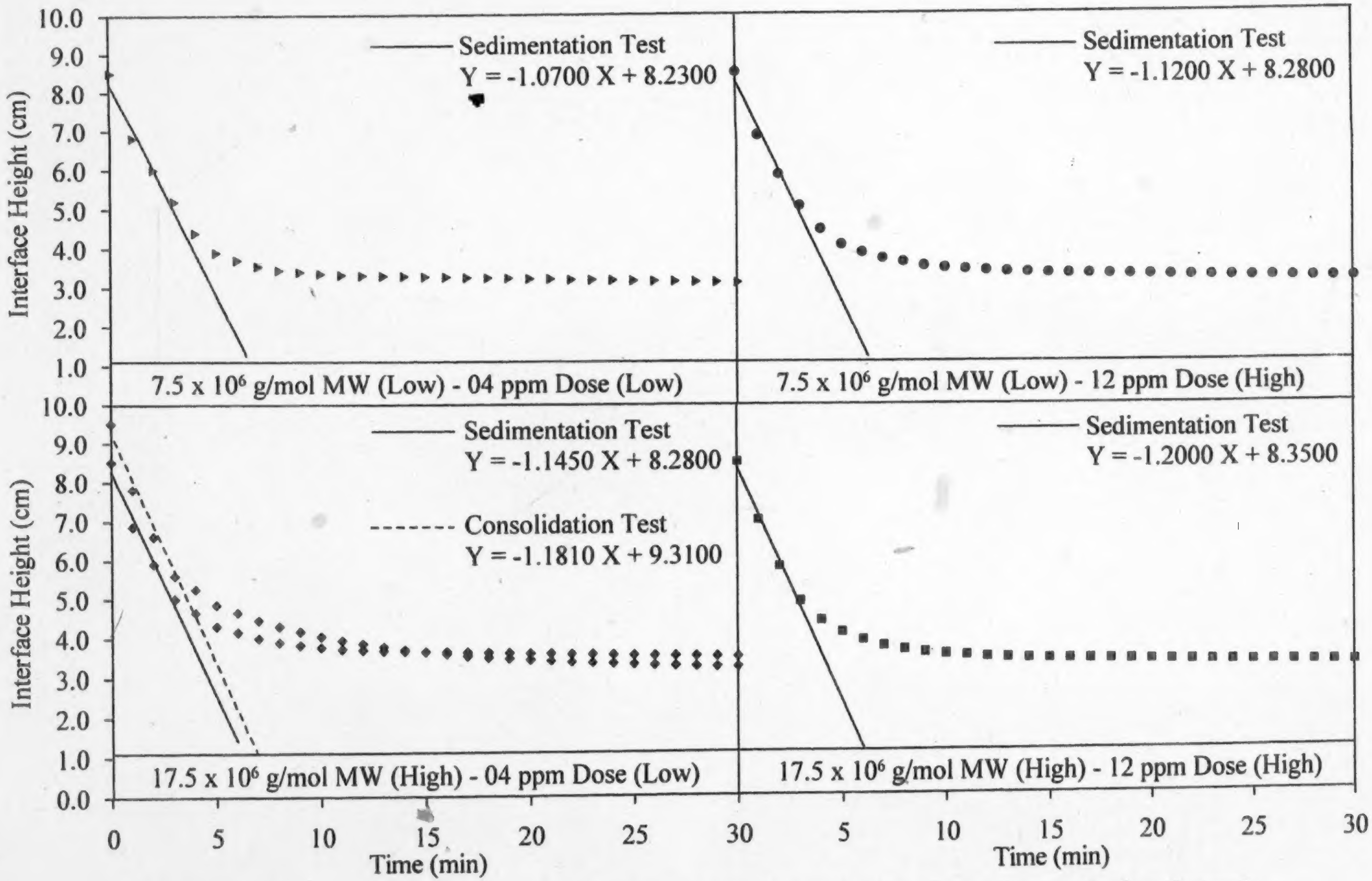

Figure B.3: Determination of k_i for laterite PAL slurry modified with 10% charge (low) cationic polymers

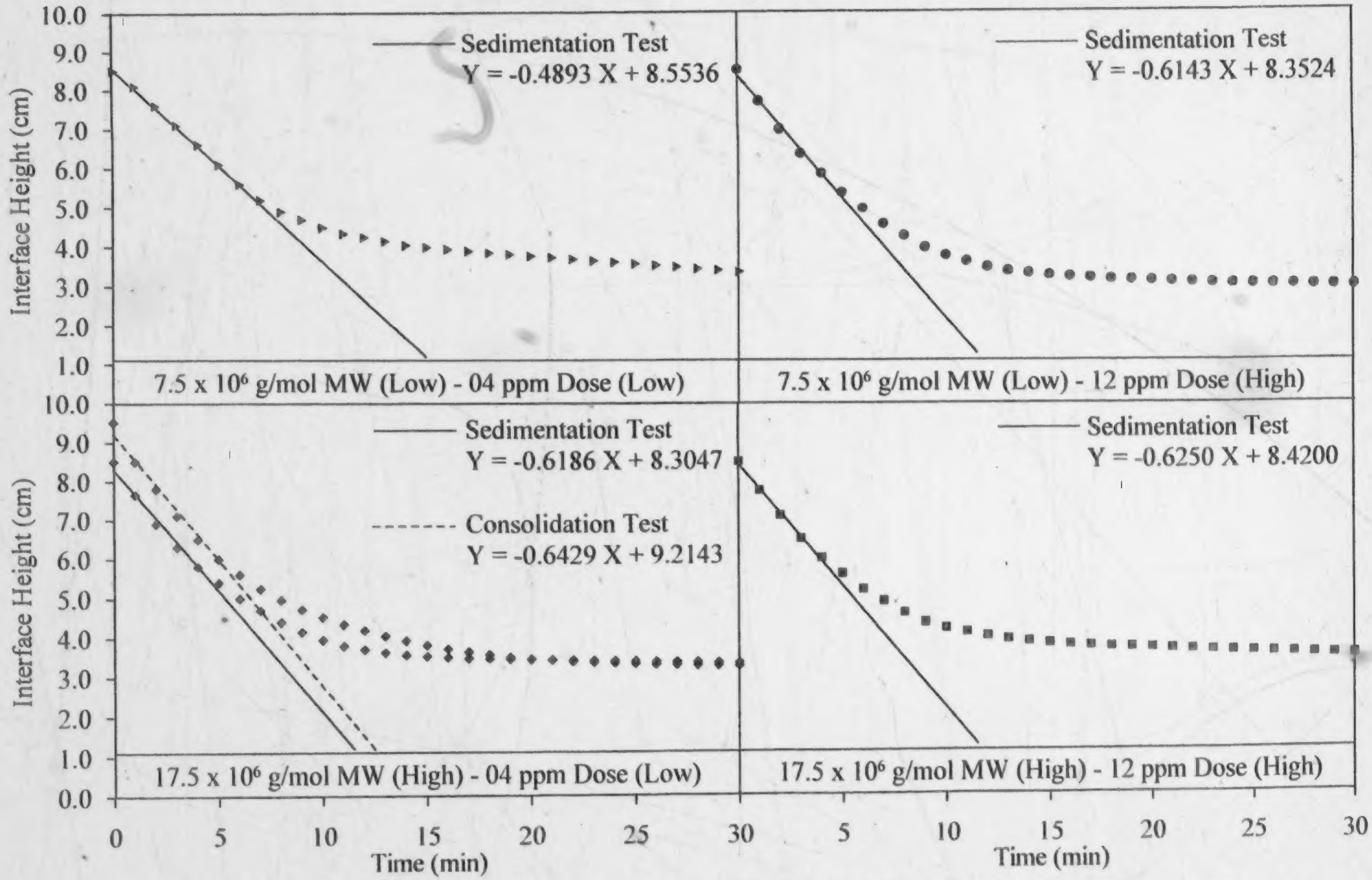

Figure B.4: Determination of k_i for laterite PAL slurry modified with 75% charge (high) cationic polymers

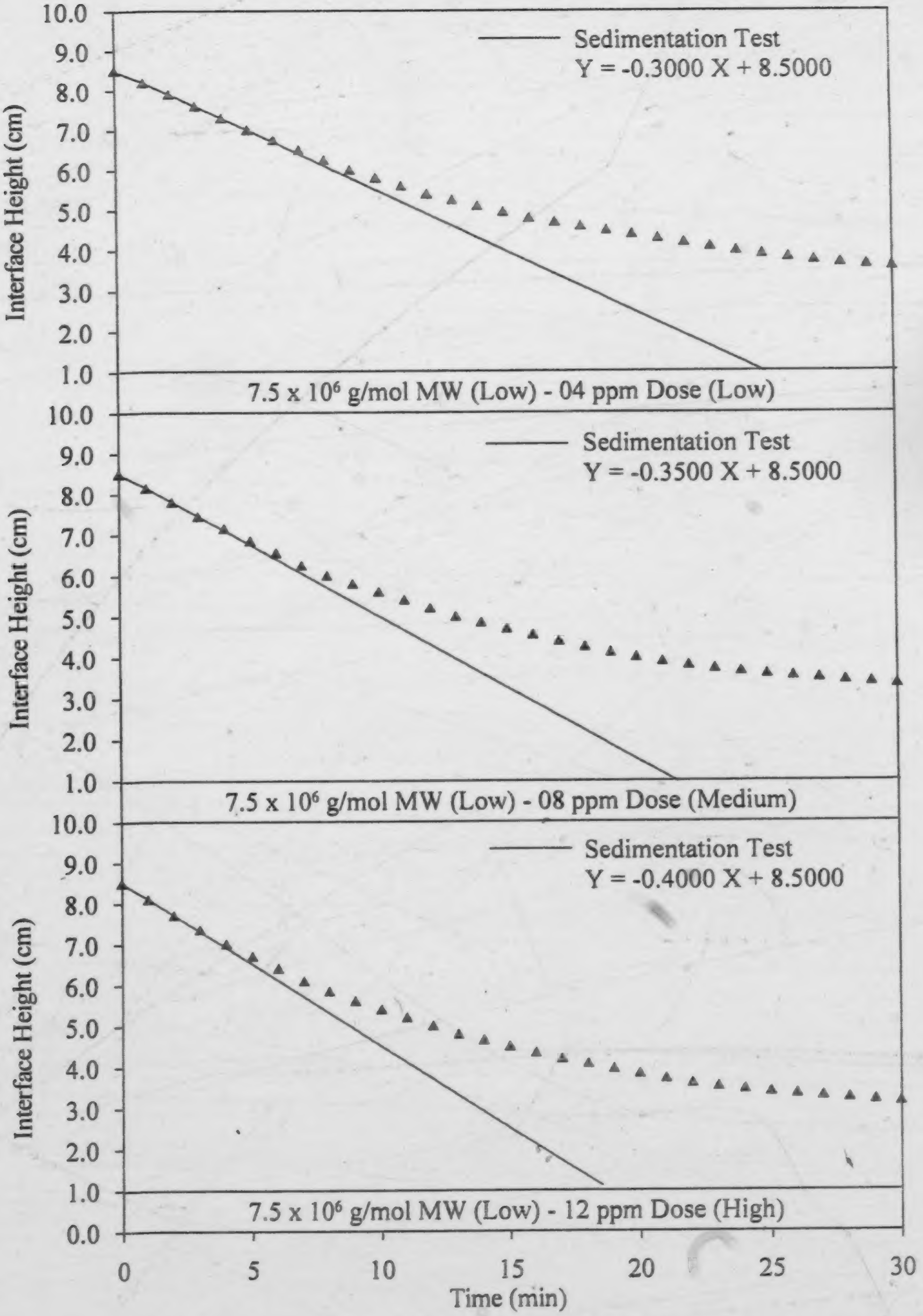

Figure B.5: Determination of k_i using low MW nonionic polymer

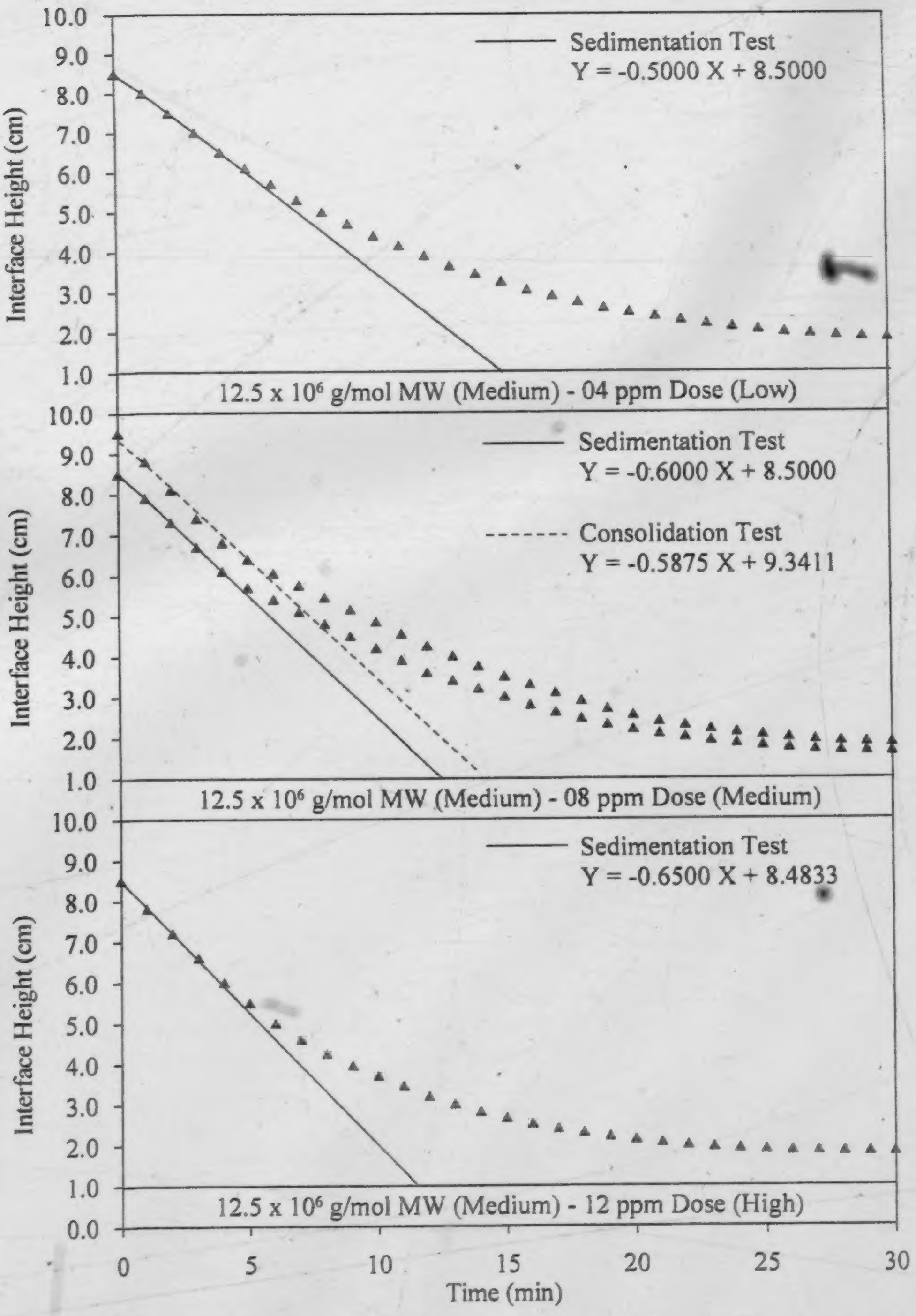

Figure B.6: Determination of k_i using medium MW nonionic polymer

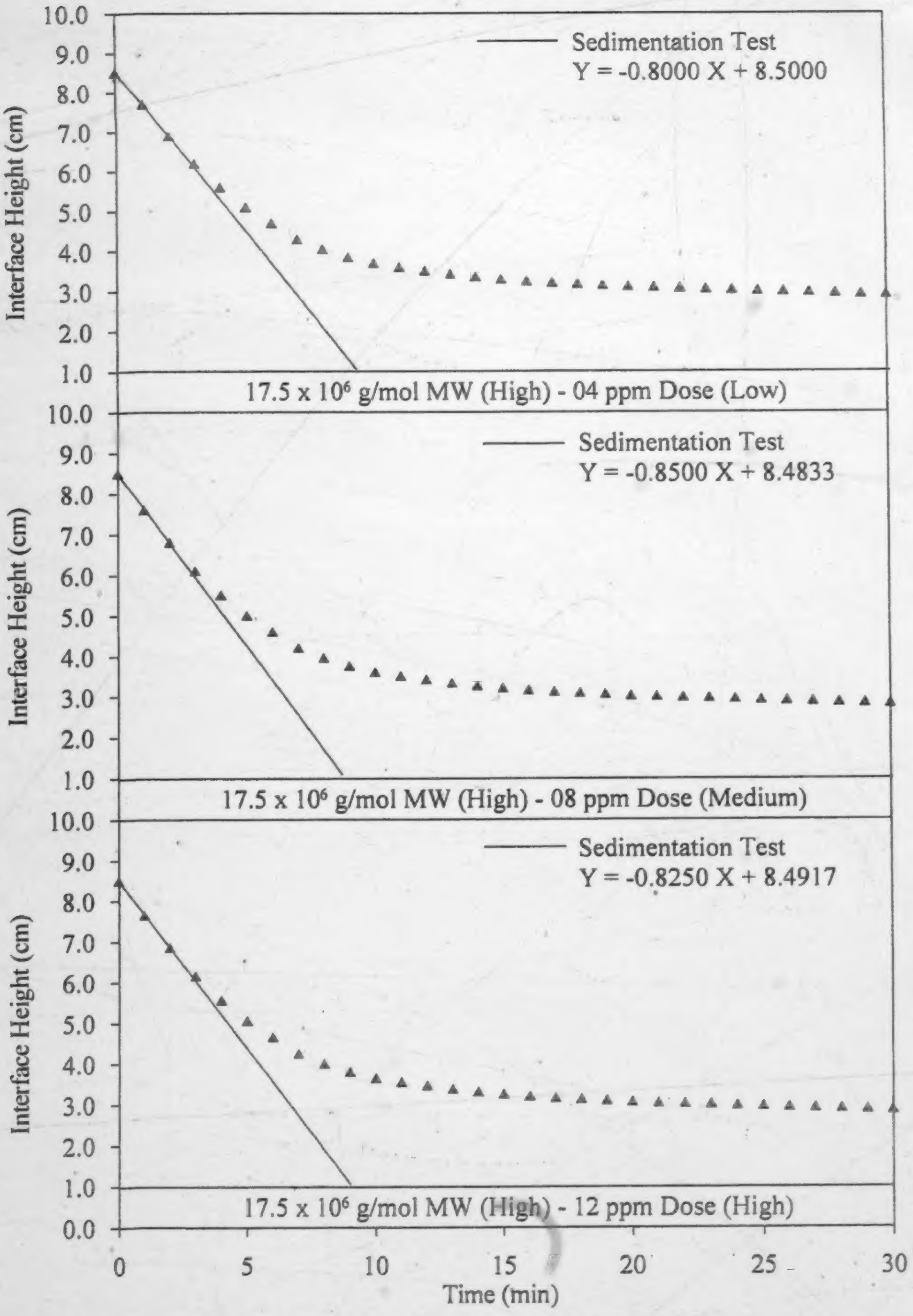

Figure B.7: Determination of k_i using high MW nonionic polymer

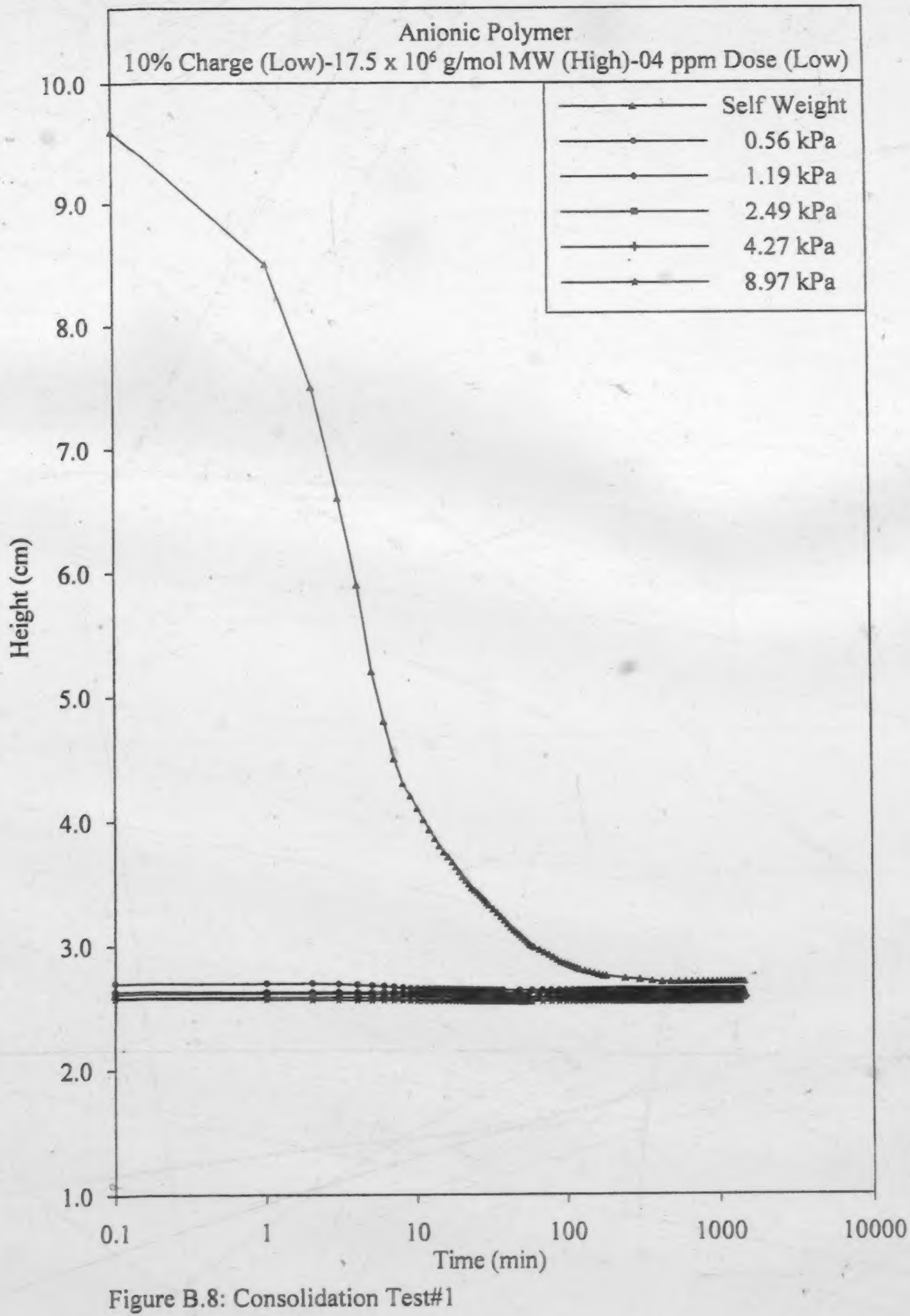

Figure B.8: Consolidation Test#1

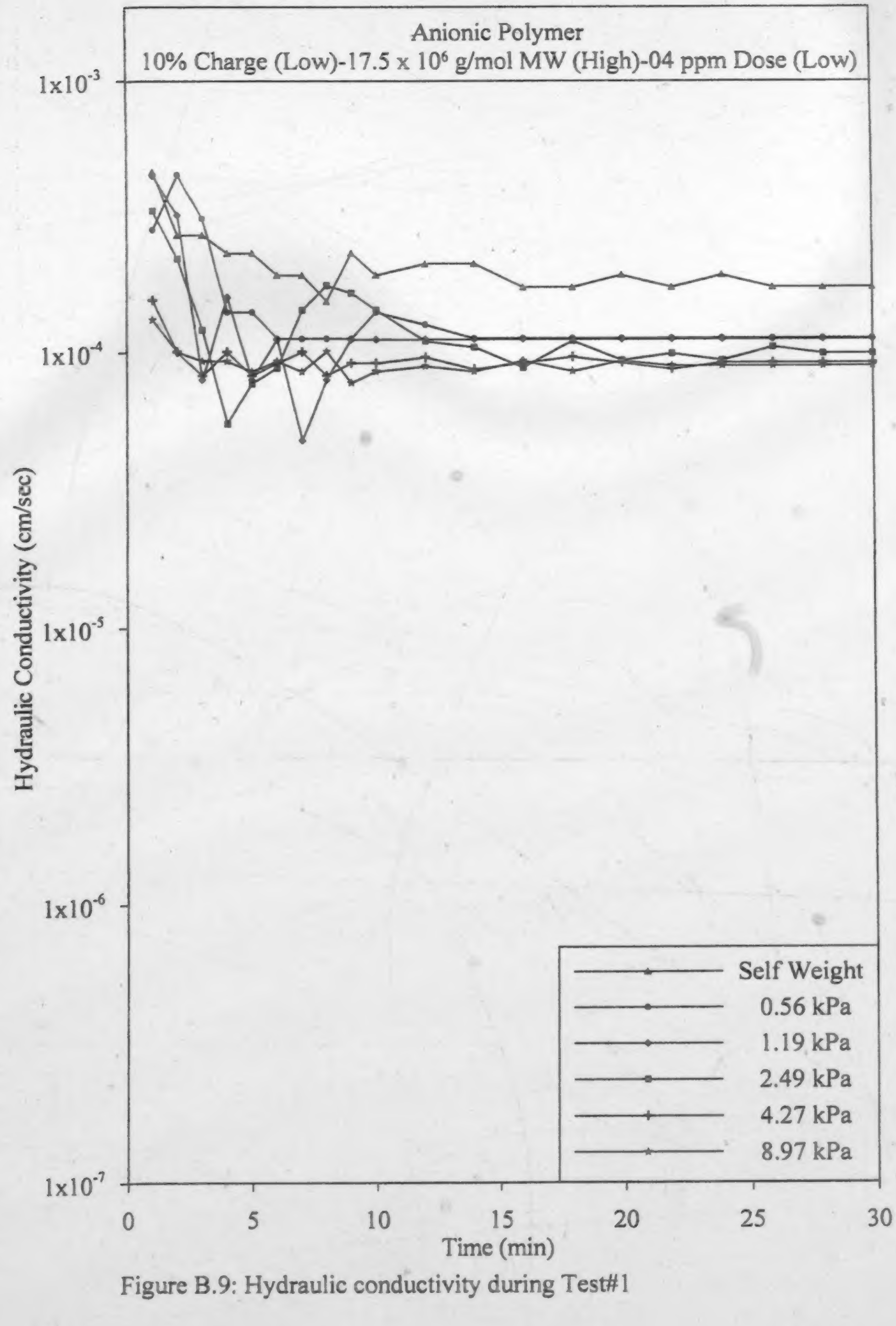

Figure B.9: Hydraulic conductivity during Test#1

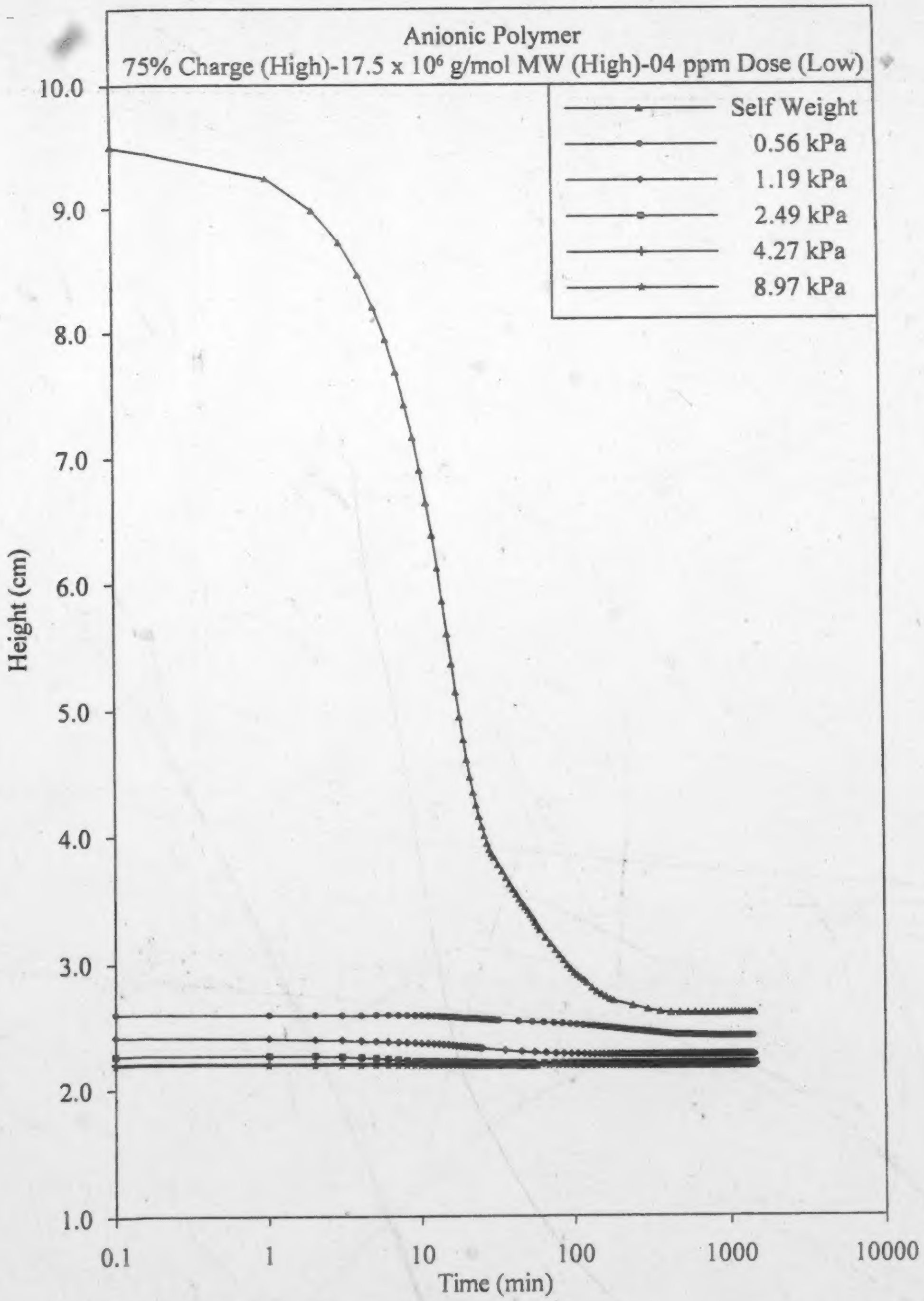

Figure B.10: Consolidation Test#2

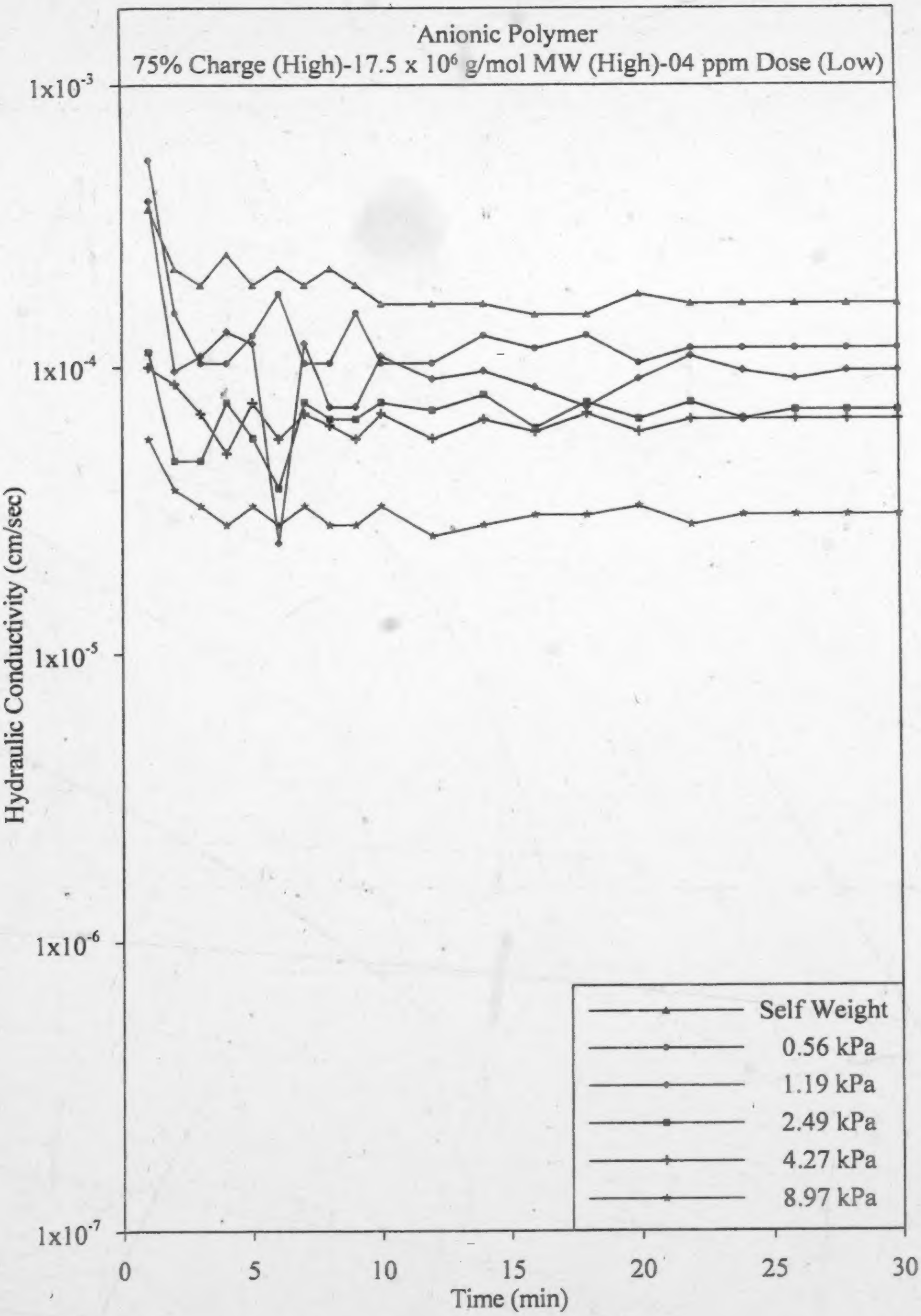

Figure B.11: Hydraulic conductivity during Test#2

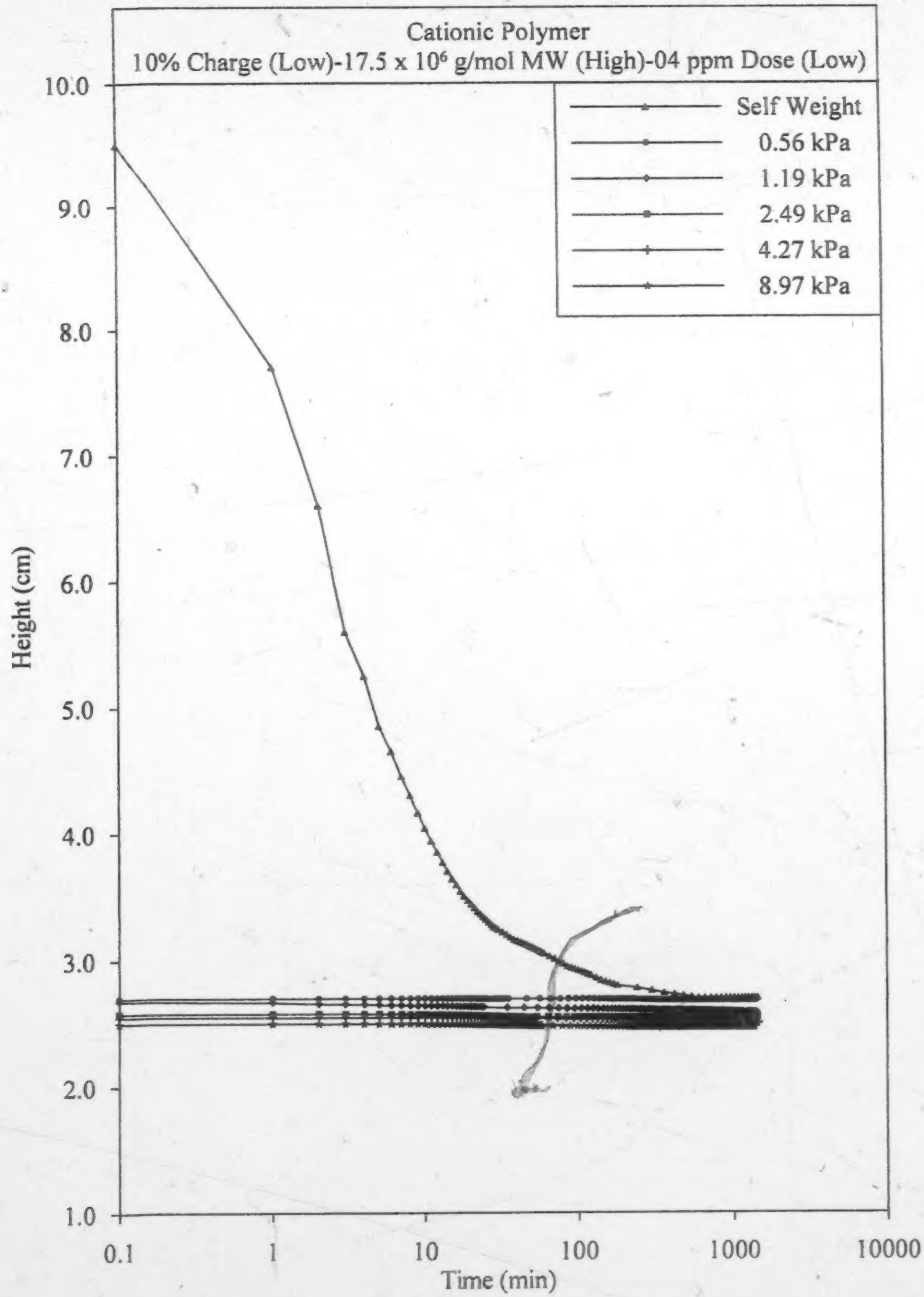

Figure B.12: Consolidation Test#3

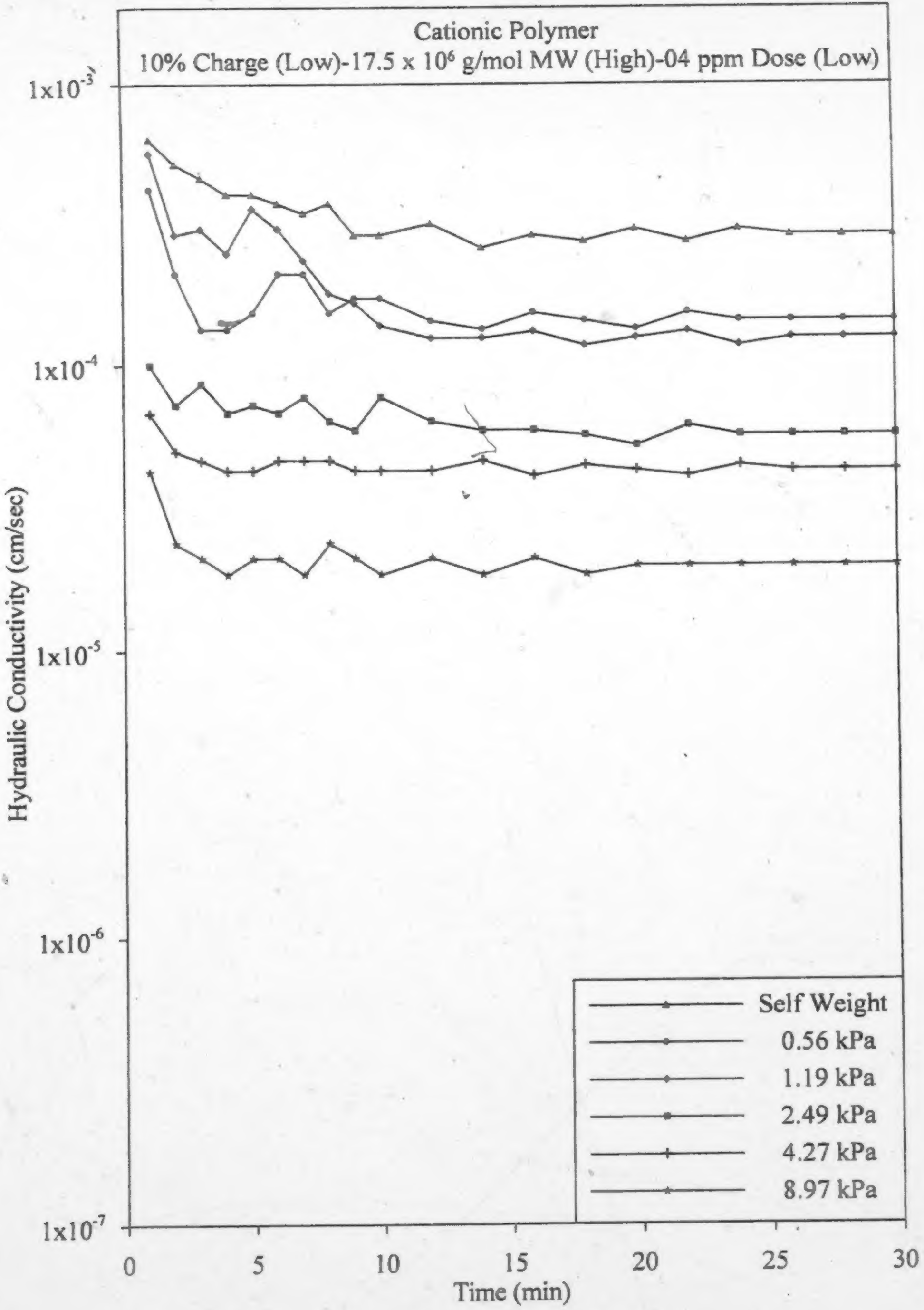

Figure B.13: Hydraulic conductivity during Test#3

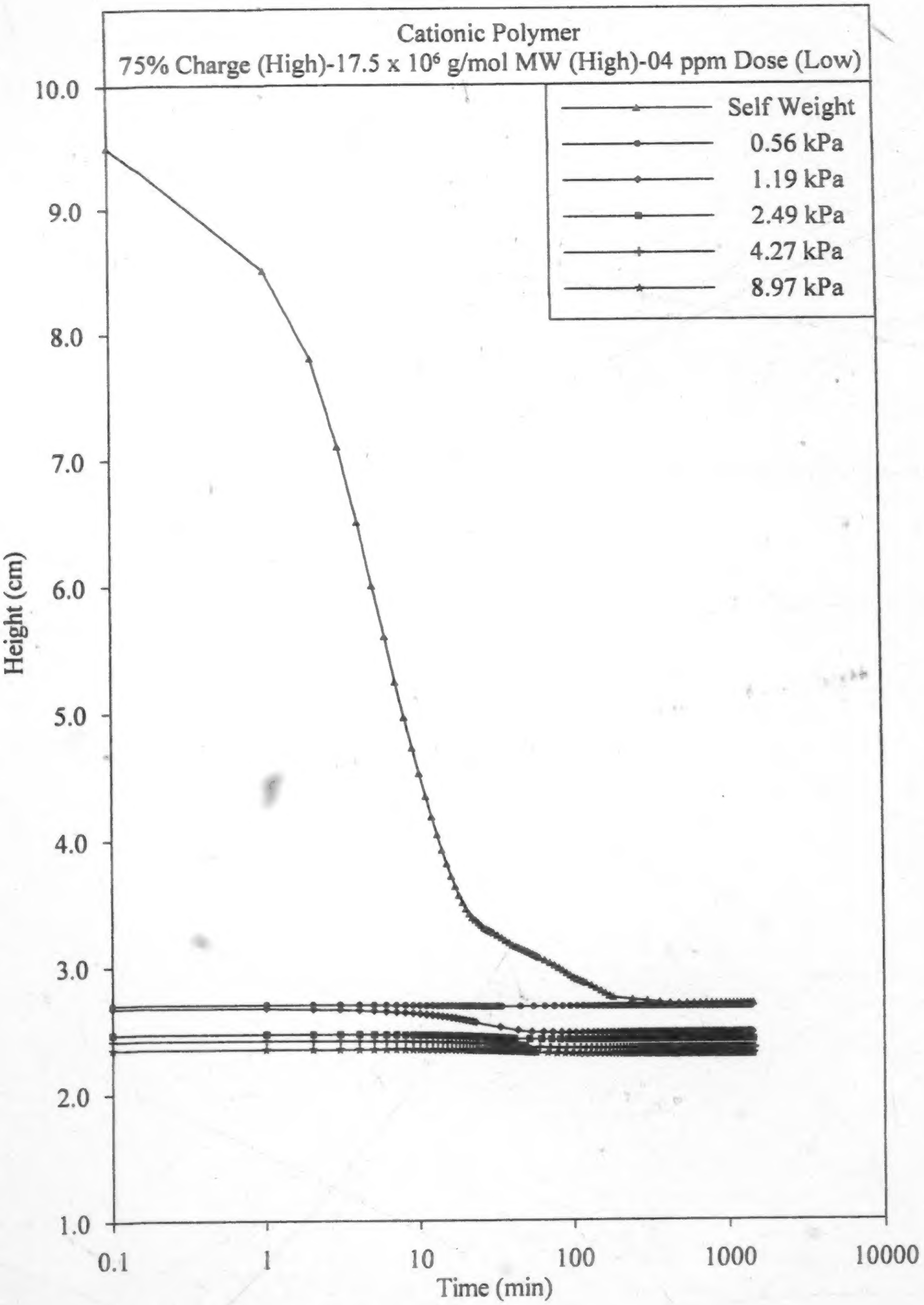

Figure B.14: Consolidation Test#4

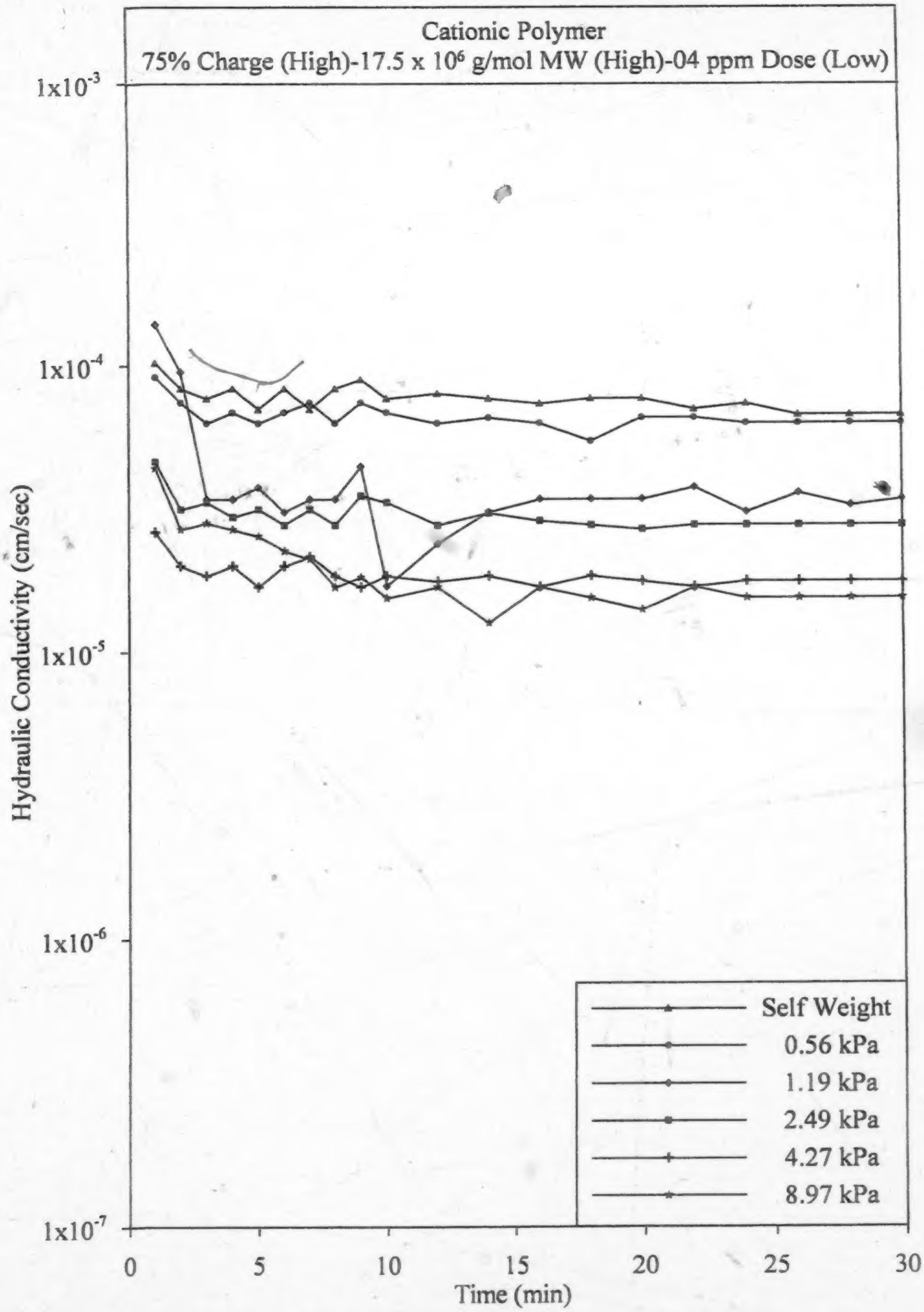

Figure B.15: Hydraulic conductivity during Test#4

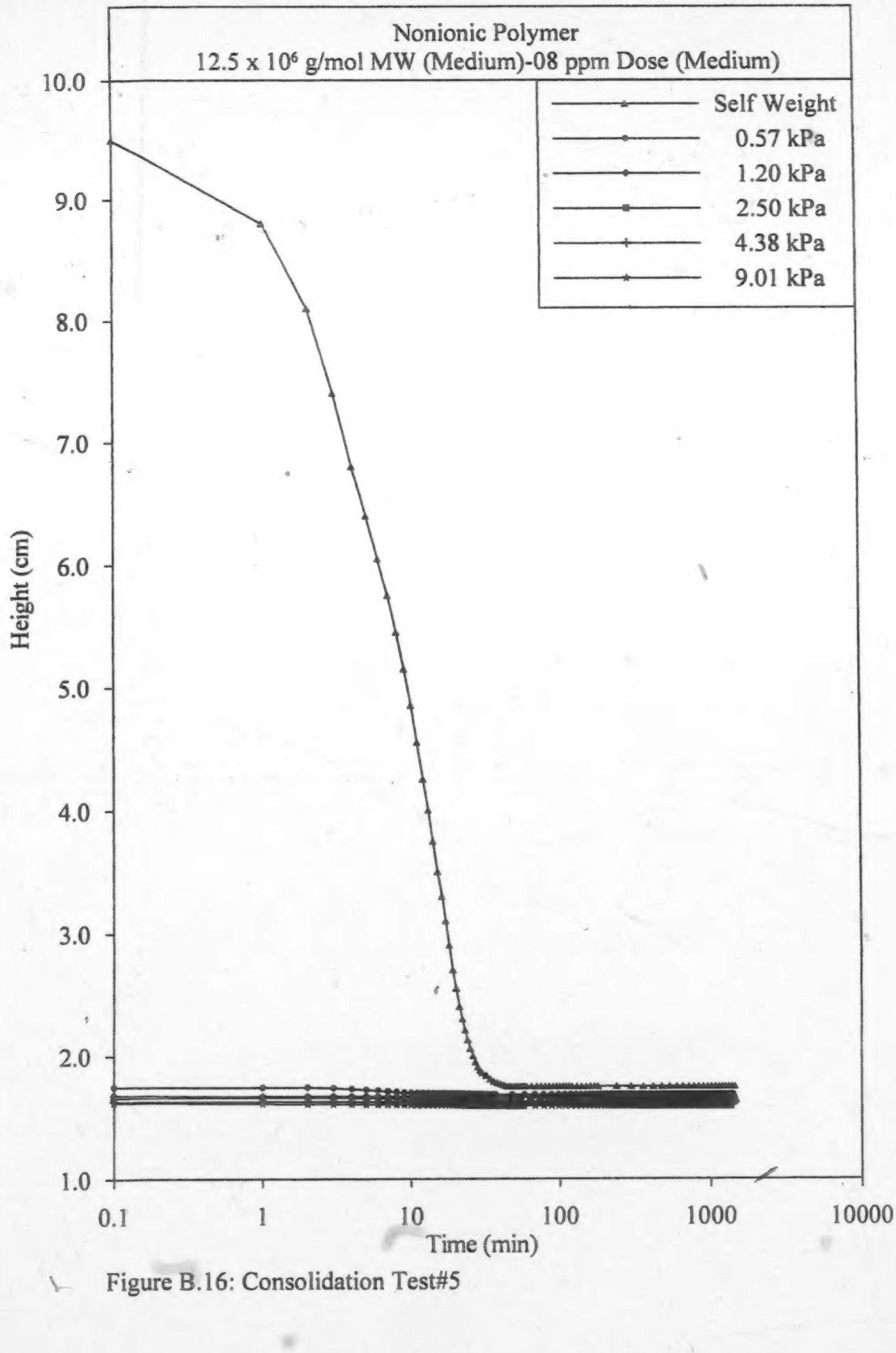

Figure B.16: Consolidation Test#5

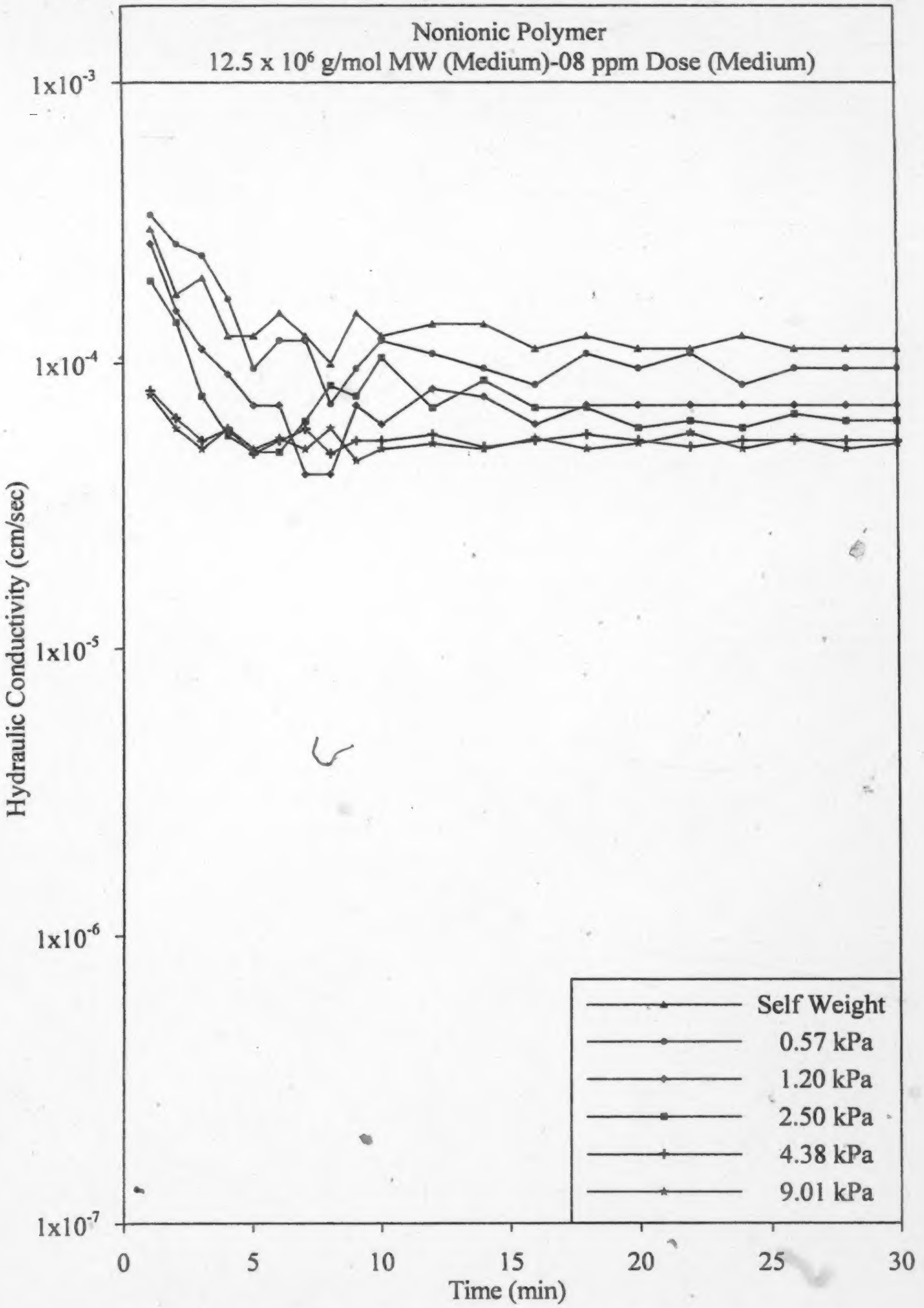

Figure B.17: Hydraulic conductivity during Test#5